THE JOURNAL OF
CHEMICAL PHYSICS

VOLUME 22 NUMBER 5

MAY, 1954

PUBLISHED BY THE
AMERICAN INSTITUTE OF PHYSICS

THE JOURNAL
OF
CHEMICAL PHYSICS

VOLUME 22, NUMBER 5 MAY, 1954

Vibrational Relaxation Times in Gases (Three-Dimensional Treatment)*

ROBERT N. SCHWARTZ, *Naval Ordnance Laboratory, White Oak, Maryland*

AND

KARL F. HERZFELD, *Catholic University of America, Washington, D. C.*

(Received December 11, 1953)

The calculations previously made by Schwartz, Slawsky, and Herzfeld are extended to three dimensions. As before, an exponential repulsion is fitted to the Lennard-Jones potential, with constants found from viscosity data. While the transition probability is determined directly by the short range repulsion forces, the attractive forces and the effect of the centrifugal quasi-potential modify the effective velocity of the colliding molecules. The agreement with experiment is fairly good, although high up on the repulsion curve (O_2,N_2) the Lennard-Jones 6–12 curve seems to be not quite steep enough.

INTRODUCTION

DESPITE the simplified geometry of the one-dimensional collision between a pair of molecules considered by C. Zener,[1] calculations of vibrational relaxation times based on this method have been fairly successful.[2,3] Zener treated the collision problem by quantum mechanics but restricted the molecules to motion along a line. In this paper this treatment is extended to a collision in three dimensions.

THE EQUATIONS GOVERNING A VIBRATIONAL ENERGY EXCHANGE IN THREE-DIMENSIONAL SPACE

In the one-dimensional treatment of the problem of an exchange of energy between the translational and vibrational degrees of freedom of a molecule during collision with another molecule, the molecules involved in the collision are taken to move along a straight line. The external motion of the pair needs but one coordinate for its description, r, the distance between the centers of mass of the pair. The particle is not permitted to rotate with respect to the line of motion. Thus, the potential of the force field between molecules can be written $V=V(r,s_1,s_2\cdots)$, where s_1, $s_2\cdots$ are internal vibrational coordinates of the molecule. This potential is approximated by a product of functions of the variables, $V=V_r(r)\cdot V_1(s_1)\cdot V_2(s_2)\cdots$.

In the present paper, the molecules are considered to move in three dimensions. Now, the relative motion of the centers of mass of the two molecules need for their description coordinates r and θ, where r is defined as above. The angle θ is the angle between the vector r and the apse-line or line joining the two molecules when at their point of closest approach. Again, the molecules are considered rotationless with respect to the apse-line. This simplification in the description of the collision, as in the one-dimensional treatment, is justified on the grounds that the actual time of "near approach" of the molecules is short compared to the period of rotation. It is therefore assumed that the rotation plays no role in the energy exchange between translation and vibration. There are experimental indications that this is so. The inclusion of rotational transitions would complicate the calculations enormously. Curtiss and Adler[4] have included the rotation in their formulas but have not yet succeeded in getting numerical results. K. Takayanagi used a classical approximation in treating the rotational problem.[5] Accordingly, the vibration is treated here as if it were a breathing vibration in a nearly spherical molecule. For a diatomic molecule, one may expect that

* Taken in part from a dissertation submitted by R.N.S. to the Faculty of the Graduate School of Arts and Sciences of the Catholic University of America in partial fulfillment of the requirements for the Ph.D. degree.

[1] C. Zener, Phys. Rev. **37**, 556 (1931).

[2] Schwartz, Slawsky, and Herzfeld, J. Chem. Phys. **20**, 1591 (1952).

[3] K. Takayanagi, Progr. Theoret. Phys. Japan **8**, 111 (1952).

[4] C. F. Curtiss and F. T. Adler, J. Chem. Phys. **20**, 249 (1952).

[5] K. Takayanagi, Progr. Theoret. Phys. Japan **8**, 497 (1952); K. Takayanagi and T. Kishimoto, ibid. **9**, 578 (1953).

the value for the transition probability so calculated ought to be multiplied by $\langle\cos^2\theta\rangle_{Av}=\frac{1}{3}$; this has been done here in the tables. The potential, then, as in the one-dimensional case, may be represented as a product of functions of the coordinates r and $s_1, s_2\cdots$. For simplicity, we shall treat a system with one internal coordinate s; the generalization to many internal coordinates is straightforward.

Let Ψ be the wave function which describes the collision of the two molecules in space. It satisfies the Schroedinger equation,

$$H^{(s)}\Psi-\frac{h^2}{8\pi^2\mu}\left(\frac{1}{r^2}\frac{\partial}{\partial r}\left(r^2\frac{\partial\Psi}{\partial r}\right)+\frac{1}{r^2\sin\theta}\frac{\partial}{\partial\theta}\left(\sin\theta\frac{\partial\Psi}{\partial\theta}\right)\right)+V\Psi=W\Psi, \quad (1)$$

where

$$V=V_r(r)\cdot V_{\text{int}}(s). \quad (2)$$

Here $H^{(s)}$ is the Hamiltonian of the internal vibrational motion and W is the total energy of the system. It is a sum of energies of the external and vibrational motion, i.e., $W=1/2\mu v_0^2+W_{\text{int}}$, where v_0 is the relative velocity of the molecules at infinite separation before collision, and W_{int}, the internal energy at that time. μ is the reduced mass of the two molecules. $\mu=M_aM_b/(M_a+M_b)$ where M_a and M_b are the masses of the two molecules.

As in the one-dimensional treatment, we seek a solution as an infinite series whose terms are products of functions of the coordinates.

$$\Psi=\sum_{i=0}^{\infty}\sum_{j=0}^{\infty}{}_j\Psi_i=\sum_{i=0}^{\infty}\sum_{j=0}^{\infty}{}_jR_i(r)\Theta_j(\theta)\psi_i(s). \quad (3)$$

Place this expression into Eq. (1). A total differential equation for Θ can be separated out. The solution of this equation yields $\Theta=P_j(\cos\theta)$, Legendre polynomials. The orbital quantum numbers, j, will not change during collision, as V does not contain a function of θ. This means that the angular momentum of the translational motion is preserved. Proceeding with the usual perturbation calculation, select as the ψ_i the unperturbed solution for the harmonic oscillator (Hermite polynomials). One then multiplies the remaining differential equation with ψ_n and integrates over the oscillator coordinates. If one then substitutes in the remaining equation the expression ${}_jf_i/r$ for ${}_jR_i$, one obtains for the ${}_jf_i$'s equations similar to those found in the one-dimensional case except that a centrifugal energy term, $j(j+1)h^2/(8\pi^2\mu r^2)$, now must be added to the potential energy V:

$$\left(\frac{h^2}{8\pi^2\mu}\frac{d^2}{dr^2}+\frac{\mu v_0^2}{2}\right){}_jf_n+\sum_{i=0}^{\infty}\left(\frac{j(j+1)h^2}{8\pi^2\mu r^2}+\int_0^{\infty}\psi_iV\psi_n ds\right){}_jf_i=0. \quad (4)$$

In the following we shall restrict ourselves to two states $i=0, n$. In the case of deactivation, ψ_0 designates the higher vibrational state, while v_0 is the relative velocity before collision. ψ_n is the lower vibrational state and v_n the relative velocity after collision. One has, in a one-quantum jump,

$$|v_0^2-v_n^2|=\frac{2}{\mu}h\nu.$$

THE TOTAL INELASTIC CROSS SECTION

The function $\sum_j({}_jf_0/r)P_j(\cos\theta)$ describes the incoming plane and the elastically scattered spherical wave; $\sum_j({}_jf_n/r)P_j(\cos\theta)$, the inelastically scattered wave. As in one dimension, we may express ${}_jf_0$ and ${}_jf_n$ in terms of solutions of the homogeneous equation (method of distorted waves):[6,7]

$$\left(\frac{d^2}{dr^2}+k_i^2-\frac{j(j+1)}{r^2}-U_r\right){}_jF_i=0, \quad i=0, n, \quad (5)$$

where

$$k_i=\frac{2\pi\mu v_i}{h},$$

and

$$U_r=V_r\frac{8\pi^2\mu}{h^2},$$

$$U_{\text{int}}=V_{\text{int}}\frac{8\pi^2\mu}{h^2}.$$

The functions ${}_jF_i$ are defined as those solutions of Eq. (5) which are regular at $r=0$ and are normalized so as to have the asymptotic form

$${}_jF_i=\cos(k_ir+\eta(i,j)), \quad r\to\infty,$$

where $\eta(ij)$ is a phase angle. Then, as the oncoming waves can be expanded into a sum of partial waves,[8] each partial wave may be treated in a manner similar to the one-dimensional case.

We take

$${}_jf_0=\frac{2j+1}{k_0}(i)^ie^{i\eta(o,j)}\,{}_jF_0$$

in order that $\sum_j({}_jf_0/r)P_j(\cos\theta)$ represent an oncoming plane and spherically reflected wave.

Then,‡ at large r,

$${}_jf_n=\frac{2j+1}{2k_0}(i)^ie^{i\eta(n,j)}\,{}_jA_{0\to n}e^{-ik_nr}, \quad (6)$$

[6] N. F. Mott and H. S. W. Massey, *The Theory of Atomic Collisions* (Clarendon Press, Oxford, 1949), second edition, Chapter VIII, p. 5.

[7] J. M. Jackson and N. F. Mott, Proc. Roy. Soc. (London) **A137**, 708 (1932).

[8] See reference 6, Chapter II.

‡ The integral $\int {}_jF_0\,{}_jF_nU_rdr$ is formally identical with the one-dimensional expression. The term $j(j+1)/r^2$ does not appear as it is independent of the internal coordinate, s. The three-dimensional nature of the integral becomes apparent when it is expressed in terms of the three-dimensional wave functions: $\int_0^{\infty}{}_jR_0\,{}_jR_nU_rr^2dr$.

where

$$ {}_jA_{0\to n}\equiv\frac{2}{k_n}\mathbf{V}_{0\to n}\int_0^\infty {}_jF_0\ {}_jF_n U_r dr, $$

and

$$ \mathbf{V}_{0\to n}\equiv\int_0^\infty \psi_0\psi_n U_{\text{int}} ds. $$

The partial wave ${}_j\Psi_n$ will become, at large r:

$$ {}_j\Psi_n=\psi_n\frac{2j+1}{2k_0r}(i)^j e^{-i(k_nr-\eta(n,j))}P_j(\cos\theta)\,{}_jA_{0\to n}. \quad (7) $$

The number of molecules inelastically scattered from a uniform beam of unit amplitude and initial velocity v_0 will be given by the integral of $\sum_j({}_j\Psi_n)^2k_n/k_0$ over a sphere. This is the inelastic cross section

$$ q_{\text{in}}=\frac{\pi k_n}{k_0^3}\sum_{j=0}^{\infty}(2j+1)[{}_jA_{0\to n}]^2. \quad (8) $$

The inelastic cross section, as usually measured, is a weighted sum of inelastic cross sections for all possible initial velocities. Assuming a normal distribution of initial velocities, v_0, in space at temperature T, we may define an over-all cross section Q_{in}:

$$ Q_{\text{in}}=2\beta^2\int_0^\infty v_0^3\exp(-\beta v_0^2)q_{\text{in}}(v_0)dv_0, \quad (9) $$

where

$$ \beta\equiv\frac{\mu}{2kT}. $$

Then, from Eq. (8),

$$ Q_{\text{in}}=2\beta^2\int_0^\infty v_0^3\exp(-\beta v_0^2)\sum_{j=0}^{\infty}\frac{2j+1}{k_0^3}k_n({}_jA_{0\to n})^2dv_0. \quad (10) $$

THE DISTORTED WAVE FUNCTIONS

The functions ${}_jF_0$, ${}_jF_n$ occurring in ${}_jA_{0\to n}$ were defined as those solutions of Eq. (5),

$$ {}_jF_i''+\left(k_i^2-U_r-\frac{j(j+1)}{r^2}\right){}_jF_i=0, \quad i=0, n, \quad (5) $$

which asymptotically approach $\cos[k_ir+\eta(i,j)]$ at large r. We now will proceed to demonstrate an approximate, but simple, relationship among the ${}_jF_0$, ${}_jF_n$ for different values of j. However, as we will be guided by the results obtained in the one-dimensional treatment, we will first briefly consider the one-dimensional problem [in the present case, proportional to the first term of Eq. (10)].

The One-Dimensional Problem

In the one-dimensional treatment, it was found that only collisions with high relative velocity contribute appreciably to the total cross section Q_{in}. On the other hand, the number of molecules of a given initial velocity in a gas sample drops off rapidly as larger initial velocities are considered. Because of this, the integrand of the $j=0$ term in Eq. (10) possesses a sharp maximum value at some velocity v_0^*.

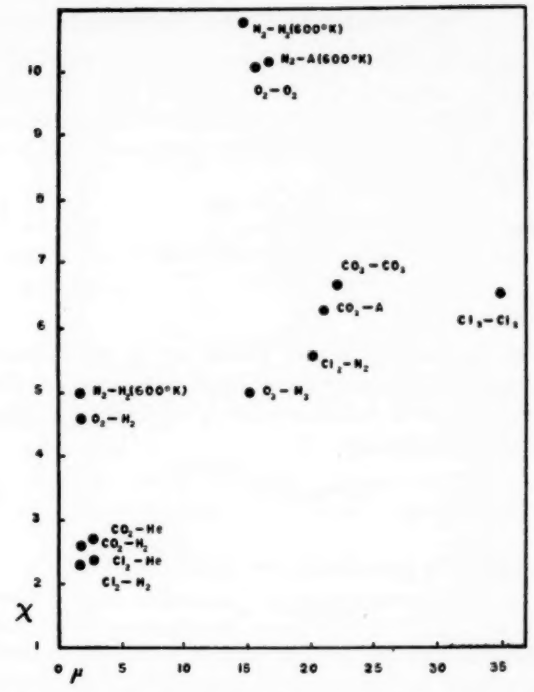

FIG. 1. The function χ for a number of collision pairs. The calculations were made for $T=288$°K unless otherwise noted.

I. Only molecules in a rather narrow range of velocities around v_0^* give a significant contribution to the inelastic cross section, and only these molecules need be considered in an approximate treatment. The velocity v_0^* may be calculated by Eq. (A-5) of reference 2. The function χ, where

$$ \chi\equiv\frac{\mu(v_0^*)^2}{2kT}, \quad (11) $$

was computed for a number of typical cases, and the results are shown in Fig. 1. As can be seen from the figure, those molecular collisions most apt to give rise to a vibrational excitation have relative translational energies several times the mean.§

II. The intermolecular potential U_r was approximated in the one-dimensional treatment by a repulsive field, $U_r=(k_0^*)^2\exp-\alpha(r-r_c)$, fitted to the experimentally determined Lennard-Jones field. This was done by matching magnitudes and slopes of these two curves at the classical distance of closest approach, $r=r_c$, for those collisions with relative velocities v_0^* and corresponding propagation constants k_0^*.

§ However, Fig. 1 shows that in cases involving collisions with the very light molecules, e.g., N_2-H_2, CO_2-He, this assumption, which had been made in reference 2, is not fulfilled. The simple theory presented in the following for the three-dimensional case is not applicable for these pairs.

The Problem in Three Dimensions

The classical distance of closest approach r_c is defined quantum mechanically as the value of r for which ${}_jF_0''=0$ in Eq. (5). For a given value of the propagation constant at infinity, k_0, r_c will be given as the value of r, for which

$$U_{(\mathrm{eff})}={}_jk_0^2, \tag{12}$$

where

$$U_{(\mathrm{eff})}\equiv U_r+\frac{j(j+1)}{r_c^2},$$

where the index j is now placed on k_0 to distinguish collisions of different orbital quantum numbers. Collisions which have the same value r_c will have propagation constants related by

$${}_jk_0^2={}_0k_0^2+\frac{j(j+1)}{r_c^2}. \tag{13}$$

We now fit a potential of the form

$$U_{(\mathrm{eff})}=a+be^{-\alpha_j(r-r_c)} \tag{14}$$

at a fixed r_c to the effective field, Eq. (12), by matching magnitudes and slopes at r_c as in the one-dimensional case. We take

$$a=\frac{j(j+1)}{r_c^2}-\frac{8\pi^2\mu\epsilon}{h^2},$$

where ϵ is the depth of the potential minimum of the Lennard-Jones potential curve. Then,

$$\alpha_j=\alpha_0\left(1+\frac{1}{r_c\alpha_0}\left(\frac{2j(j+1)}{r_c^2[({}_0k_0)^2+8\pi^2\mu\epsilon/h^2]}\right)\right); \tag{15}$$

$$b=({}_0k_0)^2+8\pi^2\mu\epsilon/h^2.$$

The additive term in the bracket is negligible because, according to Fig. 2 of reference 2, $\alpha_0 r_c>17.5$ and, as will be seen, collisions for which

$${}_0k_0^2+\frac{8\pi^2\mu\epsilon}{h^2}<\frac{j(j+1)}{r_c^2}$$

may be neglected in the calculations. Therefore,

$$\alpha_j\cong\alpha_0. \tag{15'}$$

The largest contribution to the integral,

$$\int_0^\infty {}_jF_0\,{}_jF_n U_r dr, \quad [\text{Eq. (6)}],$$

comes from the neighborhood of $r=r_c$. Equation (5) may be written in this neighborhood:

$$\left(\frac{d^2}{dr^2}+{}_jk_0^2+\frac{8\pi^2\mu}{h^2}\epsilon-\frac{j(j+1)}{r_c^2}-\left[{}_0k_0^2+\frac{8\pi^2\mu\epsilon}{h^2}\right]e^{-\alpha_0(r-r_c)}\right){}_jF_0=0 \tag{5'}$$

for collisions where the propagation constants are related by Eq. (13). We see that by choosing α as we have, the solution ${}_jF_0$ is approximated‖ in the neighborhood r_c by

$${}_jF_0({}_jk_0)=\bar{F}(\bar{k}_0),$$

where $\bar{F}$ is the solution for a purely exponential field¶ and

$$\bar{k}_0\equiv\left([{}_jk_0]^2+\frac{8\pi^2\mu\epsilon}{h^2}-\frac{j(j+1)}{r_c^2}\right)^{\frac{1}{2}}.$$

Thus, we have expressed the approximate fact that the longer-range forces (the attractive force of the Lennard-Jones potential, accounted for here by the term $8\pi^2\mu\epsilon/h^2$, and the inverse-r-squared centrifugal term) affect the solution by modifying the velocity at which the molecules enter into the range of the repulsive field, but that the short-range repulsive field in the neighborhood of r_c causes the transition.** From its definition, Eq. (6),

$${}_jA_{0\to n}(v_0)={}_0A_{0\to n}([v_0^2-\gamma_j]^{\frac{1}{2}}), \tag{16}$$

where

$$\gamma_j\equiv\frac{h^2j(j+1)}{4\pi^2\mu^2r_c^2}.$$

Furthermore, ${}_jA_{0\to n}(v_0)$ is related to the wave amplitude, $\bar{A}_{0\to n}$, entering in the one-dimensional case of a purely exponential field.

One has

$${}_jA_{0\to n}(v_0)=\bar{A}_{0\to n}([v_0^2-\gamma_j']^{\frac{1}{2}}),$$

where

$$\gamma_j'\equiv\gamma_j-\frac{2\epsilon}{\mu}.$$

$\bar{A}_{0\to n}$ has been calculated[7] and is given in reference 2.

‖ This approximation was also suggested in reference 5.

¶ In reference 2 the solution for the purely exponential field, which is now designated by $\bar{F}$, was used. From the argument given in the text one should have included the factor $\exp(\epsilon/kT)$, which appears in our final result, Eq. (22), also in reference 2, Eq. (A-7).

** This statement is well illustrated by taking an extreme example. Assume $\alpha\to\infty$. Then, in three dimensions, we have

$$U_{(\mathrm{eff})}=j(j+1)/r^2; \quad r>r_c,$$
$$=\infty; \quad r<r_c.$$

The solution of this problem is (see reference 7)

$${}_jF_0=\left(\frac{\pi}{2}k_0r\right)^{\frac{1}{2}}J_{j+\frac{1}{2}}(k_0r),$$

where k_0 is the value of the propagation constant at ∞. If $j(j+1)/(r^2k_0^2)\ll1$, this is approximately (see reference 9)

$${}_jF_0\cong\cos\bar{k}_0r,$$

where

$$\bar{k}_0=(k_0^2-j(j+1)/r_1^2)^{\frac{1}{2}}.$$

${}_jF_0$ describes, then, a wave motion that is locally a plane wave but of changing wavelength as it progresses, such that the energy at each point is the translational energy at infinity minus the quasi-potential of the centrifugal force at that point. In this example, only the value of ${}_jF_0$ at r_c enters into the probability integral. Therefore, here

$$\bar{k}_0=(k_0^2-j(j+1)/r_c^2)^{\frac{1}{2}}.$$

With the help of Eq. (16), Eq. (10) may now be summed. Placing Eq. (16) into Eq. (10), we have

$$Q_{in}=2\pi\beta^2\int_0^\infty v_0^3\exp(-\beta v_0^2)\times\left[\sum_{j=0}^{\infty}\frac{(2j+1)k_n}{k_0^3}(\bar{A}_{0\to n}([v_0^2-\gamma_j']^{\frac{1}{2}}))^2\right]dv_0.$$

First, we may replace the summation over j with an integral as it will be shown that more than 100 terms must be kept in the summation in the evaluation of Q_{in}. We may write

$$\frac{2j+1}{k_0^2}dj=\frac{r_c^2}{v_0^2}d\gamma_j'.$$

Now, by letting

$$v_0^2-\gamma_j'\equiv w_0^2$$

we have

$$Q_{in}=\pi\beta^2\int_{-\gamma_j'}^{\infty}r_c^2\exp(-\beta w_0^2)\frac{v_n}{v_0}(\bar{A}_{0\to n}(w_0))^2\times\int_{-2\epsilon/\mu}^{\infty}\exp(-\beta\gamma_j')d\gamma_j'dw_0^2. \quad (17)$$

Since in our approximation most of the contribution to Q_{in} comes from the velocities in the neighborhood of a rather large value v_0^*, r_c may be taken out of the integral and the lower limit taken as zero in the integration over w_0^2. Then Eq. (17) may be written

$$Q_{in}=\beta\pi r_c^2e^{\epsilon/kT}\int_0^\infty\exp(-\beta w_0^2)\frac{v_n}{v_0}(\bar{A}_{0\to n}(w_0))^2dw_0^2. \quad (18)$$

The probability of a vibrational change from quantum state 0 to n during a single collision is

$$P_{0\to n}=Q_{in}/Q_{el},$$

where Q_{el} is the elastic cross section. As a matter of principle, Q_{el} might be calculated once V_r is given. However, an approximate value of Q_{el} obtained from viscosity data will suffice here. We take Q_{el} as[9]

$$Q_{el}=0.93\pi r_0^2(1+C/T), \quad (19)$$

where r_0 is the zero of the Lennard-Jones curve and C is Sutherland's constant. The Sutherland correction $(1+C/T)$ is physically due to the long range force bringing molecules within interaction distance that would not have otherwise collided. Such an effect should be omitted in inelastic collisions, since only kinetic energies several times kT are important, and the attractive forces have been taken into account by the factor $\exp(\epsilon/kT)$. Therefore, we take $P_{0\to n}$:

$$P_{0\to n}=1.074(r_c/r_0)^2e^{\epsilon/kT}(1+C/T)^{-1}\beta\times\int_0^\infty\exp(-\beta w_0^2)\frac{v_n}{v_0}(\bar{A}_{0\to n})^2dw_0^2. \quad (20)$$

The factor $1.074(r_c/r_0)^2$ is not much different from one; it varies but slowly with temperature. It is given approximately by

$$1.074[\tfrac{1}{2}(1+\chi kT/\epsilon)^{\frac{1}{3}}+\tfrac{1}{2}]^{-1}. \quad (21)$$

(It varies from 0.65 for N_2 at 600°K to 0.93 for Cl_2 at room temperature.)

The integral in Eq. (20) is the same as would be obtained in a one-dimensional calculation where the velocity distribution is taken to be a one-dimensional one.

The final result will be multiplied by a geometrical factor $\frac{1}{3}$ as indicated in the second paragraph of this paper. Making use of the results of reference 2, we write the probability of a change from the first to the zeroth vibrational quantum level:

$$P_{1\to 0}=0.716(1+C/T)^{-1}(r_c/r_0)^2\left(\frac{\pi}{3}\right)^{\frac{1}{3}}\left(\frac{8\pi^3\mu h\nu}{\alpha^{*2}h^2}\right)^2\times\mathbf{V}_{1\to 0}^2\chi^{\frac{1}{3}}\exp\left[-\left(3\chi-\left[\frac{h\nu}{2kT}+\frac{\epsilon}{kT}\right]\right)\right], \quad (22)$$

where

$$\chi=\left[\frac{2\pi^4\mu(h\nu)^2}{(\alpha^*)^2h^2kT}\right]^{\frac{1}{3}}.$$

In reference 2 the transition probability for the one-dimensional case was given as

$$P_{1\to 0}=2(\pi/3)^{\frac{1}{3}}\left(\frac{8\pi^3\mu h\nu}{\alpha^{*2}h^2}\right)^2\mathbf{V}_{1\to 0}^2\chi^{\frac{1}{3}}\times\exp\left[-\left(3\chi-\frac{h\nu}{2kT}\right)\right] \quad (22')$$

in Eq. (A-7). This was obtained by summing a one-dimensional solution of the collision problem over a three-dimensional distribution of velocities, the integral

TABLE I.

Gas	T	r_0/r_c	χ	P_1 Value[a] given in reference 2	P_1 Experimental value	P_1 Value from Eq. (22)
CO_2-CO_2	288°K	1.12	6.7	4×10^{-4}	2×10^{-5}	1.1×10^{-5}
CO_2-H_2	288°K	1.11	2.6	4.5×10^{-2}	2×10^{-3}	5.7×10^{-3}
Cl_2-Cl_2	288°K	1.08	6.6	1.0×10^{-4}	3×10^{-5}	0.85×10^{-5}
Cl_2-N_2	288°K	1.11	5.6	6×10^{-4}	2.3×10^{-5}	3.7×10^{-5}
O_2-O_2	288°K	1.19	10.1	8.4×10^{-3}	$4-6\times10^{-3}$	2.3×10^{-3}
N_2-N_2	600°K	1.28	10.8	6.9×10^{-3}	3×10^{-3} [b]	1.7×10^{-10}
N_2-H_2	600°K	1.23	5	9×10^{-4}	...	10^{-5}

[a] These values do not include the factor $\exp(\epsilon/kT)(1+C/T)^{-1}$.
[b] See discussion of this value above.

[9] K. F. Herzfeld and H. M. Smallwood, in Taylor and Glasstone, *A Treatise on Physical Chemistry* (New York, 1951), 3rd edition, Vol. II, p. 84, 86.

TABLE II. Calculated fraction of effective collision at higher temperatures.

	T 288°K	600	900	1200	1800	2400	3000
N_2 in N_2 gas	$<10^{-12}$	2×10^{-10}	3.2×10^{-9}	5×10^{-8}	1.1×10^{-6}	8×10^{-6}	1.6×10^{-5}
O_2 in O_2 gas	3.0×10^{-9}	3×10^{-7}	3×10^{-6}	1.3×10^{-5}	8.6×10^{-5}	5.5×10^{-4}	1.5×10^{-3}
O_2 in N_2 gas	2×10^{-8}	3×10^{-6}	3×10^{-5}	1.2×10^{-4}	7×10^{-4}	2×10^{-3}	4×10^{-3}

being evaluated by the method of steepest descent. The present results differ from the above in the following manner:

1. The factor $1.074/3\ (r_c/r_0)^2$ is present.
2. The factor $\exp(\epsilon/kT)$ appears in the present results but was omitted in reference 2. This is a number that does not vary significantly from one.
3. The present results contain the factor $\chi^{\frac{1}{2}}$ while reference 2 contains $\chi^{\frac{3}{2}}$. This is because a three-dimensional velocity distribution was used in reference 2 instead of a one-dimensional distribution which would have made the two results identical in this respect.

Table I compares value of $P_{1\to0}$ as computed by Eqs. (22) and (22′) with experimental values for several cases. Numerically, the three-dimensional treatment yields an answer that is between $\frac{1}{5}$ and $\frac{1}{10}$ of the one-dimensional treatment. This brings collisions of moderately small probabilities as CO_2-CO_2 and Cl_2-Cl_2 into good agreement with the experiments. In N_2-N_2 and O_2-O_2, however, where the probability is very small, the theoretical value has become much smaller than the experimental value. For N_2-N_2, the measurements of Huber and Kantrowitz[10] were made with about 0.05 percent water vapor present. Using their measurements for a mixture of H_2O and N_2 from the same experiments, this concentration of water vapor itself should give about the observed probability. As this is between 50 and 100 times $P_{1\to0}(N_2, N_2)$ as computed, it should mask the effects of N_2, N_2 collisions in the experiment. However, if one believes that the experimental values are for N_2-N_2 collisions, one must consider that the effective kinetic energies involved in the N_2-N_2 collisions are equivalent to the mean energy of a gas at about 6000°K. The value of α was computed from the Lennard-Jones curve extrapolated to these values. If one accepts the experimental value of Huber and Kantrowitz[10] as correct, it would indicate a change of the value of α from 4.75×10^8 cm^{-1} to 6.14×10^8 cm^{-1} (an increase by $\frac{1}{3}$), i.e., the molecules would be "harder" than given by $(r_0/r)^{12}$. For O_2-O_2, the data of the Knoetzels[11] are for dry gas, and here the experimental value is 10–20 times the theoretical one. To make the two equal, a change of α from 5.27×10^8 to 6.15×10^8 must be made (equivalent 3000°), an increase of 16 percent.

Because of their interest in aerodynamic and combustion problems, calculations for P at high temperature are given in Table II.

[10] P. W. Huber and A. Kantrowitz, J. Chem. Phys. **15**, 275 (1947).
[11] H. Knoetzel and L. Knoetzel, Ann. Physik **2**, 393 (1948).

VALIDITY OF AN APPROXIMATION USED

The approximation that

$$j(j+1)<({}_jk_0{}^*)^2r_c{}^2$$

for the largest j value that need be considered is essential to the present treatment (see Eq. (15) and reference ††). From Eq. (17) we see that the fractional contribution from the first j partial cross sections to the total Q is

$$\beta\int_0^{(j)} e^{-\beta\gamma_j}d\gamma_j. \tag{23}$$

From the definition of χ [Eq. (11)] we may write

$$\beta\gamma_j\cong\left(\frac{j}{k_0{}^*r_c}\right)^2\chi.$$

The function χ was computed for a number of cases, and the results are shown in Fig. 1. The largest j necessary to carry (17) to 98 percent of the full value of Q is one which makes $\beta\gamma_j\sim4$. From Fig. 1 it is evident that the condition in question is satisfied for the molecular collisions considered with the notable exception of collisions involving the very light molecules He and H_2. As $k_0{}^*r_c$ is of the order of 100 for collisions of heavier molecules, j will be of the order of 100 also.

CONCLUSIONS

Ignoring the inconsequential factor $1.074(r_c/r_0)^2$, the probabilities calculated by treating the collision as a straight line motion and summing over a one-dimensional velocity distribution give nearly the same result as obtained by treating the collision process in three dimensions and summing over a three-dimensional distribution. The physical features of this inelastic collision process that permit such a simplification in treatment may be repeated here: (1) Only the collisions that enter the range of interaction with a high relative velocity give any significant contribution to a vibrational excitation, and the influence of slower collisions and collisions with large j values may be ignored in the computation. (2) The intermolecular potential is very

†† It is easily seen that the condition

$$k_0{}^2+\frac{8\pi^2\mu\epsilon}{h^2}>\frac{j(j+1)}{r_c{}^2}$$

means that the "collision" is not caused by a potential hill due to centrifugal force, but that the particle can get over such a hill and "collide" with the repulsive potential. See also Bauer and Widom (reference 12).

steep and short ranged compared to the inverse-r-squared centrifugal energy in the neighborhood of $r=r_c$. The centrifugal energy only affects the effective velocity, just as does the long range attractive force. As Landau and Teller have pointed out long ago, long range forces do not affect transition probabilities directly. However, they do have an indirect influence, because they influence the effective value of the relative velocity in the neighborhood of $r=r_c$, the attractive force increasing it and the centrifugal terms decreasing it compared to the value at large distances. Bauer and Widom[12] have pointed out that the approximation used here fails if the attractive forces are very strong. They explain the great effectiveness of small amounts of water vapor as due to this attractive force. Formally, but not quantitatively, this is represented in our present theory by the factor $e^{\epsilon/kT}$. (See Table III.) For ϵ equal to one-third of an electron volt, as assumed by Widom and Bauer for the CO_2-H_2O interaction, this factor is 1.6×10^5 which is too large, but 0.2 ev would give the right value. (3) The agreement with experiment is fairly good.

We wish to thank Dr. Z. Slawsky of the Naval Ordnance Laboratory for many enlightening and helpful discussions and for his constant encouragement.

APPENDIX I. THE Cl_2-H_2 MIXTURE

The case of the Cl_2-H_2 mixture illustrates the manner in which the assumptions behind Eq. (22) are violated when the low-energy collisions cannot be neglected. Because the relative translational energy $\mu/2(v_0^*)^2$ is *not* large compared to kT, the integrand in

$$2\beta\int_0^\infty v_0\exp(-\beta v_0^2)[{}_0A_{0\to n}]^2dv_0 \qquad (24)$$

is not a steeply peaked function; (1) it cannot be summed by the saddle point method, and (2) it is no longer proper to fit the potential by an exponential at r_c for a single velocity v_0^*. Then α_0 must be taken as a function of v_0. Because $\mu/2(v_0^*)^2$ is not large compared to $h\nu$, (3) the function $|{}_0A_{0\to n}|^2$ cannot be approximated by

$$|{}_0A_{0\to n}|^2=\text{const}\exp(-c_1/v_0) \qquad (25a)$$

as in Eq. (A-7) of reference 2. The more correct form (as evaluated for Cl_2-H_2)

$$|{}_0A_{0\to n}|^2\cong\text{const}\exp\left[-\frac{20}{\alpha}(v_0-v_n)\right] \qquad (25b)$$

[12] B. Widom and S. H. Bauer, J. Chem. Phys. **21**, 1670 (1953).

TABLE III. The factor $\exp(\epsilon/kT)(1+C/T)^{-1}$ which measures the effect of the attractive forces on P.

ϵ/kT	0	0.5	0.75	1	2	3	4
Factor	1	1.13	1.17	1.30	2.33	4.70	10.1

must be used in its place. (4) Finally, as one can see from Eq. (1), collisions for which

$$j(j+1)/r_c^2\gg({}_0k_0^*)^2+\frac{8\pi^2\mu\epsilon}{h^2}$$

cannot be ignored so that α_j varies appreciably with j. This latter point is the only one introduced by the three-dimensional nature of the problem.

In order to see the effect of these four points on the final computation, computations were carried out free of these objections. First, the integral

$$2\beta\int_0^\infty v_0\exp[-\beta v_0^2-20(v_0-v_n)/\alpha]dv_0$$

was evaluated numerically with α_0 equal to 5.5×10^8 cm^{-1} and by the saddle point method using the approximate Eq. (25a) for ${}_0A_{0\to n}$. The numerical computation yields 0.00736 for the integral against 0.0045 for the approximate computation, or an increase of 65 percent from the previous value; however, if α_0 is not taken as a constant but is recomputed for each collision, the low velocity encounters become more favorable. The numerical value of the integral is increased to 0.0145, or a factor 3 more than given by the approximate theory.

The value of ϵ used here is arbitrarily taken as

$$\epsilon=[\epsilon(Cl_2)\cdot\epsilon(H_2)]^{\frac{1}{2}}$$

and is given $\epsilon/k=105°K$. The first thirty-three partial cross sections must be included in the summation of Q_{in} to bring Q_{in} within 98 percent of its full value. α_j/α_0, as defined in Eq. (15), does not change appreciably for the first ten partial cross sections; it has a value of two for a velocity $v_0=0$ for the thirty-third partial cross section. The increase in α_j causes ${}_jF_0$ and ${}_jF_n$ to become smaller for these very low velocity collisions and the over-all effect is to lower $P_{1\to0}$ somewhat. If all collisions for which $j(j+1)/r_c^2>{}_0k_0^2+8\pi^2\mu\epsilon/h^2$ were completely excluded from the final summation, it would reduce $P_{1\to0}$ by 7 percent, which may be taken as an outside bound for this effect. The experimental value of $P_{1\to0}$ is in the neighborhood of 0.0013. The value given by a direct application of Eq. (22) is 0.003, while the more accurate numerical computation with a variable α_0 is nearly 0.01.

Approximation of Molecular Orbitals in Diatomic Molecules by Diatomic Orbitals*

RICHARD F. WALLIS, *Applied Physics Laboratory, The Johns Hopkins University, Silver Spring, Maryland*

AND

HUGH M. HULBURT,† *Department of Chemistry, The Catholic University of America, Washington, D. C.*

(Received October 22, 1953)

The constants necessary for the specification of the exact wave functions of the homonuclear one-electron diatomic molecule have been tabulated for a range of relatively large internuclear distances. A method for determining upper and lower bounds of the constants is presented. The energy of the hydrogen molecule has been calculated for the ground state using the one-electron two-center wave functions as molecular orbitals. The results of a similar calculation by Hylleraas have been confirmed and extended. It is found that the best results are obtained if the effective nuclear charges for the molecular orbital of one electron are different from the effective nuclear charges for the molecular orbital of the second electron. Somewhat less satisfactory results are obtained if the effective nuclear charges are the same in both orbitals. The application of diatomic orbitals in the calculation of the properties of other diatomic molecules is discussed. Calculations of energy appear to be prohibitively laborious; calculations of electric dipole moments and transition probabilities may be feasible.

1. INTRODUCTION

IN 1931 Hylleraas[1] published a molecular orbital calculation of the energies of various states of the hydrogen molecule. The molecular orbitals (MO's) were chosen to be the exact wave functions for an electron moving in the field of two stationary nuclei of equal charge. We shall refer to the latter one-electron wave functions as diatomic orbitals (DO's). They have been obtained as infinite series not only for the homonuclear case[1–3] but also for the heteronuclear case.[4,5]

For the ground state Hylleraas assigned one electron of H_2 to the $1s\sigma$ DO corresponding to one-half unit of positive charge on each nucleus and assigned the second electron to a similar orbital corresponding to one unit of positive charge on each nucleus. The contribution of the electronic repulsion to the electronic energy was evaluated, however, using only the first term in the infinite expansion for each orbital. Substitution into the formula given by Hylleraas [his Eq. (20)] yields a dissociation energy appropriate to the state of no zero-point vibration of 3.4193 ev.

Coulson[6] and Weinbaum[7] have computed the dissociation energy of H_2 using the LCAO form of the MO method. They assigned both $1s\sigma$ electrons to the same MO represented by the sum of the $1s$ atomic orbitals (AO's) with effective nuclear charge varied to minimize the total energy. Their result for the dissociation energy is 3.47 ev.

A striking feature of Hylleraas' calculation is that his result is comparable to that of Coulson and of Weinbaum even though he chose his effective nuclear charges on intuitive physical grounds rather than by a variation calculation. The question arises whether useful approximations to the wave functions of diatomic molecules can be constructed from DO's. The purpose of this paper is to investigate this question.

We have considered three problems. First, before one can use DO's, one must know the values of the principal coefficients in the series expansions for the orbitals. Until now no precise data have been available for the moderately large internuclear distances and nuclear charges appropriate to the diatomic molecules in the first row of the periodic table. We have carried out calculations for this range for the homonuclear case and discussed the accuracy of the results. Second, we have extended Hylleraas' calculations on the hydrogen molecule so that the merits of DO's may be more clearly appraised. Third, we have discussed the use of DO's in constructing approximate electronic wave functions for diatomic molecules more complex than the hydrogen molecule.

2. WAVE FUNCTIONS FOR THE ONE-ELECTRON TWO-CENTER PROBLEM

Let us consider one electron with charge $-e$ moving in the field of two fixed nuclei with charges $+Z_ae$ and $+Z_be$, respectively. If length is measured in terms of the Bohr radius $a_0=0.5292$A and energy in units of $e^2/a_0=27.204$ ev (atomic units, a.u.), the time independent Schrödinger equation for the problem is

$$\tfrac{1}{2}\nabla^2\psi+\left(E+\frac{Z_a}{r_a}+\frac{Z_b}{r_b}-\frac{Z_aZ_b}{R}\right)\psi=0,$$

* The major portion of the work reported in this paper is based on the dissertation submitted by Richard F. Wallis to the Faculty of the Graduate School of Arts and Sciences of The Catholic University of America in partial fulfillment of the requirements for the degree of Doctor of Philosophy. One of the authors (R.F.W.) acknowledges the recent support of the Bureau of Ordnance, Department of the Navy.

† Present address: Chemical Construction Corporation, 488 Madison Avenue, New York, New York.

[1] E. A. Hylleraas, Z. Physik **71**, 739 (1931).
[2] E. Teller, Z. Physik **61**, 458 (1930).
[3] G. Jaffé, Z. Physik **87**, 535 (1934).
[4] W. T. Baber and H. R. Hassé, Proc. Cambridge Phil. Soc. **31**, 564 (1935).
[5] C. A. Coulson and W. E. Duncanson, Proc. Roy. Soc. (London) **A165**, 90 (1938).
[6] C. A. Coulson, Trans. Faraday Soc. **33**, 1479 (1937).
[7] S. Weinbaum, quoted in L. Pauling and E. B. Wilson, Jr., *Introduction to Quantum Mechanics* (McGraw-Hill Book Company, Inc., New York, 1935), p. 347.

where the symbols have their usual significance. If one introduces the elliptic coordinates u, v, φ defined by

$$u=\frac{r_a+r_b}{R}, \quad v=\frac{r_a-r_b}{R},$$

φ = azimuth about the internuclear axis,

the Schrödinger equation becomes separable. If ψ is written as $\psi=U(u)V(v)\Phi(\varphi)$, then U, V, and Φ satisfy the ordinary differential equations

$$\frac{d^2\Phi}{d\varphi^2}+m^2\Phi=0, \tag{1}$$

$$\frac{d}{du}\left[(u^2-1)\frac{dU}{du}\right]+\left\{-p^2u^2+2R_2u+A-\frac{m^2}{u^2-1}\right\}U=0, \tag{2}$$

$$\frac{d}{dv}\left[(1-v^2)\frac{dV}{dv}\right]+\left\{p^2v^2-2R_1v-A-\frac{m^2}{1-v^2}\right\}V=0, \tag{3}$$

where m, A = separation constants, $p^2=-E_eR^2/2$, $E_e=E-(Z_aZ_b/R)$ = electronic energy, and $R_1=R(Z_a-Z_b)/2$, $R_2=R(Z_a+Z_b)/2$. The constants m, A, and p are determined by the requirement that ψ be single-valued, continuous, and finite over the entire region of space given by $1\leq u\leq\infty$, $-1\leq v\leq 1$, $0\leq\varphi\leq 2\pi$. Teller[2] has tabulated these constants for eight quantum states for values of $R_2\leq 25$. Hellmig[3] has published approximate data over the range $0\leq R_2\leq 40$.

The solution of Eq. (1) may be taken as

$$\Phi=\exp(\pm im\varphi),$$

where m is a positive integer or zero. For the solution of Eq. (2), we take the expansion given by Hylleraas:[1]

$$\begin{aligned} U(u)&=(u^2-1)^{m/2}F(x)\exp(-x/2),\\ x&=2p(u-1),\\ F(x)&=\sum_{n=0}^{\infty}c_n\frac{L_{m+n}{}^m(x)}{(m+n)!}, \end{aligned} \tag{4}$$

where the c_n are constants to be determined by the substitution of $U(u)$ into Eq. (2) and the $L_{m+n}{}^m(x)$ are the associated Laguerre polynomials of degree n and order m. As shown rigorously by Baber and Hassé[4] expansion (4) converges over the closed interval $0\leq x\leq\infty$ only if the constants m, A, and p satisfy the continued fraction relation

$$-\frac{Y}{m+1}=\frac{a_1}{b_1-}\frac{a_2}{b_2-}\frac{a_3}{b_3-}\cdots, \tag{5}$$

where

$$\begin{aligned} Y&=A-p^2+2ps+(m+1)(m+s),\\ s&=-(m+1)+R_2/p,\\ a_1&=s(m+s)/(m+1),\\ a_n&=\frac{(n-1-s)(n-1-m-s)}{(n-1)(n-1+m)}, \quad n\geq 2,\\ b_n&=\frac{2n^2+2n(2p-s)-y}{n(n+m)}, \quad n\geq 1. \end{aligned}$$

Continued fraction relation (5) possesses a denumerable infinity of roots corresponding to eigenfunctions possessing 0, 1, 2, $\cdots$ nodes in the interval $0<x<\infty$. If relation (5) is inverted 0, 1, 2, $\cdots$ times and the method of successive approximations is applied, power series expansions for Y appropriate to 0, 1, 2, $\cdots$ nodes, respectively, may be developed. If the substitution $y=1/2p$ is made, the results are

for zero nodes:

$$Y=\tfrac{1}{8}s(m+1)(m+s)\{-4y+4(1-s)y^2-[5s^2-(m+12)s-(m^2+m-6)]y^3 -[7s^3-(4m+29)s^2-(4m^2-34)s+(4m^2+4m-12)]y^4+\cdots\}; \tag{6}$$

for one node:

$$\begin{aligned} Y=2/y&+2(1-s)+\{s(m+1)(m+s)/2+(1-s)(m+2)(m-1+s)\}y\\ &-\{s(1-s)(m+1)(m+s)/2+(1-s)(3-s)(m+2)(m-1+s)\}y^2+\{[s(m+1)(m+s)/(2)]\\ &\times[(1-s)^2-s(m+1)(m+s)/4-(1-s)(m+2)m-1+s)/2]+[(1-s)(m+2)(m-1+s)/(4)]\\ &\times[4(3-s)^2+s(m+1)(m+s)+2(1-s)(m+2)(m-1+s)-3(2-s)(m+3)(m-2+s)/2]\}y^3\\ &-\{[s(1-s)(m+1)(m+s)/(2)][(1-s)^2-3s(m+1)(m+s)/4-(5-3s)(m+2)(m-1+s)/2]\\ &+[(1-s)(m+2)(m-1+s)/(4)][4(3-s)^3+s(7-3s)(m+1)(m+s)+6(1-s)(3-s)(m+2)(m-1+s)\\ &-3(2-s)(10-3s)(m+3)(m-2+s)/2]\}y^4+\cdots; \end{aligned} \tag{7}$$

[3] E. Hellmig, Z. Physik **104**, 694 (1937).

for two nodes:

$$Y=4/y+4(2-s)+\{(1-s)(m+2)(1-m-s)-3(2-s)(m+3)(2-m-s)/2\}y$$
$$+\{3(2-s)(5-s)(m+3)(2-m-s)/(2)-(1-s)(3-s)(m+2)(1-m-s)\}y^2$$
$$-\{[(1-s)(m+2)(1-m-s)/(4)][-4(3-s)^2-s(m+1)(m+s)/2+2(1-s)(m+2)(1-m-s)$$
$$-3(2-s)(m+3)(2-m-s)]+[3(2-s)(m+3)(2-m-s)/(8)][4(5-s)^2+2(1-s)(m+2)(1-m-s)$$
$$-3(2-s)(m+3)(2-m-s)+2(3-s)(m+4)(3-m-s)]\}y^3+\{[(1-s)(m+2)(1-m-s)/(4)]$$
$$\times[-4(3-s)^3-s(8-3s)(m+1)(m+s)/2+6(1-s)(3-s)(m+2)(1-m-s)$$
$$-3(2-s)(11-3s)(m+3)(2-m-s)]-[3(2-s)(m+3)(2-m-s)/(8)]$$
$$\times[-4(5-s)^3-2(1-s)(13-3s)(m+2)(1-m-s)+9(2-s)(5-s)(m+3)(2-m-s)$$
$$-2(3-s)(16-3s)(m+4)(3-m-s)]\}y^4+\cdots. \quad (8)$$

The solution of Eq. (3) will now be discussed for the homonuclear case, $R_1=0$. We shall use the expansion in associated Legendre polynomials suggested by Hylleraas:[1]

$$V(v)=\sum_{l=m}^{\infty} d_l{}^m P_l{}^m(v). \quad (9)$$

One may use the methods of Baber and Hassé[4] to show that expansion (9) converges over the range $-1\leq v\leq 1$ only if m, A, and p satisfy the continued fraction relation

$$r_{0+\delta}=\frac{q_{2+\delta}}{r_{2+\delta}-}\frac{q_{4+\delta}}{r_{4+\delta}-}\cdots, \quad (10)$$

where

$$r_{0+\delta}=\frac{(2m+2\delta+5)(2m+2\delta+3)}{(2m+\delta+2)(2m+\delta+1)}\left\{\frac{A}{p^2}+\frac{(m+\delta)(m+\delta+1)}{p^2}\right.$$
$$\left.-\left[\frac{(2\delta)(2m+2)}{(2m+5)(2m+3)}+\frac{1}{2m+3}\right]\right\},$$

$$q_{2+\delta}=\frac{2(1+2\delta)}{(2m+2\delta+1)(2m+2\delta+3)},$$

$$q_{l-m}=\frac{(l+m-1)(l-m-1)(l+m)(l-m)}{(2l-3)(2l-1)^2(2l+1)},$$

$$l=m+4+\delta,\ m+6+\delta,\ \cdots,$$

$$r_{l-m}=\frac{A}{p^2}+\frac{l(l+1)}{p^2}$$
$$-\left[\frac{(l-m+1)(l+m+1)}{(2l+3)(2l+1)}+\frac{(l+m)(l-m)}{(2l+1)(2l-1)}\right],$$

$$l=m+2+\delta,\ m+4+\delta,\ \cdots.$$

The quantity δ is zero for the even solutions and one for the odd solutions. Continued fraction relation (10) has infinitely many roots which may be correlated with the eigenfunctions possessing 0, 1, 2, $\cdots$ nodes in the interval $-1<v<1$. A useful power series expansion of relation (10) valid for large values of R_2 and appropriate to the nodeless eigenfunction is the following:

$$Y_1=[(m+1)^2/(8)]\{4y+4(m+2)y^2+(5m^2+22m+23)y^3$$
$$+(7m^3+50m^2+113m+82)y^4+\cdots\}, \quad (11)$$

where

$$Y_1=A-p^2+(m+1)(2p-1), \quad y=1/2p.$$

Each root of either continued fraction relation (5) or (10) specifies a functional relation between A and p. The common solution of a pair of such roots, one from each relation, gives the eigenvalues of A and p for a certain quantum state. The approximate specification of the eigenvalues is facilitated by interpolation or extra-

TABLE I. Separation constant A for the homonuclear one-electron, two-center problem.[a]

m	n_v	n_u	UA \ R_2	5	10	15	25	35	45
0	0	0	$1s\sigma$	4.3776937	20.133291	48.822352	143.79185	288.77943	483.77275
0	1	0	$2p\sigma$	3.5248708	20.092098	48.821469	143.79185	288.7794	483.7728
0	0	1	$2s\sigma$	1.2840020	5.1293590	12.433723	37.086084	74.444840	124.36353
1	0	0	$2p\pi$	−1.1143467	1.1610268	5.7187191	24.998904	57.349328	102.28041
0	0	2	$3s\sigma$	0.6392632	2.419251	5.720392	17.394217	35.185675	58.737096
0	1	1	$3p\sigma$	−0.1714825	4.6288373	12.333007	37.083912	74.444810	124.36358
1	0	1	$3p\pi$	−1.5664517	−0.4759749	1.4075673	9.2336787	23.514173	43.725301
0	2	0	$3d\sigma$	−4.1664667	−0.8747206	2.3361423	15.539510	42.520090	82.387826
1	1	0	$3d\pi$	−4.7347815	−1.0644561	4.8741502	24.960323	57.348428	102.28040
0	1	2	$4p\sigma$	−1.0310329	1.4701402	5.342285	17.360881	35.183481	58.736973
0	2	1	$4d\sigma$	−5.0323098	−2.8437801	−0.7733848	4.3313801	14.405110	30.987050
0	3	0	$4f\sigma$	−11.128209	−7.4964445	−1.7327624	15.026036	42.499379	82.387313

[a] n_v = number of nodes in $V(v)$ in the range $-1<v<1$, n_u = number of nodes in $U(u)$ in the range $1<u<\infty$, UA = united atom designation of the quantum state. The other symbols are defined in the text.

TABLE II. Energy parameter p for the homonuclear one-electron, two-center problem.[a]

m	n_v	n_u	UA \ R_2	5	10	15	25	35	45
0	0	0	$1s\sigma$	3.0091948	5.4798662	7.9847044	12.990452	17.993078	22.994576
0	1	0	$2p\sigma$	2.9096641	5.4767739	7.9846559	12.990452	17.993077	22.994576
0	0	1	$2s\sigma$	1.8217636	3.1993016	4.5112975	7.0863758	9.6264517	12.150831
1	0	0	$2p\pi$	2.0043228	3.4111309	4.6662460	7.1776163	9.6958008	12.207166
0	0	2	$3s\sigma$	1.3308169	2.3790916	3.3365606	5.1618569	6.9280913	8.6618644
0	1	1	$3p\sigma$	1.7178225	3.1669050	4.5055041	7.0862760	9.6264505	12.150833
1	0	1	$3p\pi$	1.4369225	2.5453918	3.5081296	5.2893894	7.0314553	8.7515895
0	2	0	$3d\sigma$	1.9558025	3.6953852	4.9652952	7.3172320	9.7834107	12.274381
1	1	0	$3d\pi$	1.6960022	3.2397289	4.6100164	7.1756386	9.6957637	12.207166
0	1	2	$4p\sigma$	1.2596060	2.3371428	3.3201924	5.1605283	6.9280119	8.6618605
0	2	1	$4d\sigma$	1.3875228	2.6883017	3.7440078	5.5096012	7.1778904	8.8648185
0	3	0	$4f\sigma$	1.3130870	3.0404495	4.6397932	7.2873802	9.7824698	12.274362

[a] n_v = number of nodes in $V(v)$ in the range $-1<v<1$. n_u = number of nodes in $U(u)$ in the range $1<u<\infty$. UA = united atom designation of the quantum state. The other symbols are defined in the text.

polation of previously published data, by the use of the above power series, and by interpolation in the table of separation constants for oblate spheroidal wave functions given by Stratton, Morse, Chu, and Hutner.[9] Precise values of A and p are then computed directly from the continued fraction relations by successive approximations. In Tables I and II we present the results of our computations for moderately large values of the parameter R_2. These data span the range of R_2 necessary for the treatment of the homonuclear diatomic molecules in the first row of the periodic table. In Table III are given additional data for the homonuclear $1s\sigma$ state.

The infinite continued fractions were, of course, broken off at a suitable approximant (convergent) in order to perform the numerical calculations. The error involved in such a procedure has apparently been inadequately treated in previous work. Although explicit statements are frequently lacking, most authors seem to have computed A using, say, the nth, $(n+1)$th, and perhaps the $(n+2)$th approximant to the continued fraction. If these calculations yielded the same value for A within the limit of accuracy, this value was regarded as the correct one. If the results did not agree, n was increased until agreement was achieved. That such a procedure may lead to unreliable conclusions is shown by the continued fraction

$$Q_1=\frac{1}{2-}\,\frac{1}{2-}\,\frac{1}{2-}\cdots,$$

which is the asymptote of the continued fraction in Eq. (5). By mathematical induction one may verify that the nth approximant to Q_1 is $n/(n+1)$. Furthermore, Q_1 converges to the value unity. Let us consider the 499th and 500th approximants to Q_1: $499/500=0.998000$, $500/501=0.998004$. We note that, although these two approximants differ among themselves only at the sixth decimal place, they differ from the value of the continued fraction at the third decimal place. It is clear that more rigorous criteria are required for estimating the proper approximant to replace the continued fraction. In the appendix we present a method for determining upper and lower bounds to the continued fractions found in Eqs. (5) and (10). These bounds enable one to give precise estimates of the error resulting from truncating the continued fractions.

The solution of Eq. (3) for the heteronuclear case, $Z_a>Z_b$, may be taken to have a form suggested by Baber and Hassé:[4]

$$V(v)=\exp(-pv)\{\sum_{l=m}^{\infty} f_l^m P_l^m(v)\}, \qquad (12)$$

where the f_l^m are expansion coefficients. The constants m, A, and p must satisfy the continued fraction relation

$$-[m(m+1)+A-p^2]=\frac{g_{m+1}}{h_{m+1}+}\,\frac{g_{m+2}}{h_{m+2}+}\cdots, \qquad (13)$$

TABLE III. Separation constant A, energy parameter p, and expansion coefficients for the homonuclear $1s\sigma$ state.[a]

WF	R_2	A	p	C_0	C_1	C_2	d_0	d_2	d_4
ψ_1	0.7000000	0.13391808	0.62828583	1.0	−0.02850893	−0.0045757	1.0	0.04440327	0.0003014
ψ_2	0.9971988	0.24873994	0.85000000	1.0	−0.03572822	−0.0045982	1.0	0.08207561	0.0010226
ψ_3	1.0325981	0.26414572	0.87507600	1.0	−0.03643386	−0.0045792	1.0	0.08710049	0.0011507
ψ_4	1.1041475	0.29634035	0.92500000	1.0	−0.03777865	−0.0045319	1.0	0.09757803	0.0014410
ψ_5	1.4000000	0.4438908	1.1218662	1.0	−0.04237207	−0.0042562	1.0	0.14518021	0.0031632

[a] WF = wave function designation. C_n = expansion coefficients of $U(u)$. d_n = expansion coefficients of $V(v)$.

[9] Stratton, Morse, Chu, and Hutner, *Elliptic Cylinder and Spheroidal Wave Functions* (John Wiley and Sons, Inc., New York, 1941).

where

$$g_{m+1}=4[p^2(m+1)^2-R_1^2],$$

$$g_l=4(l+m)(l-m)[p^2l^2-R_1^2], \quad l=m+2,\ m+3,\ \cdots,$$

$$h_l=(2l+1)[l(l+1)+A-p^2], \quad l=m+1,\ m+2,\ \cdots.$$

It does not seem worth while to attempt to construct a table of the constants A and p for the heteronuclear case.

3. DISSOCIATION ENERGY OF THE HYDROGEN MOLECULE

As a first application of DO's we have extended Hylleraas' calculation on the hydrogen molecule. Apart from an antisymmetric spin factor, our complete electronic wave function Ψ is

$$\Psi=\psi_1(1)\psi_5(2)+\psi_1(2)\psi_5(1),$$

where the homonuclear DO's ψ_1 and ψ_5 correspond to nuclear charges $Z=\frac{1}{2}$ and $Z=1$, respectively, and the numbers in parentheses refer to electrons 1 and 2. The total energy E of the hydrogen molecule is given by W/N where

$$W=\int \Psi^*\mathbf{H}\Psi dt_1dt_2,$$

$$N=\int \Psi^*\Psi dt_1dt_2,$$

$$\mathbf{H}=-\tfrac{1}{2}\nabla_1^2-\tfrac{1}{2}\nabla_2^2+\frac{1}{R}+\frac{1}{r_{12}}-\frac{1}{r_{a1}}-\frac{1}{r_{b1}}-\frac{1}{r_{a2}}-\frac{1}{r_{b2}},$$

dt_1, dt_2 = volume elements for space coordinates of electrons 1 and 2, respectively.

The normalization integral N is easily evaluated in terms of the integral $A_n(\alpha)$ discussed by Rosen.[10] The integral W may be written as

$$W=2W_1+2W_2,$$

where

$$W_1=\int \psi_1^*(1)\psi_5^*(2)\mathbf{H}\psi_1(1)\psi_5(2)dt_1dt_2,$$

$$W_2=\int \psi_1^*(1)\psi_5^*(2)\mathbf{H}\psi_1(2)\psi_5(1)dt_1dt_2.$$

The diatomic orbitals ψ_1 and ψ_5 satisfy the equations

$$\left\{-\tfrac{1}{2}\nabla^2-\frac{Z_1}{r_a}-\frac{Z_1}{r_b}\right\}\psi_1=E_{e1}\psi_1, \tag{14}$$

$$\left\{-\tfrac{1}{2}\nabla^2-\frac{Z_5}{r_a}-\frac{Z_5}{r_b}\right\}\psi_5=E_{e5}\psi_5, \tag{15}$$

[10] N. Rosen, Phys. Rev. 38, 255, 2099 (1931).

where E_{e1} and E_{e5} are the appropriate electronic energies. The integral W_1 accordingly becomes

$$W_1=N_1N_5(E_{e1}+E_{e5})+\frac{N_1N_5}{R}+W'-(1-Z_1)N_5W_1''-(1-Z_5)N_1W_5'',$$

where

$$W'=\int \psi_1^*(1)\psi_5^*(2)\left[\frac{1}{r_{12}}\right]\psi_1(1)\psi_5(2)dt_1dt_2,$$

$$W_1''=\int \psi_1^*(1)\left[\frac{1}{r_a}+\frac{1}{r_b}\right]\psi_1(1)dt_1,$$

$$W_5''=\int \psi_5^*(2)\left[\frac{1}{r_a}+\frac{1}{r_b}\right]\psi_5(2)dt_2,$$

and N_1 and N_5 are normalization integrals. We shall call the quantities $1-Z_1$ and $1-Z_5$ the screening constants for DO's ψ_1 and ψ_5, respectively.

By means of elliptic coordinates the integrals W_1'' and W_5'' may be evaluated in terms of the integrals $A_n(\alpha)$. If the Neumann expansion in elliptic coordinates is substituted for $1/r_{12}$, the integral W' may be expressed as a finite series involving the integrals $H_\tau(m,\gamma_1,n,\gamma_2)$ studied by James.[11]

The integral W_2 is treated analogously to W_1.

The result of our calculation using the above wave function is given in the second entry of Table IV. Here, as well as in our other calculations on H_2, the internuclear distance was taken to be the experimental value, 1.40 a.u. The integrals W' and W_1'' (W_5'' contributes nothing) were evaluated using two terms in the expansions for $U(u)$ and $V(v)$ as indicated in Table III. The result of Hylleraas, based on the use of only a single term in each expansion, is listed as the first entry for comparison. The apparent rates of convergence of the expansion coefficients suggest that our value of the dissociation energy is within one or two percent of the value one would obtain if the complete expansions for the DO's were employed.

TABLE IV. Energy of the hydrogen molecule computed by the DO method.[a]

No.	Wave function	n_u	n_v	Z	Total energy, a.u.	Dissociation energy, ev
1.	$\psi_1(1)\psi_5(2)+\psi_1(2)\psi_5(1)$	1	1	1.0, 0.5	−1.125710	3.41931
2.	$\psi_1(1)\psi_5(2)+\psi_1(2)\psi_5(1)$	2	2	1.0, 0.5	−1.135371	3.68209
3.	$\psi_2(1)\psi_2(2)$	1	1	0.7122849	−1.118924	3.23474
4.	$\psi_2(1)\psi_2(2)$	2	2	0.7122849	−1.121522	3.30540
5.	$\psi_3(1)\psi_3(2)$	1	1	0.7375701	−1.118047	3.21088
6.	$\psi_3(1)\psi_3(2)$	2	2	0.7375701	−1.125455	3.41238
7.	$\psi_4(1)\psi_4(2)$	1	1	0.7886768	−1.110596	3.00821
8.	$\psi_4(1)\psi_4(2)$	2	1	0.7886768	−1.115954	3.15395
9.	$\psi_4(1)\psi_4(2)$	2	2	0.7886768	−1.128060	3.48323
10.	$\psi_5(1)\psi_5(2)$	1	1	1.0	−1.018193	0.49485
11.	$\psi_5(1)\psi_5(2)$	2	2	1.0	−1.076995	2.0943

[a] n_u = number of terms used for $U(u)$, n_v = number of terms used for $V(v)$. The internuclear distance R is 1.40 a.u. in every case.

[11] H. M. James, J. Chem. Phys. 2, 794 (1934).

There do not seem to exist any LCAO calculations for the hydrogen molecule based on the use of different screening constants in the two MO's occupied by the two electrons; therefore, no direct comparison between the Hylleraas method and the LCAO method can be made at this time. It is interesting to note, however, that our result is somewhat superior to the dissociation energy 3.603 ev obtained by Coulson[12] using MO's chosen through a variational procedure. The effective nuclear charge was the same for each of Coulson's MO's. Consequently, one may infer that the two electrons of the hydrogen molecule should be assigned to MO's having different screening constants for best results. This behavior is also found with the helium atom for which the best effective nuclear charges for the two orbitals are 2.15 and 1.19, respectively.[13]

From the practical computational point of view it is simpler to use the same screening constant in both MO's than to use different screening constants. In order to compare the two procedures we have made several calculations of the dissociation energy of H_2 using the former method. The results are contained in Table IV, entries 3–11. The maximum dissociation energy D_m and the corresponding effective nuclear charge Z_m were estimated to be 3.485 ev and 0.7825, respectively, by fitting a polynomial to the data under entries 4, 6, 9, and 11. The close agreement between D_m and the dissociation energy of 3.470 ev calculated by Coulson[6] and by Weinbaum[7] using the LCAO approximation is interesting. The differences between the MO's thus far discussed are illustrated in Fig. 1 where the values of the MO's along the internuclear axis are plotted.

A significant feature of our results on the hydrogen molecule is that the wave function specified by Hylleraas' method for choosing screening constants gives a better energy value than the wave functions chosen by a variational calculation and containing only a single screening constant.

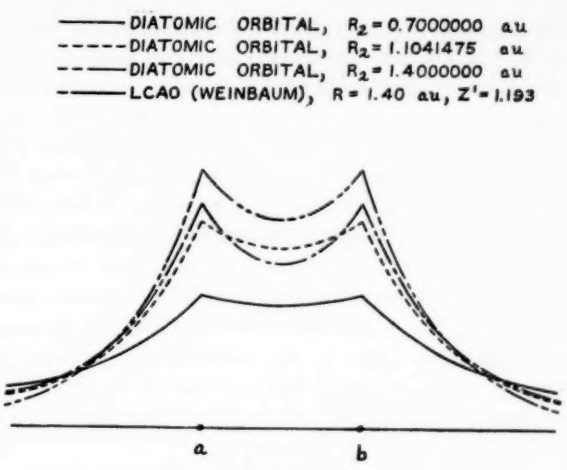
DIATOMIC ORBITAL, $R_2 = 0.7000000$ au
DIATOMIC ORBITAL, $R_2 = 1.1041475$ au
DIATOMIC ORBITAL, $R_2 = 1.4000000$ au
LCAO (WEINBAUM), $R = 1.40$ au, $Z' = 1.193$
a
b

FIG. 1. Values of molecular orbitals for H_2 along the internuclear axis.

4. THE GENERAL DIATOMIC MOLECULE

If one is interested in energy calculations, wave functions constructed from diatomic orbitals are not very satisfactory except for the hydrogen molecule. The reason is that as the parameter R_2 increases, the convergence of the infinite series for $V(v)$, Eq. (9), or Eq. (12), becomes rapidly worse. One then requires integrals $H_\tau(m,\gamma_1,n,\gamma_2)$ where $\tau>4$; these integrals are very difficult to evaluate by the usual recurrence relations because they appear as the difference of large but nearly equal numbers. The labor consequently increases very rapidly with increasing R_2. Even for the helium hydride ion, HeH^+, the labor is excessive.

For the computation of other molecular quantities such as electric dipole moments, polarizabilities, and transition probabilities, however, the convergence problem is much less troublesome because the necessary integrals are fewer in number and simpler in form.

Additional difficulties not encountered with H_2 arise, however, when one treats molecules containing more than two electrons using a generalization of Hylleraas' procedure for choosing screening constants. The complete wave function for the molecule can be expressed as a linear combination of determinants of DO's. This linear combination does not reduce to a single determinant even for ground states consisting of so-called closed shells. This behavior is similar to that found in the Heitler-London method and is due to no two DO's having the same screening constants.

Some of the coefficients specifying the linear combination of determinants can be determined by requiring the complete wave function to be an eigenfunction of operators such as the spin operators S_z and S^2 which commute with the Hamiltonian. In general, however, there will remain coefficients which would have to be determined by minimizing the energy, and this is impractical.

This difficulty may be circumvented for states consisting of closed shells by using the same screening constant in DO's having the same quantum numbers aside from spin (equivalent DO's). We shall call these constants "standard" screening constants and denote them by S_a and S_b where a and b specify the nuclei.

One may tentatively assign S_a and S_b by a modification of Hylleraas' method. Let us consider first H_2. The sum of all the screening constants in the two DO's used by Hylleraas is one unit of charge—i.e., $0+0+0.5+0.5=1.0$. Let us require that the sum of all the standard screening constants also be one unit of charge—i.e., $2S_a+2S_b=1.0$. From symmetry one takes $S_a=S_b$; hence, $S_a=0.25$ and the effective nuclear charge Z is

[12] C. A. Coulson, Proc. Cambridge Phil. Soc. 34, 204 (1938).
[13] E. A. Hylleraas, Z. Physik 54, 347 (1929); C. Eckart, Phys. Rev. 36, 878 (1930); R. S. Mulliken, Proc. Natl. Acad. Sci. U. S. 38, 160 (1952). The authors are indebted to the referee for emphasizing this point.

0.75. Interpolation in Table IV shows that this value of Z leads to a dissociation energy nearly as good as D_m.

For homonuclear molecules containing more than two electrons the standard screening constants for the various pairs of equivalent DO's may be determined successively starting with the $1s\sigma$ DO. For the latter the screening constants are the same as for the $1s\sigma$ DO of H_2. For the $2p\sigma$ DO (if this is the next higher orbital)

$$S_a=S_b=1.0+0.25=1.25,$$

where the first term is the contribution of the $1s\sigma$ electrons and the second term is that of the other $2p\sigma$ electrons. The screening constants for the higher DO's may be determined analogously.

For heteronuclear molecules whose bare nuclei have charges Z_a and Z_b, a physically reasonable assignment of screening constants to the $1s\sigma$ DO is given by

$$S_a+S_b=0.5,$$

$$S_a/S_b=Z_a/Z_b.$$

The total contribution of a $1s\sigma$ electron to the screening constant of a $2s\sigma$ DO (if this is the next higher orbital) is 1.0. This contribution may be divided between the two nuclei in the same ratio as the fractions of the $1s\sigma$ electron charge density which are in the vicinity of the respective nuclei. The total contribution of the other $2p\sigma$ electron is 0.5 which may be divided between the nuclei in the same ratio as the effective nuclear charges computed from the screening contributions of the $1s\sigma$ electrons. The higher DO's are treated in similar fashion.

The screening constants together with the internuclear distance and bare nuclear charges specify the DO's of the diatomic molecule. In general these DO's are not mutually orthogonal. In practical calculations it is perhaps convenient to construct an orthonormal set of DO's.

The above discussion presents a prescription for writing down a complete electronic wave function of molecular orbital form for a diatomic molecule, either homonuclear or heteronuclear, without a variation of parameters to minimize the energy. The value of such wave functions may be tested by computing properties such as the electric dipole moment, polarizability, and transition probabilities of molecules such as LiH, Li_2, etc., and comparing the results with experiment or with other theoretical calculations. *A priori* it seems probable that the above wave functions can be useful only when configuration interaction is small.

ACKNOWLEDGMENT

The authors wish to thank Miss Agnes Fogelgren for her assistance in the preparation of the manuscript.

APPENDIX

Let us consider the two continued fractions

$$Q_a=\frac{A_1}{B_1-}\frac{A_2}{B_2-}\frac{A_3}{B_3-}\cdots,$$

$$Q_c=\frac{C_1}{D_1-}\frac{C_2}{D_2-}\frac{C_3}{D_3-}\cdots.$$

We assume that

(i) A_k, B_k, C_k, D_k are positive for every k, $k=1, 2, 3, \cdots$,

(ii) $A_k \leq C_k$ for every k,

(iii) $B_k \geq D_k$ for every k,

(iv) $D_j-\frac{C_{j+1}}{D_{j+1}-}\frac{C_{j+2}}{D_{j+2}-}\cdots\frac{C_k}{D_k}>0$ for every j, k such that $j<k$,

(v) Q_a and Q_c converge.

Then the theorem we wish to prove states:

$$Q_a \leq Q_c.$$

Proof: From hypotheses (i) through (iv) we have

$$\frac{A_n}{B_n}\leq\frac{C_n}{D_n} \text{ for any given positive integer } n,$$

$$B_{n-1}-\frac{A_n}{B_n}\geq D_{n-1}-\frac{C_n}{D_n},$$

$$\frac{A_{n-1}}{B_{n-1}-}\frac{A_n}{B_n}\leq\frac{C_{n-1}}{D_{n-1}-}\frac{C_n}{D_n}.$$

Continuing in this manner, we conclude that $P_{an}\leq P_{cn}$ where P_{an} and P_{cn} are the nth approximants to Q_a and Q_c, respectively. Let us assume for the sake of argument that $Q_a>Q_c$. Then $Q_a-Q_c=\epsilon$ where $\epsilon>0$. By definition of convergence,

$$Q_a=\lim_{n\to\infty}P_{an},$$

$$Q_c=\lim_{n\to\infty}P_{cn}.$$

It is therefore possible to find an n, say N, such that $|Q_a-P_{aN}|<\epsilon/2$, $|Q_c-P_{cN}|<\epsilon/2$. But the latter inequalities together with $Q_a-Q_c=\epsilon$ require that $P_{aN}>P_{cN}$, which contradicts our previously derived result. Hence, $Q_a\leq Q_c$. If one can choose Q_c so that its value is easily obtained, one has a convenient upper bound for Q_a.

Considerations similar to those used in the proof of the theorem show that the nth approximants of Q_a and Q_c constitute lower bounds for the respective continued fractions.

Upper bounds to the continued fraction in Eq. (5) were generally obtained by using continued fractions of the form

$$\frac{a_1}{b_1-}\,\frac{a_2}{b_2-}\cdots\frac{a_n}{b_n-}\,\frac{a_{n+1}}{2-}\,\frac{1}{2-}\,\frac{1}{2-}\,\frac{1}{2-}\cdots.$$

Occasionally it was necessary to transform the continued fraction in Eq. (5) by the equivalence transformation[14]

$$a_1'=2a_1/b_1,$$
$$a_n'=4a_n/b_nb_{n-1}, \quad n=2, 3, \cdots,$$
$$b_n'=2, \quad n=1, 2, 3, \cdots,$$

in order to meet the conditions of the above theorem.

Upper bounds to the continued fraction in Eq. (10) were obtained with a continued fraction of the form

$$\frac{q_{2+\delta}}{r_{2+\delta}-}\,\frac{q_{4+\delta}}{r_{4+\delta}-}\cdots\frac{q_{n+\delta}}{r_{n+\delta}-}\,\frac{c}{d-}\,\frac{c}{d-}\,\frac{c}{d-}\cdots.$$

The constants c and d were chosen so that the theorem discussed above could be applied and so that as small an upper bound as possible would result. Under the conditions of this research the value of

$$\frac{c}{d-}\,\frac{c}{d-}\,\frac{c}{d-}\cdots$$

is[14]

$$\{1-[1-4c/(d^2)]^{\frac{1}{2}}\}d/2.$$

[14] H. S. Wall, *Continued Fractions* (D. Van Nostrand Company, Inc., New York, 1948).

THE JOURNAL OF CHEMICAL PHYSICS VOLUME 22, NUMBER 5 MAY, 1954

Infrared Absorption Spectra of Aqueous HF_2^-, DF_2^-, and HF*

LLEWELLYN H. JONES AND ROBERT A. PENNEMAN
Los Alamos Scientific Laboratory, University of California, Los Alamos, New Mexico
(Received November 16, 1953)

Strong infrared absorption bands of KHF_2 appear at 1233 cm^{-1} and 1473 cm^{-1} in the solid, and are observed at 1206 cm^{-1} and 1536 cm^{-1} respectively, in H_2O solution. Corresponding values for KDF_2 are 888 cm^{-1} and 1045 cm^{-1} in the solid, and 873 cm^{-1} and 1102 cm^{-1} in D_2O solution. In saturated KHF_2 and in KHF_2 solutions containing excess HF, there appear new, broad absorption bands attributed to polymeric species, e.g., $H_2F_3^-$. The HF_2^- ion is observed in concentrated aqueous HF; in addition, there is a strong absorption at 1820 cm^{-1} which is not shifted in D_2O-HF mixtures.

THE infrared absorption spectra of various inorganic complex ions in aqueous solution are being studied. It is the purpose of this letter to report the infrared absorption spectra of aqueous HF_2^-, DF_2^-, and HF.

Specific heat determinations by Pitzer and Westrum[1] showed that the $(F-H-F)^-$ ion is symmetrical. Infrared studies of solid KHF_2 have been reported by Ketelaar,[2] Coté and Thompson,[3] Ketelaar and Vedder,[4] and by Newman and Badger.[5] Raman studies of solid KHF_2 by Mathieu and Mathieu[6] have also been reported. The results can be summarized as follows: ν_1 (symmetric stretching) *ca* 600 cm^{-1}; ν_2 (bending) *ca* 1230 cm^{-1}; and ν_3 (asymmetric stretching) *ca* 1425 cm^{-1}. Ketelaar[2] also studied solid KDF_2 and reported $\nu_2=863$ cm^{-1} and $\nu_3=1023$ cm^{-1}. No Raman effect was observed by Woodward and Tyrrell[7] with concentrated aqueous solutions of KHF_2. This they interpreted as showing the H bonds are highly ionic in character. Their experiments bear repetition in view of the strong infrared absorption we observe for similar solutions.

We have observed the infrared absorption spectrum of HF_2^- ion in aqueous KHF_2 solution between silver chloride windows using the thin-film technique already described.[8] A single-beam Perkin-Elmer Model 12-C recording spectrograph converted to double pass was used. To obtain the spectrum of the aqueous DF_2^- ion, solid KHF_2 was added to saturate 99 percent D_2O. Exchange equilibrium was reached rapidly. The spectra of the solid compounds were also observed. Aqueous solutions of various concentrations of HF were studied, as were solutions containing 3 f KF (prepared from weighed amounts of $KF\cdot 2H_2O$) to which various amounts of either HF or HNO_3 were added. Results are recorded in Table I. Some of the spectra are shown in Fig. 1.

* This work was sponsored by the U. S. Atomic Energy Commission.

[1] K. P. Pitzer and E. F. Westrum, J. Chem. Phys. **15**, 526 (1947).
[2] J. A. A. Ketelaar, Rec. trav. chim. **60**, 523 (1941); J. Chem. Phys. **9**, 775 (1941).
[3] G. L. Coté and H. W. Thompson, Proc. Roy. Soc. (London) **210A**, 206 (1951).
[4] J. A. A. Ketelaar and W. Vedder, J. Chem. Phys. **19**, 654 (1951).
[5] R. Newman and R. M. Badger, J. Chem. Phys. **19**, 1201 (1951).
[6] L. C. Mathieu and J. P. Mathieu, Compt. rend. **230**, 1054 (1950).
[7] L. A. Woodward and J. V. Tyrrell, Trans. Faraday Soc. **38**, 517 (1942).
[8] L. Jones and R. Penneman, J. Chem. Phys. **21**, 542 (1953).

TABLE I. Observed infrared absorption maxima in solid and aqueous KHF_2 and KDF_2 and aqueous HF.

$HF_{(aq)}$ 1535 cm^{-1} (ν_2, HF_2^-) very weak; 1820 assignment unknown

	KHF_2		KDF_2	
	Solid	Aqueous	Solid	Aqueous
ν_2	1233±3 cm^{-1}	1206±6 cm^{-1}	888±5 cm^{-1}[a]	873±5 cm^{-1}
ν_3	1473±50[b]	1536±15	1045±50[b]	1102±8
		1105 (very broad)		780 (very broad)
		1015 (very broad)		

[a] This value, 888 cm^{-1}, does not agree with that reported by Ketelaar (reference 2) (863 cm^{-1}); however, we believe the limits of error given here are satisfactory, and the shift from solid to aqueous phase is in accord with that for KHF_2.
[b] These absorption bands are broad, and the maxima are thus uncertain.

The spectra of aqueous solutions of KHF_2 and KDF_2 gave no absorption other than the continuous absorption of H_2O and D_2O in the region 700–400 cm^{-1}. This is in accord with the assignment of 600 cm^{-1} to the HF_2^- symmetrical stretching frequency, as it should be infrared inactive.

In aqueous solution, the HF_2^- and DF_2^- asymmetric stretching vibrations (ν_3) are higher and the bending vibrations (ν_2) are lower than in solid KHF_2 and KDF_2. This indicates that in the solid the H−F bonds are weaker than in aqueous HF_2^-, probably because of interaction with neighboring potassium ions. Also, this ordering effect tends to restrict the bending motion and thus in effect increase the bending force constant, in agreement with the results given in Table I.

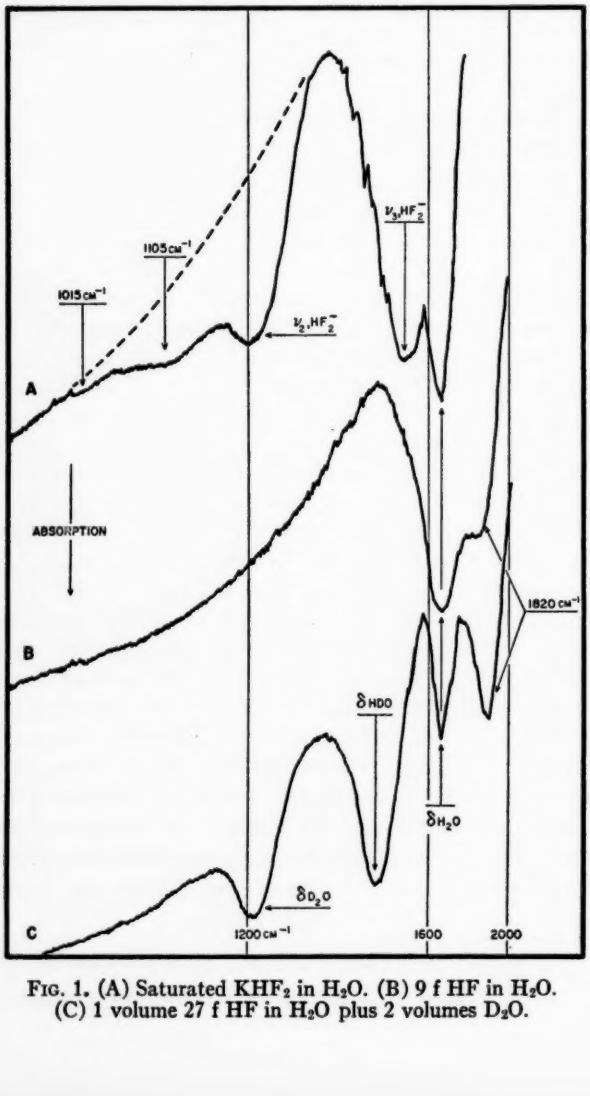

FIG. 1. (A) Saturated KHF_2 in H_2O. (B) 9 f HF in H_2O. (C) 1 volume 27 f HF in H_2O plus 2 volumes D_2O.

As noted in Table I, broad absorption maxima were observed at ~1105 cm^{-1} and 1015 cm^{-1} in aqueous KHF_2, and at 780 cm^{-1} in aqueous KDF_2. For solutions 3 formal in KF and 3 formal in HF, this absorption in the region 1000–1150 cm^{-1} was very weak, but was slightly stronger in saturated KHF_2. When the HF/KF ratio was varied from 1–3 at constant 3 f KF, the absorption in the region 1000–1150 cm^{-1} increased. Thus, it appears that this absorption probably arises from species such as $H_2F_3^-$ or higher polymers. Species KF·4HF, KF·3HF, KF·2.5HF, KF·2HF, and KF·HF were reported by Cady.[9]

The very broad absorption at 780 cm^{-1} in aqueous KDF_2 can be attributed to the same type of species.

Concentrated aqueous HF (*ca* 27 f) gave strong absorption at 1820 cm^{-1}, which was also noted in the KF solutions containing excess HF and weak absorption at 1535 cm^{-1}, but no absorption other than from H_2O from 1500 to 700 cm^{-1}. The absorption at 1535 cm^{-1} arises from HF_2^- (much less than 1 f). Broene and DeVries[10] report $HF = H^+ + F^-$, $K_1 = 6.71 \times 10^{-4}$ and $HF + F^- = HF_2^-$, $K_2 = 3.96$. Using these values an observable amount of HF_2^- is expected in concentrated HF solutions, in agreement with our observation. Also, considerable dissociation of HF_2^- in KHF_2 solution is expected, yielding HF which is available for formation of $H_2F_3^-$.

A solution of 9 f HF gave a strong absorption at 1655 cm^{-1} (H_2O bending) and a slightly weaker absorption at 1820 cm^{-1}. When deuterium was largely substituted for hydrogen (by 1:2 dilution of 27 f HF with D_2O), the peak at 1820 cm^{-1} persisted at about the same intensity. When HF was prepared from HNO_3 and NaF, or from BaF_2 and H_2SO_4, the 1820 peak was observed, on either AgCl or CaF_2 windows. This seems to rule out the presence of an impurity giving rise to the 1820 cm^{-1} absorption.

IN SUMMARY

(1) Both HF_2^- and DF_2^- have characteristic infrared absorption peaks in aqueous solution with ν_3 shifted to higher and ν_2 shifted to lower frequencies than in the respective solids. Nearly saturated solutions of KHF_2 (3–4 f) show additional absorption attributed to ions such as $H_2F_3^-$. Addition of excess HF increases the amount of these polymeric species. A similar behavior is noted for DF_2^-.

(2) Aqueous HF at concentrations of 6 f and greater shows increasingly stronger infrared absorption at 1820 cm^{-1} which is not shifted in D_2O. Weak absorption by the HF_2^- ion is also observed.

[9] G. H. Cady, J. Am. Chem. Soc. **56**, 1431 (1934).
[10] H. H. Broene and T. DeVries, J. Am. Chem. Soc. **69**, 1644 (1947).

Statistical Mechanical Theory of Transport Processes. VII. The Coefficient of Thermal Conductivity of Monatomic Liquids*

ROBERT W. ZWANZIG, JOHN G. KIRKWOOD, IRWIN OPPENHEIM,† AND BERNI J. ALDER‡
Sterling Chemistry Laboratory, Yale University, New Haven, Connecticut

(Received November 30, 1953)

A molecular theory of the coefficient of thermal conductivity is developed from the general theory of transport processes presented in the first article of this series. The thermal conductivity of liquid argon at its normal boiling point is evaluated using the Lennard-Jones intermolecular potential and a theoretically determined radial distribution function. The theory leads to an explicit expression for the product of the thermal conductivity and the friction constant of the theory of Brownian motion. With a reasonable estimate of the friction constant, the results of the theory agree satisfactorily with experiment.

I.

AMONG the objectives of the statistical mechanical theory of transport processes outlined in the first article of this series[1] (SMT-I) are the investigation of the domain of validity of the empirical Fourier law of heat conduction and the determination of the coefficient of thermal conductivity of a fluid in terms of its molecular parameters. In the present article, the theory of thermal conductivity is developed for a one-component fluid whose molecules interact with central forces, and a numerical evaluation of the coefficient of thermal conductivity of liquid argon is performed.

Our discussion starts from the generalized Chandrasekhar equations[1] for the motion through phase space of the probability distributions of sets of one, two, and more molecules. An alternate approach is provided by the theory of Born and Green.[2] While their theory duplicates some of the general results of ours, it differs in the way in which dissipative effects are to be introduced into the equations satisfied by the distribution functions. They have not succeeded in constructing solutions for the distribution functions in sufficiently explicit form to yield useful results.

In the fourth article of this series[3] (SMT-IV) an expression was derived for the heat current density in a fluid in terms of averages of molecular variables. The averages are performed with distribution functions in the phase space of a single molecule and with distribution functions in the configuration space of pairs of molecules. In order to relate the heat current density to the temperature gradient, it is necessary to determine the perturbing effect of a temperature gradient on these distribution functions. This is accomplished with the generalized Chandrasekhar equations. The derivation has been carried out in detail for the case of a one-component fluid whose molecules interact with the spherically symmetric potential energy

$$V_N=\sum_{i<j=1}^{N-1}\sum^{N}V(R_{ij})$$
$$R_{ij}=|\mathbf{R}_i-\mathbf{R}_j|, \tag{1}$$

where $V(R)$ is the potential energy of a pair of molecules. The resulting expression for the coefficient of thermal conductivity κ, is

$$\mathbf{q}=-\kappa\nabla T, \tag{2}$$

$$\kappa=\kappa_K+\kappa_V, \tag{3}$$

$$\kappa_K=\frac{k^2T}{2\zeta}\rho^{(1)}-\frac{k^2T^2}{6\zeta}\left(\frac{\partial\rho^{(1)}}{\partial T}\right)_P, \tag{4}$$

$$\kappa_V=\frac{\pi kT}{3\zeta}\rho^{(1)2}\int_0^\infty R^3\left(R\frac{dV}{dR}-V\right)g_0^{(2)}(R)\times\frac{d}{dR}\left[\frac{\partial}{\partial T}\log g_0^{(2)}(R)\right]_P dR+\frac{\pi kT}{\zeta}\rho^{(1)2}\left[\frac{\partial}{\partial T}\int_0^\infty(R^2V-R^3V')g_0^{(2)}(R)dR\right]_P, \tag{5}$$

where $\mathbf{q}$ is the heat current density, ∇T is the temperature gradient, κ_K is the momentum transport contribution to the thermal conductivity, and κ_V is the intermolecular force contribution. The other quantities in these equations are defined in this way: k is the Boltzmann constant, T is the absolute temperature, $\rho^{(1)}$ is the mean number of molecules per unit volume of the fluid, $g_0^{(2)}(R)$ is the equilibrium (unperturbed) radial distribution function of the fluid, and ζ is the friction constant. ζ is related to the coefficient of self-diffusion D of the fluid by

$$D=kT/\zeta. \tag{6}$$

The quantity $\zeta\kappa$ was evaluated for liquid argon at its normal boiling point, using experimentally determined

* This work was carried out with support from the U. S. Office of Naval Research, under contract with Yale University.

† Present address: National Bureau of Standards, Washington, D. C.

‡ Present address: Chemistry Department, University of California, Berkeley, California.

[1] J. G. Kirkwood, J. Chem. Phys. 14, 180 (1946).

[2] M. Born and H. S. Green, *A General Kinetic Theory of Liquids* (Cambridge University Press, Cambridge, 1949).

[3] J. H. Irving and J. G. Kirkwood, J. Chem. Phys. 18, 817 (1950).

equilibrium thermodynamic properties and a theoretically determined radial distribution function. The Lennard-Jones intermolecular potential was used. With an estimated value of the friction constant, $\zeta = 2.85 \times 10^{-10}$ g/sec, the final numerical result is $\kappa = 4.1 \times 10^{-4}$ cal/g sec °K. This may be compared with the experimental value $\kappa = 2.9 \times 10^{-4}$ cal/g sec °K.

II.

In SMT–IV, it was shown that the basic equations of hydrodynamics may be derived by performing the appropriate statistical mechanical averaging processes on microscopic variables. These equations are the equation of continuity,

$$(\partial\rho/\partial t) + \nabla_r \cdot \rho\mathbf{u} = 0, \tag{7}$$

where $\rho(\mathbf{r}; t)$ is the mass density and $\mathbf{u}(\mathbf{r}; t)$ is the bulk velocity of fluid; the equation of motion,

$$\frac{\partial \rho\mathbf{u}}{\partial t} + \nabla_r \cdot [\rho\mathbf{u}\mathbf{u}] = \mathbf{X} + \nabla_r \cdot \boldsymbol{\sigma}, \tag{8}$$

where $\mathbf{X}$ is the external force on the fluid and $\boldsymbol{\sigma}$ is the hydrodynamic stress tensor; and the equation of energy transport,

$$\frac{\partial E}{\partial t} + \nabla_r \cdot [E\mathbf{u} + \mathbf{q} - \mathbf{u} \cdot \boldsymbol{\sigma}] = 0, \tag{9}$$

where $E(\mathbf{r}; t)$ is the density (per unit mass) of internal energy, $\mathbf{q}$ is the heat current density, and $\mathbf{u} \cdot \boldsymbol{\sigma}$ represents the frictional work which is converted into heat. When the quantities ρ, E, $\mathbf{u}$, and $\boldsymbol{\sigma}$ are defined as averages of molecular variables, an expression for $\mathbf{q}$ in terms of averages of molecular variables may be obtained from the energy transport equation, Eq. (9). Before this expression is given, it will be necessary to define the distribution functions used in the averaging process.

The fundamental point of view of this theory is that macroscopic observables are determined by time averages of ensemble averages of molecular quantities. The averages are performed with probability densities $\bar{f}^{(n)}(\mathbf{p},\mathbf{q}; t)$ that subsets of n molecules out of an N molecule system have momenta and coordinates $(\mathbf{p},\mathbf{q})$,

$$f^{(n)}(\mathbf{p},\mathbf{q}; t) = \frac{1}{\tau}\int_0^\tau f^{(n)}(\mathbf{p},\mathbf{q}; t+s)\,ds$$
$$f^{(n)}(\mathbf{p},\mathbf{q}; t) = \int\int f^{(N)}(\mathbf{p},\mathbf{q},\mathbf{P},\mathbf{Q}; t)\,d\mathbf{P}\,d\mathbf{Q}, \tag{10}$$

where $(\mathbf{P},\mathbf{Q})$ are the momenta and coordinates of the residual set of $N-n$ molecules, and $f^{(N)}(\mathbf{p},\mathbf{q},\mathbf{P},\mathbf{Q}; t)$ is the probability density in the complete phase space of the N molecule system. (A more complete description of this theory of measurement, and the related distribution functions, is given in SMT–I.) Another useful type of distribution function is the number density

$$\rho^{(n)}(\mathbf{q}; t) = \frac{N!}{(N-n)!}\int \bar{f}^{(n)}(\mathbf{p},\mathbf{q}; t)\,d\mathbf{p}, \tag{11}$$

which is the density of systems in the $3n$-dimensional configuration space of the subset (n). In the configuration space of a single molecule, $\rho^{(1)}$ is the number density of molecules in the fluid. In the configuration space of pairs of molecules, the number density is

$$\rho^{(2)}(\mathbf{r},\mathbf{r}+\mathbf{R}; t) = \rho^{(1)}(\mathbf{r}; t)\rho^{(1)}(\mathbf{r}+\mathbf{R}; t)g^{(2)}(\mathbf{r},\mathbf{R}; t). \tag{12}$$

This defines the radial distribution function $g^{(2)}(\mathbf{r},\mathbf{R}; t)$.

Some basic macroscopic variables are the mass density ρ of the fluid,

$$\rho(\mathbf{r}; t) = m\rho^{(1)}(\mathbf{r}; t), \tag{13}$$

where m is the mass of a single molecule, and the current density $\mathbf{j}^{(1)}$,

$$\mathbf{j}^{(1)}(\mathbf{r}; t) = \rho^{(1)}(\mathbf{r}; t)\mathbf{u}(\mathbf{r}; t) = N\int \frac{\mathbf{p}}{m}\bar{f}^{(1)}(\mathbf{r},\mathbf{p}; t)\,d\mathbf{p}. \tag{14}$$

Also,

$$\mathbf{j}_1^{(2)}(\mathbf{r}_1,\mathbf{r}_2; t) = N^2\int\int \frac{\mathbf{p}_1}{m}\bar{f}^{(2)}(\mathbf{r}_1,\mathbf{r}_2,\mathbf{p}_1,\mathbf{p}_2; t)\,d\mathbf{p}_1 d\mathbf{p}_2 \tag{15}$$

is the projection on the space of molecule one of the current density in the pair space, or the current density at $\mathbf{r}_1$ when a molecule is fixed at $\mathbf{r}_2$, multiplied by the number density of molecules at $\mathbf{r}_2$.

It was shown in SMT–IV that the heat current density $\mathbf{q}$ is given by

$$\mathbf{q} = \mathbf{q}_K + \mathbf{q}_V, \tag{16}$$

$$\mathbf{q}_K(\mathbf{r}; t) = \frac{Nm}{2}\int \left|\frac{\mathbf{p}}{m} - \mathbf{u}\right|^2 \left(\frac{\mathbf{p}}{m} - \mathbf{u}\right)\bar{f}^{(1)}(\mathbf{r},\mathbf{p}; t)\,d\mathbf{p}, \tag{17}$$

$$\mathbf{q}_V(\mathbf{r}; t) = \tfrac{1}{2}\int\left[V(R)\mathbf{1} + \frac{\mathbf{R}\mathbf{R}}{R}\frac{dV(R)}{dR}\right] \cdot [\mathbf{j}_1^{(2)}(\mathbf{r},\mathbf{r}+\mathbf{R}; t) - \mathbf{u}(\mathbf{r}; t)\rho^{(2)}(\mathbf{r},\mathbf{r}+\mathbf{R}; t)]\,d\mathbf{R}, \tag{18}$$

where $\mathbf{1}$ is the unit dyad. A physical interpretation of this result is that $\mathbf{q}_K$ represents the average transport of kinetic energy relative to the bulk velocity of the fluid, and that in the expression for $\mathbf{q}_V$, the term containing $V(R)$ represents the transport of potential energy due to macroscopically imperceptible Brownian motion, while the term involving $V'(R)$ represents the work dissipated by this random motion. The Fourier heat law

$$\mathbf{q} = -\kappa\nabla T \tag{19}$$

defines the coefficient of thermal conductivity κ. It is therefore necessary to calculate the perturbation of $\bar{f}^{(1)}$ and $\bar{f}^{(2)}$ from equilibrium due to the temperature gradient ∇T.

The distribution functions $\bar{f}^{(1)}$ and $\bar{f}^{(2)}$ satisfy generalized Chandrasekhar equations [SMT–I, Eqs. (59) and (60)]. The $\bar{f}^{(1)}$ equation is

$$\frac{\partial \bar{f}^{(1)}}{\partial t}+\frac{\mathbf{p}}{m}\cdot\nabla_r f^{(1)}+\nabla_p\cdot\mathbf{F}^{(1)}\bar{f}^{(1)} =\zeta\nabla_p\cdot\left[\left(\frac{\mathbf{p}}{m}-\mathbf{u}\right)\bar{f}^{(1)}+kT\nabla_p\bar{f}^{(1)}\right], \quad (20)$$

where

$$\mathbf{F}^{(1)}={}^{(1)}\langle\mathbf{F}\rangle^0+{}^{(1)}\mathbf{F}\dagger. \quad (21)$$

The force ${}^{(1)}\langle\mathbf{F}\rangle^0$ is the average total intermolecular force on a molecule at $\mathbf{R}$ when the average is performed, in a canonical ensemble, over all the other molecules. The force ${}^{(1)}\mathbf{F}\dagger$ is a perturbation arising from the departure of $\rho^{(2)}$ from its equilibrium value. The quantity ζ is the friction constant in the space of a single molecule. Its expression in terms of intermolecular forces is given in SMT–I.

The differential equation for $\bar{f}^{(2)}$ is

$$\begin{aligned}\frac{\partial \bar{f}^{(2)}}{\partial t}&+\frac{\mathbf{p}_1}{m}\cdot\nabla_{R_1}\bar{f}^{(2)}+\frac{\mathbf{p}_2}{m}\cdot\nabla_{R_2}\bar{f}^{(2)}\\ &+\nabla_{p_1}\cdot(\mathbf{F}_1{}^{(2)}\bar{f}^{(2)})+\nabla_{p_2}\cdot(\mathbf{F}_2{}^{(2)}\bar{f}^{(2)})\\ &=\nabla_{p_1}\cdot\boldsymbol{\zeta}_1{}^{(2)}\cdot\left\{\left(\frac{\mathbf{p}_1}{m}-\mathbf{u}_1\right)\bar{f}^{(2)}+kT\nabla_{p_1}\bar{f}^{(2)}\right\}\\ &+\nabla_{p_2}\cdot\boldsymbol{\zeta}_2{}^{(2)}\cdot\left\{\left(\frac{\mathbf{p}_2}{m}-\mathbf{u}_2\right)\bar{f}^{(2)}+kT\nabla_{p_2}\bar{f}^{(2)}\right\}; \quad (22)\end{aligned}$$

$$\begin{aligned}\mathbf{F}_1{}^{(2)}&={}^{(2)}\langle\mathbf{F}_1\rangle^0+{}^{(2)}\mathbf{F}_1\dagger\\ \mathbf{F}_2{}^{(2)}&={}^{(2)}\langle\mathbf{F}_2\rangle^0+{}^{(2)}\mathbf{F}_2\dagger,\end{aligned} \quad (23)$$

where ${}^{(2)}\langle\mathbf{F}_1\rangle^0$ is the average total intermolecular force on a molecule at $\mathbf{R}_1$, when a pair of molecules are fixed at $\mathbf{R}_1$ and $\mathbf{R}_2$ and the average is performed, in a canonical ensemble, over the rest of the molecules. ${}^{(2)}\mathbf{F}\dagger$ is a perturbing force arising from the departure of $\rho^{(3)}$ from its equilibrium value. The friction tensor $\boldsymbol{\zeta}^{(2)}$ is a second-rank tensor in the six-dimensional configuration space of a pair of molecules. Its relation to intermolecular forces is described in SMT–I.

III.

The momentum contribution $\mathbf{q}_K$ to the heat current density will be evaluated in this section. The general procedure is to multiply the differential equation for $\bar{f}^{(1)}$ by various functions of momentum and then integrate the resulting equations over momentum space.

When Eq. (20) is integrated directly over momentum space, the equation of continuity is obtained. When Eq. (20) is multiplied by $N\mathbf{p}/m$ and integrated over momentum space, one obtains

$$\frac{\partial\mathbf{j}^{(1)}}{\partial t}+N\nabla_r\cdot\int\frac{\mathbf{pp}}{m^2}{}^{(1)}\bar{f}(\mathbf{r},\mathbf{p};t)d\mathbf{p}=\frac{\mathbf{F}^{(1)}\rho^{(1)}}{m}. \quad (24)$$

(In these integrations, Green's theorem is used to eliminate terms of the form $\int\nabla_p\cdot\mathbf{G}d\mathbf{p}$ when the surface integral of the quantity $\mathbf{G}$ over the boundaries of momentum space vanishes, which will always be the case in this article.) To relate the second term in this equation to macroscopic quantities, a nonequilibrium temperature $T(\mathbf{r};t)$ is defined by

$$\frac{mN}{2}\int\left(\frac{\mathbf{p}}{m}-\mathbf{u}\right)\left(\frac{\mathbf{p}}{m}-\mathbf{u}\right)\bar{f}^{(1)}d\mathbf{p}=\frac{kT\rho^{(1)}}{2}\mathbf{1}. \quad (25)$$

The temperature at $\mathbf{r}$ is therefore proportional to the average kinetic energy, relative to the bulk velocity of the fluid of a molecule at $\mathbf{r}$. When this definition of temperature and the equation of continuity are used and nonlinear terms in the bulk velocity are neglected, one obtains

$$\mathbf{F}^{(1)}=\frac{1}{\rho^{(1)}}\nabla_r(kT\rho^{(1)}). \quad (26)$$

This implies that even in the case of constant density, a gradient in temperature produces an average force on a molecule.

Next, Eq. (20) is multiplied by $|\boldsymbol{\pi}|^2\boldsymbol{\pi}$, where $\boldsymbol{\pi}=(\mathbf{p}/m)-\mathbf{u}$, and integrated over momentum space. Green's theorem and the nonequilibrium definition of temperature are used, and nonlinear terms in $\mathbf{u}$, gradients of $\mathbf{u}$, and terms of order $1/\zeta^2$ are neglected. This leads to

$$\mathbf{q}_K=\frac{5kT}{6\zeta}\nabla_r(\rho^{(1)}kT)-\frac{Nm^2}{6\zeta}\nabla_r\cdot\int|\boldsymbol{\pi}|^2\boldsymbol{\pi}\boldsymbol{\pi}\bar{f}^{(1)}d\mathbf{p}. \quad (27)$$

It is still necessary to evaluate the last term. When Eq. (20) is multiplied by $|\boldsymbol{\pi}|^2\boldsymbol{\pi}\boldsymbol{\pi}$, integrated over momentum space, and nonlinear terms and terms of order $1/\zeta^2$ are neglected, one gets

$$\int|\boldsymbol{\pi}|^2\boldsymbol{\pi}\boldsymbol{\pi}\bar{f}^{(1)}d\mathbf{p}=\frac{4k^2T^2}{Nm^2}\rho^{(1)}\mathbf{1}. \quad (28)$$

Therefore,

$$\mathbf{q}_K=\frac{5kT}{6\zeta}\nabla_r(\rho^{(1)}kT)-\frac{2}{3\zeta}\nabla_r(\rho^{(1)}k^2T^2). \quad (29)$$

Since experimental observations of thermal conduction are performed at constant pressure, the indicated differentiations must be performed at constant pressure. The result is

$$\mathbf{q}_K=-\frac{k^2T}{2\zeta}\rho^{(1)}\nabla T+\frac{k^2T^2}{6\zeta}\left(\frac{\partial\rho^{(1)}}{\partial T}\right)_P\nabla T \quad (30)$$

or

$$\kappa_K=\frac{k^2T}{2\zeta}\rho^{(1)}-\frac{k^2T^2}{6\zeta}\left(\frac{\partial\rho^{(1)}}{\partial T}\right)_P. \tag{31}$$

IV.

In this section, the intermolecular force contribution $\mathbf{q}_V$ to the heat current density will be evaluated. The object of the procedure to be described here is to obtain the expansion, in powers of the temperature gradient, of the quantity $(\mathbf{j}_1^{(2)}-\rho^{(2)}\mathbf{u}_1)$. To achieve this, the Chandrasekhar equation for $\bar{f}^{(2)}$ is multiplied by $\mathbf{p}_1$ and integrated over the six-dimensional space of $\mathbf{p}_1$ and $\mathbf{p}_2$. As in the evaluation of $\mathbf{q}_K$, some preliminary results must first be obtained.

When Eq. (22) is integrated directly over momentum pair space, the result is an equation of continuity in pair configuration space,

$$\frac{\partial\rho^{(2)}}{\partial t}+\nabla_{r1}\cdot\mathbf{j}_1^{(2)}+\nabla_{r2}\cdot\mathbf{j}_2^{(2)}=0. \tag{32}$$

When Eq. (22) is multiplied by $\mathbf{p}_1\mathbf{p}_1$, integrated over $\mathbf{p}_1$ and $\mathbf{p}_2$, and terms of order $1/\zeta^2$ are neglected, an equation is obtained,

$$N^2\int\int\frac{\mathbf{p}_1\mathbf{p}_1}{m}\bar{f}^{(2)}d\mathbf{p}_1d\mathbf{p}_2=kT\rho^{(2)}\mathbf{1}+m\mathbf{u}_1\mathbf{j}_1^{(2)}, \tag{33}$$

which is analogous to Eq. (25) in singlet space. When Eq. (22) is multiplied by $\mathbf{p}_1\mathbf{p}_2/m$ and integrated, one obtains

$$\zeta_1^{(2)}\cdot\left\{\int\int\frac{\mathbf{p}_2\mathbf{p}_1}{m}\bar{f}^{(2)}d\mathbf{p}_1d\mathbf{p}_2-\frac{\mathbf{u}_1\mathbf{j}_2^{(2)}}{N^2}\right\}+\zeta_2^{(2)}\cdot\left\{\int\int\frac{\mathbf{p}_1\mathbf{p}_2}{m}\bar{f}^{(2)}d\mathbf{p}_1d\mathbf{p}_2-\frac{\mathbf{u}_2\mathbf{j}_1^{(2)}}{N^2}\right\}=0. \tag{34}$$

At this point, it is convenient to make an approximation on the form of the friction tensor in pair space,

$$\zeta^{(2)}=\zeta\mathbf{1}_1+\zeta\mathbf{1}_2, \tag{35}$$

where ζ is the scalar friction constant in singlet space and $\mathbf{1}_1$, $\mathbf{1}_2$ are unit dyads in $\mathbf{r}_1$, $\mathbf{r}_2$ space. This means that the dependence of the friction tensor on momenta and on the relative configuration of pairs of molecules is neglected. This approximation was also used in the theory of the viscosity coefficients (SMT–III).

Now, Eq. (22) is multiplied by $\mathbf{p}_1$ and integrated over momenta. When the results of the preceding paragraphs are used, and second order terms in velocities and in $1/\zeta$ are neglected, one gets

$$\frac{m}{\zeta}\frac{\partial\mathbf{j}_1^{(2)}}{\partial t}+\frac{1}{\zeta}\nabla_{r1}(kT\rho^{(2)})-\frac{\mathbf{F}_1^{(2)}\rho^{(2)}}{\zeta}=-(\mathbf{j}_1^{(2)}-\rho^{(2)}\mathbf{u}_1). \tag{36}$$

A similar equation may be derived for the second molecule. Since the current density $\mathbf{j}^{(2)}$ is itself of order $1/\zeta$, the time derivative, which is of order $1/\zeta^2$, may be neglected. When the radial distribution function $g^{(2)}$ is introduced, and the perturbation force ${}^{(2)}\mathbf{F}\dagger$ is neglected, a simple rearrangement leads to

$$\mathbf{j}_1^{(2)}-\rho^{(2)}\mathbf{u}_1=-\rho^{(1)}(\mathbf{r}_1)\rho^{(1)}(\mathbf{r}_2)\frac{kT}{\zeta}\times[\nabla_{r_1}g^{(2)}-g^{(2)}\nabla_{R_1}{}^{(T_1)}\log g_0^{(2)}]. \tag{37}$$

The following expression from the equilibrium theory of distribution functions has been used:

$${}^{(2)}\langle\mathbf{F}_1\rangle^0-{}^{(1)}\langle\mathbf{F}_1\rangle^0=kT\nabla_{R_1}{}^{(T_1)}\log g_0^{(2)}(R_{12},T_1), \tag{38}$$

where $g_0^{(2)}$ is the equilibrium radial distribution function, and depends upon the relative separation R_{12} and on the temperature and pressure at $\mathbf{R}_1$. The notation $\nabla_R{}^{(T)}$ is used to indicate partial differentiation with respect to $\mathbf{R}$, keeping temperature T fixed. When the superscript is omitted, the differentiation is total, and may contain a term resulting from temperature gradients.

The perturbed $g^{(2)}(R)$ depends on a temperature gradient, but the equilibrium $g_0^{(2)}(R)$ depends only on a single temperature. In order to express $g^{(2)}(R)$ in terms of $g_0^{(2)}(R)$ and a perturbation, it is necessary to establish some convention about which temperature to use in $g_0^{(2)}(R)$. If $T(\mathbf{R})$ is the temperature at $\mathbf{R}$, the perturbation $g_1^{(2)}(R)$ will be defined by

$$g^{(2)}(\mathbf{R}_1,\mathbf{R}_{12},T(\mathbf{R}_1),T(\mathbf{R}_2),P;t)=g_0^{(2)}(R_{12},T(\mathbf{R}_1),P)+g_1^{(2)}(\mathbf{R}_1,\mathbf{R}_{12},T(\mathbf{R}_1),T(\mathbf{R}_2),P;t). \tag{39}$$

The pressure P is indicated as an independent variable, rather than the density, since experimental studies of thermal conduction are performed at constant pressure. When this form of $g^{(2)}$ is substituted in Eq. (37) and the differentiations are performed, the relative pair current densities are

$$\begin{aligned}\mathbf{j}_1^{(2)}-\rho^{(2)}\mathbf{u}_1&=-\rho^{(1)}(\mathbf{R}_1)\rho^{(1)}(\mathbf{R}_2)\frac{kT(\mathbf{R}_1)}{\zeta(\mathbf{R}_2)}\mathbf{A}_1\\ \mathbf{j}_2^{(2)}-\rho^{(2)}\mathbf{u}_2&=-\rho^{(1)}(\mathbf{R}_1)\rho^{(1)}(\mathbf{R}_2)\frac{kT(\mathbf{R}_2)}{\zeta(\mathbf{R}_2)}\mathbf{A}_2,\end{aligned} \tag{40}$$

where the friction constant ζ depends explicitly on temperature and hence implicitly on position, and

$$\mathbf{A}_1=\nabla_{R_1}g_1^{(2)}-g_1^{(2)}\nabla_{R_1}{}^{(T_1)}\log g_0^{(2)}(R_{12},T_1,P)+\frac{\partial g_0^{(2)}(R_{12},T_1,P)}{\partial T_1}\nabla_{R_1}T_1, \tag{41}$$

$$\mathbf{A}_2=-\nabla_{R_1}g_1^{(2)}+g_1^{(2)}\nabla_{R_1}{}^{(T_1)}\log g_0^{(2)}(R_{12},T_1,P)+\left[g_0^{(2)}(R_{12},T_1,P)\frac{\partial}{\partial T_1}\nabla_{R_1}{}^{(T_1)}\log g_0^{(2)}(R_{12},T_1,P)\right]\times(\mathbf{R}_{12}\cdot\nabla_{R_1}T_1). \tag{42}$$

In deriving these expressions, it was assumed that $g_1^{(2)}$ is of order ∇T, that higher-order terms in ∇T may be neglected, and that $\nabla_{R_1} g_1^{(2)} = -\nabla_{R_2} g_1^{(2)}$. It may be verified that $g_1^{(2)}$ actually has these properties. In the equation for $\mathbf{A}_2$, the expansion

$$\nabla_{R_2^{(T_2)}} \log g_0^{(2)}(R_{12},T_2,P) = -\nabla_{R_1^{(T_1)}} \log g_0^{(2)}(R_{12},T_1,P) - (\mathbf{R}_{12}\cdot\nabla_{R_1}T_1)\frac{\partial}{\partial T_1}\nabla_{R_1^{(T_1)}} \times \log g_0^{(2)}(R_{12},T_1,P) + O(\nabla T)^2, \quad (43)$$

where

$$T(\mathbf{R}_2) - T(\mathbf{R}_1) = \mathbf{R}_{12}\cdot\nabla_{R_1}T_1 + O(\nabla T)^2, \quad (44)$$

was carried out.

A differential equation for $g_1^{(2)}$ will now be obtained. When the equations of continuity in pair space and in singlet space are combined, one obtains

$$\nabla_{R_1}\cdot(\mathbf{j}_1^{(2)} - \rho^{(2)}\mathbf{u}_1) + \nabla_{R_2}\cdot(\mathbf{j}_2^{(2)} - \rho^{(2)}\mathbf{u}_2) = -\rho^{(1)}(\mathbf{R}_1)\rho^{(1)}(\mathbf{R}_2)\frac{Dg^{(2)}}{Dt}, \quad (45)$$

where $Dg^{(2)}/Dt$ is a generalized Stokes derivative,

$$\frac{D}{Dt} \equiv \frac{\partial}{\partial t} + \mathbf{u}_1\cdot\nabla_{R_1} + \mathbf{u}_2\cdot\nabla_{R_2}. \quad (46)$$

When the expressions for the relative pair current densities are substituted in Eq. (45) and terms of order $(\nabla T)^2$ are neglected, then

$$\frac{\zeta_1}{kT_1}\frac{Dg^{(2)}}{Dt} = \nabla_{R_1}\cdot\mathbf{A}_1 + \nabla_{R_2}\cdot\mathbf{A}_2. \quad (47)$$

When the values for $\mathbf{A}_1$ and $\mathbf{A}_2$ are substituted in this equation, a differential equation for $g_1^{(2)}$ is obtained,

$$\frac{\zeta_1}{kT_1}\frac{Dg_1^{(2)}}{Dt} = \nabla_{R_1}\cdot\Big\{-2\nabla_{R_1}g_1^{(2)} + 2g_1^{(2)} \times \nabla_{R_1^{(T_1)}} \log g_0^{(2)}(R_{12},T_1,P) - \frac{\partial g_0^{(2)}(R_{12},T_1,P)}{\partial T_1}\nabla_{R_1}T_1 + \Big[g_0^{(2)}(R_{12},T_1,P)\frac{\partial}{\partial T_1}\nabla_{R_1^{(T_1)}} \times \log g_0^{(2)}(R_{12},T_1,P)\Big]\mathbf{R}_{12}\cdot\nabla_{R_1}T_1\Big\}. \quad (48)$$

A complete solution of this equation would lead to a molecular theory of the spectrum of relaxation times associated with heat flow due to temperature gradients. In order to get the steady-state thermal conductivity, it is sufficient to obtain the time-independent solution. It can be verified by substitution that

$$g_1^{(2)} = -\frac{1}{2}\frac{\partial g_0^{(2)}(R_{12},T_1,P)}{\partial T_1}\mathbf{R}_{12}\cdot\nabla_{R_1}T_1 \quad (49)$$

is a solution. This leads to the relative pair current density

$$\mathbf{j}_1^{(2)} - \rho^{(2)}\mathbf{u}_1 = [\rho^{(1)}]^2\frac{kT_1}{2\zeta}g_0^{(2)}\nabla_{R_{12}^{(T_1)}}\frac{\partial \log g_0^{(2)}}{\partial T_1}\mathbf{R}_{12}\cdot\nabla T_1 - [\rho^{(1)}]^2\frac{kT_1}{2\zeta}g_0^{(2)}\frac{\partial \log g_0^{(2)}}{\partial T_1}\nabla T_1. \quad (50)$$

The relative pair current density must satisfy certain conditions. It must have no current sources or sinks, and it must vanish when the two molecules are infinitely separated. These conditions are satisfied if the equilibrium radial distribution function has the physically reasonable properties of vanishing strongly at $R_{12}=0$ and approaching unity at infinite separation.

This solution leads to the heat current density

$$\mathbf{q}_V = [\rho^{(1)}]^2\frac{kT}{4\zeta}\int\left(V - R\frac{dV}{dR}\right) \times \frac{\mathbf{R}}{R}\frac{d}{dR}\frac{\partial \log g_0^{(2)}}{\partial T}(\mathbf{R}\cdot\nabla T)d\mathbf{R} - [\rho^{(1)}]^2\frac{kT}{4\zeta} \times \int\left(V\mathbf{1} - \frac{\mathbf{RR}}{R^2}\frac{dV}{dR}\right)\cdot\nabla T\frac{\partial g_0^{(2)}}{\partial T}d\mathbf{R}. \quad (51)$$

When the integrations over angles are performed, the heat current density becomes

$$\mathbf{q}_V = [\rho^{(1)}]^2\frac{\pi kT}{3\zeta}\nabla T\int_0^\infty R^3\left(V - R\frac{dV}{dR}\right)g_0^{(2)}(R) \times \frac{d}{dR}\left(\frac{\partial \log g_0^{(2)}}{\partial T}\right)_P dR - [\rho^{(1)}]^2\frac{\pi kT}{\zeta}\nabla T \times \int_0^\infty R^2\left(V - \tfrac{1}{3}R\frac{dV}{dR}\right)\left(\frac{\partial g_0^{(2)}}{\partial T}\right)_P dR. \quad (52)$$

Therefore, the potential energy contribution to the coefficient of thermal conductivity is

$$\kappa_V = [\rho^{(1)}]^2\frac{\pi kT}{3\zeta}\int_0^\infty R^3(RV' - V)g_0^{(2)}(R) \times \frac{d}{dR}\left(\frac{\partial \log g_0^{(2)}}{\partial T}\right)_P dR + [\rho^{(1)}]^2\frac{\pi kT}{\zeta} \times \int_0^\infty R^2(V - \tfrac{1}{3}RV')\left(\frac{\partial g_0^{(2)}}{\partial T}\right)_P dR. \quad (53)$$

V.

The theory which was developed in the preceding sections will now be applied to the calculation of the coefficient of thermal conductivity of liquid argon at its boiling point under a pressure of one atmosphere.

The intermolecular potential which will be used in this calculation is the Lennard-Jones potential,

$$V(R)=\epsilon\gamma(x),\qquad x=R/a,\qquad \gamma(x)=4\left(\frac{1}{x^{12}}-\frac{1}{x^{6}}\right). \tag{54}$$

It is convenient to express distance in the reduced units $x=R/a$ and pressure, volume, and temperature in the reduced units

$$P^*=Pa^3/\epsilon,\qquad T^*=Tk/\epsilon,\qquad v^*=v/Na^3. \tag{55}$$

Then, the quantity $\zeta\kappa$ may be expressed in reduced units,

$$\zeta\kappa_K=\frac{k\epsilon}{a^3}(\zeta\kappa_K)^*,\qquad \zeta\kappa_V=\frac{k\epsilon}{a^3}(\zeta\kappa_V)^*, \tag{56}$$

where

$$(\zeta\kappa_K)^*=\frac{T^*}{2v^*}\left\{1+\frac{T^*}{3v^*}\left(\frac{\partial v^*}{\partial T^*}\right)_{P^*}\right\} \tag{57}$$

and

$$(\zeta\kappa_V)^*=\frac{T^*}{2v^*}\left\{\frac{2\pi}{3v^*}\int_0^\infty x^3(x\gamma'-\gamma)g_0^{(2)}(x)\times\frac{d}{dx}\left(\frac{\partial \log g_0^{(2)}(x)}{\partial T^*}\right)_{P^*}dx-\frac{2\pi}{3v^*}\int_0^\infty x^2(x\gamma'-3\gamma)\left(\frac{\partial g_0^{(2)}(x)}{\partial T^*}\right)_{P^*}dx\right\}. \tag{58}$$

The integrals may be evaluated if the radial distribution function $g_0^{(2)}(x)$ and its temperature derivative are known. Since the integrals depend rather sensitively on these quantities, it is advantageous to transform the integrals into another form in which a part may be obtained from experimentally available thermodynamic properties. The kinetic contribution $(\zeta\kappa_K)^*$ is already in such a form.

By partial integration and some simple rearrangements, $(\zeta\kappa_V)^*$ may be split into two parts,

$$(\zeta\kappa_V)^*=I_1+I_2, \tag{59}$$

where

$$I_1=\frac{\pi T^*}{3v^{*2}}\int_0^\infty (x^3\gamma-x^4\gamma')\frac{\partial g_0^{(2)}(x)}{\partial x}\times\left(\frac{\partial \log g_0^{(2)}(x)}{\partial T^*}\right)_{P^*}dx \tag{60}$$

and

$$I_2=-\frac{\pi T^*}{3v^{*2}}\left[\frac{\partial}{\partial T^*}\times\int_0^\infty (4x^3\gamma'+x^4\gamma''-6x^2\gamma)g_0^{(2)}(x)dx\right]_{P^*}. \tag{61}$$

The pressure and internal energy of this fluid are given[4] by

$$\frac{P^*v^*}{T^*}=1-\frac{2\pi}{3v^*T^*}\int_0^\infty x^3\gamma'(x)g_0^{(2)}(x)dx \tag{62}$$

and

$$E^*=\tfrac{3}{2}T^*+\frac{2\pi}{v^*}\int_0^\infty x^2\gamma(x)g_0^{(2)}(x)dx, \tag{63}$$

where $E^*=E/N\epsilon$. Since $\gamma(x)$ has the Lennard-Jones form, so that

$$x^4\gamma''=-19x^3\gamma'-72x^2\gamma, \tag{64}$$

then the quantity I_2 is

$$I_2=\frac{\pi T^*}{3v^{*2}}\left[\frac{\partial}{\partial T^*}\int_0^\infty (15x^3\gamma'+78x^2\gamma)g_0^{(2)}(x)dx\right]_{P^*}. \tag{65}$$

It is possible to express I_2 in terms of thermodynamic variables. Making use of the expressions for P^*v^*/T^* and E^*, the result is

$$I_2=\frac{T^*}{v^*}\left\{13C_P^*-12+\beta^*\left(13\Delta H^*+\frac{41}{2}T^*-41P^*v^*\right)\right\}, \tag{66}$$

where

$$C_P^*=\left(\frac{\partial H^*}{\partial T^*}\right)_{P^*};\quad H^*=H/N\epsilon,\qquad \Delta H^*=H^*-\frac{5}{2}T^*,\qquad \beta^*=\frac{1}{v^*}\left(\frac{\partial v^*}{\partial T^*}\right)_{P^*}. \tag{67}$$

These are, in reduced units, the specific heat at constant pressure, the difference in enthalpy between the liquid

[4] Zwanzig, Kirkwood, Stripp, and Oppenheim, J. Chem. Phys. **21**, 1268 (1953).

and an ideal gas, and the coefficient of volume expansion.

The integral in I_1 cannot be expressed in terms of thermodynamic quantities in this way, and therefore must be calculated by direct integration. The radial distribution function which is used in this calculation was evaluated[4] for a fluid whose molecules interact with the Lennard-Jones potential, by solving the Born-Green integral equation in the superposition approximation. Since the $g_0^{(2)}(x)$ obtained in this way does not lead to a satisfactory pressure at the density and temperature of the normal boiling point, an empirical parameter c is introduced, and all integrals are evaluated with $g_0^{(2)}(cx)$ instead of $g_0^{(2)}(x)$. The value of c which leads to the correct pressure at the normal boiling point is[4] $c=1.026$. The integral I_1 was evaluated as a function of c. The details of the calculation of $(\zeta\kappa_K)^*$, I_1, and I_2 are given in an appendix.

The Lennard-Jones parameters have been determined for argon by Michels, Wijker, and Wijker.[5] They are

$$\epsilon=1.653\times10^{-14}\text{ erg},$$

$$a=3.405\times10^{-8}\text{ cm}.$$

In cgs units, the conversion factor from $(\zeta\kappa)^*$ to $\zeta\kappa$ is $k\epsilon/a^3=5.779\times10^{-8}$. The conversion factor from ergs to calories is 4.1844×10^7 ergs per calorie. In reduced units the temperature and volume at the normal boiling point are $T^*=0.7454$ and $v^*=1.223$. The thermodynamic variables needed in the calculation of $(\zeta\kappa_K)^*$ and I_2, and the radial distribution function used to calculate I_1, were obtained for these values of the reduced temperature and volume.

The results of these calculations will now be given. The kinetic contribution to the thermal conductivity is

$$(\zeta\kappa_K)^*=0.35.$$

The contribution I_2 to the thermal conductivity is

$$I_2=10.28.$$

The contribution $I_1(c)$ was calculated for several values of c. This function is only moderately sensitive to c. The most significant values of $I_1(c)$ are

$$I_1(1.000)=50.89,$$

$$I_1(1.026)=73.06.$$

It is clear that the kinetic part of the thermal conductivity of this liquid is negligible, and that the thermodynamically evaluated part of the potential contribution is dominated by the part which must be calculated with an explicit knowledge of the radial distribution function. When the various contributions are added together, one obtains

$$(\zeta\kappa)^*=61.5 \quad (c=1.000),$$

$$(\zeta\kappa)^*=84.7 \quad (c=1.026).$$

The friction constant ζ was evaluated by the linear trajectory method, which will be described in a future article in this series. This calculation was performed for $c=1$ and $c=1.026$. The results are

$$\zeta(1)=3.53\times10^{-10}\text{ g/sec},$$

$$\zeta(1.026)=2.85\times10^{-10}\text{ g/sec}.$$

The thermal conductivity is therefore

$$\kappa(1)=2.4\times10^{-4}\text{ cal/g sec °K},$$

$$\kappa(1.026)=4.1\times10^{-4}\text{ cal/g sec °K}.$$

The thermal conductivity of argon at its normal boiling point was measured by Uhlir.[6] His result is

$$\kappa_{\text{expt}}=2.9\times10^{-4}\text{ cal/g sec °K}.$$

The agreement is quite satisfactory. For $c=1.026$, the difference between theory and experiment is forty percent. For $c=1.000$, the difference is seventeen percent.

APPENDIX

For the calculation of $(\zeta\kappa_K)^*$ and I_2, various thermodynamic properties of argon are required. The values used were obtained from the *International Critical Tables*. Although they may be somewhat inaccurate, the contribution of $(\zeta\kappa_K)^*$ and I_2 to the total thermal conductivity is only about fifteen percent, so that any errors in these values will not lead to a significant error in the final result. The values which were used are

$$C_p=10.1\text{ cal/mole °K},$$

$$\Delta H=-1500\text{ cal/mole},$$

$$\beta=-\frac{1}{v}\left(\frac{\partial v}{\partial T}\right)_p=0.00465\ 1/°\text{K},$$

$$T=89°\text{K},$$

$$v=29.0\text{ cc/mole}.$$

In the calculation of $(\zeta\kappa_K)^*$ and I_2, the thermodynamic quantities were combined in their unreduced form, and then the results were reduced.

In the calculation of I_1, the derivatives of $g_0^{(2)}(x)$ with respect to x and T^* are required. The method of calculation of $g_0^{(2)}(x)$ has been described.[4] The derivative $dg_0^{(2)}(x)/dx$ was evaluated using the differentiated form of Newton's interpolation formula, with the inter-

[5] Michels, Wijker, and Wijker, Physica **15**, 627 (1949).

[6] A. Uhlir, Jr., J. Chem. Phys. **20**, 463 (1952).

val 0.01. The derivative $[\partial \log g_0^{(2)}(x)/\partial T^*]_{P^*}$ was converted to another form

$$\left(\frac{\partial \log g_0^{(2)}(x)}{\partial T^*}\right)_{P^*}=\left(\frac{\partial \log g_0^{(2)}(x)}{\partial T^*}\right)_{v^*}+\left(\frac{\partial \log g_0^{(2)}(x)}{\partial v^*}\right)_{T^*}\left(\frac{\partial v^*}{\partial T^*}\right)_{P^*}, \quad (68)$$

since $g_0^{(2)}(x)$ is available as a function of temperature and volume,

$$\log g_0^{(2)}(x)=\psi_0(x,v^*)+\frac{1}{T^*}\psi_1(x,v^*)+\frac{1}{T^{*2}}\psi_2(x,v^*). \quad (69)$$

The differentiation with respect to temperature was performed with this expression. The derivative of $\log g_0^{(2)}(x)$ with respect to v^* was evaluated using the differentiated form of Lagrange's interpolation formula. The experimental value of $(\partial v^*/\partial T^*)_{P^*}$ was used. When this calculation was performed with the scale factor c, the equation

$$A(c)=\int_0^\infty (x^4\gamma'-x^3\gamma)\frac{\partial g_0^{(2)}(cx)}{\partial x}\times\left(\frac{\partial \log g_0^{(2)}(cx)}{\partial T^*}\right)_{P^*}dx=c^3A(1)-52c^3(c^6-1)\times\int_0^\infty \frac{1}{y^9}\frac{dg_0^{(2)}(y)}{dy}\left(\frac{\partial \log g_0^{(2)}(y)}{\partial T^*}\right)_{P^*,c}dy+O\left(\frac{\partial c}{\partial T^*}\right)+O\left(\frac{\partial c}{\partial v^*}\right) \quad (70)$$

was used. The corrections arising from the dependence of c on T^* and v^* were estimated, using experimental data on the equation of state and the internal energy to evaluate $\partial c/\partial T^*$ and $\partial c/\partial v^*$. It was found that these corrections may be neglected. The integrals were evaluated numerically, using Simpson's rule with an 0.01 interval from $x=0$ to $x=1.12$, Simpson's rule with an 0.02 interval from $x=1.12$ to $x=1.28$, and the trapezoidal rule with an 0.04 interval for $x>1.28$.

THE JOURNAL OF CHEMICAL PHYSICS VOLUME 22, NUMBER 5 MAY, 1954

Isotope Effect in Continuous Ultraviolet Absorption Spectra: Methyl Bromide-d_3 and Chloroform-d

ADON A. GORDUS* AND RICHARD B. BERNSTEIN†
Department of Chemistry, Illinois Institute of Technology, Chicago, Illinois

(Received November 17, 1953)

A comparison of the continuous ultraviolet absorption spectra of CH_3Br and CD_3Br indicated a nearly constant shift of $+280\pm50$ cm^{-1} upon deuterium substitution. In the case of $CHCl_3$ and $CDCl_3$ the shift was less than the uncertainty of ±50 cm^{-1}. These results are interpreted in terms of the Herzberg-Goodeve picture involving the carbon-halogen bond rupture.

The ultraviolet absorption spectra of CCl_4, $CFCl_3$, CH_2Cl_2, CF_2Cl_2, and $CHFCl_2$ are also reported.

INTRODUCTION

CONTINUOUS ultraviolet absorption spectra for various halogen-substituted methanes have been reported by a large number of workers.[1–14] Discussions relevant to the interpretation of these results are found in most of these papers, and others.[15–19] In the case of

* Present address: Department of Chemistry, University of Wisconsin, Madison, Wisconsin.
† Present address: Department of Chemistry, University of Michigan, Ann Arbor, Michigan.

[1] G. Herzberg and G. Scheibe, Trans. Faraday Soc. **25**, 716 (1929); CH_3I, CH_3Br, CH_3Cl.
[2] G. Herzberg and G. Scheibe, Z physik. Chem. **B7**, 390 (1930); CH_3I, CH_3Br, CH_3Cl.
[3] A. K. Dutta and M. N. Saha, Bull. Acad. Sci., United Provinces Agra and Oudh, India **1**, 19 (1931–32); Chem. Abstracts **26**, 5841; CCl_4.
[4] A. Henrici, Z. Physik **77**, 35 (1932); CH_3I, CH_3Br, CH_3Cl; CH_2I_2, CH_2Br_2, CH_2Cl_2; CHI_3, $CHBr_3$, $CHCl_3$; CBr_4, CCl_4.
[5] P. K. Sen-Gupta, Bull. Acad. Sci., United Provinces Agra and Oudh, India, **2**, 115 (1933); Chem. Abstracts **27**, 3368; CH_3Cl.
[6] N. K. Saha, Bull. Acad. Sci., United Provinces Agra and Oudh, India **2**, 233 (1933); Chem. Abstracts **27**, 4733; CCl_4, $CHCl_3$, CH_2Cl_2.
[7] Y. Hukumoto, J. Chem. Phys. **3**, 164 (1935); CH_3I, CH_2I_2; CCl_4, $CHCl_3$, CH_2Cl_2, CH_3Cl.
[8] P. K. Sen-Gupta, J. Univ. Bombay, **5**, Part 2, 22 (1936); Chem. Abstracts **31**, 2928; CH_3I, CH_3Br, CH_3Cl; CH_2I_2, CH_2Br_2, CH_2Cl_2; CBr_4, CCl_4.
[9] Y. P. Parti and R. Samuel, Proc. Phys. Soc. (London) **49**, 568 (1937); CH_3I, CH_3Br, CH_3Cl; CI_4, CBr_4, CCl_4; CHI_3, $CHBr_3$, $CHCl_3$; CH_2I_2, CH_2Br_2, CH_2Cl_2.
[10] P. Fink and C. F. Goodeve, Proc. Roy. Soc. (London) **A163**, 592 (1937); CH_3Br.
[11] D. Porret and C. F. Goodeve, Trans. Faraday Soc. **33**, 690 (1937); CH_3I.
[12] D. Porret and C. F. Goodeve, Proc. Roy. Soc. (London) **A165**, 31 (1938); CH_3I, RI, RBr.
[13] Lacher, Hummel, Bohmfalk, and Park, J. Am. Chem. Soc. **72**, 5486 (1950); CCl_4, $CHCl_3$, CH_2Cl_2; $CFCl_3$, CF_2Cl_2; $CHFCl_2$.
[14] N. Davidson, J. Am. Chem. Soc. **73**, 467 (1951); CH_2Br; CBr_2F_2, $CBrF_3$; CHF_2Br.
[15] O. K. Rice, Phys. Rev. **33**, 748 (1929); **35**, 1551 (1930).
[16] G. Herzberg, Z. Physik **61**, 604 (1930).
[17] Gibson, Rice, and Bayliss, Phys. Rev. **44**, 193 (1933).
[18] E. C. Stueckelberg, Phys. Rev. **42**, 518 (1932).
[19] C. F. Goodeve and A. W. Taylor, Proc. Roy. Soc. (London) **A152**, 221 (1935).

the halogen-substituted methanes, upon absorption of a quantum of incident light and transition to an upper (repulsive) potential curve, rupture of the weakest carbon-halogen bond is thought to occur.

According to theory, the extinction coefficient at a given frequency is proportional to the probability of the transition. The transition probability is given by an expression of the form $K\nu[\int \psi' M\psi'' d\tau]^2$ where ψ' and ψ'' are the eigenfunctions for the upper and lower states, M is the dipole moment, and ν is the frequency. The magnitude of the extinction coefficient thus depends on the extent of overlap of the eigenfunctions. Goodeve and Taylor[19] showed that the extinction coefficient could be written, to a first approximation,‡ as $\epsilon = K'[\psi_{N,0}'']^2$ where $\psi_{N,0}''$ is the nuclear eigenfunction for the ground vibrational-electronic state.

For a diatomic molecule one thus obtains the result that $\log_e \epsilon_m/\epsilon = 2\beta x^2$, where ϵ_m is the extinction coefficient at the absorption maximum. The constant β is $2\pi^2\mu\omega/h$, where μ is the reduced mass and ω is the fundamental vibrational frequency; x is the displacement from equilibrium, $r - r_e''$. Given the value of β and experimental values of ϵ/ϵ_m at various frequencies, one can then determine the slope of the upper potential curve, dU'/dx, as well as its altitude above the ground-state curve at $r = r_e''$, i.e., $U'(r_e'') - U''(r_e'')$.

Goodeve and co-workers[10–12] attempted to extend the applicability of these concepts to the alkyl halides, assuming that they could be considered pseudo-diatomic molecules, $R-X$. Fink and Goodeve[10] made a thorough study of CH_3Br, from which they were able to deduce the upper potential curve with a fair degree of reliability. They used a method of successive approximations, whereby they avoided most of the weaknesses of the simple treatment. The slope of the resulting curve in the neighborhood of r_e'', however, was quite close to that obtained by the original simplified treatment.

The influence of isotopic substitution on the continuous absorption spectrum of HI and HBr has been studied by Bates, Halford, and Anderson.[20] For DI the curve of extinction coefficient *vs* frequency was shifted from that of HI by an amount which changed from about $+1000$ cm^{-1} at 32 000 cm^{-1} to about $+360$ cm^{-1} at 36 000 cm^{-1}, the highest frequency used. Theoretically the curves should be displaced (at the maxima) by the difference in the zero-point energies $+330$ cm^{-1}. For DBr the shift decreased from about $+1400$ cm^{-1} at about 40 000 cm^{-1} to about $+1100$ cm^{-1} at the highest frequencies (*ca* 43 500 cm^{-1}). This shift was almost three times the zero-point difference of 375 cm^{-1}; the authors attributed this to the contraction of the eigenfunction to smaller values of internuclear separation for DBr.

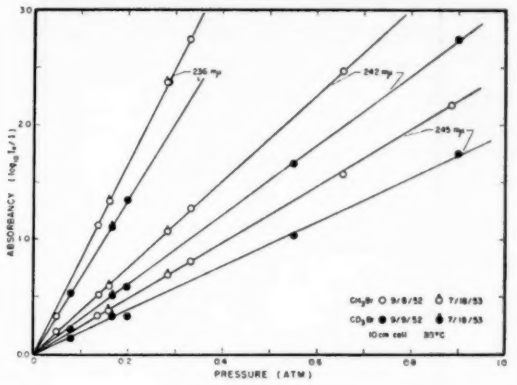

FIG. 1.

It was thought of interest to determine the effect of isotopic substitution on the continuous absorption spectra of some polyatomic molecules. For this purpose the spectra of CH_3Br and CD_3Br were obtained under identical conditions for intercomparison. Similarly, the spectra of $CHCl_3$ and $CDCl_3$ were obtained (over a smaller range). One would anticipate little or no effect upon deuterium substitution according to the generally accepted Herzberg concept, e.g., $CH_3Br + h\nu \rightarrow CH_3 + Br$. However, the mechanism of Parti and Samuel,[9] i.e., $CH_3Br + h\nu \rightarrow CH_2 + H + Br$ would imply a very large isotopic shift. It will be shown that the data support the first mentioned point of view.

In the course of the present work, the absorption spectrum of CCl_4 was also measured over a wide range; limited portions of the spectra of $CFCl_3$, CH_2Cl_2, CF_2Cl_2, and $CHFCl_2$ were also obtained for comparison with existing values in the literature.[13]

EXPERIMENTAL

Ultraviolet absorption spectra were obtained with a Cary Recording spectrophotometer (Model 11PM), and also with a Beckman DU spectrophotometer and a second Cary spectrophotometer as a check in certain cases. Quartz gas cells 10.0 cm in length were used.

Beer's law plots at various wavelengths were obtained. They were accurately linear through the origin after correction for absorption and scattering by the cell windows. A few typical Beer's law plots for CH_3Br and CD_3Br are shown in Fig. 1.

The purification procedure varied for the different compounds studied. All compounds were degassed in vacuum before use. CF_2Cl_2 (Dupont-Kinetic Chemicals) and $CHFCl_2$ (Matheson) were purified by bubbling through concentrated H_2SO_4. $CFCl_3$ (Kinetic Chemicals) was fractionated in a 12-in. Vigreux column. CH_2Cl_2 (Matheson), CCl_4 (technical), and CCl_3H (technical) were purified according to the procedures given by Vogel,[21] followed by fractionation in a 1-meter packed

‡ It is assumed that the slope of the repulsive curve is steep and constant, that the temperature is low enough so that a negligible fraction of the population is above the zero-point vibrational level, and that one is considering only transitions associated with internuclear distances near the equilibrium values.

[20] Bates, Halford, and Anderson, J. Chem. Phys. **3**, 415, 531 (1935).

[21] A. I. Vogel, *Textbook of Practical Organic Chemistry* (Longmans, Green and Company, London, 1948).

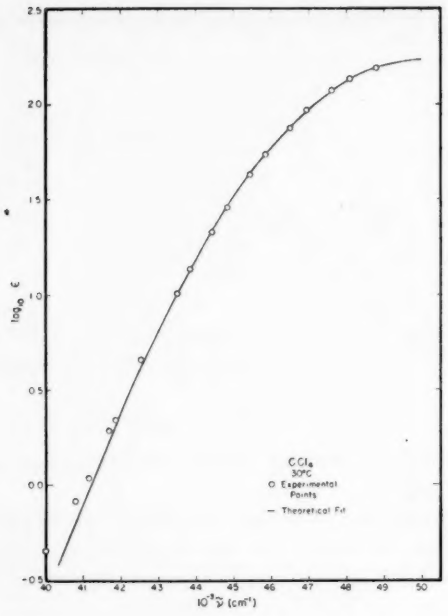

FIG. 2.

column. For purposes of comparison a synthetic sample of $CHCl_3$ was obtained by the reaction of anhydrous chloral with sodium hydroxide. Its spectrum was identical with that of the purified commercial material. $CDCl_3$ was prepared in a similar way, using NaOD under a nitrogen atmosphere. The product was found to contain approximately 1 percent $CHCl_3$ using infrared[22] and mass spectrometric techniques. The CH_3Br and CD_3Br were prepared by the bromination of methanol and methanol-d_3 (Tracerlab, Inc., stated isotopic purity

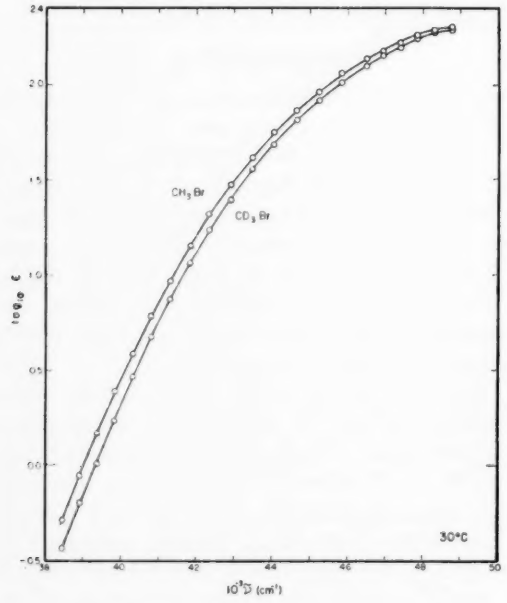

FIG. 3.

[22] Bernstein, Gordus, and Cleveland, J. Chem. Phys. **20**, 1979 (1952).

>95 percent CD_3OH) using KBr and H_2SO_4,[23] and dried by passage through P_2O_5. A yield of 75 percent CD_3Br was obtained.

Table I summarizes the physical properties of the compounds. In addition, infrared and/or mass spectral analyses obtained for most of the compounds indicated high purity, except for the sample of CCl_3F which appeared to contain approximately 0.5 percent CCl_2F_2.

RESULTS

Table II summarizes the data obtained for CCl_4, CH_3Br, and CD_3Br. The extinction coefficient is given as $\epsilon \equiv (1/LC)\log_{10}(I_0/I)$ l mole^{-1} cm^{-1} at 30°C.

Figure 2 shows the absorption spectrum for CCl_4. The solid curve is a theoretical fit to the experimental points, discussed later. Figure 3 compares the spectra of CH_3Br

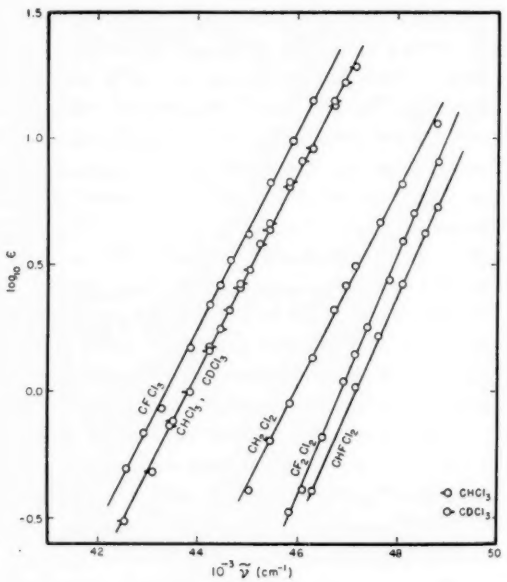

FIG. 4.

and CD_3Br. There appears to be a nearly constant shift of $+280\pm50$ cm^{-1} due to the substitution of the three deuterium atoms for protium in methyl bromide.

Figure 4 shows the spectra over a limited frequency range for a series of halogenated methanes: $CFCl_3$, $CHCl_3$, $CDCl_3$, CH_2Cl_2, CF_2Cl_2, and $CHFCl_2$. The data are summarized in Table III, which lists the frequency at which $\epsilon = 2.49$. This corresponds to a value of $\epsilon = (10/LP)\log_{10}(I_0/I)$ atmos^{-1} cm^{-1} $= 1.00$, which makes possible a direct comparison with the tabulated data of Lacher *et al.*[13] for most of these compounds. It is of interest to note that the spectra of $CHCl_3$ and $CDCl_3$ are virtually indistinguishable within the precision of the measurements.

[23] H. J. Lucas and D. Pressman, *Principles and Practice in Organic Chemistry* (John Wiley and Sons, Inc., New York, 1949), pp. 177–179.

DISCUSSION OF RESULTS

The present results for CH_3Br appear to be in fair agreement with previously published data. Fink and Goodeve[10] and Davidson[14] report values of ϵ_m of 182 and >175, respectively, compared to the present value of 200. The entire absorption curve agrees with that of Fink and Goodeve within the mutual experimental errors, but appears to be slightly higher than that of Davidson by amounts ranging from 0 to 15 percent in ϵ. Over most of the curve (from 38 500 to 46 500 cm^{-1}), however, this amounts to a frequency shift of no more than -200 cm^{-1} relative to the curve of reference 14.

TABLE I. Physical properties of compounds studied.

Compound[a]	n_D[b]		Vapor pressure[b] (cm Hg)		Molecular weight[c]
$CFCl_3$	1.3838	(17)	30.78	(0.6)	136.3
	[1.3865][d]	(18.5)	[30.73][e]	(0.6)	[137.3]
CH_2Cl_2	1.4251	(18)	...		...
	[1.4237]	(18)			
$CHCl_3$	1.4465	(18)	...		...
	[1.4450][f]	(20)			
	[1.4464][g]	(18)			
$CHCl_3$ (*s*)	1.4463	(18)	...		117.6
					[119.4]
$CDCl_3$ (*s*)	1.4462	(18)	...		...
	[1.4451][f]	(20)			
CCl_4	1.4613	(18)	...		...
	[1.4607]	(20)			
CH_3Br (*s*)	...		66.40	(0.0)	95.2
			[66.20][h]	(0.0)	[95.0]
CD_3Br (*s*)	...		68.50	(0.0)	96.5
			[68.34][i]	(0.0)	[97.9]

[a] (*s*) indicates synthesized compound.
[b] Brackets indicate literature values; parentheses indicate temperature °C.
[c] Vapor density method.
[d] S. Swarts, Bull. acad. roy. Belg. **3**, 24 (1893).
[e] A. F. Benning and R. C. McHarness, Ind. Eng. Chem. **32**, 497 (1940).
[f] M. Earing and J. B. Cloke, J. Am. Chem. Soc. **73**, 769 (1951).
[g] *International Critical Tables*, Vol. VII, p. 34.
[h] C. J. Egan and J. D. Kemp, J. Am. Chem. Soc. **60**, 2097 (1938).
[i] J. Beersmans and J. C. Jungers, Bull. soc. chim. Belges **56**, 238 (1947).

Since no information on the purity of the CH_3Br is given in reference 14, it is difficult to decide if the discrepancy is significant.

Since the CD_3Br and CH_3Br were prepared and purified by the same technique, and the spectra of the two samples were obtained under identical conditions, it is believed that the observed isotopic shift of 280 ± 50 cm^{-1} is a real one, independent of instrumental errors, and subject only to the usual uncertainty regarding the possible effect of minute traces of undetected impurities.

In the case of the isotopic molecules $CHCl_3$ and $CDCl_3$, the shift is apparently smaller than the experimental uncertainty of about ±50 cm^{-1}. The most recent data for $CHCl_3$ is that of Lacher *et al.*[13] As seen in Table III, there is somewhat of a discrepancy between the present results and those of reference 13. Because of the fact that the spectrum for the sample of $CHCl_3$ prepared synthetically was identical with that for the purified commercial material, it is felt that the present results are quite reliable. A small amount of an ab-

TABLE II. Extinction coefficients[a] at 30°C.

$\bar{\nu}$ ($cm^{-1}\times10^{-3}$)	CH_3Br		CD_3Br	
38.49	0.516	±0.05[b]	0.366	±0.03[b]
38.95	0.881	0.05	0.637	0.05
39.40	1.47	0.07	1.02	0.07
39.87	2.44	0.10	1.72	0.10
40.35	3.84	0.10	2.94	0.13
40.84	6.07	0.15	4.78	0.25
41.35	9.31	0.2	7.46	0.5
41.87	14.2	0.3	11.6	0.8
42.41	20.7	0.7	17.1	1.0
42.94	29.9	0.8	24.6	1.5
43.51	41.6	1.0	36.1	1.5
44.08	56.3	1.5	48.3	1.7
44.69	73.2	1.5	65.5	2.0
45.28	92.6	2.0	82.9	2.0
45.90	116.	2.0	102.4	2.0
46.55	137.	2.2	126.	2.5
46.99	152.	2.7	142.	2.7
47.43	167.	3.0	157.	3.2
47.89	181.	3.8	174.	3.7
48.35	193.	7.5	188.	4.5
48.82	200.	7.5	193.	5.0

$\bar{\nu}$ ($cm^{-1}\times10^{-3}$)	CCl_4	
40.03	0.451	±0.08[b]
40.84	0.827	0.15
41.19	1.08	0.19
41.70	1.93	0.16
41.87	2.19	0.11
42.58	4.56	0.37
43.51	10.1	0.5
43.89	13.6	0.6
44.49	21.2	0.9
44.89	28.6	1.0
45.49	42.3	2.7
45.90	54.1	3.0
46.55	75.8	4.2
46.99	92.0	5.5
47.66	117.	7.7
48.12	130.	9.2
48.82	153.	13.

[a] Extinction coefficient defined $\epsilon=(1/LC)\log_{10}(I_0/I)$ 1 $mole^{-1}$ cm^{-1}.
[b] Estimated uncertainty from Beer's law plots.

TABLE III. Wave number for $\epsilon=2.49$[a] for various halogenated methanes.

Compound	$\bar{\nu}$ ($cm^{-1}\times10^{-3}$) Present results	Lacher *et al.*[b]
CCl_4	41.9	42.3
$CFCl_3$	44.4	44.5
$CHCl_3$	44.9	43.7
$CDCl_3$	44.9	...
CH_2Cl_2	46.9	46.4
CF_2Cl_2	47.7	47.9
$CHFCl_2$	48.0$_5$	47.1

[a] This corresponds at 30°C to
$\epsilon=(10/LP)\log_{10}(I_0/I)$ $atmos^{-1}$ $cm^{-1}=1.00$
as employed by Lacher *et al.* (See reference 13).
[b] See reference 13.

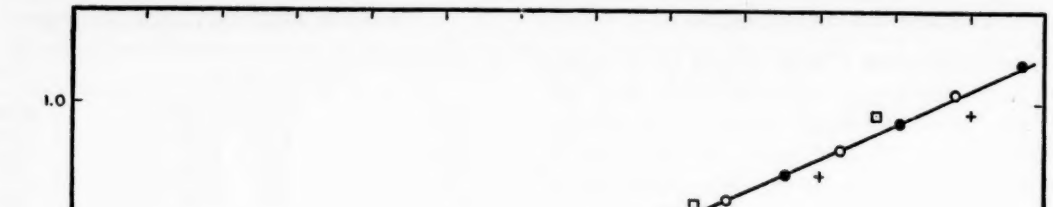

FIG. 5.

sorbing impurity in their sample would have shifted the spectrum toward lower frequencies, the correct direction to explain the discrepancy.

The spectra for most of the other compounds studied agreed fairly well with reference 13 (see Table III). It may be noted, however, that according to the present results the relative positions for $CHCl_3$ and $CFCl_3$ are reversed; similarly for CF_2Cl_2 and $CHFCl_2$.

INTERPRETATION

As shown by Porret and Goodeve[12] for the alkyl bromides and iodides, the influence of substituent groups on the carbon linked to the halogen is of secondary importance. In the neighborhood of the maximum, the spectra of ethyl and *n*-butyl bromide were displaced relative to that of methyl bromide by about +500 to +1000 cm^{-1}; the values of ϵ_m differed by an amount which was considered within experimental error. In view of these results and the present data for the isotopic compounds, it seems that the mechanism of Parti and Samuel[9] is not tenable; one would have expected a much greater isotope effect if the dissociation involved both the carbon-bromine and carbon-hydrogen (-deuterium) bonds. Thus, the general concepts of Herzberg and Goodeve and co-workers are supported by the present results.

Using the simplified expression of Goodeve and Taylor[19] for the relative intensity as a function of the displacement $(r-r_e'')$, and assuming a linear repulsive curve near $r'=r_e''$, [i.e., $U'(r')=U'(r_e'')-k(r'-r_e'')$], one obtains the following result for a diatomic or pseudodiatomic molecule:

$$\log_{10}\epsilon=\log_{10}\epsilon_m-B(\tilde{\nu}_m-\tilde{\nu})^2, \qquad (1)$$

where $B=2\beta h^2c^2/2.303k^2$ cm^2; $\beta=2\pi^2\mu\omega/h$ cm^{-2} as defined previously; $\tilde{\nu}_m=(1/hc)[U'(r_e'')-U''(r_e'')]$ cm^{-1}; and k is the slope of the repulsive curve (erg/cm). Shown in Fig. 5 is a graph of $\log_{10}\epsilon$ *versus* $(\tilde{\nu}_m-\tilde{\nu})^2$ for CH_3Br and CD_3Br, using $\tilde{\nu}_m$ values of 49 000 and 49 280 cm^{-1}, respectively. A single line has been drawn through the present data for *both* isotopic molecules.§

Since $\tilde{\nu}_m$ for CD_3Br was not actually measured, but rather deduced from the shift in frequency along the spectral curve, other values were tried in an attempt to make an alternate linearized plot. With $\tilde{\nu}_m$ assumed to be 49 000 cm^{-1}, the resulting graph was not nearly as linear as that of Fig. 5; thus one is fairly restricted in the choice of a value for $\tilde{\nu}_m$ which satisfies Eq. (1).

Following the procedure of Fink and Goodeve,[10] β was calculated using the reduced mass for the pseudodiatomic molecule CH_3-Br, $\mu=2.10\times10^{-23}$ g; the frequency $\omega_3(a_1)=611$ cm^{-1}. From the slope of Fig. 5, $B=2.19\times10^{-8}$ cm^2, one obtains a value for k, namely $k=1.33\times10^{-3}$ erg/cm or 6.70×10^4 cm^{-1}/A. Fink and Goodeve reported $k=6.25\times10^4$ cm^{-1}/A using their data with similar assumptions. The discrepancy is thus about 7 percent, as apparent from Fig. 5.

For CD_3Br, assuming a reduced mass of 2.44×10^{-23} g and $\omega=577$ cm^{-1},[24] one would predict that the slope B would be some 10 percent greater than that for CH_3Br. On the other hand, assuming the diatomic C−Br reduced mass (unchanged upon deuterium substitution), and the frequencies as above, one calculates that the slope B would be 5 percent smaller for CD_3Br. Since the slopes appear the same within experimental error, the more correct assumption must lie between the above extremes.

§ Included on the graph for comparison are the experimental points of Davidson (reference 14) and points calculated from the information given by Fink and Goodeve (reference 10), assuming $\epsilon_m=182$ and $k=6.25\times10^{-4}$ cm^{-1}/A.

[24] H. D. Noether, J. Chem. Phys. **10**, 664 (1942).

A more serious difficulty arises when one considers that, according to the simple theory, the shift in frequency at the maxima should be given by the difference in zero-point energy, associated presumably with the $\omega_3(a_1)$ C—Br stretching vibration only. This difference is only 17 cm^{-1}, compared to the observed shift of 280 cm^{-1}.

Several possible factors suggest themselves to explain this situation. First, there exists the possibility that the two curves converge at slightly higher frequencies, which were not reached because of instrumental factors. Also, slight errors in the experimental determination of extinction coefficients in the region of the maxima (near 2000A) cause very large apparent displacements in terms of frequency. Second, there may be a real difference in the absolute intensity at the maximum for the two molecules; if ϵ_m of CD_3Br were for some reason 3 percent lower than that of CH_3Br, the frequency shift would show a gradual convergence from about 280 cm^{-1} at 39 000 cm^{-1} to the expected 17 cm^{-1} near 49 000 cm^{-1}. Unfortunately, one anticipates, on the basis of qualitative considerations of the contraction of the ground state vibrational eigenfunction for the deuterated compound, that ϵ_m for CD_3Br would be slightly *higher* rather than *lower* than that for CH_3Br. The third, and possibly the most reasonable, explanation is that the diatomic approximation is inadequate when subjected to so stringent a test, and that one must include contributions from other vibrational degrees of freedom. The total difference in zero-point energy for the two molecules is calculated to be 1976 cm^{-1}; only 14 percent of this is required in order to explain the observed shift.

In the case of $CHCl_3$ and $CDCl_3$, the calculated shift of the maxima, considering only the C—Cl stretching vibrations, is less than the experimental uncertainty of ±50 cm^{-1}, in agreement with the results shown in Fig. 4 and Table III.

The results for CCl_4 may be considered briefly. Here the diatomic approximation is entirely inapplicable, since there is no unique C—Cl bond. Given the total vibrational eigenfunction and the entire repulsive potential energy surface, it might be possible, in principle, to formulate an expression for the extinction coefficient as a function of the frequency. In the absence of this information, a semi-empirical approach was used. It was assumed that only a single (unspecified) normal vibration need be considered, ω_k, and that the appropriate repulsive potential energy curve is the projection of the repulsive potential energy surface on the vertical plane which includes this normal coordinate Q_k. The usual assumption of a steep linear portion of the curve near $Q_k=0$ is made. The total vibrational eigenfunction is factorable when expressed in terms of the normal coordinates[25] so that for the ground state,

$$\psi_0''=\prod_{i=1}^{3N-6}\left(\frac{\alpha_i}{\pi}\right)^{\frac{1}{4}}\exp\left(-\frac{\alpha_i}{2}Q_i^2\right),$$

where $\alpha_i=4\pi^2\omega_i/h$, Q_i is the ith mass-reduced normal coordinate, and ω_i the ith normal vibrational frequency. Only one term, involving Q_k, is of interest; thus we assume $\log_e(\epsilon_m/\epsilon)=\alpha_k Q_k^2$. Using the assumption of the linearity of the upper curve to eliminate Q_k, one obtains an expression analogous to Eq. (1):

$$\log_{10}\epsilon=\log_{10}\epsilon_m-B'(\tilde{\nu}_m-\tilde{\nu})^2, \qquad (1')$$

where B' no longer retains its explicit meaning as in Eq. (1). Thus the absorption spectrum for CCl_4 should have the usual parabolic shape near the maximum.

Since the experimental data did not extend quite to the maximum, a slight extrapolation was needed to obtain $\tilde{\nu}_m$ and ϵ_m. Differentiating Eq. (1'),

$$d\log_{10}\epsilon/d\tilde{\nu}=2B'\tilde{\nu}-2B'\tilde{\nu}_m.$$

Thus, a graph of the slope of the absorption curve *versus* $\tilde{\nu}$ should be linear, with an intercept at $\tilde{\nu}=\tilde{\nu}_m$. From such a linear plot, tentative values for $\tilde{\nu}_m$ and B' were found: 50 000±400 cm^{-1} and $(2.9\pm0.3)\times10^{-8}$ cm^2, respectively. Using this value of $\tilde{\nu}_m$, a graph of $\log_{10}\epsilon$ *vs* $(\tilde{\nu}_m-\tilde{\nu})^2$ was plotted (similar to the procedure for methyl bromide); this is shown in Fig. 6. For comparison, graphs using $\tilde{\nu}_m=49\,600$ and 50 400 cm^{-1} are also shown. The best straight line is obtained for $\tilde{\nu}_m=50\,000$. From the slope one obtains $B'=2.90\times10^{-8}$ cm^2; from the intercept, $\log\epsilon_m=2.23\pm0.02$. The solid line of Fig. 2 was calculated using Eq. (1') with these values for the parameters. The fit is good from ϵ_m down to $1/10\epsilon_m$, below which the deviation is in the direction anticipated on the basis of transitions from levels higher than the ground state (see reference 10).

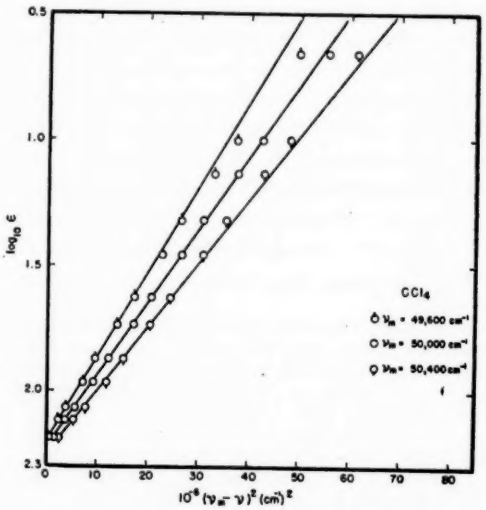

FIG. 6.

ACKNOWLEDGMENTS

This work was supported in part by the U. S. Atomic Energy Commission.

[25] K. S. Pitzer, *Quantum Chemistry* (Prentice-Hall, Inc., New York, 1953), p. 224.

Successive Orientational Transitions in Crystals*

THEODORE J. KRIEGER† AND HUBERT M. JAMES
Purdue University, Lafayette, Indiana

(Received April 17, 1953)

An extended discussion is given of a crystal model showing successive "rotational" or orientational transitions. This model consists of an array of classical rotators with next-neighbor coupling, the potential energy of coupling being

$$E(\theta_{ij}) = AP_1(\cos\theta_{ij}) + BP_2(\cos\theta_{ij}),$$

where θ_{ij} is the angle between the molecular axes of symmetry. It is treated by both the internal field approximation (Bragg-Williams approximation) and Chang's modification of Bethe's method. The internal field approximation is applied in two ways, the first involving use of consistency relations, the second involving calculations of the thermodynamic potentials. The consistency relations are shown to be equivalent to the condition that the free energy be stationary, but not necessarily a minimum, with respect to variation of the orientational distribution of the molecules. Depending on the relative values of A and B, the model shows a single second-order transition, a single first-order transition, two first-order transitions, or a second-order transition followed by a first-order transition as T rises. The treatment by Chang's method is not as complete as that by the internal field method, but gives confidence that the latter method is sufficiently accurate to indicate correctly the general behavior of the model. Transition temperatures are computed by both methods, latent heats and specific heats by the internal field method only. The relatively complex behavior of the model can be understood in general terms. In particular, when two transitions occur, the one at lower temperature marks a change from an ordered state in which molecular axes tend to be all parallel to a preferred direction ("ferromagnetic" case) or alternately parallel and antiparallel ("antiferromagnetic" case) to another ordered state in which parallel and antiparallel orientations are equally probable for each molecule; the second transition is to a state of complete long-range orientational disorder. There are suggestive similarities between the behavior of this model and the observed properties of the hydrogen and deuterium halides.

1. INTRODUCTION

THE specific heats and other properties of a number of molecular crystals show anomalies at low temperatures that are of the sort associated with order-disorder transitions. The complexity of these phenomena is well described in the review article of Eucken.[1] We shall here be concerned primarily with the existence of several successive transitions of this type below the melting point, as is observed, for example, in the hydrogen and deuterium halides.[2]

These transitions are commonly referred to as "rotational transitions," because of the attempts of Pauling[3] and of Fowler[4] to explain them as arising from the onset of free rotation of the molecules as temperature rises, due to the cumulative breakdown of constraints on molecular rotation. Observations on nuclear magnetic resonance[5] have now made it quite clear that in almost all cases the molecules are not freely rotating above the transition temperature. It is now generally agreed that the transitions are a result of changes in the orientational order of the molecules, as was first suggested by Frenkel;[6] hence they are perhaps better called "orientational transitions."

The occurrence of successive orientational transitions has been discussed in terms of special models for special crystals, by Nagamiya[7] in the case of the ammonium halides, and by Tisza[8] and by Powles[9] in the case of the hydrogen halides. These discussions are very helpful in bringing out various factors that may be involved in orientational transitions, but they do not constitute straightforward deductions of the occurrence of multiple transitions in definitely specified models. It is the purpose of this paper to present a simple model of a molecular crystal that does show single or multiple orientational transitions, of first or second order, depending on the constants that characterize the model.

The model to be treated in this paper is a generalization of that considered by Chang,[10] by Kirkwood,[11] and by Oguchi and Takagi.[12] It consists of an array of classical rotators about fixed centers, with next-neighbor interactions that depend only on the relative orientations of the two neighbors. It leaves out of account the effects of quantization of the rotational or oscillational energy of the molecules, the tunnel effect, and the dependence of the orientational coupling of two molecules on their separation, or on the direction of their line of centers. It is thus not suitable for a treatment of isotope effects, or of the interaction between lattice form or vibration and orientational order. The specific heat that one computes by its use, the rota-

* Based in part on a thesis presented by T. J. Krieger in partial fulfillment of the requirements for the degree of Doctor of Philosophy at Purdue University.

† Now at Battelle Memorial Institute, Columbus, Ohio.

[1] A. Eucken, Z. Elektrochem. **45**, 126 (1939).

[2] See, for instance, the recent measurements on HBr and DBr by J. G. Powles, J. phys. et radium **13**, 121 (1952).

[3] L. Pauling, Phys. Rev. **36**, 430 (1930).

[4] R. H. Fowler, Proc. Roy. Soc. (London) **A149**, 1 (1935).

[5] See, for instance, N. L. Alpert, Phys. Rev. **75**, 398 (1949); H. S. Gutowsky and G. E. Pake, J. Chem. Phys. **18**, 162 (1950).

[6] J. Frenkel, Acta Physicochim. U.R.S.S. **3**, 23 (1935).

[7] T. Nagamiya, Proc. Phys.-Math. Soc. Japan **24**, 137 (1942); **25**, 540 (1943).

[8] L. Tisza, Phys. Rev. **72**, 161 (1947); a different, somewhat incomplete suggestion concerning the transitions in HBr is made by Tisza in Chapter I of *Phase Transformatims in Solids* (report on Cornell symposium of National Research Council), (John Wiley and Sons, Inc., New York, 1951).

[9] J. G. Powles, Trans. Faraday Soc. **48**, 430 (1952); see, also, reference 1.

[10] T. S. Chang, Proc. Cambridge Phil. Soc. **33**, 524 (1937).

[11] J. G. Kirkwood, J. Chem. Phys. **8**, 205 (1940).

[12] T. Oguchi and Y. Takagi, J. Phys. Soc. Japan **7**, 145 (1952).

tional specific heat, is, at best, a part of the total specific heat; to it must be added the specific heat of the lattice vibrations. The model is, however, well suited for an investigation of the relation between the form of the orientational coupling of the molecules and the number and type of transitions that may occur.

In all previous work with this model, it has been assumed that the potential energy of the orientational coupling of next neighbors has the form

$$E(\theta_{ij}) = A\cos\theta_{ij} = AP_1(\cos\theta_{ij}), \tag{1.1}$$

where θ_{ij} is the angle between directed axes fixed in molecules i and j. Adjacent molecules will then tend to be parallel or antiparallel, according as A is negative or positive. Kirkwood[11] has treated this model in an approximation equivalent to that of the Bragg-Williams[13] theory of order in alloys. (The same approximation will be used in Part I of the present paper, where it will be called the internal field approximation.) Chang[10] has treated it by a method patterned after that of Bethe,[14] while Oguchi and Takagi[12] have used a method analogous to that devised by Kikuchi[15] for the treatment of alloys. All these methods lead to the same qualitative result: with rising temperature, the model shows a single second-order transition as the long-range order disappears completely. It was supposed by Chang that the qualitative behavior of the model would be independent of the assumed form of $E(\theta_{ij})$. This is, however, contrary to the fact (mentioned by Kirkwood, and easily verified) that a model with $E(\theta_{ij})$ proportional to $\cos^2\theta_{ij}$ gives a transition of the first order, rather than one of the second order. A more complete investigation of the dependence of the properties of the model on the choice of $E(\theta_{ij})$ has hitherto been lacking.

The interaction energy in Eq. (1.1) is usually thought of as representing the interaction of two dipolar molecules, though it has a somewhat simpler form than the actual dipole-dipole interaction potential. It is, however, grossly inappropriate as a representation of the interaction of homonuclear molecules such as H_2 or N_2, in which the direction of the molecular axis has no physically definite sense, and the interaction energy must be unchanged by reversal of the molecular axis, or replacement of θ_{ij} by $\pi-\theta_{ij}$. The simplest potential of this form is proportional to $\cos^2\theta_{ij}$ or to the Legendre polynomial $P_2(\cos\theta_{ij})$, which differs essentially by an additive constant. Even in the case of dipolar molecules one may expect van der Waals forces to give rise to terms of this type in the interaction potential. We have therefore chosen to investigate the effect of assuming

$$E(\theta_{ij}) = AP_1(\cos\theta_{ij}) + BP_2(\cos\theta_{ij}), \tag{1.2}$$

where A and B are arbitrary. The first term, which will be called the P_1 interaction, may be thought of as representing a polar interaction; it weights parallel configurations of the molecules favorably as compared with antiparallel configurations, or unfavorably, depending on the sign of A. The second term, which will be called the P_2 interaction, may be thought of as representing a nonpolar interaction; it weights parallel and antiparallel configurations equally favorably, or unfavorably, compared to perpendicular configurations. The two terms in Eq. (1.2) may be thought of as the first terms in an expansion of $E(\theta_{ij})$ in terms of Legendre polynomials, but there is no reason to expect further terms in such an expansion to be small.

It will be shown that, depending on the relative values of A and B, this model may show a single second-order transition, a single first-order transition, two successive first-order transitions, or a second-order transition followed by a first-order transition, as temperature rises.[16] The most complete discussion, in terms of the internal field approximation, will be found in Part I of this paper; a quantitatively more accurate, but less complete, treatment by a simplified and extended version of Chang's method is given in Part II. Part III will compare the results of these two methods, interpret the results of the theory, and indicate a possible relation to observations on the hydrogen halides.

Attention will here be limited to $A \leqslant 0$, without any real loss in generality. Many lattices can be divided into two equivalent sublattices such that a molecule in one sublattice has all its next neighbors in the other sublattice; this is true, for instance, of square and hexagonal lattices in the plane, and of simple cubic and body-centered cubic lattices in three dimensions. With such a lattice, simultaneous reversal in the sign of A and in axial direction of all molecules on one sublattice leaves E unchanged. Therefore, two models based on such a lattice and differing only in the sign of A will exhibit a one-to-one correspondence between configurations with the same energy, differing only in reversal of the molecules on one sublattice. It follows that at any temperature the two models will have the same average energy, and exhibit the same thermal properties; in particular, their transitions will have identical character and will occur at the same temperature.[17] This invariance of thermal properties to change in sign of A applies to all cases considered in this paper, since our application of Chang's method is limited to this special type of lattice, and the lattice structure is not a significant factor in the internal field approximation. We have chosen to consider the case of A negative (the "ferromagnetic" case), since then all molecules tend to lie parallel, all lattice sites are equivalent, and

[13] W. L. Bragg and E. J. Williams, Proc. Roy. Soc. (London) **A145**, 699 (1934).
[14] H. A. Bethe, Proc. Roy. Soc. (London) **A150**, 552 (1935).
[15] R. Kikuchi, Phys. Rev. **81**, 988 (1951).

[16] A preliminary description of the results has been published earlier: T. J. Krieger and H. M. James, J. Chem. Phys. **21**, 176 (1953).
[17] A similar argument will make it clear why Oguchi and Takagi found no change in the transition temperature for a square lattice when they reversed the sign of the P_1 interaction between neighbors in the same column, but not between neighbors in the same row.

all molecules have the same distribution of orientations. To pass to the case of A positive (the "antiferromagnetic" case), where all lattice sites are not equivalent, one has simply to reverse the orientational distribution for molecules on one sublattice, replacing θ by $\pi-\theta$.

PART I. THE INTERNAL FIELD APPROXIMATION

The "internal field approximation" involves (a) treatment of each molecule as taking on its orientations independently of other molecules, in an effective potential field, or orienting potential $\epsilon(\theta,\phi)$, that represents the interaction of this molecule with its neighbors, and (b) calculation of the orienting potential $\epsilon(\theta,\phi)$ as the average energy of interaction of this molecule with its neighbors, when it has the specified orientation.

Subject to this approximation, the crystal can be treated by two alternative methods: (1) consistency of the description of the molecular orientations in terms of an internal field implies certain necessary conditions on the distribution function for molecular orientations $f(\theta,\phi)$; these conditions limit $f(\theta,\phi)$ to a small number of possible forms. (2) The free energy F of the system can be computed as a functional of $f(\theta,\phi)$; the form of $f(\theta,\phi)$ is then chosen to minimize F.

Both methods will be used here, to illustrate their relation. It will become evident that solutions of the consistency relations extremalize F but do not necessarily make it a minimum. Solutions that make F a minimum have physical interest as representing stable or metastable phases of the system; the solution that makes F an absolute minimum represents the stable phase.

2. THE CONSISTENCY RELATIONS

We shall discuss states of order in the assembly that have axial symmetry about some preferred direction in space. Taking this direction as the polar axis, we shall describe the orientation of the directed axis of the ith molecule by the usual spherical coordinates θ_i, ϕ_i. We shall assume that the interaction of the ith molecule with its neighbors can be represented by an effective potential energy $\epsilon(\theta_i)$, and that the probability of its having its axis directed within a solid angle $d\omega_i$ about the direction (θ_i,ϕ_i) is $F(\cos\theta_i)d\omega_i$; that ϵ and F are independent of ϕ_i follows from the assumption of axial symmetry in the state of order.

We shall assume, further, that the functions ϵ and F have the same form for every molecule. This assumption is appropriate for $A<0$ in our model, since then the coupling forces tend to order all molecules in the same direction, and will bring them into complete parallelism when $T\to 0$. It would not be appropriate to the case of $A>0$, in which the coupling forces tend to orient neighboring molecules in opposite senses, and will make all next neighbors antiparallel as $T\to 0$. It is this assumption that restricts the validity of our detailed treatment to the case of $A<0$; the conclusions can, however, be extended to the case of $A>0$ by the symmetry argument stated in Sec. 1.

Let us fix attention on a particular molecule, with orientation described by (θ_0,ϕ_0); its next neighbors will have orientations described by (θ_i,ϕ_i), $i=1, 2, \cdots z$. Neglecting any correlation in the orientations of molecules 0 and 1, we can compute their average energy of interaction, for fixed value of θ_0, as

$$\bar{E}(\theta_0)=\int F(\cos\theta_1)E(\theta_{01})d\omega_1$$

$$=\int F(\cos\theta_1)[AP_1(\cos\theta_{01})+BP_2(\cos\theta_{01})]d\omega_1. \quad (2.1)$$

Using the addition theorem for Legendre polynomials, and integrating over ϕ, we obtain

$$\bar{E}(\theta_0)=2\pi\left[A\left\{\int_{-1}^{+1}F(x)P_1(x)dx\right\}P_1(\cos\theta_0)\right.$$

$$\left.+B\left\{\int_{-1}^{+1}F(x)P_2(x)dx\right\}P_2(\cos\theta_0)\right]. \quad (2.2)$$

The effective ordering potential energy for molecule 0 is its average interaction energy with its z neighbors:

$$\epsilon(\theta_0)=z\bar{E}(\theta_0)=z[AI_1P_1(\cos\theta_0)+BI_2P_2(\cos\theta_0)] \quad (2.3)$$

where

$$2\pi\int_{-1}^{+1}F(x)P_n(x)dx=I_n, \quad (n=1,2). \quad (2.4)$$

Self-consistency in this treatment of the crystal requires that the distribution of orientations produced by this orienting field be identical with $F(\cos\theta)$, the assumed distribution. Hence

$$F(\cos\theta)=Ce^{-\epsilon(\theta)/kT} \quad (2.5)$$

where C is a normalization constant determined from $\int F(\cos\theta)d\omega=1$. Defining

$$\alpha\equiv\frac{AzI_1}{kT} \quad (2.6)$$

and

$$\beta\equiv\frac{BzI_2}{kT}, \quad (2.7)$$

we have

$$F(\cos\theta)=\frac{e^{-\alpha P_1(\cos\theta)-\beta P_2(\cos\theta)}}{2\pi\int_{-1}^{+1}e^{-\alpha P_1(x)-\beta P_2(x)}dx}. \quad (2.8)$$

Equations (2.4), (2.6), and (2.7) then yield two simultaneous equations for α and β:

$$\frac{kT}{Az}\alpha=\frac{\int_{-1}^{+1}P_1(x)e^{-\alpha P_1(x)-\beta P_2(x)}dx}{\int_{-1}^{+1}e^{-\alpha P_1(x)-\beta P_2(x)}dx}, \tag{2.9}$$

$$\frac{kT}{Bz}\beta=\frac{\int_{-1}^{+1}P_2(x)e^{-\alpha P_1(x)-\beta P_2(x)}dx}{\int_{-1}^{+1}e^{-\alpha P_1(x)-\beta P_2(x)}dx}. \tag{2.10}$$

These will be called the "consistency equations," since they are essential for the internal consistency of the approximations used.

These relations can be made more concise by the introduction of a function $Q(\alpha,\beta)$ and quantities σ and τ defined as follows:

$$Q(\alpha,\beta)\equiv-\ln\left\{\tfrac{1}{2}\int_{-1}^{+1}e^{-\alpha P_1(x)-\beta P_2(x)}dx\right\}, \tag{2.11}$$

$$\sigma\equiv\frac{kT}{Az}, \tag{2.12}$$

$$\tau\equiv\frac{kT}{Bz}. \tag{2.13}$$

If $\partial Q/\partial\alpha$ and $\partial Q/\partial\beta$ are denoted by Q_α' and Q_β', respectively, then Eqs. (2.9) and (2.10) read simply,

$$\sigma\alpha=Q_\alpha'(\alpha,\beta), \tag{2.14}$$

$$\tau\beta=Q_\beta'(\alpha,\beta). \tag{2.15}$$

3. THERMODYNAMIC FUNCTIONS

This problem can also be approached through consideration of the thermodynamic functions. To the internal field approximation, one can assume that the molecules all take on their orientations independently, subject to a probability distribution function $F(\cos\theta)$. The free energy $U-TS$ can be computed as a functional of the distribution function $F(\cos\theta)$; the best, or physically significant, form of F will then be that which makes the free energy an absolute minimum. It will now be shown that the condition that the free energy be stationary (but not necessarily a minimum) leads to the distributions derived in the preceding section.

We first consider a particular family of orientational distribution functions,

$$F(\cos\theta)=Ce^{-\alpha P_1(\cos\theta)-\beta P_2(\cos\theta)}, \tag{3.1}$$

where α and β are to be regarded as arbitrarily adjustable parameters, and C is a normalization constant.

Neglecting orientational correlations, one has for the average interaction energy of a next-neighbor pair

$$\bar{E}_{ij}=\int\int F(\cos\theta_i)F(\cos\theta_j)E(\theta_{ij})d\omega_i d\omega_j. \tag{3.2}$$

On neglect of the internal energy of molecular rotation, which plays no significant role in a discussion of transitions, the internal energy U of our model becomes simply the average potential energy of interaction of the $Nz/2$ pairs of next neighbors:

$$U(\alpha,\beta)=\frac{Nz}{2}\bar{E}_{ij}=\frac{Nz}{2}[A\bar{P}_1^2(\alpha,\beta)+B\bar{P}_2^2(\alpha,\beta)], \tag{3.3}$$

where

$$\bar{P}_n(\alpha,\beta)=\frac{\int_{-1}^{+1}P_n(x)e^{-\alpha P_1(x)-\beta P_2(x)}dx}{\int_{-1}^{+1}e^{-\alpha P_1(x)-\beta P_2(x)}dx}, \quad (n-1,2). \tag{3.4}$$

Again neglecting orientational correlations, one can compute the contribution of molecular orientations to the entropy as

$$\begin{aligned}S&=-Nk\int F(\cos\theta)\ \ln F(\cos\theta)d\omega\\&=Nk\alpha\bar{P}_1(\alpha,\beta)+Nk\beta\bar{P}_2(\alpha,\beta)\\&\quad+Nk\ln\left(2\pi\int_{-1}^{+1}e^{-\alpha P_1(x)-\beta P_2(x)}dx\right).\end{aligned} \tag{3.5}$$

Extremalization of the free energy $U-TS$ with respect to variation of α and β requires that

$$\begin{cases}[NzA\bar{P}_1(\alpha,\beta)-NkT\alpha]\dfrac{\partial\bar{P}_1}{\partial\alpha}\\\qquad+[NzB\bar{P}_2(\alpha,\beta)-NkT\beta]\dfrac{\partial\bar{P}_2}{\partial\alpha}=0\\[NzA\bar{P}_1(\alpha,\beta)-NkT\alpha]\dfrac{\partial\bar{P}_1}{\partial\beta}\\\qquad+[NzB\bar{P}_2(\alpha,\beta)-NkT\beta]\dfrac{\partial\bar{P}_2}{\partial\beta}=0.\end{cases} \tag{3.6}$$

These equations can be regarded as simultaneous equations for the quantities in square brackets. It can be shown (Appendix B) that the determinant of coefficients,

$$\frac{\partial(\bar{P}_1,\bar{P}_2)}{\partial(\alpha,\beta)}=\begin{vmatrix}\dfrac{\partial\bar{P}_1}{\partial\alpha} & \dfrac{\partial\bar{P}_2}{\partial\alpha}\\[2ex]\dfrac{\partial\bar{P}_1}{\partial\beta} & \dfrac{\partial\bar{P}_2}{\partial\beta}\end{vmatrix}, \tag{3.7}$$

does not vanish for any values of α and β. It follows that the quantities in square brackets must vanish—which means that the consistency relations, Eqs. (2.9) and (2.10), must be satisfied.

One can treat similarly the more general distribution function

$$F(\cos\theta)=C\exp[-\sum_{i=1}^{n}\alpha_i P_i(\cos\theta)]. \tag{3.8}$$

Extremalization of the free energy is then found to require that $\alpha_j=0$, for $j>2$, while α_1 and α_2 must satisfy the conditions previously derived for α and β. It thus follows that the only distribution functions $F(\cos\theta)$ that make the free energy stationary have the form given in Eq. (3.1), with α and β satisfying the consistency relations.

4. APPLICATION OF (U,T) DIAGRAMS

For a given σ and τ—that is, for a given system at given T—Eqs. (2.14) and (2.15) can, in principle, be solved for α and β. In general, the solutions for α and β will not be unique. The solution that makes $F(\alpha,\beta)$ an absolute minimum corresponds to the stable state of order in the system.[18] Other solutions that make F a minimum with respect to small variations of α and β correspond to metastable states of order, analogous, for example, to supercooled liquids. Still other solutions, corresponding to local maxima in F or merely stationary values, are without physical significance. It will, however, be convenient to think of each solution of the consistency equations as corresponding to a "phase," deferring investigation of the nature of the extrema of F that are not immediately important to the argument.

An alternative method for discussing the significance of solutions of the consistency relations involves consideration of the internal energy as a function of T. This is particularly convenient in the case of the approximation considered in Part II of this paper. For the sake of uniformity we shall employ this method even in the present discussion.

We consider the solution $[\alpha_i(T), \beta_i(T)]$ of the consistency relations that corresponds to a particular "phase" i, as a function of temperature. Then $F[\alpha_i(T), \beta_i(T), T]$ and $U[\alpha_i(T), \beta_i(T), T]$ represent the free energy and internal energy of this phase, in the internal field approximation. It is easily verified that, since

$$\frac{\partial F(\alpha,\beta,T)}{\partial\alpha}=\frac{\partial F(\alpha,\beta,T)}{\partial\beta}=0 \tag{4.1}$$

when $\alpha=\alpha_i(T)$, $\beta=\beta_i(T)$, the approximate F and U satisfy the thermodynamic relation

$$\frac{d\{F[\alpha_i(T),\beta_i(T),T]/T\}}{d(1/T)}=U[\alpha_i(T),\beta_i(T),T]. \tag{4.2}$$

More concisely, one has the integrated form

$$\frac{F_i(T_2)}{T_2}-\frac{F_i(T_1)}{T_1}=\int_{1/T_1}^{1/T_2}U_i(T)d(1/T). \tag{4.3}$$

Consider now two solutions, say $[\alpha_1(T), \beta_1(T)]$ and $[\alpha_2(T), \beta_2(T)]$, that become identical at a particular temperature T_1, but are distinct either above or below this temperature. Since F and U are determined by the values of α, β, and T, one will have $F_1(T_1)=F_2(T_1)$, $U_1(T_1)=U_2(T_1)$. It follows from Eq. (4.3) that

$$\frac{1}{T_2}[F_1(T_2)-F_2(T_2)]=\int_{1/T_1}^{1/T_2}[U_1(T)-U_2(T)]d(1/T). \tag{4.4}$$

Let U_1 and U_2 be plotted as functions of $1/T$ (see, for instance, Fig. 1). The integral on the right can be interpreted as the total area enclosed by a path starting at the point $[U_2(T_2), 1/T_2]$, traversing the curve $U_2(T)$ to its point of intersection with $U_1(T)$, then following the latter curve to the point $[U_1(T_2), 1/T_2]$, and finally returning by a vertical path to the starting point; areas are to be taken with positive or negative sign according as they are circumscribed clockwise or counterclockwise, respectively. Thus one can easily determine, by in-

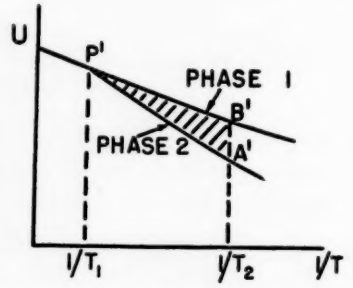

FIG. 1. $(U,1/T)$ diagram for second-order phase change.

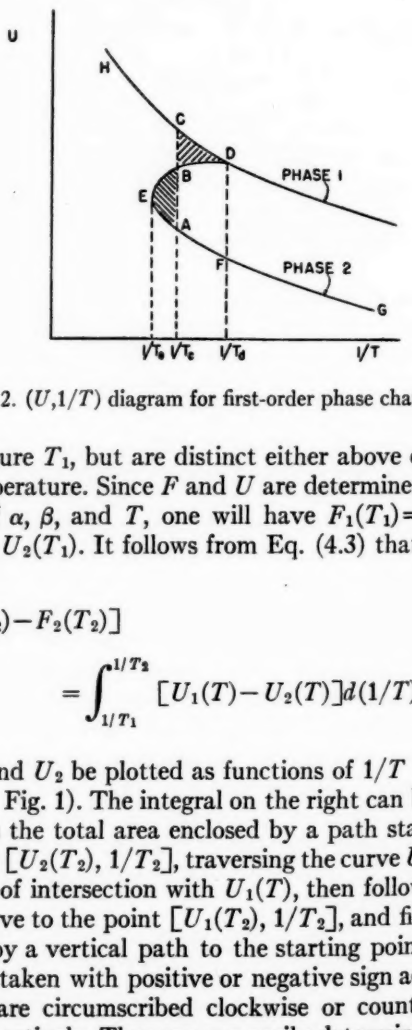

FIG. 2. $(U,1/T)$ diagram for first-order phase change.

[18] It is easily seen that $F(\alpha,\beta)$ has a lower bound; it then follows from the continuity of F and its derivatives that F attains its lowest value when (α,β) is a solution of the consistency relations.

spection of a $(U, 1/T)$ plot, which of several solutions is associated with the lower free energy.

Figure 1 represents a situation in which the consistency relation has two solutions: solution 1, changing smoothly with T for all temperatures, and solution 2, existing only for $T<T_1$ and becoming identical with solution 1 at $T=T_1$. Inspection of Fig. 1, and use of Eq. (4.4), make it clear that, while phase 1 is stable for $T>T_1$, phase 2 is stable for $T<T_1$. The plot of U against $1/T$ for the system in equilibrium consists of segments from the curves for phase 1 and phase 2, and shows a discontinuity in slope at $T=T_1$. This diagram thus represents a situation in which there is a second-order transition at $T=T_1$—a discontinuity in the specific heat, with no latent heat.

A second example is given in Fig. 2. Here the consistency conditions have one solution for $1/T<1/T_e$, and two solutions for $1/T>1/T_d$. For intermediate T there are three solutions, two of which become identical at $1/T_d$, and two of which become identical at $1/T_e$; in the latter case the two plots of U against $1/T$ join at E to form a smooth curve with vertical tangent. For $T>T_e$, the system will exist in phase 1; for $T<T_d$, phase 2 is stable. For any intermediate temperature, the rules given above show that the phase represented by point B on arc ED is not physically significant, having a free energy larger than that of phase 1 (point C) or phase 2 (point A). If the area AEB is greater than the area BCD, phase 2 has lower free energy than phase 1, and is stable; if BCD is greater than AEB, phase 1 is stable. Let T_c be so chosen that the areas AEB and BCD are equal, as shown in Fig. 2; then T_c is the temperature at which phases 1 and 2 have the same free energy, and can coexist. A plot of U against $1/T$ for the stable phase of the system will consist of the segments HC and AG of Fig. 2, with a discontinuity at $T=T_c$. It is evident that this figure represents a system with a first-order phase change at $T=T_c$, with latent heat $U_1(T_c)-U_2(T_c)$.

Cases more complicated than these arise in the present problem, as will be noted later. In presenting the results, plots of U against T (instead of $1/T$) will be given, since they permit easier representation of the situation as $T\to 0$. On these plots, positive areas are traversed counterclockwise, negative areas clockwise. It must also be remembered that differences in F/T for two phases are quantitatively represented by areas only in plots of U against $1/T$.

5. SOLUTION OF THE CONSISTENCY RELATIONS

The mathematical problem to be solved is then the following: For a given model, given A, B, and z, at given T, the parameters σ and τ [Eqs. (2.12) and (2.13)] are fixed. One needs to determine the corresponding values of α and β by solution of the consistency relations, Eqs. (2.14) and (2.15), and, using these values, to compute the internal energy U. This last

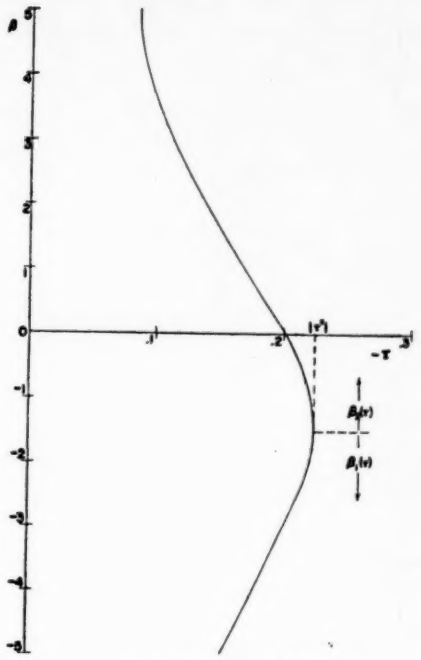

FIG. 3. $\beta_1(\tau)$ and $\beta_2(\tau)$.

calculation is conveniently made by use of relations obtained on combining Eqs. (2.6), (2.7), and (3.3):

$$U=\frac{NzB}{2}\left[\left(\frac{B}{A}\right)\alpha^2+\beta^2\right]\tau^2 \quad (A,B\neq 0), \tag{5.1}$$

$$U=\frac{NzB}{2}\tau^2\beta^2 \quad (A=0), \tag{5.2}$$

$$U=\frac{NzA}{2}\sigma^2\alpha^2 \quad (B=0). \tag{5.3}$$

Disordered solution.—From the fact that $Q_\alpha'(0,0)=Q_\beta'(0,0)=0$ (see Eq. A.11, Appendix A) it follows that $\alpha=\beta=0$ is a solution of the problem for all values of σ and τ. This solution corresponds to $F(\cos\theta)=\text{const}$, which describes a random distribution of orientations of the molecules. The corresponding phase will therefore be called the "disordered" phase. It exists at all temperatures but is stable only above the highest transition temperature, as will be seen later.

Even solutions.—Another interesting special case of solutions has $\alpha=0$, $\beta\neq 0$. If $\alpha=0$, one of the consistency relations is automatically satisfied. The other becomes

$$\tau\beta=Q_\beta'(0,\beta). \tag{5.4}$$

A numerical evaluation of $Q_\beta'(0,\beta)$, by methods indicated in Appendix A, shows that nonzero solutions of Eq. (5.4) for β exist only when $\tau^*\leqq\tau<0$, where

$$\tau^*\cong -0.2228. \tag{5.5}$$

In this range there are two solutions for β, which we shall call $\beta_1(\tau)$ and $\beta_2(\tau)$. As τ decreases from 0 to τ^*,

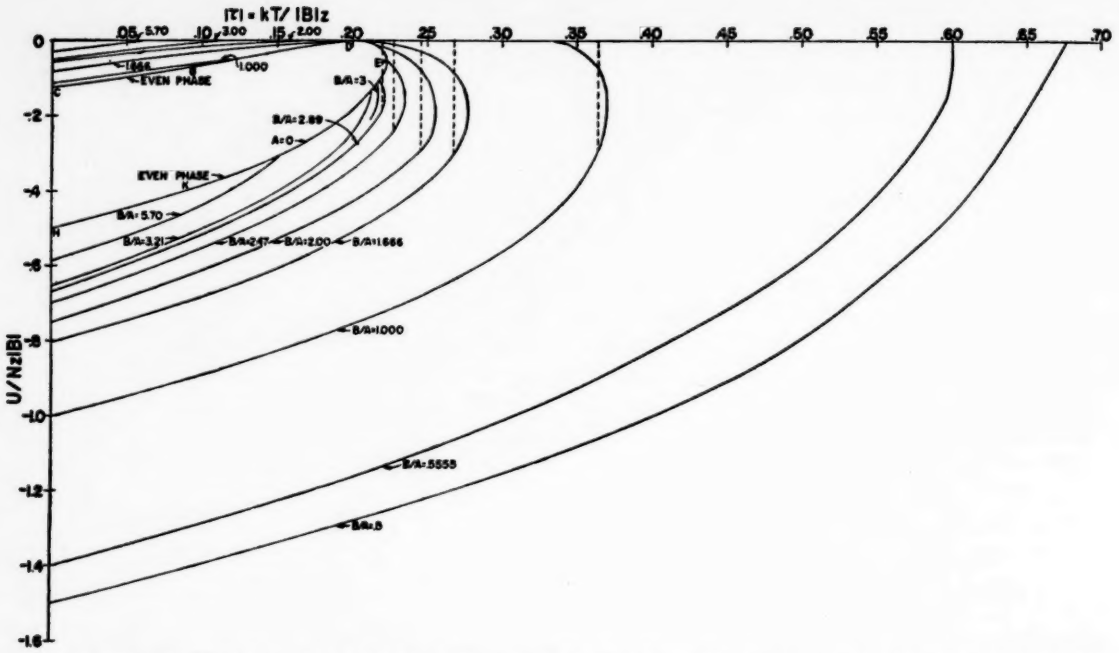

FIG. 4. Plots of $U/Nz|B|$ against $kT/|B|z$, for constant B/A and $B<0$. The horizontal axis gives U for the disordered phase. The curve labelled $A=0$ and "even phase" gives the energy of the even phase for all B/A. The other curves apply to the "mixed phase."

$\beta_1(\tau)$ and $\beta_2(\tau)$ approach each other and become identical, as is illustrated in Fig. 3. We have then the result: if $\tau^* \leqslant \tau < 0$,

$$\begin{cases} \alpha = 0 \\ \beta = \beta_1(\tau) \end{cases} \quad \text{and} \quad \begin{cases} \alpha = 0 \\ \beta = \beta_2(\tau) \end{cases}$$

are solutions of Eqs. (2.14) and (2.15). It will be observed that these solutions are independent of the value of σ or of the ratio B/A. We shall refer to them as the "even" solutions, since for them the distribution function $F(\cos\theta)$ is an even function of $\cos\theta$.

Mixed solutions.—In discussing other solutions of the problem (here called "mixed"), it is useful to note that if (α,β) is a solution of the consistency relations for given σ and τ, then so is $(-\alpha,\beta)$ a solution. It is therefore sufficient to consider solutions with $\alpha \geqslant 0$. Solutions differing in the sign of α describe the same physical situation, except for reversal in the direction of the symmetry axis of the distribution.

Graphical methods were employed in finding the mixed solutions of the consistency relations. The quantities σ and τ were first evaluated numerically as functions of α and β, using formulas given in Appendix A. Contours of constant $\sigma/\tau = B/A$ and constant τ in the (α,β) plane were next constructed; the point (or points) of intersection of a σ/τ contour and a τ contour then determined the solutions (α,β) corresponding to the given σ and τ.

6. REPRESENTATION OF PHASES ON (U,T) DIAGRAM

Figure 4 shows the (U,T) curves found by these methods for $B<0$. For the disordered solution $\alpha=\beta=0$ the (U,T) curve coincides with the T axis for all A and B, as is shown by Eq. (5.1). This equation shows also that for the even solution ($\alpha=0$, β independent of B/A), $U/Nz|B|$ is always the same function of $|\tau| = kT/|B|z$, whatever the value of B/A. The corresponding curve in Fig. 4 is labeled both $A=0$ and "even phase." In addition, Fig. 4 shows (U,T) relations for the mixed phase for several values of B/A.

It is worth while to discuss analytically for all B the form of the mixed-phase curves near the point where they branch from the $|\tau|$ axis or disordered-phase curve. At the branching point, $\alpha=\beta=0$; near this point both parameters will be small. Then, by Eq. (A.11), Appendix A,

$$\sigma = \frac{Q_\alpha'}{\alpha} = -\frac{1}{3} + \frac{2}{15}\beta + \frac{1}{45}\alpha^2 - \frac{3}{280}\beta^2 + \cdots, \tag{6.1}$$

$$\tau = \frac{Q_\beta'}{\beta} = -\frac{1}{5} + \frac{1}{35}\beta + \frac{1}{15}\frac{\alpha^2}{\beta} - \frac{3}{280}\alpha^2 + \frac{1}{175}\beta^2 + \cdots. \tag{6.2}$$

Along a contour of constant B/A one has

$$\frac{B}{A} = \frac{\sigma}{\tau} = \frac{-\frac{1}{3} + \frac{2}{15}\beta + \cdots}{-\frac{1}{5} + \frac{1}{15}\frac{\alpha^2}{\beta} + \frac{1}{35}\beta + \cdots}. \tag{6.3}$$

As one approaches the branching point, all terms in this expression except the first in the numerator and the first two in the denominator must vanish. Thus one must

have

$$\alpha^2/\beta \cong 3-5A/B, \tag{6.4}$$

for small β. Equation (6.1) then yields

$$\sigma=-\frac{1}{3}+\left(\frac{1}{5}-\frac{1}{9}\frac{A}{B}\right)\beta+O(\beta^{\frac{3}{2}}), \tag{6.5}$$

whence

$$\tau=\frac{A}{B}\sigma=-\frac{1}{3}\frac{A}{B}+\left[\frac{1}{5}\frac{A}{B}-\frac{1}{9}\left(\frac{A}{B}\right)^2\right]\beta+O(\beta^{\frac{3}{2}}). \tag{6.6}$$

Solving for β, one finds

$$\beta \cong 45\left(\frac{B}{A}\right)^2\left[9\frac{B}{A}-5\right]^{-1}\left(\tau+\frac{1}{3}\frac{A}{B}\right), \tag{6.7}$$

$$\alpha^2 \cong 45\left(\frac{B}{A}\right)\cdot\frac{3B/A-5}{9B/A-5}\cdot\left(\tau+\frac{1}{3}\frac{A}{B}\right), \tag{6.8}$$

and, by Eq. (5.1),

$$\frac{U}{NzB} \cong \frac{45}{2}\left(\frac{B}{A}\right)^2\frac{3B/A-5}{9B/A-5}\cdot\tau^2(\tau+A/3B), \tag{6.9}$$

all with neglect of terms of relative magnitude $\beta^{\frac{3}{2}}$.

The branching point is given by

$$\tau_b=-A/3B. \tag{6.10}$$

The slope of the mixed-phase curve in Fig. 4, at the branching point, is

$$\frac{d}{d|\tau|}\left(\frac{U}{Nz|B|}\right)\Bigg|_{\tau_b}=-\frac{5}{2}\frac{3B/A-5}{9B/A-5}. \tag{6.11}$$

It is negative if $5/9<B/A<5/3$, becoming 0 when $B/A=5/3$ and infinite when $B/A=5/9$; in all other cases it is positive.

7. DEPENDENCE OF THE TRANSITIONS ON B/A

In discussing the transitions that occur for $B<0$, $B/A>0$, it is convenient to consider separately five ranges of B/A, each illustrated by a curve in Fig. 4.

Range I: $0<B/A<5/9$

In this range the mixed-phase curve has a single branch, which lies below the even-phase curve everywhere and intersects the disordered-phase curve with positive slope at τ_b. The even-phase solution is never significant, and the situation is essentially like that illustrated in Fig. 1. At low T the mixed phase is stable. As T rises the system undergoes a single second-order transition to the disordered phase at a Curie temperature T_c corresponding to the value of τ_b; by Eqs. (2.13) and (6.10), one has, since $A \leqslant 0$,

$$T_c=|A|z/3k. \tag{7.1}$$

It is noteworthy that this Curie temperature is independent of the value of B. Above T_c, $U\equiv 0$ and the potential energy of orientational coupling makes no contribution to the specific heat; below T_c it does contribute to the specific heat an amount, per molecule,

$$c=\frac{1}{N}\frac{dU}{dT}=k\frac{d}{d|\tau|}\left(\frac{U}{Nz|B|}\right). \tag{7.2}$$

From Eq. (6.11) it follows that at the Curie temperature there will be a discontinuity in the specific heat per mole given by

$$\Delta C=-\frac{5}{2}R\cdot\frac{3B/A-5}{9B/A-5}, \tag{7.3}$$

which becomes infinite as B/A approaches 5/9, the upper limit of range I.

Range II: $5/9<B/A<5/3$

The form of the mixed-phase curves in Range II is illustrated in Fig. 4 for the case $B/A=1$. The mixed-phase curve falls into two isolated parts. One part lies above the even-phase curve, and is rather inconspicuous in Fig. 4; by the argument of Sec. 4, the corresponding phase has higher F than the even phase, and is never significant. The other part of the mixed-phase curve lies below the even-phase curve in Fig. 4, and represents a phase more stable than the even phase. This mixed-phase curve and the disordered-phase curve together present a situation essentially like that illustrated in Fig. 2, except for use of an abscissa proportional to T rather than to $1/T$. At low T the mixed phase is stable; as T rises the system undergoes a single first-order transition to the disordered phase at a temperature that can be determined by the rule of equal areas on a $(U,1/T)$ plot, and which obviously satisfies the inequality

$$T_c>z|B\tau_b|/k=|A|z/3k. \tag{7.4}$$

The latent heat of the transition corresponds to the length of the dashed line in Fig. 4, which connects the physically significant segment of the mixed-phase curve with the physically significant segment of the disordered-phase curve.

As B/A reaches the value 5/3 (the upper limit of Range II) the lower part of the mixed-phase curve becomes tangent to the even-phase curve at $|\tau|=0.2$. For all higher B/A, this part of the mixed-phase curve terminates where it meets the even-phase curve. The upper part of the mixed-phase curve and the arc DGC of the even-phase curve correspond to high values of F and are never significant. The remaining parts of the (U,T) curve for each $B/A>5/3$—the disordered-phase curve, the arc $DEKH$ of the even-phase curve, and the lower mixed-phase curve—are related like the curves marked disordered, even, and mixed, respectively, in Fig. 5. Reference will be made to this figure for the further qualitative discussion.

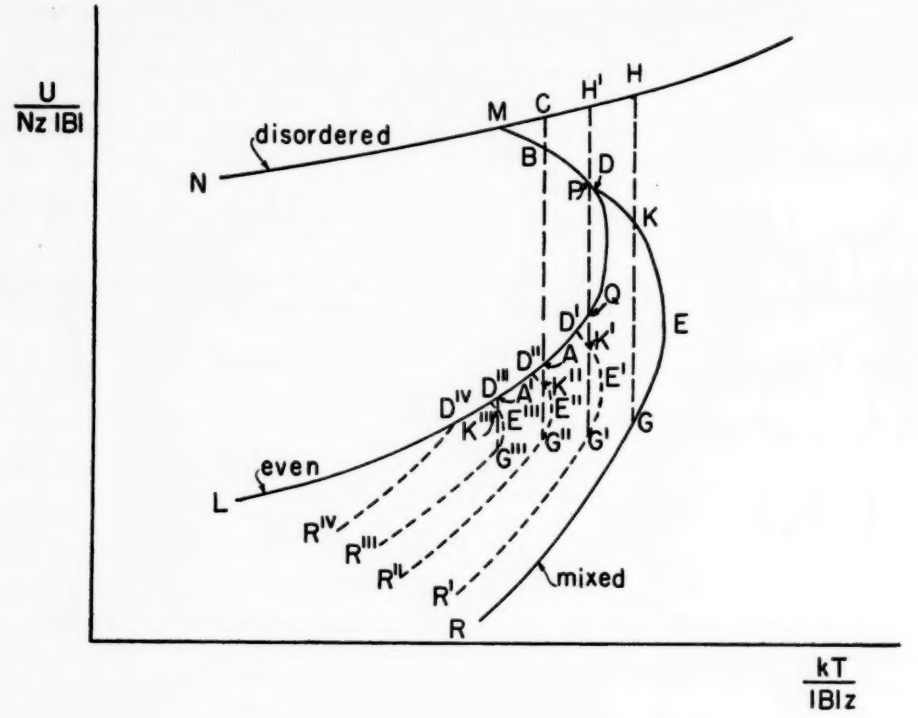

FIG. 5. Illustrative sketches of the dependence of $U/Nz|B|$ on $kT/|B|z$ for several B/A. These curves illustrate the variety of transitions that may occur, and the definitions of the ranges of B/A, as discussed in the text.

Range III: $5/3 < B/A < 2.89$

In this range, as in Range II, the system undergoes a single first-order transition from the mixed phase to the disordered phase. Typical forms for the mixed-phase curves in this range are indicated by curves $DKEGR$ and $D'K'E'G'R'$ in Fig. 5. The transition temperatures, indicated by vertical dashed lines, are determined by the rule of equal areas, in the $(U,1/T)$ plot. In the first case, equality of the areas *corresponding to* (not identical with) the areas $HMDK$ and KGE is required. In the second case, equality is required for the sum of areas in the $(U,1/T)$ plot corresponding to areas $H'MP$ and $QD'K'$ and the sum of areas corresponding to PQD and $K'G'E'$. In this latter case, there are five points on the line $H'G'$ corresponding to solutions of the consistency relations: H', P, Q, K', G'. It is easily seen, by the methods of Section 4, that P has a higher free energy than either H' or Q, and that K' has a higher free energy than either Q or G'. The construction specified for the line $H'G'$ assures that H' and G' correspond to the same free energy. The free energy of Q differs from that of H' by the area corresponding to $H'MP$ minus the area corresponding to PQD. Range III is so defined that this difference is always positive. In consequence, in this range, as the temperature rises the free energy of the mixed phase rises until it is equal to that of the disordered phase, and a first-order transition directly to the disordered phase takes place; the even phase has no significance, except possibly as a metastable state of order, because its free energy is always higher than that of one of the other two phases. The (U,T) curve for the stable phase is made up of the mixed-phase curve to the left of G', and the disordered-phase curve to the right of H'.

The upper limit of Range III, $B/A=2.89$, corresponds to the mixed-phase curve $R''D''$ in Fig. 5. It is determined by the condition that the area in the $(U,1/T)$ plot corresponding to CMB be equal to that corresponding to BAP, or that the free energies corresponding to points C, A, and G'' all be equal. For $B/A=2.89$, three phases or states of order can coexist at the transition temperature: mixed, even, and disordered. This triple point is the only one possessed by the present model. Detailed calculation shows that it occurs at a temperature T_3 given by

$$|\tau_3| = kT_3/|B|z = 0.2202. \tag{7.5}$$

Range IV: $2.89 < B/A < 3.21$

In this range the mixed-phase curve $R'''D'''$ in Fig. 5 meets the even-phase curve with negative slope, to the left of D''. The vertical line $A'G'''$ is determined by the condition that the area in the $(U,1/T)$ plot corresponding to $A'D'''K'''$ be equal to that corresponding to $K'''G'''E'''$, or that A' and G''' correspond to solutions of the consistency equations with the same free energy.

In this range the mixed phase is again the stable one at low T. As T rises to the value corresponding to point G''', the free energies of the mixed and even phases become equal, and a first-order transition to the even phase takes place, with latent heat corresponding to the length of $A'G'''$. As T rises further, the mixed phase is stable until the temperature corresponding to point A [that is, T_3 of Eq. (7.5)] is reached. Here the

free energy of the even phase becomes equal to that of the disordered phase, and a first-order transition to the disordered phase takes place, with latent heat corresponding to the length of CA. At all higher T the disordered phase is stable. The (U,T) curve of the stable phase is made up of the arcs $R'''G'''$, $A'A$, and the disordered-phase curve to the right of C.

In this range, if B/A is increased by decreasing $|A|$, the mixed-phase curve will meet the even-phase curve more nearly vertically; the low-T first-order transition will occur at lower T, and with smaller latent heat. The other first-order transition will, however, take place at temperature T_3, as before, and with the same latent heat. The upper limit of Range IV, $B/A=3.21$, is set by intersection of the mixed- and even-phase curves where the mixed-phase curve has a vertical tangent—that is, by the vanishing of the latent heat of the low-T transition.

Range V: $3.21 < B/A < \infty$

In this range the mixed-phase curve $R^{iv}D^{iv}$ meets the even-phase curve with positive slope. At low T the mixed phase is stable. As T rises to the value corresponding to D^{iv}, a second-order transition to the even phase takes place. Thereafter the even phase is stable until the temperature corresponding to point A (T_3 again) is reached, where a first-order transition to the disordered phase takes place.

$A=0$, $B/A=\infty$

Range V is characterized by the occurrence of two transitions: a second-order transition at a temperature determined by A and B, and a first-order transition at a higher temperature determined by B only. As $A\to 0$ the second-order transition temperature goes to zero, and the even phase is stable to arbitrarily low T.

For $A=0$, pure P_2 interaction of the molecules, the mixed-phase solution does not appear at all. The even phase is stable below the temperature T_3, where it goes over into the disordered phase in a single first-order transition.

Summary, $B<0$

It follows from the representation of the even and disordered phases by unique curves in the $[(U/Nz|B|), (kT/|B|z)]$ plane that the properties of these phases, except for their stability, are independent of the value of A. Thus the specific heat of the even phase, if it is stable, is independent of A; so is the temperature and latent heat of the transition between these two phases, if it occurs.

Quantitative results of our calculations for $B<0$ are summarized in three figures. Figure 6 gives the specific heat of the even phase, for $T<T_3$; the specific heat of the disordered phase, in the approximation considered here, is zero. Figure 7 summarizes the transition temperatures; note also Eq. (7.1) for Range I. Finally, Fig. 8 gives the latent heats of the first-order transitions, as they depend on B and B/A.

$B>0$, $B/A<0$

When B is positive, τ is positive, and no even solution of the consistency equation exists. For each B/A there is one mixed-phase curve in the (U,T) plane, which reaches the disordered phase curve with positive slope; two examples are shown in Fig. 9. Thus for each B/A there is a single second-order transition from the mixed phase, stable at low T, to the disordered phase. The analytic discussion of the mixed phase given in Sec. 6 and the first part of the present Section (Range I) applies also for $B>0$. Thus the transition temperature

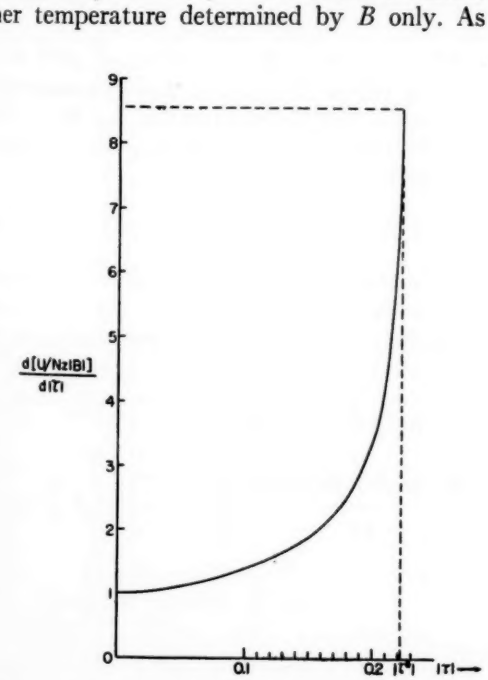

FIG. 6. Specific heat of even phase. Internal field approximation.

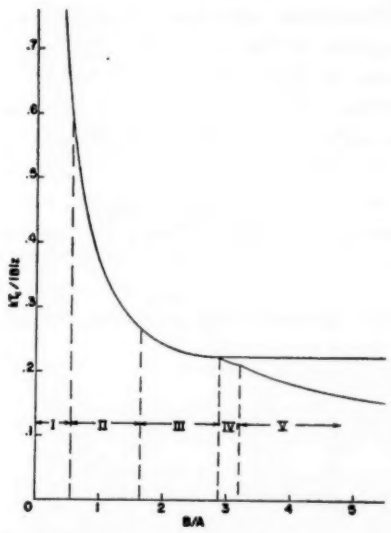

FIG. 7. Transition temperatures as functions of B/A. Internal field approximation.

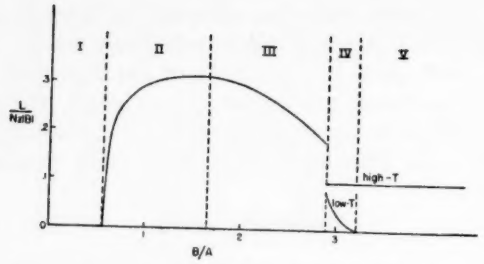

FIG. 8. Latent heats of first-order transitions, as functions of B/A. Internal field approximation.

and specific heat discontinuity are given by Eqs. (7.1) and (7.3), respectively.

In the limit of pure P_2 coupling, $B>0$, $A\to 0$, the transition temperature goes to zero. With this type of P_2 coupling no ordered phase—or, at least, none with $f=f(\theta)$—exists at any temperature.

PART II. MODIFICATION OF CHANG'S METHOD

8. DERIVATION OF THE CONSISTENCY RELATIONS

In the preceding Section each molecule was treated as taking on its orientations independently, subject to a constant orienting potential that is the average energy of interaction of the molecule with its neighbors. Actually, fluctuations in the orientations of the neighboring molecules will give rise to fluctuations in the orienting potential acting on the central molecule. Bethe's method for treating order in alloys takes account of such fluctuations, and has been extended by Chang[10] to the treatment of orientational order in a system of rotators with next-neighbor coupling energy given by $E(\theta_{ij})=AP_1(\cos\theta_{ij})$. Chang considers a small aggregate of molecules, consisting of a central molecule, labeled 0, and z nearest neighbors, forming the outer shell, and labeled $1, 2, \cdots, z$, where $z\geqslant 3$. It is assumed that no two of the z nearest neighbors are nearest neighbors of each other. Chang's basic assumption is that the small aggregate of $(z+1)$ molecules can be regarded as independent of the remainder of the crystal, except that each outer shell molecule is subject to an orienting potential $V(\theta_i)$ that represents the effect of its interaction with the external molecules. In treating our more general form of interaction potential we follow Chang in making this approximation. It will, however, be convenient to modify Chang's method in order to obtain a simpler consistency relation for the determination of $V(\theta_i)$, or of

$$g(\theta_i)=\exp[-V(\theta_i)/kT]. \tag{8.1}$$

Let θ_{i0} be the angle between the axes of the central molecule and its ith neighbor. The relative weight for a given configuration of the cluster of $(z+1)$ molecules can then be written as

$$\exp\left[-\frac{A\sum_{i=1}^{z}P_1(\cos\theta_{i0})+B\sum_{i=1}^{z}P_2(\cos\theta_{i0})}{kT}\right]\prod_{i=1}^{z}g(\theta_i). \tag{8.2}$$

The relative probability that the central molecule and one of its neighbors, say neighbor 1, take on directions θ_0, ϕ_0 and θ_1, ϕ_1, respectively, is then

$$\begin{aligned}\psi(\theta_0,\phi_0;\theta_1,\phi_1)&=\exp\left[-\frac{AP_1(\cos\theta_{10})+BP_2(\cos\theta_{10})}{kT}\right]g(\theta_1)\\&\times\int\cdots\int\exp\left[-\frac{A\sum_{i=2}^{z}P_1(\cos\theta_{i0})+B\sum_{i=2}^{z}P_2(\cos\theta_{i0})}{kT}\right]\\&\times\prod_{i=2}^{z}g(\theta_i)\prod_{i=2}^{z}\frac{d\omega_i}{4\pi}.\end{aligned} \tag{8.3}$$

This distribution function must apply to any pair of next neighbors in the system, and must assume the same form regardless of which of the two molecules is originally regarded as the 0th molecule. It follows, then, that ψ must be unchanged by interchange of the orientations of the molecules:

$$\psi(\theta_0,\phi_0;\theta_1,\phi_1)=\psi(\theta_1,\phi_1;\theta_0,\phi_0). \tag{8.4}$$

The condition that this be so is a consistency relation that serves to determine the form of $g(\theta_i)$. It can be shown to be equivalent to Chang's consistency relation, and will be used here because of its simpler form.[19]

To determine ψ, we expand the exponential in Legendre polynomials, to obtain

$$\exp\left[-\frac{AP_1(\cos\theta)+BP_2(\cos\theta)}{kT}\right]=d\sum_{k=0}^{\infty}(2k+1)c_kP_k(\cos\theta), \tag{8.5}$$

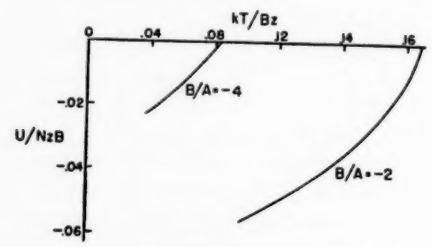

FIG. 9. Typical plots of U/NzB against kT/Bz, for $B>0$. Internal field approximation.

[19] See Letter to Editor by A. James and T. Krieger, "Equivalence of Nakamura's and Chang's Theories of Rotational Transitions," J. Chem. Phys. **22**, 764 (1954).

where

$$c_n \equiv \frac{\int_{-1}^{+1} P_n(x) \exp\left[-\frac{AP_1(x)+BP_2(x)}{kT}\right]dx}{\int_{-1}^{+1} \exp\left[-\frac{AP_1(x)+BP_2(x)}{kT}\right]dx} = \bar{P}_n, \quad (8.6)$$

and

$$d \equiv \tfrac{1}{2}\int_{-1}^{+1} \exp\left[-\frac{AP_1(x)+BP_2(x)}{kT}\right]dx. \quad (8.7)$$

We also expand $g(\theta_i)$ in Legendre polynomials:

$$g(\theta_i) = \sum_{k=0}^{\infty} a_k P_k(\cos\theta_i). \quad (8.8)$$

On substituting these expansions into Eq. (8.3) and carrying out the integrations, making use of the addition theorem for Legendre polynomials, one obtains

$$\psi(\theta_0,\phi_0;\theta_1,\phi_1) = \exp\left[-\frac{AP_1(\cos\theta_{01})+BP_2(\cos\theta_{01})}{kT}\right]$$

$$\times\left[\sum_{k=0}^{\infty} a_k P_k(\cos\theta_1)\right]\left[d\sum_{l=0}^{\infty} a_l c_l P_l(\cos\theta_0)\right]^{z-1}. \quad (8.9)$$

On use of this result, the consistency relation, Eq. (8.4), becomes, after cancellation of factors and a slight rearrangement,

$$\frac{\sum_{k=0}^{\infty} a_k P_k(\cos\theta_0)}{\left[\sum_{k=0}^{\infty} a_k c_k P_k(\cos\theta_0)\right]^{z-1}} = \frac{\sum_{k=0}^{\infty} a_k P_k(\cos\theta_1)}{\left[\sum_{k=0}^{\infty} a_k c_k P_k(\cos\theta_1)\right]^{z-1}}. \quad (8.10)$$

Since the left member of Eq. (8.10) is a function of θ_0 but not of θ_1 and the right member a function of θ_1 and not of θ_0, each must be equal to a quantity ρ independent of both θ_0 and θ_1:

$$\sum_{k=0}^{\infty} a_k P_k(\cos\theta) = \rho\left[\sum_{k=0}^{\infty} a_k c_k P_k(\cos\theta)\right]^{z-1}, \quad (8.11)$$

the subscript on θ no longer being necessary.

Equations determining the a_k and ρ are obtained by expanding the right member of Eq. (8.11) in Legendre polynomials, to obtain

$$\sum_{k=0}^{\infty} a_k P_k(\cos\theta) = \rho\sum_{k=0}^{\infty} A_k' P_k(\cos\theta), \quad (8.12)$$

where

$$A_k' = (k+\tfrac{1}{2})\int_{-1}^{+1} P_k(x)\left[\sum_{l=0}^{\infty} a_l c_l P_l(x)\right]^{z-1}dx. \quad (8.13)$$

Equating coefficients in Eq. (8.12), we have as the consistency relations on the a's

$$a_k = \rho A_k' \quad (k=0,1,2,\cdots), \quad (8.14)$$

where the A_k' are polynomials in the a_l and the known functions c_l.

9. SOLUTION OF THE CONSISTENCY EQUATIONS FOR INFINITESIMAL a_k

Symmetry of Solutions

Some general properties of the solutions of Eqs. (8.14) can be inferred immediately.

Consideration of Eqs. (8.12) and (8.13) makes it evident that the disordered solution $a_k=\delta_{k0}$ exists regardless of the value of the c_l—that is, at all temperatures.

If $a_k=0$ for all odd k, then the integrands in Eqs. (8.13) for odd k are odd functions of x, and the integrals vanish: $A_k'=0$ for all odd k. Equations (8.14) with odd k are thus automatically satisfied. Equations (8.14) with even k then serve to determine the even a's. Solutions in which only even a's differ from zero will be called "even" solutions. Solutions with only odd a's different from zero are not possible, since $a_0\equiv 1$. A solution with both even and odd a's different from zero will be called a "mixed" solution.

Let $a_k=a_k^{(0)}$ $(k=0,1,\cdots)$ be a solution of Eq. (8.14). Then it is easily seen that $a_k=(-1)^k a_k^{(0)}$ $(k=0,1,2,\cdots)$ is also a solution of Eq. (8.14). These two solutions are physically equivalent, each arising from the other on reversal of the sense of the symmetry axis.

For sufficiently high temperatures it is to be expected on physical grounds that the disordered solution will be the only solution. As the temperature is lowered, points will be reached near which mixed or even solutions exist with infinitesimal coefficients a_k $(k>0)$. These temperatures will not be called transition temperatures, since they need not correspond to phase transitions. Instead, we shall refer to them as branching temperatures, since they correspond to a branching off of one solution from another. To determine these branching temperatures, Chang's procedure of expanding the A_k' in power series in the infinitesimal a_k will be followed.

The Mixed Solution

The branching temperature T_b for a mixed solution will be discussed first. Assuming, as Chang does, that $a_k=O(a_1^k)$, and neglecting infinitesimals of higher order, one finds

$$A_0' = 1+\frac{(z-1)(z-2)}{2\cdot 3}a_1^2c_1^2+\cdots,$$

$$A_1' = (z-1)a_1c_1+\tfrac{2}{5}(z-1)(z-2)c_1c_2a_1a_2$$
$$+\tfrac{1}{10}(z-1)(z-2)(z-3)c_1^3a_1^3+\cdots,$$

$$A_2' = (z-1)a_2c_2+\tfrac{1}{3}(z-1)(z-2)c_1^2a_1^2+\cdots.$$

The consistency relation $A_0'a_1=A_1'$ in the neighborhood of the branching temperature becomes

$$\left[1+\frac{(z-1)(z-2)}{6}a_1^2c_1^2+\cdots\right]a_1 = (z-1)a_1c_1+\tfrac{2}{5}(z-1)(z-2)c_1c_2a_1a_2 +\tfrac{1}{10}(z-1)(z-2)(z-3)c_1^3a_1^3+\cdots. \quad (9.1)$$

The consistency relation $a_2=A_2'/A_0'$ reads

$$a_2=(z-1)a_2c_2+\tfrac{1}{3}(z-1)(z-2)a_1^2c_1^2+\cdots. \quad (9.2)$$

From these equations it follows that, since $a_1\neq 0$,

$$a_1^2=[1-(z-1)c_1]\Big/\left[\frac{2}{15}\frac{(z-1)^2(z-2)^2}{1-(z-1)c_2}c_1^3c_2 +\tfrac{1}{10}(z-1)(z-2)(z-3)c_1^3 -\frac{(z-1)(z-2)}{6}c_1^2\right]+\cdots. \quad (9.3)$$

Real solutions for a_1 will exist when the right member of Eq. (9.3) is positive. Branching occurs when the numerator $1-(z-1)c_1$ vanishes:

$$c_1=\tilde{P}_1=1/(z-1), \quad (9.4)$$

provided that the denominator of Eq. (9.3) does not also vanish at this temperature.

Whether the real infinitesimal solutions for a_1 exist below or above the branching temperature T_b depends on the sign of the denominator D in Eq. (9.3) at $T=T_b$. It will be seen later that $1-(z-1)c_1$ is positive for $T>T_b$ and negative for $T<T_b$. If, then, $D<0$ when $T=T_b$, a_1^2 will be negative for $T>T_b$, positive for $T<T_b$; real infinitesimal solutions for a_1 will exist below T_b, but not above. Conversely, if $D>0$ when $T=T_b$, real infinitesimal solutions for a_1 will exist only above T_b.

The Even Solution

For the even solution we have, in the neighborhood of T_b,

$$A_0'=1+\tfrac{1}{10}(z-1)(z-2)a_2^2c_2^2+\cdots$$
$$A_1'=0$$
$$A_2'=(z-1)a_2c_2+(1/7)(z-1)(z-2)a_2^2c_2^2+\cdots.$$

The consistency relation $a_2=A_2'/A_0'$ has the solution

$$a_2=\frac{1-(z-1)c_2}{c_2^2/7}. \quad (9.5)$$

Here, in contrast with the situation in Eq. (9.3), infinitesimal real solutions for a_2 exist whether the numerator on the right is positive or negative. The branching temperature is determined by

$$c_2=\tilde{P}_2=1/(z-1). \quad (9.6)$$

10. CALCULATION OF THE INTERNAL ENERGY

To construct the (U,T) diagrams in the present approximation, an expression for the internal energy is needed. This can be obtained by a method simpler than Chang's, by computing the average energy of interaction of next-neighbor pairs using the (unnormalized) distribution function $\psi(\theta_i,\phi_i;\theta_j,\phi_j)$ for next-neighbor orientations. Since there are $Nz/2$ next-neighbor pairs in the crystal, one has

$$U=\frac{Nz}{2}\frac{\int\int E(\theta_{ij})\psi(\theta_i,\phi_i;\theta_j,\phi_j)d\omega_i d\omega_j}{\int\int\psi(\theta_i,\phi_i;\theta_j,\phi_j)d\omega_i d\omega_j}, \quad (10.1)$$

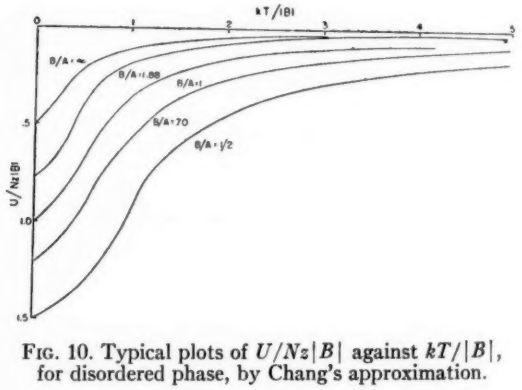

FIG. 10. Typical plots of $U/Nz|B|$ against $kT/|B|$, for disordered phase, by Chang's approximation.

where $E(\theta_{ij})$ is given by Eq. (1.2). A somewhat tedious calculation yields

$$U=\frac{Nz}{2}\Bigg[A\left\{\sum_{k=0}^{\infty}\frac{1}{2k+1}\left[\frac{k}{2k+1}c_{k-1}+\frac{k+1}{2k+1}c_{k+1}\right]a_k^2\right\} +B\left\{\sum_{k=1}^{\infty}\frac{1}{2k+1}\left[\nu_1(k)c_{k-2}+\nu_2(k)c_k +\nu_3(k)c_{k+2}\right]a_k^2\right\}\Bigg]\Big/\left\{\sum_{k=0}^{\infty}\frac{c_k}{2k+1}a_k^2\right\}, \quad (10.2)$$

where

$$\left.\begin{aligned}\nu_1(k)&=-\frac{3}{2}\frac{(k-1)k}{(2k-1)(2k+1)},\\ \nu_2(k)&=\frac{k(k+1)}{(2k-1)(2k+3)},\\ \nu_3(k)&=-\frac{3}{2}\frac{(k+1)(k+2)}{(2k+1)(2k+3)}.\end{aligned}\right\} \quad (10.3)$$

For the disordered phase $[a_k=0\ (k=1,2,\cdots)]$ this reduces to

$$U_d=\frac{Nz}{2}(A\bar{P}_1+B\bar{P}_2), \tag{10.4}$$

when one remembers that $c_n=\bar{P}_n$. The infinitesimal mixed solutions ($a_1\neq 0$) have energy

$$U_m=U_d+\frac{Nz}{2}\left[\frac{A}{3}(\tfrac{1}{3}c_0-c_1^2+\tfrac{2}{3}c_2)+\frac{B}{3}(\tfrac{2}{5}c_1-c_1c_2+\tfrac{3}{5}c_3)\right]a_1^2$$

$$+\text{terms of higher order}$$

$$=U_d+\frac{Nz}{6}\cdot kT_{b1}^2\left.\frac{d\bar{P}_1}{dT}\right|_{T_{b1}} a_1^2+\cdots. \tag{10.5}$$

The coefficient of a_1^2 is negative, because $\bar{P}_1$ decreases monotonely as T increases; thus the infinitesimal mixed solutions have lower U than the disordered solution. The infinitesimal even solutions ($a_1=0$) similarly have energy

$$U_e=U_d+\frac{Nz}{10}\cdot kT_{b2}^2\cdot\left.\frac{d\bar{P}_2}{dT}\right|_{T_{b2}} a_2^2+\cdots. \tag{10.6}$$

The derivative here is always negative when T_{b2} exists (see later sections); thus the infinitesimal even solutions also have lower U than the disordered solution.

Next we consider the value of U at $T=0$. It is obvious that

$$c_n|_{T=0}=\bar{P}_n|_{T=0}=P_n(x_{\min}), \tag{10.7}$$

where $x_{\min}$ is the value of x in the range -1 to $+1$ for which $AP_1(x)+BP_2(x)$ assumes its lowest value. One finds ($A<0$!)

$$x_{\min}=\begin{cases}-A/3B & \text{if } 0<-A/3B<1,\\ 1 & \text{otherwise.}\end{cases} \tag{10.8}$$

When $x_{\min}=1$, it follows from Eq. (10.2), and from

$$\nu_1(k)+\nu_2(k)+\nu_3(k)\equiv 1, \tag{10.9}$$

that

$$U|_{T=0}=\frac{Nz}{2}(A+B), \tag{10.10}$$

and is thus the same for all solutions, whether infinitesimal or not. This is to be contrasted with the result of calculations in the internal field approximation, which give different U for different phases at $T=0$.

The internal energy U of the disordered phase, as a function of temperature for several values of B/A, is shown in Fig. 10. In the Bragg-Williams approximation all these curves are replaced by the same line, $U=0$.

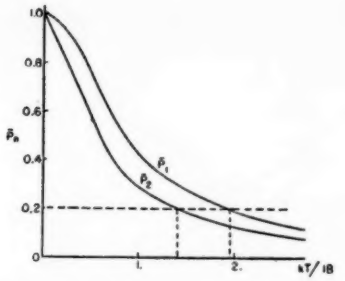

FIG. 11. $\bar{P}_1$ and $\bar{P}_2$ as functions of $kT/|B|$, for $B/A=1$.

11. DETERMINATION OF BRANCHING TEMPERATURES

Calculations made for the internal field treatment of this problem provide the numerical values required for quantitative discussion of the present approximation. Let

$$\mu_1\equiv A/kT<0,\quad \mu_2\equiv B/kT. \tag{11.1}$$

Then, by Eqs. (2.11) and (8.6), one has

$$\left.\begin{aligned}\bar{P}_1&=Q_{\mu_1}'(\mu_1,\mu_2),\\ \bar{P}_2&=Q_{\mu_2}'(\mu_1,\mu_2).\end{aligned}\right\} \tag{11.2}$$

For $B<0$, both $\bar{P}_1$ and $\bar{P}_2$ vary from 0 to 1 as T ranges from infinity to zero. A typical plot of $\bar{P}_1$ and $\bar{P}_2$ against $kT/|B|$ is shown in Fig. 11, for the ratio $B/A=1$. The branching temperatures T_{b1} and T_{b2} can be determined graphically from the intersections of the $\bar{P}_1$ and $\bar{P}_2$ curves, respectively, with the horizontal line

$$\bar{P}_n=1/(z-1) \tag{11.3}$$

[see Eqs. (9.4) and (9.6)]. This is illustrated in Fig. 11 for $z=6$.

When $B>0$, $\bar{P}_2$ assumes negative values for sufficiently large T, but $\bar{P}_1$ is always positive. Both $\bar{P}_1$ and $\bar{P}_2$ approach 1 at $T=0$ if $-3B/A<1$, as sketched in Fig. 12a. As $-3B/A$ rises above 1, the maximum values of $\bar{P}_1$ and $\bar{P}_2$ fall, as shown in Fig. 12b, and so do $kT_{b1}/|B|$ and $kT_{b2}|B|$. The branching temperature

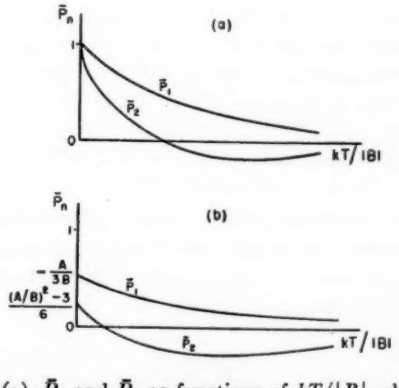

FIG. 12. (a). $\bar{P}_1$ and $\bar{P}_2$ as functions of $kT/|B|$, sketched for $B>0$, $-3B/A\leq 1$. (b). $\bar{P}_1$ and $\bar{P}_2$ as functions of $kT/|B|$, sketched for $B>0$, $-3B/A>1$.

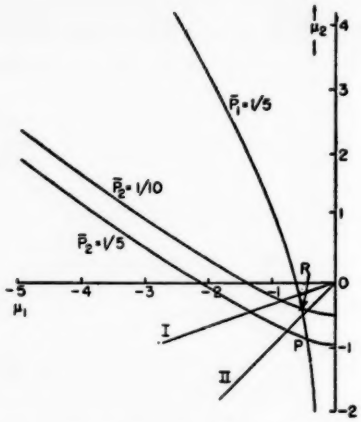

FIG. 13. Contours of constant $\bar{P}_n$ in the (μ_1,μ_2) plane.

T_{1b} goes to 0 when

$$\bar{P}_1|_{T=0}=-A/3B=1/(z-1), \tag{11.4}$$

and the branching temperature T_{2b} goes to 0 when

$$\bar{P}_2|_{T=0}=\tfrac{1}{6}(A/B)^2-\tfrac{1}{2}=1/(z-1). \tag{11.5}$$

For larger values of $-3B/A$ the corresponding infinitesimal solutions do not exist. These figures also make it clear that $d\bar{P}_2/dT|_{T_{b2}}<0$, as was mentioned in the preceding Section.

To survey the dependence of T_{b1} and T_{b2} on A and B, it is convenient to use a figure such as Fig. 13, giving contours of constant $\bar{P}_1$ and $\bar{P}_2$ in the (μ_1,μ_2) plane. The contours shown in Fig. 13 are those needed for discussion of the case $z=6$. The contour $\bar{P}_1=0$ coincides with the μ_2 axis; as $\bar{P}_1$ rises the contours move to the left. The contour $\bar{P}_2=0$ is tangent to the μ_1 axis at the origin; as $\bar{P}_2$ increases the contours move downward. To a given value of $B/A=\mu_2/\mu_1$ there corresponds a radial line in this figure. Each point on this line corresponds to a particular temperature; as T falls from ∞ to 0, the corresponding point moves out from the origin to ∞. The intersection of this line with the contours $\bar{P}_1=1/(z-1)$ and $\bar{P}_2=1/(z-1)$ fixes the values of μ_{b1} and μ_{b2} corresponding to T_{b1} and T_{b2}, and thus the values of these temperatures for given A, B, and z. It is evident from the preceding paragraph that the point of intersection with the $\bar{P}_2$ contour will recede to ∞ as $-B/A$ rises toward $[(z-1)/3(z+1)]^{\frac{1}{2}}$, and that the point of intersection with the $\bar{P}_1$ contour will recede to ∞ as $-B/A$ approaches $(z-1)/3$.

12. DEPENDENCE OF THE TRANSITIONS ON B/A AND ON z

Chang's approximation, unlike the internal field approximation, indicates that the nature of the transition depends on z as well as on B/A. As in Sec. 7, we consider first the case of $B<0$.

Range I

It is evident from the discussion in Sec. 7 that the system will show a single second-order transition (and, by definition, B/A will be in Range I) if $T_{b1}>T_{b2}$, and dU/dT for the mixed phase is positive for $T=T_{b1}$. The second condition will be met if the real infinitesimal mixed solutions exist for $T<T_{b1}$. From Eqs. (9.3) and (9.4), and the associated discussion, it follows that this condition will be met if $D<0$ when $T=T_{b1}$, or if

$$\frac{2}{15}\frac{(z-2)\bar{P}_{2b}}{1-(z-1)\bar{P}_{2b}}+\frac{1}{10}\frac{z-3}{z-1}-\frac{1}{6}<0, \tag{12.1}$$

where $\bar{P}_{2b}$ is the value of $\bar{P}_2$ at the branching temperature T_{b1}. A little calculation will show that both conditions will be met, and a second-order transition will take place, if

$$\bar{P}_{2b}<\frac{z+2}{(z-1)(3z-2)}, \quad (z\geqslant 3). \tag{12.2}$$

We now consider for a moment the case $z=6$. Figure 13 shows the following contours in the (μ_1,μ_2) plane:

$$\bar{P}_1=1/(z-1)=\tfrac{1}{5}; \quad \bar{P}_2=1/(z-1)=\tfrac{1}{5};$$
$$\bar{P}_2=(z+2)/(z-1)(3z-2)=\tfrac{1}{10}.$$

A line in the third quadrant with small B/A, such as that labelled I, intersects the contour $\bar{P}_1=\frac{1}{5}$ nearer to the origin than it does the contour $\bar{P}_2=\frac{1}{5}$; thus $T_{b1}>T_{b2}$. Further, the point of intersection clearly lies on a $\bar{P}_2$ contour, the contour $\bar{P}_2=\bar{P}_{2b}$, for which Eq. (12.2) is satisfied. The line I thus corresponds to a value of B/A in Range I, as does every radial line passing above the point R where the contours $\bar{P}_1=\frac{1}{5}$ and $\bar{P}_2=\frac{1}{10}$ intersect. The radial line through point R, with $B/A=0.70$, marks the upper limit of Range I for $z=6$.

Figure 14 shows the values of T_{b1} obtained for $z=4$, 6, 8, 10, and ∞, in Range I. The value for $z=\infty$ is that given by the internal field method, which can be shown in detail to be equivalent to Chang's method in the limit $z\to\infty$, for constant Az and Bz. It will be noted that, for given B/A, the value of $T_{b1}/|B|z$ is quite insensitive to change in z. The upper limit of Range I, which occurs for values of B/A marked by the dashed line, is somewhat more sensitive to z, but

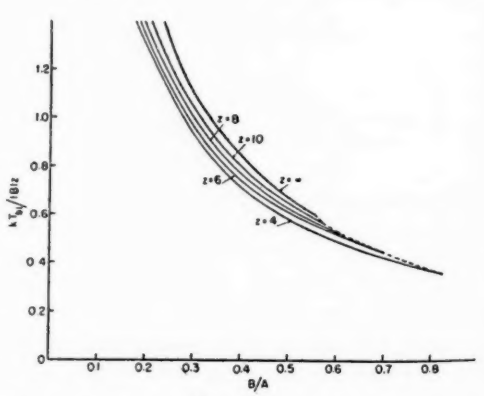

FIG. 14. Plots of $kT_{b1}/|B|z$ against B/A, for various z. Chang's approximation.

again there is little difference between the cases $z=10$ and $z=\infty$.

Range II

Range II of B/A is characterized by the occurrence of a single first-order transition in the system, plus the mathematical condition that $T_{b1}>T_{b2}$. It is obvious from the discussion in Sec. 7 that T_{b1} is not the temperature of the first-order transition, but is a *lower limit* to that temperature. Because of the condition that $T_{b1}>T_{b2}$, the actual transition temperature could be deduced from application of the law of equal areas to $(U,1/T)$ plots for the disordered and mixed phases only. This, however, is not possible on the basis of the infinitesimal solutions of the consistency relation that have been obtained here.

The radial line marked II in Fig. 13 corresponds to a value of B/A in Range II, as do all radial lines passing between point R and point P where the contours $\bar{P}_1=1/(z-1)$ and $\bar{P}_2=1/(z-1)$ intersect. The radial line through point P marks the upper limit of Range II. This limit is of little physical interest, and the corresponding values of B/A for several z are given in Table I primarily for the light they throw on the accuracy of the internal field approximation ($z=\infty$).

Ranges III, IV, V

These ranges can be discussed only by obtaining noninfinitesimal solutions of the consistency relations. Our discussion of these ranges is therefore limited to the internal field approximation, in Sec. 7.

PART III. DISCUSSION OF RESULTS

13. REASONABLENESS OF THE QUALITATIVE RESULTS

The behavior of our model has been discussed fully only in terms of the internal field approximation. The variety of predicted behaviors, for different B/A, is best seen from Figs. 7 and 8.

It is natural to ask to what degree the predicted behaviors may have been affected by the rather rough approximations of the internal field method. It appears to us that comparison with the more accurate calculations by Chang's method, as well as the inherent reasonableness of the results, lends support to the main qualitative predictions of the internal field method.

Figure 14 and Table I show that the internal field method gives quantitative results which agree fairly well with those obtained by Chang's method, particularly for lattices with large numbers of nearest neighbors. Chang's method differs mainly in indicating (a) a nonzero orientational specific heat in the disordered phase [compare Eq. (10.4)], (b) dependence of the transition temperature in Range I on B, as well as on A, (c) some dependence on z of the transition temperatures and of the values of B/A in the different ranges.

TABLE I. Upper limit of B/A for Range II.

z	B/A
4	1.96
6	1.87
8	1.73
∞	1.667

To make clear the reasonableness of the results, we shall review the behavior of the model range by range.

$B=0$; P_1 Coupling

A pure P_1-type coupling that tends to align adjacent molecules parallel to each other,

$$E(\theta_{ij})=AP_1(\cos\theta_{ij}) \quad (A<0), \tag{13.1}$$

gives rise to an internal field potential [see Eqs. (2.3) and (2.6)],

$$z\bar{E}(\theta)=\alpha kTP_1(\cos\theta) \quad (\alpha\gtrless 0), \tag{13.2}$$

which tends to align each molecule parallel to a preferred direction in space. As $T\to T_c$, α goes to zero continuously, and the internal field vanishes, remaining zero for all higher T. The internal field treatment of the model thus indicates the occurrence of a rotational transition as pictured by Pauling and Fowler, with each molecule rotating freely above the transition point.

In Chang's approximation, the molecular couplings will prevent free molecular rotation, but there will be no fixed preferred axis in the model; the orientational distribution for each molecule is independent of θ.

$A=0$; P_2 Coupling

At the opposite extreme, we have pure P_2 coupling that tends to favor equally parallel or antiparallel alignments of next-neighbor molecules:

$$E(\theta_{ij})=BP_2(\cos\theta_{ij}), \quad (B<0). \tag{13.3}$$

In the internal field approximation, this gives rise to an internal field potential,

$$z\bar{E}(\theta)=\beta kTP_2(\cos\theta), \tag{13.4}$$

which tends to align all molecules parallel or antiparallel to a preferred direction in space if $\beta<0$. At sufficiently low temperatures there exists a stable ordered phase, $\beta<0$. As T rises the internal field decreases until the ordered state of the molecules becomes unstable; then β and the internal field go discontinuously to zero, and the distribution of molecular orientations becomes uniform, in a first-order transition.

Range V

When both P_1 and P_2 coupling are present, the effective internal field is

$$z\bar{E}(\theta)=\alpha kTP_1(\cos\theta)+\beta kTP_2(\cos\theta). \tag{13.5}$$

If $B<0$ is large in magnitude and $A<0$ is small, B/A lies in Range V. If T is not too high, the strong P_2 coupling will give rise to an internal field with large negative β, which will restrict the molecules to orientations nearly parallel or nearly antiparallel to the preferred direction. In addition, the relatively weak P_1 coupling will tend to favor parallel orientations of next neighbors over antiparallel orientations. The model will then be nearly equivalent to an Ising model with $A<0$. It is well known that at sufficiently low T this Ising model gives an ordered phase with molecules predominantly parallel ($\alpha>0$), which as T rises undergoes a second-order transition to a phase in which parallel and antiparallel orientations are equally probable ($\alpha=0$). Our model gives this transition, and, in addition, the first-order transition at higher temperature in which the stronger P_2 coupling becomes ineffective and the parallel-antiparallel order gives way to random orientation of the molecules.

Range IV

For larger values of $|A|$, in Range IV, the P_1 and P_2 couplings are more nearly comparable in effect. Our model is then not equivalent to an Ising model at temperatures near the lower transition point, where the P_1 coupling is losing its effectiveness, because the effect of the P_2 coupling is there also changing with temperature. Because of the interaction of the two types of coupling, α does not go to zero continuously, but discontinuously; at the same time β changes discontinuously, but not to zero. The low-temperature transition thus becomes one of the first order. Above this lower transition point, $\alpha\equiv 0$ and the P_1 coupling is without effect on the system, to the internal field approximation. The parallel-antiparallel order due to the P_2 coupling disappears, as before, in a first-order transition.

Ranges III, II

For still larger relative values of $|A|$, in Ranges II and III, the P_1 and P_2 couplings have still stronger mutual effects. Both P_1 and P_2 terms in the internal field, and the corresponding types of order, persist to temperatures above those at which all order would have disappeared if only one or the other type of coupling were present. The internal field then disappears completely in a single first-order transition, at a temperature determined by the values of both A and B.

TABLE II.

	HCl	HBr	HI	DCl	DBr	DI
Transition temperatures (°K)	98.4	89.7 113.6 116.9	70.1 125.7	105.0	93.5 120.3	77.3 128.3
Melting temperatures (°K)	158.9	186.3	223.2	158.4	185.6	221.2

Range I

For the largest values of $|A|$ the P_1 coupling is the dominant one. The parameter β goes to zero continuously with α, and all order disappears in a second-order transition, at a temperature determined entirely by the value of A. This is to be contrasted with the disappearance of the P_1 term in the internal field in a separate transition when the P_2-type coupling is strongly dominant (Range V).

14. COMPARISON WITH EXPERIMENT

Since our model does not give a realistic representation of any particular crystal, we shall comment only very briefly on the relation of our results to experiment.

The transition and melting temperatures of the hydrogen and deuterium halides are shown in Table II. The single transition of the chlorides is of the first order; all others seem to be of second order. The fact that two transitions in HBr (at 113.6°K and 116.9°K) correspond to a single transition in DBr is clearly due to some factor not taken into account in the present model. Neither does our model show successive second-order transitions for any B/A; it approximates this behavior most closely in Range V, with a second-order transition followed by a first-order transition.

Tisza[8] has suggested that in the bromides and iodides the lower transition marks a change from an ordered phase in which next neighbors tend to be antiparallel to a phase with parallel-antiparallel order, and that the second transition is to the disordered phase. He suggests also that the lower transition is controlled by dipole forces, and the upper transition by van der Waals forces. In our model, the orientational coupling due to dipole forces is represented by P_1 coupling, and that due to van der Waals forces is represented by P_2 coupling, with perhaps a small admixture of P_1 coupling for unsymmetrical molecules; thus Tisza's suggestion corresponds exactly to our model with $A>0$ and B/A in Range V.

Powles[9] has made rough calculations of the orientational coupling due to dipole and van der Waals forces in these crystals. He finds a fair correlation of the van der Waals forces with the upper transition temperature, but a very poor correlation of the dipolar forces with the lower transition temperature. This is what our model would lead one to expect, since the upper transition temperature is independent of A in the internal field approximation, whereas the lower transition tempera-

ture depends on both B and A. Further, as the atomic weight of the halogen decreases, the dipolar forces increase and the van der Waals forces decrease. This corresponds to decreasing B/A, which carries with it decreasing separation of the transitions (as observed in passing from the iodides to the bromides) followed by merging of the two transitions into a single transition of the first order (as observed in the chlorides). In view of the correspondence of the observed behavior of these crystals to that of our model, except as concerns the order of the higher transition in the bromides and chlorides, further elaboration of our model might be worth while.

Acknowledgments

The authors are indebted to Mr. Robert S. Cohen for the use of his preliminary calculations on the problem, and to Helen R. Krieger for assistance in the numerical work.

APPENDIX A. EVALUATION OF $Q(\alpha,\beta)$ AND ITS DERIVATIVES

$\alpha>0$, $\beta>0$

Let

$$l=\left(\frac{3\beta}{2}\right)^{\frac{1}{2}}\left(\frac{\alpha}{3\beta}-1\right), \quad L=\left(\frac{3\beta}{2}\right)^{\frac{1}{2}}\left(\frac{\alpha}{3\beta}+1\right), \tag{A.1}$$

$$F(x)=\int_0^x e^{-t^2}dt. \tag{A.2}$$

$F(x)$ is extensively tabulated. Then

$$Q(\alpha,\beta)=-\frac{\beta}{2}-\frac{\alpha^2}{6\beta}+\frac{1}{2}\ln(6\beta)-\ln[F(L)-F(l)], \tag{A.3}$$

$$Q_\alpha'=-\frac{\alpha}{3\beta}-\frac{1}{(6\beta)^{\frac{1}{2}}}\frac{e^{-L^2}-e^{-l^2}}{F(L)-F(l)}, \tag{A.4}$$

$$Q_\beta'=-\frac{1}{2}+\frac{1}{6}\left(\frac{\alpha}{\beta}\right)^2+\frac{1}{2\beta}+\frac{1}{2\beta}\frac{le^{-L^2}-Le^{-l^2}}{F(L)-F(l)}. \tag{A.5}$$

$\alpha>0$, $\beta<0$

For $\alpha>0$, $\beta<0$, l and L are pure imaginary. Real quantities λ and Λ and a function $G(x)$ are defined by

$$\lambda=-il, \quad \Lambda=-iL, \tag{A.6}$$

$$G(x)=\int_0^x e^{t^2}dt. \tag{A.7}$$

The function $G(x)$ has been tabulated in the range $0\leq x\leq 4$ at intervals of 0.01.[20] Then

$$Q(\alpha,\beta)=-\frac{\beta}{2}-\frac{\alpha^2}{6\beta}+\frac{1}{2}\ln(-6\beta)-\ln[G(\Lambda)-G(\lambda)] \tag{A.8}$$

$$Q_\alpha'=-\frac{\alpha}{3\beta}+\left(-\frac{1}{6\beta}\right)^{\frac{1}{2}}\frac{e^{\Lambda^2}-e^{\lambda^2}}{G(\Lambda)-G(\lambda)} \tag{A.9}$$

$$Q_\beta'=-\frac{1}{2}+\frac{1}{6}\left(\frac{\alpha}{\beta}\right)^2+\frac{1}{2\beta}\frac{\lambda e^{\Lambda^2}-\Lambda e^{\lambda^2}}{G(\Lambda)-G(\lambda)}. \tag{A.10}$$

α, β Small

Expanding about $\alpha=\beta=0$, one finds

$$Q(\alpha,\beta)=-\frac{1}{6}\alpha^2-\frac{1}{10}\beta^2+\frac{1}{15}\alpha^2\beta+\frac{1}{105}\beta^3+\frac{1}{180}\alpha^4-\frac{3}{560}\alpha^2\beta^2+\frac{1}{700}\beta^4+\cdots. \tag{A.11}$$

APPENDIX B. PROOF THAT $\left|\frac{\partial\bar{P}_i}{\partial\alpha_j}\right|\neq 0$

Let

$$\bar{f}=\int_{-1}^{+1}dz f(z)w(z), \tag{B.1}$$

where

$$w(z)=\frac{\exp[-\sum_{k=1}^{n}a_kP_k(z)]}{\int_{-1}^{+1}dz\exp[-\sum_{k=1}^{n}\alpha_kP_k(z)]}. \tag{B.2}$$

Then

$$\frac{\partial\bar{P}_i}{\partial\alpha_j}=-\overline{P_iP_j}+\bar{P}_i\bar{P}_j=\overline{(\bar{P}_i-P_i)(\bar{P}_j-P_j)}$$

$$=\int_{-1}^{+1}dz_i[\bar{P}_i-P_i(z_i)][\bar{P}_j-P_j(z_i)]w(z_i). \tag{B.3}$$

The n-rowed determinant of the quantities

$$\partial\bar{P}_i/\partial\alpha_j \quad (i,j=1,2,\cdots,n)$$

can be written as

$$\left|\frac{\partial\bar{P}_i}{\partial\alpha_j}\right|_n=\int_{-1}^{+1}dz_1\cdots\int_{-1}^{+1}dz_n \times\{\sum_P\sigma_P P\prod_i[\bar{P}_i-P_i(z_i)]\} \times\prod_i\{[\bar{P}_i-P_i(z_i)]w(z_i)\}. \tag{B.4}$$

[20] H. M. Terrell and L. Sweeney, J. Franklin Inst. **237**, 495 (1944); **238**, 220 (1944).

where the sum is over all permutations P of the z's, and $\sigma_P=+1$ or -1 according as P is an even or odd permutation. The sum is the determinant of the quantities $\bar{P}_i-P_i(z_j)$ $(i,j=1,2,\cdots,n)$; thus

$$\left|\frac{\partial\bar{P}_i}{\partial\alpha_j}\right|_n=\int_{-1}^{+1}dz_1\cdots\int_{-1}^{+1}dz_n\left|\bar{P}_i-P_i(z_j)\right|_n \times\prod_i\{[\bar{P}_i-P_i(z_i)]w(z_i)\}. \quad (B.5)$$

Reversing the manipulation familiar in the handling of Slater determinants in the theory of atomic structure, one can write this as

$$\left|\frac{\partial\bar{P}_i}{\partial\alpha_j}\right|_n=\frac{1}{n!}\int_{-1}^{+1}dz_1\cdots\int_{-1}^{+1}dz_n \times\left|\bar{P}_i-P_i(z_j)\right|_n^2\prod_i w(z_i). \quad (B.6)$$

Since $w(z)$ is non-negative, the integral on the right is clearly positive.

THE JOURNAL OF CHEMICAL PHYSICS VOLUME 22, NUMBER 5 MAY, 1954

Flame Turbulence Measurements by the Method of Helium Diffusion*

ARTHUR A. WESTENBERG
Applied Physics Laboratory, The Johns Hopkins University, Silver Spring, Maryland
(Received December 4, 1953)

A technique is described for measuring transverse turbulence intensity in flames which makes use of the diffusion of helium. The latter is detected by a thermal conductivity method. The effects of various experimental parameters and the reliability of the technique are discussed. Results obtained in highly turbulent flames stabilized on various baffles in a 5 cm×20 cm duct are given, and compared with results obtained under comparable cold flow conditions. It appears that, under the conditions of these experiments, the amount of "flame-generated" turbulence detectable at a fixed point in the duct by this technique is probably small.

I. INTRODUCTION

THE importance of turbulence in the propagation of flames is generally recognized. Thus it is known, for example, that the rate of burning in a combustible mixture is increased by large-scale turbulence—the effect being usually attributed to greater flame front area and better mixing brought about by the turbulent fluctuations. Several attempts have been made to relate theoretically the so-called turbulent flame speed to the turbulence characteristics of the approach flow.[1–4] Recently, there have been suggestions that a flame may actually generate turbulence to a level many times greater than that present in the approach flow itself. In a study of open Bunsen flames, Karlovitz[3] found that measured values of turbulent flame speed could not be reconciled with predictions of his theory, unless much greater values of turbulence intensity than those known to exist in the approach flow were used. The assumption was then that the additional turbulence was generated by the flame itself, and a mechanism was proposed to account for this. For confined flames, Scurlock[4] has suggested the possibility of another type of flame-generated turbulence due to the high shear region set up at the boundary between a (less dense) flame accelerated by the combustion process and the unburned gas of lower velocity.

At present, neither the theories nor the interpretation of turbulent flame speed measurements may be regarded as firmly established. Conspicuously lacking in the literature are directly measured, quantitative data on the turbulence characteristics of flames. Karlovitz *et al.*[5] have reported preliminary results with an interesting technique involving an ionization probe which may prove very useful upon further development. There seem to have been no direct measurements of flame turbulence using a more or less established method, however, and the present program was undertaken to provide such data. Since the hot-wire anemometer commonly used in cold flow turbulence measurements is not suited for use in a flame, a diffusion method seemed the only other present alternative. Cold flow measurements utilizing the diffusion of heat[6–8] and the

* This work was supported by the Bureau of Ordnance, U. S. Navy.

[1] G. Damköhler, Z. Elektrochem. **46**, 601 (1940). English translation: Natl. Advisory Comm. Aeronaut. Tech. Mem. No. 1112 (1947).

[2] K. I. Shelkin, J. Tech. Phys. (U.S.S.R.) **13**, 520 (1943). English translation: Natl. Advisory Comm. Aeronaut. Tech. Mem. No. 1110 (1947).

[3] Karlovitz, Denniston, and Wells, J. Chem. Phys. **19**, 541 (1951).

[4] A. C. Scurlock and J. H. Grover, *Fourth Symposium on Combustion* (The Williams and Wilkins Company, Baltimore, 1953), 645.

[5] Karlovitz, Denniston, Knapschaefer, and Wells, *Fourth Symposium on Combustion* (The Williams and Wilkins Company, Baltimore, 1953), 613.

[6] G. B. Schubauer, Natl. Advisory Comm. Aeronaut. Rept. No. 524 (1935).

[7] D. C. Collis, Australian Council Sci. and Ind. Research, Div. Aeronaut., Report No. A-55 (1948).

[8] M. S. Uberoi and S. Corrsin, Natl. Advisory Comm. Aeronaut. Tech. Note No. 2710 (1952).

diffusion of matter[9] have been reported by several investigators, but as far as the author is aware, the diffusion method has never been applied in flames. Helium was chosen as the gas whose diffusion was to be measured for two reasons: first, it fulfilled the obvious requirement of chemical inertness, and second, its high thermal conductivity offered a convenient property to be used in detecting its presence in very small concentrations.

II. THEORETICAL BACKGROUND

The statistical theory of turbulent diffusion has been described adequately many times[10–11] so that only the bare essentials are given here. Let us assume that the diffusion is taking place in a field of homogeneous, isotropic turbulence with a steady mean velocity U along the x axis of a Cartesian coordinate system. It is customary to characterize turbulence by the quantities intensity and scale. The intensity at any point in the turbulent field is defined as $(\langle v^2\rangle_{Av})^{\frac{1}{2}}/U$, where $(\langle v^2\rangle_{Av})^{\frac{1}{2}}$ is the rms value of the fluctuating velocity component along any of the coordinate axes (the three components are equal in isotropic turbulence). The scale may be defined in various ways, but when turbulent diffusion is being treated it is convenient to define scale in terms of the Lagrangian correlation coefficient

$$R_h=\langle v(t)v(t+h)\rangle_{Av}/\langle v^2\rangle_{Av}$$

by means of the relation

$$L_t=\int_0^\infty R_h dh. \tag{1}$$

The scale L_t thus has the units of time.

Assume now that a point source at the origin of the coordinate system emits continuously a mass of fluid Q per unit time at a velocity U into such a turbulent flow. Then in a plane $x=$ constant downstream of the source, the theory of turbulent diffusion gives for the time-average concentration distribution of the diffusing fluid the expression

$$\bar{s}=\frac{Q}{2\pi U\langle y^2\rangle_{Av}}\exp\left[-\frac{(y^2+z^2)}{2\langle y^2\rangle_{Av}}\right]. \tag{2}$$

$\langle y^2\rangle_{Av}$ is the mean square displacement of fluid elements in any direction transverse to the x axis after a diffusion time $t=x/U$. This is an approximate relation which neglects diffusion in the x direction and is valid under the conditions that $(\langle v^2\rangle_{Av})^{\frac{1}{2}}/U\ll 1$, y and $z\ll x$, and that either $t\ll L_t$ or $t\gg L_t$. For intermediate values of t the distribution function depends on the correlation coefficient R_h and cannot be given explicitly without assumptions (or knowledge) regarding the functional form of R_h.

Equation (2) represents a two-dimensional Gaussian distribution with $\langle y^2\rangle_{Av}$ identified as the variance or $(\langle y^2\rangle_{Av})^{\frac{1}{2}}$ the standard deviation. In most cases of practical interest the limiting conditions on $(\langle v^2\rangle_{Av})^{\frac{1}{2}}/U$, y, and z are always fulfilled, so that those on the diffusion time t are the most important. It can be shown that for $t\ll L_t$,

$$\langle y^2\rangle_{Av}=\langle v^2\rangle_{Av}t^2=x^2\langle v^2\rangle_{Av}/U^2. \tag{3}$$

Thus the intensity of turbulence can be determined from the standard deviations of distributions taken at small diffusion times, i.e., $(\langle y^2\rangle_{Av})^{\frac{1}{2}}/x$ is independent of x and equal to $(\langle v^2\rangle_{Av})^{\frac{1}{2}}/U$. For the opposite case when $t\gg L_t$, the theory yields the result that

$$\langle y^2\rangle_{Av}=2\langle v^2\rangle_{Av}L_t t=2L_t x\langle v^2\rangle_{Av}/U. \tag{4}$$

In principle, the Lagrangian time scale of turbulence L_t can be determined—once the intensity is known—from measurements of $\langle y^2\rangle_{Av}$ taken at large diffusion times. The difficulty in practice is that both intensity and scale change with the distance x along the flow, i.e., the turbulence cannot be truly homogeneous over a long enough distance from the diffusion source to be characterized by constant values of intensity and scale.

When the turbulence is nonisotropic, then by definition, one must consider three different component intensities $(\langle u^2\rangle_{Av})^{\frac{1}{2}}/U$, $(\langle v^2\rangle_{Av})^{\frac{1}{2}}/U$, and $(\langle w^2\rangle_{Av})^{\frac{1}{2}}/U$ along the x, y, and z axes, respectively, and also three Lagrangian time scales $L_t{}^u$, $L_t{}^v$, and $L_t{}^w$. However, the distribution of a fluid diffusing downstream from a point source still retains a Gaussian form for small or large diffusion times compared to each of the three scales. The appropriate relations corresponding to (3) are then

$$\langle x^2\rangle_{Av}=\langle u^2\rangle_{Av}t^2;\quad \langle y^2\rangle_{Av}=\langle v^2\rangle_{Av}t^2;\quad \langle z^2\rangle_{Av}=\langle w^2\rangle_{Av}t^2 \tag{5}$$

for small t, and corresponding to (4),

$$\langle x^2\rangle_{Av}=2\langle u^2\rangle_{Av}L_t{}^u t;\quad \langle y^2\rangle_{Av}=2\langle v^2\rangle_{Av}L_t{}^v t;\quad \langle z^2\rangle_{Av}=2\langle w^2\rangle_{Av}L_t{}^w t \tag{6}$$

for large t.

All of the measurements reported here were found to be described by Eq. 5 and hence shown to be carried out at small enough distances from the source that they were in the range of diffusion time $t\ll L_t$, permitting turbulence intensity to be determined. Any decay of turbulence over this small region of space can be safely ignored. No attempt was made to prove or disprove isotropy. Some indication of isotropy would be given if the helium distribution in any x plane could be shown to be axially symmetric. Limitations on the sampling mechanism, however, allowed accurate measurements only along one axis transverse to the flow, so that intensities reported here refer only to this one trans-

[9] Towle, Sherwood, and Seder, Proc. Fifth Internatl. Congr. Appl. Mech. 396 (1938).

[10] The original paper in this field is that of G. I. Taylor, Proc. London Math. Soc. **A20**, 196 (1921).

[11] For a recent detailed review, see the chapter by F. N. Frenkiel in *Advances in Applied Mechanics* (The Academic Press, Inc., New York, 1953), Vol. 3.

verse component. Extension of the conclusions to the other two components of intensity could be made only by assumptions as to isotropic conditions existing in the flow both with and without a flame. Such assumptions are not warranted in the present state of our knowledge.

III. EXPERIMENTAL TECHNIQUE

1. Flow System and Accessories

The measurements were carried out in a vertical 5 cm×20 cm rectangular duct, the essential components being arranged as shown in Fig. 1. The main air flow (or premixed air and fuel) entered the test section after passage through a settling chamber containing several screens, a short contracting nozzle, and a perforated choking plate present as a safety device to prevent flashback. The various baffles used as flameholders were placed at the position shown, extending across the 5-cm dimension of the duct.

The helium source (0.040-in. i.d.×0.058-in. o.d. Inconel tubing) was brought in horizontally from the rear to the center of the duct, and then bent up at right angles so that it coincided with the duct axis and was in line with the flameholder. The vertical section of the source tube was about 4 cm long. The sampling probe was a similar piece of Inconel tubing carried on a water-cooled traversing mechanism. The probe could be moved vertically (x axis) through a distance of about 4 cm, and across the short duct dimension (z axis) about 1.5 cm, being held at the desired x, z coordinates by two independent sets of clamps. Across the 20-cm duct dimension (y axis), the probe was continuously adjustable by means of a threaded axle (through which the coolant water flowed) provided with a calibrated dial, so that increments in y could be measured to better than 0.002 cm. All profiles were taken along this axis. The separation between source and sampling probe (the distance x) was read through a window in the duct with a calibrated eye-piece accurate to 0.025 cm.

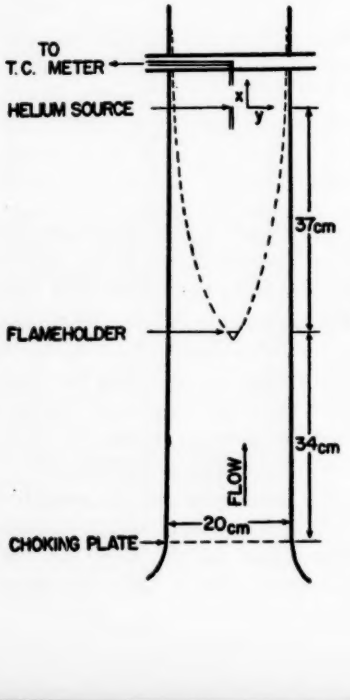

FIG. 1. Schematic diagram of 5-cm×20-cm duct.

The helium used was an "oil-free" product (specified as 99.5 percent pure) from a high-pressure tank. It was fed at the desired constant rate (convenient rates were of the order of 4×10^{-4} g/sec) to the source tube through a jeweled critical orifice of 0.06-mm nominal diameter, the pressure upstream being maintained by a Moore "Null-matic" Regulator.

The temperature in the combustion zone in the region of measurement was estimated from combustion efficiency determined with the thermal conductivity (T.C.) meter in the manner which has been described.[12] Mean flow velocities were obtained by using the sampling probe as a total pressure indicator together with a wall static tap connected to a differential oil manometer. Pentane, metered through a rotameter, was the fuel in all cases. The runs were carried out at constant pressures of $\frac{1}{2}$–$\frac{2}{3}$ atmos in the duct.

2. Helium Detection

The method used to trace out the helium profiles employed a T.C. meter which was originally designed as a combustion analyzer,[12] i.e., to measure CO_2 concentrations in air or other mixtures of O_2 and N_2. Its essential element is a commercial (Gow-Mac) thermal conductivity cell arranged in a Wheatstone bridge circuit with a reference gas (dry air) surrounding the hot wire in one leg, and the unknown sample pumped continuously by the other leg. In normal use the meter is "zeroed" with air passing through the cell. Then the admixture of any gas having a thermal conductivity less than air (e.g., CO_2) causes a positive meter deflection. Since helium has a thermal conductivity greater than air, its presence would cause a negative deflection. Hence it was necessary to modify the instrument by installing a polarity reversing switch in the bridge circuit which would allow a positive deflection with helium. Thus, for sampling in cold flow (no fuel present), the meter was simply zeroed against air with the switch in its normal position, and then helium-air mixtures were read directly from the meter with the switch reversed.

For sampling in a flame, a reference reading was taken first with no helium present. The sample withdrawn from the flame was burned to completion and dried (both furnaces and desiccant are provided as integral parts of the T.C. meter unit) so that it consisted only of CO_2 and residual air. The resulting meter reading (normal polarity) was thus a function only of equivalence ratio and provided a reference which was taken as zero. With helium present, the reading would decrease and might require reversal of bridge polarity. In any

[12] Neumann, Dembrow, Berl, and Prescott, J. Am. Rocket Soc. 23, 244 (1953).

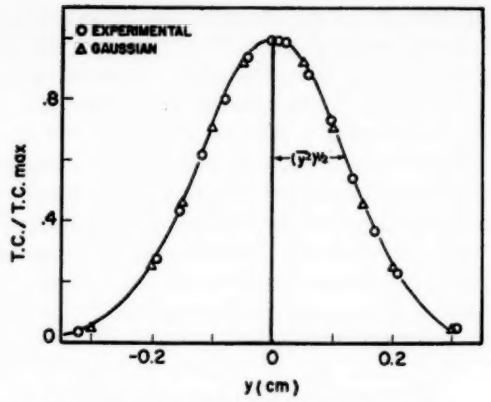

FIG. 2. Typical helium distribution in flame.

case, the reading for a given sample was the algebraic difference between the initial (reference) and final readings on the meter. The time required for the sample flowing through the cell to attain constant composition and give a steady meter reading was of the order of two minutes, so that a good time average at any sampling point was obtained.

Since all that was required were relative helium concentrations to get the desired distribution, it was not necessary to calibrate the meter absolutely; only the linearity of its response to small amounts (~0–3 mol percent) of helium had to be established. This was accomplished by using various accurately known mixtures of helium-air and helium-propane-air. The meter response in both cases was strictly linear over its useful range. In the propane-air case, two different equivalence ratios (1.0 and 0.8) were used but the meter deflection for a given helium mol fraction was the same for both. The linearity proven with propane-air would not be affected adversely with the pentane-air used in the actual experiments.

3. Treatment of the Data

Figure 2 shows a typical helium profile obtained in a flame which will serve to illustrate how the data were used. This profile was taken (as were all the others) by traversing across the y axis in the plane of the source, corresponding to $z=0$. The center of symmetry of the profile was determined by inspection when plotted with an arbitrary origin, not by assuming the source axis to represent $y=0$. This was preferable because of the difficulty of determining accurately the source axis and because profiles taken at different distances x usually had slightly different absolute centers of symmetry—probably the result of slight deviations of the mean flow from the perpendicular. Note that the ordinate of Fig. 2 has been plotted as the fraction of the maximum T.C. meter deflection measured at $y=0$, a convenient method when comparing different profiles.

As pointed out earlier, the information desired from the measured helium profiles is the standard deviation $(\langle y^2\rangle_{Av})^{\frac{1}{2}}$. For our purposes the fundamental distribution Eq. (2) can be written (for $z=0$) in terms of T.C. meter readings as

$$\text{T.C.} = \text{T.C.}_{\max} \exp(-y^2/2\langle y^2\rangle_{Av}). \tag{7}$$

There are various ways of finding the standard deviation of a Gaussian curve. One is to plot y^2 against the logarithm of the ordinate, which gives a straight line with slope equal to $-1/2\langle y^2\rangle_{Av}$. The linearity of such a plot thus provides a qualitative test as to whether or not a given experimental curve is Gaussian. Figure 3 shows this plot for the experimental data of Fig. 2. It is essentially linear and its slope gives a value of 0.122 cm for $(\langle y^2\rangle_{Av})^{\frac{1}{2}}$. Using this standard deviation, the points corresponding to a true Gaussian curve (the function $\exp[-y^2/2\langle y^2\rangle_{Av}]$) are also plotted in Fig. 2, and the closeness of fit between the two distributions is apparent. This verification of the predicted nature of the experimental data promotes confidence in the technique developed for measuring the turbulence characteristics of flames.

With the Gaussian form of the helium distributions established, a simpler procedure for obtaining $(\langle y^2\rangle_{Av})^{\frac{1}{2}}$ routinely is to make use of the fact that $y=(\langle y^2\rangle_{Av})^{\frac{1}{2}}$ at 61 percent of the maximum ordinate, i.e., $\exp(-\frac{1}{2})=0.607$. In Fig. 2 this value is 0.122 cm which, of course, checks the $(\langle y^2\rangle_{Av})^{\frac{1}{2}}$ obtained by the slope method. The "61 percent method" has been used in all cases to be reported and is believed to be more reliable than the slope method in general, because small errors in T.C. readings near the maximum of the curve cause rather large percentage errors in the logarithms, making it difficult to determine the proper slope.

IV. EFFECTS OF VARIOUS EXPERIMENTAL CONDITIONS ON THE MEASURED HELIUM DISTRIBUTION

Considerable effort has been spent in trying to establish the reliability of the technique for practical

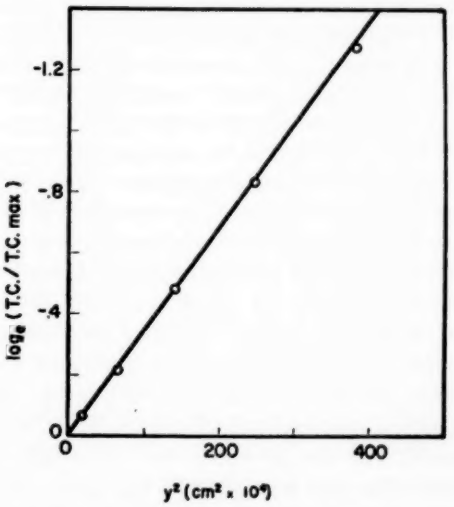

FIG. 3. Plot of y^2 *vs* $\log_e$(T.C./T.C. max) for experimental data of Fig. 2.

turbulence measurements in flames. There are several experimental conditions and variables which might conceivably affect the helium distribution measured by the thermal conductivity technique even though the turbulent flow itself remained unaltered. Since the diffusion due solely to turbulence is what one wants to measure, the effects of these other parameters had to be determined or eliminated as far as possible. This section summarizes our findings in this matter.

1. Wake of the Source

Perhaps the most obvious and serious difficulty with any diffusion method of studying turbulence is the flow disturbance and velocity wake set up by the injection source, especially when one is interested in measurements at small distances downstream. The source cannot be as small as desired because of the requirements of mechanical rigidity and ability to withstand flame temperatures. The 0.040-in. i.d.×0.058-in. o.d. Inconel tubing used as the source in most of this work proved very satisfactory in these respects.

It is apparent from both Eq. (3) and Eq. (4) that the standard deviation of a diffusion profile is an inverse function of the mean stream velocity U. Thus any traverses taken so close to the source as to be in its velocity wake will be in error—$(\langle y^2\rangle_{Av})^{\frac{1}{2}}$ will be too large. Total pressure surveys behind the source indicated that in the range of mean velocities encountered here (30–90 m/sec) the velocity profile was essentially flat beyond about 1 cm, and no helium distributions were taken closer than this. Even so, the fact remains that the diffusion process must unavoidably occur in its early stages in a region of mean velocity lower than that of the general stream so that measured values of $(\langle y^2\rangle_{Av})^{\frac{1}{2}}$ may be expected to err on the high side. It is impossible to estimate this error but some idea of its magnitude may be obtained from the experimental result mentioned below.

The question of eddy-shedding by the source must also be considered. It is known that a bluff object begins to shed eddies at a Reynolds number of about 50, based on the characteristic dimension of the object. Since the Reynolds number of the source used is of the order of 1000 in cold flow, it undoubtedly sheds eddies under these conditions, and possibly also in the flame. It is not unlikely, however, that the effect of this eddy shedding is "swamped out" by the relatively very high turbulence intensities encountered in this work.

As an actual check on the effect of the source wake on the measured helium distribution, comparative profiles were taken under exactly the same cold flow conditions and at the same distance x using a 0.023-in. i.d.×0.035-in. o.d. source, and a 0.04-in. i.d.×0.058-in. o.d. source. The smaller source had to be held rigid by means of a fine guy wire (0.0015 in.). Since, as will be shown presently, the internal diameter of the source has no effect on the profiles, this comparison should give some indication of the effect of the source wake. As expected, the larger source gave a slightly wider profile than the smaller source—the standard deviations being 0.185 cm and 0.175 cm, respectively. This shows that the source wake has a definite effect on the measurement which tends to make reported values of turbulent intensity too high. However, since we are primarily interested in comparisons between flame and no-flame turbulence in this work, and since (as we shall show) the method is definitely sensitive to rather small changes in turbulence, the error due to the source wake can be neglected for our purposes.

2. Finite Size of the Source

Besides the effect of the source as a wake producing element in the flow, one must also consider the fact that it does not furnish a point source of helium but rather an injection over a finite area. Two sets of data were taken under identical conditions but with sources 0.023-in. i.d.×0.058-in. o.d. and 0.040-in. i.d.×0.058-in. o.d., respectively. The two distributions were essentially superimposable and so had the same $(\langle y^2\rangle_{Av})^{\frac{1}{2}}$. Thus, for the values of x used in this work compared to the internal diameter of the source, one may regard the latter as a point for all practical purposes.

3. Helium Injection Rate

In deriving the theory of turbulent diffusion it is assumed that the diffusing fluid enters the turbulent flow at the mean stream velocity U. In practice it is not feasible to accomplish this matching of velocities, so that one must inject the helium at a lower velocity and assume that it very rapidly acquires mean stream velocity. Injection velocities used in this work were of the order of 5 m/sec in cold flow, and perhaps 25 m/sec in the flame (since the helium reaches approximately the flame temperature before leaving the source tube). To check the effect of this variable, two sets of data were taken at different injection rates (roughly 1.7 to 1), and although the whole distribution was multiplied by a constant ($\sim$1.7) for the higher rate as expected, the standard deviations were the same for both.

4. Sampling Rate

Ideally, it would be desirable to withdraw the sample through an extremely small probe (to attain something like point by point averaging), and at mean stream velocity. Neither of these goals can be realized in practice, the sampling probe used being 0.04-in. i.d.×0.058-in. o.d., and the sampling velocity greater than U. It was found experimentally that increasing the sampling rate caused an increase in the apparent helium concentration as read on the T.C. meter. The reason for this probably lies in the fact that the helium undergoing diffusion in the turbulent air stream constitutes a mixture which is macroscopically inhomogeneous, i.e.,

the sampling probe is exposed to a flow of fluctuating density (helium concentration) at any point. An increase in sampling velocity would thus be expected to favor the less dense pockets of fluid—those richer in helium. For absolute concentration determinations this would be a very serious difficulty, but the effect seems to be immaterial for present purposes, since the standard deviations of profiles taken at two quite different sampling rates were essentially identical. Hence one needs only to make sure the sampling rate remains constant during a particular traverse. This was accomplished by metering the total flow rate from the pump to the conductivity cell.

V. THE MOLECULAR DIFFUSION CORRECTION

In addition to the diffusion due to turbulence, that due to molecular motion is, of course, always present in an actual experiment. Since the latter also obeys a Gaussian law, the two effects are additive,[10–11] i.e.,

$$\langle y^2\rangle_{Av}=(\langle y^2\rangle_{Av})_{turb.}+(\langle y^2\rangle_{Av})_{mol}, \tag{8}$$

where $(\langle y^2\rangle_{Av})_{mol}=2Dt$, D being the molecular diffusion coefficient of (in this case) helium in the main turbulent fluid (assumed to be air in the flame as well as in cold flow). In turbulence of moderate or high intensity, the contribution of molecular diffusion to the total measured variance $\langle y^2\rangle_{Av}$ is very small† in cold flow cases even though helium has a relatively high value of D. In a flame, however, it may (as will be shown) become comparable to the turbulent contribution due to the fact that D increases rapidly with temperature—roughly as $T^{\frac{3}{2}}$.

Unfortunately, experimental data on the molecular diffusion coefficient of helium in air even at room temperature seem to be completely absent from the literature as far as the author could determine, to say nothing of values at the temperatures existing in flames. It was necessary, therefore, to use calculated values for D. This was done by means of the published tables for the Lennard-Jones interaction potential according to the method outlined by Hirschfelder *et al.*[13] The cold flow temperature used throughout was 400°K and the flame temperature estimated by means of the combustion efficiency was about 1950°K in all cases. The calculated diffusion coefficients at one atmosphere pressure were $D(400°K)=1.13$ cm²/sec and $D(1950°K)=15.7$ cm²/sec. The values of $\langle y^2\rangle_{Av}$ actually measured in all cases were corrected for molecular diffusion using the above D's (adjusted for the actual pressure in each case—$D\propto 1/P$) to give $(\langle y^2\rangle_{Av})_{turb.}$. The error introduced by the uncertainty in D at the flame temperature is probably no greater than that resulting from the temperature estimate itself or the measured values of mean stream velocity U, all of which enter into the molecular diffusion correction.

† Except for very small diffusion times, when the molecular contribution may easily be the dominant one. This is because $(\langle y^2\rangle_{Av})_{turb.}$ depends on t^2 (see Eq. (3)) for small t, while $(\langle y^2\rangle_{Av})_{mol}$ depends on t.

[13] Hirschfelder, Bird, and Spotz, J. Chem. Phys. **16**, 968 (1948).

TABLE I. Effect of mean stream velocity on cold flow turbulence.

U (m/sec)	x (cm)	$(\langle y^2\rangle_{Av})_{turb.}$ (cm² × 10³)	$[(\langle y^2\rangle_{Av})_{turb.}]^{\frac{1}{2}}/x = (\langle v^2\rangle_{Av})^{\frac{1}{2}}/U$
27	0.86	7.3	0.099
	1.12	12.3	0.099
	1.37	18.2	0.098
36	0.86	8.2	0.105
	1.12	12.5	0.100
	1.37	18.9	0.100
39	0.86	7.9	0.103
	1.12	12.1	0.098
	1.37	18.6	0.099
50	0.86	7.5	0.101
	1.12	12.7	0.101
	1.37	18.8	0.100

VI. EXPERIMENTAL RESULTS IN COLD FLOW

This section summarizes pertinent data from a large number of cold flow experiments. Since all of the helium distributions are of similar (Gaussian) nature they are not included here—just the desired information from each distribution which is the standard deviation.

1. Effect of Mean Stream Velocity

A series of profiles was taken over a range of values of U to determine its effect, if any, on the measured turbulence level. The static pressure in the test section was kept at 42 cm Hg in all the runs. A solid triangular baffle with characteristic dimension of 2.5 cm was present. Results are given in Table I. The ratios $[(\langle y^2\rangle_{Av})_{turb.}]^{\frac{1}{2}}/x$ are given to three significant figures merely to show the sort of internal consistency obtained. Since the separation x could be determined to about ±0.02 cm and $(\langle y^2\rangle_{Av})^{\frac{1}{2}}$ to about ±0.003 cm, the precision of the measurements might be expected to be of the order of 5 percent at the smallest x and slightly better for larger x.

These data show, first of all, that the ratio $[(\langle y^2\rangle_{Av})_{turb.}]^{\frac{1}{2}}/x$ is essentially independent of x over the range examined. This is characteristic of results expected for profiles taken at small diffusion time compared to the Lagrangian time scale of turbulence, with the ratio then equal to the intensity $(\langle v^2\rangle_{Av})^{\frac{1}{2}}/U$. Second, one notes from Table I that the intensity of turbulence is independent of U over the range used, i.e., the absolute value of the rms turbulent velocity fluctuations $(\langle v^2\rangle_{Av})^{\frac{1}{2}}$ measured at a fixed point in the duct is proportional to U. This has been found by others to be the case over even wider ranges of U, using both the conventional hot-wire technique[14–15] and the diffusion

[14] Dryden, Schubauer, and Mock, Natl. Advisory Comm. Aeronaut. Rept. No. 581 (1937).

[15] G. I. Taylor, Proc. Fifth Internatl. Congr. Appl. Mech., 294 (1938).

TABLE II. Experimental results in cold flow behind various baffles.[a]

Baffle	U (m/sec)	x (cm)	$\langle y^2\rangle_{Av}$ (cm$^2\times10^3$)	$(\langle y^2\rangle_{Av})_{mol.}$ (cm$^2\times10^3$)	$(\langle y^2\rangle_{Av})_{turb.}$ (cm$^2\times10^3$)	$[(\langle y^2\rangle_{Av})_{turb.}]^{\frac{1}{2}}/x$
None	44	1.27	7.7	1.2	6.5	0.063
		1.50	9.8	1.4	8.4	0.061
		1.78	13.0	1.7	11.3	0.060
		2.01	16.1	1.9	14.2	0.059
1.25 cm T.R.	51	1.40	9.8	1.4	8.4	0.065
		1.65	13.0	1.6	11.4	0.065
		1.88	16.1	1.9	14.2	0.063
1.25 cm V.G.	52	1.47	11.4	1.5	9.9	0.068
		1.73	14.8	1.8	13.0	0.066
		1.98	19.5	2.0	17.5	0.067
1.25 cm C.R.	52	1.25	8.1	1.3	6.8	0.066
		1.78	14.3	1.8	12.5	0.063
2.50 cm T.R.	37	1.27	16.4	1.4	15.0	0.096
		1.52	23.2	1.7	21.5	0.096
		1.75	30.2	2.0	28.2	0.096
		2.01	41.2	2.3	38.9	0.098
2.50 cm V.G.	49	1.22	14.6	1.4	13.2	0.094
		1.47	20.2	1.6	18.6	0.093
		1.73	32.5	1.9	30.6	0.101
2.50 cm C.R.	49	1.27	16.1	1.4	14.7	0.095
		1.78	31.6	2.0	29.6	0.097
3.75 cm T.R.	48	1.27	37.3	1.4	35.9	0.149
		1.52	57.6	1.7	55.9	0.155
		1.78	80.9	2.0	78.9	0.158
3.75 cm V.G.	48	1.42	67.1	1.6	65.5	0.180
		1.65	85.0	1.8	83.2	0.175
3.75 cm C.R.	52	1.27	37.2	1.4	35.8	0.149
		1.68	73.5	1.9	71.6	0.159

[a] T.R. =triangular rod; V.G. =V-type gutter; C.R. =circular rod.

of heat.[6] The constancy of $(\langle v^2\rangle_{Av})^{\frac{1}{2}}/U$ with U will prove useful in what follows. It should be pointed out that this property would be expected only when U is varied throughout the stream in its passage over all the main turbulence producing elements (grids, flameholders, etc.), and not when there is only a local acceleration downstream of these elements (as in a ducted flame).

2. Effect of Baffle Size and Shape

Table II summarizes a number of results obtained in cold flow with variations in the baffle present as potential flameholder. The mass flow of air entering the duct was the same in all cases, so that minor differences in static pressure resulted in corresponding differences in mean velocity.

There are several things to be noted about these data. (a) All of the cases fall into the range $t\ll L_t$, so that $(\langle v^2\rangle_{Av})^{\frac{1}{2}}/U=[(\langle y^2\rangle_{Av})_{turb.}]^{\frac{1}{2}}/x$. (b) The influence of the baffle as a turbulence producing element is clearly revealed by the markedly larger intensities measured with a baffle present than without. The smallest baffles (1.25 cm) apparently do not affect the intensity much at the point of measurement, as evidenced by the close approach of this value (6.5 percent) to the no-baffle value (6 percent). (c) The greater the characteristic dimension of the baffle, the greater is the turbulent intensity. Whether this effect is due to the baffle size per se or to increasing duct blockage is not possible to determine unambiguously from these data. Probably both play a part. However, the blockage for the largest baffle is only about 18 percent of the duct cross section so that it seems likely the major influence is the result of the size of the baffle itself. (d) The turbulence level is not affected by the geometric shape of the baffle since intensities for each size baffle are essentially the same whether open or solid triangle or cylinder. This is what one would expect, as the frequency and other features of the Karman eddies shed from a bluff object are determined mainly by its characteristic dimension for a given approach stream velocity. (e) These clearly demonstrated differences in the standard deviations of helium profiles measured in the same range of distance x and under the same mean flow conditions, but with different turbulence generating obstructions (baffles) in the upstream flow, promote confidence in the sensitivity of the method as at least a relative turbulence indicator. Further evidence along this line was provided by a series of profiles taken with no baffle present but also with the perforated choking plate removed from

the entrance to the test section. Under these conditions the measured intensity was 4.5 percent, compared to the 6 percent shown in Table II when the choking plate was present. As expected, the plate produced considerable turbulence. More important, however, is the fact that its effect was easily measurable by the helium-diffusion method, despite the admitted influence of the source wake—the main drawback to absolute intensity measurements. Thus the cold flow experiments summarized in this section prove rather conclusively that this technique is capable of detecting fairly small changes (~10 parts in 100) in transverse turbulence intensity in flows of high intensity (~4 percent or greater).

VII. EXPERIMENTAL RESULTS IN FLAME

All of the flame runs were made at an equivalence ratio of 0.70. The total mass flow through the duct was the same as in the cold flow runs, so that with the flame present the pressure was higher than in the cold flow case. This meant the approach velocity to the flameholder was lower than in cold flow, a point which will be amplified later. The temperature at the point of measurement was the same for all baffles—about 1950°K, representing nearly 100 percent combustion efficiency. Flame results are compiled in Table III.

Certain qualitative features are evident from an inspection of these data. (a) After correction for molecular diffusion, the ratio $[(\langle y^2\rangle_{Av})_{turb.}]^{\frac{1}{2}}/x$ is essentially independent of x as was the case in cold flow. Because of the greater experimental difficulties encountered in a flame, the far greater importance of the molecular diffusion correction $[(\langle y^2\rangle_{Av})_{mol}$ is of the order of 50 percent of the total measured $\langle y^2\rangle_{Av}]$, and in the greater uncertainty in its calculation, it would not be surprising if the scatter in $[(\langle y^2\rangle_{Av})_{turb.}]^{\frac{1}{2}}/x$ as x varies were considerably worse than in cold flow. Actually, comparison of Tables II and III shows that the flame results are about as good as the cold flow results, which is rather remarkable. At any rate, they clearly indicate a case of $t \ll L_t$. This is what one would expect (assuming the flame did not change L_t drastically), since in the same range of values of x the diffusion time is less in the flame than in cold flow due to the increased mean stream velocity. (b) The influence of the size of the flameholder in producing turbulence remains evident in the flame since the intensity increases with characteristic dimension of the baffle. The trend is not nearly as pronounced as in cold flow, however. For the latter case, the intensity changes by a factor of about 1.5 in going from 1.25-cm to 2.50-cm and from 2.50-cm to 3.75-cm baffles, while in the flame the intensity is practically the same for

TABLE III. Experimental results in flames stabilized on various baffles.[a]

Baffle	U (m/sec)	x (cm)	$\langle y^2\rangle_{Av}$ (cm$^2\times10^3$)	$(\langle y^2\rangle_{Av})_{mol.}$ (cm$^2\times10^3$)	$(\langle y^2\rangle_{Av})_{turb.}$ (cm$^2\times10^3$)	$[(\langle y^2\rangle_{Av})_{turb.}]^{\frac{1}{2}}/x$
1.25 cm T.R.	87	1.47	14.5	8.7	5.8	0.052
		1.73	18.1	10.2	7.9	0.051
1.25 cm V.G.	84	1.52	15.5	9.0	6.5	0.053
		1.78	21.0	10.5	10.5	0.058
		2.03	23.2	12.0	11.2	0.052
1.25 cm C.R.	92	1.57	15.8	7.8	8.0	0.057
		1.83	19.1	9.1	10.0	0.055
		2.08	22.8	10.4	12.4	0.054
2.50 cm T.R.	82	1.37	16.1	9.1	7.0	0.061
		1.63	19.5	10.8	8.7	0.057
		1.96	25.6	13.0	12.6	0.057
		2.14	29.0	14.2	14.8	0.057
2.50 cm V.G.	84	1.52	16.1	9.0	7.1	0.055
		1.78	19.9	10.5	9.4	0.054
		2.03	24.8	12.0	12.8	0.056
2.50 cm C.R.	83	1.58	18.4	8.8	9.6	0.062
		1.83	21.3	10.2	11.1	0.058
		2.08	26.4	11.6	14.8	0.059
3.75 cm T.R.	79	1.63	23.6	10.0	13.6	0.072
		1.88	29.4	11.6	17.8	0.071
		2.13	35.4	13.1	22.3	0.070
3.75 cm V.G.	78	1.68	22.4	10.1	12.3	0.066
		1.93	29.0	11.6	17.4	0.068
		2.18	34.4	13.1	21.3	0.067
3.75 cm C.R.	84	1.63	22.8	9.4	13.4	0.071
		1.85	26.1	10.7	15.4	0.067
		2.13	34.4	12.3	22.1	0.070

[a] T.R. =triangular rod; V.G. =V-type gutter; C.R. =circular rod.

TABLE IV. Comparison of flame and cold flow turbulence.[a]

Baffle	Flame			Cold flow		
	U (m/sec)	$(\langle v^2\rangle_{Av})^{\frac{1}{2}}/U$	$(\langle v^2\rangle_{Av})^{\frac{1}{2}}$ (cm/sec)	$U_{corrected}$ (m/sec)	$(\langle v^2\rangle_{Av})^{\frac{1}{2}}/U$	$(\langle v^2\rangle_{Av})^{\frac{1}{2}}$ (cm/sec
1.25 cm T.R.	87	0.052	450	37	0.065	240
1.25 cm V.G.	84	0.054	450	35	0.067	230
1.25 cm C.R.	92	0.055	500	32	0.064	210
2.50 cm T.R.	82	0.058	480	35	0.096	340
2.50 cm V.G.	84	0.055	460	32	0.096	310
2.50 cm C.R.	83	0.060	500	30	0.096	290
3.75 cm T.R.	79	0.071	560	31	0.154	480
3.75 cm V.G.	78	0.067	520	31	0.178	550
3.75 cm C.R.	84	0.069	580	31	0.154	480

[a] T.R. =triangular rod; V.G. =V-type gutter; C.R. =circular rod.

the first increment in baffle size and changes by a factor of about 1.2 for the second increment. This is undoubtedly a manifestation of the current belief that a bluff object with a flame stabilized on it becomes more effectively "streamlined" and exhibits less tendency to shed eddies than when the flame is absent.[16]

In order to determine what effect, if any, the presence of a flame has upon the turbulence level of a stream, ideally one would like to be able to compare measurements taken under exactly the same mean flow conditions with and without combustion. Specifically, it would be desirable to match mean stream velocities throughout the system in both cases, which is an obvious impossibility in a ducted flame of this sort. If the velocity of the approach flow to the flameholder is matched, then at the point of turbulence measurement the value of U will, of course, be greater with the flame than without due to the density decrease accompanying combustion. Therefore, even if nothing at all happened to the fluctuating turbulence components of the flow in passing through the flame front, the intensity measured as $(\langle v^2\rangle_{Av})^{\frac{1}{2}}/U$ by the diffusion method would have to be smaller in the flame than in cold flow. As previously pointed out, the invariance of $(\langle v^2\rangle_{Av})^{\frac{1}{2}}/U$ with U observed in cold flow would not be expected to hold when U is varied only by a local acceleration downstream of the turbulence producing elements in the flow.

Under the circumstances, it appears that the best one can do is as follows: Examine the flame and no-flame cases under the same flow conditions up to the flameholder, so that everything including the turbulence level is the same to the point where the flame begins. Then a comparison of the *absolute value* of the turbulent velocity fluctuations $(\langle v^2\rangle_{Av})^{\frac{1}{2}}$ in the two cases (instead of $(\langle v^2\rangle_{Av})^{\frac{1}{2}}/U$) should reflect any changes brought about by the presence of the flame. Such a comparison of the data is given in Table IV. As mentioned earlier, it was not convenient to carry out the two sets of measurements with the approach velocity to the flameholder exactly matched, so it was necessary to correct for this. Since the total mass flow through the duct was constant, the continuity condition was applied by multiplying the measured cold flow mean stream velocity in each case by the static pressure ratio P_{cold}/P_{flame}. This gave values of $U_{corrected}$, which are the mean stream velocities which would have existed at the point of measurement in cold flow at the same static pressure found in the corresponding flame case. The validity of this correction was proven by actually measuring the cold flow velocities at two different static pressures, 32.0 cm Hg and 52.4 cm Hg, corresponding roughly to the pressures encountered in the cold flow and flame runs, respectively. At 32.0 cm the measured U was 52 m/sec. At 52.4 cm the value of $U_{corrected}$ would be $(32.0/52.4)52 = 32$ m/sec, while the measured value was 33 m/sec.

With the values of $U_{corrected}$ thus obtained, and the property that $(\langle v^2\rangle_{Av})^{\frac{1}{2}}/U$ is independent of U in the range of cold flow velocities which are of interest, one can then compute absolute values of $(\langle v^2\rangle_{Av})^{\frac{1}{2}}$ for cold flow under the same approach conditions found with the flames, and compare them with the directly measured values of $(\langle v^2\rangle_{Av})^{\frac{1}{2}}$ found in the flames. This is what has been done in Table IV. The intensity of turbulence for each baffle was taken to be the average value of $[\langle(\langle y^2\rangle_{Av})_{turb.}\rangle]^{\frac{1}{2}}/x$ measured at the various distances x, simply to arrive at a single number characteristic of each baffle.

The data of Table IV, while admittedly providing only a rather rough comparison between turbulence with and without a flame, show several interesting things. One notes that for the 1.25-cm baffles the ratio $(\langle v^2\rangle_{Av})^{\frac{1}{2}}_{flame}/(\langle v^2\rangle_{Av})^{\frac{1}{2}}_{cold}$ is of the order of 2, while for the 3.75-cm baffles the two are approximately equal. This presumably is because the turbulence produced by the baffle is greatly diminished upon flame attachment, so that the quantity $(\langle v^2\rangle_{Av})^{\frac{1}{2}}_{cold}$ can actually become equal to $(\langle v^2\rangle_{Av})^{\frac{1}{2}}_{flame}$ with increasing baffle size. That this is so is further indicated by some measurements taken with a 5.0-cm baffle (not listed here because the flow regime was quite badly upset and the profiles rather skewed), for which $(\langle v^2\rangle_{Av})^{\frac{1}{2}}_{cold}$ definitely exceeded $(\langle v^2\rangle_{Av})^{\frac{1}{2}}_{flame}$.

[16] Williams, Hottel, and Scurlock, *Third Symposium on Combustion, Flames, and Explosion Phenomena* (The Williams and Wilkins Company, Baltimore, Maryland, 1949), p. 31.

For indications of flame-generated turbulence, the most reliable data are those for the smallest baffles. It was shown earlier that in cold flow the 1.25-cm baffles gave a turbulence intensity not very different from that with no baffle at all, so that a comparison of $(\langle v^2\rangle_{Av})^{\frac{1}{2}}_{\text{flame}}$ and $(\langle v^2\rangle_{Av})^{\frac{1}{2}}_{\text{cold}}$ for this case should be one from which the flameholder disturbance itself is fairly completely eliminated. From Table IV, then, one would conclude that the turbulence level in the flame was roughly twice that under corresponding cold flow conditions. It must be borne in mind, however, that the total elapsed time during which the turbulence can undergo decay as the flow moves from the position of the flameholder to the point of measurement of the turbulence is considerably less with the flame present than without due to the acceleration during combustion. This would tend to make $(\langle v^2\rangle_{Av})^{\frac{1}{2}}_{\text{flame}}$ somewhat higher than $(\langle v^2\rangle_{Av})^{\frac{1}{2}}_{\text{cold}}$ even in the absence of any other flame influence. On the other hand, the higher kinematic viscosity of the combustion gases compared to the cold gas ought to increase the decay rate of turbulence in the flame, which would tend to offset the effect mentioned above. In such a complicated flow as we are dealing with it would be futile to try even to estimate the relative importance of these two opposing effects. It seems clear, however, that the present data indicate some increase in transverse turbulence intensity brought about by the flame, but that the change is perhaps not as pronounced as has sometimes been expected. Certainly if the intensity were increased several fold it would have been easily measurable by this method, and this has not proven to be the case under the present conditions.

It would have been desirable to extend the measurements to several other points within the flame—nearer the flameholder, various other points on the y axis, etc. A limited series of profiles were taken with the helium source at the same distance downstream from the baffle but offset 2.5 cm along the y axis from the center of the duct. This put the region of measurement right in the center of the diffuse, luminous flame front. Neither cold flow nor flame results were appreciably different from those taken at the duct center. Flame measurements in this region were not very satisfactory, however, because the mean velocity and temperature change too rapidly over the distance required to get a diffusion profile.

VIII. CONCLUSIONS

Results of this work may be summarized briefly as follows:

(1) It has been shown that transverse turbulence intensity of fairly large magnitude (roughly 4 percent or more) may be successfully measured in a baffle-stabilized flame and in cold flow by the helium diffusion method, using thermal conductivity detection.

(2) The measured helium distributions are Gaussian within experimental error, and up to the maximum distance x used ($\sim$2 cm) exhibit the behavior expected of diffusion times small compared to the Lagrangian time scale of turbulence.

(3) The technique is quite sensitive to small changes in intensity of turbulence, but gives absolute magnitudes for this quantity which are probably too high (especially at the lower intensities) due to the flow disturbance of the source.

(4) In cold flow, the intensity $(\langle v^2\rangle_{Av})^{\frac{1}{2}}/U$ at a fixed point in the flow is essentially independent of U over the range examined.

(5) In cold flow, the intensity downstream of a baffle increases with the characteristic dimension of the baffle but is independent of its geometry.

(6) With a flame stabilized on the baffle, the above effect of baffle dimension is drastically reduced.

(7) At a fixed distance downstream of the baffle, the absolute turbulence intensity $(\langle v^2\rangle_{Av})^{\frac{1}{2}}$ is not very different whether a flame is present or not—under the conditions of these experiments.

IX. ACKNOWLEDGMENTS

Many members of the staff of the Applied Physics Laboratory have contributed to this work. Special mention is due of the invaluable assistance rendered by Mr. S. E. Matthews in the handling of instrumentation and gathering of experimental data. The author is indebted to Dr. F. N. Frenkiel for originally suggesting the problem and for advice and criticism, to Dr. J. J. Zelinski for his aid in initiating the program, and to Dr. W. H. Avery for his interest and encouragement.

Measurement of Temperature Distribution in a Low-Pressure Flat Flame

RAYMOND FRIEDMAN AND EDWARD BURKE
Westinghouse Research Laboratories, East Pittsburgh, Pennsylvania

(Received September 8, 1953)

The temperature distribution in a very lean, flat propane-air flame was measured by the thermocouple method, at a pressure of 0.0594 atmos. The temperature change occurred in a zone about 3 cm thick. Wall-quenching was minimized by employing a burner tube diam of 25 cm. The thermocouple was made from 12-micron wire, coated with ceramic to avoid catalytic effects. One hundred experimental traverse points were obtained, with a standard deviation of ± 0.016 cm.

The burning velocity was also measured, and was found to vary with the inverse 0.30 power of pressure. This is in agreement with Egerton and Sen's result, obtained over a more limited range of pressure.

The temperature pattern was analyzed mathematically to obtain the pattern of heat release rate, taking into account the variation with temperature of thermal conductivity and specific heat. It was found that the heat release began at 300°C, attained a maximum value of 1.2 cal/cm³-sec at 1100°C, was nowhere negative, and was finite over a zone about 2 cm thick. The maximum temperature of the flame was 1332°C. The result obtained for the "ignition point" was found to be extremely sensitive to the exponent giving the temperature dependence of the thermal conductivity. Some calculations relating to the chemical kinetics of the flame are described.

I. INTRODUCTION

We are concerned here with the steady-state burning of a uniform gaseous mixture in one-dimensional laminar flow. A knowledge of the temperature distribution in a flame of this idealized type would give insight into the chemical kinetics of the processes by which thermal energy is released in the flame. The interrelationship between the temperature pattern and the heat release rate has been analyzed in detail by the present writers, in a purely theoretical study.[1]

Recently, the problem of measuring the temperature distribution has been approached from a number of directions. Several workers[2,3] have attempted to measure the gradient of refractive index in the flame; this approach is limited, however, by the high degree of flatness which the flame must possess over its entire extent, if fine details of the temperature distribution are to be observed. Others[4,5] have measured the curving streamlines through a flame inclined to the direction of initial flow, using dust particles as tracers. Analysis of these streamlines yields the temperature pattern, if a somewhat questionable assumption is made concerning the component of the gas velocity parallel to the flame front. There is also a question of how well the particles follow the gas flow; for instance, the radiometer force[6] on the particles may cause a lag.

Klaukens and Wolfhard[7] have used a thermocouple for exploring temperature distribution in a flame. Their techniques were refined in several important respects by Friedman.[8] The present investigation constitutes a further refinement of the thermocouple method.

Let us consider in some detail the possibility of obtaining a reliable temperature traverse by this method. The first criterion for a significant experiment is one of relative sizes. The burner diameter must be large compared with the flame thickness (otherwise quenching effects occur and the flame is not one-dimensional); the flame thickness must be large compared with the thermocouple size (otherwise the local velocity and, hence, temperature will be perturbed); and finally, the thermocouple should be large compared with the mean free path (otherwise the heat transfer to the couple becomes poor and of uncertain magnitude). A second criterion is that the radiation corrections which must be applied to the measured temperatures should be either fairly small or known to high precision. A third criterion is that there should be no catalytic heating at the thermocouple surface.

In the earlier investigation by one of the present authors,[8] an attempt was made to satisfy these criteria as nearly as possible, while studying a very lean propane-air flat flame at atmospheric pressure, with a burner of 10-cm diameter. In that study, however, even though the thermocouple bead was only about 0.0025 cm thick, there was some doubt as to whether this was sufficiently small to make the effect of the aerodynamic wake of the couple completely negligible. In the current investigation, the burner diameter has been increased to 25 cm and the absolute pressure reduced to about 0.06 atmos; thus the flame is very much thicker than before. The distance from the 5 percent temperature rise point to the 95 percent temperature rise point is now about 2 cm. This is about 300 times the thickness of the present thermocouple bead, and about 1600 times the thickness of the thermocouple support wires;

[1] R. Friedman and E. Burke, J. Aeronaut. Sci. **18**, 239 (1951).
[2] (a) G. Dixon-Lewis, Trans. Faraday Soc. **47**, 1106 (1951). (b) G. Dixon-Lewis, *Fourth Symposium on Combustion* (Williams and Wilkins, Baltimore, 1953), pp. 263–67.
[3] J. H. Burgoyne and F. Weinberg, *Fourth Symposium on Combustion* (Williams and Wilkins, Baltimore, 1953), pp. 294–302.
[4] J. W. Andersen and R. S. Fein, J. Chem. Phys. **17**, 1268 (1949).
[5] Fristrom, Prescott, Neumann, and Avery, *Fourth Symposium on Combustion* (Williams and Wilkins, Baltimore, 1953), pp. 267–74.
[6] R. L. Saxton and W. E. Ranz, J. Appl. Phys. **23**, 917 (1952).
[7] H. Klaukens and H. G. Wolfhard, Proc. Roy. Soc. (London) **A193**, 512 (1948).
[8] R. Friedman, *Fourth Symposium on Combustion* (Williams and Wilkins, Baltimore, 1953), pp. 259–63.

therefore, the wake can hardly introduce any appreciable error, as the discussion in the earlier paper shows.

The apparatus and technique for making temperature traverses are described in detail in the following sections. Then the data are analyzed to obtain the variation of heat release rate through the flame.

II. APPARATUS

Figure 1 shows the flat-flame burner apparatus which was built for this investigation. The burner tube contains several wire screens (0.033-cm wire diam, 23 percent open area), which produce a uniform gas velocity distribution. The propane (Matheson, 99 percent purity) and air (0.5 percent water vapor by volume) were supplied by a critical-flow system similar to that described by Andersen and Friedman.[9] A water-cooled copper plate was located 10 cm above the burner rim (12 cm above the uppermost screen). A ring of holes was drilled in this plate as shown in the drawing. In the course of the study, several other hole distributions were tried, but the flames were neither as flat nor as free from vibration as with the configuration shown. With a water-cooled copper plate above the flame instead of the stainless steel screen used in the earlier study,[8] one is able to minimize the radiative preheating of the lower screens which would otherwise occur.

The burner was enclosed in a water-cooled vacuum chamber. It was essential to keep the walls of the chamber quite smooth in the vicinity of the flame; this necessitated special baffles to cover the igniter and traverse tube openings, as well as windows flush with the wall. The igniter, a hydrogen torch, was itself ignited by a spark plug. The burner pressure was controlled by the degree of throttling in the exhaust line to the vacuum pump.

The thermocouple was made of platinum and platinum plus 10 percent rhodium wire, 0.0012-cm diam, by gas-welding, and was coated with NBS Ceramic Coating A-418, to prevent catalytic effects, described earlier.[8] These fine wires were attached to larger wires supported by a movable tube as shown in Fig. 1. The fine

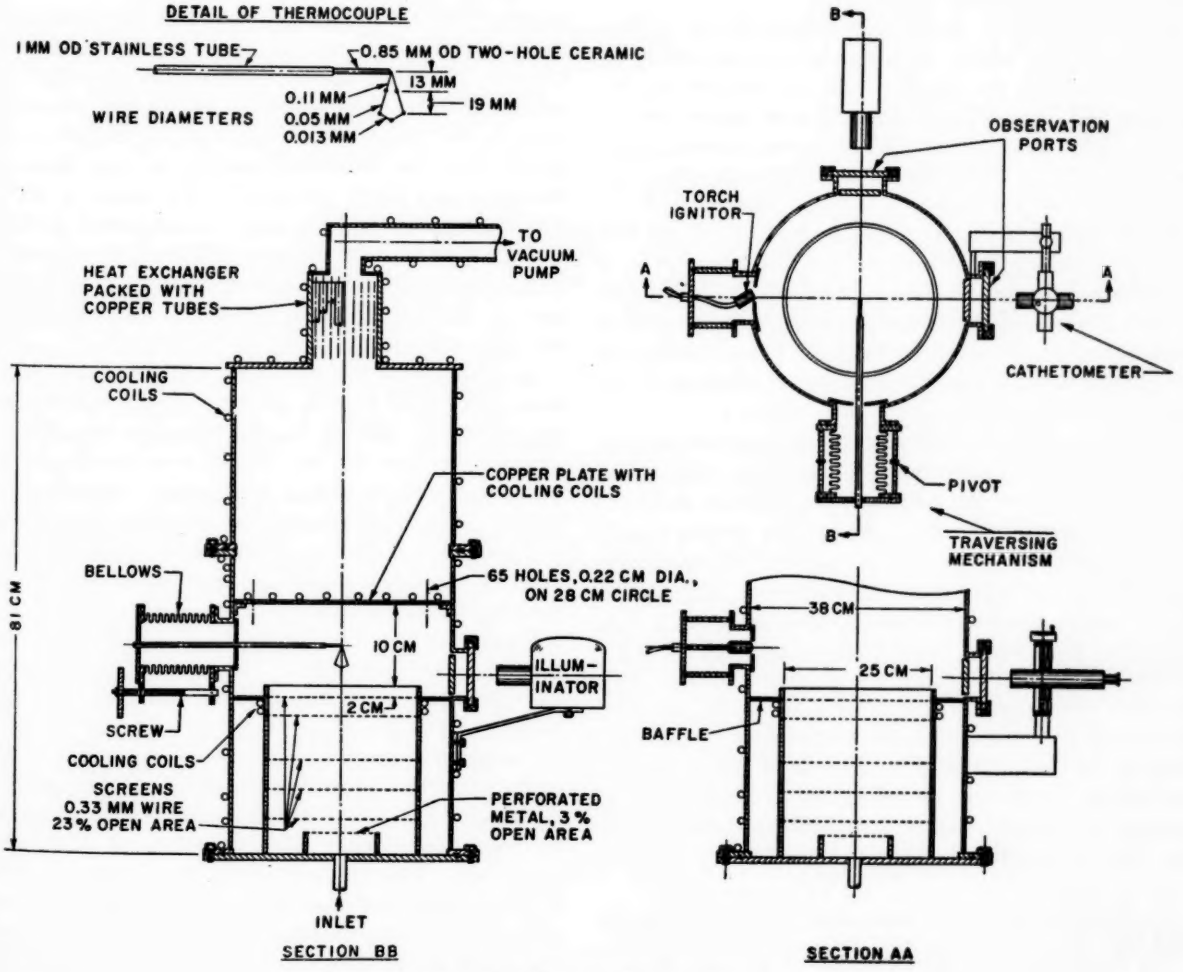

FIG. 1. Flat-flame burner apparatus.

[9] J. W. Andersen and R. Friedman, Rev. Sci. Instr. **20**, 61 (1949).

wires approaching the bead were arranged to be nearly parallel to the flame front. The support tube was always several cm above the region being traversed. This tube, consisting of a two-hole ceramic insulator inside a stainless-steel sheath of 0.10-cm diam, could be moved vertically by a mechanism involving a flexible bellows, pivots, and a lead screw.

The positions of the thermocouple bead and the beginning of the luminous zone of the flame (*vide infra*) were observed with a cathetometer equipped with a 5× eyepiece and an objective lens of 10-cm focal length and 0.63-cm aperture.

III. TRAVERSE MEASUREMENTS

A propane-air mixture was selected for study because of the large number of combustion investigations which have already been made with this system. A very lean flame was chosen, because near-stoichiometric flames would melt the thermocouple, and very rich propane-air flames are not flat, but cellular, as shown by Markstein.[10] The fact that lean flames are much thicker than stoichiometric flames facilitates a detailed determination of the temperature distribution.

Various shapes of flames are attainable on a flat-flame burner by minor variations of the apparatus or slight changes in the air-fuel ratio, as pointed out by Egerton and Thabet.[11] All our data were taken using a flame which was very nearly flat, only the extreme edges being turned up. The mass air-fuel ratio was 29.2, the pressure 0.0594 atmos, and the initial temperature 46°C. This set of conditions is outside of the flammability range determined for propane-air at this pressure in a 5-cm-diam tube by Di Piazza, Gerstein, and Weast.[12] Indeed, it was possible to burn even leaner flames at this pressure on the 25-cm-diam burner. These results are in agreement with a wall-quenching concept of flammability limits.[13]

The thermocouple temperature was continually recorded on a self-balancing potentiometer, which was recalibrated before and after each run. These temperatures were correlated with cathetometer measurements of the distance from the thermocouple to the upstream edge of the luminous zone of the flame. To obtain a datum point, the thermocouple was positioned by the traversing mechanism, and a rapid sequence of measurements was made alternately of the thermocouple position and the flame position. Direct telescopic observation of the thermocouple bead was necessary, since the readings of the calibrated lead screw of the traversing mechanism could not be relied on to give the bead position accurately enough, inasmuch as variable thermal distortion of the thermocouple lead wires occurred. Frequent observations of the flame position were required, because the thermocouple supporting structure when in certain positions slightly distorted the flame.

Although considerable effort was expended in achieving a combustion-chamber geometry which minimized the flame oscillations, there was a residual random vibration with a maximum amplitude of about ±0.02 cm and a "frequency" of about one cycle per sec. This showed up in the temperature trace on the recording potentiometer as a temperature fluctuation of varying amplitude in the different parts of the flame, the amplitude varying with the local temperature gradient. For each datum point, an average thermocouple temperature was correlated with the visual measurements of the flame position relative to the thermocouple bead.

For measuring the flame location, the telescope was set on the beginning of the intensely luminous zone, i.e., the underside of the visible flame. In preliminary runs it was found difficult for an observer to reproduce his measurements of the flame position with the desired precision, because of the flicker and the lack of distinctness of the beginning of luminosity. The reproducibility was improved by the adoption of "offset flame observations." Here the apparatus was modified to permit the telescope to be swung horizontally by approximately 4°, since the glow of the red-hot thermocouple wires interfered with observation of the flame, when both were in the same field of view. Furthermore, it was found that the measured location of the flame was dependent on slight changes in the vision of the observer. Accordingly, the room was completely darkened and the eyes of the experimenter were dark-adapted for 30 min before observations were begun. When illumination of the thermocouple bead was necessary, a dim red light was used.

As a check on the reliability of the measurements, data were taken by two different observers. At first it was especially difficult for the two observers to obtain identical settings on the flame, considerable practice being required to attain satisfactory reproducibility. Also, to preclude systematic errors arising from changes in the observers' vision, the points of a given run were taken in a random sequence rather than by proceeding straight through the flame.

Figure 2 is a plot of thermocouple reading *vs* distance normal to the flame front. (The cusp in the curve drawn through the points results from a change in scale.) Each point is based on a set of observations of the thermocouple bead and the flame (generally two of each) while the thermocouple was in a given position. An abscissa of zero thus corresponds to the bead being in coincidence with the beginning of the intense luminosity. The zone of intense luminosity was about 0.29 cm thick, and shaded off into dimmer regions both upstream and downstream of the flame. Especially on the downstream side, the dimmer luminosity persisted for a considerable distance. The presence of the dimmer luminosity was the result, in part, of the departure of

[10] G. H. Markstein, J. Aeronaut. Sci. **18**, 199 (1951).
[11] A. Egerton and S. K. Thabet, Proc. Roy. Soc. (London) **A211**, 445 (1952).
[12] Di Piazza, Gerstein, and Weast, Ind. Eng. Chem. **43**, 2721 (1951).
[13] R. Friedman and W. C. Johnston, J. Appl. Phys. **21**, 791 (1950).

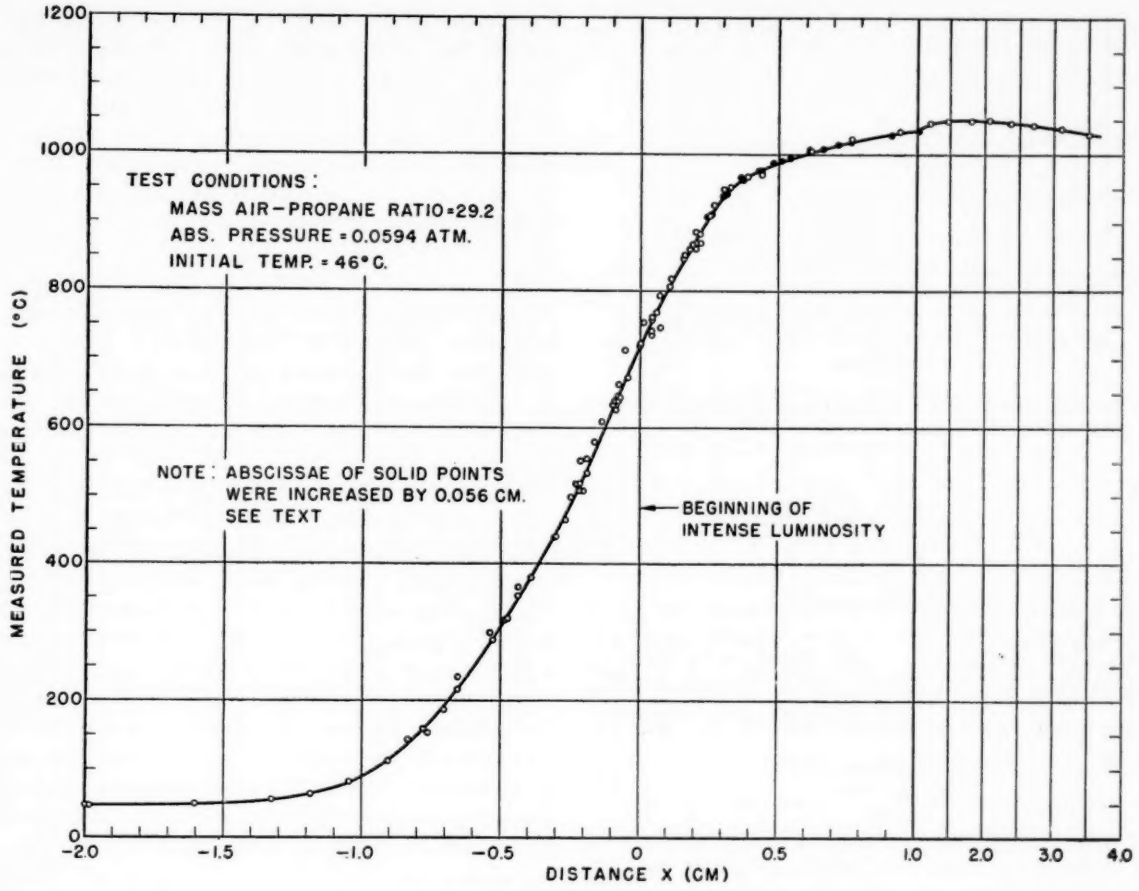

FIG. 2. Thermocouple traverse through flat flame.

the flame from perfect flatness and to the properties of the optical system. Because of these effects, it is possible that the observed position of the intensely luminous zone does not coincide precisely with its true position. However, the upstream boundary of this zone provided a convenient reference plane for the thermocouple positions.

A total of one hundred points was obtained; none was discarded in plotting Fig. 2. The standard deviation of the points from the curve between -1 cm and $+1$ cm (the region of greatest scatter) was computed and found to be ± 0.016 cm. The open points were obtained in two runs on different days. On a later occasion, the 18 solid points were obtained to determine more accurately the region of greatest curvature. Since it was not possible to obtain precisely the same test conditions, the abscissas of the solid points differed as a whole from the earlier curve by 0.056 cm. Accordingly, their abscissas were increased by this amount for plotting in Fig. 2.

IV. BURNING VELOCITY MEASUREMENTS

Before the measured temperature distribution in a flame can be analyzed to yield the heat release pattern, the burning velocity of the flame must be known. Therefore, burning velocity measurements of a series of propane-air flames at a mass air-propane ratio of 29.0 were made, at absolute pressures from 0.047 to 0.072 atmos, and an initial temperature of 46°C. The burning velocities were computed by dividing the volumetric flow at 46°C by the area of the flat flame on the 25-cm burner; this area was determined from flame photographs, the overhang of the flame relative to the burner and the departure from flatness at the edge being taken into account. The results, along with an atmospheric-pressure value taken from the previous study,[8] are plotted in log-log form in Fig. 3. From the slope, it is seen that the burning velocity varies inversely with the 0.30 power of the pressure. It is gratifying to note that this result agrees quite closely with that of Egerton and Sen,[14] who studied lean propane-air flames in the pressure range from 0.26 to 0.66 atmos, with a burner of 5.7-cm diam.

V. ANALYSIS OF DATA

Let Q (cal/cm³-sec) be the heat-release rate at any point in the flame. The steady-state energy balance

[14] A. Egerton and D. Sen, *Fourth Symposium on Combustion* (Williams and Wilkins, Baltimore, 1953), pp. 321–28.

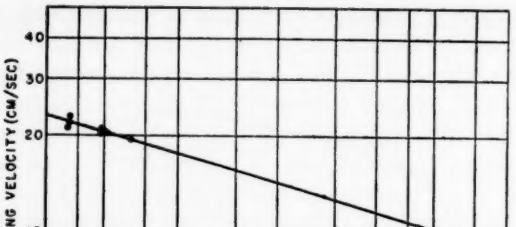

FIG. 3. Burning velocity of a lean propane-air flame as a function of pressure. (46°C, mass air-propane ratio = 29.0.)

yields

$$Q = v_u \rho_u C_p \frac{dT}{dx} - \frac{d}{dx}\left(\lambda \frac{dT}{dx}\right). \quad (1)$$

Here, x is distance normal to the flame front (cm), T is local temperature (°C), v_u is burning velocity (cm/sec), ρ_u is density of unburned gas (gm/cm³), λ is local thermal conductivity (cal/cm-sec-°C), and C_p is local effective specific heat at constant pressure (cal/gm-°C), given by

$$C_p = \sum_i G_i C_{pi}, \quad (2)$$

where G_i is the fraction of the mass rate of flow across plane x which is due to component i. In general, the G_i are difficult to evaluate because they are influenced by diffusion as well as by chemical reaction.[15] In this particular case, however, about 86 mole percent of the gas consists of nitrogen and excess oxygen which pass through the flame unchanged. Therefore, very little error is introduced by the assumption that the specific heat of the small reacting portion of the gas is the same as that of the unreacting portion. With this assumption, the G_i need not be evaluated.

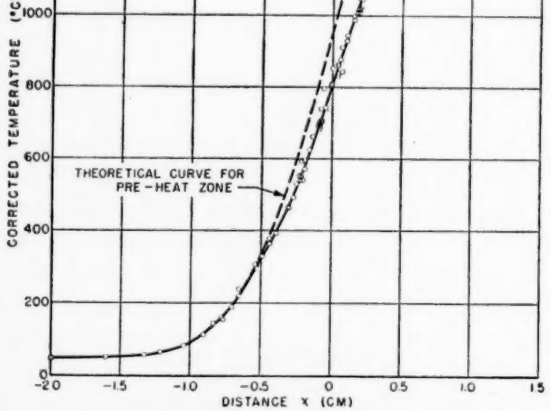

FIG. 4. Corrected temperature *vs* distance through flame.

[15] Hirschfelder, Curtiss, and Campbell, J. Phys. Chem. **57**, 403 (1953), as well as earlier papers by this group.

In the energy balance leading to Eq. (1), we have taken the terms due to the kinetic energy of the gas and radiative heat transfer to be negligible. It is easy to demonstrate that these terms are always very small for non-detonative flames free from solid particles.

Figure 2 gives $T(x)$ in the form of thermocouple readings uncorrected for radiation error. The measured maximum temperature was 1051°C, which is 281° lower than the calculated adiabatic flame temperature. It is, therefore, important to determine whether this difference is consistent with the result of heat transfer calculations.

The thermocouple bead (heavily coated with ceramic) was approximately a cylinder of 0.0066-cm diam and 0.023 cm long. (Traverses were also made with other thermocouples, yielding results consistent with these.) The Reynolds number based on the diam of the cylinder in the hot gas is about 0.02. If we use King's equation,[16] a temperature difference of the same order of magnitude as the difference between the calculated adiabatic and the measured maximum temperature is obtained. However, since (a) the bead corresponds only very roughly to an infinite cylinder, (b) the cylinder diam is only 8 times the mean free path, and (c) the emissivity of the coated bead is not known precisely, the heat transfer calculation can hardly be considered exact. Therefore, the following radiation correction formula was used:

$$\Delta T = (\Delta T)_{\max}\left(\frac{T+273}{T_{\max}+273}\right)^4.$$

Here, T is the measured temperature, $(\Delta T)_{\max} = 281$°C, $T_{\max} = 1051$°C, and ΔT is the difference in temperature between the thermocouple and the gas.

Another, rather small, correction was applied to $T(x)$. Figure 1 shows that the temperature drops slowly in the region beyond the maximum; this is probably the result of radiation losses from the gas, the emitters being CO_2 and H_2O. If it is assumed that this gas radiation also occurs in the reaction zone, at a rate proportional to the fourth power of the absolute gas temperature, an appropriate correction to $T(x)$ can be made.

The corrected data points giving $T(x)$ were plotted with high precision (Fig. 4), and were carefully fitted with a smooth curve. A theoretical curve for the preheat zone ($Q=0$) is superimposed. The derivation of the equation for this curve, which takes into account the variation of thermal properties with temperature, has been given in the earlier paper by one of the present authors.[8] It is necessary to use the measured burning velocity to obtain the theoretical preheat curve; since

[16] L. V. King, Trans. Roy. Soc. (London) **A214**, 373 (1914).

the theoretical curve agrees with the measured $T(x)$ in the low-temperature range, this constitutes a demonstration that the burning velocity measurement is consistent with the $T(x)$ measurement. The agreement of the theoretical curve with the data in the preheat zone may be observed more clearly in the semilogarithmic plot of Fig. 5.

The theoretical preheat curve is seen from Fig. 4 to deviate from the measured $T(x)$ above about 300°C. From this region onward, the smooth curve through the data points was analyzed by means of Eq. (1), dT/dx being obtained by a finite-difference method. Intervals of $dx=0.05$ cm were chosen, and corresponding values of $T(x)$ obtained from the smooth curve. Values of C_p and λ were obtained at each of these temperatures, λ being taken from the NBS-NACA tabulation for air,[17] with extrapolation above 1000°K by linear projection of the tabulated values on a log-log plot. Then, the two terms on the right-hand side of Eq. (1) were evaluated

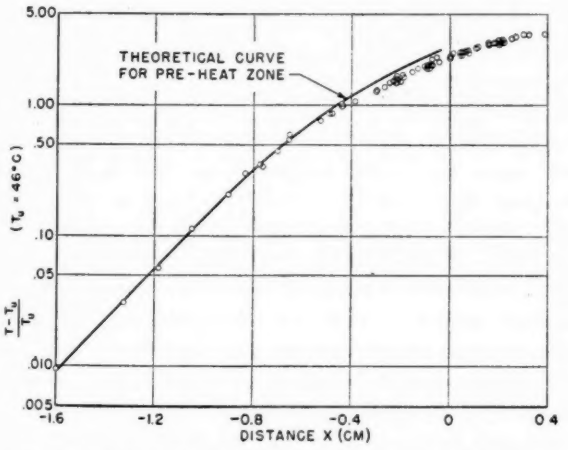

FIG. 5. Semilogarithmic plot of temperature *vs* distance.

at each interval, the differentials being treated as finite differences.

The results are plotted in Fig. 6. The vertical distance between the two curves is the local heat-release rate Q and the area between the two curves is the integrated heat-release rate

$$\int_{-\infty}^{\infty} Q dx.$$

The value of this integrated heat-release rate can be calculated separately, from the heat of combustion of propane (488 500 cal/mole) and the measured burning velocity; a value of 0.483 cal/cm²-sec is then obtained. When the area between the two curves of Fig. 6 is measured, a value of 0.486 cal/cm²-sec is obtained. This close agreement merely shows that the calculations are internally consistent.

In Fig. 7, Q is plotted directly against x. On the same curve, the fraction of the total heat release that has

[17] *The NBS-NACA Tables of Thermal Properties of Gases* (National Bureau of Standards, Washington, 1950).

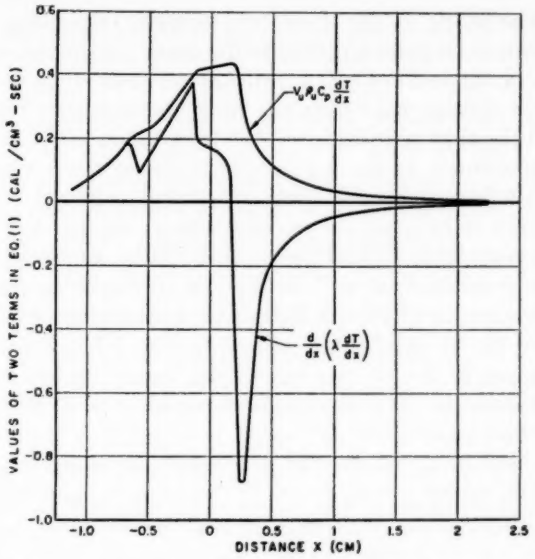

FIG. 6. Two terms in Eq. (1) as evaluated by numerical differentiation of $T(x)$.

occurred from minus infinity up to any plane x is also plotted against x. The significance of these results is discussed in the next section.

VI. DISCUSSION OF RESULTS

The "ignition point," i.e., the temperature at which heat release begins, is often considered to be a useful concept in the analysis of the combustion wave. From Figs. 4 and 5 we see that the measured $T(x)$ curve begins to deviate from the theoretical preheat curve above about 300°C, and Figs. 6 and 7 show that heat release begins in this neighborhood. This is 0.7 cm before the beginning of the intensely luminous zone, and Fig. 7 shows that 14 percent of the heat release has occurred in this preluminous zone ($T<800$°C). It is of interest to know how much of this heat release is real and how much is the result of errors of analysis.

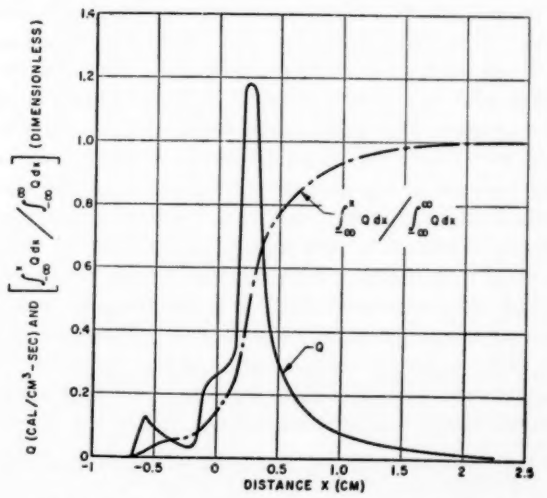

FIG. 7. Instantaneous and integrated heat release as functions of distance through flame.

The shape of the theoretical preheat curve may be shown to be quite sensitive to the nature of the assumed law of variation of λ/C_{pm} with temperature. (C_{pm} is the mean specific heat over the range between the initial and the local temperature.) We have taken λ/C_{pm} to be proportional to the $\frac{3}{4}$ power of absolute temperature, which is in extremely close agreement with the NBS-NACA tabulation of recommended values for air. However, this $\frac{3}{4}$-power law could still be incorrect, for two possible reasons. The thermal conductivity measurements on which the NBS-NACA tabulation is based may be in substantial error, or the 2.2 percent of propane in the air may have a disproportionately large influence on the temperature dependence of λ. Neither of these possibilities, of course, is very likely. However, we have made an analysis which shows that, if λ/C_{pm} is taken to vary with the 0.93 power of absolute temperature instead of the 0.75 power, the theoretical preheat curve obtained in this manner would agree with the measured $T(x)$ up to about 1000°C. For powers between 0.75 and 0.93, "ignition points" between 300 and 1000°C may be obtained. We may conclude that the temperature at which reaction begins cannot be specified with great confidence.

Now, let us consider the zone of intense reaction. The maximum value of Q, which is 1.2 cal/cm³-sec, occurs 0.25 cm beyond the beginning of intense luminosity, and at a temperature of 1100°C. At this plane, 48 percent of the heat release has occurred.

The above value for $Q_{\max}$ may be used to establish an order of magnitude for the activation energy of the combustion process. From kinetic theory, we may estimate the rate of binary collisions at 1100°C between O_2 molecules and fuel molecules, or molecules resulting from partial degradation of the fuel. Upon assuming a reasonable heat of reaction for this step, e.g., 100–200 kcal, we may calculate the fraction of the above kind of collisions which must lead to reaction, in order to account for the observed $Q_{\max}$. This fraction comes out to be $\sim 1/50\,000$. Now, on the basis of the collision theory of second-order reactions, if we assume a steric factor of unity, the corresponding activation energy is $\sim$30 kcal; for a steric factor of 0.1, the activation energy is $\sim$23 kcal. This calculation cannot be considered to yield anything more than an order of magnitude, not only because of the assumptions implied by the above method of calculation, but also because the burning velocity is known to vary with pressure (Fig. 3), clearly showing that the rate-limiting step cannot be a simple second-order reaction.[18] Still, it is encouraging that the activation energy obtained in this novel fashion is of the same order of magnitude as that computed from Dugger and Heimel's measurements[19] of temperature dependence of burning velocity.

[18] J. O. Hirschfelder and C. F. Curtiss, J. Phys. Colloid Chem. 55, 774 (1951).

[19] G. L. Dugger and S. Heimel, NACA Technical Note 2624 (February, 1952).

Now, let us turn our attention to the latter part of the reaction zone. We recall the observation that the brilliance of the luminosity appeared to decrease sharply at $x=0.29$ cm; Fig. 7 shows that only 55 percent of the heat release has occurred up to this plane. The reaction does not go to completion until more than 2 cm beyond the beginning of the luminous zone.

These observations suggest that the combustion may occur in two distinct stages:

$$C_3H_8 \xrightarrow{3.5\,O_2} 3CO + 4H_2O \xrightarrow{1.5\,O_2} 3CO_2 + 4H_2O.$$

Thermochemical data show that 58.5 percent of the total heat evolution for this reaction sequence occurs in the first stage. From Fig. 7, we find that this corresponds to $x=0.30$ cm, which is essentially at the end of the intensely luminous zone (in which the main emitters are presumably C_2 and CH). Beyond this point, then, it seems possible that the heat release is due to combustion of CO. Gas sampling in this region would be informative.*

VII. SUMMARY AND CONCLUSIONS

The temperature distribution in a lean, flat propane-air flame has been measured by the thermocouple method, at a pressure of 0.0594 atmos, an initial temperature of 46°C, and a mass air-fuel ratio of 29.2. The thickness of the zone of rapid temperature change was found to be of the order of 2 cm. Techniques were sufficiently refined so that the standard deviation of the temperature traverse points was ± 0.016 cm. The temperature pattern was analyzed mathematically to obtain the pattern of heat-release rate Q.

It was found that Q has its maximum value, 1.2 cal/cm³-sec, near the end of the intensely luminous zone; this magnitude was shown to be consistent with chemical kinetic considerations. Nowhere was Q negative; i.e., there were no regions in this flame where absorption of heat (due to dissociation of fuel or combustion products) predominated over exothermic reactions. An appreciable portion of the heat release occurred beyond the intensely luminous zone.

The analysis showed that the temperature at which heat release begins cannot be determined with high precision, even with a very reliable temperature traverse, unless the thermal conductivity λ of the gas is known to great accuracy. On the basis of a $\frac{3}{4}$-power law for the temperature dependence of λ/C_{pm}, 300°C is obtained for the "ignition point," larger powers leading to much higher "ignition points;" on the basis of the beginning of intense luminosity, 800°C is obtained.

* *Note added in proof.*—A. Egerton [Fuel **31**, 385 (1952)], has reported experiments of Burgoyne and Hirsch showing that the oxidation of CO to CO_2 is inhibited by the presence of CH_4. This is consistent with the two-stage combustion model proposed here. We are currently engaged in further experiments along these lines.

Studies of Evaporation of Small Drops*

LOUIS MONCHICK† AND HOWARD REISS‡
Department of Chemistry, Boston University, Boston, Massachusetts
(Received November 5, 1953)

The rates of evaporation of small droplets of diamyl sebecate (average radius $R\sim10^{-4}$ cm) were measured in a Millikan oil-drop chamber, and observed to obey a law of the form $dR/dT=a/(1+bR)$ which has been predicted by the theories of Fuchs and Frisch and Collins. Using a nonequilibrium distribution function of the velocities, the relationship has been rederived in a more rigorous fashion (over a limited range of conditions). Certain corrections in the constants a and b are introduced, and the validity of the Fuchs theory in this range of conditions is demonstrated. Using the formulation of Frisch and Collins, the law may be derived in the same form, subject to certain approximations.

An empirical form of the Stokes-Cunningham law for the limiting velocity of fall in a dilute medium has been obtained for dicapryl sebecate in air.

I. INTRODUCTION

LANGMUIR[1] assumed that the rate of evaporation of small drops was determined by the diffusion of vapor away from the drop. As a boundary condition he supposed that the density of vapor at the drop surface was maintained at the value characteristic of equilibrium for the temperature in question. In this manner he arrived at the result, subsequently confirmed by experiment, that the rate of diminution of surface should be invariant in time.

It soon became evident that Langmuir's rule was not at all general, being inadequate in circumstances such that the drop radius and mean free path of a diffusing vapor molecule were comparable quantities. The origin of the difficulty lies in the fact that in the steady state of spherically symmetric Fick's law diffusion, the concentration gradient at the drop varies inversely with the radius square. This gradient furnishes the driving force for the removal of vapor molecules, and it is evident that for small drops the evaporation rate must be quite large. Under these conditions, the drop is not able to maintain an equilibrium vapor concentration, even at its own surface.

It therefore would seem to be a more reasonable procedure to estimate the flux of molecules at the surface by a kinetic or stochastic theory, and obtain a boundary condition in terms of the concentration and its gradients. This was done in an approximate manner by Fuchs[2] and Bradley, Evans, and Whytlaw-Gray.[3] The method they used was actually an application of Meyer's simplified "mean free path" theory.[4] They supposed that all molecules impinging on a spherical drop, of radius R, came on the average from a concentric spherical shell, $R+\Delta$ in radius (Δ is of the order of one mean free path). The concentration of vapor at $r=R+\Delta$ (assuming spherical symmetry) can be represented by n_1^*, a value eventually to be eliminated from the analysis. In the following

$$\nu=(kT/2\pi m_1)^{\frac{1}{2}} \tag{1.1}$$

is the rate computed from a Maxwell distribution, at which vapor molecules strike unit area of surface. k is the Boltzmann constant, T, the absolute temperature, and m_1, the molecular mass of a vapor molecule.

The rate at which molecules leave the shell and condense on the surface is given by[3]

$$\alpha_0\nu n_1^*, \tag{1.2}$$

where α_0 is the condensation coefficient. To the same degree of approximation, molecules leaving the surface will travel a distance Δ before colliding. Therefore the rate at which they leave the surface and reach the shell $r=R+\Delta$ is

$$\alpha_0\nu n_1^0, \tag{1.3}$$

where n_1^0 is the equilibrium value of the vapor concentration. The net rate of arrival is

$$4\pi R^2\alpha_0\nu(n_1^0-n_1^*). \tag{1.4}$$

In the steady state of Fick's law diffusion (with $n_1=0$ at $r=\infty$)

$$n_1=\frac{\gamma}{r}, \tag{1.5}$$

$$n_1^*=\gamma/R+\Delta, \tag{1.6}$$

where γ is a constant. The net flux at $R+\Delta$, on application of Ficks law, is

$$-4\pi(R+\Delta)^2D(\partial n_1/\partial r)_{R+\Delta}=4\pi D\gamma, \tag{1.7}$$

where D is the diffusion coefficient. Equating (1.4) to (1.7) serves to determine γ.

The rate of change of radius of an evaporating drop is given by

$$dR/dt=m_1D(\partial n_1/\partial r)_R/\rho, \tag{1.8}$$

* Supported in part by the Air Force Cambridge Research Center.

† Based on a dissertation for the degree of Doctor of Philosophy at Boston University.

‡ Present address: Bell Telephone Laboratories, Murray Hill, New Jersey.

[1] I. Langmuir, Phys. Rev. **12**, 368 (1918).
[2] N. Fuchs, Physik. F. Sowjetunion **6**, 225 (1934).
[3] Bradley, Evans, and Whytlaw-Gray, Proc. Roy. Soc. (London) A198, 226 (1949).
[4] S. Chapman, Phil. Mag. **5**, 630 (1928).

where ρ is the density of the drop, and t is the time. With γ determined, substitution from (1.5) yields

$$\frac{dR}{dt}=-\frac{n_1^0 m_1 \nu \alpha_0}{\rho\left(1+\frac{R^2}{R+\Delta}\frac{\nu\alpha_0}{D}\right)}. \tag{1.9}$$

If R is large compared to Δ, (1.9) has the form

$$\frac{dR}{dt}=-\frac{A}{1+BR/D}. \tag{1.10}$$

For such large values of R that unity in the denominator can be neglected, Langmuir's law is obtained.

In a series of careful experiments, Bradley, Evans, and Whytlaw-Gray,[3] and Birks and Bradley[5] confirmed the above relation (1.10). In order to obtain the necessary relation between radius and mean free path while conserving the precision of measurement, they elected to work with large drops (10^{-2} cm) and very low pressures. As it will appear below, we have confirmed the relation for drops as small as 5×10^{-5} cm at somewhat higher pressures.

Frisch and Collins[6,7] arrived at an equation of the form (1.10) by more logical methods based on stochastics. However, their result contains certain undetermined parameters. In order to determine these parameters, we had to make certain assumptions (to be discussed later), the validities of which are not entirely clear, although apparently justified for the range of conditions involved.

On the other hand, the Fuchs method is unsatisfactory because the model on which it is based remains vague. The distance, Δ, is never clearly defined, and the limits of validity of the treatment are not apparent.

An alternate to both of these procedures is developed below, based on the use of non-Maxwellian distribution functions which are more appropriate to gases in extremely nonuniform states. Use of this type of function not only leads to a boundary condition applicable on the drop surface itself, but tends to display the limits of validity of the Fuchs method. In gases where the derivation of nonequilibrium distribution functions is feasible, this method is more convenient than that of Frisch and Collins.

In the following sections, this type of theory is developed, the limits of the Fuchs theory are examined, and the observations of Bradley and his co-workers are extended to smaller droplets.

II. EXPERIMENTAL

Evaporation measurements were performed in dry air at moderate pressures (1–10 cm Hg) in a Millikan oil-drop chamber built according to the authors' specifications by the Waltham Model Works, Waltham, Massachusetts. The entire chamber was immersed in a built-on thermostat bath through which water was circulated and regulated to ±0.005°C. Condenser plates (flat to 10^{-3} cm), fashioned of stainless steel, were 10 cm in radius, 1.5 cm thick, and separated by 3 glass spacers, 2 cm high. A paper baffle with glass windows surrounded the plates to reduce convection which was appreciable even with good temperature control. The field was supplied by a regulated high voltage power supply, Model PS-22, Scientific Specialties Corporation, Cambridge, Mass. When this operated in conjunction with a constant voltage transformer, only negligible fluctuations of voltage occurred.

The measurements were made in much the same manner as those of Woodland and Mack,[8] and Shereshefsky and Steckler.[9] Both baffle and plates were coated with a layer of absorbent-dicapryl sebecate in one series of experiments, and diundecyl sebecate in the rest. This precaution assured that the density of vapor at large distances from the drop was effectively zero.

Drops of diamyl sebecate were admitted to the chamber by passing a small amount of air through a glass frit wet with the liquid. In this manner, a cloud of drops was

TABLE I.

Drop No. $T=25.16°$	P(cm Hg)	R cm	U (min-cm^{-1})	$\langle RP\rangle_{Hg}$ (cm/cm Hg)
1	1.987	0.89×10^{-4}	$44.7\times10^{+4}$	1.76×10^{-4}
2	1.426	1.27	44.6	1.81
3	2.844	1.01	49.2	2.88
4	2.890	0.48	39.9	1.37
5	6.423	1.07	68.6	6.90
6	8.352	0.80	63.2	6.66
7	1.890	0.92	43.0	1.75
8	1.938	1.02	41.0	1.98
9	1.980	0.97	44.3	1.92
10	2.021	1.52	45.8	3.06
11	3.905	0.88	51.8	3.42
12	2.199	1.12	40.0	2.47
13	2.249	0.50	38.3	1.13
14	2.340	1.10	41.6	2.58
15	9.606	2.04	121.9	19.58
16	9.685	1.55	96.5	15.00
17	6.607	2.04	121.9	19.58
18	6.655	1.27	71.6	8.43
19	6.374	1.41	77.4	8.97
20	4.229	2.65	89.1	11.22
21	4.273	1.10	56.2	4.71
22	2.806	1.55	54.2	4.35
23	2.896	1.05	44.7	3.04
24	0.865	0.80	41.0	0.69
$T=34.92°$				
1	5.500	1.22×10^{-4}	16.6×10^{4}	6.70×10^{-4}
2	4.190	2.45	20.6	10.25
3	2.924	2.27	15.6	6.64
4	2.056	1.82	13.7	3.74
5	1.103	1.05	10.6	1.16

[5] J. Birks and R. S. Bradley, Proc. Roy. Soc. (London) **A198**, 226 (1949).
[6] H. L. Frisch and F. C. Collins, J. Chem. Phys. **20**, 1797 (1952).
[7] H. L. Frisch, Z. Elektrochem. **56**, 324 (1952).
[8] D. J. Woodland and E. Mack, J. Am. Chem. Soc. **55**, 3149 (1933).
[9] J. L. Shereshefsky and S. Steckler, J. Chem. Phys. **4**, 108 (1936).

carried to the region above the plates. No observable diminution of temperature accompanied the expansion.

As a drop, having passed through a hole in the top plate, came into view, the hole was closed by a shutter, thus preventing the entrance of additional drops. The voltage, V_0, required to hold the drop stationary was recorded at suitable intervals of time. Usually, each experiment consisted of eight such readings. The velocity of free fall was determined (several times on the same drop) so that after each measurement of V_0 a rough value could be assigned to the radius of the drop by application of the empirical Stokes-Cunningham law, discussed below. These values were refined by combining the data on V_0 with that of free fall to compute the approximate number of charges on the drop (usually 8–25), correcting to the nearest integer, and then recalculating the radius, using only V_0 and the density.

During the time, Δt, of an observation the change in drop radius, ΔR, was so small that

$$\frac{dR}{dt}\simeq\frac{\Delta R}{\Delta T}, \tag{2.1}$$

with good accuracy. This was borne out by the fact that plots of R *versus* t were invariably linear. Values of R, and dR/dt, so determined, are recorded in Table I.

Dicapryl sebecate was obtained from the Harchem Chemical Company of New York. To insure high purity, both diamyl sebecate and diundecyl sebecate were prepared in this laboratory by esterifying sebacic acid with either *n*-amyl or undecyl alcohols. The resulting mixture, washed in sodium carbonate solution, and distilled water, was distilled at 1 mm Hg. The ester (the high boiling fraction) was then purified further in a molecular still.

The density of pure di-*n*-amyl sebecate was determined in the range 15–35°C and was found to obey the relation [$\rho=0.9288-0.00053$ (T°C -20) g/cm³]. The density of dicapryl sebecate was 0.9039 g/cm³ at 25°C.

For the pressures at which these measurements were made, Stokes law for the limiting velocity of fall of small drops fails quite seriously. Millikan[10] observed that a law of the form

$$R^2+\frac{bR}{P}=9/2\frac{\eta v_f\times 10^8}{g(\rho_l-\rho_g)}=\theta, \tag{2.2}$$

was more suitable. Here, η is the viscosity (in poise) of the medium, ρ_l and ρ_g the densities of the drop and medium, respectively, g the acceleration of gravity, v_f the limiting velocity, P the pressure (in cm Hg), R the drop radius (in microns), and b the Stokes-Cunningham coefficient. At infinite pressure the formula converges on the usual Stokes law. The value of b appropriate to our measurements was determined as follows.

[10] R. S. Millikan, Phys. Rev. **15**, 525 (1960); **21**, 617, 663 (1963); **22**, 1 (1963).

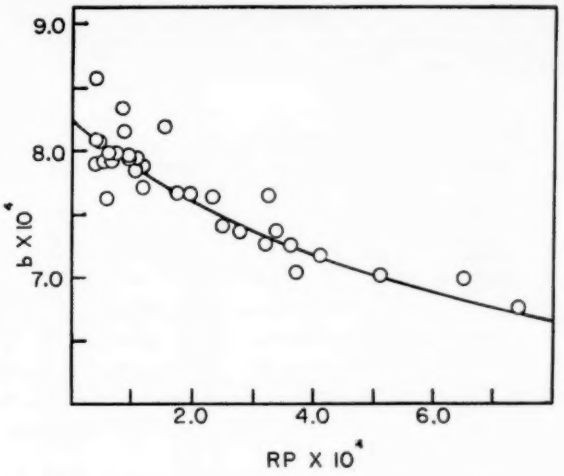

FIG. 1. Cunningham coefficient b as a function of radius and pressure. [The curve is the function $7.2[0.864+0.28\times\exp(-0.18RP)]$ cm-cm Hg.]

The velocity of fall of the same drop of dicapryl sebecate was measured at various pressures (1–10 cm Hg). Then θ was plotted against $1/P$. Extrapolation of this curve to $1/P$ equal to zero provided a rough value for R. Using this value of R, the charge was determined and corrected to the nearest integer. Then R was calculated exactly. Now the original data could be made to yield the value of b appropriate to each pressure by detailed application of (2.2). The results are given in Table II. In Fig. 1, b is plotted *versus* RP.

Millikan[10] determined b for clock oil and air, $b=7.2[0.864+0.290\exp(-0.18RP)]$. The data for dicapryl sebecate conforms more closely to $b=7.2[0.864+0.280\exp(-0.18RP)]$. The actual deviation of the actual b from this curve is about 2 percent. In view of its high rate of evaporation, b could not be measured directly for diamyl sebecate. Instead, the value measured for dicapryl sebecate was assumed to hold. This is partially justified when it is considered that the two substances are similar, and that b is not found to vary greatly even for substances which differ widely.[11]

Velocities of fall were not corrected for the effect of Brownian motion. It was observed, however, that when potentials less than V_0 were applied, so that v_f varied by a factor of 5 to 10, the calculated radii differed at most by 2 percent, and only in a random manner.

III. THEORY OF THE EVAPORATION RATE

Consider a binary gas mixture consisting of components 1 and 2, whose molecular masses are m_1, and m_2, respectively. The concentration of the two species will be denoted by $n_1(\mathbf{r},t)$ and $n_2(\mathbf{r},t)$. A spherical drop of component 1, having liquid density ρ, is placed with center at $r=0$. The gas conditions are such that no gradients of temperature and pressure exist while forces between molecules may be ignored except during

[11] C. N. Davies, Proc. Phys. Soc. (London) **57**, 659 (1945).

TABLE II.

$\eta = 183.2 \times 10^{-6}$ poise, $\rho_l = 0.9034$, $T = 25.15°$

Drop	P(cm Hg)	$\frac{9}{2}\frac{\eta v_f}{(\rho_l-\rho_0)g}$ (cm²)	Charge	R cm	b(cm/cm Hg)
1	0.802	5.67×10^{-8}	1	0.535×10^{-4}	8.07×10^{-4}
	2.134	2.24	2	0.537	7.72
2	6.147	0.950	1	0.544	7.38
	1.378	3.90	1	0.598	8.16
4	3.688	1.68	1	0.622	7.65
	5.193	1.30	1	0.620	7.66
5	0.619	8.55	2	0.607	8.34
	1.333	4.14		0.603	8.35
	2.464	2.38		0.604	8.20
6	0.525	10.56	2	0.672	7.90
	0.743	7.61		0.672	7.92
	0.934	6.17		0.672	7.94
	1.336	4.46		0.672	7.96
	1.566	3.86		0.672	7.95
	2.524	2.52		0.678	7.68
	4.408	1.60		0.679	7.38
	7.510	1.10		0.679	7.04
	9.510	0.98		0.685	7.02
7	0.777	7.67	2	0.727	7.63
	1.614	4.06		0.727	7.85
	3.406	2.11		0.727	7.43
	5.098	1.53		0.727	7.05
8	0.783	7.95	2	0.728	7.99
9	0.763	10.40	4	0.913	8.00
	0.934	8.22		0.912	7.97
	1.221	6.74		0.914	7.89
	3.002	3.08		0.915	7.38
	4.490	2.31		0.916	7.19
10	1.860	5.31	4	1.029	7.68
	3.499	3.21		1.031	7.28

encounters. Furthermore no mass motion of the mixture occurs. In these circumstances the appropriate nonequilibrium distribution function, based on Enskog's development[12] of the Boltzmann equation, is (for component 1)

$$f_1(\mathbf{r},c_1) = f_1^0\{1 - D_1(c_1)\mathbf{c}_1\cdot\nabla n_1\}, \tag{3.1}$$

where $\mathbf{c}_1$ is the velocity vector, $f_1^0(c_1)$ is the equilibrium distribution function

$$f_1^0(c_1) = n_1\left(\frac{m_1}{2\pi kT}\right)^{\frac{3}{2}}\exp(-m_1c_1^2/2kT), \tag{3.2}$$

and $D_1(c_1)$ in general depends only on the magnitude c_1. Equation (3.1) includes perturbation terms of the first order.

From (3.1) we derive

$$n_1\langle\mathbf{c}_1\rangle_{Av} = -\left\{\tfrac{1}{3}\int f_1^0(c_1)D_1(c_1)c_1^2 d\mathbf{c}_1\right\}\nabla n_1$$
$$= -D\nabla n_1, \tag{3.3}$$

where the integral covers the whole of velocity space. This is an expression of Fick's law and serves to define the diffusion coefficient, D.

In our problem n_1 and n_2 depend only on r. The net flux into the drop is then given by

$$\phi = +4\pi R^2 n_1(R)\langle c_{1n}\rangle_{Av}$$
$$= 4\pi R^2\left(\frac{\partial n_1}{\partial r}\right)_R, \tag{3.4}$$

where $\langle c_{1n}\rangle_{Av}$ denotes the average component of velocity normal to the drop surface. The flux ϕ is composed of the difference between ϕ_i, the flux of molecules condensing from the gas phase, and ϕ_l, the flux evaporating from the drop surface. For ϕ_i we obtain

$$\phi_i = 4\pi R^2\int_+ \alpha(\mathbf{c}_1)f_1(c_1)c_{1n}d\mathbf{c}_1, \tag{3.5}$$

where the positive subscript implies that the integral is to be taken only over positive directions of c_{1n} (into the drop surface). $\alpha(\mathbf{c}_1)$ is the condensation coefficient (probability of condensation) and may depend upon both the direction and magnitude of $\mathbf{c}_1$. In the absence of definite information concerning it we shall replace it by its mean value, α_1. Lennard-Jones and Devonshire[13] treated the simple case of H_2, HD, and D_2 adsorbing on copper, and found that $\alpha(\mathbf{c}_1)$ possesses a long, flat maximum, thus supporting the above simplification.

Substitution of (3.1) into (3.5) yields

$$\phi_i = 4\pi R^2\left\{\alpha_0\int_+ f_1^0 c_{1n}d\mathbf{c}_1 + \alpha_1\left(\frac{\partial n_1}{\partial r}\right)_R\int_+ f_1^0 D_1(c_1)c_{1n}^2 d\mathbf{c}_1\right\}. \tag{3.6}$$

Since $\alpha(\mathbf{c}_1)$ must be averaged differently for the two integrals α_0 in general differs from α_1. When we need to perform calculations we shall take advantage of the work of Lennard-Jones and Devonshire, and suppose α_0 equal to α_1. For the moment we shall continue to represent them by different symbols.

Substitution of the identity

$$\int c_n^2 F(c)d\mathbf{c} = \tfrac{1}{3}\int c^2 F(c)d\mathbf{c} \tag{3.7}$$

into (3.6) leads to

$$\phi_i = 4\pi R^2\left\{n_1(R)\alpha_0 v + \alpha_1\frac{D}{2}\left(\frac{\partial n_1}{\partial r}\right)_R\right\}, \tag{3.8}$$

where v has been defined in Sec. I, and D is given by (3.3).

To evaluate ϕ_l, the usual assumption is made that the rate at which molecules leave the surface is independent of the rate of condensation. ϕ_l is then evaluated most conveniently by assuming complete equilibrium to exist so that $\phi = 0$. Then $n_1 = n_1^0$, and since the rates of

[12] S. Chapman and T. G. Cowling, *Mathematical Theory of Non-Uniform Gases* (Cambridge University Press, Cambridge, 1952).

[13] J. E. Lennard-Jones and A. F. Devonshire, Proc. Roy. Soc. (London) **A156**, 6–28, 29–36 (1936).

condensation and evaporation are equal

$$\phi_l = 4\pi R^2 \alpha_0 \nu n_1^0. \tag{3.9}$$

Combining (3.9) and (3.8) with (3.4) provides the boundary condition

$$\left(\frac{\partial n_1}{\partial r}\right)_R = \frac{\alpha_0 \nu (n_1(R) - n_1^0)}{D(1-\alpha_1/2)}, \tag{3.10}$$

applicable right down to the drop surface.

Frisch and Collins[14] have shown that for the case of diffusion to a growing particle with a boundary condition of the form (3.10), it is a good approximation to assume the steady-state solution of Fick's law appropriate to a stationary boundary. Making use, therefore, of (1.5) to compute $n_1(R)$ and $(\partial n_1/\partial r)_R$, determining γ by application of (3.10) and applying (1.8), we are led to the result

$$\frac{dR}{dt} = -\frac{m_1 \alpha \nu n_1^0}{\rho(1-\alpha/2)\left(1+\dfrac{\alpha\nu}{(1-\alpha/2)D}R\right)}, \tag{3.11}$$

which is of the form (1.10). Here we have set $\alpha_0 = \alpha_1 = \alpha$.

Comparison of (3.11) and (1.10) reveals that both A and B are modified in (3.11) by the factor $(1-\alpha_1/2)^{-1}$.

The successive perturbations $f^{(0)}$, $f^{(1)}$, $f^{(2)}$, $\cdots$ in the nonequilibrium distribution function are proportional to powers of n in the order n, n^0, $n^{(-1)}$, $\cdots$.[12] At low pressures the later terms become very important. As far as first-order perturbation theory is valid, however, the form of the Fuchs theory is correct, except for some small modification of the constants A and B.

It has not been found convenient to estimate the contribution to the boundary flux due to the second-order perturbation, but some estimate may be made of the point at which (3.6) breaks down. This occurs when the flux due to $f^{(1)}$ becomes comparable to that due to $f^{(0)}$, and, from (3.6), when

$$D/R = 2\nu. \tag{3.12}$$

For heavy molecules of the kind, dibutyl phthalate and diamyl sebecate, one takes

$$D \simeq 2.8/P \text{ cm}^{-2} \text{ sec}^{-1}, \qquad \nu \simeq 3500 \text{ sec}^{-1} \text{ cm}^{-2}, \tag{3.13}$$

then if R is in microns (3.12) becomes

$$RP \simeq 4\,\mu \text{ cm Hg}, \tag{3.14}$$

where it is understood that the (3.6) is valid for RP *larger* than 4. For the case of water diffusing in air the limit is given by

$$RP \simeq 8\,\mu \text{ cm Hg}. \tag{3.15}$$

[14] H. L. Frisch and F. C. Collins, J. Chem. Phys. (to be published).

It is also to be pointed out that in the limit of zero pressure, Eq. (3.11) does not converge to the vacuum rate of evaporation.

$$\frac{dR}{dt} = -\frac{m_1 n_1^0 \nu \alpha_0}{\rho}.$$

The same analysis may be applied to plane surfaces. In this case, due to the small concentration gradient, the boundary condition is applicable to pressures of the order 10^{-4} cm Hg under normal conditions.

Subject to the validity of certain assumptions we have used the method of Collins and Frisch to obtain (3.11). In their treatment ϕ is given by[6]

$$\phi = \alpha_0 \nu' \int_0^\infty \int_0^{\sin^{-1}R/r} \int_{r\cos\theta - (R^2 - r^2\sin^2\theta)^{\frac{1}{2}}}^\infty 2\pi r^2 \times \sin\theta c(r,t)\psi(s) ds d\theta dr, \tag{3.16}$$

where $\psi(s)ds$ is the probability of a molecule moving the distance s in the time $\Delta t = 1/\nu'$. In order to evaluate this integral we have made the following assumptions. Thus it is supposed that:

(1) $c(r,t) = n_1(R)\dfrac{R}{r} - n_1^0$, (3.17)

(2) a steady state exists,

(3) the distribution of velocities following each jump is Maxwellian,

(4) $\psi(s)$ is isotropic.

This procedure is equivalent to an *equilibrium* theory of rate corrected for a distribution of free paths.

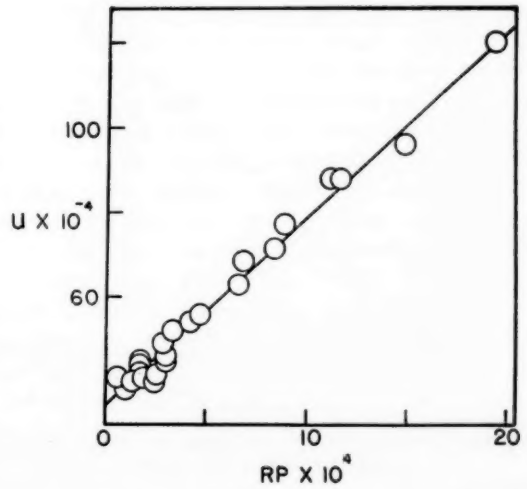

FIG. 2. Plot of $u = \exp(2\sigma V/RkT)/dR/dt$ for diamyl sebecate at 25.15°C. RP in cm cm Hg.

The rate law obtained is

$$\frac{dR}{dt}=-\frac{m_1\alpha_0\nu'\langle s\rangle n_1^0}{4\rho\left(1-\frac{\alpha_0}{2}\right)\left(1+\frac{\alpha_0\nu'}{2(1-\alpha_0/2)D}x\right)}, \quad (3.18)$$

where

$$x=\int_0^\infty \Psi(s)\left\{\frac{R^2}{2}\log\frac{(s^2+R^2)^{\frac{1}{2}}+s}{R}+\frac{R}{6}s(s^2+R^2)^{\frac{1}{2}}+\frac{R^2}{3}\left(\frac{R-(s^2+R^2)^{\frac{1}{2}}}{s}\right)\right\}ds$$

$$\simeq\frac{R\langle s\rangle}{2}, \quad R\gg\langle s\rangle, \quad (3.19)$$

and

$$D\equiv\frac{\nu'}{6}\langle s^2\rangle,$$

$$\langle s^n\rangle=\int_0^\infty s^n\Psi(s)ds. \quad (3.20)$$

Thus

$$\frac{dR}{dt}\simeq-\frac{\alpha_0\nu'\langle s\rangle m_1 n_1^0}{4\rho\left(1-\frac{\alpha_0}{2}\right)\left(1+\frac{\alpha_0\nu_1'\langle s\rangle}{4(1-\alpha_0/2)D}R\right)}, \quad (3.21)$$

and it is seen that (3.21) reduces to (3.11) when $\nu'\langle s\rangle$ is set equal to the mean thermal velocity, $\langle c_1\rangle_{Av}$, since $\nu=\frac{1}{4}\langle c_1\rangle_{Av}$.

IV. DISCUSSION

Assuming D to vary inversely with the pressure, and using the Kelvin equation giving the dependence of the partial pressure of the drop on the radius

$$n_{1R}^0=n_{1R=\infty}^0 e^{2\sigma V/RkT}, \quad (4.1)$$

where σ is the surface tension and V, the molecular volume (3.11), predicts an evaporation rate equation of the form

$$u=e^{2\sigma V/RkT}\Big/\frac{dR}{dt}$$

$$=a(1+bRP). \quad (4.2)$$

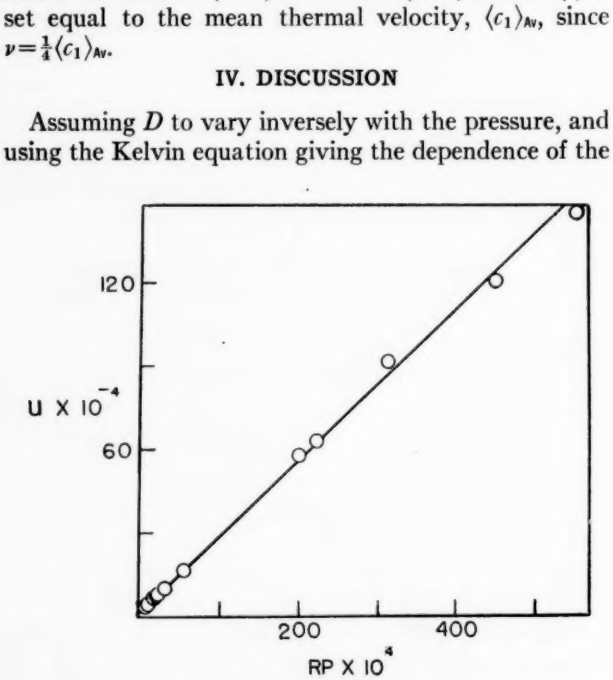

FIG. 3. Plot of $u=\exp(2\sigma V/RkT)/dR/dt$ for dibutyl phthalate at 19.92°C. RP in cm cm Hg.

TABLE III.

Cpd	T°C	P_1^0 (mm Hg)	$\frac{\alpha}{1-\frac{\alpha}{2}}$	D at (76 cm Hg)	α
diAS	25.16	1.1×10^{-6} [a]	0.67	0.0237	0.50
diAS	34.92	4.0×10^{-6} [a]	0.68	0.0254	0.50
diBP[b]	19.90	1.42×10^{-5} [b]	1.27	0.0340	0.76
diBP[b,c]	19.90	1.42×10^{-5} [b]			0.69

[a] E. S. Perry and W. H. Weber, J. Am. Chem. Soc. **71**, 3726 (1950).
[b] See reference 5.
[c] Flat surface.

Figure 2 illustrates that drops of diamyl sebecate obey this law even though the range of RP included, extends, at times, below 4 μ cm Hg. The data of Birks and Bradley[5] have been plotted in the same fashion in Fig. 3. Their range of RP extends from 6 to 550 μ cm Hg. From the slope and intercept, α and D may be evaluated if the equilibrium vapor pressure is known. The results are tabulated in Table III, together with a value for α measured by Birks and Bradley in the evaporation of dibutyl phthalate from a flat surface. This last value of α, 0.69, agrees well with the α calculated from (3.11), 0.76, as contrasted with α calculated from (1.9), 1.00. The values of D calculated from (3.11) and (1.9) are much the same: the chief difference then lies in the values of the condensation coefficient. D and α were obtained in the same manner for diamyl sebecate, but the results here are to be regarded only as qualitative for the following reasons: The asymptote and slope were obtained for data which extended partly over a range where it is not certain that (3.11) holds. Secondly, the values of vapor pressure used were extrapolated from data obtained at higher temperatures.

The condensation coefficient of mercury on mercury has been observed by Knudsen[15] to be highly dependent on the condition of the surface. However, the factor $\alpha/(1-\alpha/2)$ for organic liquids as obtained here and by Bradley and his co-workers has been found to be reproducible to within 4 percent.

[15] M. Knudsen, Ann. Physik **47**, 697 (1915).

The Thermodynamics of Boron Nitride; Low-Temperature Heat Capacity and Entropy; Heats of Combustion and Formation

A. S. Dworkin, D. J. Sasmor, and E. R. Van Artsdalen
Chemistry Division, Oak Ridge National Laboratory, Oak Ridge, Tennessee

(Received November 9, 1953)

The low-temperature heat capacity of microcrystalline boron nitride has been measured up to 300°K. It has been found that in the range from 20 to 65°K the heat capacity follows a T^2 relationship rather than the usual Debye T^3 law, and this has been explained as resulting from the layered, quasi-two-dimensional lattice of boron nitride. The Debye-type characteristic (two-dimensional) temperature is $\theta_2=598$°K. At 298.16°K $C_p=4.78_3$ cal/mole deg and $S^0=3.67_3$ eu, of which 0.034 has been extrapolated below 20°K. Derived thermodynamic functions have been tabulated at 10° intervals between 20 and 300°K. The heat of combustion of boron nitride in a conventional bomb calorimeter to yield amorphous boric oxide and elemental nitrogen has been determined to be 90.2±0.5 kcal/mole. From this value and other established thermal data the heat of formation of boron nitride is exothermic 60.7±0.7 kcal/mole.

INTRODUCTION

In recent years numerous studies of the chemistry of boron-nitrogen compounds have been made and we have been intrigued by the structural and physical similarity between borazole and its derivatives on the one hand and corresponding benzene compounds on the other, while noting the rather considerable differences in a number of their chemical properties. In line with earlier studies[1] on the heat of formation of *B*-trichloroborazole we decided to continue the investigation of thermodynamic properties of compounds containing the borazole ring. Boron nitride represents the ultimate in fused borazole ring compounds just as graphite represents the ultimate in fused benzene ring compounds. Boron nitride is not only isoelectronic with graphite but it resembles graphite structurally[2] to a remarkable extent, although differing sharply in color and electrical conductivity. It seemed to us to be particularly desirable to determine both the low-temperature heat capacity and the heat of formation of boron nitride. It was of interest to learn whether or not boron nitride would show a T^2 low-temperature heat capacity dependence as is the case with graphite.

Boron Nitride Sample

The sample of boron nitride used in our studies was kindly placed at our disposal by Mr. C. T. Henson of the Norton Company. Both spectrographic and wet chemical analysis in our laboratories showed that this boron nitride contained 1.5 percent of iron as Fe_3O_4; indeed the sample was very slightly magnetic. X-ray investigation indicated that the boron nitride was satisfactorily microcrystalline, good agreement being obtained with the data given by Pease[2] for recrystallized boron nitride. Although our sample was a little less well crystallized than the one reported by Pease, the purposes of our studies did not seem to warrant recrystallization since such small imperfections as did exist could not have caused observable effects in heat capacity or heat of formation. The sample showed a reasonably uniform particle size of about 1-micron diameter.

[1] E. R. Van Artsdalen and A. S. Dworkin, J. Am. Chem. Soc. 74, 3401 (1952).
[2] R. S. Pease, Acta Cryst. 5, 356 (1952).

LOW-TEMPERATURE HEAT CAPACITY AND ENTROPY

Experimental

The low-temperature, adiabatic calorimeter used by us has been described in the literature by Oliver and Grisard.[3] The actual calorimeter can, fabricated of copper and given a copper and silver plate, was slightly larger than the one used by Oliver and Grisard. Before making runs the can was tested and proved vacuum tight. Our temperature scale was established by using a small calorimetric-type platinum resistance thermometer which had been certified from 10°K to 500°C by the National Bureau of Standards.

Heat capacities were obtained by measuring the temperature rise produced by supplying a carefully measured quantity of electrical energy to the calorimeter heater. The relation 1 calorie equals 4.1840 absolute joules was used to convert electrical to thermal energy.

The calorimeter can, including thermometer and heater, weighed 56.3980 g and was calibrated by making adiabatic runs from about 15°K to room temperature. Liquid hydrogen was the refrigerant below about 50°K and liquid nitrogen above this temperature. After calibration the can was charged with 20.1034 g (weighed in air against brass weights) of the finely powdered and carefully dried and outgassed boron nitride. (A correction to *in vacuo* weights would make a difference of only 0.04 percent and has been neglected.) After evacuation about 3 to 5 mm of helium at room temperature was admitted to the calorimeter can in order to insure sufficiently rapid heat transfer.

The over-all accuracy with this calorimeter is better than 0.2 percent above 50°K,[3] but the error increases to about 0.5 percent at 20°K.

[3] G. D. Oliver and J. W. Grisard, J. Am. Chem. Soc. 73, 1688 (1951).

Results and Discussion

The raw data for the heat capacity of one mole* (24.828 g) of our sample of boron nitride are given in Table I. The data in this table have not been corrected for the presence of 1.5 percent iron as Fe_3O_4; however, results given in later tables have been corrected as described below. The data of Table I are shown in the order in which they were obtained and it will be noted that nine separate series of determinations of heat capacity were carried out, two series of which were made in the liquid hydrogen range and the others in the liquid nitrogen range. T_m is the mean temperature of each determination, and by comparing successive values of T_m one notes that the temperature rise of each individual C_p measurement was approximately 5 to 7°, except at the lowest temperatures where it was less.

The analytical result of 1.50 percent iron in the boron nitride sample can be used to show that the presumed one mole of BN in Table I actually contained 0.9793 mole BN and 0.00222 mole Fe_3O_4. Milar's[4] determination of the heat capacity of Fe_3O_4 was then used to correct these data for the presence of 0.00222 mole Fe_3O_4 in the boron nitride. It develops that the correction is quite small over most of the range, since the Fe_3O_4 amounts to less than 0.23 mole percent impurity. However, there was a very slight hump in the raw data heat capacity curve near 100°K, corresponding with a lambda transition at 110–120°K in Fe_3O_4.

The corrected molar heat capacities are plotted in Fig. 1 and smoothed values obtained from a large scale plot are given in Table II. High-temperature (400–900°C) heat capacity determinations of boron nitride have been made by Magnus and Danz.[5] Calculated

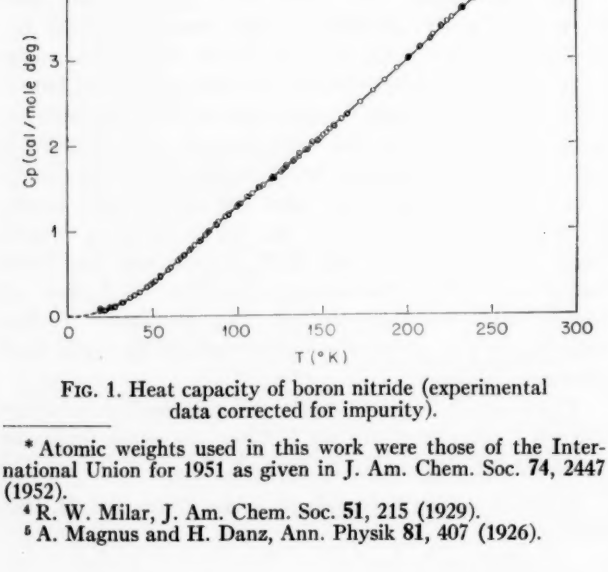

FIG. 1. Heat capacity of boron nitride (experimental data corrected for impurity).

TABLE I. Heat capacity of 1 mole (24.828 grams) BN. (Raw data, uncorrected for impurity).

T_m (°K)	C_p (cal/mole deg)	T_m (°K)	C_p (cal/mole deg)	T_m (°K)	C_p (cal/mole deg)
65.99	0.678	164.95	2.361	18.97	0.099
72.40	0.787	172.55	2.498	21.99	0.079
78.09	0.889	180.23	2.633	25.26	0.107
83.28	0.988	187.14	2.757	27.65	0.121
88.75	1.100	194.17	2.899	32.59	0.168
94.71	1.186	201.03	3.017	39.32	0.251
100.31	1.297	207.75	3.137	46.25	0.341
105.63	1.389	214.35	3.247	51.43	0.419
112.57	1.509	220.81	3.380		
121.03	1.639	227.16	3.481	201.65	3.032
129.04	1.766	233.39	3.601	208.33	3.144
136.68	1.904			215.92	3.284
144.13	2.029	49.94	0.391	224.44	3.437
147.20	2.046	54.53	0.463	232.77	3.588
152.47	2.141	60.54	0.574	240.91	3.731
		67.75	0.705	248.90	3.872
54.47	0.468			256.73	4.013
58.99	0.545	200.89	3.012	264.41	4.166
64.92	0.651	214.19	3.234	271.97	4.276
71.47	0.768	220.65	3.369	279.25	4.436
77.26	0.876	226.96	3.480	286.54	4.589
82.52	0.977	233.19	3.591	293.72	4.703
87.39	1.066	239.32	3.693	300.80	4.791
92.69	1.162	245.36	3.805		
99.28	1.271	251.31	3.909	68.58	0.718
106.39	1.391	257.17	4.014	74.64	0.834
113.09	1.507	262.95	4.117	80.90	0.944
119.46	1.609	268.65	4.230	87.44	1.063
125.58	1.687	282.57	4.494	94.39	1.181
132.42	1.807	289.82	4.615	101.79	1.313
139.95	1.935	296.97	4.742	108.68	1.431
147.21	2.059			115.23	1.535
154.21	2.181	18.56	0.078	121.48	1.620
161.41	2.303	21.42	0.073	128.45	1.733
		24.56	0.104	136.11	1.864
120.86	1.622	27.75	0.117	143.46	1.988
126.92	1.712	31.91	0.170	150.49	2.112
133.70	1.823	36.67	0.220	157.42	2.222
141.18	1.945	42.16	0.282	164.65	2.349
148.98	2.076	48.27	0.371		
157.11	2.221				

extrapolations of our data and those of Magnus and Danz show very reasonable consistency of both the high- and low-temperature measurements. It should be noted that the equation for the heat capacity of boron nitride given by Magnus and Danz is actually for ½ mole of BN and that a derived equation given by Kelly[6a] in an early paper is in error by the factor 2, although this has been corrected in his later compilations.[6b]

Values of the thermodynamic functions S^0, $-(F^0-H_0^0)/T$, and $(H^0-H_0^0)/T$ have been derived from the C_p determinations. Smoothed values of these functions as well as values of C_p are listed in Table II at ten-degree intervals from 20 to 300°K. S^0 was obtained by integrating the area under a large-scale plot of C_p/T *vs* T in which each individual C_p value, corrected for impurity as described above, was used. C_p values below 20°K were estimated by a T^2 extrapolation to 0°K (see following). Then a large plot of S^0 *vs* T was made and used to evaluate $-(F^0-H_0^0)/T$

* Atomic weights used in this work were those of the International Union for 1951 as given in J. Am. Chem. Soc. **74**, 2447 (1952).

[4] R. W. Milar, J. Am. Chem. Soc. **51**, 215 (1929).

[5] A. Magnus and H. Danz, Ann. Physik **81**, 407 (1926).

[6a] K. K. Kelly, U. S. Bur. Mines Bull. No. 371, **14** (1934); [b] No. 407, **31** (1935); No. 476, **28** (1949).

TABLE II. Smoothed thermodynamic functions of BN.[a]

T (°K)	C_p (cal/mole deg)	S^0 [b] (cal/mole)	$-\frac{(F^0-H_0^0)}{T}$ (cal/mole deg)	$\frac{(H^0-H_0^0)}{T}$ (cal/mole deg)
20	0.065	0.034	0.012_0	0.022_0
30	0.144	0.074	0.025_7	0.048_3
40	0.257	0.131	0.047_3	0.083_7
50	0.396	0.203	0.070_8	0.132_2
60	0.563	0.290	0.100_0	0.190_0
70	0.743	0.390	0.134_4	0.255_6
80	0.928	0.501	0.173_6	0.327_4
90	1.108	0.621	0.217	0.404
100	1.280	0.747	0.264	0.483
110	1.444	0.876	0.314	0.562
120	1.596	1.009	0.366	0.643
130	1.754	1.143	0.421	0.722
140	1.926	1.280	0.477	0.803
150	2.096	1.418	0.535	0.883
160	2.270	1.559	0.595	0.964
170	2.451	1.702	0.656	1.046
180	2.631	1.847	0.718	1.129
190	2.812	1.994	0.782	1.212
200	2.994	2.143	0.846	1.297
210	3.176	2.294	0.912	1.382
220	3.357	2.446	0.978	1.468
230	3.539	2.599	1.045	1.554
240	3.721	2.754	1.113	1.641
250	3.904	2.910	1.182	1.728
260	4.087	3.066	1.251	1.815
270	4.268	3.224	1.322	1.902
273.16	4.326	3.274	1.344	1.930
280	4.450	3.382	1.392	1.990
290	4.633	3.542	1.464	2.078
298.16	4.783	3.673	1.523	2.150
300	4.815	3.702	1.536	2.166

[a] All values have been corrected for presence of 1.50 percent Fe as Fe_3O_4.
[b] The value at 20°K was obtained by graphical extrapolation described in the text.

at the same ten-degree intervals. $(H^0-H_0^0)/T$ was computed from S^0 and $-(F^0-H_0^0)/T$. Thus, $S^0_{298.16}=3.67_3\pm0.02$ cal/mole.

T^2 Dependence of C_v

The significant observation has been made that in the range from 20 to 65°K the heat capacity of boron nitride follows a T^2 dependence rather than the usual Debye T^3 relationship.[7] This is shown clearly in Fig. 2 where C_v is plotted against T^2.

In our previous publication[7] we calculated C_v by use of the equation

$$C_p-C_v=\alpha^2VT/\beta, \qquad (1)$$

where the coefficient of cubical expansion α and the molar volume V were obtained from the x-ray crystallographic data of Pease[2] and the compressibility β was assumed to be the same as that of graphite,[8] since no data could be found for boron nitride. It was pointed out that this approximation of β appeared reasonable and in any case it alone should not introduce any very appreciable error. However, the use of this equation at very low temperatures requires the extrapolation of Pease's data beyond the range of measurement so that the difference C_p-C_v becomes approximately a linear function of absolute temperature. This has been demonstrated to be true with some substances, as for instance in the case of germanium.[9] C_v was found to be about 1 percent less than C_p for boron nitride by this method. A second method of computation commonly used assumes the validity of the Nernst-Lindemann formula[10]

$$C_p-C_v=ATC_p^2, \qquad (2)$$

where A is an empirical constant. A can be evaluated by equating (1) and (2) at some temperature at which C_p, α, V, and β have been measured, and then C_v may be computed from any C_p value by Eq. (2). In this paper we have chosen the Nernst-Lindemann method because of its wide acceptance. In the case of boron nitride this method leads to the conclusion that below 80°K C_v equals C_p within less than our experimental error.

A T^2 dependence of the heat capacity in the low-temperature region has been observed in the cases of graphite[11] and gallium,[12] both of which have layer structure with a high degree of anisotropy. We believe

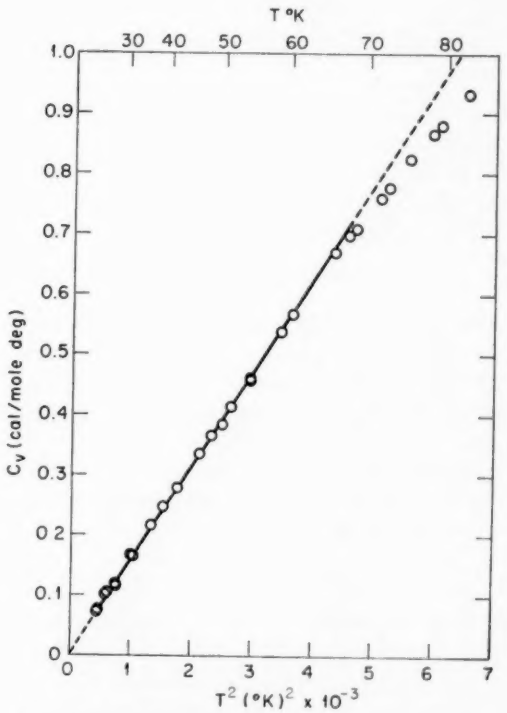

FIG. 2. T^2 dependence of low-temperature heat capacity of boron nitride.

[7] Dworkin, Sasmor, and Van Artsdalen, J. Chem. Phys. **21**, 954 (1953).
[8] T. W. Richards, J. Am. Chem. Soc. **37**, 1643 (1915) gives for graphite $\beta=3\times10^{-6}$ cm²/kg.
[9] M. E. Fine, J. Chem. Phys. **21**, 1427 (1953).
[10] W. Nernst and F. A. Lindemann, Z. Elektrochem. **17**, 817 (1911).
[11] W. DeSorbo and W. W. Tyler, Phys. Rev. **83**, 878 (1951) and report No. RL-847, General Electric Research Laboratory, April, 1953, J. Chem. Phys. **21**, 1660 (1953).
[12] W. DeSorbo, J. Chem. Phys. **21**, 168 (1953).

that the T^2 dependence of the heat capacity of boron nitride at low temperatures is the direct result of its pronounced layered structure, which makes it a quasi-two-dimensional crystal. Such a view has been expressed previously by Tarassov[13] in the case of several other substances, but there are numerous flaws in his arguments, among them the choice of data which extended only as low as 50°K. Tarassov claimed that published heat capacity data for $FeCl_2$,[14] $MgCl_2$,[14] and MoS_2,[15] followed a T^2 dependence. However, all of these data were obtained at temperatures above 50°K and when plotted against T^2 they do not show a linear relationship. Hence it is clear that the heat capacity of these substances does not follow a T^2 dependence above 50°K, and the question of whether or not the heat capacity depends on T^2 in some lower temperature range must remain unanswered in the absence of data below 50°K. Very recently DeSorbo[16] has shown that Tarassov's ideas are inadequate in the case of selenium, which Tarassov claimed showed a first-power temperature dependence of its heat capacity. Gurney[17] has presented a theory of the T^2 law for graphite using the concept of a two-dimensional lattice in an otherwise conventional Debye treatment of low-temperature heat capacity. He has derived for a monatomic lattice the expression

$$C_v = 9.60RT^2/\theta_2^2, \tag{3}$$

where subscript 2 on theta refers to the two-dimensional case. A thorough investigation of the lattice vibrations of graphite has been made by Krumhansl and Brooks,[18] who have been able to present a coherent theory for the T^2 heat capacity dependence based on their analysis of graphite lattice vibrations. By making certain simplifying approximations their theory reduces to

$$C_v = 14.4RT^2/\theta_2^2 \tag{4}$$

for a certain range of low temperature. Krumhansl and Brooks have pointed out errors in Gurney's work which lead to the erroneous constant 9.6 rather than 14.4. Equation (4) can also be derived by an approximate method.

We believe that an approximate theory for the low-temperature heat capacity of any quasi-two-dimensional crystal can be given in the form

$$C_v = 14.4aRT^2/\theta_2^2, \tag{5}$$

where C_v is the "molar" heat capacity, a is the number of atoms per "molecule," and θ_2 is a two-dimensional Debye-type characteristic temperature. Thus, a will be 2 in the case of boron nitride BN, and Eq. (5) should apply rather well because boron and nitrogen have nearly the same size and atomic weight.

Values of θ_2 for boron nitride were calculated according to Eq. (5). We have assumed for this purpose that C_v can be computed by the Nernst-Lindemann equation and thus in the temperature range in question C_v equals C_p. Good constancy of θ_2 was obtained up to about 66°K and this is illustrated also by Fig. 2. From these data it is found that the characteristic temperature θ_2 for boron nitride is 598°K with a mean deviation of ±7°K. (It is found that $\theta_2 = 604$°K when C_v values calculated by Eq. (1) are used with extrapolated constants.) This is to be compared with $\theta_2 = 767$°K calculated from the results of DeSorbo and Tyler[11] in the case of graphite by using Eq. (4). The difference between the value of $\theta_2 = 598$°K reported here, and that given by us[7] in an earlier communication is the result of our previously using the erroneous equation (3).

HEAT, FREE ENERGY, AND ENTROPY OF FORMATION

Experimental

The heat of combustion of boron nitride to yield amorphous boric oxide and elemental nitrogen was measured in a Parr calorimeter modified in such a way that it operated with an isothermal jacket rather than adiabatically. The oxygen bomb was a standard Parr double-valve type. The temperature of the isothermal water jacket around the calorimeter was maintained constant at approximately 27°C by means of a thermistor as the temperature-sensitive element in a bridge circuit employing a variable zero-suppression Speedomax recorder-controller operating a low-lag knife-blade heater at about 25 volts. It was observed that random temperature fluctuations of the order of somewhat less than 0.001°C occurred in both directions around the control temperature, but no drift was found during combustion. Temperature in the calorimeter was measured with a precision Mueller bridge and a calibrated copper resistance thermometer constructed so as to have an extremely small time constant. This particular thermometer has the designation CUV-7 and has been described by Van Artsdalen and Dworkin.[1] The calorimeter was operated so that the final temperature after combustion was somewhat lower than the isothermal jacket temperature and in this way vaporization from the calorimeter was minimized.

The calorimeter was calibrated according to Bureau of Standards recommendations by combustion of NBS certified benzoic acid (heat of combustion 6318 cal/g) when one gram of water was present in the bomb, and the initial oxygen pressure was 30 atmos at room temperature. The bomb was flushed three times with oxygen at 10 atmos before final filling for each combustion. The standard amount of water in the calorimeter was 2067 g for all combustions. Corrections were applied for slight deviations (less than 0.5 g) from this

[13] V. V. Tarassov, Compt. rend. acad. sci. U.R.S.S. **46**, 20, 110 (1945); **54**, 795 (1946); Doklady Akad. Nauk. U.R.S.S. **58**, 577 (1947); Zhur. Fiz. Khim. **24**, 111 (1950).
[14] K. K. Kelly and G. E. Moore, J. Am. Chem. Soc. **65**, 1264 (1943).
[15] C. T. Anderson, J. Am. Chem. Soc. **59**, 486 (1937).
[16] W. DeSorbo, J. Chem. Phys. **21**, 1144 (1953).
[17] R. W. Gurney, Phys. Rev. **88**, 465 (1952).
[18] J. Krumhansl and H. Brooks, J. Chem. Phys. **21**, 1663 (1953).

amount of water, for the amount of heat introduced by combustion of the ignition wire, for the presence of the small amount of water in the bomb, and for the difference of the mean temperature of the combustion from a standard mean of 24.5°C. No correction was applied for heat introduced by the current through the ignition wire prior to its rupture since actual experiment showed this to be entirely negligible. A series of nine calibrations made during the course of measuring the heat of combustion of boron nitride gave 2519.7±4.3 (±0.17 percent) cal for the thermal equivalent of the calorimeter.

In the combustion of boron nitride 30 atmos of oxygen was used, but no water was added to the bomb, since its presence would have caused an indeterminate amount of hydrolysis of the product boric oxide. Combustion was effected without promoters, the BN being ignited directly by the fuse wire. The combustion process was complicated by the fact that complete combustion was not achieved and hence the actual amount of boron nitride burned had to be determined after each combustion by analysis of the products for boric oxide after its hydrolysis to boric acid. Following combustion of boron nitride, the gases in the bomb were vented slowly through aqueous bubbler bottles which were subsequently titrated for nitric acid. It was found in this way that the amount of nitrogen dioxide produced during combustion of BN was entirely negligible (heat produced less than 0.4 cal) and the same as that produced during calibration; hence no correction was made for it. On opening the bomb a white, fluffy solid was found sublimed onto the walls. X-ray examination of this solid showed it to be amorphous and to correspond to the product formed when elemental boron was burned similarly, where the product is known to be amorphous boric oxide. Some of this product from burning of boron nitride was dissolved in water in a small calorimeter whereby its heat of solution was measured and found to agree closely with that for amorphous boric oxide reported by Van Artsdalen and Anderson.[19] X-ray study of some of the unburned boron nitride clinker remaining after a bomb combustion showed lines of BN only.

In runs used for measuring the heat of combustion of boron nitride the amount of BN burned was determined by analysis of the solid products remaining in the bomb. The bomb was washed out thoroughly with water and the solid digested a few minutes in water at about 80°C to break up any clinker. After filtering, the solution was diluted to 1 liter, and 100 ml aliquots were titrated for boric acid with standardized $N/10$ sodium hydroxide using phenolphthalein as indicator and mannitol to convert H_3BO_3 to a strong acid by complexing. At the end point a little additional mannitol was added to insure complete complexing. This is a standard method for determining boric acid. Separate studies showed that the method was probably reliable to about 0.1 to 0.15 percent. The residue which remained on the filter from the hot water digestion was dried and weighed. Perhaps the best proof of identity of the products of combustion lies in the fact that the weight of unburned residue remaining on the filter plus the weight of burned BN computed from the analytical result for B_2O_3 was equal to the original weight of BN taken for combustion. One is thus led to the conclusion that the combustion process reported here in fact does yield amorphous boric oxide and elemental nitrogen to the exclusion of all other products.

Corrections were made in runs with boron nitride as in calibrations and in addition for difference in specific heats of materials in the bomb during calibration and boron nitride combustion, respectively.

[19] E. R. Van Artsdalen and K. P. Anderson, J. Am. Chem. Soc. 73, 579 (1951).

Results and Discussion

The results of six combustions of boron nitride are given in Table III. In the first column t_m is the mean temperature of the combustion. The number of moles of BN burned, as determined by analysis, is listed in the second column while the third indicates about how much of the BN was burned and Δt in the fourth column lists the temperature rise of the calorimeter following combustion. This temperature rise has been converted to calories of heat produced Q_t by using the thermal equivalent of the calorimeter obtained in its calibration. However, this amount of heat must be corrected by subtraction of the heat introduced by the fuse wire, and the corrected heat produced by combustion of BN alone is listed as Q_c in column six. ΔH was computed from this figure and the moles of BN burned. Actually, for purposes of computation one more significant figure was used than is recorded in Table III, but because of the inherent uncertainties it is felt that the precision is not better than indicated by the table.

The value for the heat of combustion in Table III must be corrected for the change in the number of moles of gas according to the reaction

$$BN_{(c)}+\tfrac{3}{4}O_2=\tfrac{1}{2}B_2O_{3(\text{amorph})}+\tfrac{1}{2}N_2. \qquad (6)$$

TABLE III. Heat of combustion of boron nitride.

t_m (°C)	BN burned (Moles)	Approx % burned	Δt (°C)	Q_t (cal)	Q_c (cal)	$-\Delta H$ (kcal/mole)
24.3	0.01722	79	0.630	1587	1570	91.2
24.6	0.02077	84	0.741	1868	1848	89.0
24.1	0.01554	86	0.563	1419	1405	90.4
24.4	0.02238	88	0.804	2026	2009	89.8
24.6	0.01626	87	0.588	1483	1466	90.1
24.3	0.02311	88	0.833	2099	2082	90.1
					Average	90.1±0.5

One then writes

$$\Delta H^0_{298.16} = -90.1 + \Delta nRT = -90.1 + (-\tfrac{1}{4})(0.5926)$$
$$\Delta H^0_{298.16} = -90.2 \text{ kcal/mole.}$$

The heat of formation of amorphous boric oxide has been given most recently as $\Delta Hf_{298.16} = -301.75 \pm 0.75$ kcal/mole by Prosen, Johnson, and Pergiel,[20] so we may write at 298.16°K

$BN_{(c)} + \frac{3}{4}O_2 = \frac{1}{2}B_2O_{3(\text{amorph})} + \frac{1}{2}N_2$	$\Delta H^0_{298.16} = -90.2$
$B_{(c)} + \frac{3}{4}O_2 = \frac{1}{2}B_2O_{3(\text{amorph})}$	$= -150.9$
$B_{(c)} + \frac{1}{2}N_2 = BN_{(c)}$	$\Delta H^0_{298.16} = -60.7.$ (7)

Assuming the over-all ± error to be equal to the square root of the sum of the squares of all individual errors, we estimate a probable error of ±0.7 kcal/mole. Thus the best value for the heat of formation of boron nitride in its standard state at 25°C is exothermic 60.7±0.7 kcal/mole.

Previously Lorenz and Woolcock[21] obtained 28.1 kcal/mole for the heat of formation of BN, and Satoh,[22] who recalculated the results using different heat capacity values, obtained 28.5 kcal/mole. The method used by Lorenz and Woolcock is open to serious question. It involved a presumed determination of the dissociation equilibrium

$$BN_{(c)} = B_{(c)} + \tfrac{1}{2}N_2 \qquad (8)$$

with experiments performed in the range 1695 to 2045°C by measuring the pressure of permanent gas produced. Lorenz and Woolcock did not prove that reaction (8) was the only reaction to occur, nor, indeed, that it was the most important one. It is now known that BN can be sublimed at such elevated temperatures; hence it is conceivable that Lorenz and Woolcock may have been measuring a combination of heat of sublimation and heat of dissociation of a gaseous species. Furthermore, only recently has relatively high-purity boron nitride been available and it is clear that a volatile or unstable impurity could have caused spurious results. Also technical problems of outgassing at the high temperatures involved are extremely difficult to overcome.

Roth[23] has proposed the value of 33.5 kcal/mole for the heat of formation of boron nitride. However, some rather vague assumptions were made and it is not clear how Roth arrived at this value.

[20] Prosen, Johnson, and Pergiel, Natl. Bur. Standards Rept. No. 1552, March 26, 1952.
[21] R. Lorenz and J. Woolcock, Z. anorg. u. allgem. Chem. **176**, 289 (1928).
[22] S. Satoh, Sci. Papers Inst. Phys. Chem. Research (Tokyo) **29**, 53 (1936).
[23] W. A. Roth, Z. Naturforsch. **1**, 574 (1946).

The free energy of formation of boron nitride has been calculated from its heat of formation and entropy by using Bureau of Standards[24] values for the entropy of elemental boron and nitrogen. We compute that for reaction (7) $\Delta S = -20.77$ eu and $\Delta F = -54.5$ kcal/mole. This large negative value for the free energy of formation is consistent with the great stability of boron nitride.

The question of bonding in boron nitride has been discussed by several people, notably recently by Pease,[2,25] who felt it was impossible to decide between double or single B-N links. Cartledge[26] has shown that in very many cases it is possible to correlate heats of formation per equivalent of particular series of compounds (e.g. chlorides, oxides, etc.) with the ionic potential of the cation, and he has given some data for nitrides. Such a correlation is most satisfactory with strictly ionic compounds, but Cartledge has been able to use it in other cases and to draw important conclusions about bonding type, as for instance in the notable case of boron trifluoride. Cartledge's curves for nitrides were based on meager data and leaned rather heavily on the old value for boron nitride. However, new determinations of heats of formation of several nitrides make relocation of these curves necessary. When this is done it becomes clear that our value for the heat of formation of boron nitride fits the curve if it is assumed that there is appreciable double bond character to the boron-nitrogen link. Although heats of formation of other nitrides with high ionic potentials are greatly to be desired for quantitative considerations, we believe our data are consistent with partial double bond character in boron nitride.

ACKNOWLEDGMENT

We wish to express our thanks to Mr. George Oliver and Mr. J. W. Grisard for their help in initial operation of the low-temperature calorimeter. Further, we acknowledge our appreciation to Dr. H. A. Bernhardt and Dr. F. W. Hurd of the K-25 Laboratories of Carbide and Carbon Chemicals Company for certain facilities placed at our disposal. Important x-ray diffraction studies were made for us by Mr. R. Ellison and Dr. M. A. Bredig of this laboratory. We also thank Professors Krumhansl and Brooks for their courtesy in giving us a copy of their manuscript prior to publication. We have had stimulating discussions with Dr. G. H. Cartledge.

[24] *Selected Values of Chemical Thermodynamic Values*, Circular 500, Natl. Bur. Standards (1952).
[25] R. S. Pease, J. Am. Chem. Soc. **74**, 4219 (1952).
[26] G. H. Cartledge, J. Phys. Chem. **55**, 248 (1951) and earlier papers.

The Intermolecular Potentials for Some Simple Nonpolar Molecules*

EDWARD A. MASON† AND WILLIAM E. RICE‡
Naval Research Laboratory, Department of Chemistry, University of Wisconsin, Madison, Wisconsin
(Received December 16, 1953)

Experimental data on the crystal properties, second virial coefficients, and viscosity coefficients of Ne, A, Kr, Xe, CH_4, N_2, CO, O_2, and CO_2 were analyzed for the purpose of obtaining values of the parameters in the exp-six intermolecular potential, $\varphi(r)=\frac{\epsilon}{1-6/\alpha}\left[\frac{6}{\alpha}e^{\alpha(1-r/r_m)}-\left(\frac{r_m}{r}\right)^6\right]$. For gases whose molecules are spherical, it was possible to reproduce, with a single set of potential parameters, not only the crystal, second virial, and viscosity data, but also data on other transport properties with fair accuracy. For gases whose molecules deviate appreciably from spherical symmetry it was necessary to choose at least two different sets of potential parameters in order to reproduce different types of properties. Such behavior was taken to indicate the inadequacy of the assumptions, made in the fundamental gas theories, that intermolecular forces are central and that intermolecular collisions are elastic.

RECENT calculations of the transport property collision integrals[1] and the second virial coefficients[2] for gases whose molecules obey an exp-six intermolecular potential, have enabled the intermolecular potentials of helium and hydrogen to be determined from experimental values of the viscosity and second virial coefficients.[3] The exp-six potential may be written in the form

$$\varphi(r)=\frac{\epsilon}{1-6/\alpha}\left[\frac{6}{\alpha}e^{\alpha(1-r/r_m)}-\left(\frac{r_m}{r}\right)^6\right], \qquad (1)$$

where $\varphi(r)$ is the potential energy of two molecules at a separation distance r, ϵ is the depth of the potential energy minimum, r_m is the position of the minimum, and α is a parameter which is a measure of the steepness of the repulsion energy. Corner[4] has shown how such calculations of intermolecular potentials may be improved by the use of crystal data in addition to gas properties data, and has used this method to determine the potentials of neon and argon from crystal, second virial coefficient, and Joule-Thomson coefficient data. In the present paper we extend the application of Corner's procedure to include experimental transport property results for the evaluation of the intermolecular potentials of a number of simple, nonpolar molecules.

DETERMINATION OF POTENTIAL PARAMETERS

The crystal data used in Corner's method are the lattice distance of the crystal, R, and the heat of sublimation E_0 both at 0°K. The heat of sublimation is corrected for the zero-point energy by taking it to be the sum of the experimental heat of sublimation at 0°K (in units of energy/mole) and the quantity $(9N_0k\Theta_D/8)$, where N_0 is the Avogadro number, k is the Boltzmann constant, and Θ_D is the experimental value of the characteristic Debye temperature as determined at low temperatures. Knowledge of the two quantities R and E_0 permits the calculation of the two potential parameters r_m and ϵ as a function of the third parameter α by solving the transcendental equation

$$\frac{6C_6}{R^{*7}}-72(\theta-\theta')e^{\alpha(1-R^*)}+\left(\frac{R^*}{R}\right)\left[\frac{3h^2(\alpha-6)}{8\pi^2m\epsilon\alpha}\right]^{\frac{1}{2}}\times\left[72\left(\frac{\alpha}{2}-\frac{1}{R^*}\right)e^{\alpha(1-R^*)}-\frac{15C_8}{R^{*8}}\right]^{-\frac{1}{2}}\times\left[\frac{120C_8}{R^{*9}}+72\left(\frac{1}{R^{*2}}+\frac{\alpha}{R^*}-\frac{\alpha^2}{2}\right)e^{\alpha(1-R^*)}\right]=0, \qquad (2)$$

where C_6 and C_8 are constants tabulated by Lennard-Jones and Ingham,[5] θ and θ' are functions of (αR^*) tabulated by Corner,[4] R^* is the reduced lattice distance R/r_m, h is Planck's constant, and m is the mass of one molecule. The value of the parameter ϵ appearing in the third term of Eq. (2) is given as a function of α and R^* by the equation

$$E_0=\frac{N_0\epsilon}{2(\alpha-6)}\left[\frac{C_6}{R^{*6}}-72\theta e^{\alpha(1-R^*)}\right]. \qquad (3)$$

Equations (2) and (3) are subject to the conditions that the crystal is cubic and that the zero-point energy is small.[6]

The procedure for finding the potential parameters r_m, ϵ, and α is then as follows:

(1) For a chosen arbitrary value of α, the value of R^* which satisfies Eq. (2) is found by trial and error. The parameter r_m is found from the relation $r_m=R/R^*$.

* This work was supported in part by contract N7onr-28511 with the U. S. Office of Naval Research.
† National Research Fellow, 1952–1953. Present address: Department of Chemistry, Pennsylvania State University, State College, Pennsylvania.
‡ Present address: Experiment Incorporated, Richmond, Virginia.
[1] E. A. Mason, J. Chem. Phys. **22**, 169 (1954).
[2] W. E. Rice and J. O. Hirschfelder, J. Chem. Phys. **22**, 187 (1954).
[3] E. A. Mason and W. E. Rice, J. Chem. Phys. (to be published).
[4] J. Corner, Trans. Faraday Soc. **44**, 914 (1948).
[5] J. E. Lennard-Jones and A. E. Ingham, Proc. Roy. Soc. (London) **A107**, 636 (1925).
[6] This condition prevents the use of crystal data in determining the potential parameters of helium and hydrogen.

TABLE I. Exp-six potential parameters for some simple, nonpolar molecules.

Substance	Parameters α	r_m (A)	ϵ/k °K	Exptl. data used for detn. of parameters: Visc.	2nd virial	Crystal
Ne	14.5	3.147	38.0	a	b	c
A	14.0	3.866	123.2	d	e	c
Kr	12.3	4.056	158.3	f	g	c
Xe	13.0	4.450	231.2	h	i	c
CH_4	14.0	4.206	152.8	j	k	l
N_2	16.2	4.040	113.5	···	m	l
	17.0	4.011	101.2	n	···	···
CO	>17	<4.10	>132	···	o	l
	17.0	3.937	119.1	p	···	···

[a] R. S. Edwards, Proc. Roy. Soc. (London) **A119**, 578 (1928); M. Trautz and H. E. Binkele, Ann. Physik **5**, 561 (1930); M. Trautz and R. Zink, *ibid.* **7**, 427 (1930); M. Trautz and H. Zimmermann, *ibid.* **22**, 189 (1935); A. van Itterbeek and O. van Paemel, Physica **7**, 265 (1940); R. Wobser and F. Müller, Kolloid-Beihefte **52**, 165 (1941); H. L. Johnston and E. R. Grilly, J. Phys. Chem. **46**, 948 (1942); van Itterbeek, van Paemel, and van Lierde, Physica **13**, 88 (1947); J. W. Buddenberg and C. R. Wilke, J. Phys. & Colloid Chem. **55**, 1491 (1951).

[b] H. K. Onnes and C. A. Crommelin, Leiden Comm. **147d** (1915); Crommelin, Martinez, and Onnes, *ibid.* **154a** (1919); L. Holborn and J. Otto, Z. Physik **33**, 1 (1925); **38**, 359 (1926).

[c] G. Kane, J. Chem. Phys. **7**, 603 (1939).

[d] Y. Ishida, Phys. Rev. **21**, 550 (1923); M. Trautz and W. Ludewigs, Ann. Physik **3**, 409 (1929); M. Trautz and H. E. Binkele, *ibid.* **5**, 561 (1930); M. Trautz and R. Zink, *ibid.* **7**, 427 (1930); A. van Itterbeek and O. van Paemel, Physica **5**, 1009 (1938); R. Wobser and F. Müller, Kolloid-Beihefte **52**, 165 (1941); H. L. Johnston and E. R. Grilly, J. Phys. Chem. **46**, 948 (1942); V. Vasilesco, Ann. phys. **20**, 137, 292 (1945).

[e] H. K. Onnes and C. A. Crommelin, Leiden Comm. **118b** (1910); L. Holborn and J. Otto, Z. Physik **23**, 77 (1924); **30**, 320 (1924); **33**, 1 (1925); Michels, Wijker, and Wijker, Physica **15**, 627 (1949).

[f] A. O. Rankine, Proc. Roy. Soc. (London) **A83**, 516 (1910); **A84**, 181 (1910); A. G. Nasini and C. Rossi, Gazz. Chim. Ital. **58**, 433, 898 (1928).

[g] Beattie, Brierley, and Barriault, J. Chem. Phys. **20**, 1615 (1952).

[h] A. O. Rankine, Proc. Roy. Soc. (London) **A83**, 516 (1910); **A84**, 181 (1910); A. G. Nasini and C. Rossi, Gazz. Chim. Ital. **58**, 433 (1928); M. Trautz and R. Heberling, Ann. Physik **20**, 118 (1934).

[i] Beattie, Barriault, and Brierley, J. Chem. Phys. **19**, 1222 (1951).

[j] A. O. Rankine and C. J. Smith, Phil. Mag. **42**, 615 (1921); Y. Ishida, Phys. Rev. **21**, 550 (1923); G. Jung and H. Schmick, Z. physik. Chem. **B7**, 130 (1930); M. Trautz and R. Zink, Ann. Physik **7**, 427 (1930); M. Trautz and K. G. Sorg, *ibid.* **10**, 81 (1931); H. L. Johnston and K. E. McCloskey, J. Phys. Chem. **44**, 1038 (1940); R. Wobser and F. Müller, Kolloid-Beihefte **52**, 165 (1941).

[k] F. A. Freeth and T. T. H. Verschoyle, Proc. Roy. Soc. (London) **A130**, 453 (1931); A. Michels and G. W. Nederbragt, Physica **2**, 1000 (1935); Beattie, Stockmayer, and Ingersoll, J. Chem. Phys. **9**, 871 (1941); J. A. Beattie and W. H. Stockmayer, *ibid.* **10**, 473 (1942).

[l] Landolt-Bornstein, *Physikalisch-Chemische Tabellen;* K. Clusius, Z. physik. Chem. **B3**, 41 (1929); J. O. Clayton and W. F. Giaque, J. Am. Chem. Soc. **54**, 2610 (1932); **55**, 4875, 5071 (1933).

[m] H. K. Onnes and A. T. van Urk, Leiden Comm. **169d, e** (1924); L. Holborn and J. Otto, Z. Physik **10**, 367 (1922); **23**, 77 (1924); **30**, 320 (1924); **33**, 1 (1925); Michels, Wouters, and de Boer, Physica **1**, 587 (1934).

[n] C. J. Smith, Proc. Phys. Soc. (London) **34**, 155 (1922); M. Trautz and P. B. Baumann, Ann. Physik **2**, 733 (1929); M. Trautz and W. Ludewigs, *ibid.* **3**, 409 (1929); M. Trautz and A. Melster, *ibid.* **7**, 409 (1930); M. Trautz and R. Zink, *ibid.* **7**, 427 (1930); M. Trautz and R. Heberling, *ibid.* **10**, 155 (1931); M. Trautz and E. Gabriel, *ibid.* **11**, 606 (1931); A. van Itterbeek and W. H. Keesom, Physica **2**, 97 (1935); P. J. Rigden, Phil. Mag. **25**, 961 (1938); H. L. Johnston and K. E. McCloskey, J. Phys. Chem. **44**, 1038 (1940); R. Wobser and F. Müller, Kolloid-Beihefte **52**, 165 (1941); V. Vasilesco, Ann. phys. **20**, 137, 292 (1945); van Itterbeek, van Paemel, and van Lierde, Physica **13**, 88 (1947).

[o] T. T. H. Verschoyle, Proc. Roy. Soc. (London) **A111**, 552 (1926); G. A. Scott, *ibid.* **A125**, 330 (1929); D. T. A. Townend and L. A. Bhatt, *ibid.* **A134**, 502 (1931); Michels, Lupton, Wassenaar, and de Graaf, Physica **18**, 121 (1952).

[p] C. J. Smith, Proc. Phys. Soc. (London) **34**, 155 (1922); M. Trautz and P. B. Baumann, Ann. Physik **2**, 733 (1929); M. Trautz and W. Ludewigs, *ibid.* **3**, 409 (1929); M. Trautz and A. Melster, *ibid.* **7**, 409 (1930); R. Wobser and F. Müller, Kolloid-Beihefte **52**, 165 (1941); H. L. Johnston and E. R. Grilly, J. Phys. Chem. **46**, 948 (1942); van Itterbeek, van Paemel, and van Lierde, Physica **13**, 88 (1947).

(2) The value of ϵ is next calculated directly from Eq. (3).

(3) Another value of α is chosen and the procedure repeated. A pair of values of r_m and ϵ is thus obtained for each value of α selected.

(4) The value of α is finally found from experimental values of the viscosity and second virial coefficients by the method of translation of axes described in reference 3. In this method a plot of experimental quantities, for example $\log B(T)$ *vs* $\log T$ where $B(T)$ is the second virial coefficient and T is the absolute temperature, is moved until it coincides with one of a family of theoretical curves; the amount of translation parallel to each axis determines r_m and ϵ, and the particular curve chosen from the family determines α. In the present case r_m and ϵ are already known for a given α, so the experimental curve is moved the corresponding amount and examined to see if it coincides with the theoretical curve corresponding to the same α as do r_m and ϵ. If not, a new value of α is selected and the process repeated until the values of α coincide.

The above procedure obviously overspecifies the potential parameters; either the viscosity or the second virial coefficient would be sufficient to determine α, whereas we have used both. This fact in itself affords a test of the usefulness of the potential form used, since an unsuitable potential form would be unable to accomplish the simultaneous fit of more than the minimum number of properties needed to evaluate the potential parameters.

Table I lists the potential parameters found by the above procedure for some simple nonpolar molecules, and Table II gives a brief summary of the crystal data used to determine the parameters. For comparison, the potential parameters obtained by Corner[4] from crystal, second virial, and Joule-Thomson coefficient data for neon and argon for the Buckingham-Corner potential[7] (which is very similar to the exp-six potential except at small values of the separation distance) are

Ne: $\alpha=13.6$, $r_m=3.16$A, $\epsilon/k=37.1$°K;
A: $\alpha=13.9$, $r_m=3.87$A, $\epsilon/k=123.2$°K.

The agreement with the exp-six parameters of Table I is satisfactory.

In some cases it was not possible to fit all measured properties with only one set of potential parameters;

TABLE II. Summary of crystal data used for the determination of potential parameters.

Substance	R (A)	E_0 (cal/mole)	Θ_D (°K)
Ne	3.20	591	64
A	3.81	2029	80
Kr	3.94	2719	63
Xe	4.33	3901	55
CH_4	4.16	2508	78
N_2	4.02	1804	68
CO	4.08	2083	79.5

[7] R. A. Buckingham and J. Corner, Proc. Roy. Soc. (London) **A189**, 118 (1947).

this failure is discussed in the next section. It was necessary to extrapolate the tables in references 1 and 2; the supplementary tables obtained by the extrapolations are given in the appendix.

COMPARISON WITH EXPERIMENT

A. Spherical Molecules

Included in the category of spherical molecules are neon, argon, krypton, xenon, and methane. Strictly speaking, the theories which relate the second virial coefficients and transport properties to the intermolecular potential are not really applicable to the methane molecule, which has internal degrees of freedom. However, the internal degrees of freedom do not seem to have much effect except in the case of the thermal conductivity, for which the theory fails.

The test of the suitability of Eq. (1) as a potential form is its ability to reproduce gas properties data, since the crystal data are automatically reproduced by the procedure used to determine the potential parameters. Figure 1 shows a comparison of measured values of the second virial coefficient, $B(T)$, and values calculated from the parameters of Table I according to the equations

$$B(T)=b_m B^*(\alpha,T^*), \tag{4}$$

$$b_m=(2\pi/3)N_0 r_m^3, \tag{5}$$

where $B^*(\alpha,T^*)$ is a dimensionless quantity tabulated in reference 2 as a function of α and $T^*(=kT/\epsilon)$, and the other factors are as previously defined. Also shown are the values of $B(T)$ calculated for the widely used Lennard-Jones (12-6) potential[8]

$$\varphi(r)=\epsilon\left[\left(\frac{r_m}{r}\right)^{12}-2\left(\frac{r_m}{r}\right)^{6}\right], \tag{6}$$

where $\varphi(r)$, ϵ, and r_m are as defined in connection with Eq. (1). Different values of the parameters r_m and ϵ of the L.-J. (12-6) potential are often available for the same substance, depending on which properties were used to evaluate the parameters. We have chosen the values based, at least in part, on crystal data; these are listed in Table III. The agreement between the observed and calculated values of $B(T)$ is excellent in the cases of neon and argon for both the exp-six and the L.-J. (12-6) potentials. The agreement is only fair for methane and xenon; for xenon the exp-six potential fits $B(T)$ better at low temperatures, whereas the L.-J. (12-6) potential fits better at high temperatures. The agreement in the case of krypton is good for the exp-six potential, but rather poor for the L.-J. (12-6) potential. On the whole, however, neither potential is markedly superior to the other as judged on the basis of second virial coefficients.

TABLE III. Lennard-Jones (12-6) potential parameters for spherical, nonpolar molecules.

Substance	Parameters r_m (A)	Parameters ϵ/k (°K)	Ref.
Ne	3.16	36.3	a
A	3.87	119.3	a
Kr	4.04	159	b
Xe	4.46	228	b
CH_4	4.22	148	b

[a] "Best" values calculated from crystal and second virial coefficient data by J. Corner (reference 4).
[b] Calculated from crystal data by the method given by J. Corner in Trans. Faraday Soc. 35, 711 (1939).

[8] All tabulations necessary for calculating properties of gases obeying a Lennard-Jones (12-6) potential may be found in Hirschfelder, Curtiss, Bird, and Spotz, *The Molecular Theory of Gases and Liquids* (John Wiley and Sons, Inc., New York, 1954).

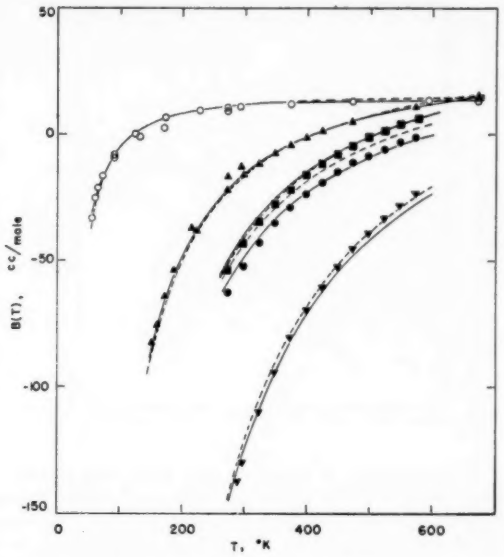

FIG. 1. Comparison of observed and calculated values of the second virial coefficients of spherical molecules. Solid line: exp-six potential; broken line: Lennard-Jones (12-6) potential. Observed values: ○ neon, ▲ argon, ● krypton, ▼ xenon, ■ methane.

Figure 2 shows a similar comparison between the experimental values of the viscosity and those calculated from the exp-six parameters of Table I according to the equation

$$10^7\eta=\frac{266.93(MT)^{\frac{1}{2}}}{r_m^2}\frac{f_\eta^{(3)}(\alpha,T^*)}{\Omega^{(2,2)*}(\alpha,T^*)}, \tag{7}$$

where η is the viscosity in g-cm^{-1}-sec^{-1}, M is the molecular weight, r_m is in angstroms, and $f_\eta^{(3)}(\alpha,T^*)$ and $\Omega^{(2,2)*}(\alpha,T^*)$ are dimensionless functions which may be obtained from the tabulations in reference 1. Also shown are the values calculated from the L.-J. (12-6) parameters of Table III. All the experimental values were corrected to a uniform relative basis in which the viscosity of air at 23°C was taken as 1833.0×10^{-7} g-cm^{-1}-sec^{-1}. Several discrepancies between experiment and theory are apparent. The measured values for argon deviate badly from the calculated curves at high temperatures. In this region forces of repulsion dominate, and the slope of the experimental curve implies an extremely steep repulsion energy at close distances of ap-

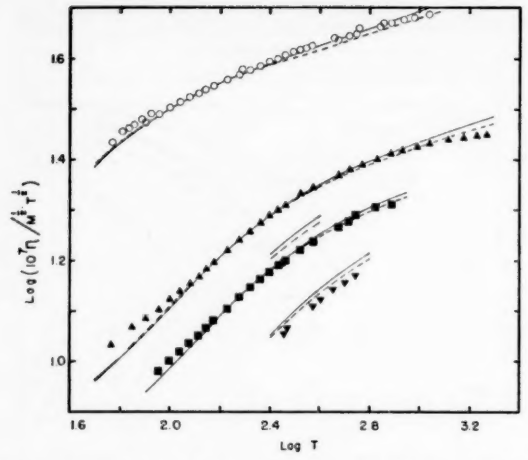

FIG. 2. Comparison of observed and calculated values of the viscosities of spherical molecules. Solid line: exp-six potential; broken line: Lennard-Jones (12-6) potential. Observed values: ○ neon, ▲ argon, ● krypton, ▼ xenon, ■ methane.

proach of two molecules. However, experiments on the scattering of high-velocity argon beams in argon gas[9] give information on the intermolecular potential in this region of strong repulsion, and no indication of such a steep repulsion is found. It therefore seems likely that the experimental viscosity results for argon are low at high temperatures. The deviations at low temperatures for argon and methane are greater than the estimated experimental error; we can think of no explanation for this. The rather scanty measurements of the viscosities of krypton and xenon are also seen to deviate from the theoretical curves. Since these gases are difficult to obtain pure, it is possible that some light gas impurities were present. Further experiments would be helpful in clarifying this point. Within the experimental error, the exp-six and the L.-J. (12-6) potentials are about equally successful in reproducing the experimental viscosities.

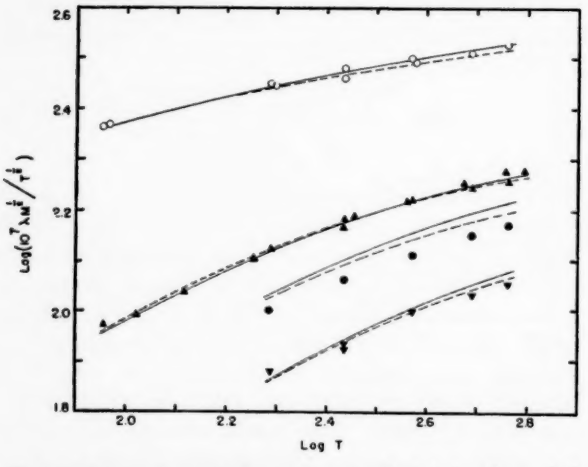

FIG. 3. Comparison of observed and calculated values of the thermal conductivities of spherical molecules. Solid line: exp-six potential; broken line: Lennard-Jones (12-6) potential. Observed values: ○ neon, ▲ argon, ● krypton, ▼ xenon.

[9] I. Amdur and E. A. Mason, J. Chem. Phys. (to be published).

A more important test of an intermolecular potential function is its ability to reproduce properties other than the ones used in determining the potential parameters. Figure 3 shows a comparison between the experimental values[10] of the thermal conductivity and those calculated from the exp-six parameters of Table I according to the equation

$$10^7\lambda=\frac{1989.1T^{\frac{1}{2}}}{M^{\frac{1}{2}}r_m^2}\frac{f_\lambda^{(3)}(\alpha,T^*)}{\Omega^{(2,2)*}(\alpha,T^*)}, \tag{8}$$

where λ is the thermal conductivity in cal-cm^{-1}-sec^{-1}-deg^{-1}, $f_\lambda^{(3)}(\alpha,T^*)$ is a dimensionless function tabulated in reference 1, and the other terms are as defined in connection with Eq. (7). Also shown in Fig. 3 are the values of λ, calculated for the L.-J. (12-6) potential. The theory from which Eq. (8) is derived takes no account of energy transported in the molecular internal degrees of freedom, so methane is excluded from this comparison. No exact method for calculating the transport of energy by the internal degrees of freedom has yet been worked out.

Experimental values of λ are much more difficult to determine accurately than values of η, but within the experimental error the exp-six and L.-J. (12-6) potentials reproduce the measured values of λ about equally well. The agreement is excellent for neon and argon, only fair for xenon, and poor for krypton. It should be pointed out that according to Eqs. (7) and (8) values of λ and η for the same gas are not independent, but instead are directly proportional (except for the functions $f_\lambda^{(3)}$ and $f_\eta^{(3)}$, which are very nearly equal). Thus comparison of observed and calculated values of λ is not an independent test of the suitability of potential parameters derived from observed values of η, but is more a check on the consistency of the measured values of λ and η according to the fundamental theory from which Eqs. (7) and (8) are derived. Comparison of Figs. 2 and 3 shows that such measurements are not always consistent. For example, the agreement between experiment and calculation for the thermal conductivity of xenon is better than the agreement for the viscosity, which incidentally furnishes some support for our suspicion that the measured viscosities are low. On the other hand, the observed values of λ and η for krypton are consistent, but the agreement with the calculated values is poor, which is surprising. One explanation for this discrepancy is of course that both sets of measurements are in error by approximately the same amount, but a more likely

[10] A. Eucken, Physik. Z. **12**, 1101 (1911) (A); S. Weber, Ann. Physik **54**, 437, 481 (1917) (Ne, A); Leiden Comm. Suppl. **42b** (1918) (Ne); M. Curie and A. Lepape, Compt. rend. **193**, 842 (1931); J. phys. radium **2**, 393 (1931) (Ne, A, Kr, Xe); B. G. Dickens, Proc. Roy. Soc. (London) **A143**, 517 (1934) (A); W. G. Kannuluik and L. H. Martin, Proc. Roy. Soc. (London) **A144**, 496 (1934) (Ne, A); W. G. Kannuluik and E. H. Carman, Proc. Phys. Soc. (London) **B65**, 701 (1952) (Ne, A, Kr, Xe); F. G. Keyes, Project Squid Tech. Mem. Mass. Inst. Technol.-1 (Oct. 1, 1952) (A); F. G. Keyes and B. G. Humphrey, private communication from B. G. Humphrey (November 2, 1953) (A).

explanation is that the crystal data used to evaluate the potential parameters are in error.

A property which serves as a better test of the suitability of our exp-six potential parameters than the thermal conductivity is the coefficient of self-diffusion, given by the relation

$$10^4 D=\frac{26.280T^{\frac{1}{2}}}{M^{\frac{1}{2}}r_m^{\,2}}\frac{f_D^{(3)}(\alpha,T^*)}{\Omega^{(1,1)*}(\alpha,T^*)}, \tag{9}$$

where D is the self-diffusion coefficient in cm^2/sec at a pressure of one atmosphere, $f_D^{(3)}(\alpha,T^*)$ and $\Omega^{(1,1)*}(\alpha,T^*)$ are dimensionless functions which may be obtained from the tabulations in reference 1, and the other quantities are as defined in connection with Eq. (7). Figure 4 is a comparison of the experimental values[11] of the self-diffusion coefficient with those calculated for the exp-six potential and the L.-J. (12-6) potential. The agreement is excellent for argon, fair for neon, and rather poor for krypton, xenon, and methane, for which the scatter of the experimental points is large. Within the scatter of the observed values, both potentials are about equally satisfactory.

A final quantity suitable as a test of potential parameters is the thermal diffusion ratio k_T. For a binary mixture of heavy isotopes, the mth approximation to the thermal diffusion ratio $[k_T]_m$ may be written as

$$[k_T]_m=[k_T^*]_m\left(\frac{M_1-M_2}{M_1+M_2}\right)x_1x_2, \tag{10}$$

correct to the first order of the small quantity $(M_1-M_2)/(M_1+M_2)$, where M_1 and M_2 are the molecular weights of the two isotopes, and x_1 and x_2 are their mole fractions in the mixture. The quantity $[k_T^*]_m$ is a reduced thermal diffusion ratio, and is tabulated in reference 1 for the exp-six potential as a function of α and T^* for $m=2$. A similar function, designated as R_T, is tabulated for the L.-J. (12-6) potential to a first approximation in reference 8; the relation between k_T^* and R_T is $[k_T^*]_1=(105/118)R_T$. Experimental values of k_T^* have been obtained[12] for neon, argon, and methane by measurement of the thermal separation of isotopic mixtures between two absolute temperatures T and T'. An experimental value of k_T^* is thus a mean value over the temperature range of T to T', but it may be shown[13] that such a mean value is equal to the actual value at an

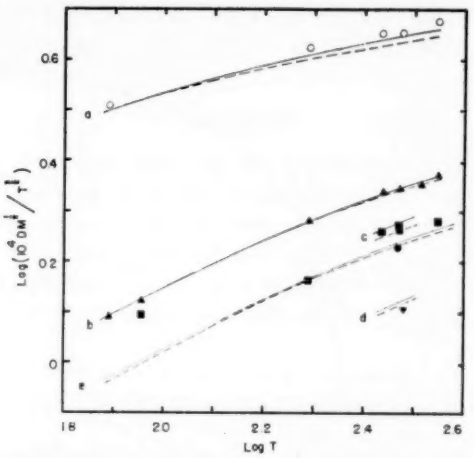

FIG. 4. Comparison of observed and calculated values of the self-diffusion coefficients of spherical molecules. Solid line: exp-six potential; broken line: Lennard-Jones (12-6) potential. Observed values: ⊙ neon, ▲ argon, ● krypton, ▼ xenon, ■ methane. Curves *a*, *b*, *c*, *d*, and *e* represent neon, argon, krypton, xenon, and methane, respectively.

intermediate temperature $\bar{T}$ given by

$$\bar{T}=\frac{TT'}{T'-T}\ln(T'/T). \tag{11}$$

Figure 5 is a comparison of the experimental and calculated values of the reduced thermal diffusion ratio k_T^* as a function of $\bar{T}$. The agreement for argon and methane is slightly better for the exp-six potential than for the L.-J. (12-6) potential; for neon the agreement is poor for both potentials. The continued increase of k_T^* for neon at high temperatures implies a very steep repulsive potential;[14] the existence of such a steep repulsion is supported neither by the viscosity data shown in Fig. 2 nor by results obtained from the scattering of

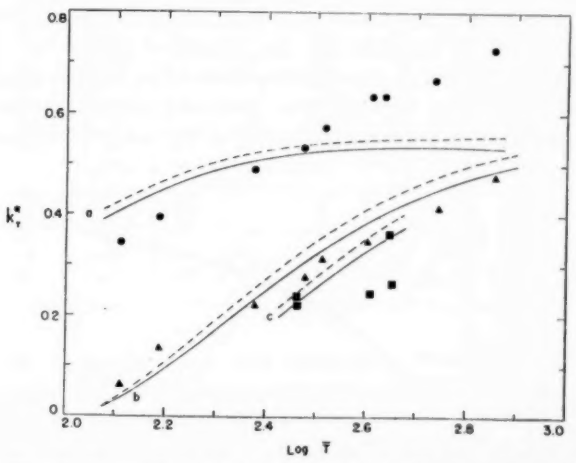

FIG. 5. Comparison of observed and calculated values of the reduced thermal diffusion ratios for spherical molecules. Solid line: exp-six potential; broken line: Lennard-Jones (12-6) potential. Observed values: ⊙ neon, ▲ argon, ■ methane. Curves *a*, *b*, and *c* represent neon, argon, and methane, respectively.

[11] W. Groth and P. Harteck, Z. Elektrochem. **47**, 167 (1941) (Kr); E. B. Winn and E. P. Ney, Phys. Rev. **72**, 77 (1947) (CH_4); F. Hutchinson, Phys. Rev. **72**, 1256 (1947), J. Chem. Phys. **17**, 1081 (1949) (A); E. B. Winn, Phys. Rev. **80**, 1024 (1950) (Ne, CH_4); S. Visner, Phys. Rev. **82**, 297 (1951) (Xe).

[12] A. O. Nier, Phys. Rev. **56**, 1009 (1939) (CH_4); Phys. Rev. **57**, 338 (1940) (Ne); L. G. Stier, Phys. Rev. **62**, 548 (1942) (Ne, A); A. K. Mann, Phys. Rev. **73**, 413 (1948) (Ne, A); A. N. Davenport and E. R. S. Winter, Trans. Faraday Soc. **47**, 1160 (1951) (CH_4).

[13] H. Brown, Phys. Rev. **58**, 661 (1940). See also A. N. Davenport and E. R. S. Winter, Trans. Faraday Soc. **47**, 1160 (1951).

[14] T. Kihara, Revs. Modern Phys. **25**, 831 (1953).

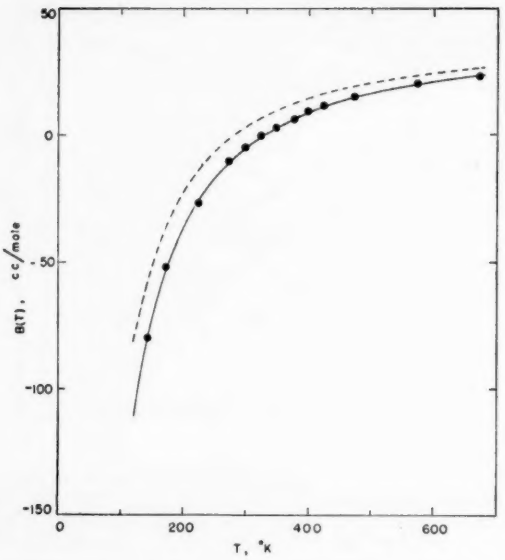

FIG. 6. Comparison of the observed second virial coefficients of nitrogen with those calculated for the exp-six potential. Solid line: calculated using the parameters derived from crystal properties and second virial coefficients; broken line: calculated using the parameters derived from viscosity.

beams of high velocity neon atoms by neon gas.[9] Further measurements of k_T^* for neon at high temperatures would seem to be desirable.

B. Nonspherical Molecules

Included in this category are nitrogen, carbon monoxide, oxygen, and carbon dioxide. There are of course many other nonspherical, nonpolar molecules, but only for these four does there exist a sufficient quantity of experimental data to justify the assignment of three disposable parameters (α, r_m, ϵ) on the basis of the measured properties.

The L.-J. (12-6) potential has not been completely successful in reproducing the measured properties of gases composed of nonspherical molecules, the principal difficulty being that different potential parameters are required to fit different properties of the same substance.

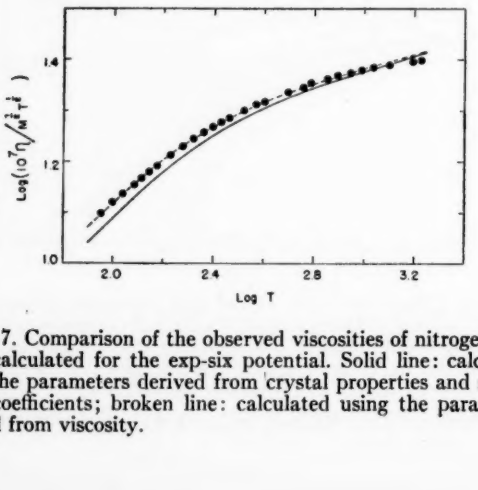

FIG. 7. Comparison of the observed viscosities of nitrogen with those calculated for the exp-six potential. Solid line: calculated using the parameters derived from crystal properties and second virial coefficients; broken line: calculated using the parameters derived from viscosity.

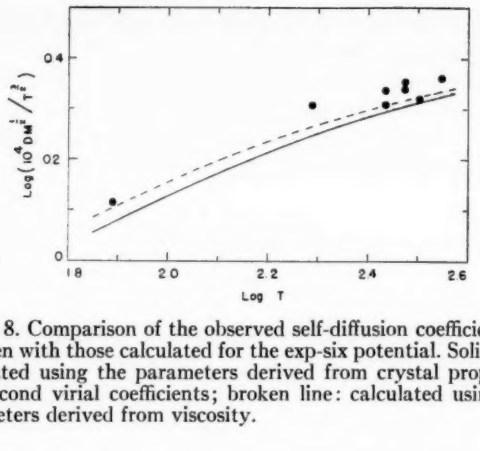

FIG. 8. Comparison of the observed self-diffusion coefficients of nitrogen with those calculated for the exp-six potential. Solid line: calculated using the parameters derived from crystal properties and second virial coefficients; broken line: calculated using the parameters derived from viscosity.

The question arises whether the fault is primarily that the potential form is inadequate, or that the basic theory is inapplicable because of its assumptions of spherically symmetric intermolecular potentials and elastic intermolecular collisions. Some light might be thrown on this question by the use of the exp-six potential, which is more realistic and contains more disposable parameters than the L.-J. (12-6) potential. If the exp-six potential fails for nonspherical molecules in the same way as does the L.-J. (12-6), it might reasonably be supposed that the trouble lies primarily with the basic theory rather than with the potential form.

It is not necessary to look far to see that the exp-six potential is not entirely successful in dealing with nonspherical molecules. Oxygen and carbon dioxide cannot be handled by the method used for spherical molecules because they do not crystallize in the cubic form. Clearly the nonspherical nature of the molecule has a strong effect on the crystal properties, but it is not even possible to fit both the second virial and the viscosity coefficients of oxygen and carbon dioxide with a single set of potential parameters. The best that can be done is to assign different parameters for each property, thereby reducing the exp-six potential to the status of an unnecessarily complicated interpolation function.

The situation is somewhat better for nitrogen and carbon monoxide, which crystallize in the cubic system. Now it is possible to fit both the crystal properties and the second virial coefficients with a single set of potential parameters, but impossible to fit both the crystal properties and the viscosities for any reasonable value of the parameter α. This behavior is shown by our assign-

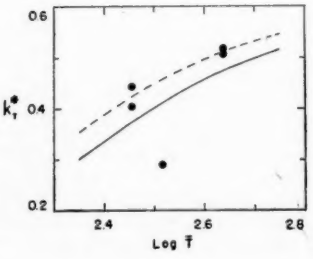

FIG. 9. Comparison of the observed reduced thermal diffusion ratios of nitrogen with those calculated for the exp-six potential. Solid line: calculated using the parameters derived from crystal properties and second virial coefficients; broken line: calculated using the parameters derived from viscosity.

ment of two sets of potential parameters for nitrogen and carbon monoxide in Table I. The situation is more clearly illustrated in Figs. 6 and 7, where the experimental second virial and viscosity coefficients of nitrogen are compared with the values calculated from the two sets of parameters in Table I. Each set of parameters accurately reproduces the experimental results for which the parameters were evaluated, but fails to fit the other experimental results.

Although the exp-six parameters derived from viscosity do not reproduce the crystal properties and second virial coefficients for nonspherical molecules, they may be fairly successful in reproducing other transport properties, as is illustrated in Figs. 8 and 9, where

TABLE IV. The reduced second virial coefficients.

T^*	$B^*(\alpha,T^*)$ $\alpha=16$	$\alpha=17$
0.40	−8.60	−8.28
0.45	−6.68	−6.44
0.50	−5.40	−5.19
0.60	−3.82	−3.67
0.70	−2.88	−2.77
0.80	−2.26	−2.16
0.90	−1.83	−1.75
1.0	−1.505	−1.429
1.2	−1.063	−1.000
1.4	−0.772	−0.717
1.6	−0.568	−0.518
1.8	−0.420	−0.375
2.0	−0.302	−0.259
2.5	−0.107	−0.070
3.0	0.016	0.048
3.5	0.099	0.128
4.0	0.159	0.188
4.5	0.201	0.227
5	0.236	0.261
6	0.284	0.307
7	0.316	0.338
8	0.338	0.360
9	0.354	0.375
10	0.366	0.387
20	0.397	0.417
30	0.393	0.412
40	0.383	0.402
50	0.373	0.393
60	0.364	0.384
70	0.356	0.376
80	0.348	0.368
90	0.341	0.361
100	0.334	0.355

experimental self-diffusion coefficients[15] and thermal diffusion ratios[16] of nitrogen are compared with the values calculated from the two sets of parameters for nitrogen. The parameters derived from the viscosity give better agreement than those derived from crystal and second virial coefficient data. Thus if it is necessary to calculate some property of a gas composed of nonspherical molecules, it is probably best to use parameters derived from equilibrium measurements if the desired property is an equilibrium one, and to use parameters derived from the viscosity for calculating transport properties.

[15] E. B. Winn, Phys. Rev. **74**, 698 (1948); **80**, 1024 (1950); E. R. S. Winter, Trans. Faraday Soc. **47**, 342 (1951).

[16] A. K. Mann, Phys. Rev. **73**, 413 (1948); A. N. Davenport and E. R. S. Winter, Trans. Faraday Soc. **47**, 1160 (1951).

SUMMARY

The three-parameter exp-six intermolecular potential has been shown to be able to predict, with a single set of potential parameters, the properties of gases composed of spherical molecules with fair accuracy. For the gases considered here, however, the simpler two-parameter L.-J. (12-6) potential is scarcely inferior (in contrast to the case of helium and hydrogen).[3] For gases whose molecules deviate appreciably from spherical symmetry, a single set of potential parameters is not able to reproduce all the measured properties. Since the form of the exp-six potential is physically realistic and quite flexible, such behavior would seem to indicate that the assumptions of central intermolecular forces and elastic intermolecular collisions made in the basic theory are inadequate to describe the behavior of most real gases.

TABLE V. Collision integral functions.

	$\alpha=16$				$\alpha=17$			
T^*	$Z^{(1,1)}$	$Z^{(1,2)}$	$Z^{(2,2)}$	$Z^{(2,3)}$	$Z^{(1,1)}$	$Z^{(1,2)}$	$Z^{(2,2)}$	$Z^{(2,3)}$
0	1.187	1.055	1.195	1.095	1.187	1.055	1.195	1.095
0.1	1.167	1.029	1.197	1.099	1.160	1.025	1.190	1.092
0.2	1.153	1.012	1.204	1.107	1.148	1.010	1.196	1.100
0.3	1.129	0.977	1.207	1.105	1.125	0.977	1.201	1.102
0.4	1.100	0.937	1.198	1.082	1.099	0.943	1.196	1.084
0.5	1.070	0.903	1.178	1.051	1.074	0.912	1.180	1.058
0.6	1.043	0.876	1.154	1.021	1.050	0.888	1.159	1.031
0.7	1.019	0.856	1.130	0.995	1.029	0.871	1.138	1.007
0.8	1.000	0.841	1.108	0.974	1.012	0.858	1.119	0.988
0.9	0.984	0.831	1.088	0.958	0.998	0.849	1.101	0.974
1.0	0.971	0.824	1.072	0.946	0.987	0.844	1.087	0.963
1.2	0.952	0.818	1.048	0.931	0.971	0.839	1.065	0.950
1.4	0.941	0.817	1.032	0.925	0.962	0.840	1.052	0.946
1.6	0.935	0.820	1.023	0.925	0.957	0.844	1.044	0.947
1.8	0.932	0.825	1.019	0.928	0.956	0.850	1.041	0.951
2.0	0.932	0.831	1.017	0.933	0.957	0.858	1.041	0.958
2.5	0.938	0.849	1.023	0.951	0.966	0.878	1.050	0.978
3.0	0.949	0.867	1.036	0.972	0.979	0.899	1.065	1.002
3.5	0.962	0.886	1.052	0.993	0.994	0.920	1.083	1.025
4	0.975	0.903	1.069	1.014	1.010	0.940	1.102	1.048
5	1.002	0.936	1.103	1.053	1.041	0.976	1.139	1.090
6	1.028	0.964	1.135	1.088	1.070	1.007	1.175	1.129
7	1.053	0.990	1.165	1.119	1.097	1.036	1.208	1.163
8	1.075	1.013	1.193	1.147	1.122	1.061	1.238	1.194
9	1.096	1.034	1.219	1.172	1.145	1.085	1.266	1.221
10	1.115	1.053	1.242	1.195	1.167	1.106	1.292	1.247
12	1.149	1.086	1.284	1.236	1.205	1.144	1.339	1.292
14	1.180	1.115	1.321	1.272	1.239	1.177	1.379	1.331
16	1.207	1.142	1.354	1.304	1.270	1.207	1.415	1.366
18	1.231	1.165	1.384	1.332	1.298	1.233	1.448	1.398
20	1.254	1.186	1.411	1.358	1.323	1.258	1.478	1.426
25	1.303	1.233	1.470	1.415	1.379	1.311	1.543	1.489
30	1.345	1.273	1.520	1.463	1.427	1.357	1.598	1.542
35	1.381	1.307	1.564	1.506	1.468	1.397	1.647	1.589
40	1.413	1.339	1.603	1.544	1.506	1.434	1.689	1.630
45	1.443	1.367	1.639	1.578	1.540	1.466	1.728	1.668
50	1.470	1.393	1.671	1.610	1.571	1.497	1.764	1.703
60	1.518	1.440	1.730	1.668	1.627	1.552	1.828	1.766
70	1.561	1.482	1.782	1.719	1.677	1.601	1.885	1.822
80	1.600	1.520	1.828	1.765	1.722	1.645	1.936	1.873
90	1.635	1.554	1.871	1.807	1.763	1.685	1.983	1.919
100	1.667	1.587	1.910	1.847	1.801	1.723	2.026	1.962

TABLE VI. The functions A^*, C^*, and the reduced thermal diffusion ratio, $[k_T^*]_1$.

	$\alpha=16$			$\alpha=17$		
T^*	A^*	C^*	$[k_T^*]_1$	A^*	C^*	$[k_T^*]_1$
0	1.006	0.889	0.311	1.006	0.889	0.311
0.1	1.031	0.886	0.286	1.036	0.886	0.287
0.2	1.047	0.880	0.251	1.050	0.882	0.262
0.3	1.070	0.866	0.170	1.070	0.870	0.193
0.4	1.089	0.852	0.097	1.088	0.858	0.127
0.5	1.101	0.844	0.052	1.099	0.850	0.084
0.6	1.107	0.840	0.034	1.104	0.846	0.066
0.7	1.108	0.840	0.032	1.106	0.846	0.064
0.8	1.108	0.842	0.042	1.105	0.848	0.074
0.9	1.106	0.845	0.060	1.104	0.851	0.091
1.0	1.104	0.849	0.081	1.102	0.855	0.111
1.2	1.100	0.859	0.130	1.097	0.864	0.158
1.4	1.097	0.868	0.179	1.093	0.873	0.206
1.6	1.094	0.877	0.223	1.091	0.882	0.249
1.8	1.093	0.885	0.263	1.089	0.889	0.289
2.0	1.092	0.891	0.299	1.088	0.896	0.323
2.5	1.091	0.905	0.368	1.087	0.909	0.391
3.0	1.092	0.914	0.417	1.087	0.918	0.439
3.5	1.094	0.921	0.453	1.089	0.925	0.475
4	1.096	0.927	0.478	1.091	0.930	0.500
5	1.100	0.934	0.513	1.095	0.937	0.534
6	1.104	0.938	0.531	1.098	0.941	0.553
7	1.107	0.940	0.544	1.101	0.944	0.566
8	1.110	0.942	0.550	1.104	0.946	0.572
9	1.112	0.944	0.557	1.106	0.947	0.580
10	1.114	0.944	0.560	1.108	0.948	0.582
12	1.118	0.945	0.564	1.111	0.949	0.588
14	1.120	0.946	0.563	1.113	0.950	0.587
16	1.122	0.946	0.564	1.114	0.950	0.590
18	1.124	0.946	0.564	1.116	0.950	0.589
20	1.125	0.946	0.564	1.117	0.951	0.591
25	1.128	0.946	0.563	1.119	0.951	0.591
30	1.131	0.946	0.563	1.120	0.951	0.591
35	1.133	0.947	0.564	1.121	0.952	0.593
40	1.134	0.947	0.564	1.121	0.952	0.595
45	1.136	0.947	0.564	1.122	0.952	0.596
50	1.137	0.948	0.567	1.123	0.953	0.598
60	1.139	0.949	0.569	1.124	0.954	0.602
70	1.141	0.949	0.572	1.124	0.954	0.605
80	1.143	0.950	0.574	1.124	0.955	0.609
90	1.145	0.951	0.578	1.125	0.956	0.613
100	1.146	0.952	0.582	1.125	0.957	0.618

ACKNOWLEDGMENTS

The authors wish to express their thanks to Dr. J. O. Hirschfelder for many helpful discussions and suggestions throughout the course of the work. For help with some of the calculations they are indebted to Miss Elaine Petersen and Mr. Donald Jepson.

APPENDIX

The tabulations of transport property collision integrals and second virial coefficients given in references 1 and 2 for the exp-six potential extend from $\alpha=12$ to 15. This range of the parameter α is sufficient for all spherical molecules so far investigated, but nonspherical molecules seem to require larger values of α. We have, therefore, extended the tabulations by extrapolation, with a consequent reduction in accuracy. Whereas the tabulations for $\alpha=12$ to 15 were for the most part accurate to within a few tenths of one percent, the extrapolations may well involve uncertainties amounting to several percent.

The reduced second virial coefficients, $B^*(\alpha,T^*)$, defined by Eq. (4) were extrapolated graphically to $\alpha=17$. The values of $B^*(\alpha,T^*)$ are nearly linear in $(\log\alpha)$, so that the extrapolation is simple. Values of $B^*(\alpha,T^*)$ are given in Table IV for $\alpha=16$, 17.

Some of the reduced collision integrals, $\Omega^{(l,n)*}(\alpha,T^*)$, two of which appear explicitly in Eqs. (7)–(9), were extrapolated to $\alpha=16$, 17. These functions are nearly linear in α. The functions $\Omega^{(l,n)*}$ are not tabulated directly, but instead the related functions,

$$Z^{(l,n)}=[T^*(1-6/\alpha)]^{\frac{1}{2}}\Omega^{(l,n)*}, \tag{12}$$

which are more suitable for interpolation purposes, are given in Table V.

In Table VI are given the values of the following ratios of collision integrals which occur frequently:

$$A^*=\Omega^{(2,2)*}/\Omega^{(1,1)*},$$
$$C^*=\Omega^{(1,2)*}/\Omega^{(1,1)*}. \tag{13}$$

TABLE VII. Functions for calculating higher approximations to the transport coefficients.

	$\alpha=16$			$\alpha=17$		
T^*	$f_\eta^{(2)}$	$f_\lambda^{(2)}$	$f_D^{(2)}$	$f_\eta^{(2)}$	$f_\lambda^{(2)}$	$f_D^{(2)}$
0	1.0017	1.0026	1.0020	1.0017	1.0026	1.0020
0.1	1.0018	1.0028	1.0018	1.0018	1.0028	1.0018
0.2	1.0020	1.0031	1.0014	1.0020	1.0030	1.0015
0.3	1.0016	1.0025	1.0007	1.0017	1.0027	1.0009
0.4	1.0008	1.0012	1.0002	1.0010	1.0016	1.0004
0.5	1.0003	1.0005	1.0001	1.0005	1.0007	1.0002
0.6	1.0001	1.0001	1.0000	1.0002	1.0003	1.0001
0.7	1.0000	1.0000	1.0000	1.0001	1.0002	1.0001
0.8	1.0000	1.0000	1.0000	1.0001	1.0001	1.0001
0.9	1.0000	1.0000	1.0001	1.0001	1.0001	1.0002
1.0	1.0001	1.0001	1.0002	1.0001	1.0002	1.0003
1.2	1.0002	1.0003	1.0004	1.0003	1.0005	1.0006
1.4	1.0004	1.0007	1.0008	1.0006	1.0009	1.0010
1.6	1.0008	1.0013	1.0012	1.0010	1.0016	1.0015
1.8	1.0013	1.0019	1.0016	1.0015	1.0023	1.0020
2.0	1.0017	1.0027	1.0021	1.0020	1.0030	1.0024
2.5	1.0029	1.0045	1.0032	1.0032	1.0049	1.0036
3.0	1.0039	1.0060	1.0041	1.0042	1.0065	1.0045
3.5	1.0047	1.0073	1.0049	1.0051	1.0079	1.0053
4	1.0054	1.0083	1.0054	1.0057	1.0089	1.0059
5	1.0062	1.0096	1.0063	1.0066	1.0103	1.0068
6	1.0067	1.0105	1.0068	1.0072	1.0111	1.0073
7	1.0071	1.0110	1.0072	1.0075	1.0117	1.0077
8	1.0073	1.0113	1.0073	1.0077	1.0120	1.0079
9	1.0074	1.0115	1.0076	1.0078	1.0122	1.0081
10	1.0074	1.0116	1.0077	1.0079	1.0123	1.0082
12	1.0075	1.0117	1.0078	1.0080	1.0124	1.0084
14	1.0075	1.0117	1.0078	1.0080	1.0124	1.0084
16	1.0075	1.0117	1.0079	1.0080	1.0124	1.0085
18	1.0075	1.0117	1.0079	1.0080	1.0124	1.0085
20	1.0075	1.0117	1.0079	1.0079	1.0123	1.0086
25	1.0075	1.0117	1.0079	1.0079	1.0123	1.0086
30	1.0075	1.0117	1.0079	1.0079	1.0123	1.0086
35	1.0076	1.0117	1.0080	1.0079	1.0123	1.0087
40	1.0076	1.0118	1.0080	1.0080	1.0124	1.0087
45	1.0076	1.0119	1.0080	1.0080	1.0124	1.0088
50	1.0077	1.0119	1.0081	1.0080	1.0124	1.0088
60	1.0078	1.0121	1.0082	1.0081	1.0126	1.0090
70	1.0079	1.0123	1.0083	1.0082	1.0128	1.0091
80	1.0081	1.0125	1.0084	1.0083	1.0130	1.0092
90	1.0081	1.0126	1.0085	1.0084	1.0131	1.0093
100	1.0082	1.0128	1.0087	1.0085	1.0133	1.0095

Table VI also gives the values of the first approximation to the reduced thermal diffusion ratio $[k_T^*]_1$ as calculated from a simple, accurate formula derived by Kihara:[17]

$$[k_T^*]_1=\frac{15}{16}\frac{(6C^*-5)}{A^*}. \tag{14}$$

This expression gives values of k_T^* which differ from the values calculated from the elaborate expressions for $[k_T^*]_2$ in reference 1 by no more than the uncertainties involved in the extrapolations of the $\Omega^{(l,s)*}$.

The quantities $f^{(m)}(\alpha,T^*)$ which appear in Eqs. (7)–(9) are functions of the reduced collision integrals, $\Omega^{(l,s)*}$, and are used for calculating higher approximations to the transport coefficients. The superscript indicates the order of approximation used in computing these functions. Kihara[17] has given simple expressions for these functions which differ from the more elaborate expressions used in reference 1 by less than the uncertainty involved in the extrapolations of the $\Omega^{(l,s)*}$. The values of the f's were therefore calculated according to Kihara's expressions

$$f_\eta^{(2)}=1+\frac{3}{49}\left[\frac{4\Omega^{(2,3)*}}{\Omega^{(2,2)*}}-\frac{7}{2}\right]^2,$$

$$f_\lambda^{(2)}=1+\frac{2}{21}\left[\frac{4\Omega^{(2,3)*}}{\Omega^{(2,2)*}}-\frac{7}{2}\right]^2, \tag{15}$$

$$f_D^{(2)}=1+\frac{(6C^*-5)^2}{16A^*+40},$$

and are tabulated in Table VII.

[17] T. Kihara, *Imperfect Gases*, originally published in Japanese (Asakusa Bookstore, Tokyo, 1949) and translated into English by the U. S. Office of Air Research, Wright-Patterson Air Force Base.

THE JOURNAL OF CHEMICAL PHYSICS VOLUME 22, NUMBER 5 MAY, 1954

Determination of Adsorption Energy Heterogeneity of Solid Surfaces

JURGEN M. HONIG* AND EDWARD L. HILL
School of Chemistry and Department of Physics, University of Minnesota, Minneapolis, Minnesota
(Received October 5, 1953)

A revision of the theory for the distribution of adsorption energies among the surface sites of a solid is presented. It is postulated that the distribution function for the adsorption energies is independent of the temperature. With this requirement, and a knowledge of the pressure-temperature dependence of empirical isotherm data, it is possible to determine simultaneously the distribution function and the dependence of the partition function of the adsorbed phase on the adsorption energy. Several examples are presented in illustration of the theory.

1. INTRODUCTION

THE distribution of adsorption energies for the surface sites on solids is a quantity of considerable interest. The aim of the present paper is to present a modification of current theories for the determination of this distribution function from experimental adsorption isotherms. The mathematical aspects of this problem have been studied repeatedly.[1–10] In the present discussion the procedure employed by Sips[7] will be followed closely.

The coverage of a solid surface by adsorbed molecules and the distribution of adsorption energies for the available sites are related functionally by an integral equation. The method used by Sips consists in a reformulation of this integral equation as a Stieltjes transform of the distribution function, which is then inverted by standard techniques. The assumptions basic to this formulation are the following: (a) adsorption occurs on a fixed number of sites; (b) the coverage is limited to a monolayer; (c) each site is associated with a fixed adsorption energy, which is the energy required to remove the adsorbed molecule from the surface back into the gas phase; (d) no lateral interactions occur between adsorbed molecules; (e) each adsorbed particle is bound rigidly to its site and does not move laterally over the surface; (f) the distribution of adsorption energies is not altered during the adsorption process; (g) the partition function of the adsorbed phase is independent of the adsorption energies.

The simultaneous applicability of all of these assumptions is open to doubt in most real systems.

* Present address: Department of Chemistry, Purdue University, Lafayette, Indiana.

[1] J. Zeldowitsh, Acta Physicochim. U.R.S.S. **1**, 961 (1934).
[2] E. Cremer and S. Flügge, Z. phys. Chem. **B41**, 453 (1938); E. Cremer, J. chim. phys. **46**, 411 (1949).
[3] S. Roginsky, Doklady Akad. Nauk. S.S.S.R. **45**, 61, 194 (1944).
[4] M. Temkin and V. Levich, Zhur. Fiz. Khim. **20**, 1441 (1946).
[5] G. D. Halsey and H. S. Taylor, J. Chem. Phys. **15**, 624 (1947).
[6] O. M. Todes and A. K. Bondareva, Zhur. Priklad. Khim. **21**, 693 (1948).
[7] R. Sips, J. Chem. Phys. **16**, 490 (1948); **18**, 1024 (1950).
[8] G. D. Halsey, J. Chem. Phys. **16**, 931 (1948).
[9] T. L. Hill, J. Chem. Phys. **17**, 762 (1949).
[10] F. C. Tompkins, Trans. Faraday Soc. (London) **46**, 569 (1950).

Attempts at the elimination of assumptions (b),[11–13] (d),[8–10,14] and (e)[10,14] have met with some success, but the rigorous modifications of the integral equation give rise to intractable mathematical complications. Some special set of simplifying assumptions or the use of a special model becomes necessary before numerical calculations are feasible. A brief remark concerning the possible elimination of assumption (g) was given in Sips' second paper.[7]

A difficulty which arises in Sips' inversion method is that the temperature appears as a parameter in the calculated distribution function. It seems to us to be more in consonance with the physical interpretation of the adsorption process to require that this function be independent of temperature, at least so long as the temperature range is not so great as to produce physical changes in the surface. In the first place, the forces of van der Waals type which are responsible for the physical adsorption mechanism are temperature independent. Furthermore, under assumption (f) the distribution function is a property of the surface alone, and so should be independent of external factors.

The object of the present discussion is to introduce the requirement that the distribution function be independent of the temperature. This requirement has two consequences: (1) the isotherm equations which can be used to represent experimental adsorption data are limited to special classes of functions satisfying quite stringent requirements; (2) it is possible to determine both the distribution of adsorption energies among surface sites and the dependence of the partition function for the adsorbed phase on the adsorption energy. Assumption (g) can thus be eliminated.

In order to avoid excessive mathematical complications the other assumptions will be retained. Since we shall restrict ourselves to physical adsorption processes, assumptions (a) and (f) should be applicable. At sufficiently low temperatures (e) is probably valid if (b) is satisfied, while by a judicious choice of the adsorbate and by selection of data in the region of low surface coverage, the importance of assumptions (b) and (d) can be minimized. It has been shown[10,14] that even when (e) is not valid the analysis is not altered fundamentally. In fact, Halsey[14] has suggested that if the distribution function diminishes sufficiently rapidly with increasing adsorption energy, the inapplicability of (d) leads to no observable consequences. It can thus be hoped that under suitable experimental conditions the mathematical procedures and physical concepts discussed below can be tested.

[11] W. G. McMillan, J. Chem Phys. **15**, 390 (1947).
[12] W. C. Walker and A. C. Zettlemoyer, J. Phys. & Colloid Chem. **52**, 47, 58 (1948).
[13] J. M. Honig, J. Phys. Chem. **57**, 353 (1953).
[14] G. D. Halsey, J. Am. Chem. Soc. **73**, 2693 (1951).

2. THEORY

Under assumptions (a) to (f) the fraction of the surface covered by adsorbate is given by the integral

$$\theta(p,T)=\int_0^\infty \frac{f(\epsilon)d\epsilon}{1+[\beta(\epsilon,T)/p]e^{-\epsilon/kT}}, \tag{1}$$

with the quantity β defined as

$$\beta(\epsilon,T)=\left(\frac{2\pi mkT}{h^2}\right)^{\frac{3}{2}}\cdot kT\cdot\frac{j_g(T)}{j_s(\epsilon,T)}. \tag{2}$$

In these relations p is the gas pressure, $f(\epsilon)d\epsilon$ is the fraction of sites associated with adsorption energies in the range from ϵ to $\epsilon+d\epsilon$, while j_g and j_s are the internal partition functions of the gaseous and adsorbed species, respectively.

More generally, if the smallest energy of adsorption on the surface has the value $\epsilon=\epsilon_0>0$, this is allowed for by writing

$$\eta=\epsilon-\epsilon_0\geqslant 0. \tag{3}$$

Since the distribution function now has the property that $f(\epsilon)=0$ for $0\leqslant\epsilon<\epsilon_0$, it becomes convenient to alter its formal definition by writing

$$F(\eta)=f(\eta+\epsilon_0). \tag{4}$$

We note for future reference that this function satisfies the normalization condition

$$\int_0^\infty F(\eta)d\eta=1. \tag{5}$$

With this notation Eq. (1) becomes

$$\theta(p,T)=\int_0^\infty \frac{F(\eta)d\eta}{1+[\alpha(\eta,\epsilon_0,T)/p]e^{-\eta/kT}}, \tag{6}$$

in which we have made the definition

$$\alpha(\eta,\epsilon_0,T)=\beta(\eta+\epsilon_0,T)\exp(-\epsilon_0/kT). \tag{7}$$

It is desirable to convert the integral in Eq. (6) to the Stieltjes transform of the distribution function before inverting it as an integral equation. This is accomplished by the substitutions

$$\lambda=(\alpha_0/\alpha)e^{\eta/kT}-1,\quad 0\leqslant\lambda\leqslant\infty, \tag{8}$$

$$y=(\alpha_0/p)+1, \tag{9}$$

in which

$$\alpha_0=\alpha(0,\epsilon_0,T). \tag{10}$$

The solution of Eq. (8) for η will be indicated as

$$\eta=Q(\lambda,T), \tag{11}$$

from which we have, taking T to be constant,

$$d\eta=(\partial Q/\partial\lambda)_T d\lambda. \tag{12}$$

The substitutions

$$L(y,T)=\theta\left(\frac{\alpha_0}{y+1},\,T\right), \tag{13}$$

$$g(\lambda,T)=(\lambda+1)\cdot F(\eta)\cdot(\partial Q/\partial\lambda)_T, \tag{14}$$

now bring Eq. (6) to the form

$$L(y,T)=\int_0^\infty \frac{g(\lambda,T)d\lambda}{\lambda+y}. \tag{15}$$

This relation is now treated as an integral equation, the left-hand side being supposed known from empirical measurements. On applying standard procedures[15,16] for its inversion, we find the solution in symbolic form

$$g(\lambda,T)=\phi(\eta,T)=(i2\pi)^{-1}[L(\lambda e^{-i\pi},T)-L(\lambda e^{i\pi},T)]. \tag{16}$$

The symbol $\phi(\eta,T)$ denotes the function which is obtained from $g(\lambda,T)$ by elimination of λ through use of definition (8). Insertion of Eqs. (8) and (14) into (16) now yields the solution for the distribution function

$$F(\eta)=\left(\frac{\partial\ln(\lambda+1)}{\partial\eta}\right)_T\phi(\eta,T)$$

$$=\left[\frac{1}{kT}+\frac{\partial\ln j_s}{\partial\eta}\right]\phi(\eta,T). \tag{17}$$

Equation (17) contains two unknown functions, F and j_s, which can be obtained individually only when some other relation is imposed on them. For this purpose we employ the requirement that the distribution function be independent of the temperature. One finds from (17) that this condition is

$$\left(\frac{\partial F}{\partial T}\right)_\eta\equiv\left(\frac{1}{kT}+\frac{\partial\ln j_s}{\partial\eta}\right)\frac{\partial\phi}{\partial T}$$

$$+\left(-\frac{1}{kT^2}+\frac{\partial^2\ln j_s}{\partial\eta\partial T}\right)\phi=0. \tag{18}$$

The problem of determining the functions F and j_s from empirical adsorption isotherm data has now been solved, at least in principle. It is seen from Eqs. (17) and (18) that the dependence of the isotherm data on both the pressure and the temperature must be known to provide for the evaluation of the functions ϕ and $\partial\phi/\partial T$ from Eqs. (13) and (16). It is clear, however, that the actual detailed procedures required for finding the explicit solutions may become extremely complicated. The investigation of the analytical solutions of Eqs. (17) and (18) is beyond the scope of this paper. We shall confine ourselves to the illustration of the theory by a few special cases of physical interest. These will be limited to the adsorption of a monatomic gas, the analogous treatment for even a diatomic gas being considerably more difficult.

[15] E. C. Titchmarsh, *Theory of Fourier Integrals* (Oxford University Press, Oxford, 1948), second edition, Sec. 11.8.

[16] D. V. Widder, *The Laplace Transform* (Princeton University Press, Princeton, 1941), Chap. 8.

3. APPLICATIONS

In the absence of electronic degeneracy the partition function associated with a surface site of adsorption energy ϵ is given by the formula

$$j_s(\epsilon,T)=\prod_{r=1}^{3}\left[1-\exp\left(-\frac{h\nu_r(\epsilon)}{kT}\right)\right]^{-1}, \tag{19}$$

in which the quantities $\nu_r(\epsilon)$, with $r=1,2,3$, are the three vibration frequencies of an adsorbed atom on this site. Two of these frequencies can be referred to oscillations in the plane of the surface while the third is a vibration normal to the surface. One has from (19)

$$\frac{\partial\ln j_s}{\partial\eta}=-\sum_{r=1}^{3}\frac{(h/kT)}{\gamma_r-1}\frac{d\nu_r(\eta+\epsilon_0)}{d\eta}, \tag{20}$$

with

$$\gamma_r=\exp[h\nu_r(\eta+\epsilon_0)/kT]. \tag{21}$$

Case 1

We consider first the case in which the vibration frequencies can be assumed to be independent of the adsorption energy. In this event Eqs. (17) and (18) reduce to

$$F(\eta)=\phi/kT,\quad \partial\phi/\partial T=\phi/T. \tag{22}$$

Integration of these relations gives the result

$$F(\eta)=\psi_1(\eta)/k,\quad \phi(\eta,T)=T\psi_1(\eta), \tag{23}$$

in which ψ_1 is an arbitrary function of η.

It follows that if j_s is to be independent of η then the admissible isotherm equations must be limited to those which satisfy Eq. (23) through (13) and (16). Furthermore, the function ψ_1 must be so restricted that (a) the distribution function $F(\eta)$ does not have a positive lower bound as $\eta\to\infty$, since otherwise the integrals (1) and (6) would diverge, and (b) the condition (5) must be preserved.

Case 2

This is an illustration of the more general case for which ν_r is a function of ϵ. T. L. Hill[9] has suggested the dependence $\nu_r=B_r\epsilon^{\frac{1}{3}}$ on theoretical grounds, while Drain and Morrison[17] assumed ν_r to be proportional to ϵ in their interpretation of thermodynamic data. Both cases can be covered by the postulate that $\nu_r=B_r\epsilon^n$, with B_r and n as suitable constants. It will be assumed for simplicity that the three modes of vibration are degenerate ($B_1=B_2=B_3=B$); this is undoubtedly a poor approximation to the real case.

[17] L. E. Drain and J. A. Morrison, Trans. Faraday Soc. (London) **49**, 654 (1953).

Make the substitutions

$$\nu = B\cdot(\eta+\epsilon_0)^n, \tag{24}$$

$$A(\eta+\epsilon_0) = 3nBh\cdot(\eta+\epsilon_0)^{n-1}, \tag{25}$$

$$C(\eta+\epsilon_0) = Bh\cdot(\eta+\epsilon_0)^n/k. \tag{26}$$

Equations (17) and (18) now reduce to the forms

$$F = \frac{1}{kT}\left[1-\frac{A}{e^{C/T}-1}\right]\phi, \tag{27}$$

$$\frac{\partial\phi}{\partial T} = \frac{\phi}{T}\left\{1+\left[\frac{AC}{T}e^{C/T}\Big/(e^{C/T}-1)(e^{C/T}-1-A)\right]\right\}. \tag{28}$$

Integration of Eq. (28) leads to the result

$$\phi = T\psi_2(\eta)\left[1-\frac{A}{e^{C/T}-1}\right]^{-1}, \tag{29}$$

and on insertion of this into (27) we find

$$F(\eta) = \psi_2(\eta)/k. \tag{30}$$

Again, ψ_2 is an undetermined function which must be so chosen that Eq. (30) satisfies conditions (a) and (b) as stated in *case 1*. Since the function ϕ must satisfy Eq. (29), this limits the isotherm equations which are consistent with the assumed dependence of ν on ϵ and of F on T.

In order that localized adsorption may prevail, the quantity $A=(3nBh)\cdot(\eta+\epsilon_0)^n/(\eta+\epsilon_0)=3nh\nu/\epsilon$ must be small; i.e., the lowest vibrational energy level must lie well below the top of the potential barrier which confines the adsorbed particle to its surface site. Equation (29) may thus be considered to be identical with the second of Eqs. (23) except for a small correction term. It may be difficult in practice to distinguish between adsorption data which are compatible with conditions (22) or (29) since ϕ is not very sensitive to the assumed dependence of ν on ϵ.

4. EXAMPLES

The methods discussed in the last section will be illustrated by considering some examples. It will be assumed that the adsorption temperature is low, in order to avoid excessive mathematical complications.

(a) Consider the isotherm equation

$$\theta(p,T) = \left[1+\frac{T}{A}\ln\left(\frac{\alpha_0}{p}+1\right)\right]^{-1}. \tag{31}$$

This relation satisfies the conditions

$$\theta(0,T)=0, \quad \lim_{p\to\infty}\theta(p,T)=1, \tag{32}$$

while for a fixed value of p the function θ decreases monotonically with increasing T, as is required by the physical interpretation of the adsorption process. Use of Eqs. (9) and (15) leads to the relations

$$L(y,T) = (A/T)[(A/T)+\ln y]^{-1}, \tag{33}$$

$$g(\lambda,T) = \frac{A}{i2\pi T}\left\{\left[\ln(\lambda e^{-i\pi})+\frac{A}{T}\right]^{-1} - \left[\ln(\lambda e^{i\pi})+\frac{A}{T}\right]^{-1}\right\}. \tag{34}$$

The function $\phi(\eta,T)$ can now be obtained from Eq. (34) by use of relations (8) and (16). In the limit of low temperatures the ratio α_0/α is approximately unity, regardless of the functional relation between ν and ϵ. Then[18]

$$\lambda \simeq e^{\eta/kT}-1 \simeq e^{\eta/kT}. \tag{35}$$

Substitution of this approximation into (34) yields

$$\phi(\eta,T) = \frac{A}{T}\left[\left(\frac{\eta}{k}+A\right)^2\frac{1}{T^2}+\pi^2\right]^{-1} \simeq Ak^2T/[\eta+kA]^2. \tag{36}$$

This is of the form of (23) with $\psi_1 = Ak^2/[\eta+kA]^2$. The distribution function is now obtained from the combination of (36) and (22) in the form

$$F(\eta) = Ak/(\eta+kA)^2. \tag{37}$$

This function is clearly independent of T, and also satisfies condition (5).

(b) As a second example consider the isotherm equation

$$\theta(p,T) = \left(\frac{\alpha_0}{p}+1\right)^{-cT}. \tag{38}$$

Conditions (32) are satisfied and θ is a monotonically decreasing function of T for fixed p, as is required. Following the procedure sketched in example (a) one finds in the limit of low temperature

$$L(y,T) = y^{-cT}, \tag{39}$$

$$g(\lambda,T) = \sin(\pi cT)\cdot e^{-cT}/\pi, \tag{40}$$

$$\phi(\eta,T) = \sin(\pi cT)\cdot e^{-c\eta/k}/\pi \simeq cTe^{-c\eta/k}, \tag{41}$$

$$F(\eta) = (c/k)e^{-c\eta/k}. \tag{42}$$

Once more all of the conditions are satisfied by this distribution function.

[18] The second approximation of Eq. (35) obviously breaks down for very small adsorption energies. As a result, the calculated distribution (37) will be incorrect at the lower end of the energy spectrum; i.e., for $\eta<2.3kT$. However, since this approximation is acceptable over most of the range of η, the relation $\lambda=\exp(\eta/kT)$ will be adopted for simplicity.

Equilibria in the Formation of Molybdenum and Thorium Iodides from the Elements

THOMAS L. ALLEN* AND DON M. YOST
Gates and Crellin Laboratories of Chemistry, California Institute of Technology, Pasadena, California
(Received December 4, 1953)

An investigation has been made of the reaction of molybdenum and iodine to form molybdenum diiodide in the temperature interval from 1086°K to 1914°K, and the reaction of thorium and iodine to form thorium tetraiodide in the temperature interval from 1395°K to 1706°K. Thermodynamic properties of molybdenum diiodide and thorium tetraiodide were determined from measurements of the equilibria in these reactions. For the reaction $Mo(s)+2I(g)=MoI_2(g)$ at 1200°K, $\Delta F^0=-13.6$ kcal/mole, $\Delta H^0=-25.0$ kcal/mole, and $\Delta S^0=-9.5$ cal/mole °K. For the reaction $Th(s)+4I(g)=ThI_4(g)$ at 1500°K, $\Delta F^0=-83$ kcal/mole. Using an estimated value for ΔS^0 of -82 cal/mole °K, $\Delta H^0=-206$ kcal/mole. The average Mo—I bond energy in $MoI_2(g)$ and the average Th—I bond energy in $ThI_4(g)$ are both 89 kcal/mole.

INTRODUCTION

IN order to determine the thermodynamic properties of molybdenum diiodide and thorium tetraiodide, measurements were made of equilibria in the reactions

$$Mo(s)+2I(g)=MoI_2(g)$$

and

$$Th(s)+4I(g)=ThI_4(g).$$

The experimental method consisted in passing iodine vapor, entrained in a stream of inert gas, over the metal at elevated temperatures. The iodine content of the gas stream was determined both before and after reaction, and the partial pressure of the metallic iodide was determined by difference.

APPARATUS

Figure 1 shows the arrangement of apparatus. Helium from a cylinder passed through a reducing valve to a capillary flowmeter, excess helium escaping to the atmosphere through a pressure stabilizer. Purification of helium was achieved by an activated charcoal trap which was cooled by liquid air.[1] The charcoal was outgassed by heating it to 300°C under a high vacuum. From the charcoal trap the helium passed through an iodine saturator, a quartz reaction tube, a dust filter, and finally a light absorption cell. By means of a pair of three-way stopcocks it was possible to by-pass the iodine saturator, reaction tube, and dust filter, or by-pass only the iodine saturator.

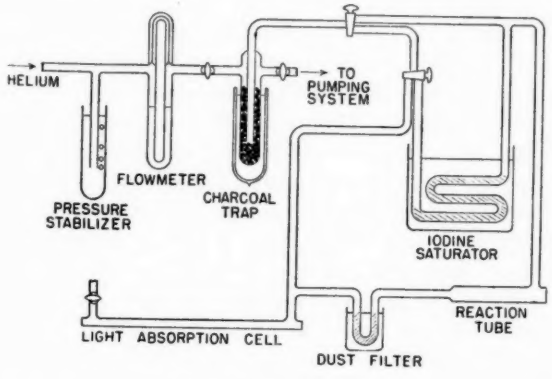

FIG. 1. Flow diagram.

The iodine saturator consisted of a glass coil containing iodine crystals, which was immersed in a water thermostat at 25.90°C. Temperature fluctuations amounted to ±0.02°C. The room temperature was kept above 25.9°C to prevent condensation of iodine beyond the saturator. Measurements showed that the iodine content of the helium was independent of helium flow rate over a wide range, indicating that saturation of the helium was achieved.

Figure 2 is a detailed cross section of the reaction tube. Surrounding the reaction tube was a water-cooled copper coil, through which passed a 400-kilocycle current from a 10-kilowatt Westinghouse radio-frequency generator. The radio-frequency current inductively heated a heavy wall molybdenum tube which was axially centered within and insulated from the quartz tube by zirconium dioxide powder. Rings of sintered zirconium dioxide were used to insulate the ends of the molybdenum tube. The temperature of the molybdenum was controlled manually by means of a phase shifter on the radio-frequency generator.

A molybdenum rod, in one end of which a hole ($\frac{3}{4}$ inch deep, $\frac{1}{16}$ inch diameter) had been drilled, was centered within the molybdenum tube by strips of molybdenum or thorium. Because of the large depth:width ratio of the hole, it acted as a blackbody radiator. The temperature was measured by viewing this hole through a

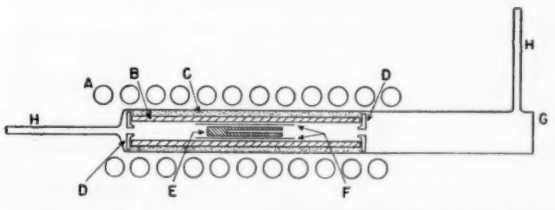

FIG. 2. Reaction tube: A, copper coil for induction heating; B, molybdenum tube; C, zirconium dioxide powder; D, zirconium dioxide rings; E, blackbody radiator; F, molybdenum or thorium strips; G, quartz window; H, graded seals.

*Present address: Department of Chemistry, University of California, Davis, California.

[1] D. M. Yost and H. Russell, *Systematic Inorganic Chemistry* (Prentice-Hall, Inc., New York, 1944), p. 8.

quartz window with a Leeds and Northrup optical pyrometer, which had been calibrated with an accuracy of ±3°C. Temperatures were corrected for absorption of light by the window.

A plug of glass wool in the line between the reaction tube and the light absorption cell served to remove particles of metallic iodide from the gas stream. It was heated with an oil bath to 100°–150°C in order to decrease adsorption of iodine on the glass wool.

The light absorption cell was a tube 6 mm in diameter and 1 meter in length. Pyrex windows were sealed to each end with beeswax and rosin.

Light from a headlight bulb (powered by five 6-volt storage batteries connected in parallel) was focused on a 0.2-mm diameter hole in a piece of aluminum foil. A 6 percent cupric sulfate solution in a 1 cm thick cell was interposed between the light source and the pinhole to remove heat rays from the beam. From the pinhole the light then passed successively through a positive lens, a 3-mm diameter aperture, a shutter mechanism, the light absorption cell, and a pair of colored glass plates to a 1P21 multiplier phototube, placed near the focal point of the lens. The colored glass plates transmitted only a sharp peak between 430 and 480 millimicrons. In the wavelength region of this peak the absorption of light by iodine is continuous, and the variation of absorption coefficient with wavelength is small.

TABLE I. Reaction of iodine with molybdenum.

T, °K	Number of experiments	Flow rate (cc/min)	d/d_0
1086	2	28	0.640±0.019
	2	46	0.580±0.041
	3	55	0.472±0.014
	8	64	0.616±0.073
	1	142	0.621
			Av. 0.588±0.069
1189	2	55	0.682±0.002
1292	1	10	0.844
	1	17	0.787
	1	28	0.863
	1	46	0.863
	2	55	0.801±0.005
	5	64	0.852±0.030
	1	108	0.863
	1	194	0.891
			Av. 0.844±0.031
1395	2	55	0.872±0.012
1498	2	10	0.905±0.038
	1	17	0.948
	2	28	0.993±0.016
	1	46	0.977
	2	55	0.923±0.010
	3	64	0.974±0.011
			Av. 0.954±0.030
1706	1	55	0.957
1914	1	55	0.966

TABLE II. Reaction of iodine with thorium.

T, °K	Number of experiments	Flow rate (cc/min)	d/d_0
1395	1	65	0.015
1447	1	65	0.058
1498	1	65	0.155
	2	93	0.087±0.087
	1	100	0.102
			Av. 0.108±0.057
1550	1	65	0.383
1602	4	65	0.540±0.153
1706	1	70	1.684
	1	74	1.582

A bank of twelve 67½-volt B batteries connected in series supplied power to the multiplier phototube. The anode current of the phototube passed through a 1-megohm resistor, and the potential drop across this resistor was measured by a Type K potentiometer. At the current levels used in these experiments the anode current of the 1P21 multiplier phototube, after correction for dark current, varies linearly with the light intensity at the cathode.[2] Fluctuations in the anode current were less than ±0.2 percent.

MATERIALS

Molybdenum was obtained from the Fansteel Metallurgical Corporation, thorium from A. D. Mackay, Inc., and helium (98.3 percent minimum purity) from the Air Reduction Sales Company. A cp grade of iodine was used. Zirconium dioxide was obtained from the Titanium Alloy Manufacturing Company. The manometer fluid was Molecular Lubricant, a type of diffusion pump oil.

PROCEDURE

In order to calibrate the photometer, the glass tubing was connected directly from the iodine saturator to the light absorption cell. The helium-iodine gas stream was passed through the cell until the potential drop across the 1-megohm resistor in the phototube circuit reached a steady value v_1. Then the cell was swept out with helium, and the potential drop v_2 was measured. With no light striking the phototube, a dark current caused a potential drop v_3. From these measurements the optical density of iodine vapor d_0 at a partial pressure p_0 is obtained from the relation $d_0=\log[(v_2-v_3)/(v_1-v_3)]$. p_0 is equal to the vapor pressure of iodine at the temperature of the iodine saturator (25.90°C), which is 4.42×10^{-4} atmos.[3]

After connecting the flow system as shown in Fig. 1, the reaction tube was heated to the desired temperature,

[2] R. W. Engstrom, J. Opt. Soc. Am. **37**, 420 (1947).

[3] *International Critical Tables* (McGraw-Hill Book Company, Inc, New York, 1928), Vol. III, p. 201.

TABLE III. Equilibrium data for $Mo(s)+2I(g)=MoI_2(g)$.

T, °K	P_{I_2}(atmos) $\times 10^4$	P_I(atmos) $\times 10^4$	P_{MoI_2}(atmos) $\times 10^4$	log$K$
1086	0.20	4.80±0.60	1.82±0.30	2.90±0.18
1189	0.07	5.88±0.02	1.41±0.01	2.61±0.01
1292	0.03	7.40±0.28	0.69±0.14	2.10±0.13
1395	0.01	7.70±0.10	0.56±0.05	1.98±0.06
1498	···	8.44±0.26	0.20±0.13	1.45±0.49

and helium was passed through the iodine saturator to the reaction tube and thence to the dust filter and light absorption cell. The measurements described in the previous paragraph were repeated, and the optical density d corresponding to a partial pressure of iodine vapor p was obtained. From Beer's law, $p=p_0d/d_0$.

In order that this equation hold it is necessary that the temperature of the gas in the light absorption cell be the same during the various measurements as in the calibration, although this temperature need not be the same as that of the iodine saturator. A fluctuation in temperature leads to an error in the calculated value of the iodine pressure, the relative error being equal to the relative deviation in absolute temperature. The time necessary for the gas to reach the cell was sufficient to allow the gas to cool to room temperature, and since relative deviations in the absolute temperature of the room were small, the errors introduced by this factor were also small.

A series of measurements was made from 1086°K to 1914°K, where molybdenum was the only metal in the reaction tube. Then the molybdenum strips inside the molybdenum tube were replaced with thorium strips, and another series of measurements was made from 1395°K to 1706°K.

RESULTS AND DISCUSSION

Table I gives the results of measurements with molybdenum, and Table II the results with thorium. Where more than one measurement was made under a given set of conditions, the arithmetic mean and the average deviation from the mean is given in the last column. In the two experiments with thorium at 1706°K, d/d_0 was greater than unity. This was apparently caused by outgassing of iodine which had been adsorbed at some point in the flow system.

The data show no trend with flow rate, indicating that equilibrium was reached. Furthermore, the equilibrium partial pressure of iodine should increase with an increase in temperature for the exothermic reactions which are occurring, whereas if equilibrium is not reached, an increase in temperature should accelerate the reaction and result in a decrease in iodine partial pressure. The data show that the iodine partial pressure increases with increasing temperature, providing further evidence that equilibrium was attained.

As the gas stream leaves the molybdenum tube and is cooled, the equilibrium shifts toward the metallic iodide. However, there is no metal at this point with which the iodine may react, and the equilibrium is thus effectively "frozen."

Tables III and IV list the partial pressures of the various molecular species, and the calculated values of the appropriate equilibrium constants. The extent of the dissociation of diatomic iodine was calculated from thermodynamic data.[4] Partial pressures were used in place of fugacities in thermodynamic calculations. The partial pressures of molybdenum diiodide and thorium tetraiodide were obtained from the difference between p_0 and p. It is considered that these are the iodides which are formed in the reactions on the basis of the previously reported properties of the iodides of molybdenum and thorium. Of the two known molybdenum iodides, molybdenum tetraiodide decomposes to iodine and molybdenum diiodide at only slightly elevated temperatures (*ca* 100°C), whereas molybdenum diiodide does not undergo appreciable decomposition at the melting point of glass.[5,6] Both thorium diiodide and thorium triiodide disproportionate at temperatures above 600°C to thorium tetraiodide and metallic thorium.[7,8]

If, after the gas stream has left the reaction tube, iodine and the metallic iodide should react to form a higher iodide, then appreciable errors would be introduced into the calculated values of the various partial pressures. However, the iodides were partly condensed on the walls shortly after leaving the reaction tube, and partly entrained as a dust which was trapped in the dust filter. In either case the temperature was too high for the formation of molybdenum tetraiodide from iodine and molybdenum diiodide. The tetraiodide is the highest known iodide of thorium. Therefore it appears that no such reaction occurred in either the molybdenum or thorium experiments.

The two experiments with molybdenum at 1706°K and 1914°K are not included in Table III because of the low values and consequent large relative uncertainties in the molybdenum diiodide partial pressures; the single experiment with thorium at 1395°K is not included in Table IV because of the low value and large relative uncertainty in the iodine partial pressure.

TABLE IV. Equilibrium data for $Th(s)+4I(g)=ThI_4(g)$.

T, °K	P_I(atmos) $\times 10^4$	P_{ThI_4}(atmos) $\times 10^4$	log$K$
1447	0.51	2.08	13.5
1498	0.95±0.50	1.97±0.13	12.4±1.3
1550	3.38	1.36	10.0
1602	4.78±1.36	1.02±0.34	9.3±0.7

[4] G. M. Murphy, J. Chem. Phys. **4**, 344 (1936).
[5] M. Guichard, Compt. rend. **123**, 821 (1896).
[6] M. Guichard, Ann. chim. et phys. [7], **23**, 498 (1901).
[7] J. S. Anderson and R. W. M. D'Eye, J. Chem. Soc. **1949** (Suppl. Issue No. 2), S 244.
[8] Hayek, Rehner, and Frank, Monatsh. Chem. **82**, 575 (1951)

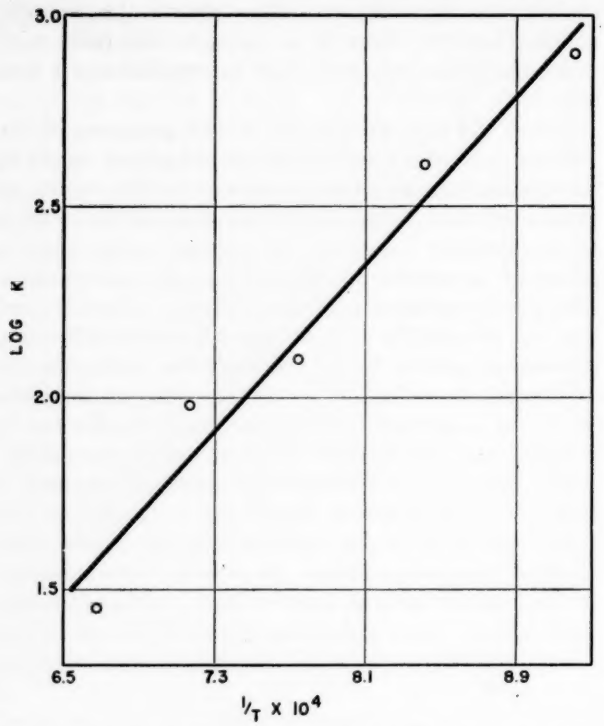

FIG. 3. Temperature dependence of the equilibrium constant for the reaction $Mo(s)+2I(g)=MoI_2(g)$.

From the data for the reaction of molybdenum and iodine, it can be shown that the partial pressure of molybdenum diiodide in the thorium experiments was negligible.

In Figs. 3 and 4 the logarithms of the equilibrium constants are plotted against the reciprocal of absolute temperature, and straight lines are drawn as close as possible to the several experimental points, the points being weighted according to the number of experiments which they represent and the mean deviations in the results of the experiments.

From the straight line of Fig. 3, the following thermodynamic results are obtained for the reaction $Mo(s)+2I(g)=MoI_2(g)$:

$$\Delta F^0_{1200°K}=-13.6 \text{ kcal/mole}$$

$$\Delta H^0_{1200°K}=-25.0 \text{ kcal/mole}$$

$$\Delta S^0_{1200°K}=-9.5 \text{ cal/mole °K}.$$

Combination of the entropy change with the entropies of molybdenum and monatomic iodine[9] gives

$$S^0_{1200°K}(MoI_2,g)=106.0 \text{ cal/mole °K}.$$

These results may be compared with values obtained from the estimated thermodynamic properties of molybdenum diiodide:[10]

$$\Delta F^0_{1200°K}=-0.6 \text{ kcal/mole}$$

$$\Delta H^0_{1200°K}=-25.8 \text{ kcal/mole}$$

$$\Delta S^0_{1200°K}=-21.0 \text{ cal/mole °K}$$

$$S^0_{1200°K}(MoI_2,g)=94.5 \text{ cal/mole °K}.$$

The heats of reaction are in excellent agreement; the estimated value for the entropy of molybdenum diiodide is 11 percent lower than the experimental value.

The heat of vaporization of molybdenum at 1200°K is 153.7 kcal/mole.[11] Combination of this value with ΔH^0 for the above reaction gives $\Delta H^0_{1200°K}=-178.7$ kcal/mole for $Mo(g)+2I(g)=MoI_2(g)$. Thus the heat of atomization of $MoI_2(g)$ is 178.7 kcal/mole, and the average Mo—I bond energy is 89.4 kcal/mole.

These results are obtained from the straight line of Fig. 4 for the reaction $Th(s)+4I(g)=ThI_4(g)$:

$$\Delta F^0_{1500°K}=-83 \text{ kcal/mole}$$

$$\Delta H^0_{1500°K}=-314 \text{ kcal/mole}$$

$$\Delta S^0_{1500°K}=-154 \text{ cal/mole °K}.$$

Combining this entropy change with the entropies of thorium and monatomic iodine[9] gives $S^0_{1500°K}(ThI_4,g)=78$ cal/mole °K.

The values obtained from the estimated thermo-

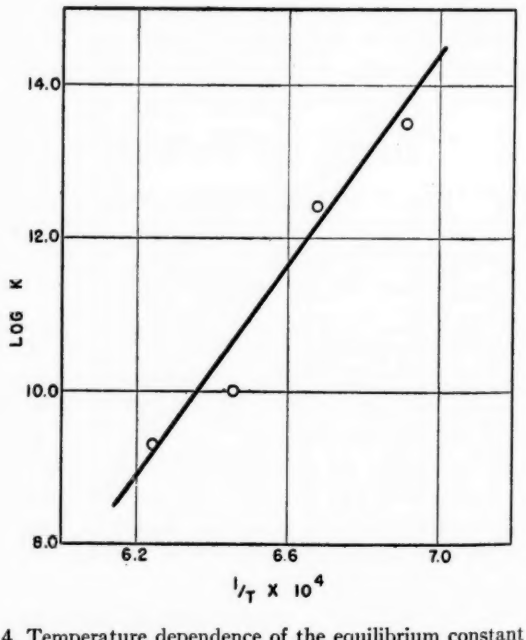

FIG. 4. Temperature dependence of the equilibrium constant for the reaction $Th(s)+4I(g)=ThI_4(g)$.

[9] L. Brewer in *The Chemistry and Metallurgy of Miscellaneous Materials*, edited by L. L. Quill (McGraw-Hill Book Company, Inc., New York, 1950), Natl. Nuclear Energy Ser., Div. IV, Vol. 19B, pp. 16, 62.

[10] Brewer, Bromley, Gilles, and Lofgren in *The Chemistry and Metallurgy of Miscellaneous Materials*, reference 9, Papers 6 and 8.

[11] K. K. Kelley, U. S. Bur. Mines Bull. 383 (1935).

dynamic properties of thorium tetraiodide[12] are:

$$\Delta F^0_{1500°K} = -\ 96 \text{ kcal/mole}$$
$$\Delta H^0_{1500°K} = -219 \text{ kcal/mole}$$
$$\Delta S^0_{1500°K} = -\ 82 \text{ cal/mole °K}$$
$$S^0_{1500°K}(ThI_4,g) = 150 \text{ cal/mole °K}.$$

Although the estimated and experimental values for the free energy change are in reasonably good agreement, the heats of reaction and entropies differ widely. This appears to be caused by error in the slope of the straight line of Fig. 4, which results from uncertainties in the equilibrium constants and the short temperature interval covered.

[12] Brewer, Bromley, Gilles, and Lofgren in *The Chemistry and Metallurgy of Miscellaneous Materials*, reference 9, Papers 6 and 7.

A more reliable value for the heat of reaction may be obtained by combining the estimated value for the entropy change with the experimental value for the free energy change. This results in $\Delta H^0_{1500°K} = -206$ kcal/mole. Subtracting this heat of reaction from the heat of vaporization of thorium[13] results in a heat of atomization of $ThI_4(g)$ of 356 kcal/mole, or an average Th—I bond energy of 89 kcal/mole.

ACKNOWLEDGMENTS

It is with pleasure that the authors acknowledge the financial assistance of a grant-in-aid from the Research Corporation, and a Research Fellowship to one of us (T.L.A.) from the Shell Oil Company.

[13] Reference 9, p. 34.

THE JOURNAL OF CHEMICAL PHYSICS VOLUME 22, NUMBER 5 MAY, 1954

Quenching of Mercury Resonance Radiation. IV. Unsaturated Compounds*

B. deB. Darwent,† M. K. Phibbs,‡ and F. G. Hurtubise§
Division of Chemistry, National Research Laboratories, Ottawa, Canada
(Received January 28, 1954)

The cross sections for quenching mercury resonance radiation by a number of mono- and di-olefins, acetylenes, substituted olefins, and other compounds containing multiply bonded atoms have been measured. The quenching cross sections of mono-olefins increase with increasing molecular weight but not with increased branching of the carbon skeleton. The position of the double bond has little or no effect on the cross section. The substitution of fluorine for hydrogen decreases the cross section of olefins. The presence of a second double bond does not alter the cross section. The double bond is more effective when between two carbon atoms than when it is between two nitrogens or carbon and oxygen. The cross sections of acetylenes are essentially the same as those of the corresponding olefins but here the substitution of N for CH does not appear to alter the effective cross section.

INTRODUCTION

IT has recently been shown[1] that the quenching cross sections of paraffins increase with increasing molecular weight and branching and that substitution by atoms other than carbon or hydrogen[2] lead to significant changes in the cross sections. It has long been recognized that olefins are much more efficient than paraffins in quenching mercury resonance radiation, but there is very little information on the effects of molecular weight or branching on the effective cross sections of olefins other than the measurements of Bates[3] and Steacie[4] on two heptenes and ethylene, respectively. There is no information available about the effects of substituents on the cross sections of olefins, and nothing is known about the quenching cross sections of acetylenes. In this communication we present the results obtained from studies of the quenching of mercury resonance radiation by a number of olefins, di-olefins, substituted olefins, and acetylenes which provide information about the effects of molecular weight, branching, position of the double bond, the presence of more than one double bond, and the relative efficiencies of double bonds and triple bonds in the quenching of mercury resonance radiation.

EXPERIMENTAL AND RESULTS

The apparatus and experimental details were identical with those already described.[2] Two separate series of experiments were done in which the values of the constant α, which defines the relationship between the quenching (Q) and τZ_Q, were 0.09 (series A) and 0.16 (series B). The details of these measurements have already been given.[2]

The experimental results are shown in the accom-

* Contribution No. 3267 from the National Research Council, Ottawa, Canada.
† Present address: Olin Industries, Inc., New Haven, Connecticut.
‡ Present address: E. I. du Pont de Nemours and Company, Wilmington, Delaware.
§ Summer student, 1951, from Carleton College, Ottawa.
[1] B. deB. Darwent, J. Chem. Phys. **18**, 1532 (1950).
[2] B. deB. Darwent and M. K. Phibbs, J. Chem. Phys. (to be published).
[3] J. R. Bates, J. Am. Chem. Soc. **54**, 569 (1932).
[4] E. W. R. Steacie, Can. J. Research **B18**, 44 (1940).

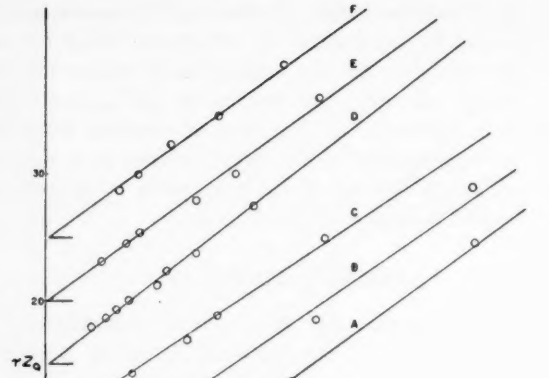

FIG. 1. Quenching of mercury resonance radiation—lower olefins and di-olefins. A—C_2H_4; B—C_3H_6; C—1—C_4H_8; D—*Trans* 2—C_4H_8; E—Iso—C_4H_8; F—C_4H_6. *All expts. in series* A.

panying graphs as plots of τZ_Q as functions of pressure The quenching cross sections (σ_Q^2) were derived from those graphs, as already described,[2] and the values of the slopes, the reduced masses and the quenching cross sections are given in Tables I to III.

The experimental results obtained with ethylene, propene, the isomeric butenes and butadienes are shown in Fig. 1. The slopes of the straight lines (Table I) vary from 1.32 (1-butene) to 1.54 (2-butene), the average slope of the six lines (Fig. 1) being 1.40. We do not consider the results to be accurate to better than ±10 percent to 15 percent, and so these differences in slopes may not be real.

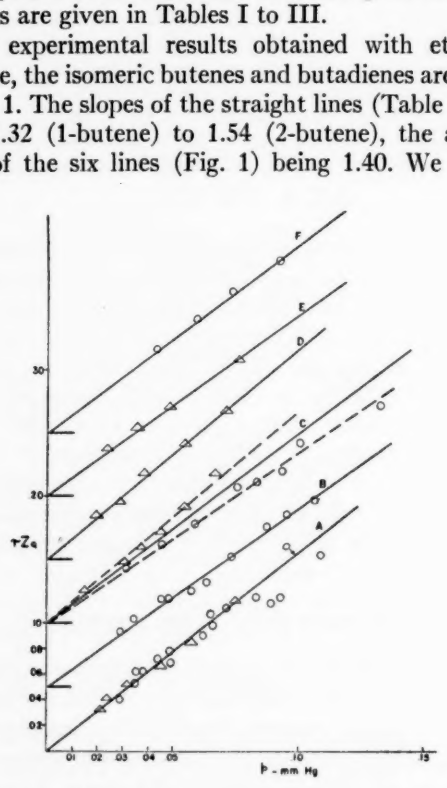

FIG. 2. Quenching of mercury resonance radiation—higher olefins and di-olefins. A—1—C_5H_{10}; B—1,4—C_5H_8; C—1—C_6H_{12}; D—2—C_6H_{12}; E—$(CH_3)_2C=C(CH_3)_2$; F—1,5—C_6H_{10}. *Circles*—"A" *series expts.; triangles*—"B" *series expts.*

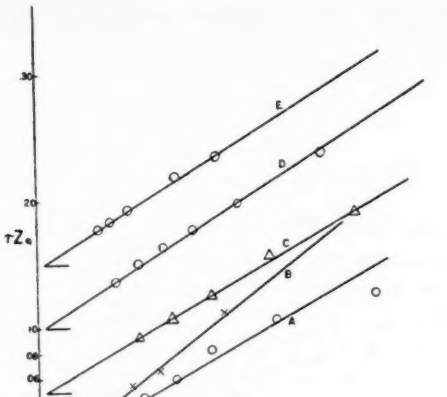

FIG. 3. Quenching of mercury resonance radiation—unsaturated compounds. A—C_2F_4; B—C_2HCl_3; C—$CH_3N=NCH_3$; D—$CH_3 \cdot CO \cdot CH_3$; E—CS_2. *All expts. in series* A.

The experimental results for pentene, the isomeric hexenes, pentadiene, and hexadiene are shown in Fig. 2. Quenching by 1-pentene and 1-hexene was measured in both series of experiments. The two series were found to be in excellent agreement in the 1-pentene experiments and so it may be assumed that, as in our previous paper[2] there is no consistent difference in the results as obtained from the two sets of experiments. With 1-hexene, however, the series *B* experiments are about 20 percent lower than series A. This is about the limit of the accuracy (±10 percent to 15 percent) of the experiment. The slopes (Table I), except for 2-hexene, all lie between

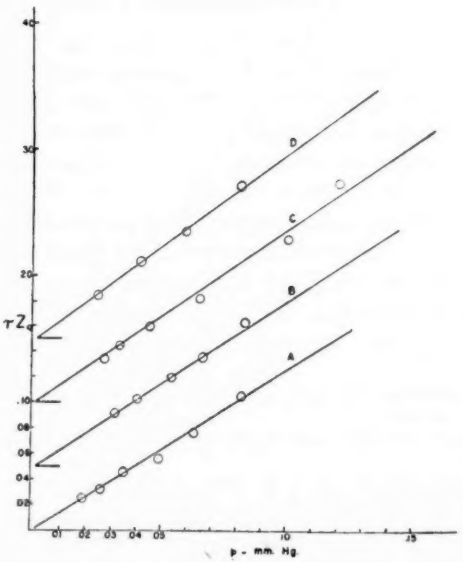

FIG. 4. Quenching of mercury resonance radiation—triple bonded compounds. A—$CH \equiv CH$; B—$CH \equiv C \cdot CH_2CH_3$; C—$CH_3-C \equiv C-CH_3$; D—$CH_3 \cdot C \equiv N$. *All expts. in series* A.

1.41 and 1.54, the average value being 1.50±0.10. Again because of the experimental uncertainty, it is difficult to say whether there is any significant difference between slopes of the lines in Fig. 2 or, indeed, between the slopes for any of the olefins or di-olefins in Table I since all, except 2-hexene which differs from the average by 0.21, fall within the limits 1.46±0.16.

The experimental results for substituted olefins and other compounds with double bonds, including azomethane, acetone and carbon disulfide, are shown in Fig. 3. Here we find (Table II) definite differences in the slopes, tetrafluorethylene ($\tau Z_Q/p=0.25$) having the smallest and trichlorethylene ($\tau Z_Q/p=1.52$) the largest of the slopes.

The results for the acetylenes and acetonitrile are presented in Fig. 4 and the slopes given in Table III. As with the olefinic hydrocarbons it is quite likely that acetylene and the two butynes all have the same slope (1.32±0.06) whereas acetonitrile may be larger.

TABLE I. The quenching of λ2537 by olefins and di-olefins.

Olefin	Expt. No.	$\frac{\tau Z_Q}{p}$	$\mu^{\frac{1}{2}}\times10^{11}$ ($g^{\frac{1}{2}}$)	$\sigma_Q^2\times10^{16}$ (cm^2)
$CH_2=CH_2$	A22	1.43	1.57	26
$CH_3\cdot CH=CH_2$	A23	1.36	1.32	31
$C_2H_5\cdot CH=CH_2$	A26	1.32	1.18	33.5
$CH_3CH=CH\cdot CH_3$	A28	1.54	1.18	39
$(CH_3)_2C=CH_2$	A24	1.44	1.18	37
$CH_2=CH\cdot CH=CH_2$	A27	1.42	1.20	36
$CH_2=CH(CH_2)_2\cdot CH_3$	{PA30, B32} {PB34, B35}	1.54	1.08	43
$CH_2=CH\cdot CH_2\cdot CH=CH_2$	B38, 39	1.41	1.09	39
$CH_2=CH(CH_2)_2\cdot CH_3$	A29, B30 B31	1.50	1.01	45
$CH_3\cdot CH=CH(CH_2)_2\cdot CH_3$	A31	1.67	1.01	50
$(CH_3)_2C=C(CH_3)_2$	A25	1.44	1.01	43
$CH_2=CH\cdot CH_2\cdot CH_2\cdot CH=CH_2$	B29	1.49	1.02	44

DISCUSSION

The cross sections of ethylene[4] and 1-heptene[3] have been measured previously and found to be 48(±5) $\times10^{-16}$ cm² and 45.8$\times10^{-16}$ cm² respectively. This may be taken to indicate that the cross sections of the olefins do not increase with increasing molecular weight. However, the value for ethylene was obtained by the 90° method which has been criticized by Zemansky[5] as giving results which are too high because of imprisonment. In the same experiments Steacie found $\sigma_Q^2=8.9\times10^{-16}$ cm² for H_2 whereas Zemansky[5] had found that cross section to be 6.0×10^{-16} cm². Assuming that resonance radiation was imprisoned in the 90° experiments and that the extent of imprisonment was the same for both H_2 and C_2H_4 then Steacie's result for ethylene should be reduced by one third. This leads to 32(±3) $\times10^{-16}$ cm² a value which is not in too bad agreement with that found in the present experiments when the accuracy of the measurements is taken into consideration.

The quenching cross sections of the 1-olefins, as measured in the present experiments, increase regularly with increasing molecular weight from ethylene to 1-hexene. Bates[3] found that 1-heptene had a cross section of 46×10^{-16} cm², which is approximately the same as we have found for 1-hexene. This may indicate that the cross sections do not continue to increase with molecular weight after hexene but, because of the inherent inaccuracy of the measurements, this may be illusory. The square root of the quenching cross section (σ_Q) is shown as a function of the number of carbon atoms in the straight chained olefins (Fig. 5) and, for comparison, the similar quantities are shown for the *n*-paraffins. For both olefins and paraffins the relationship appears to be approximately linear, the rate of increase of σ_Q being much greater for the paraffins than for the olefins. This indicates that the cross sections of the olefins and paraffins will be approximately equal when there are 10 to 11 carbon atoms in the chain and that, above this number, the paraffins will quench more efficiently than the olefins. This conclusion would be wrong only if the line for the olefins were concave upwards and/or that for the paraffins concave downwards instead of being straight. The results do not support that possibility, and so the above conclusion, although unexpected, appears to be valid.

The reason for the lower rate of increase in σ_Q with N for the olefins compared with the paraffins is not clear. Previous results[1] have indicated that the presence of a tertiary C—H bond in paraffins leads to an increase in σ_Q, presumably because such bonds are weaker than the secondary or primary bonds. It is likely that the C—H bonds once removed from the double bond in olefins are as weak or weaker than the tertiary C—H bond in, say, iso-butane so that one would have expected a similar rate of increase of σ_Q with N. This does not appear to be the case.

TABLE II. The quenching of λ2537 by substituted olefins and other compounds with double bonds.

Compound	Expt. No.	$\frac{\tau Z_Q}{p}$	$\mu^{\frac{1}{2}}\times10^{11}$ ($g^{\frac{1}{2}}$)	$\sigma_Q^2\times10^{16}$ (cm^2)
$CF_2=CF_2$	A27	0.25	0.95	7.9
$CHCl=CCl_2$	A51	1.52	0.88	52
$CH_3\cdot N=N\cdot CH_3$	A62	1.12	1.16	29
$CH_3\cdot \overset{O}{\overset{\|}{C}}\cdot CH_3$	A49	1.25	1.16	32
$S=C=S$	A53	1.23	1.05	35

TABLE III. The quenching of λ2537 by acetylenes and acetonitrile.

Compound	Expt. No.	$\frac{\tau Z_Q}{p}$	$\mu^{\frac{1}{2}}\times10^{11}$ ($g^{\frac{1}{2}}$)	$\sigma_Q^2\times10^{16}$ (cm^2)
$CH\equiv CH$	A50	1.26	1.62	23
$CH\equiv C\cdot CH_2\cdot CH_3$	A40	1.32	1.19	33
$CH_3\cdot C\equiv C\cdot CH_3$	A39	1.38	1.19	35
$CH_3\cdot C\equiv N$	A63	1.48	1.33	35

[5] M. W. Zemansky, Phys. Rev. **36**, 919 (1930).

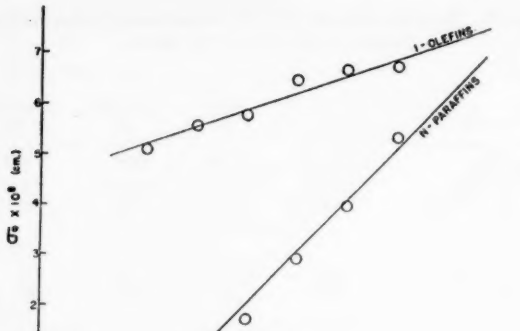

FIG. 5. Quenching of mercury resonance radiation. Effect of number of carbon atoms in chain on σ_Q for 1-olefins (point for 1-heptene from Bates) and *n*-paraffins (Darwent).

The following results, which include Bates' earlier data[3] for the 1- and 3- heptenes, show the effect of the position of the double bond on the quenching efficiency.

	Butenes		Hexenes		Heptenes	
Double-bond position	1	2	1	2	1	3
σ_Q^2—cm$^2\times10^{16}$	31	39	45	50	46	56
Ratio	1.26		1.11		1.22	

In all cases the double bond appears to enhance the cross section less when terminal than when it is further within the molecule. This difference amounts to at most 26 percent, which is about the limit of accuracy (±10 to 15 percent) claimed in these experiments, but with both the butenes and hexenes, measured in these experiments, as well as with the heptenes, measured independently by Bates, the 1-olefins were in all cases smaller than the 2- and 3-isomers so that the effect is probably real.

The results indicate that branching of the carbon skeleton has little or no influence on the quenching cross section. Thus the cross section of iso-butene is intermediate between those of 1- and 2-butene and 2,3:dimethyl-2-butene is smaller than either 1- or 2-hexene.

Since ethylene is much more efficient than ethane it may have been expected that further increase in unsaturation would have lead to a significant increase in σ_Q^2. Information on this point is obtained by comparing butadiene with the butenes, pentadiene with 1-pentene, and hexadiene with the hexenes. The results show that butadiene is slightly larger than 1-butene but is no larger and actually may be smaller than 2-butene, pentadiene is smaller than 1-pentene, and hexadiene is about the same size as 1-hexene and apparently smaller than 2-hexene. Thus it may be concluded that the presence of a second double bond, whether far removed from or conjugated with the first, does not increase perceptibly the cross section of the molecule. Hence, either the second double bond itself is ineffective even though it is quite remote from, and so presumably uninfluenced by, the first, or the influence of the first double bond extends over the entire molecule and, even in a C_6 chain, its efficiency is unimpaired by the process of extention.

The results provide information about the effect of substituting the hydrogen atoms in ethylene by other atoms or groups. We find that tetrafluorethylene is much smaller and trichlorethylene much larger than ethylene. The increase in cross section on chlorination may be caused largely or even entirely by the increase in the physical size of the molecule but it is unlikely that tetrafluorethylene is, physically, significantly smaller than ethylene whereas its cross section is only about one-third that of ethylene. This effect of fluorine substitution is similar to that observed previously with the substituted paraffins.[4]

The results given in Table II also allow us to draw conclusions concerning the effect of the nature of the atoms involved in the double bond on the quenching efficiency. We may compare asomethane with 2-butene and acetone with iso-butene.

	σ_Q^2-(cm$^2\times10^{16}$)		σ_Q^2-(cm$^2\times10^{16}$)
2-butene	39	iso-butene	37
azo-methane	29	acetone	32

Assuming that the compounds in each group are approximately the same size the double bond between two carbon atoms (2-butene) is more efficient in quenching than when it is between two nitrogen atoms. Similarly the effectiveness of C=C and C=O in quenching may be compared by considering iso-butene and acetone; again, providing the physical sizes of the molecule are the same, we see that the C=C appear to be more effective than C=O.

The transformation of a double to a triple bond does not alter the quenching cross section; thus acetylene, 1-butyne and 2-butyne (Table III) have essentially the same cross sections as ethylene, 1-butene and 2-butene respectively. However, if we assume that methylacetylene has the same cross section as propylene (31 $\times10^{-16}$ cm^2), then the substitution of N for CH does not reduce σ_Q^2 as found with the olefins, since azo-methane has an effective cross section of 35×10^{-16} cm.

Analysis of the Near Ultraviolet Absorption Spectrum of Acetylene

K. KEITH INNES*
Division of Physics, National Research Council, Ottawa, Canada
(Received October 16, 1953)

The absorption spectrum of acetylene in the region 1970–2470A has been photographed in the fourth and fifth orders of a twenty-one-foot grating spectrograph with absorbing paths of 0.007 to 70 m-atmos.

It has been possible to extend the arguments which led King and Ingold to conclude that in the upper electronic state the molecule is bent and has C_{2h} symmetry. The upper electronic state is A_u or, possibly A_g.

The effective moment of inertia I_a of the excited state is small, causing sub-band separations of 50 to 150 cm^{-1}. These sub-bands all have P, Q, and R branches, are well resolved, and have the appearance of bands of diatomic molecules. The following rotational constants of the upper state are derived:

$$A_0=12.94, \quad B_0=1.1247, \quad C_0=1.0297 \text{ cm}^{-1}.$$

If the C—H distance is assumed to be between 1.070 and 1.090A, one finds

$$r_{CC}=1.38_3\text{A}, \quad \sphericalangle\text{CCH}=120°.$$

Ground-state combination differences are in agreement with precise values derived from infrared data. Some new lower state B values are obtained.

The O—O vibrational transition is shown to be at 42 197.69 cm^{-1}. The sub-bands form v_4'' progressions and v_3' progressions. Analysis gives two upper state vibrational frequencies

$$\nu_3(\text{CCH})=1047.70 \text{ cm}^{-1} \quad \text{and} \quad \nu_2(\text{CC})=1389 \text{ cm}^{-1}.$$

The following lower state vibrational constants are obtained:

$$\omega_4^0=608.2_6, \quad x_{44}=+3.29, \quad g_{44}=+0.1_7 \text{ cm}^{-1}.$$

The fundamental frequency ν_4'' is the sum of these constants, that is, 611.7_2 cm^{-1}.

A. INTRODUCTION

THE paucity of even partial rotational analyses of electronic transitions of polyatomic molecules is well known.[1] In no case has it been possible to obtain combination differences which are in satisfactory agreement with those obtained previously from infrared data. The present research was undertaken in the hope that the complicated, discrete ultraviolet absorption spectrum of acetylene[2] would not only be resolvable and capable of rotational analysis but could be fitted into a consistent vibrational scheme. This was indeed found to be the case.

The preliminary report[3] of this work coincided with a summary publication of a more complete interpretation of the spectrum by King and Ingold.[4] A few weeks later Dr. King and Professor Ingold kindly made available to us the convincing details[5] of their work. They were the first to recognize that in the upper electronic state of the near ultraviolet bands the acetylene molecule is nonlinear and has the shape illustrated in Fig. 1(b). In the ground state, the molecule has long been known to be linear [Fig. 1(a)]. The conclusion with regard to the upper state has been confirmed in many ways in the present work. The maximum absorbing path and the practical resolving power used in this work were three times those attained by King and Ingold. Therefore, it was often possible, apart from verifying their conclusions, to obtain additional information and higher

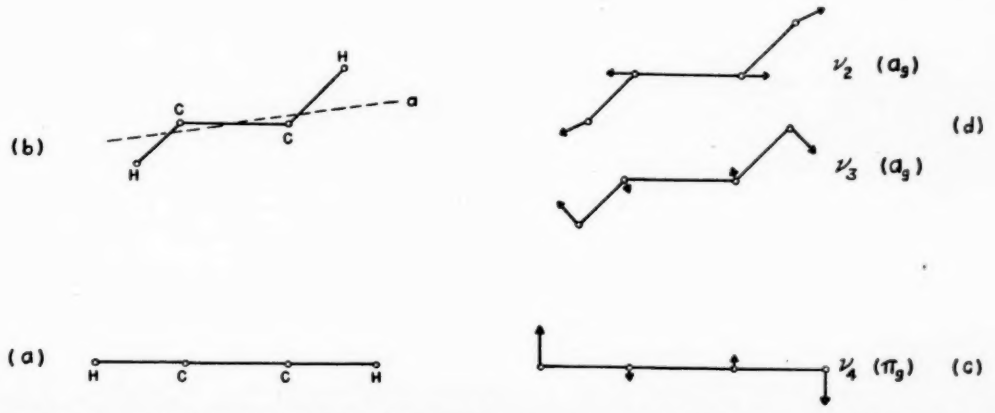

FIG. 1. Geometrical structure of C_2H_2 (a) in the electronic ground state, (b) in the excited electronic state, and approximate vector diagrams (c) and (d) of three vibrations in these states. The vibrations are numbered according to the convention of reference 7, page 271.

*National Research Laboratories Postdoctorate Fellow, 1951–53. Now at the Department of Chemistry, University of Oklahoma, Norman, Oklahoma.

[1] J. B. Coon, J. Chem. Phys. **14**, 665 (1946).
[2] Woo, Liu, Chu, and Chih, J. Chem. Phys. **6**, 240 (1938).
[3] K. K. Innes, Symposium on Molecular Structure and Spectroscopy, Columbus, Ohio (1952).
[4] G. W. King and C. K. Ingold, Nature **169**, 1101 (1952).
[5] G. W. King, thesis, University College, London (June, 1952).

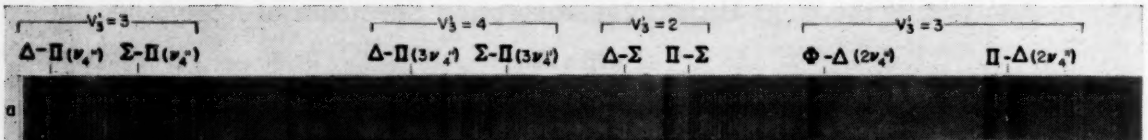

FIG. 2. Representative portions of the absorption spectrum of acetylene (a) at 25°C, (b) at −80°C. The region shown extends from about 44750 cm^{-1} to about 44050 cm^{-1}. For both spectra, the absorbing path was 100 cm and the pressure 240 mm Hg (at 25°C). The leading lines point to the Q heads of the sub-bands.

accuracy of the molecular constants. For this reason it appeared worth while to report on our work, emphasizing the results which go beyond those of King and Ingold.

B. EXPERIMENTAL

Matheson acetylene was bubbled slowly through concentrated sulfuric acid and used without further purification. Two Pyrex absorption cells with quartz windows were used: a simple one-meter tube and a five-meter multiple reflection cell, allowing up to twenty traversals. The pressure varied from 5 mm to 53 cm Hg. The temperature dependence of a representative part of the spectrum was investigated by cooling the short cell with solid CO_2.

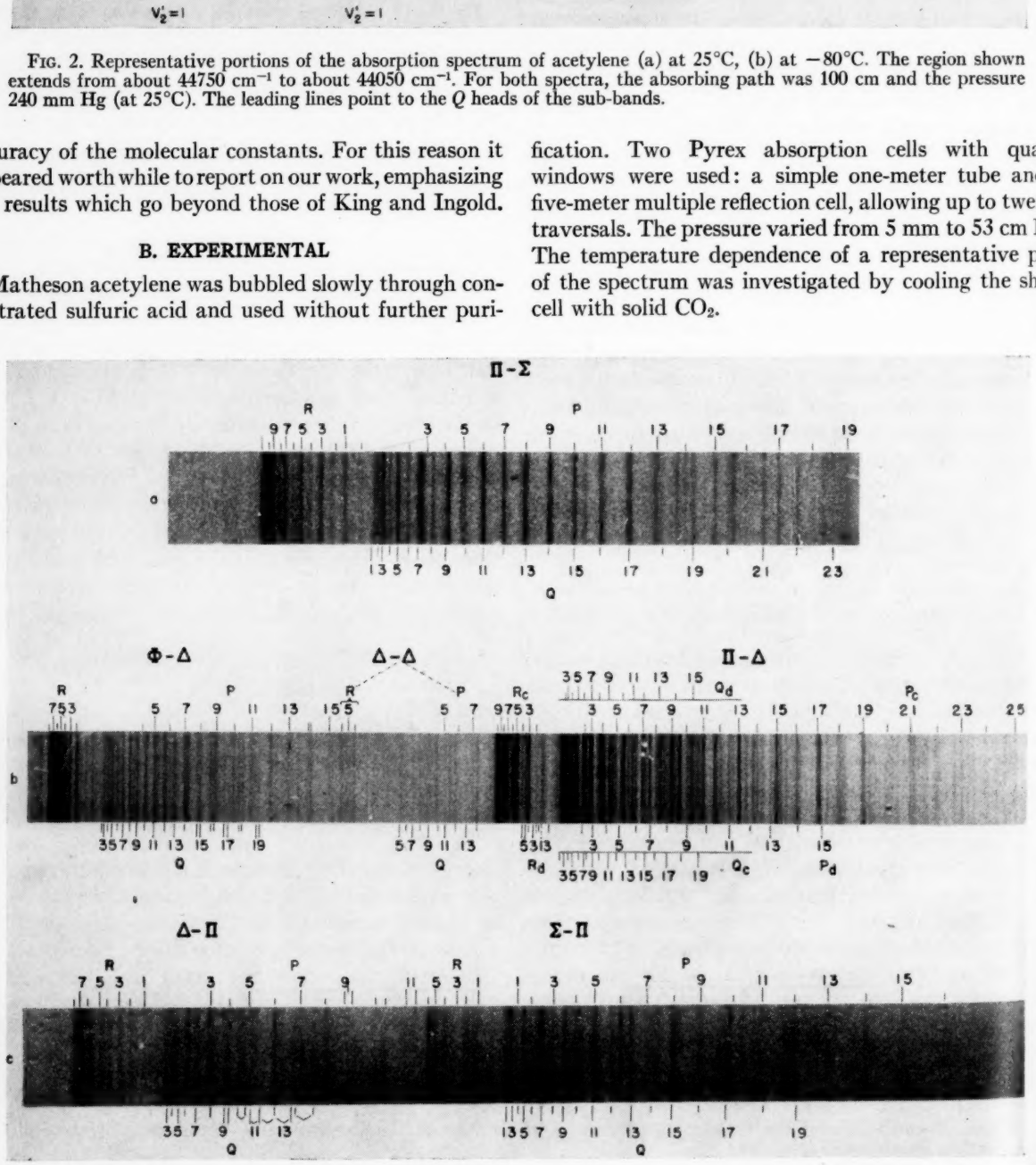

FIG. 3. Fine structure of important types of sub-bands: (a) Π−Σ band at 43 258 cm^{-1}, $v_3'=1$, $K'=1$; $v_4''=0$, $L''=0$; (b) Π−Δ, Δ−Δ, and Φ−Δ bands in the region 43 185–42 950 cm^{-1}, $v_3'=2$, $K'=1, 2, 3$; $v_4''=2$, $L''=2$; (c) Σ−Π and Δ−Π bands in the region 41 460–41 320 cm^{-1}, $v_3'=1$, $K'=0, 2$; $v_4''=3$, $L''=1$. The spectrograms (a) and (c) have approximately the same wave-number scale; (b) has a somewhat smaller scale in order to accommodate all three bands shown.

A hydrogen discharge tube of conventional design was used to supply the continuous background. The spectrum in the region 1970–2470A was photographed in the fourth and fifth orders of a 21-ft grating spectrograph using Kodak 103a-0 and 103a-0 uv plates. A cylindrical lens before the slit separated overlapping orders.[6] Second and third order iron lines were juxtaposed with the absorption spectra. Measurements were made on a Gaertner comparator using the M.I.T. wavelengths of the Fe lines as standards. The estimated relative accuracy of the vacuum wave numbers of the absorption lines is about 0.06 cm^{-1}.

C. DESCRIPTION OF THE SPECTRUM

In Fig. 2 a representative section of the spectrum is shown both at room temperature and at the temperature of solid CO_2. Figure 3 reproduces enlargements of portions of the spectrum. The apparent bands which, as will be shown later, are really not complete bands but only sub-bands, have a clearly defined fine structure. All sub-bands are shaded to the red. They show a simple P, Q, R structure with the exception of a few in which more than three branches can be recognized. The separation of R and Q heads varies from 12 to 18 cm^{-1}.

Each of the strong sub-bands of Fig. 3 is a member of a long progression of similar sub-bands. The spacing in each progression is about 1050 cm^{-1}, the interval decreasing at higher frequencies. In only one of the strong progressions do the lines in the sub-bands show an intensity alternation. The alternation can be seen particularly clearly in the R branches, as is shown in Fig. 3(a). This same progression is the only strong one that is not affected by cooling to −80°C showing, as has been recognized by King and Ingold,[4,5] that it is the only progression that arises from the vibrationless ground state. These sub-bands have the same structure as $\Pi-\Sigma$ bands of diatomic molecules. The sub-bands of most other progressions arise from vibrationally excited molecules. They have the structure of $\Sigma-\Pi$, $\Delta-\Pi$, $\Pi-\Delta$, and $\Phi-\Delta$ bands.

The wave numbers of sub-band heads have already been tabulated with good accuracy both by Woo, Liu, Chu, and Chih,[2] and by King.[5] In addition, we have observed an important pair of sub-bands with Q heads at 40 343.0 and 40 390.5 cm^{-1}. The wave numbers of the individual lines of twenty measured sub-bands, grouped according to sub-band type, are listed in Table I. Visually estimated relative intensities are included to indicate intensity alternations and blending of lines. The origins of the sub-bands are collected in Table II.

D. VIBRATIONAL ANALYSIS

As mentioned before, all ultraviolet sub-bands of C_2H_2 have the appearance of normal bands of a molecule that is linear in both upper and lower state. It is only on consideration of finer details of both the vibrational and the rotational structure of the spectrum that the conclusion emerges that the molecule is nonlinear in the upper state.

While Woo, Liu, Chu, and Chih[2] have found the seven main progressions from low dispersion work, the clue to the vibrational analysis is supplied by the low temperature spectra as was shown by King and Ingold.[4,5] At low temperature only one strong progression and two weaker ones retain their room temperature intensities. Each of these progressions consists of a number of sub-bands with a spacing of about 1050 cm^{-1}. The sub-bands of the two weak progressions are separated from the corresponding sub-bands of the main one by about 1390 cm^{-1} and 40 to 60 cm^{-1}. At room temperature each "main" sub-band is accompanied by six other strong sub-bands which clearly arise from excited vibrational levels of the lower state. Four such "hot" sub-bands are seen in Fig. 2(a), two at the extreme left of the figure and two at the right end. These pairs are, respectively, about 600 and 1200 cm^{-1} to the red of a main $\Pi-\Sigma$ sub-band. Two more pairs can be found at further successive intervals of about 600 cm^{-1}. From the diminution of intensities at low temperature one concludes that, in each pair, the two sub-bands arise from the same lower level, and that the pairs arise from successively higher multiples of a lower state frequency of about 600 cm^{-1}. The lowest vibrational frequency of acetylene is the bending fundamental ν_4'' which has been found from infrared difference bands to be 611.8 cm^{-1}.[7] It therefore appears that the lower states of the progressions discussed above are the ground state and a number of excited states of the ν_4 vibration. The upper state must consist of progressions of pairs of levels. Figure 4 incorporates the preceding observations into a vibrational energy level diagram which shows examples of the main transitions. The choice given there for the vibrational angular momentum quantum number $L=l_4+l_5$ of each lower level and of the symmetry types for the upper levels was dictated by the apparent sub-band types. The types are also labeled in Fig. 2(a). This interpretation is substantially the same as that of King and Ingold, but was arrived at independently. The latter fact is stressed only for its value in establishing the uniqueness of the vibrational analysis.

The important and novel feature of the vibrational analysis is that it leads to a series of levels in the upper state which is clearly rotational in character and which can be immediately understood if the molecule is assumed to be nonlinear in the upper state. In that case we have an approximately symmetric top with one very small moment of inertia. The approximate rotational energy formula is

$$F(J,K)=\bar{B}J(J+1)+(A-\bar{B})K^2, \qquad (1)$$

[6] J. Curry and G. Herzberg, Ann. Physik. 19, 800 (1934).

[7] G. Herzberg, *Infrared and Raman Spectra of Polyatomic Molecules* (D. Van Nostrand, Inc., New York, 1945).

TABLE I. Wave numbers of the lines in the C_2H_2 sub-bands (ν_{vac}, cm^{-1}).[a]

(a) $K'=1$; $v_4''=0$, $l_4''=0$[b] $(\Pi-\Sigma)$

	$v_3'=0$ $\nu_0=42209.58$ cm^{-1}			$v_3'=1$ $\nu_0=43258.05$ cm^{-1}			$v_3'=2$ $\nu_0=44289.24$ cm^{-1}		
J	$R(J)$	$P(J)$	$Q(J)$	$R(J)$	$P(J)$	$Q(J)$	$R(J)$	$P(J)$	$Q(J)$
0	42211.84(0)			43261.09(?)			44291.30(0)		
1	13.72(3)		42209.34(1)	62.20(3)	43254.25(3)[c]	43257.58(2)[c]	93.54(2)		44288.58(0)[c]
2	15.93(1)	42205.27(0)	08.70(0)	64.31(1)		57.58(2)[c]	95.48(1)	44283.94(1)[c]	88.58(0)[c]
3	17.49(3)	201.87(0)	08.04(4)	65.98(3)	50.37(0)	56.49(3)	97.21(2)	82.04(4)[c]	87.77(2)
4	19.05(0)	199.35(0)	07.04(1)	67.59(1)	47.81(0)	55.47(1)	298.80(0)	79.00(1)	86.67(1)
5	20.39(3)	96.18(4)[c]	05.88(4)	69.00(3)	44.85(2)	54.25(3)	300.17(2)	76.01(1)	85.49(3)
6	21.70(0)	93.28(5)[c]	04.43(1)	70.16(1)	41.46(4)[c]	52.74(1)[c]	01.38(ob)	72.48(4)[c]	83.94(1c)
7	22.87(3)	90.09(4b)[c]	02.67(5)	71.33(3)	38.41(3)[c]	51.17(3)	02.57(2)	69.49(4)[c]	82.05(4c)
8	23.58(0)	86.29(1)	200.72(2)	72.25(1)	35.03(4)[c]	48.98(2)	03.45(0)[c]	65.98(4)[c]	80.14(2)
9	24.56(2)	82.88(3)	198.51(5)	73.20(3)[c]	31.38(4)[c]	46.67(4)	04.43(1)[c]	62.52(3)[c]	77.74(3)
10	25.05(2)	78.99(2)	96.18(4)[c]	73.84(3)[c]	27.64(4)[c]	44.18(2)	04.94(0)[c]	58.59(2)[c]	75.22(1)
11	26.06(4)[c]	75.26(3)	93.28(5)[c]	74.69(4)[c]	23.60(4)[c]	41.46(4)[c]	05.55(5)[c]	55.07(2)	72.48(4)[c]
12	26.06(4)[c]	71.49(4)[c]	90.09(4b)[c]	74.69(4)[c]	19.39(4)[c]	38.41(3)[c]	05.90(5)[c]	50.84(0)	69.49(4)[c]
13	26.06(4)[c]	67.01(3)[c]	87.03(5)	74.69(4)[c]	15.38(2)	35.03(4)[c]	05.90(5)[c]	46.75(2)	65.98(4)[c]
14	26.06(4)[c]	62.70(1)	83.78(2)	74.69(4)[c]	10.99(0)	31.38(4)[c]	05.90(5)[c]	42.17(2)	62.52(3)[c]
15	26.06(4)[c]	58.17(2)	79.83(3)	74.69(4)[c]	06.43(2)	27.64(4)[c]	05.90(5)[c]	37.85(2)	58.59(2c)
16		53.41(1)	76.04(1)	73.84(3)[c]	201.78(1)	23.60(4)[c]	05.55(5)[c]	33.36(1)	54.31(0)
17		48.56(1)	71.49(4)[c]	73.20(3)[c]	196.80(1)	19.39(4)[c]	04.43(1)[c]	28.34(0)	49.75(4)
18			67.01(3)[c]		91.61(0)	14.52(0)	03.45(0)[c]	23.63(1)[c]	45.24(0)
19			62.12(2)		86.26(1)	09.69(1)		17.93(1)[c]	40.22(2)
20			56.83(1)			204.49(0)		12.69(0)	35.07(?)
21			51.70(2)			199.08(3)		06.69(?)	29.50(0)
22			45.90(0)			93.94(1)			23.63(1)[c]
23						87.29(1)			17.93(1b)[c]

(a) $K'=1$; $v_4''=0$, $l_4''=0$ $(\Pi-\Sigma)$

	$v_3'=3$ $\nu_0=45301.00$ cm^{-1}			$v_3'=4$ $\nu_0=46288.10$ cm^{-1}			$v_3'=5$ $\nu_0=47259.94$ cm^{-1}		
J	$R(J)$	$P(J)$	$Q(J)$	$R(J)$	$P(J)$	$Q(J)$	$R(J)$	$P(J)$	$Q(J)$
0	45303.13(1)			46290.87(0)					
1	05.16(5)		45300.32(5b)[c]	92.28(2)		46287.87(1)	47264.16(4)		47259.65(1)
2	07.22(2)		300.32(5b)[c]	94.34(0)	46284.17(4)[c]	87.30(0)	65.95(0)		59.09(1)
3	09.02(5)	45293.73(5b)[c]	300.32(5b)[c]	95.88(3)	80.78(5)[c]	86.61(2)	67.65(4)	47252.24(5)[c]	58.31(4)
4	10.52(2)	90.55(1)	298.37(3)	97.56(1)	77.74(0)	85.41(1)	69.19(0)		57.17(2)
5	11.92(5)	87.70(4)	97.18(5)	298.97(3)	74.72(1)	84.17(4)[c]	70.46(4)	46.48(1)	55.81(4)
6	16.13(6)[c]	84.09(5b)[c]	95.48(4)	300.32(1)	71.66(0)	82.58(1)	71.91(0)	43.15(1)	54.13(2)
7	16.13(6)[c]	81.06(5b)[c]	93.73(5b)[c]	01.33(3)	68.43(2)	80.78(5)[c]	73.14(4)	39.80(2)	52.24(5)[c]
8	16.13(6)[c]	77.65(4)[c]	91.72(4)	02.31(2)	64.90(0)	78.86(1)	73.88(1)		50.14(2)
9		74.15(5b)[c]	89.40(5)	03.19(4)	61.34(1)	76.09(5)	74.46(4)	33.06(2)	47.75(4)
10		69.87(5b)[c]	86.82(4)	03.84(1)	57.58(0)	73.48(2)	75.07(4)	29.20(2)[c]	44.69(1)
11		66.73(4)	84.09(5b)[c]	04.33(6)	53.77(2)	70.61(4)	75.31(4)	25.08(3)	41.88(4)
12		62.90(3)	81.06(5b)[c]	04.67(6)[c]	49.70(0)	67.53(1)	75.56(5)		38.69(2)
13		58.49(4)	77.65(4)[c]	04.67(6)[c]	45.51(1)	64.02(4)			36.05(0)
14		54.17(2)	74.15(5b)[c]	04.67(6)[c]	40.98(00)	60.32(0)			29.20(2)[c]
15		49.52(3)	69.87(5b)[c]		36.53(2)	56.31(3)			27.11(3)
16		44.86(1)	65.60(3)		32.14(0)[c]	52.06(0)			
17		40.13(6)[c]	61.08(4)			47.46(3)			
18		34.85(2)[c]	56.26(2)			42.65(0)			
19		29.63(3)	51.22(3)			37.49(1)			
20		24.23(0)	45.98(1)			32.14(0)[c]			
21		18.73(2)	40.13(6)[c]			26.44(2)			
22		12.78(1)	34.85(2)[c]						
23		06.77(1)	28.34(3)						
24			22.64(1)						
25			15.13(2)						
26			07.88(0)						

[a] ( ) Visually estimated relative intensities.
[b] Unspecified quantum numbers are equal to zero.
[c] Blended lines.

where $\bar{B}=\frac{1}{2}(B+C)$, and $A\gg B\simeq C$. The constants A, B, and C are related in the usual way to the effective moments of inertia. For $K=0, 1, 2, 3, \cdots$ the resultant states are entirely similar to Σ, Π, Δ, Φ, $\cdots$ states, respectively, of a linear molecule; that is, for a given value of K there is a series of rotational levels with $J=K, K+1, K+2\cdots$. Since A is large, these K levels are fairly widely separated. Therefore, the transitions which connect them with the lower state vibrational levels (Σ, Π, Δ, $\cdots$ depending on whether L is 0, 1, 2, $\cdots$) appear as well-separated *sub-bands* which have a structure very similar to $\Pi-\Sigma$, $\Sigma-\Pi$, $\cdots$ bands of diatomic molecules. For example, the main progression which corresponds to transitions from the ground state

TABLE I.—*Continued.*

(b) $K'=0$; $v_4''=1$, $l_4''=1$ ($\Sigma-\Pi$)

	$v_3'=0$ $\nu_0=41585.80$ cm^{-1}			$v_3'=3$ $\nu_0=44673.88$ cm^{-1}		
J	$R(J)$	$P(J)$	$Q(J)$	$R(J)$	$P(J)$	$Q(J)$
1	41589.29(0)	41583.76(0)[e]	41585.35(0)[e]	44678.04(1)	44671.15(4)[e]	44673.43(3)[e]
2	91.21(0)	81.65(0)[e]	85.35(0)[e]	79.62(4)	68.72(1)	73.43(3)[e]
3	92.41(0)	78.61(1*d*)[e]	84.66(1)	81.21(2)	66.66(4)	72.87(4)
4	94.38(1)	75.24(2*d*)[e]	83.76(0)[e]	82.55(5)	63.29(3)	71.87(2)
5	95.40(1)	72.33(4)[e]	82.77(2)	83.71(4)	60.18(6)[e]	71.15(4)[e]
6	96.59(2)	68.50(3)	81.65(0)[e]	84.53(4)	56.61(4)	69.72(2)
7	97.75(2)[e]	64.40(1*d*)[e]	80.21(3)	85.23(5)	53.14(1)	68.26(2)
8	97.75(2)[e]	61.15(5)[e]	78.61(3)[e]	85.61(5)[e]	49.03(5)	66.17(3)
9	97.75(2)[e]	57.25(2)[e]	76.84(3)	85.61(5)[e]	45.01(3)[e]	64.69(5)
10		52.73(1)	75.24(2*d*)[e]		41.02(5)[e]	62.26(3)
11		48.24(0)	72.33(4)[e]		35.98(2)	60.18(6)[e]
12		43.51(0)	70.00(1*b*)		31.30(4)	57.77(2)
13		38.24(0)	67.23(2)		26.20(2)	55.04(3)
14		33.28(0)	64.40(1*d*)[e]		20.86(3)	51.85(3)
15		27.41(0)	61.15(5)[e]		15.23(1)	48.52(5)
16		21.84(0)	57.25(2)[e]		09.52(4)	45.01(3)[e]
17		16.40(0)			603.17(2)	41.02(5)[e]
18		09.62(0)			596.93(3)	36.90(3)
19		502.99(0)				32.43(4)
20		496.22(0)				27.67(2)
21		88.25(0)				22.58(2)
22						17.30(4)
23						11.85(3)
24						605.90(1)
25						599.47(1*b*)

(c) $K'=2$; $v_4''=1$, $l_4''=1$ ($\Delta-\Pi$)

	$v_3'=0$ $\nu_0=41633.70$ cm^{-1}			$v_3'=3$ $\nu_0=44735.43$ cm^{-1}		
J	$R(J)$	$P(J)$	$Q(J)$	$R(J)$	$P(J)$	$Q(J)$
1	41637.78(1)[e]			44739.49(5)[e]		
2	39.31(1)[e]			41.23(4)[e]		44734.74(2)[e]
3	41.09(1)[e]	41626.28(1)[e]	41632.55(0)[e]	42.83(3)[e]	44727.78(4)[e]	34.20(2)[e]
4	42.31(1)[e]	23.43(0)[e]	31.70(1)[e]	44.09(4)[e]	24.76(1)[e]	33.40(2)[e]
5	43.71(1)[e]	20.00(0)[e]	30.66(1)[e]	45.35(2)[e]	21.42(3)[e]	32.46(3)
	43.71(1)[e]	20.00(0)[e]	30.66(1)[e]	45.35(2)[e]	21.43(3)[e]	32.10(3)
6	44.54(1)[e]	16.45(0)[e]	29.48(1)[e]	46.15(3)[e]	18.16(1)[e]	31.02(4)[e]
	44.54(1)[e]	16.45(0)[e]	29.48(1)[e]	46.15(3)[e]	18.16(1)[e]	31.02(4)[e]
7	45.48(1)[e]		28.27(1)[e]	46.93(2)[e]	14.70(2)[e]	29.76(5)
	45.48(1)[e]		28.27(1)[e]	46.93(2)[e]	14.70(2)[e]	29.42(1)
8	46.30(4)[e]		26.28(1)[e]	47.39(2)[e]	10.76(2)[e]	28.34(1)
	46.30(4)[e]		26.28(1)[e]	47.39(2)[e]	10.76(2)[e]	27.78(4)[e]
9			24.99(0)[e]	47.94(4)[e]	07.28(0)	26.50(3)
			24.99(0)[e]	47.94(4)[e]	06.84(2)	25.82(1)
10			22.29(1)[e]		02.77(4)[e]	24.76(1)[e]
			22.29(1)[e]		702.35(4)	23.76(4)
11			20.00(0)[e]		698.49(5)	22.44(3)
			20.00(0)[e]		98.05(1)	21.42(3)[e]
12			17.58(0)[e]		93.97(1)	20.16(0)
			17.58(0)[e]		93.42(4)	18.78(5)
13					89.12(3)	17.78(6)
					88.66(1)	16.04(1)

(Σ) to the upper states with $K=1$, consists of bands of the $\Pi-\Sigma$ type.

The fact that the vibration ν_4'' of the lower state is excited up to $v_4=4$ gives strong support to the preceding argument and is a basis for the assumption that the actual configuration of C_2H_2 in the upper state is the C_{2h} structure of Fig. 1(b). Only for such a structure will the Franck-Condon principle allow transitions with widely different v_4'' for a given upper vibrational level. The excitation of ν_4'' also strongly suggests that the long v' progression corresponds to a similar vibration of the upper state, i.e., $\nu_3(a_g)$ of Fig. 1(d). That the first sub-band of the main progression has $v_3'=0$ is suggested by the fact that an increased absorbing path does not bring out new sub-bands from lower vibrational levels and is confirmed by the rotational analysis (see below). Since the main sub-bands go to $K=1$ of the upper state, their separations do not give exactly the vibrational quanta of the upper state but give $\Delta G+\Delta(A_v-\bar{B}_v)$. Correcting for this on the basis of the rotational analysis one finds that the energy of the $K=0$ level of the lowest vibrational level of the upper

TABLE I.—*Continued.*

(d) $K'=1$; $v_4''=2$, $l_4''=2$ $(\Pi-\Delta)$
$v_3'=1$
$\nu_0=42027.67$ cm^{-1}

J	$R_c(J)$	$R_d(J)$	$P_c(J)$	$P_d(J)$	$Q_c(J)$	$Q_d(J)$
2	42033.73(1)				42026.71(0)[e]	42027.56(0)
3	35.44(2)[e]				25.97(3)[e]	26.71(0)[e]
4	37.14(2)[e]	42035.44(2)[e]		42016.90(1)	25.11(2)[e]	25.97(3)[e]
5	38.39(5)	36.31(2)	42014.27(2)[e]	13.33(1)[e]	23.75(5)	25.11(2)[e]
6	39.49(2)	37.14(2)[e]	11.21(1)	09.53(1)	22.02(4)	
7	40.65(4)		07.49(5)	06.25(4)	20.27(5)[e]	
8	41.57(3)		03.87(2)[e]	01.63(1)	17.95(4)[e]	
9	42.47(3)[e]		00.45(4)	41997.01(2)[e]	15.92(3)	20.27(5)[e]
10	42.47(3)[e]		41997.01(2)[e]		13.33(1)[e]	17.95(4)[e]
11	43.22(5)[e]		92.71(4)		10.38(2)[e]	
12			88.56(0)		07.49(5)[e]	14.27(2)[e]
13			83.98(5)		02.72(2)	12.50(4)
14			79.63(2)		41998.90(4)[e]	10.38(2)[e]
15			74.96(5)		96.02(1)[e]	07.49(5)[e]
16			70.92(2)			04.86(1)
17			65.88(3)			01.63(1)
18			60.71(3)			41998.90(4)[e]
19			55.20(3)			96.02(1)

(d) $K'=1$; $v_4''=2$, $l_4''=2$ $(\Pi-\Delta)$
$v_3'=2$
$\nu_0=43058.90$ cm^{-1}

J	$R_c(J)$	$R_d(J)$	$P_c(J)$	$P_d(J)$	$Q_c(J)$	$Q_d(J)$
2	43065.01(1)	43064.45(1)			43058.08(3)[e]	43048.80(3)
3	66.70(4)[e]	65.94(0)			57.26(4)[e]	58.08(3)[e]
4	68.37(3)[e]	66.70(4)[e]		43048.16(1)	56.35(3)[e]	57.26(4)[e]
5	69.78(4)	67.50(2)	43045.44(2)[e]	44.36(2)[e]	54.92(6)	56.35(3)[e]
6	70.80(3)	68.37(3)[e]	42.34(3)	40.49(3)	53.24(5)	55.52(0)
7	71.93(6)		38.88(5)[e]	37.10(5)	51.24(4)[e]	?
8	72.86(4)		35.30(1)	32.86(1)[e]	49.42(2)[e]	52.81(1)
9	73.60(4)		31.69(4)	27.99(2)[e]	47.05(3)	51.24(4)[e]
10	74.10(1)		27.99(2)[e]	23.10(0)[e]	44.36(2)[e]	49.42(2)[e]
11	74.69(4)[e]		23.97(4)	17.66(2)	41.40(3)[e]	?
12			19.73(1)	12.63(0)	38.23(1)	45.44(2)[e]
13			15.27(2)	06.76(1)	34.36(2)	43.58(5)
14			10.80(2)	00.38(1)	30.86(0)	41.40(3)[e]
15			06.08(4)	94.71(0)	26.66(2)[e]	38.88(5)[e]
16			01.18(5)		22.47(1)	35.73(1)
17			96.09(5)		17.66(2)[e]	32.86(1)[e]
18					12.63(0)[e]	29.73(4)
19					07.50(2)	26.66(2)[e]
20					02.56(0)	23.10(0)[e]

(e) $K'=3$; $v_4''=2$, $l_4''=2$ $(\Phi-\Delta)$

	$v_3'=1$ $\nu_0=42132.06$ cm^{-1}		$v_3'=2$ $\nu_0=43171.90$ cm^{-1}		
J	$R(J)$	$Q(J)$	$R(J)$	$P(J)$	$Q(J)$
2	42137.93(5)		43177.69(4)		
3	39.65(5)	42130.84(2)	79.30(3)		43170.87(1)
4	40.73(5)	30.01(3)	80.55(3)		69.85(1)
5	41.85(5)	28.96(4)	81.74(3)		68.84(2)
6	42.83(5)	27.77(4)	82.52(3)	43154.79(0)	67.57(2)
7	43.66(4)	26.37(4)	84.20(4)	51.05(2)	66.17(3)
8	44.37(5)	24.69(4)		47.25(2)[e]	64.54(3)
9		22.93(4)		43.25(1)	62.69(3)
10		20.85(4)		39.08(1)	60.64(3)
11		18.62(4)		34.58(1)	58.46(2)
12		16.12(4)		30.05(1)	55.98(3)
13				25.52(1)	53.43(2)
14				20.03(1)	50.23(2)
15					47.25(2)[e]
16					43.92(1)

TABLE I.—*Continued.*

(f) $K'=0$; $v_4''=3$, $l_4''=1$ ($\Sigma-\Pi$)
$v_3'=1$
$\nu_0=41390.71$ cm^{-1}

J	$R(J)$	$P(J)$	$Q(J)$
1	41394.60(0)	41388.42(0)[e]	41390.16(0)[e]
2	96.18(0)		90.16(0)[e]
3	97.89(0)	83.06(1)[e]	89.38(1)
4	399.33(1)	79.60(2)[e]	88.42(0)[e]
5	400.70(1)[e]	76.91(3)[e]	87.49(1)
6	00.70(1)[e]	72.97(2)	86.34(0)
7	01.70(2)[e]	68.11(2)[e]	84.90(2)
8		65.13(3)[e]	83.06(1)[e]
9		61.16(1)[e]	81.38(3)
10		56.66(2)	79.60(2)[e]
11		52.01(0)	76.91(3)[e]
12		46.99(0)	74.31(1)
13		42.03(0)	71.43(2)
14			68.11(2)[e]
15			65.13(3)[e]
16			61.16(1)[e]
17			57.40(1)
18			53.16(0)
19			48.71(1)
20			43.74(0)

(g) $K'=2$; $v_4''=3$, $l_4''=1$ ($\Delta-\Pi$)
$v_3'=1$
$\nu_0=41442.15$ cm^{-1}

J	$R(J)$	$P(J)$	$Q(J)$
1	41446.10(2)[e]		
2	47.77(2)[e]		41440.95(2)[e]
3	49.32(2)[e]	41434.20(1)[e]	40.95(2)[e]
4	50.59(2)[e]	31.25(0)[e]	39.84(1)[e]
5	52.08(2)[e]	28.16(0)[e]	39.08(1)[e]
6	52.89(0)[e]	24.61(2)[e]	37.72(2)[e]
7	53.73(5)[e]	20.90(0)[e]	36.18(1)[e]
8	53.73(5)[e]	16.97(2)[e]	34.20(1)[e]
9	54.59(2)[e]	13.73(0)	33.24(0)
		12.48(0)	32.06(0)
10		09.67(0)	31.25(0)[e]
		08.35(0)	29.95(0)
11		05.14(0)	29.19(0)
		03.75(0)	27.36(0)[e]
12			27.36(0)[e]
			24.61(2)[e]
13			24.61(2)[e]
			21.90(0)[e]
14			21.90(0)[e]
			18.79(0)[e]
15			18.79(0)[e]
			15.67(0)[e]
16			15.67(0)[e]

(h) $K'=1$; $v_4''=4$, $l_4''=0$ ($\Pi-\Sigma$)
$v_3'=2$
$\nu_0=41803.54$ cm^{-1}

J	$R(J)$	$P(J)$	$Q(J)$
1	41807.59(0)		
2	809.38(?)		
3	811.35(2)	41795.83(2)[e]	41801.72(1)
4	812.72(1)	792.01(0)	800.69(1)
5	814.18(2)	790.03(0)	799.31(2)
6	815.29(1)	786.75(1)	797.65(2)
7	816.39(2)	783.33(1)	795.83(2)[e]
8	817.33(2)	779.54(1)	793.53(2)
9	818.19(?)	775.88(2)	791.00(1)
10		771.95(0)	788.08(3)[e]
11		767.78(2)	785.16(2)
12			781.58(2)
13			778.20(1)
14			774.18(2)
15			769.68(0)

TABLE I.—*Continued.*

(i) $K'=1$; $v_4''=0$, $l_4''=0$ ($\Pi-\Sigma$)
$v_2'=1$
$v_3'=4$
$\nu_0=47677.41$ cm^{-1}

J	$R(J)$	$P(J)$	$Q(J)$
0	47680.47(0)		
1	81.58(2)		47677.17(1)
2	83.74(0)	47673.30(5)[e]	76.53(0)
3	85.15(3)	69.71(5)[e]	75.74(3)
4	86.56(1)	67.51(1)[e]	74.69(1)
5	87.85(5)	64.03(3)	73.30(5)[e]
6	89.06(2)	60.72(0)	71.62(1)
7	90.06(4)		69.71(5)[e]
8	90.88(2)		67.61(1)[e]
9	91.58(4)		65.15(5)
10	92.26(4)[e]		62.40(3)
11			59.51(5)

(j) $K'=2$; $v_4''=0$, $l_4''=0$ ($\Delta-\Sigma$)
$v_3'=4$
$\nu_0=46337.10$ cm^{-1}

J	$R(J)$	$P(J)$	$Q(J)$
1	46341.35(2)		46336.80(0)
2	43.11(0)		
3	44.81(2)		335.40(1)
4	46.36(0)		34.20(0)
5	47.64(1)	46322.67(2)[e]	32.72(3)
6	48.42(0)	20.10(4)[e]	31.11(2)
7	49.45(2)	17.44(3)[e]	29.28(4)
8	50.44(4)[e]	13.58(0)	27.25(2)
9		09.83(2)	25.04(5)
10		05.56(3)	22.67(2)[e]
11			20.10(4)[e]
12			17.44(3)[e]
13			14.39(4)
14			11.46(1)
15			08.24(2)

(k) $K'=2$; $v_4''=2$, $l_4''=2$ ($\Delta-\Delta$)
$v_3'=2$
$\nu_0=43101.03$ cm^{-1}

J	$R(J)$	$P(J)$	$Q(J)$
4	43109.49(1)		
5	111.20(0)	43087.42(0)[e]	43098.10(1)
6	112.48(1)[e]	083.06(0)	96.58(0)
7		080.39(0)	95.13(0)
8			93.46(1)
9			91.28(1)
10			89.24(1)
11			87.42(0)
12			84.62(0)
13			82.06(0)
14			79.22(0)

state is 42 197.69 cm^{-1}, and the vibrational constants associated with v_3' are

$$\omega_3^{0\prime}=1056.27, \quad x_{33}'=-8.7_1 \text{ cm}^{-1}.$$

Another vibration of the upper state, which gives rise to a second progression from the ground state as well as weak, "hot" sub-bands similar to those already discussed, is in all probability the CC stretching vibration, $v_2'(a_g)$, of Fig. 1(d). A few of these sub-bands are assigned at the bottom of Fig. 2. A precise value has been obtained from the rotational analysis only for the difference $[(v_2'+4v_3')-4v_3']_{K=1}$, which is 1389.31 cm^{-1}.

Three of the lower state levels, $2v_4^2$, $3v_4^1$, $4v_4^0$, of Fig. 4 have not previously been observed. Accurate values for them are obtained after rotational analysis from the sub-band origins of Table II. The frequencies

$2\nu_4^2$ and $4\nu_4^0$ are direct differences of the origins of sub-bands which have common upper levels with $K=1$. However, the sub-bands for $v_4''=3$ go to $K=0$ and $K=2$ rather than to $K=1$, so that in order to find $3\nu_4^{1''}$ one must add $(A-\bar{B})$ to the $\Sigma-\Pi$ sub-band origin before subtracting from the appropriate $\Pi-\Sigma$ origin [see below for the correct $(A-\bar{B})$ to be used]. In this way $3\nu_4^{1''}$ was found to be 1854.57 cm^{-1}.[8] Using a similar procedure for deriving the level ν_4'' one finds the frequency 611.8$_5$ cm^{-1}; a value that agrees quite well with that obtained from infrared difference bands. From the new levels $v_4''=2$, 3, 4 the following vibrational constants are obtained:

$$\omega_4^{0''}=608.2_6, \quad x_{44}''=3.29, \quad g_{44}''=0.1_7 \text{ cm}^{-1}.$$

The sum of these values, 611.7$_2$ cm^{-1},[8] gives a good check of ν_4''. One unusual feature is to be noted, namely, the positive sign of x_{44}.

In the scheme of Fig. 4 there are no sub-bands corresponding to transitions from the vibrationless ground state (Σ_g^+) to the upper levels with $K=0$ (levels of type Σ). The strongest transitions which are found are those in which $K-L=\pm1$, that is, transitions which in a symmetric top molecule would form a perpendicular band. To be sure, the rotational analysis shows that weak $\Delta-\Sigma$ and $\Delta-\Delta$ sub-bands do exist, but it is likely that their occurrence is the result of the deviations from the symmetric top in the upper state.

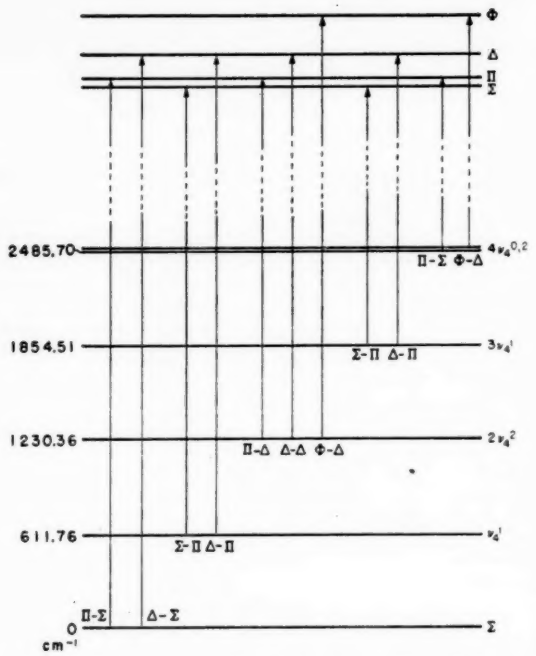

FIG. 4. Energy level diagram of C_2H_2 representing the observed sub-bands. Only one vibrational level of the upper electronic state is shown. The coarse rotational structure of this level is shown on a larger scale than the vibrational structure of the electronic ground state except that the splitting of the $4\nu_4''$ level is exaggerated.

E. ROTATIONAL ANALYSIS

1. Strong Sub-Bands Originating in the Ground State ($\Pi-\Sigma$)

It has been noted in Section C that the one progression of strong sub-bands which is unchanged at low temperature shows a clear intensity alternation in the fine structure of each sub-band. This is in agreement with the assumption (see Section D) that these sub-bands arise from the ground state which has the symmetry type Σ_g^+. In this state, as is well known, the odd rotational levels have three times the statistical weight of the even levels, just as in the case of hydrogen. Therefore, the first strong lines of the three branches of the $\Pi-\Sigma$ sub-bands are $R(1)$, $Q(1)$, and $P(3)$. This gives a check on the numbering after the three regular series have been picked out. Another check is the coincidence of ν_0, as determined from the P and R branches and the Q branch. Finally, the combination differences $\Delta_2F''(J)=R(J-1)-P(J+1)$ give a very critical test of the whole analysis since they must agree for each J value with those obtained from infrared bands involving the same vibrationless state. Table III shows that this is indeed the case. The second column of this table gives the average $\Delta_2F''(J)$ values from the seven $\Pi-\Sigma$ sub-bands of Table I, while the third column gives the average $\Delta_2F''(J)$ values obtained by Herzberg and Spinks[9] from three strong photographic infrared bands.

The agreement is most satisfactory particularly if it is considered that the wave-number accuracy in the ultraviolet is much less than in the infrared. The average B'' obtained from the $\Delta_2F''(J)$ values of the ultraviolet sub-bands is 1.177 cm^{-1}, compared to the infrared value of 1.1769 cm^{-1}.

TABLE II. Origins ν_0 of the sub-bands which have been measured and analyzed.

		Assignment				
		Upper state			Lower state	
ν_0(cm^{-1})	Type	v_2'	v_3'	K	v_4''	L
41390.71	$\Sigma-\Pi$	0	1	0	3	1
41442.15	$\Delta-\Pi$	0	1	2	3	1
41585.80	$\Sigma-\Pi$	0	0	0	1	1
41633.70	$\Delta-\Pi$	0	0	2	1	1
41803.54	$\Pi-\Sigma$	0	2	1	4	0
42027.67	$\Pi-\Delta$	0	1	1	2	2
42132.06	$\Phi-\Delta$	0	1	3	2	2
42209.58	$\Pi-\Sigma$	0	0	1	0	0
43058.90	$\Pi-\Delta$	0	2	1	2	2
43101.03	$\Delta-\Delta$	0	2	2	2	2
43171.90	$\Phi-\Delta$	0	2	3	2	2
43258.05	$\Pi-\Sigma$	0	1	1	0	0
44289.24	$\Pi-\Sigma$	0	2	1	0	0
44673.88	$\Sigma-\Pi$	0	3	0	1	1
44735.43	$\Delta-\Pi$	0	3	2	1	1
45301.00	$\Pi-\Sigma$	0	3	1	0	0
46288.10	$\Pi-\Sigma$	0	4	1	0	0
46337.10	$\Delta-\Sigma$	0	4	2	0	0
47259.94	$\Pi-\Sigma$	0	5	1	0	0
47677.41	$\Pi-\Sigma$	1	4	1	0	0

[8] Note that this is a slight refinement of Fig. 4.

[9] G. Herzberg and J. W. T. Spinks, Z. Physik. **91**, 386 (1934).

If, on the assumption that the molecule is linear in both upper and lower state, B' values are determined in the usual way from the Q branch on the one hand and from P and R branches on the other, one finds for each $\Pi-\Sigma$ sub-band that the two values obtained differ by about 5 percent. This splitting of the two components of the Π states appears far too large to be explained as due to an L-type or Λ-type doubling in the upper state; (in the ground state the L-type doubling amounts to only 0.5 percent of the rotational energy). Moreover, the magnitude of the splitting changes very little in the main progression of sub-bands. King and Ingold[4,5] noticed this effect despite their lower resolution and concluded that it was a result of the nonlinearity of the molecule in the excited state. For a slightly asymmetric top the splitting of the levels with $K=1$ is large enough to account for this observed doubling. It is found that Q-branch lines involve the lower component levels, and P and R branch lines the upper ones.

For a transition between linear configurations:

$$Q(J)=\nu_0+(B'-B'')J(J+1)-(D'-D'')J^2(J+1)^2, \quad (2)$$

where the last term is usually very small. Similar behavior is expected if the molecule is an exact symmetric top in the upper state. If, however, the molecule is an asymmetric top, the rotational energy levels should not be so closely proportional to $J(J+1)$. Figure 5 shows, for one of the $\Pi-\Sigma$ sub-bands, a plot of $Q(J)-aJ(J+1)$ against $J(J+1)$, where a is an approximation to $(B'-B'')$. The scatter of points at low J is due to blending of lines. Similar plots have been obtained for each $\Pi-\Sigma$ sub-band, though usually there is more blending of lines for the high J values and less for low J values. The plot exhibits a marked departure from linearity at rather low J, showing that Eq. (2) might account for the observed points only if the last term happens to be large. The dotted curve of Fig. 5 was calculated using $D'=4.50\times10^{-6}$ cm^{-1}, which compares to 1.87×10^{-6} for the ground state. An even larger D' appears to be necessary to bring the dotted curve near to coincidence with the experimental one in the region for which the latter is narrowly defined. On the other hand, the dashed curve of Fig. 5, which was calculated using the asymmetric top energy expression discussed below, follows the observed curve quite closely.

Wang has given an expression for the separation of the K doublets of an asymmetric top.[10] It takes a particularly simple form for $K=1$,

$$\Delta\nu=\tfrac{1}{2}(B-C)J(J+1). \quad (3)$$

It can be shown that for low J the splitting is symmetric about the energy given by the symmetric top approximation. If $\Delta\nu/2$ is added to and subtracted from the energy given by Eq. (1), one obtains for the energies of the upper levels of the $\Pi-\Sigma$ sub-bands:

$$F_{P,R}(J)=\left(\frac{3B+C}{4}\right)J(J+1)+(A-\bar{B}), \quad (4)$$

$$F_Q(J)=\left(\frac{B+3C}{4}\right)J(J+1)+(A-\bar{B}). \quad (5)$$

From these equations one derives that the slope of the extrapolated line of Fig. 5 gives the correction to the assumed values of $[(B+3C)/4]-B''$. Similarly, a plot of $R(J-1)+P(J)$ *vs* J^2 gives a curve with a linear part of slope $2\{[(3B+C)/4]-B''\}$. The constants B' and C' may be determined to within ±0.002 cm^{-1} from these expressions. Actually we have here used the alternative derivation of $(3B+C)$ from $[R(J)-P(J)]/(J+\frac{1}{2})$.

These determinations are based on lines with J less than 12. An improvement in the accuracy of the constants can be obtained by fitting the lines of higher J using the asymmetric top formulas in a stochastic manner closely similar to that used by Cross[11] and by Allen, Cross, and Wilson[12] for the rotation-vibration spectrum of a strongly asymmetric top. Golden[13] has derived approximate expressions for the rotational energy which are quite accurate for high J and low K, that is, for the case considered here. For the nearly prolate symmetric top, Golden's expression reduces to

$$F(J,\alpha)=\bar{B}J(J+1)+(A-\bar{B})\alpha, \quad (6)$$

where $\alpha=b-\frac{1}{2}s$ replaces K^2 of Eq. (1). Here

$$s=\frac{B-C}{A-\bar{B}}\left\{J(J+1)-\left[1+\frac{1}{2J(J+1)}\right]\right\}$$

and b can be found as a function of s in tables of Mathieu functions.[14]

The procedure is briefly as follows. The energy levels of the upper state are calculated from Eq. (6) with the

TABLE III. Comparison of combination differences $\Delta_2F''(J)$ obtained from ultraviolet and infrared bands.

J	Ultraviolet	Infrared
1	...	6.91
2	11.84	11.73
3	16.57	16.50
4	21.19	21.16
5	25.93	25.90
6	30.60	30.60
7	35.22	35.26
8	40.02	40.00
9	44.66	44.72
10	49.37	49.40
11	54.14	54.11
12	58.82	58.80

[10] See, for example, S. C. Wang, Phys. Rev. **34**, 243 (1929); R. B. Lawrance and M. W. P. Strandberg, Phys. Rev. **83**, 363 (1951).

[11] P. C. Cross, Phys. Rev. **47**, 7 (1935).

[12] Allen, Cross, and Wilson, J. Chem. Phys. **18**, 691 (1950).

[13] S. Golden, J. Chem. Phys. **16**, 78 (1948).

[14] *Tables Relating to Mathieu Functions* edited by the National Bureau of Standards. (Columbia University Press, New York, 1951).

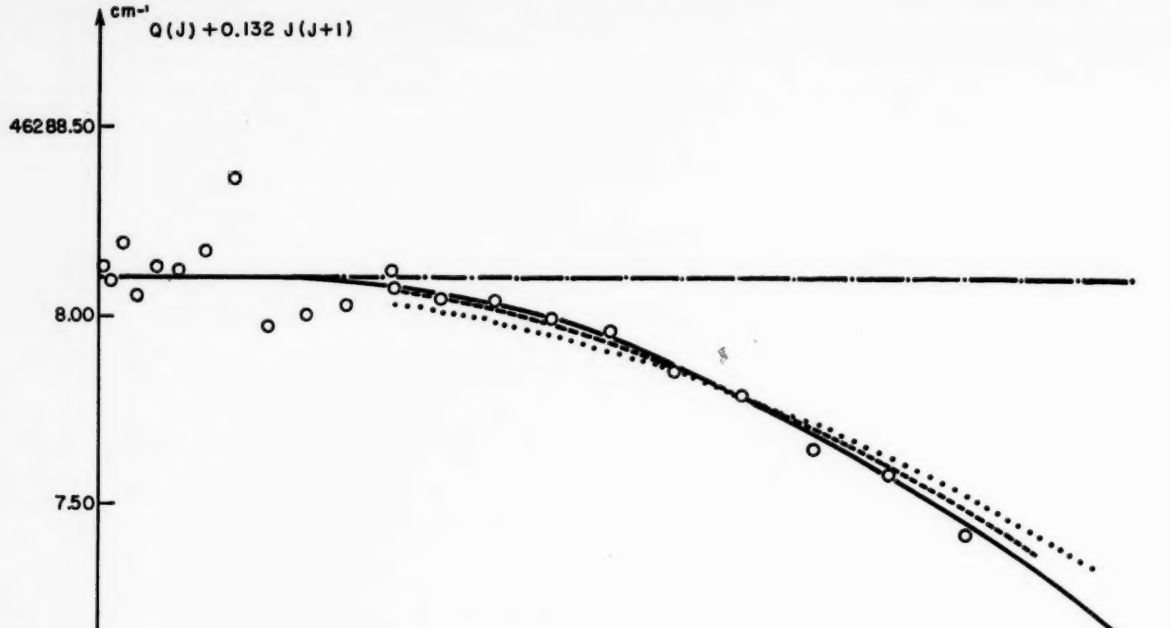

FIG. 5. Plot of the Q branch of the $\Pi-\Sigma$ sub-band with $v_3'=4$, $v_4''=0$ against $J(J+1)$, after addition of $0.132J(J+1)$. The full-line curve represents the observed data, the dotted curve represents $Q(J)=46\,288.10-0.132J(J+1)-2.67\times10^{-6}J^2(J+1)^2$, and the broken-line curve was calculated from Eq. (6) using $B'=1.1275$ and $C'=1.0176$ cm^{-1}.

approximate B' and C' values determined earlier, and approximate A values from the separations of the Q heads of the sub-bands of a given band. The energy levels of the ground state are calculated from the accurate constants of Herzberg and Spinks.[9] The calculated transitions are then compared with the observed ones and with the help of the derivatives $\partial F/\partial B$ and $\partial F/\partial C$ obtained from (6), corrections are made to B' and C' to bring observed and calculated lines into coincidence.[15] In this way the B' and C' values of Table IV were obtained. It may be noted that the P and R branch lines are most sensitive to B' while the Q-branch lines are most sensitive to C'. Small changes in A' affect the relative positions of the individual lines of a sub-band very little since $\partial F/\partial A$ is very small and almost independent of J. An improvement of A' can therefore not be obtained by this method.

The observed B' and C' values may be represented by the formulas

$$B'_{[v]}=1.1247+0.0008v_3', \quad C'_{[v]}=1.0297-0.0030v_3'.$$

The agreement of calculated and observed values in Table IV is very satisfactory showing that

$$B_0'=1.1247 \quad \text{and} \quad C_0'=1.0297 \text{ cm}^{-1}$$

are probably correct to ±0.0004 and ±0.0001 cm^{-1}, respectively.

[15] Only changes of B' and C' up to 0.005 cm^{-1} are possible by use of the derivatives.

2. Strong Sub-Bands Originating in Excited Vibrational Levels ("Hot" Sub-Bands)

The spectrograms of Fig. 3(b) and 3(c) show the rotational fine structure of the four important types of "hot" sub-bands, namely, $\Sigma-\Pi$, $\Delta-\Pi$, $\Pi-\Delta$, and $\Phi-\Delta$. Table I gives the measured and assigned lines of these sub-bands.

In spite of the overlapping by $\Delta-\Pi$ sub-bands, the simple structure of the $\Sigma-\Pi$ sub-bands is readily recognizable. Just like the $\Pi-\Sigma$ sub-bands, they consist of three branches P, Q, R except that now the R branch is weakest since $K-L=-1$. On account of the l-type doubling in the lower state,[16] the Q lines have slightly different lower levels from the P and R lines. Because of the weakness of the R branch, it was not possible to determine all rotational constants directly. Therefore, again the stochastic method mentioned in the preceding subsection was used this time considering the upper state constants as accurately known from the $\Pi-\Sigma$ sub-bands and adjusting lower state constants which are known approximately from infrared data.[9] One finds

$$\text{for } v_4''(L=1): \quad B_c''=1.1750, \quad B_d''=1.180_8 \text{ cm}^{-1},$$
$$\text{for } 3v_4''(L=1): \quad B_c''=1.1785, \quad B_d''=1.187_5 \text{ cm}^{-1}.$$

Here the subscript c designates the levels which are positive for even J, that is the lower level of each pair, while d designates the upper levels. The l-type doubling

[16] G. Herzberg, Revs. Modern Phys. 14, 219 (1942).

constant q_4'' is seen to be 0.005_3 cm^{-1} for ν_4'', and 0.009_0 cm^{-1} for $3\nu_4''$. The first of these values is in agreement with the value given by Herzberg.[16] The value for $3\nu_4''$ is approximately twice that for ν_4'' in agreement with theory.[17]

It is important for the later discussions to emphasize that in the $\Sigma-\Pi$ sub-bands it is observed that the even-numbered lines are strong in the P and R branches, while the odd-numbered lines are strong in the Q branches.

The $\Delta-\Pi$ sub-bands should consist of six branches, because of the K-type doubling in the upper and the l-type doubling in the lower state. However, most of these sub-bands do not show a doubling of the branches except for high J values of those sub-bands originating in the level $3\nu_4''$. The reason for the apparently vanishing splitting is that the doubling in the $K=2$ upper level is, according to Eq. (6), very small and the splitting in the lower level, ν_4'', is not sufficient to be resolved. Since the unresolved branches have opposite intensity alternations, no alternation is observed. A calculation of the lines of the branches from B', C' values of Table IV, and the B'' values of Herzberg and Spinks[9] gives excellent agreement with the measured lines within experimental accuracy. It is evident in Fig. 3(c), and even more so for the strong $\Delta-\Pi$ sub-band of Fig. 2, that the $R(0)$ transitions are missing. It may be remarked here that the successful calculation of fine structure for these and other "hot" sub-bands (below), using the same B' and C' values for each of the four upper state levels of Fig. 4, is further strong evidence that the four levels belong to a single vibrational level, a circumstance possible only if acetylene is nonlinear in the upper state.

The $\Pi-\Delta$ sub-bands are the only ones for which six branches are fairly well resolved. This is due to the very large splitting of the upper level already observed in the $\Pi-\Sigma$ sub-bands. In the $\Pi-\Delta$ sub-bands the two P (and R) branches are separated by the sum of the Π and Δ splittings, while the two Q branches are separated by the difference of the splittings. The sub-bands appear complicated, as can be seen from Fig. 3(b), and many lines are blended. Since the upper state energy levels are known to $J=20$–23, from analyses of the $\Pi-\Sigma$ sub-bands, the simplest method of assigning lines was by a calculation of the spectrum using an approximate B'' value. Again a slight adjustment of B'' was necessary to obtain the best agreement. The following B'' values of the level $2\nu_4''$ ($L=2$) were found from the $\Pi-\Delta$ sub-band of Fig. 3(b) [$v_3'=2$ in Table I(d)]:

$$B_c''=1.183_6, \quad B_d''=1.185_2 \text{ cm}^{-1}.$$

The slight difference of these values is probably not significant. At any rate, the l-type doubling of a state with $L=2$ is expected to be negligibly small. It appears significant that the average B'' value (1.184_4 cm^{-1}) is appreciably larger than would have been expected from the B'' values of $\nu_4''(L=1)$ and $3\nu_4''(L=1)$. This behavior suggests an appreciable dependence of B on L.

The $\Phi-\Delta$ sub-bands were analyzed in a way very similar to the $\Delta-\Pi$ sub-bands. For $\Phi-\Delta$ also the splitting is not resolved except at high J values. It may be recognized in Fig. 3(b) for the Q branch from $J=15$ up. In the same figure the absence of the lines $R(0)$ and $R(1)$ is particularly clear, confirming the $\Phi-\Delta$ character of the sub-band.

3. Miscellaneous Weak Sub-Bands

Several progressions of weak sub-bands were found and a few of these were analyzed.

One sub-band of a progression involving the 1389 cm^{-1} vibration of the upper state was analyzed [Table I(i)]. It is of the $\Pi-\Sigma$ type and yields values for B' and C' which are somewhat smaller than those of the corresponding sub-band of the main progression (see Table IV). This difference is in the direction expected for excitation of a CC stretching vibration.

The members of a still weaker progression, also originating in the ground state, appear regularly at about 50 cm^{-1} to the violet of the main $\Pi-\Sigma$ transitions. In Fig. 2 the heads are barely discernible at both temperatures. One such sub-band was measured and analyzed as shown in Table I(j). There are three branches of comparable intensities. The origin is 49.00 cm^{-1} to the violet of the $\Pi-\Sigma$ sub-band belonging to $v_3'=4$. This separation fits the assignment as a $\Delta-\Sigma$ sub-band, since from head measurements $A-\bar{B}$ for $v_3'=4$ is about 16.5 cm^{-1}.

In Fig. 3(b) there is further weak structure which has been measured and analyzed as a $\Delta-\Delta$ sub-band [see Table I(k)]. The structure agrees with that computed from the known constants of the upper and lower states.

Finally, the fine structure of one weak $\Pi-\Sigma$ sub-band with lower level $4\nu_4''(L=0)$ was measured and analyzed [Table I(h)]. The constants of the upper state were known from the corresponding main sub-band and the lower state B value was found to be 1.189 cm^{-1}.

4. Determination of A' Values

From the origins of the sub-bands discussed in the preceding three sub-sections and listed in Table II, precise values of $A'-\bar{B}'$, and therefore of A' can be

TABLE IV. Rotational constants for the upper state of the ultraviolet bands of acetylene.

v_2'	v_3'	A'_{obs} cm^{-1}	B'_{obs} cm^{-1}	C'_{obs} cm^{-1}	B'_{calc} cm^{-1}	C'_{calc} cm^{-1}
0	0	12.94	1.1243	1.0297	1.1247	1.0297
0	1	13.82	1.1250	1.0267	1.1255	1.0267
0	2	14.91	1.1270	1.0237	1.1264	1.0237
0	3	16.36	1.1278	1.0205	1.1272	1.0206
0	4	...	1.1275	1.0176	1.1280	1.0176
1	4		1.118	1.014		

[17] H. H. Nielsen, Revs. Modern Phys. **23**, 90 (1951).

obtained for each upper vibrational level for which at least two sub-bands were analyzed. In deciding which of the numerous sub-bands should be measured, care was taken to have pairs of sub-bands with the same upper and lower vibrational levels. From the origins of two such sub-bands (e.g., $\Phi-\Delta$ and $\Pi-\Delta$, or $\Delta-\Pi$ and $\Sigma-\Pi$), $A'-\bar{B}'$ is immediately obtained with the use of Eq. (1) [e.g., $\nu_0(\Phi-\Delta)-\nu_0(\Pi-\Delta)=8(A'-\bar{B}')$ and $\nu_0(\Delta-\Pi)-\nu_0(\Sigma-\Pi)=4(A'-\bar{B}')$]. In one case two pairs of sub-bands belonging to the same upper vibrational level ($v_3'=1$, $K=0, 2; 1, 3$) were analyzed. From the first pair $A'-\bar{B}'=12.86$ cm^{-1}, from the second pair $A'-\bar{B}'=13.05$ cm^{-1}. This apparent discrepancy is probably due to an additional term $+D_K K^4$ in Eq. (1) which causes the apparent $A'-\bar{B}'$ to be different, depending on the K values used. The somewhat surprising result is that, contrary to expectation, D_K is required to be positive.[18] More particularly one finds from the above two apparent $(A'-\bar{B}')$ values that $D_K=0.03$ cm^{-1}. A very similar value is obtained from the three sub-bands with $v_3'=2$. Using $D_K=0.03$ cm^{-1}, one finds a corrected $A'-\bar{B}'=12.74$ cm^{-1} for $v_3'=1$. Correcting in the same way for the other vibrational levels and adding $\bar{B}'$, the final A' values of Table IV were obtained. The rapid increase of A' with v_3' is very striking.

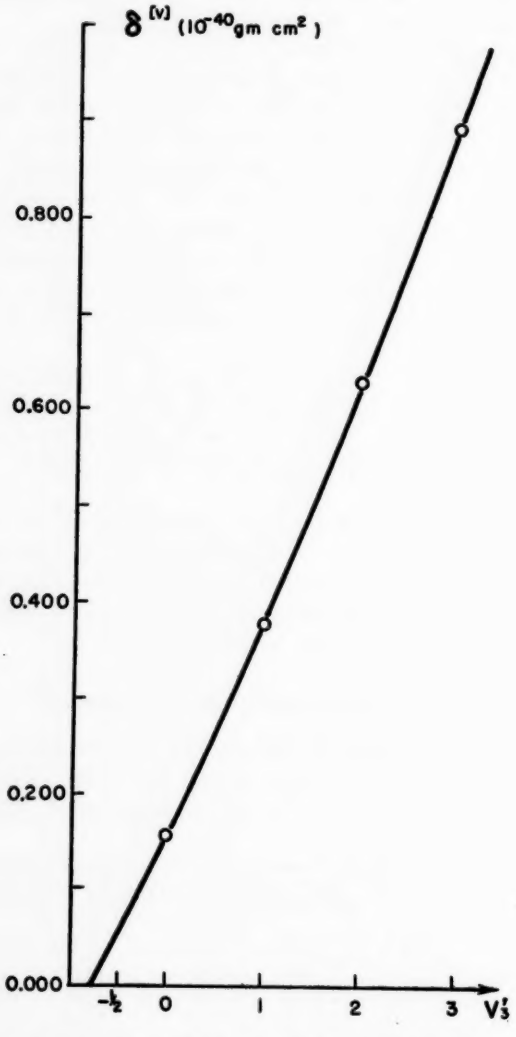

FIG. 6. Defect $\delta^{[v]}=I_c-I_a-I_b$ as a function of v_3'.

F. GEOMETRICAL STRUCTURE OF THE MOLECULE IN THE UPPER STATE

In the preceding sections conclusive evidence has been presented showing that the acetylene molecule is nonlinear in the upper state of the ultraviolet bands. We must now consider the question of the particular way in which the molecule deviates from linearity. It is conceivable that the molecule is not only nonlinear but also nonplanar, that is, that the angle φ between the two H—C—C planes is different from 0° (*cis* configuration) or 180° (*trans* configuration). From calculations by Giguère[19] for the similar case of H_2O_2, it can be seen that for angles φ between 45° and 135° the C_2H_2 molecule would be nearly a symmetric top. Since the spectrum shows C_2H_2 to be a distinctly asymmetric top with about 10 percent difference between I_b and I_c, it follows that φ is not between 45° and 135° and that therefore the molecule is likely to be planar with either $\varphi=0$ (point group C_{2v}) or $\varphi=180°$ (point group C_{2h}). For $\varphi=0$ the twofold axis of symmetry is clearly that of the intermediate moment of inertia (b axis), while for $\varphi=180°$ it is that of the largest moment of inertia (c axis). The transition from the b to the c axis takes place near $\varphi=90°$.

The over-all species classification of the rotational levels is different for these two cases and conversely therefore a decision can be made from the observed intensity alternation as to which case actually applies. Let 1_d and 1_c be the levels of the asymmetric top into which the symmetric top levels with $K=1$ are split, such that the 1_c levels are the lower ones [see Eqs. (4) and (5)]. It can easily be shown from figures similar to Fig. 144 of ref. 7 that when the c axis is the symmetry axis the over-all species classification (A, B of ref. 7), and therefore, the alternation of statistical weights, follows the same pattern for the $K=0$ and 1_c levels. In other words, in both sets, the levels with even J are "strong," those with odd J are "weak" or, conversely, in both sets, the levels with even J are "weak," those with odd J "strong." On the other hand, when the b axis is the symmetry axis, the symmetries and therefore the alternation of statistical weights are opposite in the $K=0$ and 1_c sets of a given vibrational level. The observation shows clearly that in the Q branches of both the $\Pi-\Sigma$ and the $\Sigma-\Pi$ sub-bands, the even lines are weak. Therefore, since the Q branches of $\Pi-\Sigma$ sub-bands belong to 1_c in the upper state, while those of $\Sigma-\Pi$ belong to $K=0$, it follows that the first case applies, i.e., that the c axis is the symmetry axis and

[18] C. Reid, J. Chem. Phys. **18**, 1544 (1950).

[19] P. A. Giguère, J. Chem. Phys. **18**, 92 (1950).

hence, φ must be either equal to 180° (C_{2h} structure, Fig. 1b), or be between 135° and 180°.

For a planar molecule, unlike a nonplanar one, in the equilibrium position the largest moment of inertia I_c^e is the sum of the two other moments of inertia, I_b^e and I_a^e. The corresponding effective moments of inertia for a vibrational level $[v]$ do not follow this sum rule, but there is a defect $\delta^{[v]}=I_c^{[v]}-I_a^{[v]}-I_b^{[v]}$. Figure 6 shows the observed values of $\delta^{[v]}$ for the upper levels of the main progression as a function of v_3'. It is seen that $\delta^{[v]}$ becomes very small for $v_3'=-\frac{1}{2}$. This value is, of course, not δ^e since the zero point vibrations of the other normal vibrations are still included. Considering, however, that ν_3 is probably the vibration with the greatest effect on the moments of inertia, it seems probable that δ^e is zero, that is, that the molecule is planar and has C_{2h} symmetry [Fig. 1(b)].

Proceeding on the assumption that C_{2h} is the correct point group, we can obtain from the observed rotational constants, the C−C−H angle θ, and the C−C distance in the excited state, if an assumption is made about the C−H distance. Using the convenient expressions of Hirschfelder[20] for the principal moments of inertia,

TABLE V. C−C distance and C−C−H angle in the upper state of the ultraviolet C_2H_2 bands.

r(CH) assumed	From I_c^0 and I_a^0		From I_c^0 and I_b^0	
	r_0(CC)	θ	r_0(CC)	θ
1.060A	1.391_9A	120°18′	1.397_9A	117°59′
1.070	1.387_6	120°55′	1.393_5	118°38′
1.080	1.383_3	121°30′	1.389_1	119°14′
1.090	1.378_9	122°3′	1.384_6	119°51′

one finds for the present case [Fig. 1(b)],

$$I_c=\tfrac{1}{2}(m_C+m_H)r_{CC}^2+2m_Hr_{CH}^2+2m_Hr_{CC}r_{CH}\cos(180°-\theta),$$

$$I^2-I_cI+m_Cm_Hr_{CH}^2r_{CC}^2\sin^2(180°-\theta)=0,$$

where the two values of I obtained from the last equation are I_a and I_b. For the lowest vibrational level we have from A_0, B_0, C_0 of Table IV (using $h/8\pi^2c=27.9832_{45}\times10^{-40}$) the moments of inertia,

$$I_a^0=2.143\times10^{-40},\quad I_b^0=24.881\times10^{-40},$$
$$I_c^0=27.176\times10^{-40}\text{ g cm}^2.$$

Since $\delta^0=I_c^0-I_a^0-I_b^0$ is not zero, slightly different values for the geometrical parameters are obtained depending on whether I_c and I_a or I_c and I_b are used. Table V gives the values obtained for four assumptions about r_0(CH).

It appears almost certain that the C−H distance is between the extreme values assumed in Table V, and therefore it is seen that $r_0(CC)=1.38_8\pm0.00_8$A while $\sphericalangle$C−C−H=120°±2°. For comparison, the ground state values $r_0(CH)=1.058$, $r_0(CC)=1.208$A, and

[20] J. O. Hirschfelder, J. Chem. Phys. **8**, 431 (1940).

TABLE VI. Intercomparison of C_2H_2 bands with $^1\Pi-{}^1\Sigma$ bands of N_2 and CO and similar bands of HCN.

	Path required (m atmos)	ν^{00} (cm^{-1})	ω'/ω''	r'/r''
C_2H_2	1.0	42200	0.70	1.15
N_2	0.3	69290	0.72	1.11
HCN	0.1	52260	0.71	1.13
CO	0.001	65075	0.70	1.10

$\sphericalangle$C−C−H=180° may be quoted.[21] In view of the photochemical polymerisation of acetylene to benzene, it is of interest that r_0(CC) for the upper state of the ultraviolet C_2H_2 bands is very close to r_0(CC) in the ground state of benzene which, according to recent work of Stoicheff,[22] is 1.398±0.003A.

G. NATURE OF THE UPPER ELECTRONIC STATE

From the intensity alternation discussed in the preceding section, we can determine the vibronic species of the upper states of the $\Pi-\Sigma$ and $\Sigma-\Pi$ sub-bands: since the odd rotational levels of $K=0$ and 1_e have the higher statistical weight (just as in the ground state of C_2H_2) the upper state must be symmetric with respect to rotation by 180° about the twofold axis of symmetry, i.e., must have species A_g or A_u. Of these two, A_g is immediately eliminated if electric dipole radiation is assumed for the transition. Since, in addition, the small value of the defect $\delta^{[v]}$ strongly suggests that the first band of the main progression is the O−O band, it would follow that the species of the upper electronic state is A_u as was already recognized by King and Ingold. This identification also accounts for the fact that transitions with $\Delta K=\pm1$ are the most intense since the transition moment is perpendicular to the plane of the molecule.

There is one argument against this identification. There appears to be a close analogy between the C_2H_2 bands under discussion and the $^1\Pi-{}^1\Sigma$ bands of the isoelectronic molecules N_2, CO, and HCN. This analogy is illustrated by Table VI which gives the required path length, the ratio of the frequencies of corresponding vibrations, and the ratio of the internuclear distances for the central bonds in the upper and lower states. The data for HCN are from a recent analysis[23] of a band system quite similar to that of C_2H_2. The upper state of the N_2 bands has been shown to be $^1\Pi_g$.[24] On going from linear to C_{2h} symmetry this state would split into two states, A_g and B_g. The upper electronic state of the ultraviolet C_2H_2 bands could be A_g or B_g only if it were assumed (a) that the bands, like those of N_2, are due to magnetic dipole radiation, or (b) that they are vibronic transitions of a forbidden electronic transition made possible by the interaction of vibrational and electronic motion. The first possibility, (a), seems unlikely since, for a molecule of

[21] B. D. Saksena, J. Chem. Phys. **20**, 95 (1952).
[22] B. P. Stoicheff, J. Chem. Phys. **21**, 1410 (1953).
[23] G. Herzberg and K. K. Innes (to be published).
[24] G. Herzberg, Phys. Rev. **69**, 362 (1946).

point group C_{2h}, no electronic orbital angular momentum and therefore no large magnetic dipole moment can arise. The second possibility, (b), would involve that the first main band is not the O−O band, but includes in the upper state the excitation of an A_u vibration so that the vibronic species would be A_u as observed. This assumption would imply that the defect δ contributed by the A_u vibration is small (see Fig. 6). An additional difficulty is the apparent absence of the second of the two states into which $^1\Pi_g$ splits. However, the observed low intensity favors the forbidden character of the transition.

The simplest assumption appears to be that the upper state is A_u. It cannot at present be ascertained whether it is a singlet or a triplet state. It should be mentioned, however, that it cannot be the analog of the lowest triplet state of N_2 which is $^3\Sigma_u^+$ since the latter would go over into ^3B_u in point group C_{2h}.

On the basis of molecular orbital calculations, Ross[25] has recently found a $^1\Sigma_u^-$ state to be the lowest singlet state of a linear C_2H_2 molecule. Such a state would go over into an ^1A_u state of a C_{2h} molecule and is likely to be the one observed here.

ACKNOWLEDGMENTS

Dr. G. Herzberg, F.R.S., suggested this problem to me and gave freely of ideas and busy hours in seeing it to completion. Dr. A. E. Douglas read and improved this manuscript and made the experimental part of the work much easier. Dr. D. A. Ramsay pointed out some errors in the manuscript. I am also very grateful for the cooperation of Dr. King and Professor Ingold. Finally, I should like to thank my wife for her assistance with measurements and calculations.

[25] I. G. Ross, Trans. Faraday Soc. 48, 973 (1952).

THE JOURNAL OF CHEMICAL PHYSICS VOLUME 22, NUMBER 5 MAY, 1954

Microwave Spectrum and Dipole Moment of Pyridine*

BILLY B. DEMORE, W. S. WILCOX,† AND J. H. GOLDSTEIN
Emory University, Emory University, Georgia

(Received December 11, 1953)

The microwave spectrum of pyridine has been studied in the region from 20 000 to 40 000 Mc. Twelve low-J R-branch lines have been identified. Analysis of the spectrum requires that the dipole moment lie in the a axis, and leads to the following values of rotational constants: $a=6039.436$ Mc, $b=5804.997$ Mc, $c=2959.210$ Mc, and $\kappa=+0.847781$. The dipole moment of pyridine vapor was found to be 2.15 ± 0.05 D from quantitative Stark effect studies.

INTRODUCTION

PYRIDINE is a planar molecule, somewhat asymmetric spectroscopically, and possessing a rich rotational spectrum. As a starting point in the study of this spectrum, preliminary values of rotational constants were estimated, using as a model: $r_{C-C}=1.39$A, $r_{C-N}=1.37$A, and $r_{C-H}=1.09$A, all ring angles 120°.[1] According to this calculation, $a=5910$ Mc, $b=5727$ Mc, $c=2907$ Mc; $\kappa=+0.89$; and the dipole moment lies in the intermediate or b axis. These results enabled us to predict a number of low-J R-branch transitions in the 20 000–40 000 Mc region. Because of the complexity of the spectrum and the many possible complications, such as distortion effects, it seemed apparent that the most effective way to determine the spectroscopic parameters would be to concentrate upon these R-branch lines, to be identified by their resolved Stark effect patterns.

The equipment used was the usual square-wave modulated spectrograph and associated apparatus. The pyridine used was of commercial grade but carefully examined spectroscopically to insure the absence of ammonia.

OBSERVED SPECTRUM AND ANALYSIS

The portion of the pyridine spectrum selected for analysis is given in Table I.

The assignments and calculated frequencies shown are based on our final model. Because of the complexity of the spectrum, interference of closely spaced lines, and of Stark lobes with lines of interest impeded the most accurate frequency measurements in some cases. Final computations did not involve such measurements, however.

The lines listed were recognized as arising from levels of low J by virtue of their resolvable Stark-effect pattern. Tentative identifications were made on the basis of the assumed model, with dipole in the b axis. However, it turned out to be impossible to fit the spectrum with b-selection rules. No set of rotational constants calculated from any given three lines could satisfactorily predict the remainder of the spectrum.

* This work was sponsored by the Office of Ordnance Research, U. S. Army.

† Present address: Southern Research Institute, Birmingham, Alabama.

[1] V. Schomaker and L. Pauling, J. Am. Chem. Soc. 61, 1769 (1939).

All these difficulties were resolved immediately, and in striking fashion, when a-selection rules were adopted. When this procedure was followed an acceptable fit of the entire spectrum followed and led to sensible values of rotational constants. The final values of our constants were calculated from lines 2, 6, and 11 in Table I, selected because of confidence in the frequency measurements and because of the relatively wide frequency range involved. The measurements utilized are estimated to be known to within about 0.10 Mc. (See Table II.)

The uncertainty in these constants is estimated as about ± 0.05 Mc, three decimals being retained for purposes of calculation. Planarity was not assumed initially but was used to check the final constants. The calculated moments are, in amu-A^2, 83.6847, 87.0643, and 170.7918. The small defect of only 0.0428 is in accord with a planar model.

STARK EFFECT

A quantitative study of the Stark effect for pyridine was carried out on the $M=3$ component of the $3_{21}-4_{22}$ transition, and the $M=1$ component of the $2_{11}-3_{30}$ transition, selected because these lobes were distinct and free of interference over a reasonable range of frequency. The maximum displacements measured were 52.72 Mc at 4.857 esu/cm, and 18.49 Mc at 3.504 esu/cm, respectively. The effect was found to be quadratic over the entire range studied.

The values of $\Delta\nu/E^2$ were obtained graphically and the dipole moment value was calculated following the method of Golden and Wilson.[2] These values were found to be 2.19D and 2.09D, ± 0.05D, for the two lines studied, respectively. We adopt the average of these two values, 2.15 ± 0.05D, as the dipole moment of pyridine vapor.

Most of the previously reported values of the dipole moment of pyridine fall in the range 2.20–2.33D.[3] These determinations were made in various solvents and at several temperatures. The agreement between our results and these values is regarded as satisfactory.

TABLE I. Microwave spectrum of pyridine.

	Transition	Obs freq., Mc	Calc freq., Mc
1	$1_{10}-2_{11}$	20 374.2	20 374.20
2	$2_{21}-3_{22}$	26 292.62	26 292.62
3	$3_{03}-4_{04}$	26 634.66	26 634.31
4	$3_{13}-4_{12}$	26 634.66	26 634.82
5	$1_{01}-2_{20}$	26 783	26 782.99
6	$2_{11}-3_{12}$	26 926.78	26 926.78
7	$2_{20}-3_{21}$	31 862.31	31 862.04
8	$3_{22}-4_{23}$	32 531	32 527.95
9	$3_{12}-4_{13}$	32 594	32 593.50
10	$3_{31}-4_{32}$	37 788.10	37 787.77
11	$2_{11}-3_{30}$	38 917.12	38 917.12
12	$3_{21}-4_{22}$	38 988.91	38 985.54

TABLE II. Rotational constants of pyridine.

a	6039.436 Mc
b	5804.997
c	2959.210
κ	+0.847781

DISCUSSION

Our study of the pyridine spectrum has been designed to minimize errors and ambiguities in the analysis of a complex spectrum. The lines studied should exhibit little centrifugal distortion and can in most cases be calculated from exact energy-level expressions. The use of resolved Stark-effect patterns facilitates the selection of low-J R-branch transitions. Possibilities for error do remain, as, for example, in the case of line No. 8 in Table I, which is one of three closely spaced lines. In addition the weakness of some lines affects the accuracy of the frequency measurement. Nevertheless, for ten of the twelve lines studied, the mean deviation between calculated and observed values is 0.16 Mc, representing a very good over-all agreement. The dipole moment value, as calculated from two different transitions is in good agreement with published values.

Recently two communications have reported quite conflicting analyses of the same spectrum.[4,5] Our results are in excellent agreement with those of McCulloh and Pollnow, who also conclude that the dipole moment lies in the a axis and whose reported rotational constants coincide very closely with ours. It is significant that these two concordant conclusions were obtained from essentially different portions of the spectrum and by somewhat different methods.

It is very interesting to consider the structural implications of these results. If the dipole moment is to lie in the a axis it is apparently necessary to alter slightly the reported structural parameters[1] in such a way as to narrow the molecule, while keeping the rotational constants unchanged. It is also reasonable to require that the electron-diffraction values be not too greatly changed, in the absence of other structural information. We have found that a reasonable model satisfying our results could be based on the following parameters: $r_{C-C}=1.39$A, $r_{C-N}=1.35$–1.36A, $r_{C-H}=1.08$A, $\angle CNC=114$–$117°$.

Although this model is not unique, it seems quite possible that its principal feature, the decrease of the angle at the N atom, is necessary to achieve the desired result. It may be remarked that this model does not greatly change the principal electron-diffraction distances, but does modify slightly the "meta" distances in the ring.

[2] S. Golden and E. B. Wilson, Jr., J. Chem. Phys. **16**, 669 (1948).

[3] *Tables of Electric Dipole Moments* (Technology Press, Cambridge 1948), p. 23.

[4] B. Bak and J. Rastrup-Andersen, J. Chem. Phys. **21**, 1305, (1953).

[5] K. E. McCulloh and G. F. Pollnow, J. Chem. Phys. **21**, 2082 (1953).

Thermodynamics of Equilibrium in the Ultracentrifuge*

T. FRASER YOUNG, KURT A. KRAUS, AND JAMES S. JOHNSON
The George Herbert Jones Chemical Laboratory, University of Chicago, Chicago, Illinois and Chemistry Division, Oak Ridge National Laboratory, Oak Ridge, Tennessee

(Received November 9, 1953)

An exact equation has been derived which can be used for the determination of the ratio of the activity of substance i in a solution of molality m_β to the activity in a solution of molality m_α. Here m_β and m_α are the respective molalities observed at two positions x_β and x_α within a two-component solution which has come to equilibrium in an ultracentrifuge. The calculation involves the densities of the solution at all positions between x_β and x_α and the partial molal volumes of i for the two molalities m_β and m_α. For each of these molalities partial volumes are required for the range of pressure between the equilibrium pressure acting on the solution of that molality and the pressure (ordinarily one atmosphere) of interest to the investigator. Some information concerning a solution containing more than two components can be derived from ultracentrifugal experiments if adequate density data are available.

THE potentialities of the ultracentrifuge for the determination of thermodynamic properties of binary solutions have been discussed by Pedersen[1] and by Drucker.[2] To calculate activity coefficients or molecular weights from their observations they used an approximate formula derived by Svedberg;[3–5] variations of the partial molal volume with concentration and with pressure were neglected.

The principal purpose of this paper is to present an exact equation relating activities in binary solutions at any specified (constant) pressure to the equilibrium concentrations observed in the centrifuge. Tiselius[6] and Pedersen,[1,3] among others, have called attention to the need for the complete equation. Two derivations are included here. The first, somewhat cumbersome one, is based upon the line integral along the actual equilibrium curve. The second, shorter derivation, employs integration along another path.

DERIVATION I

The (chemical) potential μ as defined by Gibbs[7] is not a function of position x in a gravitational or centrifugal field. The partial molal free energy as used by Lewis,[8] however, does include the energy of position in the field. The relation between the functions is shown by the equation,

$$\bar{F}=\mu-\int Mgdx, \tag{1}$$

in which M denotes the mass of one mole, g the acceleration resulting from a centrifugal or gravitational field, and x a distance measured in the direction of the field, e.g., vertically *downward* in a gravitational field. In the centrifuge g is $\omega^2 x$, the product of the distance x from the center of rotation and the square of the angular velocity ω. Relative values of the Lewis activity are given by

$$RT\ln\frac{a}{a_\alpha}=\bar{F}-\bar{F}_\alpha=\mu-\mu_\alpha-\int_{x_\alpha}^{x}Mgdx. \tag{2}$$

Here μ_α and $\bar{F}_\alpha$ are values of the potential and partial molal free energy of any constituent at a position x_α chosen as a reference position. It is convenient, for this discussion, to choose x_α where the pressure P is one atmosphere. Since $\bar{F}$ and a are uniform throughout the cell when equilibrium has been reached, $\bar{F}-\bar{F}_\alpha$ is zero. Hence

$$d\ln a=\left(\frac{\partial\ln a}{\partial P}\right)_{x,m}dP+\left(\frac{\partial\ln a}{\partial\ln m}\right)_{P,x}d\ln m+\left(\frac{\partial\ln a}{\partial x}\right)_{P,m}dx=0. \tag{3}$$

Note also that

$$(\partial\ln a/\partial x)_{P,m}=-Mg/RT \tag{4}$$

and

$$(\partial\ln a/\partial P)_{m,x}=\bar{V}/RT. \tag{5}$$

Substitution of Eqs. (4) and (5) in Eq. (3) yields[9]

$$\left(\frac{\partial\ln a}{\partial\ln m}\right)_{P,x}=\frac{Mg}{RT}\frac{dx}{d\ln m}-\frac{\bar{V}}{RT}\frac{dP}{d\ln m}. \tag{6}$$

* This document is based on work performed for the U. S. Atomic Energy Commission.

[1] K. O. Pedersen, Z. physik. Chem. **A170**, 41 (1934).
[2] C. Drucker, Z. physik. Chem. **A180**, 359 (1937); Z. physik. Chem. **A180**, 378 (1937).
[3] Th. Svedberg and K. O. Pedersen, *The Ultracentrifuge* (The Clarendon Press, Oxford, 1940), p. 51; R. J. Goldberg, J. Phys. Chem. **57**, 194 (1953).
[4] Th. Svedberg, Kolloid Z. (Zsigmondy Festschrift) **36**, 53 (1925).
[5] Th. Svedberg, Z. physik. Chem. **121**, 65 (1926).
[6] A. Tiselius, Z. physik. Chem. **124**, 449 (1926).
[7] J. W. Gibbs, *The Collected Works of J. Willard Gibbs* (Longmans, Green and Company, New York, 1928), Vol. 1, pp. 144–150; E. A. Guggenheim, *Thermodynamics* (North-Holland Publishing Company, Amsterdam, 1949), pp. 355–360.
[8] G. N. Lewis and M. Randall, *Thermodynamics and the Free Energy of Chemical Substances* (McGraw-Hill Book Company, Inc., New York, 1923), pp. 242–4.
[9] Note that the derivative $(\partial\ln a/\partial\ln m)_{P,x}$ is not the total derivative, $d\ln a/d\ln m$, which is zero. It is a partial derivative whose value is a function of P and of x. The derivatives on the right-hand side of (6) are total derivatives.

The partial derivative $(\partial \ln a/\partial \ln m)_{P,x}$ may be evaluated directly from the usual measurements made during an investigation with the ultracentrifuge, i.e., values of molality m, acceleration g, pressure P, and partial molal volume $\bar{V}$ for each value of x. The molality m is usually determined from an integration of observed refractive index gradients, from optical densities, or from the refractive index itself; g is calculated from x and ω; and P from g and ρ, the density of the solution γ by the equation

$$dP=\rho g dx=\rho\omega^2 x dx. \tag{7}$$

It is our objective to determine the ratio of the activity of each constituent in a binary solution of molality m_β to its activity in a solution of molality m_α when both solutions have been removed from the centrifuge and are held under the same pressure P'' and at equivalent values of x, i.e., the ratio $a(m_\beta,P'',x'')/a(m_\alpha,P'',x'')$.

It is necessary to determine the difference between $(\partial \ln a/\partial \ln m)_P$ at the chosen pressure P'', e.g., one atmosphere, and at the equilibrium pressure P' which exists at any point x' in the cell where the molality is m'. The variation of $(\partial \ln a/\partial \ln m)_P$ with pressure is

$$\frac{\partial}{\partial P}\left(\frac{\partial \ln a}{\partial \ln m}\right)_P=\frac{\partial^2 \ln a}{\partial \ln m\,\partial P}=\frac{1}{RT}\left(\frac{\partial \bar{V}}{\partial \ln m}\right)_P. \tag{8}$$

Integration of (8) between P' and P'' leads to

$$\left(\frac{\partial \ln a}{\partial \ln m}\right)_{P''}-\left(\frac{\partial \ln a}{\partial \ln m}\right)_{P'}=\frac{1}{RT}\int_{P'}^{P''}\left(\frac{\partial \bar{V}}{\partial \ln m}\right)_P dP \tag{9}$$

for any constant m and constant x. Combination of (6) and (9) leads to an expression for the variation of $\ln a$ with $\ln m$ at the constant pressure P'' and at any constant x,

$$\left(\frac{\partial \ln a}{\partial \ln m}\right)_{P''}=\frac{Mg'}{RT}\frac{dx}{d\ln m}-\frac{\bar{V}'}{RT}\frac{dP}{d\ln m}+\frac{1}{RT}\int_{P'}^{P''}\left(\frac{\partial \bar{V}}{\partial \ln m}\right)_P dP. \tag{10}$$

Here again the primes indicate values of the variables for the equilibrium curve. Equation (10) may be integrated, with respect to $\ln m$, at constant P'' and constant x to obtain the ratio of a_β at m_β to a_α at any arbitrarily chosen molality m_α.

$$\left.\begin{aligned}\left(RT\ln\frac{a_\beta}{a_\alpha}\right)_{P''}&=M\int_{m_\alpha}^{m_\beta} g\frac{dx}{d\ln m}d\ln m\\&-\int_{m_\alpha}^{m_\beta}\bar{V}'\frac{dP}{d\ln m}d\ln m\\&+\int_{m_\alpha}^{m_\beta}\left[\int_{P'}^{P''}\left(\frac{\partial \bar{V}}{\partial \ln m}\right)_P dP\right]d\ln m\end{aligned}\right\}. \tag{11}$$

The last term of Eq. (11) may be written more simply if the order of the integration is reversed (the transformation can be readily visualized with the aid of a 3-dimensional model of P, $\ln m$, and $(\partial \bar{V}/\partial \ln m)_P$):

$$\int_{m_\alpha}^{m_\beta}\left[\int_{P'}^{P''}\left(\frac{\partial \bar{V}}{\partial \ln m}\right)_P dP\right]d\ln m=\int_{P_\beta}^{P_\alpha}(\bar{V}_\beta-\bar{V}')dP+\int_{P''}^{P_\alpha}(\bar{V}_\beta-\bar{V}_\alpha)dP. \tag{12}$$

Here P_α denotes the pressure existing in the centrifuge tube where the molality is the chosen m_α. $\bar{V}_\beta$ and $\bar{V}_\alpha$ are the partial molal volumes (both functions of the pressure) when the molalities are m_β and m_α, and $\bar{V}'$ is the partial molal volume at any level x' when equilibrium has been established. For the special case when $P_\alpha=P''$ the last term of Eq. (12) is zero. Substitution[10] of (12) in (11) yields the exact[11] equation

$$RT\ln\frac{a_\beta}{a_\alpha}=M\int_{x_\alpha}^{x_\beta} g dx-\int_{P_\alpha}^{P_\beta}\bar{V}_\beta dP. \tag{13}$$

DERIVATION II

The first derivation was based upon the fact that the total derivative of the escaping tendency with respect to x or m is zero. The second derivation depends upon the equivalent fact that the escaping tendency at any point in the cell is equal to that at any other point. For variety the escaping tendency is expressed in terms of the partial molal free energy $\bar{F}$. When equilibrium exists

$$d\bar{F}=\left(\frac{\partial \bar{F}}{\partial x}\right)_{P,m}dx+\left(\frac{\partial \bar{F}}{\partial P}\right)_{m,x}dP+\left(\frac{\partial \bar{F}}{\partial \ln m}\right)_{P,x}d\ln m=0. \tag{14}$$

Note also that

$$(\partial \bar{F}/\partial x)_{P,m}=-Mg \tag{15}$$

and

$$(\partial \bar{F}/\partial P)_{m,x}=\bar{V}. \tag{16}$$

Consider the transfer of an infinitesimal amount of constituent J from any point in the centrifuge to any other. If equilibrium has been attained, $\Delta\bar{F}=0$. Let

[10] The $\bar{V}'$ term in Eq. (12) results in the cancellation of the corresponding term of Eq. (11). Hence, it is not necessary to determine $\bar{V}'$ for the respective values of x' along the equilibrium line.

[11] Equation (13) is exact if the only factors affecting the partial molal free energy are pressure, temperature, and composition. There is still one factor which has been neglected; very large values of g or of dg/dx might produce small orientations or distortions of unsymmetrical molecules—especially very large ones. If these changes should in turn affect the escaping tendency, e.g., partial molal free energy, of a molecular species it is possible that Eq. (13) might not be entirely perfect. Effects large enough to be observable seem to be highly improbable unless fields can be produced which are several orders of magnitude larger than any now obtainable.

x_β, m_β, P_β, and $\bar{F}_\beta$ represent particular values of the respective variables at the first position and x_α, m_α, P_α, and $\bar{F}_\alpha$ represent values for the second position.

Now consider the following three processes and $\Delta\bar{F}$ which corresponds to each:

$$J(x_\beta,P_\beta,m_\beta)\rightarrow J(x_\alpha,P_\beta,m_\beta)$$

$$(\Delta\bar{F})_x=-\int_{x_\beta}^{x_\alpha} Mgdx, \qquad (17)$$

$$J(x_\alpha,P_\beta,m_\beta)\rightarrow J(x_\alpha,P_\alpha,m_\beta)$$

$$(\Delta\bar{F})_P=\int_{P_\beta}^{P_\alpha} \bar{V}(x_\alpha,m_\beta)dP, \qquad (18)$$

$$J(x_\alpha,P_\alpha,m_\beta)\rightarrow J(x_\alpha,P_\alpha,m_\alpha)$$

$$(\Delta\bar{F})_m=RT\ln(a_\alpha/a_\beta). \qquad (19)$$

For the summation of the three processes,

$$J(x_\beta,P_\beta,m_\beta)\rightarrow J(x_\alpha,P_\alpha,m_\alpha)$$

$$\Delta\bar{F}=(\Delta\bar{F})_x+(\Delta\bar{F})_P+(\Delta\bar{F})_m=0. \qquad (20)$$

Hence for the transfer of J from m_β to m_α at constant P_α and constant x_α,

$$J(m_\beta)\rightarrow J(m_\alpha)$$

$$(\Delta\bar{F})_m=RT\ln\frac{a_\alpha}{a_\beta}=-\int_{x_\alpha}^{x_\beta} Mgdx+\int_{P_\alpha}^{P_\beta}\bar{V}_\beta dP. \qquad (21)$$

The pressure P can be computed from Eq. (7). Substitution of (7) into (21) (and change of algebraic sign) yields

$$RT\ln\frac{a_\beta}{a_\alpha}=\int_{x_\alpha}^{x_\beta} Mgdx-\int_{P_\alpha}^{P_\beta}\bar{V}_\beta dP$$

$$=\int_{x_\alpha}^{x_\beta} Mgdx-\int_{P_\alpha}^{P_\beta}\bar{V}_\beta g\rho dx \qquad (22)$$

or

$$RT\ln\frac{a_\beta}{a_\alpha}=M\int_{P_\alpha}^{P_\beta}(1-\bar{v}_\beta\rho)\omega^2 x dx, \qquad (23)$$

which is equivalent to Eq. (13). Because of the similarity of this equation to the one used previously,[1-6] it must be pointed out that $\bar{v}_\beta$ is not the partial volume of one gram of species J in the solution which has come to equilibrium at each level, x', within the cell; it is the partial volume of one gram of J in the solution of constant composition m_β. It must be known, of course, as a function of P over the range between P_α and P_β but need not be evaluated for other values of m. The density, on the other hand, which affects the pressure is a function of both m and P and must be known for each value of x.

Although Eqs. (22) and (23) are derived here only for a binary solution, they are valid for any constituent of a solution of any number of components. The subscripts α and β refer to solutions which actually exist at some two levels x_α and x_β within the cell. In general, the molality of each solute in the solution at x_α must differ from the molality of that constituent at x_β. Since the molalities at x_β cannot be varied independently and arbitrarily when those at x_α are fixed, the centrifuge cannot yield directly the values of a_β/a_α for any two arbitrarily chosen compositions. Nevertheless, it can yield information concerning multicomponent systems which cannot be obtained from conventional methods. If such information concerning a ternary solution (for example) is to be obtained, it is necessary that two methods of analysis be used simultaneously, e.g., refractive index and light absorption. If additional methods should be devised, still more complex mixtures could be analyzed. New methods may not become available in the near future but they are not inconceivable. For some mixtures, conductivity or radioactive tracer techniques might be utilized. If an ingenious procedure for withdrawal of small samples should be developed, it could be used for systems of any reasonable number of components. Of course, the necessary partial molal volume data must always be available.

To apply the ultracentrifuge to thermodynamic problems the investigator must bear in mind that a solution which can be considered to be a two-component system in the absence of a centrifugal field may behave in the centrifuge as a three-component (or even a more complex) system. This phenomenon occurs when a solute reacts to yield two or more substances which can be distributed independently in the centrifugal field. For example, hydrolysis of a metal ion may result in an increased concentration of a base at one end of the cell and an increased concentration of acid at the other. A solution in the ultracentrifuge cell may be thought of as an infinite series of solutions of different compositions in equilibrium with one another. With respect to each of these layers the hydrolysis products may be regarded as new "components" since they need not enter the layer in equivalent amounts. When an electrolyte is centrifuged in the presence of a supporting electrolyte the possibilities of reactions of this kind may be enhanced. It may be necessary in some cases to demonstrate the presence or absence of reactions by chemical analysis. When hydrolysis is the only likely reaction simple determinations of hydrogen ion concentration may suffice.

A recent application of the ultracentrifuge to the determination of activity coefficients is described in a forthcoming article.[12]

[12] Johnson, Kraus, and Young, J. Am. Chem. Soc. **76**, 1436 (1954).

Further Results on Monte Carlo Equations of State

MARSHALL N. ROSENBLUTH AND ARIANNA W. ROSENBLUTH
Los Alamos Scientific Laboratory, Los Alamos, New Mexico
(Received September 15, 1953)

The equation of state of three-dimensional hard spheres has been obtained by the Monte Carlo method. Some qualitative results for a system of two-dimensional molecules with Lennard-Jones interaction are also given, as well as a general discussion of the usefulness and limitations of the Monte Carlo method.

I. INTRODUCTION

THE purpose of this paper is to present some further results obtained by the Monte Carlo method.[1] Some qualitative results have been obtained for the system of two-dimensional molecules with Lennard-Jones interaction, and the equation of state for three-dimensional rigid spheres has been obtained.

II. QUALITATIVE RESULTS FOR THE SYSTEM OF TWO-DIMENSIONAL MOLECULES WITH LENNARD-JONES INTERACTION

Some work has been done on a two-dimensional system of fifty-six molecules with intermolecular potential:

$$V=(a/r^{12})-(b/r^{6}). \quad (1)$$

This work has been pursued far enough to obtain quantitative results, but does show some interesting qualitative features.

In particular, it was possible to observe the existence of the liquid-gas phase transition. Figure 1 is a typical plot of the positions of the fifty-six molecules at a temperature equal to one-half the well depth and for various values of A/A_0. Here, A is the area per molecule, and A_0 is the area per molecule in a close-packed lattice when the molecules are a distance apart, such that $V=0$.

Figure 1(a) ($A/A_0=1$) represents a quite tightly packed configuration, hence the molecules are nearly in a regular lattice. (It should be borne in mind that due to our periodicity condition,[1] molecules near one edge of the square are neighbors of those near the opposite edge of the square.)

Figure 1(b) ($A/A_0=1.6$) shows the molecules in a more expanded configuration in which they continue to fill up the square, although in a more irregular fashion. This configuration is close to the boiling point.

Figures 1(c) and 1(d) ($A/A_0=2$ and $A/A_0=2.52$) represent still more expanded configurations. It will be observed that the molecules no longer continue to fill the square but that cavitation occurs. This presumably is the result of the phase transition—the area of the square becomes greater than the area of the liquid at its boiling point, and hence the liquid does not fill the square. Since the density of the gas is very low, the gaseous phase appears as holes in the fluid.

The critical temperature phenomenon is also observed. Thus for high temperatures (the critical temperature appears very roughly equal to the well depth) cavitation no longer occurs.

The general shape of the isotherms is also in agreement with typical liquid-gas isotherms. However, it seems very difficult to obtain accurate quantitative results in the interesting transition regions.

There are several reasons for this:

(1) For our small sample of molecules the surface between fluid and bubbles is quite large and many molecules are on the surface. Thus, a large surface energy and pressure is introduced.

(2) The process of forming or destroying bubbles is a lengthy one, requiring many moves. Thus, it is difficult to reach equilibrium. In fact, over a considerable region of density a bubble will not be formed spontaneously but will persist once introduced into the fluid.

(3) For densities where the molecules are a distance apart corresponding to the potential minimum one must expect large fluctuations in the pressure. This comes about because the virial, rdV/dr, whose average value determines the pressure, varies strongly with the intermolecular distance while the energy and hence the probability factor $\exp(-E/kT)$ does not.

Thus, one cannot expect the Monte Carlo method to give great detail in the neighborhood of phase transitions, or certainly in the critical region, though it should be possible, for example, to determine the critical constants withinin 20 percent. In a one-phase region the Monte Carlo method should be feasible with an arbitrary intermolecular potential.

In view of the somewhat academic nature of the two-dimensional Lennard-Jones system, and the large amount of work which would be necessary to obtain quantitative results, no further work is contemplated on this case.

III. THREE-DIMENSIONAL RIGID SPHERES

Most of the work on three-dimensional rigid spheres was done with a sample of 256 molecules starting from a face-centered-cubic lattice. About twenty different densities were computed, and at each density each

[1] Metropolis, Rosenbluth, Rosenbluth, Teller, and Teller, J. Chem. Phys. **21**, 1087 (1953). This paper discusses in detail the Monte Carlo method.

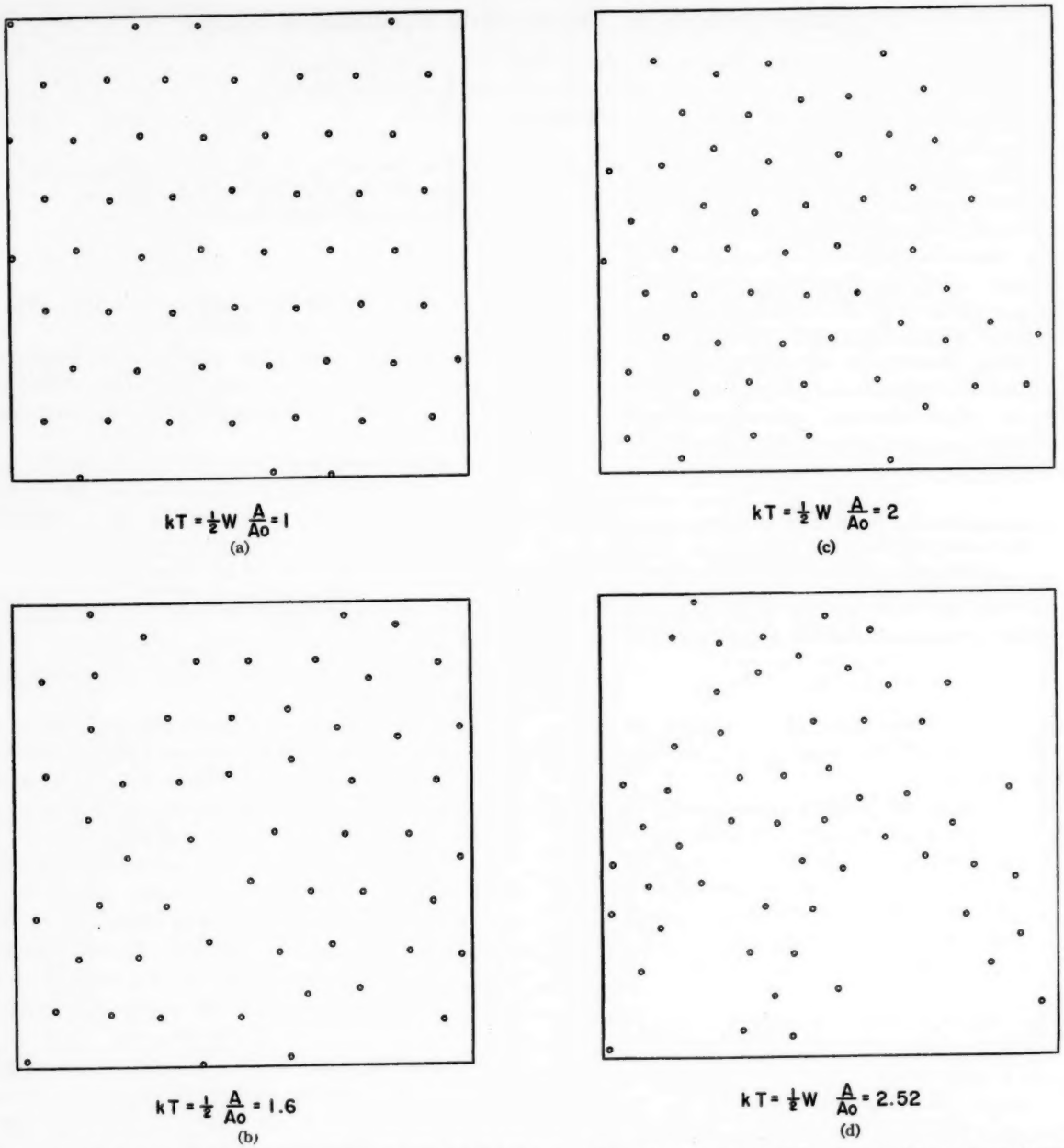

FIG. 1. Typical plots of the positions of the 56 molecules for a two-dimensional system with a Lennard-Jones type interaction between pairs. The temperature is one-half the well depth. The ratio A, the area, to A_0, the area in a close packed system with the nearest neighbor distance such as to make the potential energy of nearest neighbors zero, is varied from 1 to 2.52 in the four diagrams.

molecule was moved about 100 times. This seemed quite sufficient for attaining equilibrium and reducing the statistical error below 5 percent. This program required about 150 hours of computing time on the Los Alamos MANIAC.

At each density the radial distribution function was obtained, and from it the pressure by means of the well known formula:

$$\frac{pV}{kT}-1=\frac{2\pi}{3}d_0^3 n(1). \qquad (2)$$

Here, d_0 is the molecular diameter, and $n(1)$ is the density of surrounding molecules at the surface of a molecule.

The equation of state is shown in Fig. 2 and Table I. Here $(pV/kT)-1$ is plotted against $(V/V_0)-1$. V is the volume per molecule, and V_0 the volume per molecule at the closest possible packing.

The equation of state agrees at low densities with the virial expansion as it should. At high densities it agrees fairly well with the free volume equation of state,[2]

[2] W. W. Wood, J. Chem. Phys. **20**, 1334 (1952).

although not nearly as well as in the two-dimensional case. At high densities it disagrees strongly with the superposition theory of Kirkwood and Born-Green.[3] It should be noted that liquids have specific volumes about twice the close-packed specific volume of their "equivalent hard sphere repulsive cores," in which region the superposition theory does not deviate too much from our results.

Our equation of state shows no sign of a phase transition but a transition involving only a small change in volume, or a higher-order transition, would not have been observed, so this evidence is not conclusive.

Figure 3 shows some radial distribution functions. Here, n, the density of molecules surrounding a given molecule, is plotted as a function of the distance from the center of the given molecule. n is normalized so that it would equal one for a uniform distribution, and R is in units of the molecular diameter.

The curve at $V/V_0=1.145$ is quite crystalline in structure, showing the various layers of neighbors only slightly smeared out from their lattice positions. Another interesting feature of the distribution is that its maximum value does not occur at $R=1$ but rather at a slightly greater radius. This shift of the maximum does not occur in the two-dimensional case. Its occurrence in three dimensions is clearly a complex many-body phenomenon, and we have not been able to fully explain it.

At the highest compressions $[(V/V_0)<1.1]$ the shape of the distribution function near $R=1$ is given approximately by

$$n=\frac{1}{V-V_0}\left\{1.1-0.15\left[\frac{R-1}{0.2\left(\frac{V}{V_0}-1\right)}-1\right]^2\right\}. \quad (3)$$

As the density is decreased, the maximum becomes less proncounced and finally disappears at about $V/V_0=1.25$. At this point there is still a negative curvature to the distribution function at the origin but as the density is decreased still further to $V/V_0=1.5$, the curvature becomes positive.

The importance of the shape of the distribution function near the origin is, of course, that $pV/kT-1$ is proportional to the molecular density at $R=1$ [see Eq. (2)]. Thus, the existence of the shifted maximum means a lowering of molecular density at $R=1$ and hence a decrease in pressure. In fact, the behavior of the equation of state at high densities—its rise relative to the free volume equation of state as V is increased—can be ascribed to the manner in which the distribution function becomes successively more peaked at the origin.

TABLE I. Equation of state of three-dimensional hard spheres.

$\frac{V}{V_0}-1$	0.05	0.1	0.25	0.5	0.75	1	1.5	2	3
$\frac{pV}{kT}-1$	58	31	13.8	7.85	5.50	4.25	2.82	2.02	1.21

[3] Kirkwood, Maun, and Alder, J. Chem. Phys. **18**, 1040 (1950).

The curve at $V/V_0=1.32$ still shows the crystalline structure though at this volume the peaks are quite smeared out.

The curve at $V/V_0=1.8$ looks quite different. Here the distinctive peaks have disappeared and one has a smoothly oscillating distribution function similar to those observed in liquids and to those obtained by the superposition theory.[3] The results differ from those of the superposition theory chiefly in that the magnitude of the oscillations is quite a bit larger for our radial distribution functions.

The transition between the solid and liquid type distribution functions seems to occur at about $V/V_0=1.5$. It occurs fairly gradually, however, so that we have not been able to say on this basis, either, whether a discontinuous phase transition takes place. It is interesting to note that $V/V_0=1.5$ is also where molecules were first able to slip past each other, another indication of lattice breakup. This fact facilitated the computation at high densities since here the original nearest neighbors of a molecule remained its nearest neighbors so that it was unnecessary to search through the lattice to determine the nearest neighbors of a molecule.

As has been mentioned earlier the indicated statistical error in the equation of state is about 5 percent. It is more difficult to estimate possible systematic errors. These might include the finite number of molecules and

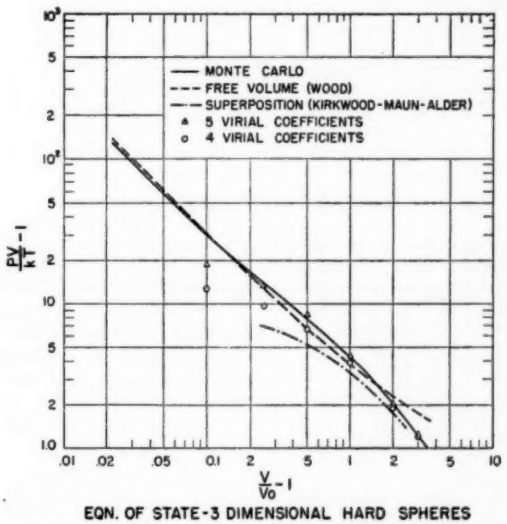

FIG. 2. A log-log plot of $(PV/kT)-1$ *versus* $(V/V_0)-1$ for hard spheres in three dimensions. Here V_0 is the volume per molecule at the closest possible packing. The solid line is the result of the Monte Carlo method as discussed in this paper; as compared to the free volume theory (dashed line), the superposition theory of Kirkwood (dot-dashed line), and to a 4 term (circles) and 5 term (triangles) virtual expansion.

the possibility that equilibrium was not reached, i.e., that what we calculated was a metastable configuration close to the initial lattice structure.

At low densities where only fairly small clusters are important our results should be good. At very high densities where the configuration must be nearly a regular lattice and where our periodicity condition should eliminate surface effects for a regular lattice our results should also be good. It is therefore in the intermediate density region where lattice breakup phenomena may be occurring that systematic errors might be large.

In order to check the effect of the finite number of molecules some runs were made using 32 and 108 molecules. These gave results within statistical error of the results obtained with 256.

In order to check the possibility that the system "remembered" its initial configuration some runs were made with the molecules initially crammed into one corner of the cell, instead of starting from a regular lattice. Here, too, the results were within statistical error. While these checks are not conclusive, they are an indication that systematic errors are not large.

Some runs were also made starting from a hexagonal-close-packed lattice. The pressures obtained were the same as for the face-centered cubic.

FIG. 3. Radial distribution functions *versus* distance for three-dimensional hard spheres. Here n, the density of molecules surrounding a given molecule, is normalized to one for a uniform distribution. The distance R is given in units of the molecular diameter. Distribution functions for three volumes are shown.

The fifth virial coefficient was calculated by Monte Carlo evaluation of the cluster integrals.[1] One obtains thus:

$$\frac{pV}{kT}-1=2.962\left(\frac{V_0}{V}\right)+5.483\left(\frac{V_0}{V}\right)^2+7.455\left(\frac{V_0}{V}\right)^3+8.9\left(\frac{V_0}{V}\right)^4.$$

The value of the coefficient of the last term, the one we calculated, has a statistical error of about 10 percent. Some values of $(pV/kT)-1$ as given by the four- and five-term virial expansions are shown on Fig. 2. It will be seen that the five-term expansion agrees very well with our equation of state at low densities. Moreover, the fact that the five-term expansion lies slightly above the equation of state at some densities indicates that some higher virial coefficients are negative.

IV. CONCLUSIONS

The equation of state for three-dimensional hard spheres casts doubt on the adequacy of the superposition approximation at high densities. The radial distribution functions obtained show a clear evolution with increasing volume from a crystalline structure to a liquid type structure with the transition being completed at about $V/V_0=1.5$. It is not possible to say, however, whether a discontinuous phase transition occurs.

Results obtained thus far lead us to feel strongly that the Monte Carlo method is a useful tool for solving statistical mechanical problems, although it does not appear to be feasible to obtain detailed results in transitions regions. The authors are now working on a modification of the method which will make it applicable to Bose-Einstein substances at zero temperature.

We would like to thank Professor Edward Teller for his invaluable interest and help. We would also like to thank Dr. Nicholas Metropolis for making available to us the computing facilities of the Los Alamos MANIAC, and Mr. Walter Orvedahl and Mr. James Richardson for their untiring efforts to keep the machine running at top efficiency.

Organic Photoconductors. I. The Kinetics of Photoconductivity in Rhodamine B*

R. C. NELSON
The Ohio State University, Columbus, Ohio
(Received October 1, 1953)

The behavior of rhodamine B undergoes a change at about 60°C below which temperature it is complicated by memory effects. Above 60°C the decay process is strictly bimolecular. Three activation energies were measured: for conduction, for decay, and for rise of conductivity, and each was approximately 0.55 ev. The observed second-order character and the absolute rate of the decay process can be accounted for by a model having a large density of monoenergetic traps lying 0.55 ev below the conduction band. There is evidence that the slowness of reaching a steady state in light is to be associated with a redistribution of charge carriers from the random sites in which they are formed into preferred sites or configurations.

INTRODUCTION

ALTHOUGH Petrikalu[1] found a number of ionic dyes to be photoconductive as early as 1930, there is very little work of a quantitative nature reported in the literature upon which to base a discussion of the nature of the phenomenon. It seems certain that there must be important differences between these materials and such inorganic ionic photoconductors as cadmium sulfide, because their rates of rise and decay of conductivity are often several orders of magnitude slower. The phenomena which take place in them are also of interest in connection with photochemistry, with the sensitization of inorganic crystal photoconductors by dyes, and with some aspects of the broad problem of the conversion of radiant energy to chemical free energy.

Rhodamine B (Rdm) is of particular interest because it shows in some measure most of the peculiarities found in dye photoconductors and hence is a suitable subject for an introductory study; and furthermore, because it is possible to give a fairly satisfactory account of many of its properties using a simple model of the "homogeneous" type in which conductivity results from the liberation in light of mobile charge carriers which recombine in darkness. For these reasons, its properties will be considered in some detail in an attempt to make clear wherein the simplicities and complexities lie and to provide a background for a later discussion of the triphenylmethane dyes, in which the phenomena are appreciably more complicated.

Rhodamine B has the structural formula

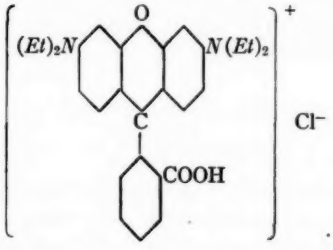

It is commercially available in biological stain quality and may be further purified by vacuum sublimation. Films prepared by sublimation or by drying from solution are continuous and glossy with a characteristic golden luster. In solution it shows a strong absorption band peaking at 5500A.

EXPERIMENTAL METHODS

Photoconductive cells were prepared in Pyrex blanks of the sort shown in Fig. 1. Three types of cells were tested: those prepared by evaporating an alcoholic solution of commercial-purity Rdm between the electrodes, those prepared in the same way from Rdm which had been purified by vacuum sublimation, and cells in which the dye was sublimed directly from the outer wall of the blank onto the interelectrode space. The first two types were essentially equivalent although an improvement in stability followed purification. Spectroscopic examination showed that a substantial degree of purification resulted from the sublimation process. Cells prepared by direct sublimation differed somewhat quantitatively but were similar qualitatively to the others. The data of this paper were taken largely on purified films deposited from alcoholic solution.

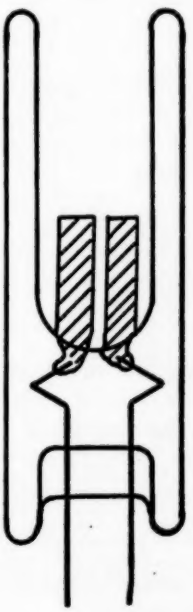

FIG. 1. Blank used in preparing photoconductive dye films. The hatched electrodes are of chemically deposited platinum.

* This work was supported by the Charles F. Kettering Foundation.
[1] Z. Petrikalu, Z. physik. Chem. **B10**, 9 (1930).

The alcohol was evaporated off at room temperature under a stream of purified nitrogen in subdued light, and the system opened to the pumps as soon as the film was dry. Cells were pumped in an oven at 50°C at a pressure of less than 10^{-4} mm of mercury for two hours before sealing off. Since the cells could not be heated to outgas them with the dye film in place, there could be no hope of achieving a permanent vacuum, but the drifts in cell characteristics were slow enough so that they could be neglected for a series of experiments lasting an hour or two.

Resistances were measured with a simple circuit in which the cell and a battery were placed in series with the grid resistor of a Victoreen 5803 electrometer triode. Two triodes in a bridge arrangement were used in the preamplifier, the output of which was measured with a General Radio dc amplifier and recorded with an Esterline-Angus recording milliammeter. The electrode spacing was about 1.0 mm and the voltage across the cell, 5.0 volts.

The temperature of the cell was controlled with a stream of heated air passed into the cavity.

In the dark, thin Rdm films showed no measurable conductivity even at 100°C. A conductance was observed at higher temperatures which proved to be the same whether or not the Rdm film was present; it was attributed to the glass blank and corrected for by subtracting it from the measured values.

THE KINETICS OF A DARK-INSULATING PHOTOCONDUCTOR

In the simple case in which the absorption of a quantum leads to the appearance of an electron in the conduction band and a hole in the valence band, and where the disappearance of conductivity is due to the recombination of the hole and the electron, the expression for the rate of change of charge carrier density is

$$dn/dt = bI - \alpha n^2,$$

where I is the rate at which quanta are absorbed and b and α are constants. If we assume the conductance to be a linear measure of the charge carrier density, we may write

$$d\sigma/dt = \gamma I - a\sigma^2. \quad (1)$$

Upon integrating, the rate of decay in the dark from a steady state in light is found to be

$$\sigma_t^{-1} - \sigma_s^{-1} = at, \quad (2)$$

a being the rate constant (in ohms/sec). Likewise, the rate of rise of conductance in constant illumination from the dark-insulating state is

$$\ln\frac{\sigma_s+\sigma_t}{\sigma_s-\sigma_t} = 2a\sigma_s t. \quad (3)$$

The logarithmic term will be referred to as the rise characteristic.

EXPERIMENTAL RESULTS

a. Activation Energy for Conduction

Since the rate of decay of conductance in Rdm is slow, it is possible to demonstrate directly, as has been done for several other dye photoconductors,[2] the existence of an activation energy for conduction. If an Rdm cell is illuminated strongly at room temperature and allowed to decay in the dark, a state will be reached in which the time rate of change of conductance is small, although a significant part of the original photoconductivity remains. If now the temperature of the cell is changed as rapidly as possible, a reversible dependence of conductance on temperature can be demonstrated. Levin[3] in this laboratory has made careful measurements of this property on cells having long interelectrode areas to give high conductances at low decay rates, and has arrived at a value of 0.57 ± 0.03 ev for the activation energy.

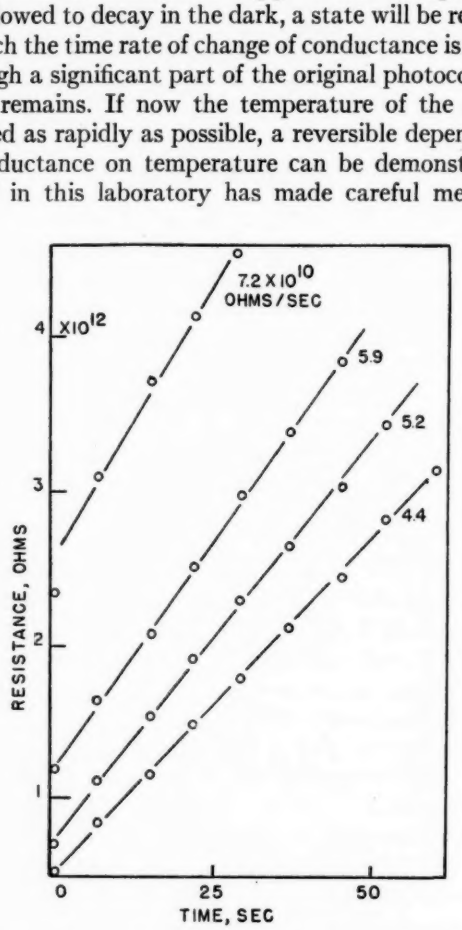

FIG. 2. Decay plots for a cell at 80°C, showing the dependence of decay rate on initial conductance.

b. Decay of Photoconductivity in the Dark

At temperatures higher than 60°C, the decay of conductivity in Rdm obeys the second-order law of Eq. (2) to within experimental error for a single given decay process from a steady state in illumination. This is true during the decay of at least 95 percent of the conductance, or the whole range in which it is possible to

[2] R. C. Nelson, J. Chem. Phys. **19**, 798 (1951).
[3] V. Levin, Master of Science thesis, Ohio State University, 1952 (unpublished).

make reasonably accurate measurements. However, there are three types of deviations from it that limit the general applicability of this law. At temperatures below 60°C the rate for the first few seconds is materially faster than the constant rate which applies thereafter. This effect becomes more pronounced as the temperature decreases.

The second type of deviation has to do with the fact that for a series of decay processes from steady-state conditions at a given temperature, the "rate constant" is not truly constant, but is a function of the steady-state conductance. Figure 2 shows this effect. It is to be noted that while the time rate of change of resistance is constant for a given process, it is larger for decays from initial states of higher resistance. At temperatures over 60°C the rate constant varies roughly as $\sigma_s^{-\frac{1}{2}}$. The dependence becomes more pronounced at lower temperatures, being $\sigma_s^{-\frac{1}{2}}$ at 30°C and apparently approaching σ_s^{-1} at temperatures below 0°C.

The third type of deviation is found when the decay rate is measured otherwise than from a steady state in illumination. Consider an experiment in which a cell is illuminated strongly and the light is cut off when the conductance has reached some level much less than that which would be reached if the cell were allowed to come to a steady state. If the decay rate is measured, and if the process is repeated several times by illuminating to the same conductance with the same source, it is found that the rate of decay becomes progressively slower with each successive illumination until a limit is approached and that this limiting rate is faster than that which is found if the cell is brought to a steady state at the same value of conductance with illumination of appropriate intensity. The series of curves in Fig. 3 illustrates this type of behavior.

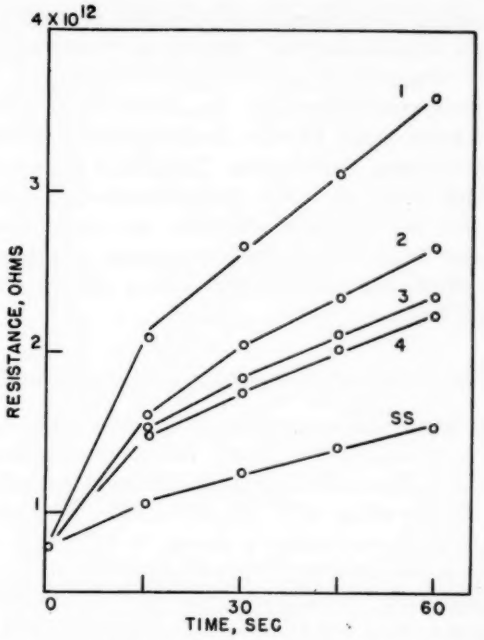

FIG. 3. Decay plots for a cell following successive brief illuminations at 40°C, (1) being the first illumination, etc., and *SS* the decay from a steady state in light at the same initial conductance.

c. Relation between Illumination and Photoconductance

Since from Eq. (1), at the steady state in light $\gamma I = a\sigma_s^2$, the steady-state conductance should vary as $I^{\frac{1}{2}}$. However, the initial slope of the rise of photoconductance upon illumination should vary directly as I, since it is determined only by the rate of formation of charge carriers. In Fig. 4, the initial rise slope plot shows the expected slope of 1.0, while that found for $\log\sigma_s$ *vs* $\log I$ is 0.53 as compared with the predicted value of 0.50.

d. The Rise of Photoconductivity in Light

A steady state in light is reached rather slowly in Rdm films. It will be noted in Fig. 5 that the rate of rise decreases sharply in the early stages, soon reaching a constant slow value. Also shown is a theoretical rise curve calculated from Eq. (3), using the decay rate constant measured from the steady state. The fact that the slope of the linear portion of the experimental curve is much less than that of the calculated curve suggests that in this portion of the buildup process the rate of production of charge carriers is not the limiting process. Experiment has in fact shown that at a given temperature, the slope of the linear portion of the curve is constant and independent of the intensity of illumination.

e. Memory Effects

Since at room temperature the rate constant for decay is strongly dependent on the steady state con-

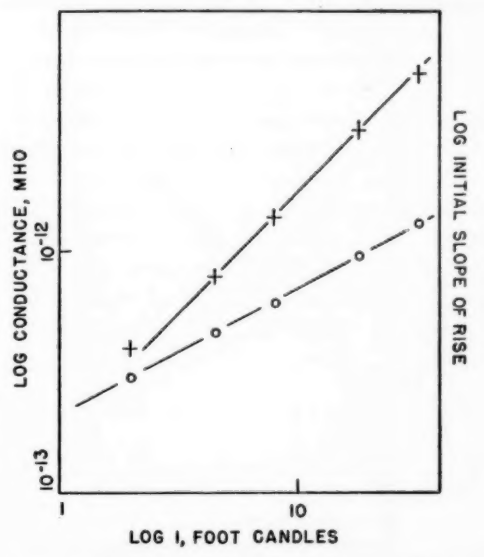

FIG. 4. Log initial slope of rise of conductance following illumination (in arbitrary units)+; together with the corresponding log steady-state conductance O; plotted against log illuminance. Temperature, 80°C.

ductance, it is of interest to note that if a cell is first strongly illuminated and allowed to decay, and then weakly illuminated immediately thereafter, its decay rate is unexpectedly slow. In other words, the rate still retains some of the character given it by the previous strong illumination. This effect disappears by standing overnight, or is easily erased by heating to 80°C for five minutes, and this was done wherever pertinent in performing the experiments here described. Such effects are of little importance at temperatures over 60°C.

f. The Effect of Temperature on Rates in Rdm

The steady-state conductance of Rdm films at constant illumination rises slowly with increasing temperature up to about 60°C, and remains substantially constant in the range 60°C to 100°C. The rate constant for decay also undergoes a change at 60°C as is shown in Fig. 6 where its logarithm is plotted against $1/T$ in the usual way. Below this temperature the activation energy for decay is 0.31 ev, and above it becomes 0.54 ev.

In Fig. 7 is shown a similar plot of the slope of the rectilinear portion of the rise curve; this process also has an activation energy of 0.54 ev.

DISCUSSION

In what follows, no attempt will be made to give an account of the behavior of Rdm films at temperatures below 60°C, since the complications met with in this range are apparently related to the memory effect, which can be more effectively discussed in connection with triphenylmethane dyes. Although it is likely that both holes and electrons are mobile and trapped, we shall speak only of electrons, for the sake of simplicity; the same line of reasoning may be used in either case.

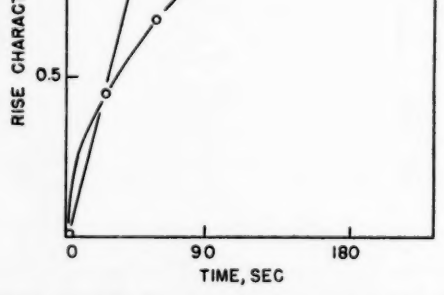

FIG. 5. Rise characteristic, log $[(\sigma_s+\sigma_t)/(\sigma_s-\sigma_t)]$, measured at 40°C, and calculated (solid line).

It has been noted that any single decay process from a steady state obeys a second-order law as simple theory suggests, but in view of the observed activation energy for decay and the slow rate, it remains to be explained why this should be so. Let us consider a system having a valence band, a conduction band, and a high density of trapping levels 0.55 ev below the conduction band. If the density of traps and the probability of trapping are high, we can consider the motion of the electron in an applied field to be a succession of jumps between traps. If the lifetime of an electron in a bound state is relatively long compared with its lifetime in the conduction band, its mean mobility must be low, and will be a function of temperature, since its lifetime in the bound state will be determined in part by the temperature. Alternatively, one might say that since the temperature affects the distribution of the electrons between bound and mobile states, the system will show the observed activation energy for conduction. The diffusivity of the electrons and, hence, the rate at which they make encounters with holes will be affected in the same way, and an activation energy for decay will be observed. Since $\sigma_s=(\gamma I/a)^{\frac{1}{2}}$, and since temperature dependent factors of this sort are implicit in both the constants, one would expect the steady-state conductance to be independent of temperature, as is observed.

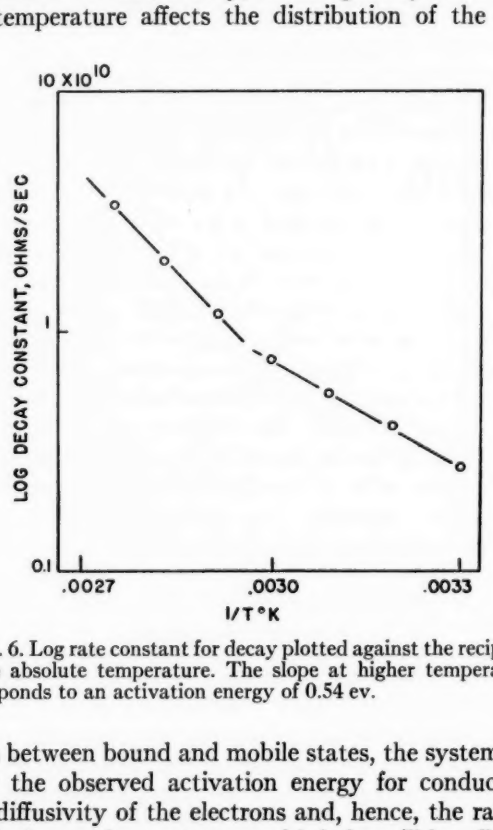

FIG. 6. Log rate constant for decay plotted against the reciprocal of the absolute temperature. The slope at higher temperatures corresponds to an activation energy of 0.54 ev.

We may inquire under what circumstances a system of this sort would display a strictly second-order decay process, having an activation energy of 0.55 ev. It is apparent that this will be so, if the rate at which electrons are liberated from traps thermally does not limit the decay rate, and if the traps are all of approximately the same depth. If an electron which was freed

from a trap is much more likely to recombine than to be retrapped, the decay process will be of the first order, since its rate is limited by a first-order process. On the other hand, if it is much more likely to be retrapped than to recombine, the process will be of the second order, and the rate will be determined by the mean diffusivity, which will depend on the temperature and the trap depth. If the process is to be strictly of the second order over its whole life, then the mean diffusivity, and hence the trap depth must be constant.

It is possible to make a rough estimate of the decay rate expected from this model. If for the sake of simplicity we take K to be a first-order rate constant corresponding to the initial rate of decay of conductance, E the trap depth f, a frequency factor, and Y the relative probability of recombination to retrapping, then

$$K = Yf \exp(-E/kT).$$

(Since a second-order process is being approximated by one of the first order, K will vary directly as the initial conductance, as will Y.) There is no unarguable basis upon which the frequency factor may be chosen. For traps 0.55 ev deep, 10^8/sec is probably a reasonable guess in the light of values measured for inorganic crystal phosphors.[4] If we take Y to be 0.1, which is of the order of the maximum value it can have if the second-order decay character is to be preserved, then K is of the order of 0.1/sec at 80°C, which agrees well enough with the value of 0.2 to 0.3/sec found experimentally under strong illumination.

The fact that much more time is required to reach a steady state in light than can be accounted for by the processes of formation and recombination of charge carriers is of considerable interest; Ewald[5] has observed a similar phenomenon in thallous sulfide cells. The observation that this process has an activation energy equal to that found for conduction and decay suggests the possibility that what is happening is a redistribution of the charge carriers from the sites in which they were randomly formed into positions or configurations in which they are in some sense more stable with respect to decay. It seems likely that the relationship between decay constant and steady-state conductance is connected with this phenomenon.

[4] R. H. Bube, Phys. Rev. **80**, 655 (1950).
[5] A. W. Ewald, Phys. Rev. **81**, 607 (1951).

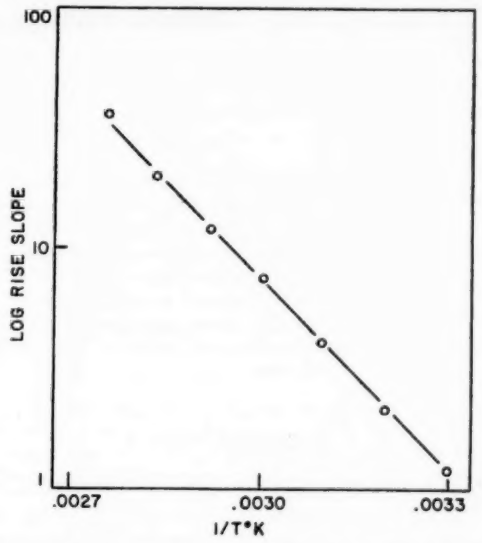

FIG. 7. The ordinate is the logarithm of the slope of the final rectilinear portion of the rise characteristic plot (in arbitrary units) and the abscissa, $1/T$°K. The activation energy is 0.54 ev.

CONCLUSION

While much remains to be explained about the behavior of Rdm as a photoconductor, it is apparent that there are in it large simplicities as compared with many inorganic ionic crystals. The existence of a well defined rate constant for decay and the single trapping level greatly simplify the discussion of the processes involved and it seems likely that the mechanisms are at least in broad outline those of the proposed model.

It appears at the moment most useful to consider the dye film as a doubly periodic system having short range order in the conjugated system of the dye molecule, which determines the optical properties, and a long range order in the arrangement of the molecules, which leads to the electrical properties. The weak interactions between molecules are reflected in the apparently very low mobility and the tendency for the carriers to become localized in traps, which are probably to be associated with the dye molecules themselves. A variety of considerations have led to the tentative conclusion that only a minute fraction of the charge carriers produced ever reaches the electrodes, and that in the larger sense, the effect of illumination on the film is the production of an excited state in it which is communal and long-lived by virtue of the diffusibility of the carriers.

Organic Photoconductors. II. Crystal Violet*

R. C. NELSON
The Ohio State University, Columbus, Ohio
(Received October 1, 1954)

Photoconductivity in crystal violet is a volume effect primarily, and surface or electrode complications have not been recognized. Donor and trapping impurities may be introduced into films, but the highly purified substance shows a large photoconductivity. The thermoelectric effect is normal. On the other hand, rates are extremely slow, there is a prominent long-lived memory effect, and under certain circumstances the second-order rate constant for a particular decay process is inversely proportional to the initial conductance. A hypothesis is proposed to account for the last-mentioned peculiarity, in terms of which structures are formed in the film which have the property of maintaining a constant initial density of charge carriers; the steady-state conductance being no longer a measure of their density but only of their total number.

INTRODUCTION

THE triphenylmethane dyes form a large class of which many members are known to be photoconductive and to display qualitatively similar behavior. In working with this class it is often convenient to study different characteristics each upon the dye having the response rate or sensitivity to illumination best suited to the problem. Crystal violet has a very large response to light which makes it possible to show with relative ease that it is in many respects unexceptional as a photoconductor. It is also an excellent material for demonstrating those peculiarities of the class which have no parallel in the behavior of inorganic photoconductors.

Basic fuchsin was selected for the kinetic studies of the succeeding paper because of its substantially faster rates of buildup and decay, but much experience has shown that the photoconductive phenomena in these dyes are essentially alike except for rates. Although data are available for many experiments demonstrating this parallelism, it will here merely be assumed that what can be shown readily to be true of crystal violet can also with more difficulty be shown to be true of basic fuchsin, and vice versa; and that the essential problem of reconciling the apparent simplicities observed to the apparent complexities is the same in detail for each substance.

Crystal violet (Xlv) is 4,4′,4″-tri(dimethylamino)triphenylmethyl chloride. It forms continuous films having a characteristic green-gold luster. The material used in this work was purified according to the method of Lewis *et al.*[1] The other experimental procedures were in general those described in the first paper of this series.[2]

CRYSTAL VIOLET AS A PHOTOCONDUCTOR

There is strong evidence that the photoconductivity of Xlv is a volume effect, and that there are no significant peculiarities associated with the dye-electrode interface. If a dye film lying between widely spaced electrodes is explored with a small spot of light, it is found that illumination of any small area of it makes the cell conductive. If a film is made thick enough to be opaque to the eye, its response is found to be the same whether it is illuminated upon its outer surface or upon the side next to the glass, including the dye-electrode interface. For thin films the level of conductance which can be reached at a given illumination is roughly proportional to the thickness of the film. Polarization effects are absent or negligible, in carefully prepared cells never exceeding a few millivolts.

Photoconductivity is to be associated with absorption of visible radiation in the dye film. The effects produced by illumination with the sodium *D* line radiation are the same as those produced with incandescent lamps.

While this paper will be concerned principally with the behavior of the pure dye as a photoconductor, two types of impurity effects are of interest. It has been noted[3] that while the chloride of Xlv is a dark insulator, its normal sulfate (Xlv_2SO_4) is a semiconductor with a thermal activation energy of 0.36 ev for conduction. Chloride films containing a small amount of sulfate show a dark conductance proportional to the sulfate content, and in fact the sulfate ion acts as though it were a donor impurity in the chloride film. Films made from dyes of commercial purity often show dark resistances a hundred times less than those made from the pure dye.

Purified crystal violet in alcoholic solution seems to be indefinitely stable. The solid dye is susceptible to oxidation, rapidly in the light and in oxygen or slowly in the dark and in air. This oxidation does not greatly change the appearance of the film, but it exerts a profound effect on the rate at which a steady state in light is reached and upon the rate of decay of conduction, increasing both by a factor of the order of 100. Partially oxidized films show a gradation in trapping depths as measured by the thermal activation energy for conduction,[4] this energy being about 0.5 ev at low levels of conductance, decreasing to 0.36 ev at moderate levels

* This work was supported by the Charles F. Kettering Foundation.
[1] Lewis, Magel, and Lipkin, J. Am. Chem. Soc. **64**, 1774 (1942).
[2] R. C. Nelson, J. Chem. Phys. **22**, 885 (1954).
[3] R. C. Nelson, J. Chem. Phys. **20**, 1327 (1952).
[4] R. C. Nelson, J. Chem. Phys. **19**, 798 (1951).

(where the deeper traps are full), while that for the pure dye remains constant at 0.36 ev to 0.38 ev over the same range. The oxygen in the film is apparently acting as a trapping impurity.

The work of Schroeder[5] on the thermoelectric effect in Xlv tends to support the point of view that the photoconductivity of this dye is not essentially different from that of more conventional photoconductors. All the films he examined showed thermoelectric powers close to -0.3 mv/°C, of the expected magnitude, and indicating conduction predominantly by electrons. He found no asymmetries in his films. The thermoelectric power was approximately independent of temperature in the range 20°–80°C when measured at constant conductance, and varied inversely with the conductance when measured at constant temperature.

THE DECAY OF PHOTOCONDUCTIVITY IN Xlv

If the conductance of a fresh, pure Xlv cell is brought to some low level by strong illumination for a few seconds, and the decay in darkness is followed, it is found that the initial rate is high, but that it decreases rapidly during the first few minutes, finally becoming constant (as expressed in ohms/sec) for the remainder of the process. If these operations are now repeated at a series of increasing levels of conductance, it is found that as the initial conductance increases, the rate constant for the slow end-process decreases. The product of the slow rate constant and the conductance obtained by extrapolating the slow process to time zero is approximately constant. This product has the dimensions sec^{-1} and is the reciprocal of the half-life of the (slow) decay process. It is thus a sort of first-order rate constant, and will be referred to as such without further qualification.

After illumination to a steady state, the initial rate of decay becomes very slow, and, for a series of such illuminations in order of increasing intensity, the product of the initial decay rate and the initial conductance is also constant and of the same magnitude as that found for the slow part of the decay following brief illumination, about 10^{-4} sec^{-1} at 30°C. Figure 1 shows the results of some experiments of this sort. At very high light intensities the decay rate becomes independent of the initial conductance. This saturation takes place at about the same illumination in each case, the corresponding conductance varying with the thickness of the film.

Although a set of decay processes may be described by a first-order constant, it is not to be inferred that the fraction of conductance disappearing in unit time is constant, but rather that the processes follow parallel courses; after a given time has elapsed, the percentage of conductance remaining in each case is the same.

The second-order rate equation $\sigma_t^{-1}-\sigma_0^{-1}=at$ may be rewritten as $(\sigma_0-\sigma_t)/\sigma_t=a\sigma_0 t=(\text{constant})\times t$ for the case where the rate constant is inversely proportional to

[5] C. Schroeder, unpublished M.S. thesis, Ohio State University, 1952.

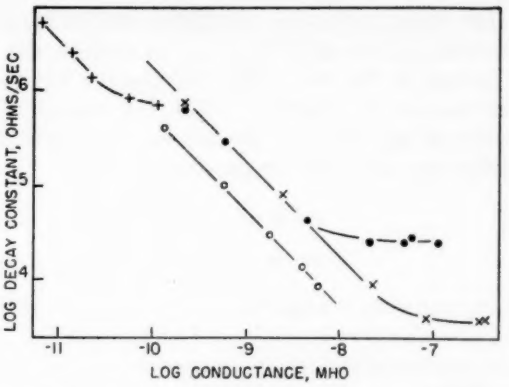

FIG. 1. Second-order rate constant for decay plotted against initial level of conductance for several cells. × and ●, dye of commercial purity. + and ○, purified dye, very thin and very thick films, respectively.

the initial conductance. This implies that the film has a memory which regulates the decay process, since its rate depends not only upon the state existing at a given time but also on the initial state. Conversely, knowing the first-order constant, and measuring the conductance at two different times, one can determine both the initial conductance and the elapsed time since the decay process began.

It is easy to show that this memory is a real property of the illuminated film and has a lifetime of many days. If a cell during the course of a week is given a number of illuminations of an hour or so duration, it is found that to a fair approximation the decay rate observed is determined by the strongest previous illumination and not by the most recent, even though the conductance is allowed to reach a low level between illuminations. This effect may be erased by heating the cell at 100°C for 24 hours, after which a new "memory" may be established by reillumination.

In a case such as this, where the cell retains the imprint of a previous illumination for many days, it would seem necessary to suppose that we are dealing with some sort of structural change produced in the film either by quanta or by charge carriers. The "structure" would seem to have the property of accomodating a limited number of carriers in some state in which they are stabilized with respect to decay.

DISCUSSION

It is apparent that while there is much evidence to suggest that the photoconductivity of Xlv is not dissimilar to that found in inorganic photoconductors, the very low rates of buildup and decay of photoconductivity raise serious problems, while the observed inverse dependence of the decay rate on the initial conductance must create real doubt as to whether the conductance is indeed a measure of the charge carrier density.

Let us suppose that there is a "true" or microscopic process in the photoconduction of Xlv which does involve the production of mobile charge carriers by quanta

and that these carriers do actually recombine according to an ideal second-order law. Let us assume also that this process is the one which we observe by making measurements of resistance. The microscopic decay process and the observed process can be described by the following equations, respectively:

$$dn/dt = -\alpha n^2,$$
$$d\sigma/dt = -a\sigma^2.$$

If we make the reasonable assumption that the half-life of the microscopic process is the same as that found for the measured process, then we may write

$$\alpha n_0 = a\sigma_0 = \text{constant}. \quad (2)$$

Since for the ideal process the rate constant α is a constant, if Eq. (2) is to be satisfied, then the initial charge carrier density n_0 must also be constant. If this were true, then the observed conductance could increase with increasing illuminance only if the mobility also increased, or if the spatial distribution of the carriers in the film were altered. If the carriers are not distributed uniformly throughout the volume of the film, but are segregated in regions of constant density in such a way that, as the conductance increases with increasing illuminance, the number of these regions, or their total volume increases, then σ is a measure not of the charge carrier density but of the total number of carriers. The decay rate is determined by the charge carrier density but is measured in terms of the reciprocal of the total number of charge carriers. If the ratio of the total number of carriers to the density is not constant but increases with increasing illumination, then even though the process on the level of the carriers may follow an ideal second-order law, the rate of the total measured process expressed in the customary units must be inversely proportional to the initial conductance.

Of the above two possibilities, it can be shown that assuming an effect of level of illumination upon mobility leads to contradictions, while the hypothesis that the carriers are not uniformly distributed in the bulk of the film finds support in the observations of a memory effect of long duration which survives the disappearance of the conductance itself. The possibility would thus seem to exist that the simple kinetics which were proposed to account for the behavior of rhodamine B could be extended to the much more complex phenomena found in the triphenylmethane dyes by the introduction of an additional assumption regarding the spatial distribution of the charge carriers in the dye film.

THE JOURNAL OF CHEMICAL PHYSICS VOLUME 22, NUMBER 5 MAY, 1954

Organic Photoconductors. III. The Kinetics of Basic Fuchsin*

R. C. NELSON
The Ohio State University, Columbus, Ohio
(Received October 1, 1953)

To account for the influence of temperature on rates and levels of conductance in basic fuchsin, two activation energies are required; for diffusivity and for quantum yield of charge carriers, and these are approximately equal having a value near 0.38 ev. Two regimes of behavior with respect to light intensity are found, one in which the response is proportional to the illumination, and another, which may be established by strong pre-illumination of the film, in which the response is as the square root of the light intensity. These observations are in accord with the hypothesis which was proposed to account for the inverse dependence of rate constant on initial conductance in crystal violet.

INTRODUCTION

IN the preceding paper of this series[1] a hypothesis was proposed to account for the inverse dependence of rate constant for decay upon steady-state conductance which is characteristic of dyes of the triphenylmethane class. In the present paper, the effects of temperature and illuminance on the conductance and decay constant of basic fuchsin are measured and considered in the light of this hypothesis.

Basic fuchsin (Bfs) is 3-methyl,4,4′,4″-triaminotriphenylmethyl chloride. It is well suited to studies of this sort because its responses are fast enough so that the effects of the irreversible drifts of cell characteristics which are inescapable in this work, may be minimized by proper design of experiments. The decay of photoconductivity in Bfs follows a second-order law to within experimental error over its whole lifetime. Its thermal activation energy for conduction is 0.38 ev.[2] Thin films show negligible dark currents at temperatures up to 80°C.

The general experimental techniques used have already been described.[3]

* This work was supported by the Charles F. Kettering Foundation.
[1] R. C. Nelson, J. Chem. Phys. **22**, 890 (1954).
[2] R. C. Nelson, J. Chem. Phys. **19**, 798 (1951).
[3] R. C. Nelson, J. Chem. Phys. **22**, 885 (1954).

EXPERIMENTAL RESULTS

a. The Buildup of Conductivity in Light

Some idea of the time scale of experiments on Bfs may be had from Fig. 1 where *A* is the plot of the rise characteristic for a cell which had not previously been illuminated. After this cell had reached a steady state, it was darkened and decay was allowed to proceed until it was 97 percent complete with respect to conductance. It was then re-illuminated in precisely the same way as before. The new rise curve obtained is *B*. It resembles *A* in form but the slopes are much greater. That the same final state was reached by both illuminations was shown by the fact that the steady-state conductance and the decay rate were the same for both.

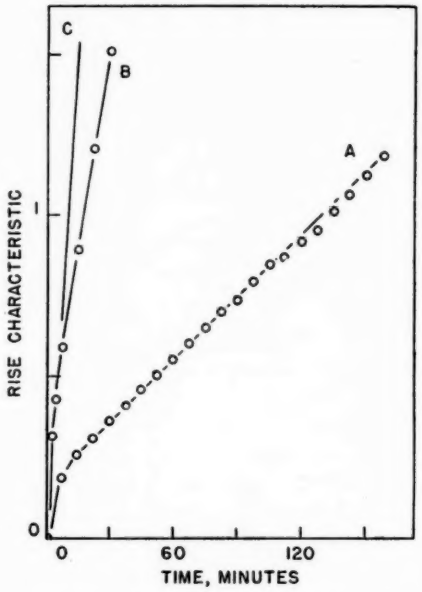

FIG. 1. Rise characteristic, $\log[(\sigma_s+\sigma_t)/(\sigma_s-\sigma_t)]$ *vs* time; *A*, for the first illumination of the cell. *B*, a like illumination immediately following the decay from the first illumination. *C*, as calculated from the decay rate and the steady-state conductance.

The straight line *C* indicates the theoretical rise characteristic calculated from the observed steady-state conductance and decay rate on the basis that the rates of production and disappearance of charge carriers determine the rise process. This assumption is quite certainly not applicable to the first slow rise, but it approximates the second, preconditioned rise process in a rough fashion.

It is found that this preconditioning disappears gradually as the cell is stored in darkness, and after several days the rise has become almost as slow as that for a cell which has never been illuminated.

b. Decay of Photoconductivity in the Dark

Figure 2 shows an experiment in which a Bfs cell was illuminated at 40°C, and the decay rate followed until about 80 percent of the conductance was gone. The

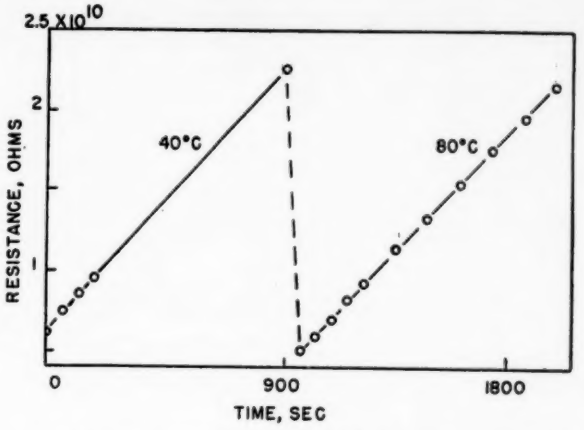

FIG. 2. Decay rates at 40° and 80°C for a basic fuchsin cell.

temperature of the cell was then raised quickly from 40°C to 80°C. Since Bfs has an activation energy for conduction of about 0.38 ev, the resistance was lowered to approximately the original level. The decay rate measured at 80°C was identical with that measured at the lower temperature.

In another experiment a cell was brought to a steady state in constant illumination at a series of temperatures. Figure 3 shows the results. The steady-state resistance decreases with increasing temperature, showing an activation energy for conduction identical with that measured in the ordinary way. The rate constant for decay is approximately independent of temperature when measured in this way. However, if the rate constant is measured over a range of temperatures at constant initial conductance rather than at constant illuminance, it also is found to have an activation energy of 0.38 ev.

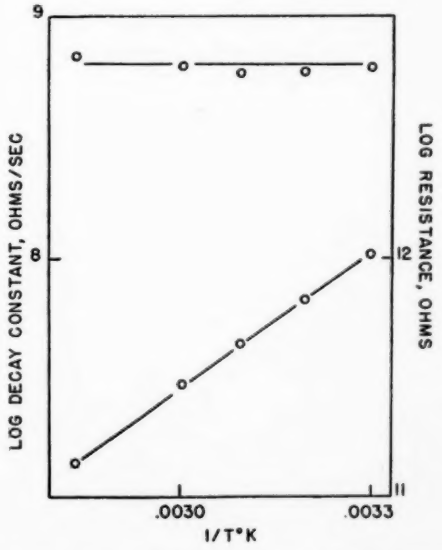

FIG. 3. Upper curve, log rate constant for decay *vs* $1/T°K$, at constant illumination. Lower curve, corresponding values of steady-state resistance.

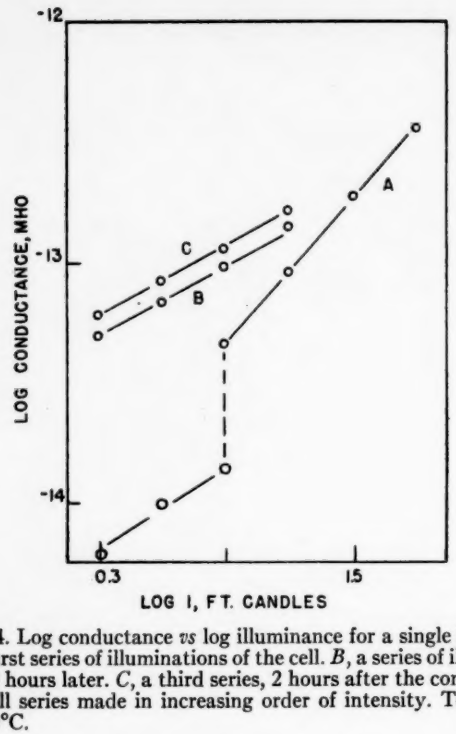

FIG. 4. Log conductance *vs* log illuminance for a single Bfs cell. *A*, the first series of illuminations of the cell. *B*, a series of illuminations 18 hours later. *C*, a third series, 2 hours after the completion of *B*. All series made in increasing order of intensity. Temperature, 80°C.

c. Illumination Experiments

A new Bfs cell was illuminated with a small source under such conditions that the inverse square law could be used to estimate relative light intensities. In Fig. 4 the discontinuous curve *A* shows the conductances which were reached at the steady state for the first series of illuminations, which were in order of increasing intensity. At the two lowest levels indicated by large circles there was a rapid response to light, the cell reaching in a few seconds a steady state which was not altered by an additional exposure to light of forty-five minutes. At the next level of illumination, the large circle marks the conductance which was reached quickly. After another five minutes of illumination the conductance began to rise slowly, and finally after several hours reached the upper level shown at the same illumination. For each irradiation thereafter a time of the order of hours was required to reach a steady state, and the resulting conductance was proportional to the light intensity. Figure 5 shows the corresponding decay rates, which are inversely proportional to the steady-state conductance. The decay rates for the first two illuminations were too rapid to measure using the strip recorder, and that for the lower conductance level at the third illumination was estimated to be 25×10^{10} ohms/sec, or about ten times greater than the final rate at the same light intensity.

Following the completion of this portion of the experiment, the cell stood overnight in the dark. When the same series of illuminations was repeated the following day, the results shown by *B* were obtained. Now the conductance varies as the square root of the illumination as shown by the slope of 0.5 for the plot. The corresponding decay rates are almost independent of the conductance. At illuminations greater than that at which *A* and *B* intersect, the regime of the previous day holds.

The cell was then put in the dark for two hours, and the illuminations were repeated once more, with the results shown by *C*. It should be noted that in the regime in which the conductance varied as the square root of the illumination, a steady state was reached in a few minutes rather than in an hour or two.

After this cell had stood in the dark for a week, the whole series of phenomena could be duplicated, with the exception of the discontinuity at low illuminations.

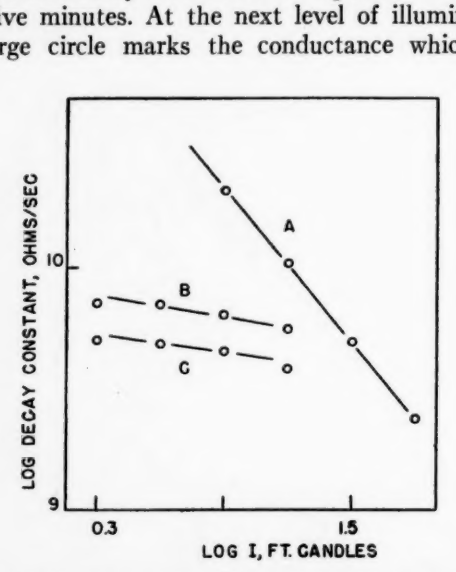

FIG. 5. The rate constants for decay corresponding to the conductances shown in Fig. 5. The key is the same.

DISCUSSION

The foregoing phenomena are readily accounted for in terms of the hypothesis proposed in II in connection with the behavior of crystal violet. We consider a model in which the processes involving charge carriers follow the simple theory for a photoconducting insulator, but in which the carriers are not distributed uniformly through the film; at the steady state in illumination they are segregated into regions of constant carrier density. These regions are supposed to be localized as some sort of relatively long-lived structural change in the film which survives the disappearance of the conductance with which it is associated in its formation in light. We must in each case consider not only the immediate treatment of the film but also its history in determining how it will respond.

In a given instance, if the light intensity is greater than that required to fill the existing structure with carriers, the structure will be enlarged slowly until a steady state is reached both with respect to formation and disappearance of structure and to the formation and decay of charge carriers. The measured rate constant for decay, as has been shown, will diminish in

proportion as the quantity of structure increases. Since $\gamma I = a\sigma_0^2$, it is obvious that if the product $a\sigma_0$ remains constant, the conductance must increase as the first power of the illuminance.

Conversely, if the light intensity is less than that required to fill the existing structure, a steady state (with respect to charge carriers) is reached quickly since the rate is now determined by the rate of production and decay of charge carriers only. The decay rate constant remains constant to a fair approximation in this regime because it has been established by the previously formed structure, and will not be affected by illuminations too weak to enlarge it. Correspondingly, since the decay rate remains constant, the conductance must increase as the square root of the illuminance.

Let us consider this model in more detail, restricting the discussion to the regime in which the amount of structure is being determined by the illumination, and assuming that only the structured part of the film need be considered, presumably because carriers formed in other parts of the film quickly find their way to the structure. Let N be the volume of structure present in the film, and μ be the product of the mean mobility of the carriers and the electronic charge, while the other symbols have their previous significance. μ and α are both proportional to the carrier diffusivity and hence will vary with temperature in the same way.

The observed conductance will now be given by $\sigma = N\mu n$. From Eq. (2) of II, $\alpha n_0 = a\sigma_0$ and by substitution we obtain $a = \alpha/N\mu$. Considering the experiment illustrated by Fig. 2, we see that in this case, where N may be assumed to have remained unchanged, the observed rate constant for decay has remained unchanged by temperature because the change in the microscopic rate constant α was exactly compensated for by the change in the mobility, and hence in the units in which the observed constant was measured.

If I is the luminous flux on the film, then the appropriate flux density is I/N and the microscopic steady-state relationship is given by

$$bI/N = \alpha n_0^2$$

By substitution, we obtain $\mu bI = a\sigma_0^2$, which is the measured steady-state relationship.

In the case of rhodamine, the steady-state conductance was independent of temperature at constant illuminance because the increased mobility was compensated for by the increased decay rate at higher temperatures. With Bfs we have seen that the steady-state conductance increases with temperature while the decay rate, as measured, remains constant. Since it can be shown with the proposed model that

$$\sigma_0 = \mu(NbI/\alpha)^{\frac{1}{2}},$$

and

$$a = bI/(N^2\mu n_0^2),$$

the immediate inference is that b, the quantum yield of charge carriers must also be a function of temperature, and have the same activation energy as the diffusivity. This implies that optical excitation takes place to a short-lived bound state which does not lead to the production of charge carriers unless further thermal excitation takes place within its lifetime. It is not known whether the equality of the two activation energies is coincidental or is causally determined.

CONCLUSION

It would seem clear at least that the interpretation of the photoconductivity of ionic organic dyes in terms of the formation of mobile electrons and holes by light is appropriate and justified. There is ample evidence that in the triphenylmethane dyes some change related to the conductive phenomenon, but distinct from it, is produced in illumination. The assumption that this change is one which leads to a constant charge carrier density at the steady state in light, enables one to account for the rather complex behavior of these dyes in a fairly direct fashion, preserving the essential features of the simple model proposed for rhodamine B. While it is possible to arrive at the formalism used here starting from other initial assumptions, the present hypothesis has advantages in simplicity.

However, attempts to explain the very slow rate of decay observed in the triphenylmethane dyes by the same line of reasoning used for rhodamine are not very satisfactory, and this problem continues under investigation.

The Infrared Spectrum of Crystalline Nitrogen Pentoxide*

ROY TERANISHI AND J. C. DECIUS
Department of Chemistry, Oregon State College, Corvallis, Oregon

(Received December 12, 1953)

The infrared absorptions of thin films of crystalline $N_2{}^{14}O_5$ and $N_2{}^{15}O_5$ maintained at liquid nitrogen temperature have been investigated between 4 and 20 microns. The spectrum is readily interpreted on the basis of the $NO_2{}^+NO_3{}^-$ structure previously indicated by Raman and x-ray data. All the constants of the most general quadratic potential functions for the two ions have been evaluated, and the relatively large errors in these constants and their significance in relation to the electronic structure is discussed.

INTRODUCTION

EARLY studies[1] of the Raman spectrum of nitrogen pentoxide revealed a marked difference between the molecular structure in nonpolar solvents on the one hand, and in concentrated aqueous solutions or the crystalline state on the other. More recently, it has been shown that some of the Raman lines of the crystalline state may be assigned to the nitrate ion; the remaining features of the Raman spectrum were attributed to the nitronium ion, $NO_2{}^+$, by comparison with the Raman spectrum of nitronium perchlorate, etc.[2] An x-ray diffraction study[3] has confirmed the nitronium nitrate structure and established the space group as $D_{6h}{}^4$ with two molecules per unit cell. In a preliminary report[4] the present authors have assigned the fundamental infrared active molecular modes of $NO_2{}^+$ and $NO_3{}^-$ ions, although the sample observed was apparently contaminated with nitric acid. In this communication, the spectra of strictly anhydrous films of $N_2{}^{14}O_5$ and of the pentoxide enriched to about 63.5 percent in N^{15} will be reported.

EXPERIMENTAL

Nitrogen pentoxide was prepared by oxidizing nitrogen dioxide with ozone. Nitrogen dioxide was generated by pyrolysis of lead nitrate or of potassium nitrate mixed with lead chloride. In some experiments, potassium nitrate containing 63.5 percent N^{15} was employed (Eastman Organic Chemicals). Although the ozonization was not carried out in a closed system, severe precautions were taken to exclude moisture. The oxygen stream to the electrical discharge was dried with concentrated H_2SO_4, followed by KOH pellets and P_2O_5. Immediately after leaving the discharge tube the ozone-oxygen mixture passed through a trap cooled with dry ice. Complete reaction of the ozone with nitrogen dioxide was assured by an excess flow rate of O_3 relative to NO_2, and by provision of a long reaction section at room temperature before the trap which condensed the pentoxide. The excess ozone and oxygen stream then passed through a dry ice trap and chemical drying agents to protect the product from moisture on the downstream side.

When sufficient N_2O_5 had been collected it was sealed off from the reaction system in a bomb provided with a break-seal leading to a standard taper joint which was later attached to the infrared sample cell. The N_2O_5, which had been trapped at the dry ice temperature, was cooled to the liquid N_2 temperature until final sublimation into the infrared cell.

The infrared cell employed was similar to that described by Wagner and Hornig.[5] A side arm with standard taper joint was provided as close as possible to the sample window holder. After attachment of the N_2O_5 bomb and evacuation and cooling of the cell with liquid N_2 had been completed, the seal was broken and the N_2O_5 was cautiously sublimed by removing the liquid nitrogen from the bomb. In some cases of too rapid sublimation, unjustified optimism was aroused by the very clear appearance of the sample film, which yielded an absorption spectrum similar to that of gaseous N_2O_5. It was evidently a metastable, perhaps glassy solid with completely covalent structure. These films could be transformed to the stable crystalline form ($NO_2{}^+NO_3{}^-$) by warming to the dry ice temperature. The nitronium nitrate films always scattered visible light noticeably, but yielded infrared spectra with satisfactorily low background (less than 5 percent absorption between the major absorptions.

The sample windows employed were 0.25-mm sheets of silver chloride, and the cell was refrigerated with liquid N_2 or O_2 throughout the absorption experiments.

The spectrometer employed was a Perkin-Elmer Model 12C, LiF, NaCl, and KBr prisms, used over suitable ranges.

RESULTS

The absorption spectra are presented graphically in Fig. 1. More precise values of the absorption maxima may be read from Table I.

There is no difficulty in assigning the nitrate ion fundamentals as $\nu_2{}^- = 824$ cm^{-1} (out-of-plane bending),

* Published with the approval of the Monographs Publication Committee, Oregon State College, as Research Paper No. 240, School of Science, Department of Chemistry.

[1] J. Chedin, thesis, Paris, (1937); Compt. rend. **200**, 1397 (1935).

[2] Goddard, Hughes, and Ingold, J. Chem. Soc. **1950**, 2559. Ingold, Millen, and Poole, J. Chem. Soc. **1950**, 2576. D. J. Millen, J. Chem. Soc. **1950**, 2606.

[3] Grison, Eriks, and de Vries, Acta. Cryst. **3**, 290 (1950).

[4] R. Teranishi and J. C. Decius, J. Chem. Phys. **21**, 1116 (1953).

[5] E. L. Wagner and D. F. Hornig, J. Chem. Phys. **18**, 296 (1950).

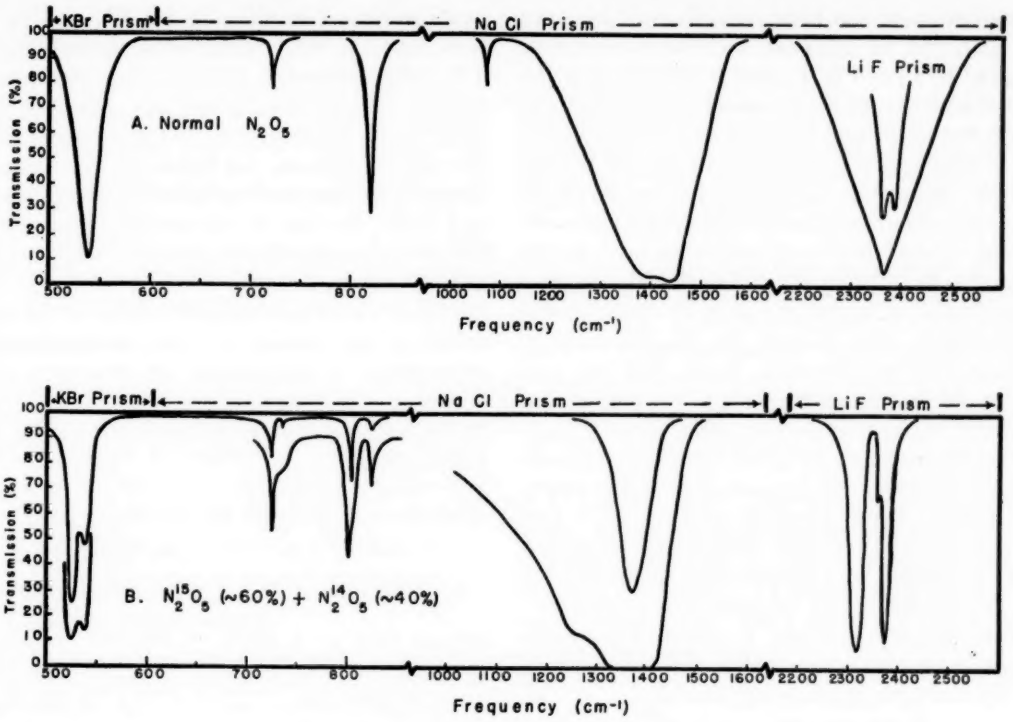

FIG. 1. The infrared spectrum of crystalline N_2O_5 at approx 90°K. A. Natural N^{14}:N^{15} ratio. B. N^{15} enriched to approx 60 percent.

$\nu_3^-=1413$ cm^{-1} (degenerate stretching), and $\nu_4^-=722$ cm^{-1} (degenerate bending), since these frequencies, and, indeed, the relative intensities and breadths of the bands agree very closely with the results of investigations of many nitrate salts.[6]

There remain the strong bands at 2375 cm^{-1} and at 538 cm^{-1}. The agreement of the former with the antisymmetric stretching frequency of the isoelectronic CO_2 molecule is striking; in fact, the presence of an apparent shoulder at about 2365 cm^{-1} in the case of a thinner sample is probably the result of incomplete compensation for atmospheric carbon dioxide. On the other hand, 538 cm^{-1} is remarkably lower than the frequency of the CO_2 bending mode, but there is no reason to doubt the assignment of this absorption to ν_2^+, the bending mode of NO_2^+. It may be mentioned here that no doublet structure in ν_1^+ has been reported by the Raman investigators[2] which is to be expected, since $2\nu_2^+=1076$ cm^{-1} which is much too far from $\nu_1^+=1400$ cm^{-1}.

These assignments are confirmed by the quantitative agreement of the measured $N^{14}-N^{15}$ isotope shifts with the theoretically predicted values. In the site group[7] approximation the modes of frequency ν_2^+, ν_3^+, and ν_2^- all occur in one-dimensional secular equations, so that the shifts in frequency are independent of the force constants. Table II indicates that the observed shifts agree with the calculated shifts well within the experimental error.

A precise measurement of the isotope shift of the degenerate stretching mode of the nitrate ion, ν_3^-, is impossible because of the relatively great breadth of this band for the sample thickness employed. However, it is noteworthy that ν_4^-, of the same symmetry species, exhibits a practically negligible shift, a fact which is in agreement with the results of N^{15} isotope studies on $Ba(NO_3)_2$.[8]

TABLE I. Fundamental frequencies of NO_2^+ and NO_3^-.

Mode	N^{14}, obs (cm^{-1})	N^{15}, obs (cm^{-1})	Shift, obs (cm^{-1})	Shift, calc (cm^{-1})
ν_1^+	1400[a]	...	...	0
ν_2^+	538	526	12	13
ν_3^+	2375	2319	56	56
ν_1^-	1050[a]	...	...	...
ν_2^-	824	802	22	21.5
ν_3^-	1413	1378	35	...
ν_4^-	722	722	0	...

[a] Raman data of references 1 and 2.

TABLE II. Comparison of the force constants of NO_2^+, N_2O, and CO_2.

	(Millidynes/A)		
	NO_2^+	N_2O	CO_2
ϕ_r	17.32±0.3	(17.9) NN (11.4) NO	15.5
ϕ_r'	1.14±0.3	1.36	1.3
ϕ_α	0.42±0.01	0.49	0.57

[6] F. A. Miller and C. H. Wilkins, Anal. Chem. **24**, 1253 (1952).

[7] R. S. Halford, J. Chem. Phys. **14**, 8 (1946). D. F. Hornig, J. Chem. Phys. **16**, 1063 (1948).

[8] Y. H. Inami, thesis, Oregon State College (1954).

This distribution of the total isotopic shift between ν_3^- and ν_4^- parallels the situation with the isoelectronic gas molecules,[9] $B^{10}F_3$ and $B^{11}F_3$, and is significant in the subsequent calculation of force constants. Although the transmission curve for normal N_2O_5 reveals no higher frequency shoulder on ν_4^-, as is the case for the N^{15} enriched sample, in several experiments a suggestion of such a shoulder (about comparable with the noise level) was observed. Therefore, the apparent increase in the intensity of the shoulder in the N^{15} enriched case may not be real, but it is interesting to note that this degenerate frequency may be split by the translational lattice modes and that it seems likely that the perturbation would be increased by the unsymmetrical environment of $N^{15}O_2^+$ and $N^{14}O_2^+$ molecules.

In addition to the bands reported here, in one experiment the 722 cm^{-1} band was apparently found at nearly 740 cm^{-1}, a weak band appeared at 1740 cm^{-1} (apparently $\nu_1^-+\nu_4^-$), and the weak band shown in Fig. 1A at 1078 cm^{-1} occurred with rather more fine structure. Moreover, ν_3^- exhibited a shoulder at 1260 cm^{-1}. Possibly this unique spectrum is evidence of polymorphism or of some structure which is disordered with respect to the orientation of the nitrate ions.

FORCE CONSTANTS OF NO_2^+ AND NO_3^- IONS

Both the nitronium and nitrate ions occupy sites of symmetry D_{3h}, which implies that in the site group approximation the fundamentals will obey the same selection rules as those for the "free molecule." More particularly, the secular determinant for NO_2^+ will be completely factored by the symmetry, thus allowing a complete evaluation of the force constants in the potential function:

$$2V=\phi_r(r_1^2+r_2^2)+2\phi_r'r_1r_2+\phi_\alpha l^2\alpha^2, \qquad (1)$$

where l is the equilibrium NO distance. Since the frequencies are uncorrected for anharmonicity, the accuracy of the force constants, particularly of the interaction term, is somewhat uncertain, but the positive sign of ϕ_r' is certain.

The force constants of NO_2^+ are compared with those of (gaseous) N_2O [10] and CO_2 [11] in Table II. One might expect that the most important resonating structures of the three molecules would be $O=C=O$, $O^--C\equiv O^+$, $O^+\equiv C-O^-$; $N\equiv N^+-O^-$, $N^-=N^+=O$; $O=N^+=O$, since Pauling's adjacent charge rule excludes $N^{-2}-N^+\equiv O^+$ and both $O^--N^+\equiv O^+$ and $O^+\equiv N^+-O^-$. If we interpret this to mean that, as far as the force constant is concerned, we are dealing with bonds of the following mean orders: 2 in CO_2, $2\frac{1}{2}$ for NN and $1\frac{1}{2}$ for NO in N_2O, and 2 in NO_2^+, then the values seem not unreasonable after allowing for differing electronegativities. Here it may be mentioned that the NO distance[3] in NO_2^+ is in agreement with the adjacent charge rule. On the other hand, the approximate constancy of the interaction constant is a little surprising, since in CO_2 [12] and N_2O[11], the sign of this constant has been associated with the increase in the order of one bond when the other one is stretched.

Finally, it is interesting to observe the uniform decrease in the bending constant accompanying the disappearance of contribution of structures of the type $-X\equiv$.

The complete potential function of the nitrate ion has the form:

$$\begin{aligned}2V=&\phi_s(s_1^2+s_2^2+s_3^2)+2\phi_s'(s_1s_2+s_2s_3+s_3s_1)\\&+\phi_\beta l^2(\beta_1^2+\beta_2^2+\beta_3^2)+2\phi_\beta' l^2(\beta_1\beta_2+\beta_2\beta_3+\beta_3\beta_1)\\&+2\phi_{s\beta}l(s_1\beta_1+s_2\beta_2+s_3\beta_3)+2\phi_{s\beta}'l(s_1\beta_2+s_2\beta_3\\&+s_3\beta_1+s_2\beta_1+s_3\beta_2+s_1\beta_3)+\phi_t l^2, \qquad (2)\end{aligned}$$

in which the s_i are bond elongations, the β_i are in-plane ONO deformations, and t is the displacement of the nitrogen atom perpendicular to the plane of the three oxygens. Because of the redundancy, $\beta_1+\beta_2+\beta_3=0$, there are only five independent potential constants, and after the introduction of symmetry coordinates and solution of the secular determinants for both $N^{14}O_3^-$ and $N^{15}O_3^-$, numerical values of $\phi_s+2\phi_s'$, $\phi_s-\phi_s'$, $\phi_\beta-\phi_\beta'$, $\phi_{s\beta}-\phi_{s\beta}'$, and ϕ_t can be found.

In calculations of the present type there are several reasons why it may be more convenient to carry out the numerical work in terms of a generalized central force (GCF) rather than a generalized valence force (GVF) potential function. In the first place, the evaluation of the **G** matrix is somewhat simpler in the GCF system, since, with the exception of the out-of-plane motions, only two types of G elements are required, namely a "bond" with itself, which has the form $\mu_\alpha+\mu_\beta$ where the μ's are the reciprocal masses of the two atoms involved, and the interaction of two "bonds" having a single common atom, α, in which case the G element is simply $\mu_\alpha\cos\phi$, where ϕ is the equilibrium angle between the two "bonds." For the GVF system no less than 11 distinct types of G elements may occur.[13] Moreover, the final expressions relating force constants, reciprocal masses, and frequencies, are in general slightly more complicated functions of the masses in the GVF than in the GCF case. Finally, it will be shown that the task of converting numerically to the GVF system after the GCF constants have been determined is not particularly difficult, especially in highly symmetric cases.

In the present example, the GCF function for nitrate

[9] D. M. Gage and E. F. Barker, J. Chem. Phys. **7**, 455 (1939). Yost, DeVault, Anderson, and Lassettre, J. Chem. Phys. **6**, 424 (1938).

[10] For N_2O: W. S. Richardson and E. Bright Wilson, Jr., J. Chem. Phys. **18**, 694 (1950).

[11] For CO_2: G. Herzberg, *Infrared and Raman Spectra of Polyatomic Molecules* (D. Van Nostrand Company, Inc., New York, 1945).

[12] H. W. Thompson and J. W. Linnett, J. Chem. Soc. 1384. 1947.

[13] J. C. Decius, J. Chem. Phys. **16**, 1025 (1948).

ion assumes the form:

$$2V=f_s(s_1^2+s_2^2+s_3^2)+2f_s'(s_1s_2+s_2s_3+s_3s_1)+f_u(u_1^2+u_2^2+u_3^2)+2f_u'(u_1u_2+u_2u_3+u_3u_1)+2f_{su}(s_1u_1+s_2u_2+s_3u_3)+2f_{su}'(s_1u_2+s_2u_3+s_3u_1+s_2u_1+s_3u_2+s_1u_3)+f_t l^2, \quad (3)$$

in which u_i represents the change in an oxygen-oxygen distance.

In order to obtain the transformation between the two sets of potential energy constants, a relation between u and β is needed. For small displacements, such a relation has the form

$$u_1=(3^{\frac{1}{2}}/2)(s_2+s_3)+(l/2)\beta_1, \quad (4)$$

together with similar expressions obtainable by suitable permutation of indices. It then follows that the symmetry coordinates in the two bases are equal, with the exception of those numbered $4a$ and $4b$, for which the relation is

$$S_{4a}(\mathrm{GCF})=-(3^{\frac{1}{2}}/2)S_{3a}(\mathrm{GVF})+(1/2)S_{4a}(\mathrm{GVF}), \quad (5)$$

with an identical relation in which b replaces a. But if $\mathbf{T}$ is a matrix which transforms the GVF symmetry coordinates into the GCF symmetry coordinates,

$$\mathbf{\Phi}=\mathbf{T}'\mathbf{F}\mathbf{T} \quad (6)$$

where $\mathbf{T}'$ is the transpose of $\mathbf{T}$. The relations between the two sets of potential constants are therefore

$$\begin{aligned}\Phi_{11}&=F_{11}\\ \Phi_{22}&=F_{22}\\ \Phi_{33}&=F_{33}-3^{\frac{1}{2}}F_{34}+(3/4)F_{44}\\ \Phi_{34}&=(1/2)F_{34}-(3^{\frac{1}{2}}/4)F_{44}\\ \Phi_{44}&=(1/4)F_{44}.\end{aligned} \quad (7)$$

The equations from which the F_{ij} are evaluated, are easily obtained after setting up the $\mathbf{G}$ matrix in the GCF system and transforming to symmetry coordinates:

$$\begin{aligned}&\mu_0F_{11}=\lambda_1\\ &(3\mu_N+\mu_0)F_{22}=\lambda_2\\ &(3/2)\mu_NF_{33}+\mu_0[F_{33}-3^{\frac{1}{2}}F_{34}+(3/2)F_{44}]=\lambda_3+\lambda_4\\ &(3/4)\mu_0(3\mu_N+\mu_0)(F_{33}F_{44}-F_{34}^2)=\lambda_3\lambda_4,\end{aligned} \quad (8)$$

in which $\lambda_k\equiv 4\pi^2\nu_k^2$.

A few words about the numerical solution now seem appropriate. The constants F_{11} and F_{22} may be determined with a percent error about double (ν^2) the percent error in the frequencies ν_1 and ν_2. The precision of the determination of F_{33} is much lower, however, since it depends upon the percentage error in $\lambda_3+\lambda_4-\lambda_3^*-\lambda_4^*$. This is especially embarrassing inasmuch as the shift in λ_3 was not measured directly but deduced by application of the product rule in view of the fact that the shift in λ_4 was negligible.

Finally, there is the problem of the quadratic equation encountered in determining F_{34} and F_{44}.

TABLE III. Nitrate ion force constants in N_2O_5.

(Millidynes/A)		
$F_{11}=10.4\pm0.2$	$\Phi_{11}=10.4\pm0.2$	$\phi_s=6.5\pm0.2$
$F_{22}=1.445\pm0.005$	$\Phi_{22}=1.445\pm0.005$	$\phi_s'=1.9\pm0.1$
$F_{33}=8.5\pm0.2$	$\Phi_{33}=4.6\pm0.3$	$\phi_t=1.445\pm0.005$
$F_{34}=4.9\pm0.1$	$\Phi_{34}=-0.19\pm0.1$	$\phi_\beta-\phi_\beta'=1.53\pm0.03$
$F_{44}=6.1\pm0.1$	$\Phi_{44}=1.53\pm0.03$	$\phi_{s\beta}-\phi_{s\beta}'=-0.19\pm0.1$

Unfortunately, it is found that no real solution exists employing Eq. (8), and the data of Table I!

Therefore, an approximate method based on first order perturbation theory[14] for small mass changes has been employed. It can be shown that

$$\Delta\lambda_4/\lambda_4=\sum_{t,t'=3,4}L_{4t}^{-1}L_{4t'}^{-1}\Delta G_{tt'}=(L_{43}^{-1})^2(3/2)\Delta\mu_N, \quad (9)$$

in which $\mathbf{L}^{-1}$ is the transformation matrix from symmetry to normal coordinates, and $\Delta\lambda$ and $\Delta\mathbf{G}$ are the changes in the respective quantities due to isotopic substitution ($\mathbf{G}$ is here the kinetic energy matrix in symmetry coordinates). Since $\Delta\lambda_4=0$, $L_{43}^{-1}=0$, which leads to the conclusion that

$$\begin{aligned}F_{33}G_{33}+F_{34}G_{34}&=\lambda_3\\ F_{33}G_{34}+F_{34}G_{44}&=0\\ F_{43}G_{34}+F_{44}G_{44}&=\lambda_4.\end{aligned} \quad (10)$$

From these equations one finds the following force constants: $F_{33}=8.52$, $F_{34}=4.92$, $F_{44}=6.11$. Now this set of potential constants fits the data very well indeed, the calculated frequencies employing Eqs. (8) being 1415 and 722 cm^{-1} for N^{14}, and 1378 and 721 for N^{15}. In order to estimate the error in the force constants, we shall therefore assume that the error involved in the approximate Eqs. (10) is negligible compared with the experimental error in λ_3 and λ_4. This leads to the results finally expressed in Table III, in which the force constants are finally reduced to GVF form. It has been assumed, quite arbitrarily, that the errors in the experimental frequencies are ±2 cm^{-1} in ν_2^- and ν_4^-, and ±10 cm^{-1} in ν_1^- and ν_3^-. Although such an estimate makes some allowance for anharmonicity, it must be noted that ν_3^- and ν_4^- in different nitrate salts[6] exhibit an even larger range of variation than is covered by the above estimate. The relatively great breadth of ν_3^- indicates strong anharmonic coupling with lattice modes, and in all likelihood the error in this frequency exceeds the above estimate.

The structure of nitrate ion is usually described as a resonant mixture of the three equivalent forms:

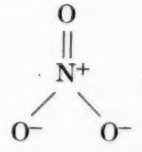

[14] See, for example, W. Edgell, J. Chem. Phys. **13**, 539 (1945).

Thus, its NO bond force constant should fall between the values for pure single and pure double bond as indeed seems to be the case ($\phi_s=6.5$), although the numerical value seems rather low. Furthermore, a preliminary extension of bonds 2 and 3 should confer more double bond character upon bond number 1, which is agreement with the large positive value of the interaction constant, $\phi_s'=1.9$. A further discussion seems inapproprate in view of the rather large experimental uncertainty in the remaining constants, although one may conclude by remarking that the omission of interaction constants, especially of the bond-bond type, is certainly not justified for molecular structures of this type.

THE JOURNAL OF CHEMICAL PHYSICS VOLUME 22, NUMBER 5 MAY, 1954

Infrared Spectrum of $S^{16}O^{18}O$ and the Potential Constants of SO_2†

SANTIAGO R. POLO AND M. KENT WILSON
Mallinckrodt Chemical Laboratory, Harvard University, Cambridge, Massachusetts
(Received December 11, 1953)

An investigation of the infrared spectrum of $S^{16}O^{18}O$ results in the following frequency assignment:

$\nu_1=1122\pm1$ cm^{-1}, $\nu_2=506.8\pm0.5$ cm^{-1}, $\nu_3=1341\pm0.5$ cm^{-1}.

These data combined with the fundamental frequencies of $S^{16}O_2$ have been used to calculate the potential constants for sulfur dioxide. These are

$$f_d=10.02,\quad f_{dd}=0.03,\quad \frac{1}{d}f_{d\alpha}=0.20,\quad \frac{1}{d^2}f_\alpha=0.793.$$

INTRODUCTION

THE determination of the potential energy constants of molecules is of fundamental importance to molecular structure. The force constants and anharmonicity coefficients can be calculated for diatomic molecules if the frequencies of the fundamental and one or more overtones are known. However, for polyatomic molecules, even in the harmonic oscillator approximation, the number of potential constants is greater than the number of fundamental vibrations. If the number of vibrations in a given symmetry class is n_i, the number of potential constants related to them is $\frac{1}{2}n_i(n_i+1)$.* Therefore, if there is a symmetry class for which $n_i\geq 2$, a knowledge of the vibrational frequencies is not sufficient for the determination of the potential constants.

As centrifugal distortion coefficients and Coriolis coupling coefficients are related to the molecular potential constants, studies of centrifugal distortion and vibration-rotation interaction can yield the required additional information. Recently, a systematic treatment of centrifugal distortion in polyatomic molecules has been developed,[1] and the relations between the centrifugal distortion coefficients and the potential constants have been established. Also a convenient analytical method dealing with the Coriolis coupling coefficients and their relations to the potential constants has been given.[2]

The investigation of the vibrational spectra of molecules in which one or more atoms have undergone isotopic substitution yields additional data. Since it is assumed that no change in force constant takes place with isotopic substitution the vibrational frequencies of the normal and isotopic molecules may be combined to yield the potential constants. Deuterium has been the most widely used isotope,[3] but in recent years several compounds containing ^{13}C or ^{15}N have been studied.[4–6]

As part of a general program to investigate the properties of sulfur-oxygen and silicon-oxygen bonds the infrared spectrum of $S^{16}O^{18}O$ has been obtained and the quadratic potential constants of SO_2 determined within comparatively narrow ranges.

EXPERIMENTAL TECHNIQUES

The $S^{16}O^{18}O$ was prepared from an oxygen sample enriched to about 23 atom percent in the ^{18}O isotope.‡

The isotopic sulfur dioxide was prepared by heating the oxygen over an excess of sublimed sulfur in a closed

† This work was supported in part by the U. S. Air Force under contract AF 18(600)-590.

* The number of potential constants is smaller when to the approximation considered the potential energy function has a higher symmetry than the molecule itself. A convenient example is afforded by the isotopic species $S^{16}O^{18}O$ studied in the present investigation.

[1] D. Kivelson and E. B. Wilson, Jr., J. Chem. Phys. **21**, 1229 (1953).

[2] S. R. Polo and J. A. Hawkins, Presented at the Symposium on Molecular Structure and Spectroscopy, Ohio State University, Columbus, Ohio, June, 1953.

[3] F. Halverson, Revs. Modern Phys. **19**, 87 (1947).

[4] W. S. Richardson and E. B. Wilson, Jr., J. Chem. Phys. **18**, 155 (1950).

[5] W. S. Richardson and E. B. Wilson, Jr., J. Chem. Phys. **18**, 694 (1950).

[6] W. S. Richardson, J. Chem. Phys. **19**, 1213 (1951).

‡ The enriched oxygen was prepared by Professor A. O. Nier of the University of Minnesota under a grant from the American Cancer Society acting through the Committee on Growth of the National Research Council.

all-glass system. Assuming 23 atom percent of ^{18}O in the original sample, the isotopic composition of the sulfur dioxide is calculated to be 60 mole percent $S^{16}O_2$, 35 mole percent $S^{16}O^{18}O$, and 5 mole percent $S^{18}O_2$.

The infrared spectra of SO_2 and isotopic species were measured with a Perkin-Elmer Model 12C single-beam spectrograph modified for double-pass operation and with a Baird Associates double-beam spectrophotometer. KBr, NaCl, and CaF_2 prisms were employed in both instruments. The spectrographs were calibrated immediately before or after each run by means of H_2O, NH_3, and HBr lines in their respective absorption regions.

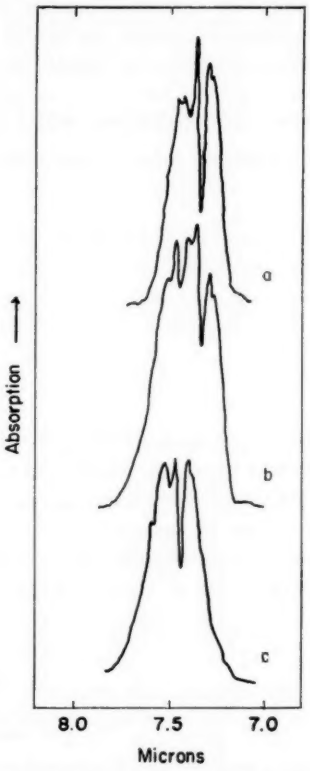

FIG. 1. The infrared absorption spectra of the antisymmetrical stretching vibrations in (a) $S^{16}O_2$, $p=16$ mm; (b) $S^{16}O_2+S^{16}O^{18}O$, $p=30$ mm; (c) $S^{16}O^{18}O$, $p=10.5$ mm. Path length is 4.0 cm.

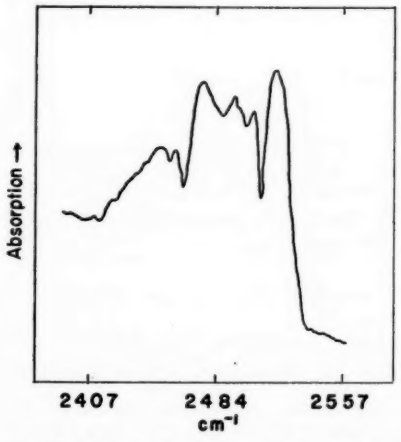

FIG. 2. The infrared absorption spectra of the combination bands $\nu_1+\nu_3$ and $(\nu_1+\nu_3)^*$ in the $S^{16}O_2-S^{16}O^{18}O$ mixture. Pressure was 562 mm in a 4.0-cm cell.

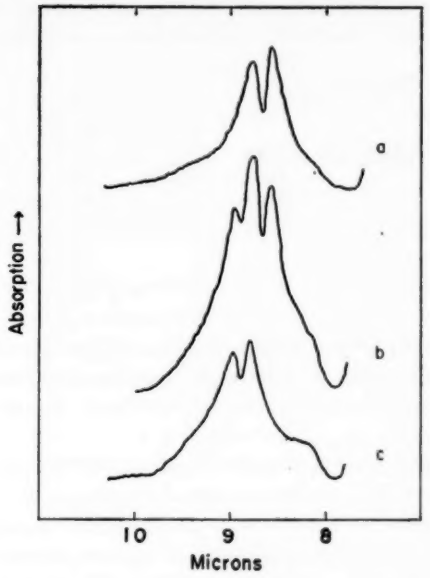

FIG. 3. The infrared absorption spectra of the symmetrical stretching vibrations in (a) $S^{16}O_2$, $p=84$ mm; (b) $S^{16}O_2+S^{16}O^{18}O$, $p=153$ mm; (c) $S^{16}O^{18}O$, $p=54$ mm. Path length is 4.0 cm.

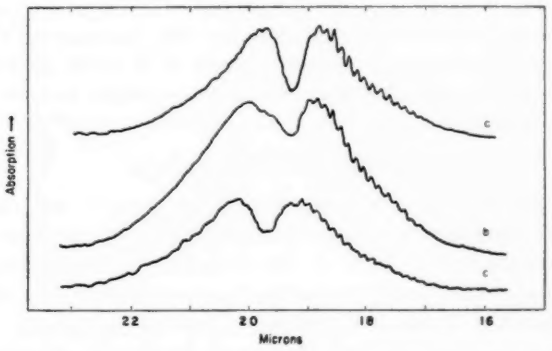

FIG. 4. The infrared absorption spectra of the bending vibrations in (a) $S^{16}O_2$, 83.5 mm; (b) $S^{16}O_2+S^{16}O^{18}O$, $p=152$ mm; (c) $S^{16}O^{18}O$, $p=53$ mm. Path length is 4.0 cm.

Gas cells 10 cm in length with KBr windows were used with the Perkin-Elmer spectrograph and two identical 4-cm cells, also with KBr windows, were used with the Baird Associates spectrophotometer.

The fundamental bands ν_3 of $S^{16}O_2$, ν_3* of $S^{16}O^{18}O$, and ν_3** of $S^{18}O_2$,§ as well as the combination bands $\nu_1+\nu_3$ and $(\nu_1+\nu_3)$* have well defined PQR structures and the prominent Q branches stand out clearly in the spectrum of the mixture. The frequencies of these Q branches were determined from measurements with the single-beam

§ In numbering the fundamentals of $S^{16}O^{18}O$ we have not followed the usual convention of numbering the vibrations starting with ν_1 as the highest frequency but have numbered them to correspond to the normal compound.

TABLE I. Observed spectra of $S^{16}O_2$ (frequencies in cm^{-1}).

Assignment	Raman, gas G and N[a]	Infrared, gas B, C, and A[b]	Infrared, gas Barker[c]	Infrared, gas Present work	Adopted values
ν_2	...	...	517.84	518.0±0.5	517.8
ν_1	1150.5±0.5	1152	1151.38	1152 ±1	1151.4
ν_3	...	1361	1361.50	1360.5±0.5	1360.5
$\nu_1+\nu_3$	...	2499	...	2497 ±0.5	

[a] See reference 8.
[b] See reference 7.
[c] See reference 9.

TABLE II. Observed spectra of $S^{16}O^{18}O$ and $S^{18}O_2$.

$S^{16}O^{18}O$ Assignment	$S^{16}O^{18}O$ Frequency (cm^{-1})	$S^{18}O_2$ Assignment	$S^{18}O_2$ Frequency (cm^{-1})
ν_2*	506.8±0.5		
ν_1*	1122 ±1		
ν_3*	1341.1±0.5	ν_3**	1316
$(\nu_1+\nu_3)$*	2451 ±0.5		

instrument, although the traces of Fig. 1 are those obtained with the double-beam spectrophotometer. The combination bands $\nu_1+\nu_3$ and $(\nu_1+\nu_3)$* are illustrated in Fig. 2.

The fundamental bands ν_1 and ν_2 of $S^{16}O_2$ and ν_1* and ν_2* of $S^{16}O^{18}O$ exhibit doublet structures. To measure these bands of the $S^{16}O^{18}O$ molecule the spectra were obtained with the double-beam spectrophotometer by placing in the sample beam the cell containing the isotopic mixture and in the comparison beam an identical cell filled with $S^{16}O_2$ to a pressure equal to its partial pressure in the isotopic mixture. As can be seen in Fig. 3 and Fig. 4 the sensitivity of the spectrograph was not seriously diminished by this procedure. The expected structure of both bands of $S^{16}O^{18}O$ appears clearly defined although the spectrum of the mixture is quite complex.

EXPERIMENTAL RESULTS

The data on $S^{16}O_2$ obtained in the present investigation together with those obtained by previous workers[7–9] are collected in Table I. The frequency values adopted for the force constant calculations are listed in the last column of Table I. Essentially they are those from the high resolution work of Barker, except for the vibration ν_3 for which Barker's data appear to be in doubt as the published frequencies do not agree with the values read from the figure of the spectra.[10] For this frequency the data obtained here have been preferred. The data for $S^{16}O^{18}O$ and $S^{18}O_2$ are given in Table II.

NORMAL COORDINATE TREATMENT

The most convenient choice of symmetry coordinates is

$$s_1=\frac{1}{\sqrt{2}}(\Delta d_1+\Delta d_2),$$

$$s_2=\Delta\alpha,$$

$$s_2=\frac{1}{\sqrt{2}}(\Delta d_1-\Delta d_2).$$

For $S^{16}O_2$ and $S^{18}O_2$, s_1 and s_2 belong to the A_1 and s_3 to the B_1 irreducible representations of the C_{2v} group, while for $S^{16}O^{18}O$ they all belong to the A' irreducible representation of the C_s group.

With this choice of symmetry coordinates the F matrix[11] is the same for all three isotopic species

$$F=\begin{bmatrix} f_d+f_{dd} & \sqrt{2}f_{d\alpha} & 0 \\ & f_\alpha & 0 \\ & & f_d-f_{dd} \end{bmatrix}.$$

The G matrix for $S^{16}O^{18}O$ is

$$G=\begin{bmatrix} \frac{1}{2}(\mu_{16_0}+\mu_{18_0})+(1+\cos\alpha)\mu_S & \frac{-\sqrt{2}}{d}\sin\alpha\mu_S & \frac{1}{2}(\mu_{16_0}-\mu_{18_0}) \\ & \frac{2}{d^2}[\frac{1}{2}(\mu_{16_3}+\mu_{18_0})+(1-\cos\alpha)\mu_S] & 0 \\ & & \frac{1}{2}(\mu_{18_0}+\mu_{16_0})+(1-\cos\alpha)\mu_S \end{bmatrix}.$$

The G matrices for $S^{16}O_2$ and $S^{18}O_2$ have not been reproduced. They can be easily obtained by appropriate substitution of masses.

The μ's are the reciprocal masses of the atoms, α the OSO angle and d the S–O distance. The values of the atomic masses used in the calculations are those given by Li.[12] The structural parameters used are those given by Kivelson,[13] which are

$$\alpha=119°\,32',\quad d_{S-O}=1.4321\text{A}.$$

In order to better estimate the influence of the experimental errors the procedure used in the determination

[7] Bailey, Cassie, and Angus, Proc. Roy. Soc. (London) **130**, 142 (1931).
[8] H. Gerding and W. J. Nijveld, Nature **137**, 1070 (1936).
[9] E. F. Barker, Revs. Modern Phys. **14**, 198 (1942).
[10] G. Herzberg, *Infrared and Raman Spectra of Polyatomic Molecules* (D. Van Nostrand Company, Inc., New York, 1945), p. 285.
[11] E. B. Wilson, Jr., J. Chem. Phys. **7**, 1047 (1939); **9**, 76 (1941).
[12] C. W. Li, Phys. Rev. **88**, 1038 (1952).
[13] D. Kivelson, J. Chem. Phys. **13**, 904 (1954), following paper.

of the potential constants has been the following. Different sets reproducing the adopted frequencies of $S^{16}O_2$ were computed, and for each set the frequencies of $S^{16}O^{18}O$ were calculated, as also the difference $(\nu_1+\nu_3)-(\nu_1+\nu_3)$*. These frequencies can be plotted as a function of F_{11}, as shown in Fig. 5. The possible range of values of F_{11} (and consequently of F_{12} and F_{22}) will depend on the errors which are considered for the frequency measurements. If they are taken as those given in Table II, it is seen that the possible set corresponds to $F_{11}=10.06$ millidynes/angstrom within rather narrow limits. If the errors are taken twice as large, the approximate range for F_{11} is from 9.74 to 10.36, and the best value (average) will then be $F_{11}=10.05$. It is then reasonable to conclude that $F_{11}=10.0\pm0.3$, taking $F_{11}=10.05$ as determining the best set.

When the results of previous calculations are used to determine the centrifugal distortion coefficients, as described in the following paper,[13] it turns out that these are rather sensitive to the potential constants. It appears possible to determine the parameter F_{11} within much narrower limits, that is $F_{11}=10.030\pm0.005$ millidynes/angstrom.

DISCUSSION

When the best microwave values and the best infrared values for the potential constants are compared, as given in Table III, they are found to be remarkably close. It is perhaps worthwhile to point out that the two ways of determining the potential constants are independent. In both cases, the infrared frequencies of $S^{16}O_2$ are used as data in order to express F_{12} and F_{22} as functions of a single parameter F_{11}, and then the best value of F_{11} is determined in one case by fitting the infrared frequencies of $S^{16}O^{18}O$, in the other by fitting the centrifugal distortion coefficients (or rather the deviations of the microwave frequencies from those of the rigid rotor).

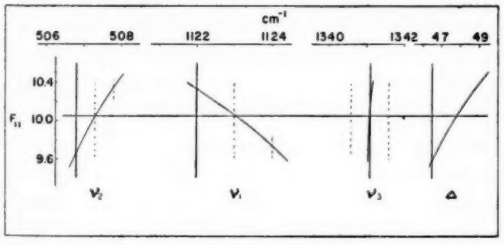

FIG. 5. The calculated frequencies of the $S^{16}O^{18}O$ fundamentals as a function of F_{11}. The measured frequencies of the bands are indicated by full vertical lines and the dotted lines indicate the ranges of experimental errors (see text). It is unnecessary to indicate the lower-frequency limits of ν_1 and ν_2, and therefore the corresponding dotted lines have not been drawn.

TABLE III. Potential constants of SO_2.[a]

	f_d	f_{dd}	$\frac{1}{d}f_{d\alpha}$	$\frac{1}{d^2}f_\alpha$
Best infrared values	10.02	0.03	0.20	0.793
Best microwave values	10.006	0.0236	0.189	0.7933

[a] f_d and f_{dd} are given in millidynes/angstrom, $f_{d\alpha}$ in millidynes, f_α in millidynes angstrom.

Even though such a degree of agreement as one might infer by inspecting Table III cannot be claimed (due to the previously discussed effect of the experimental errors, the neglect of anharmonicity, etc.), the consistency of microwave and infrared results is as satisfactory as can possibly be expected.

Coulson, Duchesne, and Manneback[14] consider that the cross terms in the potential function arise from three distinct causes (1) resonance effects, (2) changes in hybridization, and (3) interactions between nonbonded atoms. The first two appear to result in positive bond-bond interaction constants, as does repulsion between nonbonded atoms. However, attraction between nonbonded atoms leads to a negative interaction constant. Since Moffitt[15] has calculated that a charge of about $\frac{1}{4}e^-$ is associated with each oxygen in SO_2, attraction between the oxygen atoms is highly unlikely. Therefore, if one wishes to apply the Coulson-Duchesne-Manneback picture to sulfur dioxide it seems that there is no cancellation of effects. The smallness of f_{dd} would then indicate that all three effects are very small in the present case.

It should also be noted that the smallness of f_{dd} and $f_{d\alpha}$ as compared with f_d explains why calculations made under the simplifying assumption $f_{dd}=f_{d\alpha}=0$ may be carried out successfully.[16]

The authors wish to thank Professor Alfred O. C. Nier of the University of Minnesota for supplying the sample of oxygen-18, Dr. Raymond Ferguson for preparing the enriched sulfur dioxide sample, Dr. D. Z. Robinson and Mr. Edward Merrill of Baird Associates, Inc., for use of the spectrophotometer with KBr and CaF_2 optics, and Professor William Moffitt for helpful discussions.

[14] Coulson, Duchesne, and Manneback, *Victor Henri Commemorative Volume* 33 (Maison Desoer, Liège, 1947); Nature **160**, 793 (1947).

[15] W. Moffitt, Proc. Roy. Soc. (London) **A200**, 409 (1950).

[16] G. Herzberg, see reference 10, p. 170.

The Determination of the Potential Constants of SO_2 from Centrifugal Distortion Effects*

DANIEL KIVELSON †
Mallinckrodt Chemical Laboratory, Harvard University, Cambridge, Massachusetts
(Received December 11, 1953)

The microwave spectrum of SO_2 was reanalyzed with particular emphasis upon the effect of centrifugal distortion. It was possible to fit the rotational spectrum to within a mean deviation of ± 0.23 Mc using the energy expression given by Kivelson and Wilson. The rotational constants so determined are $a=60778.79$ Mc, $b=10318.10$ Mc, and $c=8799.96$ Mc. The four distortion constants could not be uniquely determined directly from the rotational spectrum.

The sets of potential constants determined by Wilson and Polo were used to calculate distortion constants and these in turn used to calculate frequency shifts due to centrifugal distortion. These shifts are critically dependent upon the set of potential constants used. By choosing a set of potential constants compatible with the infrared spectrum which also yield distortion frequency shifts in accord with those obtained from a direct analysis of the rotational spectrum, a very sensitive determination of the potential constants may be made. The resulting force constants are: $f_d=10.006\times 10^5$ dyne cm^{-1}; $f_\alpha/d_0^2=0.7933\times 10^5$ dyne cm^{-1}; $f_{dd}=0.0236\times 10^5$ dyne cm^{-1}; $f_{d\alpha}/d_0=0.189$ dyne cm^{-1}.

THE microwave spectrum of SO_2 has been studied previously by several investigators.[1–3] Crable and Smith[2] studied the low J transitions and determined structural parameters on the basis of a rigid rotor model. Sirvetz considered high J transitions using a semirigid model with constants of centrifugal distortion calculated from infrared vibrational data. The present investigation treats the SO_2 spectrum in a third way; it also employs a semirigid rotor model, but the constants of centrifugal distortion are determined directly from the rotational spectrum and used to obtain estimates of the vibrational frequencies. Finally, the information obtained from the pure rotational spectrum is combined with results derived from the vibrational spectrum to give precise information about the quadratic force field.

The Hamiltonian in the symmetric rotor representation for a semirigid rotor of orthorhombic symmetry is a complicated matrix[4] with $(K|K)$, $(K|K\pm 2)$, and $(K|K\pm 4)$ elements where K is the quantum number corresponding to the component of angular momentum along the z axis. Sirvetz used the Mathieu function method proposed by Golden[5] to evaluate the contribution of the $(K|K\pm 4)$ elements and the continued fraction method discussed by King, Hainer, and Cross[6] to evaluate the contribution arising from the rest of the energy matrix. Since the constants of centrifugal distortion appear both on and off the diagonal in the Hamiltonian matrix used above, it would be an almost impossible task to determine these constants empirically from the rotational spectrum without making some approximations.

Recently an approximate form of the Hamiltonian for the semirigid rotor has been proposed.[7] In this form the effect of centrifugal distortion on the energy levels may be treated as an additive perturbation in which the distortion constants (τ's) enter linearly. This form permits the determination of the τ's from the rotational data.

THEORY

The energy of a semirigid rotor is given by Eq. (I-17). Rewriting this equation in a more convenient form one has

$$\begin{aligned} W=W_0&-[D_J+2R_6]J^2(J+1)^2\\ &-[D_{JK}-4R_6]J(J+1)\langle \mathbf{P}_z^2\rangle\\ &-[D_K+2R_6]\langle \mathbf{P}_z^4\rangle+2\sigma\delta_J J(J+1)(p_z^2-\eta)\\ &+4R_5\sigma(-p_z^4+K^2\eta+K^2p_z^2+p_z^2\eta)\\ &+4R_6\sigma^2(p_z^4-2K^2p_z^2+\eta^2-2p_z^2\eta), \end{aligned} \tag{1}$$

where

$$p_z^2=\langle \mathbf{P}_z^2\rangle-K^2, \tag{2}$$

$$p_z^4=\langle \mathbf{P}_z^4\rangle-K^4, \tag{3}$$

$$\eta=\frac{2\lambda}{3-\kappa}-K^2, \tag{4}$$

κ is the asymmetry parameter and λ the reduced energy defined by King, Hainer, and Cross,[6] K is the limiting symmetric rotor quantum number, and the remaining quantities in Eq. (1) are defined in I.

The distortion constants appearing in Eq. (1) are linear combinations of the distortion constants $\tau_{\alpha\beta\gamma\delta}$ introduced by Wilson and Howard.[8] Explicit formulas for the evaluation of these τ's in terms of the four

* This research was supported in part by the U. S. Office of Naval Research.
† Present address: Department of Physics, Massachusetts Institute of Technology.
[1] Dailey, Golden, and Wilson, Phys. Rev. **72**, 871 (1947).
[2] G. Crable and W. Smith, J. Chem. Phys. **19**, 502 (1951).
[3] M. Sirvetz, J. Chem. Phys. **19**, 938 (1951).
[4] E. B. Wilson, Jr., J. Chem. Phys. **5**, 617 (1937).
[5] S. Golden, J. Chem. Phys. **16**, 250 (1948); and erratum, J. Chem. Phys. **17**, 586 (1949).
[6] King, Hainer, and Cross, J. Chem. Phys. **11**, 27 (1943).
[7] D. Kivelson and E. B. Wilson, Jr., J. Chem. Phys. **20**, 1575 (1952). Hereafter referred to as I.
[8] E. B. Wilson, Jr., and J. B. Howard, J. Chem. Phys. **4**, 260 (1936).

independent force constants of SO_2 have been given in a previous paper.[9] Since there are only four force constants, the seven τ's that enter into Eq. (1) are connected, the relations being as follows:

$$\tau_{yyyy}=\tau_{xxxx}\frac{c^4}{b^4}+\tau_{zzzz}\frac{c^4}{a^4}+2\tau_{xxzz}\frac{c^4}{a^2b^2}, \tag{5}$$

$$\tau_{yyxx}=\tau_{xxxx}\frac{c^2}{b^2}+\tau_{xxzz}\frac{c^2}{a^2}, \tag{6}$$

$$\tau_{yyzz}=\tau_{zzzz}\frac{c^2}{a^2}+\tau_{xxzz}\frac{c^2}{b^2}; \tag{7}$$

where a, b, c are the usual reciprocal principal moments of inertia, $a\geqslant b\geqslant c$ and the I^r representation of King, Hainer, and Cross has been used.

Combining Eqs. (5)–(7) with Eq. (1) one finds that the energy of the system is equal to the rigid rotor energy (W_0) plus terms linear in the four distortion constants τ_{xxxx}, τ_{zzzz}, τ_{xxzz}, τ_{xxzz}. The coefficients of these constants can be readily calculated since J and K are the rotational quantum numbers, λ is the rigid rotor reduced energy and can be calculated from previously determined approximate rigid rotor parameters, and $\langle \mathbf{P}_z^2\rangle$ and $\langle \mathbf{P}_z^4\rangle$ can be calculated from the rigid rotor parameters by means of Eq. (I-23).

ITERATION PROCEDURE

The rigid rotor parameters determined by Crable and Smith from the three lowest J transitions, which are only slightly affected by centrifugal distortion, were used as zeroth-order rotational constants. The four highest J transitions were then calculated on this basis and the discrepancy between calculated and observed frequencies ($\delta\nu$) was attributed to centrifugal distortion. $\langle \mathbf{P}_z^2\rangle$ and $\langle \mathbf{P}_z^4\rangle$ were calculated using these parameters and Eq. (1) was used to solve for the four independent τ's. The distortion of the three lowest J transitions was then computed and new rigid rotor parameters determined. The procedure was then repeated with these parameters. The initial coefficients of the τ's were used throughout since the change in rigid rotor parameters did not affect these quantities appreciably. The cycle was repeated three times. The mean deviation between the observed frequencies and those calculated by this method is 1.25 megacycles for all these lines.

A least squares calculation on seven of the levels with the four τ's as parameters did not reduce the mean deviation. Since the reported mean experimental[2] error on the three lowest J lines is 0.12 Mc and the mean discrepancy between the present calculation and observed values for these low J lines is 0.15 Mc, it was not thought profitable to continue the iteration procedure.

[9] D. Kivelson and E. B. Wilson, Jr., J. Chem. Phys. **21**, 1229 (1953).

TABLE I. SO_2 rotational transitions.

Transition	Computed frequency "Least-squares method" (Mc)	Observed frequency (Mc)
$0_{0,0}\rightarrow 1_{1,1}$	69576.01	69576.06[a]
$2_{0,2}\rightarrow 2_{1,1}$	53529.00	53529.16[a]
$3_{1,3}\rightarrow 4_{0,4}$	29321.44	29321.22[a]
$4_{0,4}\rightarrow 4_{1,3}$	59224.96	59225.00[a]
$6_{1,5}\rightarrow 5_{2,4}$	23414.08	23414.30[b]
$7_{2,6}\rightarrow 8_{1,7}$	25393.22	25392.80[b]
$9_{1,9}\rightarrow 8_{2,6}$	24083.65	24083.39[b]
$13_{2,19}\rightarrow 12_{3,9}$	20335.07	20335.47[b]
$16_{3,13}\rightarrow 17_{2,16}$	28858.10	28858.11[b]
$22_{4,18}\rightarrow 21_{5,17}$	24040.08	24039.50[b]
$23_{5,19}\rightarrow 24_{4,20}$	22482.68	22482.51[b]
$24_{5,19}\rightarrow 25_{4,21}$	26776.80	26777.20[b]
$34_{7,27}\rightarrow 35_{6,30}$	25049.31	25049.13[b]

[a] Measured by Crable and Smith.
[b] Measured by Sirvetz.

The rotational parameters determined in this manner are

$$a=60778.79 \text{ Mc},$$
$$b=10318.03 \text{ Mc},$$
$$c=\ 8799.74 \text{ Mc},$$

which are, respectively, 2.2, 0.4, and 0.3 megacycles larger than those reported by Crable and Smith.

LEAST-SQUARES PROCEDURE

In order to get a more reliable set of constants a more extended least-squares calculation was carried through with seven variables, the four distortion constants and three functions of the rotational constants. The rigid rotor energy was differentiated with respect to the rotational parameters and only linear variations of the energy with respect to these parameters were considered.[10] It is convenient to take $(a-c)$, $(b+c)$, and the asymmetry parameter κ as the rigid rotor variables. The least-squares calculations were performed on a system of eleven lines, that is all but the $4_{04}\rightarrow 4_{13}$ and the $9_{19}\rightarrow 8_{26}$ lines in Table I. The resulting rigid rotor parameters are

$$a=60778.79 \text{ Mc},$$
$$b=10318.10 \text{ Mc},$$
$$c=\ 8799.96 \text{ Mc},$$

and the distortion constants are given in Table II. The transition frequencies calculated on the basis of these parameters are given in Table I along with the observed frequencies. These agree much better with the observed frequencies than do the preceding set. The mean deviation from the experimental frequencies is

[10] The rigid rotor energy W_0 is given by the relation

$$W_0=(\tfrac{1}{2})(b+c)J(J+1)+(\tfrac{1}{4})(a-c)\lambda(\kappa),$$

where $\lambda(\kappa)$ is the reduced energy. With the use of $\partial W_0/\partial a=\langle \mathbf{P}_z^2\rangle$ it can be shown that

$$d\lambda/d\kappa=(\lambda-2\langle \mathbf{P}_z^2\rangle)/(1+\kappa)$$

$\langle \mathbf{P}_z^2\rangle$ can be evaluated by Eq. (I-23).

TABLE II. SO_2 distortion and potential constants.

		Iteration procedure	Least-squares procedure	Combined infrared microwave results
τ_{xxxx}	(Mc)	−0.037617	−0.035615	−0.039696
τ_{zzzz}	(Mc)	−10.1548	−10.1557	−9.8098
τ_{zzxx}	(Mc)	0.46515	0.46436	0.41170
τ_{xxzz}	(Mc)	−0.061484	−0.048496	−0.053203
f_d	($\times 10^{-5}$ dyne cm^{-1})	11.3558	13.4146	10.006
f_α/d_0^2	($\times 10^{-5}$ dyne cm^{-1})	0.7524	0.7614	0.7933
f_{dd}	($\times 10^{-5}$ dyne cm^{-1})	2.7174	2.4628	0.0236
$f_{d\alpha}/d_0$	($\times 10^{-5}$ dyne cm^{-1})	0.2384	0.3288	0.189
$\nu_1(s)$	(cm^{-1})	1361	1445	1151[a]
$\nu_2(s)$	(cm^{-1})	505	506	519[a]
$\nu_3(a)$	(cm^{-1})	1276	1437	1361[a]

[a] Observed infrared frequencies are 1151, 519, 1361 cm^{-1} for the $\nu_1(s)$, $\nu_2(s)$, and $\nu_3(a)$ vibration, respectively.

0.23 Mc, which is just above the range of experimental accuracy.

RESULTS

Table II gives the values of the τ's determined by the procedures outlined above. It is found that the relations between the τ's and the frequencies are not sufficiently independent to permit the determination of a unique set of τ's, although one may obtain τ's that yield frequencies in good agreement with the observed microwave frequencies. Since the τ's can be explicitly related to the force constants that enter into a general quadratic potential field,[9] (see Appendix) the force constants corresponding to the various sets of τ's have been evaluated and are given in Table II.[11] The interatomic parameters used were derived from the "effective" inverse moments of inertia a and b. They turn out to be $d_{S-O}=1.4321$A and $\measuredangle O-S-O=119.536°$. The force constants have been used to calculate the vibrational frequencies of SO_2. These results are given in Table II.

The predicted vibrational frequencies are the right order of magnitude but differ appreciably from the observed values. This is understandable since the various sets of τ's calculated from the rotational spectrum yield quite different vibrational frequencies. Thus very great accuracy could not be expected since a unique set of τ's cannot be determined from the rotational spectrum and since centrifugal distortion only adds a small correction term to the rotational energy.

The effect of centrifugal distortion on the rotational frequencies of SO_2 is small even for high J values. Thus a small error in the microwave frequency introduces a large error in the τ's and hence in the vibrational frequencies. It should be noted that although the frequency shift of the lines arising from distortion is small, the corresponding shift in the energy levels is large, e.g., about 7000 Mc for $35_{6,30}$. The τ's have been reported to many places in spite of the fact that even the second place is in doubt because the distortion frequencies depend on rather small differences of large numbers.

COMBINED INFRARED-MICROWAVE RESULTS

Microwave data together with infrared measurements can be combined to yield more information concerning

TABLE III. Centrifugal distortion frequency shifts (Mc).

Transition	Calculated on basis of sets determined by F_{11}: 10.2×10^5 dyne cm^{-1}	10.0×10^5 dyne cm^{-1}	9.8×10^5 dyne cm^{-1}	"Iteration" procedure (Mc)	"Least-Squares" procedure (Mc)	Final results combined infrared-microwave data (Mc)
$0_{0,0}\rightarrow1_{1,1}$				−2.45	−2.45	−2.39
$2_{0,2}\rightarrow2_{1,1}$				−1.77	−1.73	−1.77
$3_{1,3}\rightarrow4_{0,4}$				−0.31	−0.25	−0.38
$4_{0,4}\rightarrow4_{1,3}$				+0.15	+0.30	−0.10
$6_{1,5}\rightarrow5_{2,4}$				−22.84	−23.03	−22.05
$7_{2,6}\rightarrow8_{1,7}$				+1.85	+2.35	+1.62
$9_{1,9}\rightarrow8_{2,6}$				−13.43	−12.37	−12.90
$13_{2,19}\rightarrow12_{3,9}$	−64.67	−52.15	−41.11	−56.15	−54.64	−53.92
$16_{3,13}\rightarrow17_{2,16}$	+34.16	+21.29	+9.96	+27.89	+23.39	+23.11
$22_{4,18}\rightarrow21_{5,17}$	−225.96	−141.96	−68.21	−155.96	−157.62	−153.84
$23_{5,19}\rightarrow24_{4,20}$	−24.53	−123.74	−210.39	−117.10	−112.39	−109.75
$24_{5,19}\rightarrow25_{4,21}$	+59.05	−30.50	−108.88	−16.28	−18.24	−17.86
$34_{7,27}\rightarrow35_{6,30}$	+160.73	−114.02	−354.40	−79.90	−78.61	−75.25

[11] In making these and subsequent calculations the following constants were used: $c=2.997902\times10^{10}$ cm/sec; $N=6.02544\pm0.00011\times10^{23}$ g mole^{-1}; $m_0=16$ amu; $m_s=31.9823$ amu; $h=6.62377\pm0.00018\times10^{27}$ erg sec.

the force field than can be obtained from either approach individually. In the preceding paper Polo and Wilson[12] have analyzed the infrared spectra of $O^{16}-S-O^{16}$ and of $O^{16}-S-O^{18}$ and have obtained potential constants describing a general quadratic force field. However, the infrared data allow the determination of the potential constants only within a range of values corresponding to $F_{11}=(10.0\pm0.2)\times10^5$ dynes cm^{-1}.

These potential constants have been used to compute the four independent τ's entering into the expression for the frequency shift due to centrifugal distortion. This is the reverse of the process described in the previous sections of this paper. The τ's were computed for each of three sets of potential constants obtained by Polo and Wilson, corresponding in turn to $F_{11}=9.8\times10^5$, 10.0×10^5, or 10.2×10^5 dyne cm^{-1}. The frequency shift due to distortion was then calculated for each set of distortion constants τ. In Table III it is readily seen that frequency shifts due to centrifugal distortion depend critically upon the particular set of force constants used. It is difficult to decide exactly what the frequency shifts should be but also included in Table III are the frequency shifts calculated from the two sets of τ's derived directly from the rotational sepctrum. (See Table II.) This should give an estimate of the uncertainty in the frequency shift due to centrifugal distortion. Even without too much precision in estimating the "true" frequency shifts, it can be seen that the correct set of potential constants can be obtained with great accuracy by interpolation. Thus the best value of F_{11} can be set at $10.030\pm0.005\times10^5$ dyne cm^{-1}. With this value of the potential constant, the other potential constants were readily obtained. The force constants[13] turn out to be

$$f_d=10.006\pm0.0025\times10^5 \text{ dyne cm}^{-1},$$
$$f_\alpha/d_0^2=0.7933\pm0.00015\times10^5 \text{ dyne cm}^{-1},$$
$$f_{dd}=0.0236\pm0.0025\times10^5 \text{ dyne cm}^{-1},$$
$$f_{d\alpha}/d_0=0.189\pm0.005\times10^5 \text{ dyne cm}^{-1}.$$

The estimated errors are based solely on the uncertainty in the determination of F_{11}. (See Fig. 1.) The distortion constants were recalculated on the basis of these force constants and are given in Table II.

Table III gives the distortion frequencies calculated with these constants. The mean deviation between the observed frequencies and the frequencies calculated with these constants is 1.32 Mc for all the transitions considered.

DISCUSSION

It has been seen that Eq. (1) can be used to yield calculated frequencies in very good agreement with the observed microwave frequencies of SO_2. However, no unique set of τ's can be obtained in this way, and the derived vibrational frequencies differ considerably from the observed infrared frequencies. At the same time it is seen that if the τ's are to be calculated from force constants derived from the vibrational frequencies, the force constants must be known with great accuracy because the resulting distortion frequencies depend critically on the values of the force constants used. This accounts for the difficulty Sirvetz[3] had in fitting the rotational spectrum of SO_2.

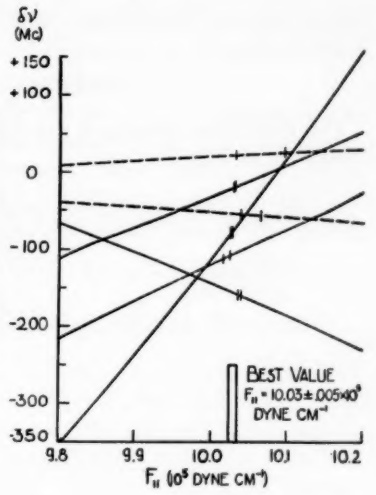

FIG. 1. Centrifugal distortion frequency shifts ($\delta\nu$) calculated for various values of F_{11}. The values are taken from Table III. The space between vertical lines give the uncertainty in F_{11} due to the uncertainty in $\delta\nu$. The solid curves were used to calculate the best F_{11} value.

The infrared data[12] were used to yield interrelations between the potential constants. With these interrelations the number of parameters to be determined in the calculations of centrifugal distortion effects was reduced to one. This parameter could be determined accurately by the analysis of the effect of centrifugal distortion in the rotational spectrum. (See Fig. 1.) In this way accurate values of the potential constants were obtained. The accuracy reported is somewhat deceptive since it assumes that the theory is exact when in fact such factors as the anharmonicity of the potential function have been totally omitted. The use of a, b, and c in Eqs. (5)–(7) rather than the equilibrium values of the moments of inertia and the use of nonequilibrium interatomic parameters also affects the results. Furthermore, the accuracy of the interrelations of the force constants determined from the infrared results are limiting factors on the final precision.

The methods used in this analysis are quite general and should be applicable to other cases although the calculations become quite formidable for more complicated molecules.

The author would like to thank Dr. Santiago Polo and Professor M. K. Wilson for their cooperation and aid in the final determination of the potential constants from the combined infrared-microwave data. He would also like to acknowledge the most valuable and frequent

[12] S. Polo and M. K. Wilson, preceding paper, J. Chem. Phys. 22, 900 (1954).
[13] See definition given in reference 12.

advice given throughout by Professor E. Bright Wilson, Jr.

APPENDIX

The distortion constants are related to the potential constants as follows:[9]

$$-R\tau_{aaaa}a^{-2}=2F_{11}^{-1}+\tan^2\theta F_{22}^{-1}-2\sqrt{2}\,\tan\theta F_{12}^{-1},$$

$$-R\tau_{bbbb}b^{-2}=2F_{11}^{-1}+\mathrm{ctn}^2\theta F_{22}^{-1}+2\sqrt{2}\,\mathrm{ctn}\theta F_{12}^{-1},$$

$$-R\tau_{aabb}a^{-1}b^{-1}=2F_{11}^{-1}-F_{22}^{-1}+\sqrt{2}(\mathrm{ctn}\theta-\tan\theta)F_{12}^{-1},$$

$$-R\tau_{abab}a^{-1}b^{-1}=2Mm_s^{-1}(1+2m_0m_s^{-1}\sin^2\theta)^{-2}F_{33}^{-1},$$

where

$$R=\tfrac{1}{2}d^2h^{-1}10^{-22}.$$

θ is one-half the O—S—O angle and d is the S—O distance expressed in angstrom units and $M=2m_0+m_s$. $\mathbf{F}^{-1}$ is the inverse of the potential constant matrix $\mathbf{F}$ given by Polo and Wilson.[12]

THE JOURNAL OF CHEMICAL PHYSICS VOLUME 22, NUMBER 5 MAY, 1954

The Photolysis of Ammonia at 1849A in a Flow System*

C. C. McDonald, A. Kahn, and H. E. Gunning
Department of Chemistry, Illinois Institute of Technology, Chicago 16, Illinois

(Received October 26, 1953)

An investigation has been made of the photolysis of ammonia at 1849A in a flow system at room temperature. The products of the reaction were found to be hydrazine, hydrogen, and nitrogen. The rate of decomposition of ammonia was independent of the linear flow rate but depended upon the ammonia pressure in the reaction zone. The fraction of ammonia decomposed which was recovered as hydrazine, while independent of ammonia pressure, increased markedly with increasing linear flow rate from zero in the static system to 0.84 at a linear flow rate of 1750 cm/sec.

It was found that the quantum yield of ammonia consumption under flow conditions was consistently higher by a factor of approximately two than for the static conditions at the same pressures.

A separate system was used to determine the extinction coefficient of ammonia at 1849A over the pressure range of the experiments. The value obtained was 1.21×10^3 liters-mole^{-1}—cm^{-1}.

A mechanism has been proposed which is in qualitative agreement with the observed facts.

INTRODUCTION

THE photolysis of ammonia has been extensively investigated in static systems, under which conditions the final products are nitrogen and hydrogen.[1] It is generally agreed that the primary process involves the formation of an amino radical and a hydrogen atom. The subsequent elementary reactions leading to the formation of stable products are apparently partially heterogeneous so that, despite many excellent studies made on the static photolysis, a definitive reaction mechanism has not been established.

Differences in the final products under flow conditions were found by Gedye and Rideal.[2] They obtained identifiable quantities of hydrazine as a third product in the flow system. Other investigators have also reported small or trace quantities of a reducing substance, presumably hydrazine, for the flow photolysis.[3,4]

The present investigation was undertaken in the hope that some additional insight could be obtained into the mechanism of the reaction by a systematic study under flow conditions. The shorter wavelength resonance line of mercury, at 1849A, was chosen for the photolysis since it falls within the region of maximum absorption for ammonia.[1] In view of the fact that no previous photochemical studies have been made on ammonia at this wavelength, it was necessary to measure the extinction coefficient of ammonia at 1849A. In addition, data on the static reaction, for comparison purposes, have been obtained. The details of the investigation follow.

EXPERIMENTAL

Apparatus for Measuring the Extinction Coefficient of Ammonia at 1849A

For these measurements an independent mercury-free high-vacuum system was used. The light source was a Hanovia "Biosteritron" mercury-in-quartz resonance discharge, operated by a Sola neon sign transformer with a 3000-volt, 30-ma secondary, coupled with a Sola constant voltage transformer. Two absorption cells were used,—a Hanovia Biosteritron cell, with path length of 0.02±0.003 cm, and an Aminco precision quartz absorption cell, style *F*, class 3, with a path length of 1.0002±0.0005 cm. A Westinghouse WL789

* This work was supported by Contracts N7-onr-32908, N7-onr-329 Task Order 3, and N7-onr-32912, with the U. S. Office of Naval Research, U. S. Navy.

[1] For an excellent discussion of the ammonia photolysis, reference should be made to *The Photochemistry of Gases*, W. A. Noyes, Jr. and P. A. Leighton (Reinhold Publishing Corporation, New York, 1941), 370 *et seq.*

[2] G. R. Gedye and E. K. Rideal, J. Chem. Soc. **135**, 1158 (1932).

[3] J. R. Bates and H. S. Taylor, J. Am. Chem. Soc. **49**, 2438 (1927).

[4] A. Koenig and T. Brings, Z. physik. Chem. Bodenstein Festband, 541 (1931).

platinum cathode phototube, which shows no response above 2100A, was used to measure the intensity at 1849A. The minute currents from the phototube were conveniently measured with a Beckman ultrohmeter. Satisfactory collimation was obtained by interposing sets of apertures between the lamp and cell, and between the cell and phototube. The lamp-cell-phototube assembly was rigidly mounted within a brass box, blackened on the inside with Kodacoat. During the measurements nitrogen was passed through the box to eliminate absorption of the 1849A radiation by oxygen in the optical path.

The absorption cell was connected to the manifold of the high-vacuum system. High vacua were achieved with a three-stage, all-glass, oil diffusion pump, backed by a Welch two-stage mechanical pump. Pressure measurements were made with an Alphatron radio-ionization gauge for the low pressure region, and a mercury manometer, with the mercury in each limb covered by a 10-cm layer of Octoil manometer fluid, for the high-pressure region.

The Light Source for the Photolyses

A mercury-in-quartz rare gas resonance lamp was designed for use as an internal source, eliminating thereby any air path between the light source and the reaction cell. The lamp is shown in Fig. 1. It consisted essentially of a U-tube fabricated of 10-mm i.d. Hanovia, S.R. grade optical quartz, with 1-mm walls. Thee lectrode arms were ring-sealed into the tubing attached to a male quartz 45/50 standard taper joint. One of the electrode arms was provided with a 5-mm i.d. sidearm for filling the lamp. The large male joint was fitted into a Pyrex reaction tube by means of a female, 45/50, Pyrex standard taper joint. The lamp, as finally used, contained a drop of mercury and 4 mm of argon. The discharge was maintained by a General Electric luminous tube transformer with a 5000-volt, 120-ma secondary. The primary input to the transformer was stabilized by interposing a Sola constant voltage transformer between the line and the transformer primary. The lamp intensity could be changed by varying the primary voltage with a Variac transformer.

The lamp is essentially dichromatic, emitting the two resonance lines of mercury at 1849A and 2537A. Since ammonia is transparent at 2537A, the discharge can be regarded as a monochromatic source at 1849A, with respect to ammonia. During operation the lamp temperature did not exceed 40°C. The design of the lamp as an internal source was dictated by the fact that 1849A radiation is strongly absorbed by oxygen, and furthermore it is strongly absorbed by quartz. It was therefore necessary to eliminate the air path and keep the thickness of quartz traversed by the radiation at a minimum to obtain photochemically-useful intensities. Such an arrangement lacks the flexibility of the external collimated source; for example, the zinc and cadmium spark sources in the 2100–2200A region used, among others, by Wiig[1] in his important series of studies on the static photolysis of ammonia.

The ammonia used throughout the investigation was the highest purity obtainable from the Matheson Company, East Rutherford, New Jersey. It had a minimum purity of 99.5 percent and gave no test for the presence of trace quantities of hydrazine or other reducing materials.

Flow Experiments at Atmospheric Pressure

The apparatus for these runs was briefly described in an earlier communication.[5] These preliminary runs were designed to ascertain whether the lamp would produce sufficient quantities of hydrazine for chemical characterization and for accurate analytical determination. The ammonia, at atmospheric pressure and at a measured flow rate was allowed to traverse the irradiated zone of the lamp-cell assembly, whereupon it condensed together with any hydrazine formed on a large cold finger containing dry ice-acetone slush at −78°C. The liquid ammonia-hydrazine mixture dripped from the cold finger into a removable collector below through a drip tube. Sufficient liquid ammonia was condensed in the collector before the lamp was turned on to cover the exit of the drip tube. Excess ammonia gas was vented into a fume hood at such a rate that the liquid level in the collector remained constant during an experiment. The flow rate of ammonia was measured by a capillary manometric flowmeter.

In one series of experiments, a trap containing hydrazine of determined purity was connected to the apparatus described above so that the hydrazine was injected into the flow stream at a point before the irradiation zone. This trap was maintained at 0°C by an ice-water bath. Both ammonia and nitrogen were used as carrier gases to sweep the hydrazine through the system so that its photolytic decomposition could be studied. The amount of hydrazine passed through the system was determined by the change in the weight of the trap containing hydrazine. The amount of hydrazine swept over was sufficiently large so that the

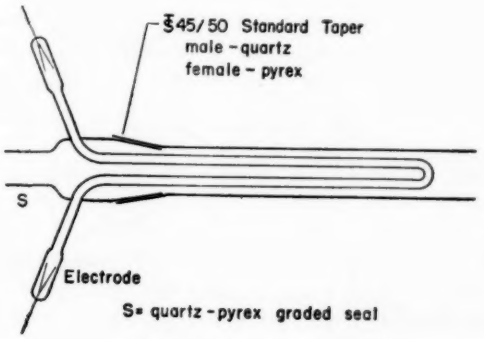

FIG. 1. The lamp system.

[5] A. Kahn and H. E. Gunning, J. Chem. Phys. 18, 392 (1950).

quantity of hydrazine produced by the photolysis of the ammonia carrier gas was negligible. When ammonia was used as the carrier gas, the effluent gases passed through liquid ammonia, but when nitrogen was used as the carrier gas the gases passed through a dilute solution of hydrochloric acid.

The hydrazine in the collector flask was analyzed by titration as described in the following section.

Flow Experiments in the Closed System

This part of the investigation was designed to study variations in the rates of formation of hydrazine, hydrogen and nitrogen as a function of reaction pressure and linear flow rate in the photolysis of ammonia. A large number of modifications of the original system were made during the course of the investigation to improve the precision of the analyses of the products and to obtain better control of the flow variables. The final modification of the apparatus, and that which was used for the main body of results to be reported here, is shown in Fig. 2.

The system was evacuated by a two-stage mercury diffusion pump, backed by a Welch Duoseal mechanical pump. Traps $T1$ and $T2$ were kept immersed in liquid nitrogen whenever stopcock A, leading to the photolysis system, was opened. Previous work had shown that under these conditions no mercury photosensitization occurs in the reaction system.

The lamp was operated at a current of 90 ma, using a Variac transformer to control the current. The pressure measurements were made with an Alphatron radio-ionization gauge, and an Octoil-mercury manometer as in the absorption measurements. The pressure measuring devices were connected to the system via stopcock B.

Variations in linear flow rates were achieved by altering the diameter of the orifice immediately below the lamp-cell assembly.

The mass flow of ammonia through the system was read from a calibrated Hoke flowmeter covering the range from 5 to 35 cu ft/hr for ammonia. The inlet needle valve was used to vary the mass flow rate.

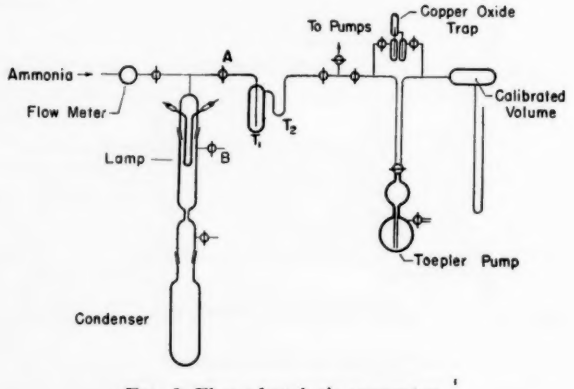

FIG. 2. Flow photolysis apparatus.

Before making an experiment the system was evacuated and the condenser flask was surrounded with liquid nitrogen. The system was flushed out with ammonia to saturate the walls and was evacuated again. The lamp was then turned on and warmed up to constant intensity. Isolation of the photolysis system was achieved by closing stopcock A. An electric timer was started simultaneously with the flow of ammonia through the reactor via the flow meter. The liquid nitrogen was maintained at a fixed level about the condenser flask in which the ammonia was condensed. At the end of the run the timer and lamp were shut off. Ammonia was allowed to flow for several more minutes while the walls of the reaction system were gently heated to drive off adsorbed hydrazine.

After the ammonia flow had been stopped, the condensables were frozen down for an additional hour. The noncondensables were transferred to a calibrated volume by the Toepler pump and their pressure in this calibrated volume was measured. Hydrogen was removed by combustion over cupric oxide, deposited on glass wool. The resulting water vapor was frozen out in a trap surrounded by liquid nitrogen. The pressure of the residual gas was measured in the calibrated volume and was assumed to be nitrogen. Repeated blank runs showed that no detectable quantities of noncondensables were present in the original ammonia.

For the hydrazine analysis, the condenser was removed and the ammonia allowed to evaporate until only a few ml remained. It was found that up to 10 percent of the hydrazine could be carried off with the voltatilizing ammonia. Tests showed that the loss of hydrazine could be prevented simply by allowing the effluent vapor to bubble through a trap containing distilled water. The residue in the condenser and the contents of the water trap were combined, diluted with water and acidified with concentrated hydrochloric acid. This solution was made up to a known volume and aliquots were titrated with 0.1 N potassium iodate following the method of Penneman and Audrieth.[6] Analyses made with synthetic solutions of hydrazine at concentrations similar to those obtained in the photolyses showed that the error in the titrations did not exceed 2 percent.

Static Experiments

To compare relative quantum yields under static and dynamic conditions, a series of runs was done in the above apparatus under static conditions.

A sample of ammonia was subjected to two trap-to-trap distillations, a middle fraction being saved in each case. The desired pressure of ammonia was admitted to the system from a storage reservoir and the photolysis was carried out on the static sample with the condenser at room temperature. At the end of a run

[6] R. A. Penneman and L. F. Audrieth, Anal. Chem. **20**, 1058 (1948).

the noncondensable and condensable products were analyzed in the same manner as in the flow runs. It should be noted that the results obtained with the ammonia, which had been subjected to two trap-to-trap distillations, were identical, within experimental error, to those found for the ammonia taken directly from the tank.

A static photolysis was also done on hydrazine to determine whether it was decomposed by 2537A radiation. A sample of Matheson's anhydrous hydrazine was thoroughly degassed and the hydrazine vapor, at 14 mm pressure, was admitted to an evacuated quartz tube attached to a mercury-free vacuum system. The tube was closed off from the liquid hydrazine and was exposed to the radiation from a mercury resonance lamp fashioned of Vycor 7910. The Vycor glass removes 1849A radiation but transmits 2537A radiation. At the end of the experiment, a sidearm from the tube was immersed in dry ice and acetone for 30 minutes. The noncondensable products were transferred by Toepler pump to a calibrated volume and measured. These gases were then passed through a trap at liquid nitrogen temperature to remove ammonia and the residual noncondensable gas was analyzed for nitrogen and hydrogen as in the ammonia photolysis experiments.

TABLE I. Production of hydrazine in the photolysis of ammonia at 1849A in an open flow system at atmospheric pressure.

Mass flow rate moles/hr	Lamp current ma	Rate of hydrazine formation moles/hr $\times 10^4$
7.7	30	0.32
13.4	30	0.39
13.4	115	0.85

RESULTS

The Extinction Coefficient of Ammonia at 1849A

The extinction coefficient ϵ is defined by the relation

$$I_t \equiv I_0 10^{-\epsilon c d},$$

where I_0 and I_t are the intensities of the 1849A radiation incident on and transmitted through the quartz absorption cell containing ammonia. The optical path length through the ammonia at a concentration of c moles/liter is d cm.

In Fig. 3, the results of absorption measurements using the Aminco cell with $d=1.0002$ cm are shown as a plot of $\frac{\log I_0/I_t}{d}$ *vs* c. The left-hand ordinate figures and the lower abscissa figures represent the results for the 1.000-cm cell. The concentration range corresponds to ammonia pressures from 1 to 40 mm. Within experimental error the points fall on a straight line the slope of which gives a value of ϵ of 1.21×10^3 liters-moles^{-1} cm^{-1}.

The absorption of ammonia in the range from 40 to 200 mm was measured with the Hanovia quartz cell which had a d value of 0.02 ± 0.003 cm. The values of ϵ calculated therefrom agree within experimental error with the value reported for the 1.000-cm cell. Beer's law is therefore obeyed at least over the range from 1 to 200 mm pressure of ammonia.

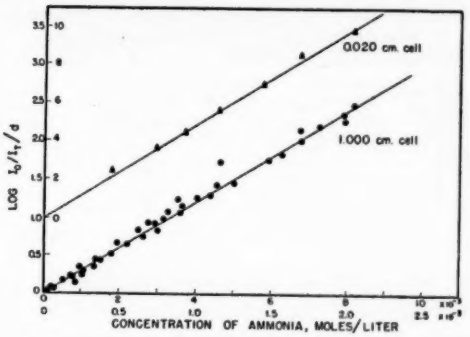

FIG. 3. The extinction coefficient of ammonia at 1849A.

From the value, 1.21×10^3 liters-moles^{-1} cm^{-1} for the extinction coefficient, and the geometry of the reactor, it was estimated that a minimum ammonia pressure of 8–10 mm was required for absorption of more than 95 percent of the 1849A radiation.

Preliminary experiments on the absorption of 1849A radiation by hydrazine indicate that the extinction coefficient is about six times as large as the corresponding ammonia value.

Flow Experiments at Atmospheric Pressure

The results obtained in these experiments are summarized in Table I.

The hydrazine formed in the reaction was characterized by preparing the derivative with benzaldehyde. The benzalazine obtained had a melting point of 91–92°C in agreement with reported values for the melting point of this compound. Furthermore, mixed melting point determinations, made by admixing a pure sample of benzalazine, showed no depression of the melting point.

These experiments showed that the system was capable of producing hydrazine in sufficient quantities for accurate analysis. The rates of hydrazine formation are in agreement with those in the closed systems if the pressure and linear flow rates used are considered. The linear flow rate in these experiments was about 7 cm/sec.

Flow Photolysis of Hydrazine

The results of the experiments in which hydrazine was swept through the irradiated zone by a carrier gas are recorded in Table II.

The amount of hydrazine passing the lamp per unit time was about 100 times greater in these experiments than the amount produced in unit time in the ammonia photolysis. It should be emphasized that the hydrazine may be decomposed by the 2537A radiation from the

TABLE II. The photolysis of hydrazine in the presence of a carrier gas at atmospheric pressure.

Mass flow rate of carrier gas moles/hr	Carrier gas	Hydrazine flow rate moles/hr $\times 10^4$	Hydrazine decomposed (percent)
13.4	NH_3	49	24
13.4	NH_3	32	20
13.4	N_2	46	27

lamp as well as by the 1849A radiation. When the runs were repeated with the lamp off, no hydrazine was decomposed. The accuracy of the measurement of the hydrazine decomposed is estimated to be $\pm$ 5 percent.

These runs, while of a qualitative nature, show that hydrazine is extensively decomposed on flowing through the irradiated zone.

The Flow Photolysis of Ammonia in the Closed System

The mass flow rate of ammonia was converted to volume flow at the temperature and pressure of the reaction zone. This quantity divided by the cross-sectional area of the irradiated zone gave the linear flow rate of the ammonia.

In the range of mass flow rates and ammonia pressures used the linear flow rate depends essentially on the resistance to flow of the tubing between the lamp and the ammonia condenser. Thus, the linear flow rate could be varied by changing the diameter of an orifice in this tubing. With a given orifice size, the pressure rise in the reaction zone on increasing the mass flow rate was just that required for the linear flow rate to remain constant. Fluctuation of the calculated linear flow rate for one orifice size at various mass flow rates in the results may therefore be attributed to error in the readings of the mass flow rates and reaction pressures.

The linear flow rates were varied from 7.05 to 11 150 cm/sec. The contact time for the gas in the irradiated zone obtained by dividing the length of the irradiated zone (26 cm) by the linear flow rate varied from 3.69 to 2.33×10^{-3} sec.

In the analysis of the products, the amounts of the total noncondensable gas, the nitrogen and the hydrazine produced per unit time were measured. Two quantities of interest can be calculated from these data using the stoichiometric equations

$$2\,NH_3 \rightarrow N_2 + 3\,H_2$$

$$2\,NH_3 \rightarrow N_2H_4 + H_2.$$

1. The apparent amount of ammonia decomposed is given by twice the sum of the hydrazine and nitrogen produced.

2. The fraction of the ammonia decomposed which is recovered as hydrazine is given by the ratio of the hydrazine to the sum of the hydrazine and nitrogen.

Since the total noncondensable gas minus the nitrogen gives the quantity of hydrogen produced, the amount of hydrazine produced can be calculated from the gas analysis only since from the stoichiometry

$$(N_2H_4) = (N_2 + H_2) - 4(N_2).$$

It was found that more accurate values for the amount of hydrazine produced were obtained by calculation from the gas analysis in the above manner than by recovery and titration of the hydrazine. Both procedures were followed in each run, but the value for the hydrazine used in calculating the ammonia decomposed and the percentage of the decomposed ammonia recovered as hydrazine was the value calculated from the gas analysis. The error in the recovery and titration of the hydrazine was shown to arise largely from loss of hydrazine in the evaporation of the liquid ammonia. When the ammonia was bubbled through water in the later runs, and this water was added to the residual hydrazine, the measured and calculated amounts of hydrazine agreed within about 5 percent.

A summary of the results of the flow photolysis of ammonia in the closed system is given in Table III. The runs are grouped according to the orifice size (i.e., with the same linear flow rate). Within the groups, the mass flow rate and hence the reaction pressure was varied over the range permitted by the apparatus.

It is evident that the percentage of the decomposed ammonia which is recovered as hydrazine (percent hydrazine) is essentially independent of the reaction pressure at any given linear flow rate but increases with the linear flow rate. The percentage conversion to hydrazine and linear flow rate values were averaged in each group. Figure 4 is a plot of percentage conversion to hydrazine *vs* log (linear flow rate) based on these averaged results. A relationship, which is approximately linear, is obeyed up to a linear flow rate of about 1750 cm/sec, at which value the conversion is about 84 percent. Runs 31 and 32 were carried out at considerably higher linear flow rates, but the conversion did not increase. To achieve these high linear flow rates, these runs had to be carried out at such low reaction pressures that there was incomplete absorption of the 1849A radiation. Small amounts of noncondensable gas were therefore obtained and the error in alalysis was larger

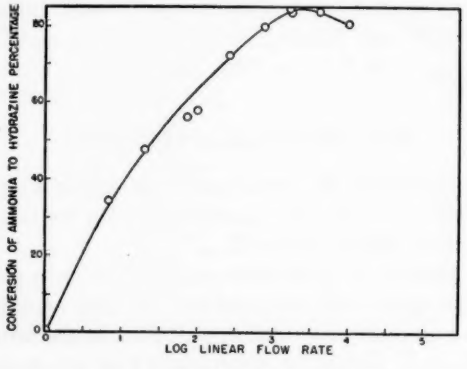

FIG. 4. Conversion of ammonia to hydrazine.

TABLE III. Results from the photolysis of ammonia at 1849A in a closed flow system.

Run No.	Mass flow rate moles/hr	Reaction pressure mm	Linear flow rate cm/sec	Total gas per hr moles $\times 10^4$	N_2 per hr moles $\times 10^4$	Measured hydrazine per hr moles $\times 10^4$	Ammonia decomp. per hr moles $\times 10^4$	Percent hydrazine
30	12.7	560.	7.05	13.15	2.91	1.27	8.82	34.2
28	12.7	188.	21.0	14.07	2.87	2.30	10.92	47.4
25	12.7	52.2	75.3	15.61	2.90	3.50	13.82	58.
26	25.3	104.	76.2	13.23	2.59	3.11	10.92	52.6
27	38.2	159.	76.6	11.62	2.18	2.71	10.16	57.2
24	6.33	22.5	87.7	16.00	2.85	4.45	14.90	61.7
20	19.0	56.8	104.	14.62	2.62	4.06	13.52	61.2
21	31.7	94.0	105.	12.85	2.34	3.23	11.66	59.9
23	38.2	112.	106.	11.91	2.35	3.00	9.72	51.7
22	44.3	131.	106.	11.75	2.33	...	9.52	51.0
18	12.7	13.8	285	15.12	2.35	4.80	16.40	71.4
19	19.0	20.3	292	15.21	2.38	4.90	16.14	70.6
13	25.3	26.9	291	15.35	2.45	5.19	16.00	69.4
14	31.7	34.5	279	13.99	2.15	4.78	15.08	71.6
15	38.2	40.6	285	13.46	2.06	5.04	14.56	71.8
16	44.3	48.2	284	12.88	1.82	4.56	14.84	75.5
5	19.0	6.91	803	12.80	1.56	5.53	16.75	81.5
6	25.4	11.6	685	13.97	1.60	6.34	18.34	82.5
8	38.2	15.7	755	14.39	1.69	6.34	16.70	76.0
9	44.3	19.2	721	14.42	1.64	7.08	17.84	79.3
29	44.3	8.	1730	15.07	1.59	8.03	20.60	84.7
2	44.3	7.5	1850	12.82	1.25	7.55	18.14	86.2
3	44.3	7.5	1870	12.96	1.06	6.96	16.94	82.2
31	12.7	0.5→2.5	7810→1580	4.30	0.48	...	5.72	83.3
32	25.3	0.70→0.85	11 150→9200	3.28	0.41	0.66	4.10	80.1

than in the other runs. Thus it is not clear whether the percent hydrazine would increase to 100 percent with high linear flow rates or whether it does in fact level off at about 84 percent.

The amount of ammonia decomposed in each run was plotted against reaction pressure in Fig. 5. The points fall on a smooth curve, independent of the linear flow rate of the run. Thus, the relative quantum yield for ammonia decomposition is independent of linear flow rate and has a constant value of about 10×10^{-4} mole/hr from 100 mm to 560 mm pressure of ammonia in the reaction zone (Run 30 at 560 mm pressure is not shown in Fig. 5). At lower pressures, the relative quantum yield rises rapidly to a value almost twice that at 100 mm. Below about 10 mm pressure there is incomplete absorption of the 1849A radiation, and therefore the ratio falls off.

For the runs reported in Table III, the surface-to-volume ratio in the zone between the lamp and the orifice was 0.95 cm^{-1}. Two experiments were made with this zone packed with Pyrex rods, thereby increasing the surface-to-volume ratio to 8.65 cm^{-1}. The results for these runs are given in Table IV together with the comparable data for the unpacked system.

While these experiments, in which the surface-to-volume ratio was changed, were not extensive, the results indicate that neither the amount of ammonia decomposed nor the percentage conversion to hydrazine was greatly affected by packing the volume immediately following the radiation zone.

STATIC PHOTOLYSIS OF AMMONIA AT 1849A

The summary of the analyses of the noncondensable products of a series of static photolyses of ammonia is given in Table V. The condensable residue gave no test for hydrazine.

The relative quantum yield for ammonia decomposition is plotted as a function of pressure in Fig. 5. The

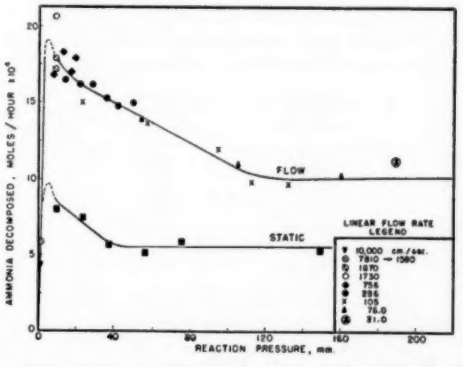

FIG. 5. Rate of ammonia decomposition as a function of pressure.

TABLE IV. Effect of altering surface-to-volume ratio.

Run No.	Mass flow rate moles/hr	Reaction pressure mm	Linear flow rate cm/sec	Total gas/hr moles $\times 10^4$	N_2/hr moles $\times 10^4$	Measured N_2H_4/hr moles $\times 10^4$	Ammonia decomposed per hr moles $\times 10^4$	Percent hydrazine
33	25.3	15.8	495	14.76	1.83	7.04	18.30	80.0
Unpacked		15.8	495				17.00	77.0
34	31.6	56	159	12.92	2.00	5.32	13.84	71.1
Unpacked		56	159				13.75	67.5

same pressure variation as in the flow runs was observed. At comparable pressures the relative quantum yield in the static system is about half the value obtained in the flow system.

The fact that the nitrogen is almost exactly 25 percent of the total noncondensable product indicates the absence of hydrazine and shows that the gas analysis is reliable.

The products of the static photolysis of hydrazine at 14 mm pressure by 2537A radiation were in exact agreement with the following equation.

$$2\,N_2H_4 \rightarrow 2\,NH_3 + H_2 + N_2.$$

In a similar experiment with no radiation, no hydrazine was decomposed. The light intensity at 2537A was 4×10^{-4} einsteins/min, and 5×10^{-6} moles of hydrazine were decomposed per minute. If the quantum yield of the hydrazine decomposition was about 2, as found by Wenner and Beckman,[7] the rate of radiation absorption was 2.5×10^{-6} einsteins/min. From the cell geometry, the percentage absorption of the 2537A radiation, and the hydrazine pressure, the extinction coefficient of hydrazine at 2537A was estimated to be 5 liters-mole^{-1} cm^{-1}.

DISCUSSION

Any discussion of the mechanism of the secondary reactions in the photolysis of ammonia at 1849A must be in consonance with the following facts:

(1) The rate of ammonia decomposition in the flow system is independent of linear flow rate.

(2) From 560 mm to 100 mm pressure the rate of ammonia decomposition is constant. At lower pressures the rate rises to a value which is almost twice the rate at 100 mm pressure. Below 10 mm pressure the rate of decomposition decreases again because of incomplete absorption of the 1849A radiation.

(3) The percentage conversion of the ammonia to hydrazine is independent of the reaction pressure but increases almost linearly with the logarithm of the linear flow rate. This conversion increases from zero in the static system to 84 percent at a linear flow of 1750 cm/sec, but may not increase further at greater flow rates.

(4) The rate of ammonia decomposition in the flow system is about twice that in the static system at the same pressure. This relationship holds over the whole of the pressure range investigated.

(5) A tenfold increase in the surface-to-volume ratio in the zone immediately following the irradiated zone has very little effect on the rate of ammonia decomposition or on the conversion to hydrazine.

(6) The extinction coefficient for ammonia at 1849A is 1.21×10^3 liters-moles^{-1} cm^{-1} between 1 mm and 200 mm pressure. The extinction coefficient of hydrazine at 1849A is about six times that for ammonia and at 2537A has a value of about 5 liters-moles^{-1} cm^{-1}.

(7) When hydrazine was passed through the flow system at a pressure some one hundred times greater than the partial pressure of hydrazine in the ammonia photolysis experiments, twenty-five percent of this hydrazine was decomposed by photolysis.

(8) The static photolysis of hydrazine at 2537A obeyed the equation

$$2\,N_2H_4 \rightarrow 2\,NH_3 + N_2 + H_2.$$

(9) If the static quantum yield for ammonia decomposition at 100 mm is about 0.25 as proposed by Wiig and others,[1] then the quantum yield in the flow system approaches unity at low pressures.

The investigation of the flow photolysis of ammonia has shown that hydrazine and hydrogen can be the major products of the reaction. The percentage of the decomposed ammonia that is recovered as hydrazine depends only on the linear flow rate of the ammonia through the system. An increase in the linear flow rate dilutes the radicals and products of the reaction with ammonia and also causes them to spend a shorter time in the irradiated zone. Dilution of the radicals and

TABLE V. The static photolysis of ammonia at 1849A.

Ammonia pressure mm	Total gas per hr moles $\times 10^4$	Percent N_2 in total gas	Ammonia decomposed per hr moles $\times 10^4$
10	16.14	25.0	8.07
24	15.12	25.0	7.56
38	11.41	25.0	5.71
57	10.60	24.8	5.30
76	11.80	···	5.90
150	10.52	···	5.26
264	11.70	···	5.70

[7] R. R. Wenner and A. O. Beckman, J. Am. Chem. Soc. **54**, 2787 (1932).

hydrazine would decrease the decomposition of hydrazine by radical attack if the radicals also disappear on collision with the wall. A decrease in the hydrazine partial pressure and a shorter contact time in the irradiated zone would lead to less photolysis of the hydrazine by the 1849A and 2537A radiation. It seems probable, therefore, that the relatively large amounts of nitrogen obtained at low linear flow rates arise from the decomposition of hydrazine either by photolysis or by radical attack. Some nitrogen may also arise by an independent reaction path since the minimum conversion of ammonia to nitrogen was 15 percent.

The over-all quantum yield of ammonia decomposition appears to approach unity at low pressure in the flow system. It is probable, therefore, that the primary quantum yield for the photolysis of ammonia into hydrogen atoms and amino radicals is unity. The lower experimental quantum yields then arise from ammonia reforming steps. These steps are pressure dependent but are independent of the linear flow rate. Since the conversion to hydrazine does depend on the linear flow rate, the decomposition of hydrazine in the flow system does not produce ammonia. The hypothesis that the hydrazine produced is partially decomposed in the flow system by photolysis was examined. It was shown that, when relatively large amounts of hydrazine were swept through the system by nitrogen or ammonia, twenty-five percent of the hydrazine was decomposed. Moreover, 2537A radiation decomposed hydrazine to produce ammonia, hydrogen, and nitrogen.

First the possibility of hydrazine photolysis by the 1849A radiation was investigated. The assumption was made that the rate of ammonia decomposition (1.5×10^{-7} moles/sec) at 100 mm pressure in the static system represented a quantum yield of 0.25. The 1849A radiation intensity incident on the flowing gas was therefore 6.0×10^{-7} einsteins/sec. Next, it was necessary to calculate the maximum possible partial pressure of hydrazine in the flow stream at various linear flow rates. It was assumed that the initial step was

$$NH_3+h\nu_{1849}\rightarrow NH_2+H,$$

with a quantum yield of one and that all the amino radicals recombined to give hydrazine. The maximum rate of production of hydrazine was, therefore, 3.0×10^{-7} moles/sec. From the volume flow rate of the ammonia through the reaction zone, it is possible to calculate the volume in which this amount of hydrazine was distributed, assuming a uniform distribution, and hence the partial pressure of the hydrazine in the flow stream. This partial pressure varied from 4.8×10^{-2} mm at a linear flow rate of 7 cm/sec to 2.5×10^{-5} mm at a flow rate of 10 000 cm/sec.

If the ammonia and hydrazine are in competition for the 1849A radiation, the absorption equation is given by the following equation:

$$I_t=I_0\cdot10^{-(\epsilon_1c_1d+\epsilon_2c_2d)}.$$

1 represents ammonia
2 represents hydrazine

The fraction of the 1849A radiation available to the hydrazine is approximately $\epsilon_2c_2/\epsilon_1c_1$. For the experiment with the highest partial pressure of hydrazine in the flow stream this fraction is 5×10^{-4}.

Thus, 3×10^{-11} einsteins/sec were available to the hydrazine, and if the quantum yield for hydrazine decomposition was unity, less than 0.01 percent of the hydrazine produced was photolyzed.

The mercury lamp puts out about ten times as much radiation at 2537A as at 1849A and at this wavelength the ammonia does not compete with the hydrazine for the radiation. The possibility of photolysis of the hydrazine by 2537A radiation was therefore examined. Using a value of 6×10^{-6} einsteins/sec as the input intensity of 2537A radiation, the extinction coefficient from the static photolysis of hydrazine (5 liters-mole^{-1} sec^{-1}), and the calculated partial pressure of hydrazine in the slowest linear flow rate experiment, it was calculated that less than 1 percent of the hydrazine could be decomposed by the 2537A radiation. This result was not in conflict with the experiments in which hydrazine was decomposed when swept through the lamp zone in a carrier gas because in these experiments the partial pressure was about one hundred times greater than in the ammonia photolysis experiments. The same method of calculation, when applied to these hydrazine flow runs, predicts that 26 percent of the hydrazine should be decomposed.

As a result of the above calculations it seems reasonable to say that the photolysis of hydrazine in the flow system cannot account for the decomposition of hydrazine and thus the hydrazine must be decomposed as a result of radical attacks.

In view of the experimental results and calculations discussed above, the following reaction mechanism was adopted as the basis for a qualitative explanation of the flow photolysis of ammonia:

(1) $NH_3+h\nu_{1849}\rightarrow NH_2+H$

(2) $H+NH_2\rightarrow NH_3^*$

(3) $NH_3^*+M\rightarrow NH_3+M$

(4) $NH_3^*\rightarrow NH_2+H$

(5) $NH_2+NH_2\rightarrow N_2H_4$

(6) $N_2H_4+H\rightarrow N_2H_3+H_2$

(7) $N_2H_3+H\rightarrow N_2+2\,H_2$

(8) $N_2H_3+N_2H_3\rightarrow 2\,NH_3+N_2$

(9) $H+\text{wall}\rightarrow\frac{1}{2}\,H_2+\text{wall}.$

According to this mechanism, if hydrazine is a product of the reaction, there is an excess of hydrogen atoms which diffuse to the wall and form molecular hydrogen. The amino radicals are removed rapidly by combination to hydrazine, whereas the homogeneous recombination of hydrogen atoms requires a three body collision and is therefore negligible. Since there is an excess of hydrogen atoms, the attack of amino radicals on hydrazine and hydrazyl radicals is unimportant. Moreover, reaction (8) is unimportant compared to reaction (7).

The assumption has already been made that the quantum yield of reaction (1) is unity. If (8) is neglected, the only ammonia reforming reaction is (3) which is pressure dependent. The flow experiments indicate that, at pressures higher than 100 mm, reaction (3) is much more important than reaction (4). At lower pressures, reaction (4) becomes important and the over-all quantum yield approaches unity.†

Reaction (3), the ammonia reforming step, depends on the hydrogen atom concentration which in turn depends on the extent of reactions (6) and (7). It will be shown below that the latter reactions depend only on the linear flow rate. Thus, the hydrogen atom concentration and hence the net rate of ammonia decomposition should depend on the linear flow rate. This effect was not found experimentally and the explanation may be that in the range of linear flow rates used the total concentration of hydrogen atoms did not vary by more than 25 percent because of removal in reactions (6) and (7).

As the linear flow rate is increased, the reaction products are diluted with ammonia causing a reduction of the partial pressure of hydrazine in the flow stream. Reactions (6) and (7) become less important compared to reaction (9) as the hydrazine partial pressure is decreased. Thus the conversion to hydrazine increases with linear flow rate and is independent of the reaction pressure.

The experiments in which the surface-to-volume ratio was increased in the zone following the lamp indicate that most of the reaction is complete in the irradiated zone. If this were not the case, the increase in the rate of hydrogen atom removal would result in an increase in the net rate of ammonia decomposition and in the conversion to hydrazine. A small increase may be noted in these experiments but the increase is scarcely greater than the experimental error.

In the static photolysis of ammonia, the mechanism must explain the fact that no hydrazine is obtained and that the rate of ammonia decomposition is lower than in the flow runs although it has the same pressure dependence. The partial pressure of hydrazine is probably much higher in the static system than in the flow system and the hydrazine formed must remain in the reaction zone. Hence, reaction (6) is very important and causes a decrease in the hydrogen atom concentration. Reaction (8) is then able to compete successfully with reaction (7) and, since reaction (8) results in ammonia reformation, the net rate of ammonia decomposition is decreased. This effect is pressure independent but reaction (3) is also in operation so that the rate of ammonia decomposition has the same pressure dependence as it has in the flow experiments. It is possible that the photolysis of hydrazine may also become important in the static system.

While the mechanism which has been presented is in qualitative agreement with the experimental facts, it is quite possible that complex homogeneous and heterogeneous reaction steps are involved which would give a more complete explanation of the results which have been obtained in the ammonia photolysis. Since the apparatus used in this investigation was somewhat different from that used by other investigators, a quantitative comparison with their results does not seem justified.

ACKNOWLEDGMENTS

The authors wish to thank Dr. C. Luner of this department for assistance in the measurement of the extinction coefficient of ammonia. They also wish to thank Dr. H. Oppenheimer, Michael Reese Hospital, Chicago, for the loan of apparatus used in these measurements.

† The authors would like to thank one of the referees of this paper who very aptly pointed out that our experimental results could also be satisfactorily described in terms of a mechanism wherein reactions (1) and (4), are replaced by the following:

$$(1)\quad NH_3 + h\nu_{1849} \rightarrow NH_2 + H$$
$$(10)\quad NH_3 + h\nu_{1849} \rightarrow NH_3^*$$
$$(11)\quad NH_3^* + M \rightarrow NH_3 + M$$
$$(12)\quad NH_3^* \rightarrow NH_2 + H.$$

Curie Point Transitions in Phosphides and Arsenides of Manganese*

KEITH H. SWEENY† AND ALLEN B. SCOTT
Department of Chemistry, Oregon State College, Corvallis, Oregon
(Received March 9, 1953)

The relative permeability of several alloys of manganese with phosphorus and arsenic have been measured in the region of the Curie point. The alloys were heated and cooled very slowly to eliminate, as much as possible, irreversible effects. The composition range investigated included alloys of higher phosphorus and arsenic content than have previously been investigated. Ferromagnetism in the phosphorus alloys appears to be due to the compound MnP over the range 27–58 mole percent *P*, and the magnetic and density transitions exhibit no temperature hysteresis. The temperature hysteresis in the magnetic transformation of manganese arsenide is confirmed. The Curie point-composition relation for the arsenides is discussed and evidence presented for the existence of a manganese-rich compound, perhaps Mn_8As_7, rather than a solid solution of Mn in MnAs.

INTRODUCTION

ALLOYS of manganese with the elements of the nitrogen group have received much attention because they are in many cases ferromagnetic.[1,2] Some of the Curie points of these alloys are in the neighborhood of room temperature; processes which take place very rapidly at the elevated Curie points of the more common ferromagnetic materials may be slow enough in the manganese alloys so that time effects are of great importance.

Several definite compounds of manganese and phosphorus have been reported. Berak and Heumann[3] present evidence for the existence of MnP, Mn_3P_2, Mn_2P, and Mn_3P. Guillaud and Creveaux[4] studied the magnetic properties of manganese-phosphorus alloys as a function of composition in the range 17–33.7 percent *P*, and found the Curie temperature (25°) to be independent of composition. They were unable to prepare MnP by direct combination of the elements, but they found that the saturation magnetization increased with increasing phosphorus content, and they obtained a value for the atomic moment of Mn in MnP by extrapolation.

Guillaud[5] reports the definite compounds MnAs, $Mn_{29}As_{21}$ or Mn_4As_3, Mn_2As, and Mn_3As_2. Mn_2As was not ferromagnetic. The highest content of As obtained by direct combination of the elements was 49.54 mole percent As.

Bates and his co-workers studied the specific heat,[6] resistivity,[7] thermoelectric and thermogalvanic potentials[8,9] of manganese arsenide passing through the Curie temperature, and Whitmore[10] studied the specific heat of manganese phosphide. Each of these properties undergoes an abrupt change in magnitude or in temperature coefficient at or near the magnetic transformation temperature. Smits, Gerding, and Vermast[11] studied volume changes of MnAs passing through the Curie temperature, and observed a temperature hysteresis.

Guillaud and Wyart[12] found the Curie transition of MnAs to be irreversible. Spontaneous magnetization disappeared at 45° when the alloy was warmed and reappeared at 34° as the sample was cooled. X-ray diffraction measurements showed that a lattice contraction occurred at 45°, which was not reversed until the temperature was reduced to 34°. Measurements with a dilatometer[5] confirmed these observed volume changes.

Guillaud[13] has recently shown that the magnetization data for MnAs can be interpreted as being due to a change from ferromagnetism to antiferromagnetism.

The experiments reported in this paper were undertaken to extend the range of information about Curie transitions in the alloys of manganese with phosphorus and arsenic, to include alloys richer in phosphorus and arsenic than could be prepared by previous methods. The transitions were made to occur very slowly to determine whether irreversible effects previously noted could be eliminated. The time involved in making such measurements upon a single alloy was so great that the number of compositions studied was necessarily limited, but it was decided that extended studies on a few alloys might reveal as much useful information as a more rapid investigation of a larger number of compositions. Measurements of relative permeability, density, thermoelectric potential, and thermogalvanic potential were made in a range of temperatures including the Curie point of each of the alloys.

Rhenium antimonide was prepared and found to be nonferromagnetic according to qualitative tests.

* Published with the approval of the Oregon State Monographs Committee as Research Paper No. 239, Department of Chemistry, School of Science. From the Ph.D. thesis of Keith H. Sweeny.
† Du Pont Fellow in Chemistry 1948–1949.
[1] S. Hilpert and T. Dieckman, Ber. deut. Chem. Ges. **44**, 2378 (1911).
[2] E. Wedekind and T. Veit, Ber. deut. Chem. Ges. **40**, 1259 (1907).
[3] J. Berak and T. Heumann, Z. Metallkunde **41**, 19 (1950).
[4] C. Guillaud and H. Creveaux, Compt. rend. **224**, 266 (1947).
[5] C. Guillaud, Ann. phys. [12] **4**, 671 (1949).
[6] L. F. Bates, Proc. Roy. Soc. (London) **117A**, 680 (1928).
[7] L. F. Bates, Phil. Mag. **6**, 593 (1928).
[8] L. F. Bates, Phil. Mag. **13**, 393 (1932).
[9] L. F. Bates, Phil. Mag. **16**, 657 (1933).
[10] B. G. Whitmore, Phil. Mag. **7**, 125 (1929).
[11] Smits, Gerding, and Vermast, Z. Physik. Chem., Bodenstein Festband, 357 (1931).
[12] C. Guillaud and J. Wyart, Compt. rend. **219**, 393 (1944).
[13] C. Guillaud, J. phys. et radium **12**, 223 (1951).

EXPERIMENTAL

Preparation of Materials

The composition range of greatest interest to us was that lying near the equiatomic ratio and extending toward low manganese content. Several methods of preparation have been described for these alloys, including direct combination by fusion, reaction of solid manganese with vapors of the other element entrained in H_2, metathesis (e.g. the reaction of $MnCl_3$ with PH_3 in ether solution), reduction of the phosphates or arsenates of manganese in aqueous solution, reaction of powdered manganese with the boiling trichlorides, and electrochemical reduction of fused phosphates or arsenates. Each of these methods was tried and was rejected as unsuitable for the preparation of alloys rich in arsenic or phosphorus.

Arrivaut[14] mentioned the possibility of making the arsenide by passing $AsCl_3$ vapors over manganese at 400°. This process has the advantage of being carried out at atmospheric pressure and thus avoiding explosions such as were frequently encountered during experiments in which the elements were fused in sealed tubes. Further, the reagents can be obtained in a state of high purity; it also became apparent that the composition could be regulated by varying the reaction temperature to give alloys of arsenic or phosphorus content considerably greater than 50 mole percent. The effect of the reaction temperature on the phosphorus or arsenic content of the alloys is shown in Table I.

Electrolytic manganese, supplied by the Electromanganese Corporation and containing less than 0.001 percent iron, was ground to approximately −100 mesh, mixed with about 10 volumes of cp MgO to serve as a mechanical diluent, and brought to the desired temperature in a tubular combustion furnace. PCl_3 or $AsCl_3$, Baker's cp grade, containing less iron than the manganese was vaporized and passed over the manganese; most of the residual vapors were trapped in an ice trap before entering the hood. The reaction proceeds with incandescence. In the absence of MgO, a crust of $MnCl_2$ formed on the surface and prevented further reaction. The product was leached twice with dilute HCl, washed repeatedly with distilled water, and dried.

TABLE I. Effect of tube furnace temperature on alloy composition.

Temperature of furnace °C	Mn−P alloys Mole percent phosphorus
370	58.2
460	56.5
660	50.5
	Mn−As alloys Mole percent arsenic
460	57.3
660	50.8

[14] G. Arrivaut, Chimie & Industrie Special No. Sept. 1925, 284.

The arsenic alloys were kept at temperatures above 45° (the approximate Curie point) during all these procedures and were finally stored at room temperature. The phosphorus alloys were stored at −30°. In this way, all of the samples passed through the Curie point only once and were stored well below the transition temperature.

The alloys were dissolved in boiling aqua regia and analyzed for Mn by standard methods.[15] The other element was determined by difference, since P and As were partially lost by volatilization during the dissolving process. Qualitative tests for chloride, magnesium, and silica all were negative. The iron content, as evaluated by the colorimetric thiocyanate method, was about the same as in the original manganese. The arsenic alloys were found to contain 47.3, 50.8, and 57.3 mole percent As, and the phosphorus alloys contained 47.1, 50.5, 56.5, and 58.2 mole percent P.

An alloy of Re and Sb was prepared by direct combination, in the proportion 1:1 by weight, at 800° under a layer of $BaCl_2$.

Temperature Control

A five-gallon water thermostat was regulated by means of the circuit of Coates[16] adapted to American components. It permitted bringing the bath to any desired temperature in the range 10° to 60° by the variation of a resistor comprising one arm of an ac bridge; the temperature then remained constant within 0.02°. The second arm of the bridge was a thermistor whose resistance varied from 283 ohms at 0° to 41 ohms at 50°. Temperature was measured by means of a copper resistance thermometer of No. 40 Formvar-covered wire, calibrated at the ice point, the transition temperature of sodium sulfate, the boiling point of pure ethanol, and the steam point.

Permeameter

A conventional heterodyne-beat apparatus[17] for measuring dielectric constants was modified to permit the measurement of relative permeabilities on small samples of alloys while in the thermostat. The coil in the tunable circuit was replaced by a coil of 500 turns, 13 mm in diameter, 5 cm in length, and of about 300μH inductance. The coil was shielded by a cylindrical copper shield filled with mineral oil to improve heat transfer when placed in the thermostat. The sample, contained in a small test tube and brought to the temperature of the thermostat, was placed in the coil without being removed from the bath. Both the coil

[15] N. H. Furman, *Scott's Standard Methods of Chemical Analysis* (D. Van Nostrand Company, Inc., New York, 1939), 5th ed., pp. 559–560, 574.

[16] G. E. Coates, J. Sci. Instr. **21**, 86 (1944).

[17] J. Y. Chien, J. Chem. Educ. **24**, 494 (1947).

and the variable precision-type 1500$\mu\mu$f condenser used to tune the circuit to the frequency of the reference oscillator were connected to the oscillator by coaxial cable.

Since the inductance of the empty coil unit varied considerably with temperature, the relative permeability of the alloy at a particular temperature was expressed in terms of ΔC, the change in capacitance necessary to rebalance the circuit upon insertion of the sample. Differences in the degree of packing of the samples introduced some error into actual magnitude of ΔC, but should not affect the shape of ΔC-temperature curves for a particular sample. No absolute calibration was made, but ΔC for powdered carbonyl nickel ranged from 115 to 254 $\mu\mu$f, depending on particle size, which shows that some of the alloys have a permeability approaching that of nickel. On the other hand, 30 percent $NiCl_2$ solution which is paramagnetic, gave a ΔC of only 1.3 $\mu\mu$f. The ΔC values for the alloys could be reproduced within 0.1 $\mu\mu$f for a given sample without repacking, so that this method was particularly satisfactory for measuring small temperature and time effects on a particular sample of alloy.

Results

The effect of temperature upon the permeability of manganese-phosphorus alloys is shown in Fig. 1. Points designated as "equilibrium" values were obtained by repeatedly observing ΔC at each temperature until it became constant and then moving to the next temperature. In most cases well removed from the Curie temperature, equilibrium was established in about an hour after each temperature change, but in the transition region equilibrium was reached more slowly. In one case four days were required. For the alloy of composition approximating MnP, 12 days were required for the heating and cooling cycle; for the others, from 5 to 9 days were required. However, only a few minutes were required at any temperature for the permeability to approach to within a few percent of the equilibrium value as was shown by repeating the measurements more rapidly. This was done by heating or cooling the alloy at a constant rate so as to traverse the entire cycle in about four hours. The permeability was measured every 10 minutes (every 5 minutes in the transition zone). It will be seen there are no marked differences between the equilibrium values and those obtained during the rapid cycle except that the slope of the ΔC-temperature curves are somewhat less in the transition zone for the rapid cycle. The transition temperature is the same for heating and cooling even for the rapid transition, and is virtually identical for the four alloys.

The transition temperature may conveniently be taken as the temperature for which $d\Delta C/dT$ is a maximum and the average value for the phosphorus alloys is 18°. The Curie point is frequently defined in another way[18] and the value chosen will vary by several degrees depending upon the definition used.

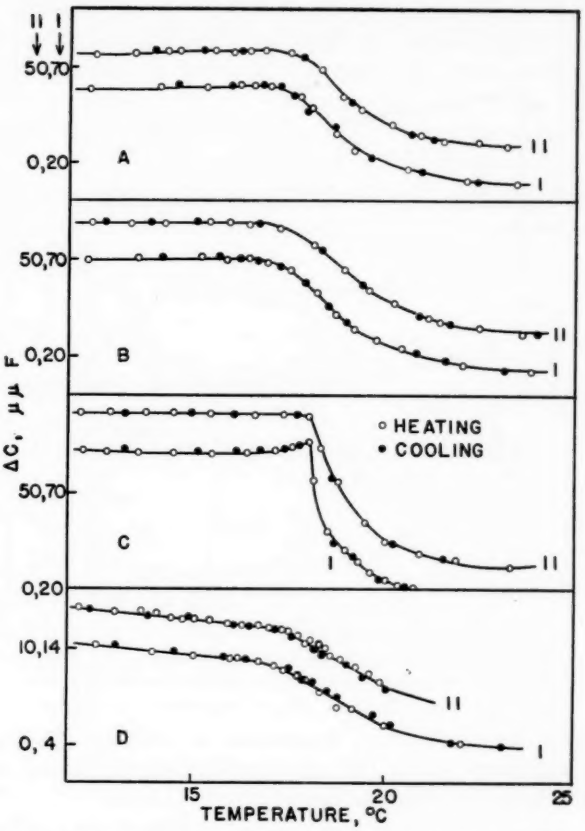

FIG. 1. Relative permeability of magnaese-phosphorus alloys. Composition, mole percent P: A: 58.2; B: 56.5; C: 50.5; D: 47.1. Curves I: Equilibrium measurements. Curves II: Rapid cycle.

The data for the 47.1 mole percent P alloy are not quantitative, as insufficient alloy was available for filling the sample tube, and the measured values of ΔC were roughly corrected by multiplying by the ratio of the volume of the tube to the volume of the material.

Figure 2 shows the results of permeability measurements on the arsenic alloys. The curves were all obtained by the "equilibrium" method, as the arsenic alloys approached equilibrium much more slowly, and from 16 to 29 days were required for the complete cycle. It is doubtful if true equilibrium was reached at any temperature, even though constancy with time was observed, as the transition temperature displays the marked temperature "hysteresis" noted by Guillaud and others. Of particular interest is the appearance of two transitions in each of the alloys of 47.3 and 57.3 mole percent As and of only one in the alloy which was nearly of equiatomic proportions.

Measurements of the density, thermoelectric potential, and thermogalvanic potential were also made; in every case anomalous changes were observed in the neighborhood of the Curie temperature but the changes

[18] R. M. Bozorth, *Ferromagnetism* (D. Van Nostrand Company, Inc., New York, 1951).

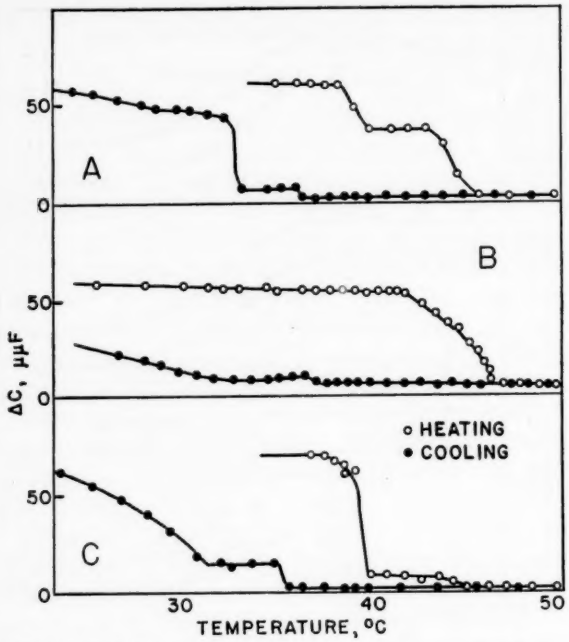

FIG. 2. Relative permeability of manganese-arsenic alloys. Composition, mole percent As: *A*: 57.3; *B*: 50.8; *C*: 47.3.

were not sufficiently systematic to warrant drawing conclusions about the relation of these properties to the loss of ferromagnetism.

DISCUSSION

Phosphorus Alloys

The results for these alloys may be combined satisfactorily with those of Guillaud and Creveaux. Their highest phosphorus composition was 45.1 mole percent; our lowest was 47.1 percent. In the range above 27.4 percent, the transition temperature is found to be independent of composition at least to 58.2 mole percent P. This datum is in disagreement with the observation of Nowotny[19] that Mn_2P (33 mole percent P) is ferromagnetic and has a Curie temperature of about 40°. The Curie point reported by Guillaud and Creveaux, 25°, was evidently obtained by the method of Weiss and Forrer[20] and should be several degrees higher than the temperature of maximum decrease in the permeability which we find to be 18°. Hilpert and Dieckman[1] also observed the rapid decrease of permeability with temperature at 18° for their phosphorus alloy. It may be concluded that in the entire range of compositions now investigated, only one ferromagnetic compound exists above 10° and that the alloys are mixtures of this compound with nonferromagnetic forms.

Guillaud and Creveaux observed that the saturation magnetization increased with phosphorus content up to the limits of their composition somewhat below that for the compound MnP. We find the relative permeability and the abruptness of the permeability decrease to be distinctly greater in MnP than in compositions to either side, so that it is likely that the ferromagnetism is due to the definite equiatomic compound. Further studies with compositions in the range MnP—$MnP_{1.3}$ would be desirable, as a composition of higher relative permeability may lie in this range. No definite compounds have been reported, however, in this range, and the constancy of the transition temperature rules out the possibility of solid solutions.

Arsenic Alloys

Guillaud[5] has presented a diagram showing the variation of the atomic saturation moment of manganese and the Curie points of its arsenic alloys as a function of composition up to 49.54 mole percent As. The results observed for our lowest arsenic composition, 47.4 mole percent, show some interesting differences from Guillaud's results, which we believe are due to time effects made apparent by the extended period over which our measurements were performed.

In the range 47–50 mole percent As, Guillaud found a regular increase in the Curie temperature with increasing arsenic content, which he interpreted as showing that a solid solution of Mn in MnAs exists in this composition range. On the other hand, we find two abrupt changes in permeability for the alloy of 47.4 mole percent As, and only one for the alloy nearly corresponding to MnAs. This indicates that at 47.4 mole percent As there are two ferromagnetic forms rather than a solid solution. One of these is MnAs, whose Curie temperature agrees quite well with the value of 45° given by Guillaud, and the other may be the alloy of 47 percent As for which Guillaud found a Curie point of 40°. This composition would correspond most nearly to the formula Mn_8As_7.

For both of the forms there is a temperature hysteresis of about 9°, the transitions occurring upon cooling at about 36° for MnAs and 31° for the manganese-rich alloy. Since at 47.4 mole percent the mixture would be about 90 percent Mn_8As_7, it is to be expected that the 40° fall and 31° rise in permeability are much more pronounced than the changes at 45° and 36°. With increasing arsenic content the changes for MnAs will become more important; upon passing through the transition more rapidly the two steps would merge and the Curie temperature would appear to shift to higher temperatures gradually with increasing arsenic content. This may explain the results of Guillaud.

The addition of excess arsenic to MnAs results in the appearance of another phase of Curie point about 40°; lacking data for alloys richer in arsenic than 53.7 mole percent, we cannot establish the composition of the phase. It is significant that both the arsenic-rich and manganese-rich phases have Curie points and hysteresis behavior which are virtually identical and which are not much different from those of MnAs.

[19] H. Nowotny, Z. Elektrochem. **49**, 254 (1943).
[20] P. Weiss and R. Forrer, Compt. rend. **178**, 1670 (1924).

It appears that the lattice characteristics of MnAs responsible for its ferromagnestism are very little altered by the incorporation of the excess element and are more or less independent of the nature of the excess element.

ACKNOWLEDGMENT

The authors wish to express their gratitude to the E. I. du Pont de Nemours Company for the assistance given to one of us (K.H.S.) in the form of a fellowship, which made possible a major part of this work. The authors are also grateful to the Research Corporation for the assistance given one of us (K. H. S.) during the investigation of the methods of preparation of the alloys. The assistance of Professor J. J. Witkopf and Mr. Ben Ballard in the design and testing of the thermoregulator is gratefully acknowledged.

THE JOURNAL OF CHEMICAL PHYSICS VOLUME 22, NUMBER 5 MAY, 1954

Photon-Induced Diffusion in Thin Films and Single Crystals of Potassium Iodide

C. J. DELBECQ AND P. H. YUSTER
Chemistry Division, Argonne National Laboratory, Lemont, Illinois
(Received February 1, 1954)

Thin films of potassium iodide have been prepared at both room and liquid nitrogen temperatures. Absorption spectra are presented which show that films deposited at liquid nitrogen temperature are quite disordered, but after warming to room temperature are very similar to those films deposited at room temperature. Evidence is given which shows that in thin films and also in single crystals of potassium iodide diffusion is promoted by the absorption of light. It is proposed that diffusion is caused by point thermal spikes at the absorbing centers.

INTRODUCTION

RECENTLY Seitz,[1] using data from Martienssen,[2] has proposed that in certain instances the absorption of light by a crystal can cause diffusion. Work in this laboratory on the change of absorption spectra of thin films and single crystals of potassium iodide by the exposure to light can be interpreted on the basis of the above-stated hypothesis.

I. THIN FILMS

Apparatus and Experimental Procedure

The thin films used in these experiments were formed in a modified evacuated Dewar flask[3] by vaporization from a single crystal of potassium iodide onto a suitable substrate. The evaporating furnace, which consisted essentially of a coiled filament of platinum wire, was mounted in place of the beryllium window while the substrate was mounted in the crystal holder. The substrates used in these experiments were fused quartz plates and single crystals of potassium bromide and lithium fluoride; these substrates were kept either at room temperature or liquid nitrogen temperature during the vaporization. Absorption measurements were taken at liquid nitrogen temperature (except where otherwise noted) with a Cary Recording Spectrophotometer. A General Electric AH-4 mercury lamp, operating at 135 v without the glass envelope, was used to irradiate films.

Results

Figures 1, 2, and 3 show some typical absorption spectra of thin films of potassium iodide when they are formed and treated as described. It has been found that the shape of the absorption curve of a thin film, obtained by the evaporation of potassium iodide on a particular substrate held at liquid nitrogen temperature, depends to some extent on the rate at which the evaporation is carried out. Figure 1(a) shows the absorption of a film formed by fairly slow evaporation of potassium iodide on quartz held at liquid nitrogen temperature (the slower the evaporation the more pronounced the hump in the long wavelength tail of the fundamental band). It should be noted that the peak absorption occurs at 213 mμ. The effect on the absorption spectrum of warming the film for 5 min successively to -165, -135, and -90°C is shown in Fig. 1(a) through (d); and Fig. 1(e) shows the absorption spectrum of the fundamental band with peak at 214.2 $m\mu$ after the film was allowed to stand for 15 hours at room temperature. There is a continuous decrease in the long wavelength tail and a continuous growth and sharpening of the fundamental band through the warming process and for at least an hour after room temperature has been reached.

Figure 2(a) also corresponds to a potassium iodide film evaporated fairly slowly on a quartz plate held at liquid nitrogen temperature (Type I film). When such a film is warmed to about -135°C and irradiated with

[1] F. Seitz, Phys. Rev. **89**, 1299 (1953).
[2] W. Martienssen, Nachr. Akad. Wiss. Göttingen, Math.-physik. Kl. 11, 111 (1952).
[3] See J. Chem. Phys. **18**, 888 (1950), for description of modified Dewar flask used.

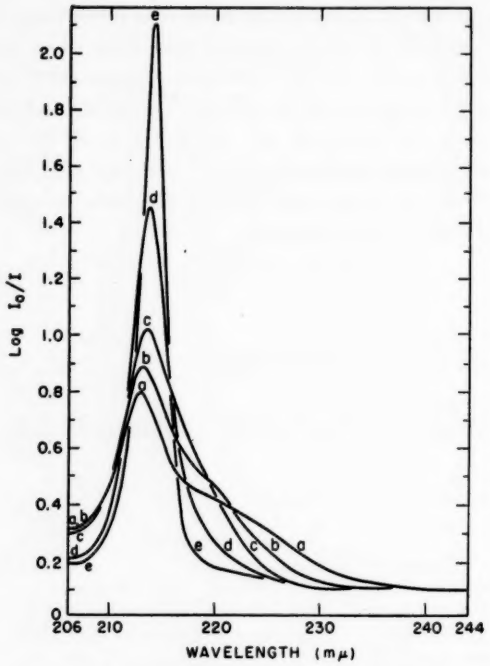

FIG. 1. Absorption spectra of potassium iodide film at liquid nitrogen temperature after the following treatments: (a) potassium iodide evaporated on quartz plate held at liquid nitrogen temperature during the evaporation. (b) Film warmed to −165°C and held at this temperature for 5 min. (c) Film warmed to −135°C and held at this temperature for 5 min. (d) Film warmed to −90°C and held at this temperature for 5 min. (e) Film at room temperature for 15 hours.

the unfiltered light of a General Electric AH-4 mercury lamp, a relatively broad band develops with peak at 216.5 mμ [Fig. 2(b) and (c)]. An investigation was carried out to determine the relative effectiveness of light of different wavelengths in inducing these alterations in the absorption spectrum. By using appropriate filters, it was found that light of wavelength less than 220 mμ was of approximately the same importance as light of wavelength between 220 and 226 mμ in causing these changes in absorption, and that light of wavelength

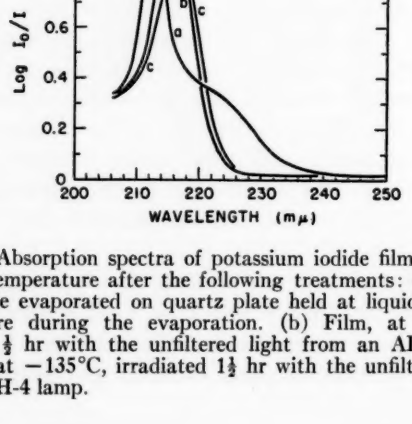

FIG. 2. Absorption spectra of potassium iodide film at liquid nitrogen temperature after the following treatments: (a) potassium iodide evaporated on quartz plate held at liquid nitrogen temperature during the evaporation. (b) Film, at −135°C, irradiated ½ hr with the unfiltered light from an AH-4 lamp. (c) Film, at −135°C, irradiated 1½ hr with the unfiltered light from an AH-4 lamp.

greater than 226 mμ was ineffective by comparison. If a Type I film is held at liquid nitrogen temperature during the irradiation, the hump in the long wavelength tail decreases while the absorption in the vicinity of 214 mμ increases to give an absorption spectrum similar to Fig. 1(c); the broad band at 216.5 mμ does not appear under these conditions.

Figure 3(a) shows the absorption spectrum of a film of potassium iodide which had been evaporated on a quartz substrate held at room temperature (Type II film). When such a film is cooled to −135°C and irradiated with the unfiltered light from a General Electric AH-4 mercury lamp, the sharp fundamental band with peak at 213.8 mμ disappears and a broad band is again formed at 216.5 mμ. It has been found that in this case the change in absorption is caused in the main by light of wavelength less than 220 mμ and that light of longer wavelength is of relatively little importance. When a film showing the broad absorption band at 216.5 mμ (produced as described in either this paragraph or the preceding one) is warmed to room temperature for an hour, the broad band disappears and the relatively sharp fundamental band appears with peak at 214.2 mμ.

The shapes of the absorption curves described above did not vary appreciably for the different substrates, quartz, lithium fluoride, and potassium bromide; however, the positions of the peaks were somewhat affected by the substrate used (Table I). The half-width of the first fundamental band is about 0.2 ev at room temperature and about 0.1 ev at liquid nitrogen temperature and appears to be independent of the substrate. The half-width of the "new" band with peak at 216.5 mμ is about 0.3 ev at liquid nitrogen temperature.

Discussion

It is generally accepted that the first fundamental absorption band in the alkali halides is due to an electronic transition within halide ions located in relatively perfect regions of the crystal lattice, and that the long wavelength tail of the fundamental band is due to perturbed transitions within halide ions—the perturbations being due to the fact that these halide ions are in less perfect regions of the crystal, for example near vacancies, vacancy aggregates, dislocations, surfaces, impurities, etc. When dealing with thin films of potassium iodide of reasonable purity, we can omit consideration of impurity imperfections since their concentrations are so low that, in the region of the fundamental band, the halide ion absorption overshadows all other absorption. In Fig. 1(a) the absorption near the peak is due to iodide ions in relatively perfect regions of the lattice, and the absorption in the hump on the long wavelength side of the peak is due to iodide ions located near vacancies, vacancy aggregates, etc.

Thus it appears that in a Type I film there are a large number of imperfections "frozen in," although in

certain regions through the film there has been appreciable diffusion of ions resulting in a relatively perfect lattice. It has been observed that the more rapid the evaporation of the potassium iodide onto the film the less prominent the hump on the long wavelength side of the fundamental band. This fact seems readily understandable, since a higher rate of deposition of ions results in higher local temperatures in the surface of the film and consequently the ions have a chance to rearrange themselves and one would expect fewer imperfections to remain in the film. The changes which take place in a film, such as the one represented in Fig. 1, as it warms up also presumably result from diffusion and the formation of a more nearly ideal structure as the temperature rises.

It has been pointed out in the previous section that a Type II film has an absorption peak at 213.8 mμ, while a film which is either formed on a substrate held at liquid nitrogen temperature or irradiated with ultraviolet light at −135°C gives, upon warming to room temperature, an absorption peak at 214.2 mμ. Evidently warming a Type I film or one irradiated at −135°C to room temperature does not reduce disorder as effectively as do the high local temperatures which obtain during the deposition of a Type II film. A Type I film has an absorption peak at 213 mμ. In view of the behavior of the absorption spectrum of such a film on warming (see Fig. 1) one would tend to identify the transition associated with the 213-mμ peak with the transition giving rise to the first fundamental band, but then one must attempt to explain the shift in wavelength. It is possible, in the case of the Type I films, that (1) the transition corresponding to the absorption peak does take place in an iodide ion in a nearly perfect lattice but that there is some perturbation which is sufficiently uniform through the region to preserve the peak but which shifts it to shorter wavelength, or (2) in some regions the lattice is more nearly perfect than in the Type II film.

In the formation, at −135°C, of the broad band with peak at 216.5 mμ represented in Figs. 2(c) and 3(c), a diffusion process again seems to occur which involves (1) the dissolution of the vacancy aggregates giving a more nearly uniform distribution of vacancies through the film and (2) the diffusion of vacancies from the surface into the film.

The symmetry (disregarding the short wavelength tail which is probably due to overlapping with the broadened second fundamental band) of this "new" absorption band suggests that the absorption is due to a single well-defined center (i.e., each absorbing center and its neighborhood is identical to every other). In order to investigate the plausibility of this suggestion, let us consider the α center[4] and its associated absorption. The α band, which is due to the absorption by a halide ion adjacent to a negative ion vacancy, is a fairly narrow, symmetrical, bell-shaped band; consequently, it seems probable that the perturbing influence of the negative ion vacancy does not extend appreciably beyond the nearest halide ion neighbors. One can probably extrapolate from the case of α centers in single crystals to the case of imperfections in films and say that the perturbing influence of vacancies, and vacancy aggregates in films, does not extend appreciably farther than two lattice spacings. Then, since it is clear that in the case of the film represented in Figs. 2(c) and 3(c) essentially every iodide ion is perturbed, one concludes that the concentration of vacancies in such a film is of the order of 10 percent. With such a high concentration of vacancies it is unlikely that many single positive or negative ion vacancies would be able to exist because of attractive forces, and it seems probable, therefore, that the vacancies are in the form of small vacancy aggregates (pairs, triplets, quartets, etc.). It is difficult to imagine an arrangement of these small vacancy aggregates which will give rise to a single well-defined absorbing center, and thus the broad band probably consists of several narrower absorption bands. It may be that the strong rise observed on the

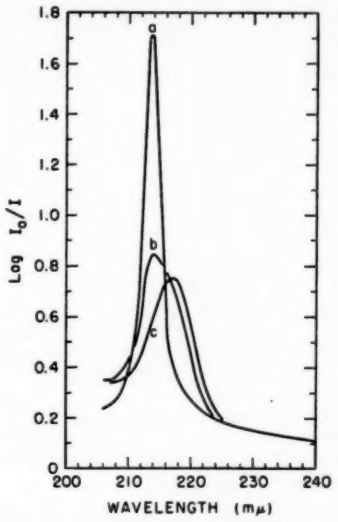

FIG. 3. Absorption spectra of potassium iodide film at liquid nitrogen temperature after the following treatments: (a) potassium iodide evaporated on quartz plate held at room temperature during the evaporation. (b) Film, at −135°C, irradiated 15 min with the unfiltered light from an AH-4 lamp. (c) Film, at −135°C, irradiated 40 min with the unfiltered light from an AH-4 lamp.

TABLE I. Characteristics of potassium iodide thin films deposited on various substrates. Data for liquid nitrogen temperature except where noted.

Substrate	LiF	KBr	Quartz
First fundamental band of KI	213.5 mμ (220.5 mμ at room temp.)	213 mμ	213.8 mμ
"New" band	216 mμ		216.5 mμ

[4] Delbecq, Pringsheim, and Yuster, J. Chem. Phys. **19**, 574 (1951).

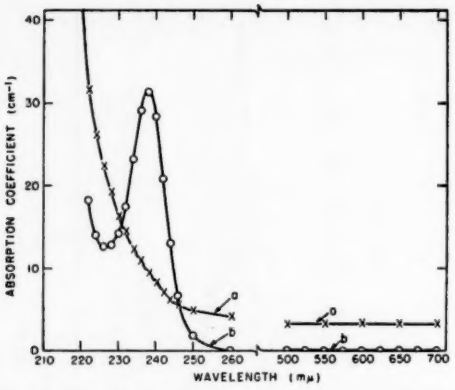

FIG. 4. Absorption spectra of pure and irradiated potassium iodide. (a) Absorption spectrum of pure potassium iodide single crystal. (b) Absorption introduced by one-half hour exposure at −170°C to unfiltered AH-6 lamp.

short wavelength side of the β band,[5] when F centers are produced photochemically in a potassium iodide single crystal at temperatures below dry ice temperature, is due to the presence of small vacancy aggregates.

Seitz has suggested a mechanism to account for the bleaching of the α band in single crystals when irradiated with α light; the same mechanism can be used to account for the photodiffusion of vacancies in thin films. The mechanism is as follows: (1) in the case of an iodide ion near a vacancy or vacancy aggregate, the rearrangments of the adjacent ions and the lattice vibrations subsequent to absorption of a photon by the iodide ion may give a sufficiently high local temperature to cause diffusion; and the transition from the excited to the ground state, particularly in the case of a radiationless transition, may set up sufficiently energetic lattice vibrations to allow diffusion to take place; and (2) in the case of an iodide ion in a perfect lattice, absorption of a photon would produce an exciton which, upon decay after being trapped at a vacancy, vacancy aggregate, or surface, may produce (as above) a sufficiently energetic thermal spike to cause diffusion.

The temperature of the film plays an important part in photodiffusion. As Fig. 3 shows, a Type II film irradiated at −135°C with the unfiltered light of an AH-4 lamp will change its absorption considerably.

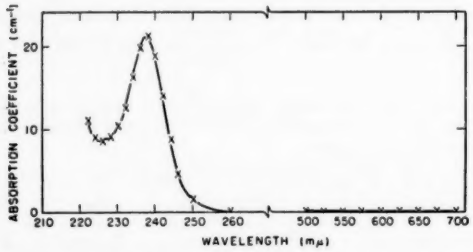

FIG. 5. Absorption introduced into a potassium iodide single crystal at −170°C by exposure to AH-6 lamp plus Corning No. 7910 filter for two hours.

[5] Compare Figs. 2 and 3 of reference 4.

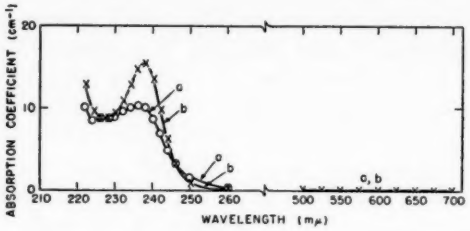

FIG. 6. Absorption introduced into a potassium iodide single crystal at −170°C by exposure to AH-6 lamp plus Corning No. 9863 filter .(a) One-half hour. (b) Two hours.

However, if one performs exactly the same experiment but with the film held at the temperature of liquid nitrogen, no large change in absorption occurs. (Actually, the height of the peak does decrease somewhat and there is some broadening of the band, but the change which takes place, relative to the change which occurs at −135°C, is very small.) There is no appreciable difference in the width of the absorption band of a film made at room temperature and measured either at −135°C or liquid nitrogen temperature, so that the above difference in behavior cannot be attributed to a difference in the amount or wavelength of light absorbed in the two films. Evidently at −135°C the ambient thermal energy coupled with the energy obtained from the point thermal spike is sufficient to cause extensive diffusion of vacancies, while at liquid nitrogen temperature this is not the case.

II. SINGLE CRYSTALS

Procedure and Results

Single crystals of potassium iodide grown in this laboratory by the Kyropoulos method as well as crystals obtained from the Harshaw Chemical Company were exposed to the unfiltered light of a GE AH-6 high-pressure mercury arc lamp. Fig. 4(b) shows the absorption introduced into the crystal by a one-half-hour exposure at −170°C to the above light. A very considerable change has occurred in the absorption spectrum of the crystal, and the α band is formed at 238 mμ.

Experiments were also performed in which filtered light was used to irradiate potassium iodide crystals. Figures 5 and 6 show the effects of irradiations using the AH-6 lamp plus Corning filters No. 7910 ($\lambda > 2200$A) or 9863 ($\lambda > 2300$), respectively. In both cases an α band is formed; however, the time necessary to obtain

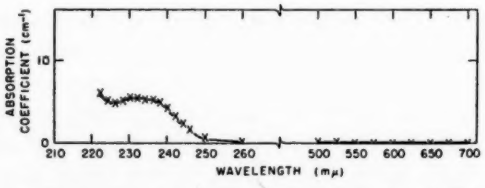

FIG. 7. Absorption introduced into a potassium iodide single crystal at −170°C by exposure to monochromatic light (about 235 mμ) for five and one-half hours.

equivalent heights of the α band is increased because of absorption of light by the filters. Figure 7 shows the effects of irradiation using monochromatic light. Light from an AH-6 lamp was sent through a Central Research Laboratory Double Monochromator, and since intensity was a problem, very wide slits were used on the monochromator. The energy distribution of the emergent light used to irradiate the crystals was roughly 20 mμ wide with a peak at about 235 mμ.

Discussion

The changes in absorption of potassium iodide crystals upon exposure to ultraviolet light are quite similar to those obtained when the same crystals are exposed to x-rays. However, one important difference in the former is the absence of F centers in the spectrum. In the case of the exposure to unfiltered AH-6 light, the incident light contains wavelengths that could bleach any F centers if they were formed. It is thus not clear from the above-mentioned experiment whether the α band is formed directly or is formed due to bleaching of F centers. It is also not clear whether the α centers are distributed throughout the bulk of the material or whether they are a skin effect due to absorption directly in the fundamental band. If the α centers were only in a very thin surface layer, one would expect that irradiation from both sides of the crystal would double the absorption change. Such an effect is not observed. From the results shown in Figs. 5 and 6, it was established that the light most effective in the formation of the α band was in the neighborhood of 235 mμ. As can be seen from the absorption of a potassium iodide crystal [Fig. 4(a)], the above wavelength light should be absorbed in the bulk of a crystal of 1 mm and should give, as is observed, an α band which is distributed throughout the whole crystal. In an attempt to determine whether α centers are formed directly or via F centers, a crystal was irradiated with ultraviolet light free from visible light. Figure 7 shows the results of such an experiment. No F centers were formed, and although the change in absorption is not as great as that observed in Figs. 4, 5, and 6, it is clear from a comparison of a short exposure of a potassium iodide crystal to filtered ultraviolet [Fig. 6(a)], that a similar change in absorption is taking place.

It is clear that, in the experiments with single crystals, diffusion has been promoted by the absorption of light, since no free negative ion vacancies (α centers) are present in the untreated crystal, while after irradiation with ultraviolet light, free negative ion vacancies are present. In single crystals as well as in thin films, this photodiffusion process is sensitive to temperature. The production of α centers is greater in a crystal maintained at -150°C than in one irradiated at liquid nitrogen temperatures. However, it is not so clear by what mechanism these vacancies are formed. Since no F centers are observed to form, it is assumed that no electron is freed into the conduction band. Also, since the α band is formed by light absorbed in the tail of the fundamental band, the original act is not one of formation of an exciton which can move through the lattice, be trapped at a dislocation or vacancy cluster, and either generate or free vacancies. It is believed, therefore, that a process occurs in single crystals similar to that previously discussed for thin films in which light is absorbed in a halide ion perturbed by a dislocation or vacancy cluster, a thermal spike is developed, and a vacancy or vacancies are freed.

THE JOURNAL OF CHEMICAL PHYSICS VOLUME 22, NUMBER 5 MAY, 1954

A Theoretical Evaluation of the Normal Frequencies of Vibration of the Ethylene Oxide Molecule*

SAMUEL A. STONE
Bradford Durfee Technical Institute, Fall River, Massachusetts
(Received April 27, 1953)

A theoretical evaluation of the normal frequencies of vibration of the ethylene oxide molecule is made. The evaluation is accomplished by assuming a generalized valence force field containing twelve force constants. Values for two of the constants are assumed, and the values of the other ten are calculated so as to give values of the computed frequencies in good agreement with observed values.

1. THE STRUCTURE

THE ethylene oxide molecule consists of seven atoms: one oxygen atom, two carbon atoms, and four hydrogen atoms. We assume for this molecule the following structure.[1] The two carbon atoms and the oxygen atom form an isosceles triangle. Two hydrogen atoms are attached to each carbon atom in such a way that the CH_2 planes are perpendicular to the C_2O plane. Table I and Fig. 1, which give internuclear distances

* Details of the calculations and of the methods used in the evaluation of the frequencies as well as calculations of the modes of vibration (not submitted here) are contained in a thesis submitted (1953) by the author to the Boston University Graduate School in partial fulfillment of the requirements for the Ph.D. degree.

[1] G. Herzberg, *Infrared and Raman Spectra* (D. Van Nostrand Company, Inc., New York, 1945), p. 340.

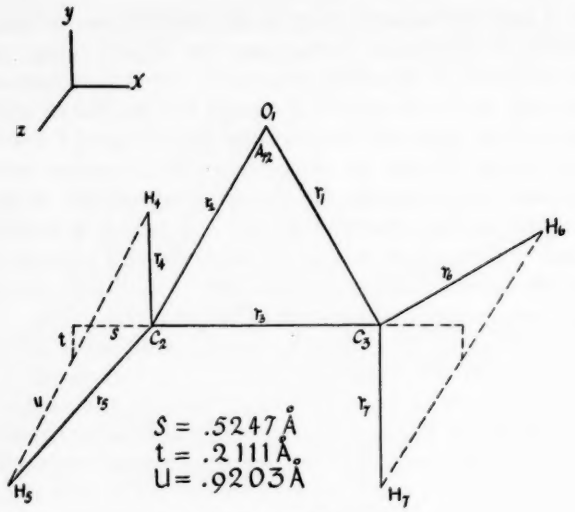

FIG. 1. The C_2H_4O molecule.

and angles, were constructed from data given by Cunningham *et al.*[2]

2. THE SYMMETRY

The ethylene oxide molecule belongs to the C_{2v} point group. The character table for this point group as well as a method for evaluating the number of vibrations in each species of vibration are given by Rosenthal and Murphy.[3] A method for determining the activity or inactivity of the infrared and Raman fundamentals is given by Bhagavantam.[4]

The ethylene oxide molecule has four species of vibration: A_1, A_2, B_1, B_2. The A_1 species has 5 fundamental frequencies; the A_2 species has 3; the B_1 species has 4; and the B_2 species has 3. The fundamental frequencies of the A_2 species are inactive in the infrared but these fundamentals are Raman active. The fundamental frequencies of the other three species are both infrared and Raman active.

3. THE POTENTIAL ENERGY FUNCTION

Since ethylene oxide resembles cyclopropane in its geometrical structure as well as in other respects,[5] it seems logical to assume a force field for ethylene oxide

TABLE I. Internuclear distances and angles for C_2H_4O molecule.

CO distance	1.4363A
CC distance	1.4728A
CH distance	1.0802A
Angle OCC	59°9′.4
Angle COC	61°41′.2
Angle HCH	116°51′
Angle OCH	114°38′
Angle CCH	119°3′.7

[2] Cunningham, Boyd, Gwinn, and LeVan, J. Chem. Phys. **17**, 211 (1949). A more complete report appears in Cunningham, Boyd, Myers, Gwinn, and LeVan, J. Chem. Phys. **19**, 676 (1951).
[3] J. E. Rosenthal and G. M. Murphy, Revs. Modern Phys. **8**, 317 (1936).
[4] S. Bhagavantam, *The Scattering of Light and the Raman Effect* (Chemical Publishing Company, Brooklyn, New York, 1942).
[5] A. D. Walsh, Trans. Faraday Soc. **45**, 184 (1949).

TABLE II. The B_2 vibration frequencies.

Computed frequencies in cm^{-1}	Observed frequencies in cm^{-1}	Force constants in dyne ÷ cm × 10^5
685	685	$K_{CH}=4.91$
1172	1164	$H_{OCH} \div (OC)(CH)=0.411$
3062	3062	$H_{CCH} \div (CC)(CH)=0.267$

similar to one used successfully for cyclopropane. Saksena[6] obtained fairly good results for cyclopropane by using a generalized valence force field involving cross products. For ethylene oxide this type of force field takes the following form:

$$\begin{aligned}2V=&K_{OC}(\Delta r_1^2+\Delta r_2^2)+K_{CC}(\Delta r_3^2)\\&+K_{CH}(\Delta r_4^2+\Delta r_5^2+\Delta r_6^2+\Delta r_7^2)\\&+H_{OCH}(\Delta A_{16}^2+\Delta A_{17}^2+\Delta A_{24}^2+\Delta A_{25}^2)\\&+H_{CCH}(\Delta A_{34}^2+\Delta A_{35}^2+\Delta A_{36}^2+\Delta A_{37}^2)\\&+H_{HCH}(\Delta A_{45}^2+\Delta A_{67}^2)+H_{COC}\Delta A_{12}^2\\&+H_{OCC}(\Delta A_{13}^2+\Delta A_{23}^2)+G_1[\Delta r_1(\Delta r_6+\Delta r_7)\\&+\Delta r_2(\Delta r_4+\Delta r_5)]+G_2(\Delta r_3)(\Delta r_4+\Delta r_5+\Delta r_6+\Delta r_7)\\&+G_3[(\Delta r_1)(\Delta A_{67})+(\Delta r_2)(\Delta A_{45})]\\&+G_4(\Delta r_3)(\Delta A_{45}+\Delta A_{67}).\end{aligned}$$

The r_i are shown in Fig. 1, and A_{ij} is the angle formed by r_i and r_j.

Of the twelve force constants appearing above, only two can be safely taken from values previously computed for other molecules. These two are $K_{OC}=4.430\times10^5$ dyne÷cm [7] and $K_{CH}=4.910\times10^5$ dyne÷cm.[6] Thus there are ten force constants to be evaluated for a molecule which has fifteen normal vibrations. This leaves five vibrations as a check on results.

4. THE SECULAR EQUATION

In the theory of small oscillations[8] it is shown that the frequencies of the normal vibrations are given by the solutions of the determinantal equation

$$|V_{ij}-w^2T_{ij}|=0.$$

V_{ij} is the second partial derivative of the potential energy with respect to the "ith" and "jth" displacement coordinates evaluated at the equilibrium position; T_{ij} is twice the coefficient of $\dot{q}_i\dot{q}_j$ in the kinetic energy equation; and w is $2\pi c$ times the frequency, where c is the velocity of light.

TABLE III. The A_2 vibration frequencies.

Computed frequencies in cm^{-1}	Observed frequencies in cm^{-1}
698	704
1243	Not observed
3069	3062

[6] B. D. Saksena, Proc. Indian Acad. Sci. **A10**, 449 (1939).
[7] L. G. Bonner, J. Chem. Phys. **5**, 293 (1937).
[8] H. Goldstein, *Classical Mechanics* (Addison-Wesley Press, Cambridge, 1950).

TABLE IV. The B_1 vibration frequencies.

Computed frequencies in cm^{-1}	Observed frequencies in cm^{-1}	Force constants in dyne ÷cm $\times 10^5$
787	807	$H_{HCH} \div (CH)^2 = 0.291$
1119	1122	$H_{OCC} \div (OC)(CC) = 0.804$
1485	1461	$G_1 = -1.000$
2985	3000	$G_3 \div CH = -0.463$

The q_i, the displacements from the respective equilibrium positions, are not all independent. For each species of vibration there are as many independent coordinates as there are vibration frequencies. If the dependent coordinates are eliminated, then the secular determinant takes the form of Fig. 56, page 147 in Herzberg.[1] The secular determinant is now factored into four (one of each species) determinants and each is solved separately. When each of these determinants is expanded, the coefficients of the frequencies in the equations will be functions of the unknown force constants. The solutions to these equations are found by first setting up the relationships between the roots and the coefficients[9] and then selecting the values of the force constants that give solutions for the frequencies in good agreement with observed values[10] (average of a number of observers[11]).

5. THE B_2 VIBRATIONS

The potential energy function contains only three force constants,[12] K_{CH}, H_{OCH}, and H_{CCH}. The secular equation is a third-degree equation since there are three fundamental vibrations.

The results of the computations are given in Table II.

6. THE A_2 VIBRATIONS

The potential energy function for the A_2 vibrations contain the same three force constants as the function for the B_2 vibrations.

The results of the computations are given in Table III.

TABLE V. The A_1 vibration frequencies.

Computed frequencies in cm^{-1}	Observed frequencies in cm^{-1}	Force constants in dyne ÷cm $\times 10^5$
521	509	$K_{CC} = 5.600$
851	868	$H_{COC} \div (OC)(CC) = -1.844$
1269	1270	$G_4 \div (CH) = -0.231$
1500	1490	
3000	3000	

[9] J. V. Uspensky, *Theory of Equations* (McGraw-Hill Book Company, Inc., New York, 1948), p. 63.

[10] The assignment used in this report is based on (1) the assignment suggested by Linnett (see reference 11), (2) the assignment suggested by Herzberg (see reference 1), and (3) the author's own preliminary calculations based on the assumed potential energy function of Sec. 3.

[11] B. Timm and R. Mecke, Z. Physik **97**, 221 (1935); R. Ananthakrishnan, Proc. Indian Acad. Sci. **A4**, 82 (1936); L. G. Bonner, J. Chem. Phys. **5**, 704 (1937); K. Kohlrausch and A. Reitz, Proc. Indian Acad. Sci. **A8**, 225 (1938); J. W. Linnett, J. Chem. Phys. **6**, 692 (1938).

[12] Hs. H. Günthard *et al.* evaluate these three force constants by assuming a simple valence force field. See Helv. Chim. Acta **33**, 1809 (1950).

7. THE B_1 VIBRATIONS

The potential energy function for the B_1 vibrations contains eight force constants. Three of these constants were evaluated in solving for the B_2 frequencies and a fourth one, K_{OC}, is taken from Bonner.[7] Thus the secular equation contains the remaining four force constants as quantities to be evaluated. (Since there are four fundamental frequencies, it is possible to select force constants to give computed frequencies in exact agreement with the observed values. These values of the force constants, however, are not in agreement with the values of similar force constants found for other molecules.)

The values of the force constants selected and the observed and computed frequencies are given in Table IV.

8. THE A_1 VIBRATIONS

The potential energy function contains all twelve of the force constants, eight of which are already evaluated. Preliminary calculations indicate that a ninth force constant, G_2, has an effect only on the highest frequency (3000 cm^{-1}) and that a good value for G_2 is zero. Thus the secular equation contains only three force constants.

The results are given in Table V.

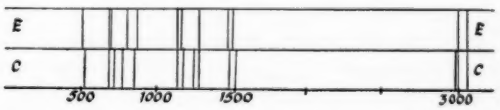

FIG. 2. The observed spectra on which the computations were based, and the computed spectra. The E lines are observed frequencies in cm^{-1}, and the C lines are computed frequencies in cm^{-1}.

SUMMARY

Comparison of the computed frequencies with the observed frequencies is summarized in Fig. 2. The maximum difference between a computed and observed frequency is 24 cm^{-1}. These satisfactory results are due in part to the potential energy function selected, and indicates that a similar function might be successful for other molecules with constructions similar to ethylene oxide. However, the large number of force constants at the disposal of the computer must also be considered in evaluating the results. This latter factor is diminished somewhat by the fact that the values of force constants are in agreement with the usual values of force constants found for other molecules. The negative values for the cross-product constants is customary, and the negative value of H_{COC} is due to the strain in the COC bond.

The author wishes to express his appreciation to Professor Charles A. Ahonen† of the Department of Physics, Northeastern University, for many helpful discussions during the progress of the research.

† Formerly at Boston University, Boston, Massachusetts.

Photochemical Activity of Salts of Uranium in Solutions at the Temperature of Liquid Nitrogen*

SIMON FREED AND KENNETH M. SANCIER †
Chemistry Department, Brookhaven National Laboratory, Upton, L. I., N. Y.

(Received January 18, 1954)

Anhydrous chlorides of hexavalent (UO_2^{++}), quadrivalent, and trivalent uranium ions are photochemically active when in a solution fluid at 77°K. The solvent consisted of 10 percent *n*-propanol, 45 percent propane, and 45 percent propene. It was shown spectroscopically and also chemically that quadrivalent uranium was reduced to the trivalent form. There were indications that trivalent and hexavalent uranium were transformed photochemically to the tetravalent state.

A SOLUTION of anhydrous uranium tetrachloride (7 mg/ml) in 10 percent *n*-propanol and 1:1 propane, propene is a bluish green fluid at 77°K and has a spectrum which is more diffuse than that of a rare earth in the same solvent. In the region between 2970A and about 7000A, absorption bands of various degrees of sharpness are present (Fig. 1); between 7000A and 11 000A, the solution is transparent; below 2970A, there is a continuum of absorption except for a faintly transparent window about 220A wide with center at 2760A.

When the solution was placed before a source of continuous ultraviolet radiation, a hydrogen discharge tube, a greenish yellow fluorescence was noticeable which quickly diminished in intensity and disappeared after several minutes. The origin of this fluorescence was in all probability a little uranyl salt present as an impurity. After about an hour of irradiation it was observed that the side of the solution nearest the source of radiation had become purple. Its boundary with the green solution moved roughly at 0.05 mm per hour despite the fact that the solution was more fluid at 77°K than is glycerine at 300°K. After irradiation for 60 hours, the solution, now intensely purple throughout, was removed from the coolant, liquid nitrogen, and evaporated at room temperature in a vacuum line. Chemical analysis of the residue for the atomic ratio of chlorine to uranium gave 3.2. It seems then that about eighty percent of the tetravalent uranium had been reduced to the trivalent state and 0.8 unit of chlorine atom had entered into a substance volatile at room temperature.

To confirm the nature of this transformation, anhydrous uranium trichloride was prepared chemically, dissolved in the same solvent as above, and cooled to the same temperature. The solution had an absorption band in the near infrared 8950A where uranium tetrachloride was transparent. Prolonged irradiation of the solution of the tetrachloride had produced a rather strong narrow band centered at about 9000A (Fig. 2). The structures of the absorption bands in the two solutions were not identical, which was scarcely to be expected since the spectra of uranium ions and also of transuranium ions are strongly responsive to the microfields of their environments, and these would be expected to be different in the two solutions at the low temperatures.

It is probable that the radiation effective in the photochemical reduction lay in the continuum below 3000A. Since uranium trichloride in solution has a continuum below about 4000A, the rate of production of U^{+3} from U^{+4} was retarded by the absorption of the product U^{+3}.

Figure 3 shows the spectrum of the purple solution of uranium trichloride 8 mg/ml in 30 percent *n*-propanol and 1:1 propane, propene at 77°K. Irradiation of this solution with white light also induced photochemical transformations. We did not determine what these were. However, Fig. 3 shows the diminution in the intensity of the characteristic absorption of U^{+3} in the ultraviolet region where uranium tetrachloride in solution is transparent, suggesting that reaction may be the inverse $U^{+3} \rightarrow U^{+4}$ of that which took place when the solution consisted of the tetrachloride. Some confirma-

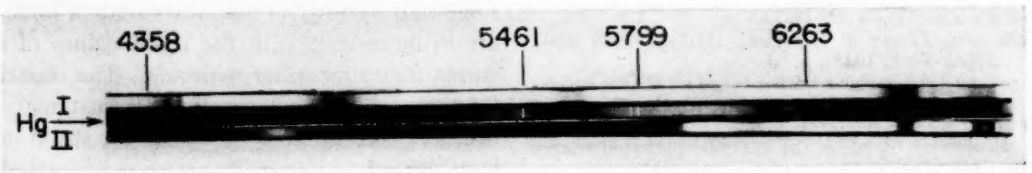

FIG. 1. I—The absorption spectrum of solution of anhydrous uranium tetrachloride in 10 percent *n*-propanol, 45 percent propane and 45 percent propene at 77°K. II—The spectrum of the same solution of irradiation 60 hours. Hg—The emission spectrum of mercury for reference. Both spectra had equal times of exposure.

* Work performed under the auspices of the U. S. Atomic Energy Commission.
† Present address: Stanford Research Institute, Stanford, California.

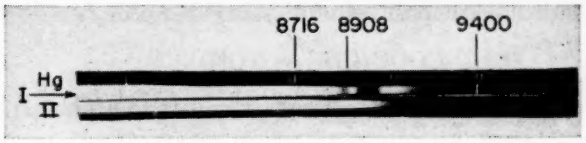

FIG. 2. Hg—The emission spectrum of mercury for reference. I—Absorption spectrum of solution of anhydrous uranium tetrachloride in 10 percent *n*-propanol, 45 percent propane, and 45 percent propene at 77°K which had been irradiated 60 hours. II—The absorption spectrum of the solution before irradiation. Both spectra had equal times of exposure.

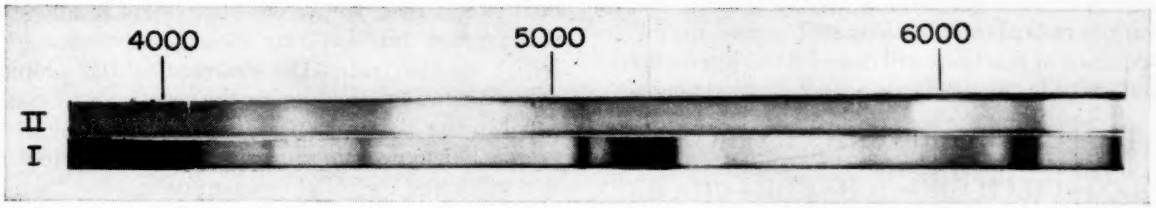

FIG. 3. I—Absorption spectrum of a solution of anhydrous uranium trichloride in 15 percent *n*-propanol, in 1:1 mixture propane and propene at 77°K. II—Absorption spectrum of the same solution after irradiation for 40 hours. Both spectra had equal times of exposure.

tion was noted in the simultaneous increase in transparency of the solution of the trichloride at about 5000A where the green solution is also transparent.

EXPERIMENTAL

The fused quartz optical cell 1 mm×10 mm×20 mm was at the end of a tube provided with stopcock and ball joint. Also sealed onto the cell was a train of tubing about 10 mm in diameter containing the uranium tetrachloride which was completely dehydrated by passing hydrogen chloride over it at from 100°C to 200°C. By attaching the ball joint to a vacuum line, the system was evacuated and the dry tetrachloride was twice sublimed along the tube at 450°C and finally into the optical cell which was then sealed off from the train. About 0.1 mm *n*-propanol was condensed on the salt which subsequently dissolved. The temperature of the solution was lowered to that of dry ice (190°K) and equal volumes of propane and propene gases were then condensed into the solution diluting it until the total volume was 1 ml.

The uranium trichloride was made in two ways, one by reducing the dried uranium tetrachloride with hydrogen gas and subliming at about 650°C; the other started with uranium metal disintegrating it by forming uranium hydride with hydrogen and pumping off the hydrogen at a higher temperature and then passing hydrogen chloride over this. Finally the salt was sublimed at 650°C. Since we found it difficult to sublime into the optical cell which was only 1 mm wide, we condensed *n*-propanol on the trichloride in the larger tubing. Part of the resulting solution was siphoned into the cell. Then propane and propene were condensed into the alcoholic solution as in the preparation of the solution of the tetrachloride.

THE JOURNAL OF CHEMICAL PHYSICS VOLUME 22, NUMBER 5 MAY, 1954

Reactions of Free Radicals with Aldehydes. II. The Reactions of Methyl Radicals with Propionaldehyde

DAVID H. VOLMAN AND ROBERT K. BRINTON
Department of Chemistry, University of California, Davis, California

(Received August 28, 1953)

The reaction of radicals derived from the thermal decomposition of di-*t*-butyl peroxide with propionaldehyde in the gas phase has been studied. The gaseous products were carbon monoxide, methane, ethane, propane, butane, and ethylene. A mechanism to account for the induced chain decomposition and product formation involving H atom abstraction by radicals and radical decomposition, combination and disproportionation is given. The energetics of H atom abstraction by methyl and ethyl were similar and lead to an activation energy of about 7.5 kcal/mole and a steric factor of about 10^{-3}. These values are in good agreement with those found for H atom abstraction from acetaldehyde. Evidence is presented that H atom abstraction takes place with the carbonyl attached H for both acetaldehyde and propionaldehyde.

INTRODUCTION

A RECENT investigation[1] of the induced decomposition of acetaldehyde and acrolein by di-*t*-butyl peroxide has been extended to include the analogous decomposition of propionaldehyde. In this latter study reported in this paper, as well as in the previous work, methyl and *t*-butoxy radicals were generated by the

[1] D. H. Volman and R. K. Brinton, J. Chem. Phys. **20**, 1764 (1952).

thermal decomposition of di-*t*-butyl peroxide,[2]

$$(CH_3)_3COOC(CH_3)_3 = 2(CH_3)_3CO, \quad (1)$$

$$(CH_3)_3CO = CH_3 + CH_3COCH_3. \quad (2)$$

If it is assumed that a chain mechanism similar to the acetaldehyde decomposition is operating and that all the various radical combinations are possible, the following sequence of reactions will describe the interaction of methyl and *t*-butoxy radicals with propionaldehyde:

$$CH_3 + CH_3CH_2CHO = CH_4 + CH_3CH_2CO, \quad (3)$$

$$(CH_3)_3CO + CH_3CH_2CHO = (CH_3)_3COH + CH_3CH_2CO, \quad (4)$$

$$CH_3CH_2CO = CH_3CH_2 + CO, \quad (5)$$

$$CH_3CH_2 + CH_3CH_2CHO = C_2H_6 + CH_3CH_2CO, \quad (6)$$

$$2CH_3 = C_2H_6, \quad (7)$$

$$2CH_3CH_2 = C_4H_{10}, \quad (8)$$

$$CH_3 + CH_3CH_2 = C_3H_8, \quad (9)$$

$$CH_3 + CH_3CH_2CO = CH_3CH_2COCH_3, \quad (10)$$

$$CH_3CH_2 + CH_3CH_2CO = CH_3CH_2COCH_2CH_3, \quad (11)$$

$$2CH_3CH_2CO = CH_3CH_2COCOCH_2CH_3. \quad (12)$$

The reactions involving the combination of a *t*-butoxy radical with another radical have not been included. Although such a combination seems likely, no trace of the resultant products, e.g., methyl *t*-butyl ether, could be found in similar type systems previously investigated.[3]

The experiments described in this paper were designed to test the validity of the proposed reaction scheme and to investigate in detail the hydrogen abstraction reactions (3) and (6).

EXPERIMENTAL METHOD

The apparatus and experimental procedure used in this work have been previously described.[1,3] The mixture of aldehyde and peroxide was reacted in a one liter glass bulb immersed in a silicone oil bath thermostat. At the termination of the reaction the mixture was expanded into a sample bulb. The portion of the aliquot in the sample bulb which could be pumped off at −65°C by use of a Toepler pump was used in the product analysis. This volatile portion was treated at about 5 mm pressure with 98 percent sulfuric acid for 2 to 3 hours, at atmospheric pressure with a sintered glass bead saturated with 98 percent sulfuric acid, and finally at atmospheric pressure with a potassium hydroxide bead. This procedure eliminated all oxygenated compounds present, and only the hydrocarbon gases and carbon monoxide remained in the final sample. The purified sample was measured at low pressure and analyzed in a consolidated mass spectrometer.

The reaction rates were taken as $\Delta C/\Delta t$ over the time interval of each experiment. The percent reaction was held to less than 10 percent completion in all cases so the average reaction rate closely approximated the initial reaction rate. The decrease in the propionaldehyde concentration during the reaction was assumed equal to the carbon monoxide formed, and the average propionaldehyde concentration was calculated from this value and its initial concentration.

Propionaldehyde and di-*t*-butyl peroxide were both commercial products which were purified by fractional distillation.

RESULTS AND DISCUSSION

The above reactions postulate that ethane is formed by two processes: methyl radical combination (7) and hydrogen abstraction by ethyl radicals (6). One other source of ethane production is the process

$$2CH_3CH_2 = C_2H_4 + C_2H_6. \quad (13)$$

This ethyl radical disproportion reaction has been studied in detail by Ivin, Wijnen, and Steacie[4] who found that the ratio of the rate of formation of ethylene to rate of formation of butane, by competing reaction (8), was about 0.10 for diethyl ketone over the range 25 to 300° while it varied from 0.36 to 0.46 for mercury diethyl over the range 75 to 200°.

The ethylene yield was determined on a separate aliquot sample of the reaction products for one experiment at 122.3° and one at 155.7°. The volatile fraction of these aliquots were separated at −120° and the treatment with sulfuric acid eliminated so as to insure against any loss of ethylene. The ratio $R_{C_2H_4}/R_{C_4H_{10}}$ was 0.15 at 155.7° and 0.13 at 122.3° which agrees quite well with the results on diethyl ketone reported above. It is felt that the accuracy of these ratios is of the order of ±20 percent because of the difficulty of determining small amounts of ethylene in mixtures of hydrocarbons by mass spectrometric analysis.

Since methane is produced by (3) only

$$\frac{d[CH_4]/dt}{(d[C_2H_6]^c/dt)^{\frac{1}{2}}} = \frac{R_{CH_4}}{(R^c_{C_2H_6})^{\frac{1}{2}}} = \frac{k_3}{k_7^{\frac{1}{2}}}[CH_3CH_2CHO],$$

where $[C_2H_6]^c$ and $R^c_{C_2H_6}$ refer to the concentrations and rates of formation of that part of the total ethane produced by methyl radical combination. Also

$$\frac{d[C_2H_6]^a/dt}{(d[C_4H_{10}]/dt)^{\frac{1}{2}}} = \frac{R^a_{C_2H_6}}{R_{C_4H_{10}}{}^{\frac{1}{2}}} = \frac{k_6}{k_8^{\frac{1}{2}}}[CH_3CH_2CHO]$$

[2] Raley, Rust, and Vaughan, J. Am. Chem. Soc. **70**, 88 (1948).
[3] R. K. Brinton and D. H. Volman, J. Chem. Phys. **20**, 25 (1952).
[4] Ivin, Wijnen, and Steacie, J. Phys. Chem. **56**, 967 (1952).

TABLE I.

Exp. no.	Temp. deg. C	Av. conc. aldehyde mole $cc^{-1}\times10^{7}$	Rates mole cc^{-1} $sec^{-1}\times10^{11}$ R_{CO}	R_{CH_4}	$R^t_{C_2H_6}$	$R_{C_2H_6}$	$R_{C_4H_{10}}$
23	122.3	0	...	0.031	0.435	...	...
24	122.3	3.9[9]	0.65	0.348	0.219	0.130	0.093
25	122.3	8.8[4]	1.00	0.402	0.450	0.071	0.114
26	122.3	20.5	1.31	0.334	0.725	0.042	0.082
27	122.3	32.3	1.50	0.297	0.863	0.015	0.062
28	122.3	49.2	1.68	0.274	1.04	Trace	0.037
7	133.9	0		0.12[5]	1.62		
8	133.9	3.4[0]	1.70	0.95[6]	0.60[7]	0.541	0.209
9	133.9	7.5[6]	3.21	1.69	1.13	0.528	0.412
4	133.9	12.1	3.99	1.69	1.55	0.417	0.472
10	133.9	17.2	4.36	1.63	1.95	0.249	0.427
11	133.9	28.0	4.93	1.45	2.62	0.118	0.323
12	133.9	40.2	5.42	1.26	3.08	0.063	0.229
6	133.9	55.4	5.67	0.99	3.44	0.048	0.154
14	155.7	0	...	0.45	17.8		
20	155.7	9.7[0]	22.9	13.9	8.3[1]	6.46	3.43
16	155.7	10.5	24.1	15.6	9.0[3]	6.26	3.38
21	155.7	20.5	32.1	17.7	12.9	4.15	4.60
17	155.7	21.0	33.0	17.6	13.5	4.55	4.26
18	155.7	34.9	39.8	17.0	19.0	2.94	3.88
22	155.7	41.3	43.0	17.2	21.7	1.98	4.18
19	155.7	46.1	45.1	16.7	22.6	1.93	3.55

and

$$\frac{(d[CH_4]/dt)(d[C_4H_{10}]/dt)^{\frac{1}{2}}}{d[C_3H_8]/dt}=\frac{R_{CH_4}(R_{C_4H_{10}})^{\frac{1}{2}}}{R_{C_3H_8}}$$

$$=\frac{k_3k_8^{\frac{1}{2}}}{k_9}[CH_3CH_2CHO],$$

if $[C_2H_6]^a$ and $R^a_{C_2H_6}$ represent the concentrations and rates of formation of that part of the ethane which is produced by hydrogen atom abstraction from propionaldehyde by ethyl radicals. The total ethane production, $R^t_{C_2H_6}$, must be the sum $R^c_{C_2H_6}+R^a_{C_2H_6}+R_{C_2H_4}$ since an amount of ethane equal to the ethylene is produced by (13). In each case the $R^t_{C_2H_6}$ must be corrected by the value of $R_{C_2H_4}$ to give the value of $R_{C_2H_6}$ which is the sum of $R^c_{C_2H_6}$ and $R^a_{C_2H_6}$. The values of $R_{C_2H_4}$ were taken as 0.15, 0.14, and 0.13 times $R_{C_4H_{10}}$ at the three temperatures, 155.7, 133.9, and 122.3°.

The values of the rates of formation of the various products are listed in Table I and are shown graphically as a function of aldehyde pressure in Figs. 1, 2, and 3. The 155.7° experiments were run at a peroxide concentration of 5.61×10^{-7} mole/cc for 360 sec, the 133.9° experiments at 6.10×10^{-7} mole/cc for 1800 sec, and the 122.3° experiments at 5.75×10^{-7} mole/cc for 7200 sec. Table II shows the values of the various calculated

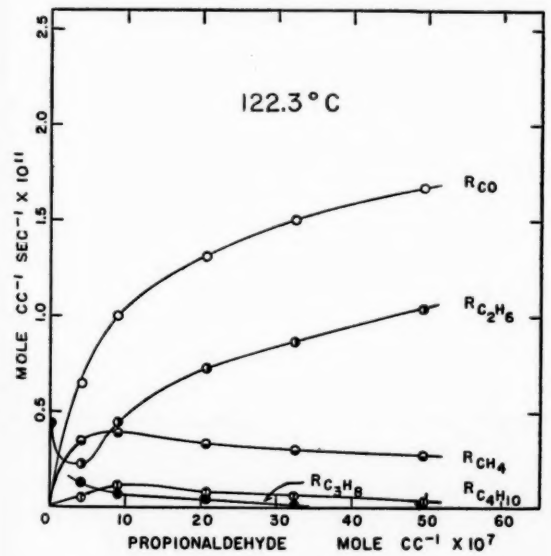

FIG. 1.

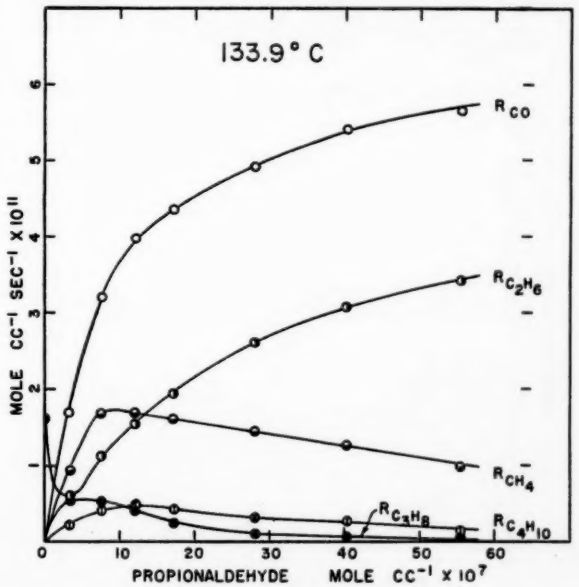

FIG. 2.

TABLE II.

Exp. no.	R_{CH_4} / $[CH_3CH_2CHO]R^c_{C_2H_6}{}^{\frac{1}{2}}$ mole$^{-\frac{1}{2}}$ cc$^{-\frac{1}{2}}$ sec$^{-\frac{1}{2}}$	Rates mole cc^{-1} sec^{-1} $\times 10^{11}$ $R_{C_2H_6}$	$R^c_{C_2H_6}$	$R^a_{C_2H_6}$	Mole$^{\frac{1}{2}}$ cc$^{-\frac{1}{2}}$ sec$^{-\frac{1}{2}}$ $\times 10^6$ $R^a_{C_2H_6}/R_{C_4H_{10}}{}^{\frac{1}{2}}$	$R_{CH_4}R_{C_4H_{10}}{}^{\frac{1}{2}}/R_{C_3H_8}$
24	11.4	0.207	0.0582	0.149	1.55	2.58
25	11.4	0.435	0.0159	0.419	3.92	6.04
26	11.4	0.713	0.0020	0.711	7.87	7.20
27	11.4	0.855	0.0006[5]	0.854	10.9	15.6
28	11.4	1.035	0.0002[4]	1.035	22.2	...
8	15.0	0.57[0]	0.353	0.21[7]	1.57	1.45
9	15.0	1.07	0.222	0.84[8]	4.19	2.03
4	15.0	1.48	0.087	1.39	6.43	2.17
10	15.0	1.89	0.040	1.85	8.95	2.07
11	15.0	2.58	0.012	2.57	14.2	1.80
12	15.0	3.05	0.004[4]	3.05	20.1	1.52
6	15.0	3.42	0.001[4]	3.42	27.6	1.24
20	24.5	7.80	3.43	4.37	7.50	5.85
16	24.5	8.52	3.66	4.86	8.51	5.71
21	24.5	12.2	1.25	10.9[5]	16.1	6.78
17	24.5	12.9	1.17	11.7[3]	17.7	6.52
18	24.5	18.4	0.39[3]	18.0	28.9	6.22
22	24.5	21.1	6.28[8]	20.8	32.2	6.46
19	24.5	22.1	0.21[8]	20.9	36.8	5.95

quantities some of which have been plotted as a function of aldehyde concentration in Figs. 4 and 5. The upper three lines of Fig. 4 representing $R_{CH_4}/R^c_{C_2H_6}{}^{\frac{1}{2}}$ were drawn as straight lines from which the values of $R^c_{C_2H_6}$ could be calculated. The slopes of these upper lines were selected so that the ratios of $R^a_{C_2H_6}/R_{C_4H_{10}}{}^{\frac{1}{2}}$ calculated from the values of $R^a_{C_2H_6}=R_{C_2H_6}-R^c_{C_2H_6}$ produced the best straight lines for the lower three curves of Fig. 4. Inspection of the various data shows that at higher aldehyde pressures the values of $R^a_{C_2H_6}$ are little influenced by the slopes chosen for the values of the $R_{CH_4}/R^c_{C_2H_6}{}^{\frac{1}{2}}$ curves since almost all ethane produced at these higher aldehydes pressures is a result of the abstraction reaction. The accuracy of the ratio $R^a_{C_2H_6}/R_{C_4H_{10}}{}^{\frac{1}{2}}$ is by and large dependent on the accuracy of $R_{C_4H_{10}}$ at these higher aldehyde concentrations since $R^a_{C_2H_6}\cong R_{C_2H_6}\cong R^t_{C_2H_6}$ and the high ethane concentration may be accurately determined by mass spectrometric analysis. At 122.3° the percentage of butane in the reaction products is low and the points determining the lowest curve of Fig. 4 are somewhat less accurate than the other two curves.

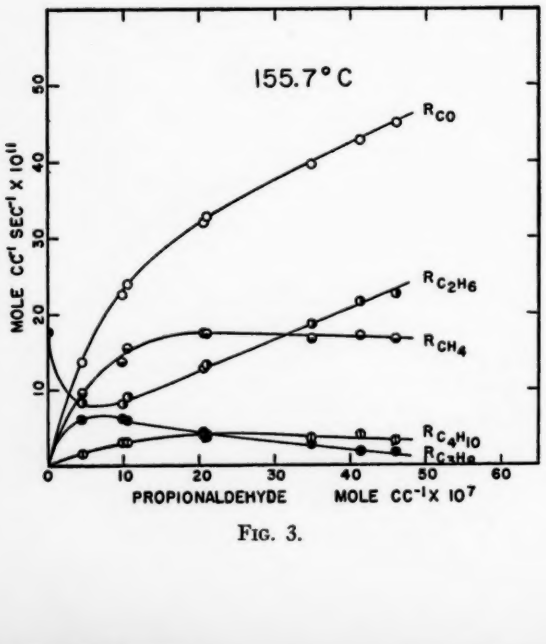

FIG. 3.

The value of the activation energy, $E=E_3-\frac{1}{2}E_7$, determined from the upper three curves of Fig. 4 is 7.5 kcal/mole. This value is not too significant since the slopes may be altered enough to change this energy by 2 to 3 kcal without affecting the lower curves to any large extent. The activation energy, $E=E_6-\frac{1}{2}E_8$, determined from the lower 155.7 and 133.9° curves of Fig. 4 is 7.60 kcal/mole while that from the 133.9 and 122.3° curves is approximately 8.6 kcal. It is felt that the best value of

$$\frac{k_6}{k_8{}^{\frac{1}{2}}}=5.9\times10^4\exp(-7600/RT)\ \text{mole}^{-\frac{1}{2}}\ \text{cc}^{\frac{1}{2}}\ \text{sec}^{-\frac{1}{2}}$$

is determined from the 155.7 and 133.9° curves with an over-all accuracy of ±1 kcal in the activation energy. If the pre-exponential factor for the combination of ethyl radicals is 1.6×10^{13} cc mole^{-1} sec^{-1} and the activation energy is about zero as indicated by Ivin and Steacie,[5] the steric factor for reaction (6) is approximately 10^{-3}.

Figure 5 shows the plot of the relation $R_{CH_4}(R_{C_4H_{10}})^{\frac{1}{2}}/R_{C_3H_8}$ for the 155.7 and 133.9° experiments. Although the points calculated for the 122.3° experiments show the correct trend, the very low accuracy of the determination of the small amounts of propane makes for a scattering of the points so that these data have not been included. The curves drawn for these two temperatures

[5] K. J. Ivin and E. W. R. Steacie, Proc. Rov. Soc. (London) A208, 25 (1951).

lead to the value of

$$\frac{k_3 k_8^{\frac{1}{2}}}{k_9} = 7.6\times 10^4 \exp(-7600/RT) \text{ mole}^{-\frac{1}{2}} \text{ cc}^{\frac{1}{2}} \text{ sec}^{-\frac{1}{2}}.$$

The divergence of the points from the 155.7° curve limit the accuracy of the value of $E_3+E_8^{\frac{1}{2}}-E_6$ to about ± 2 kcal/mole.

The fit of the experimentally determined rates to the treatment given above substantiates the proposed mechanisms well. It is certain that the chain ending mechanisms (10), (11), and (12) are all important processes. The testing of these mechanisms is rather difficult because of the analytical problems involved in determining small amounts of methylethyl ketone,

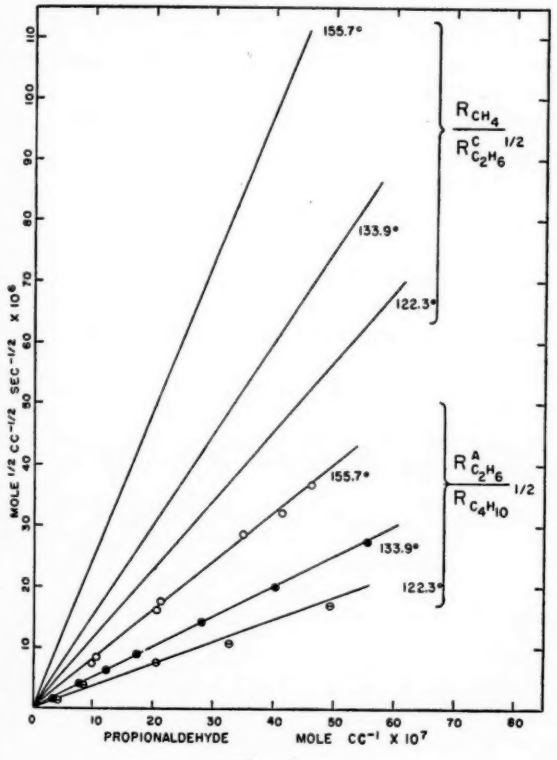

FIG. 4.

diethylketone, and bipropionyl in a large excess of propionaldehyde and acetone. Although the inherent complexities of this study do not allow the determination of the energetics to a precision comparable to the similar investigation of acetaldehyde,[1] it does appear that the hydrogen atom abstraction energy is about the same for both the methyl and ethyl radicals. Furthermore these abstraction energies are within experimental error the same as for the abstraction from acetaldehyde. This similarity lends credence to the postulate that has been tacitly assumed in writing the propionaldehyde reaction mechanisms: that abstraction occurs on the hydrogen atom attached to the carbonyl group. In the case of acetaldehyde this seems quite logical in view of the low abstraction energy of 7.5 kcal/mole compared to about 9.7 for acetone[6] since all hydrogens on

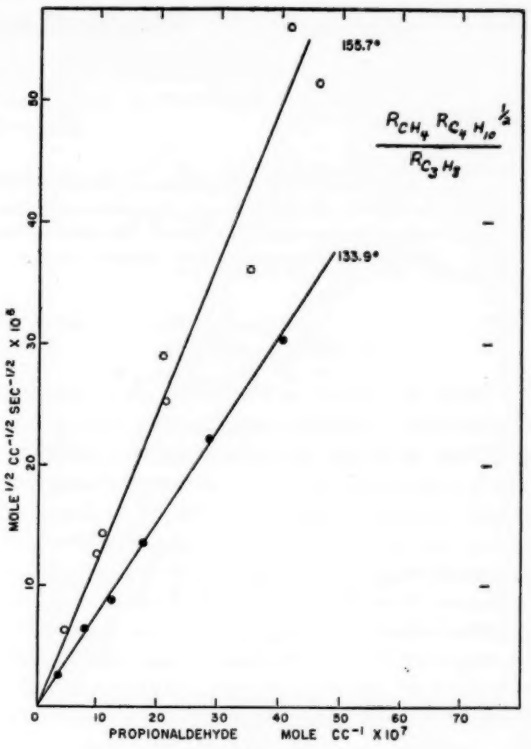

FIG. 5.

these two compounds are of similar type structurally except the carbonyl attached atom. On the other hand the reaction with propionaldehyde may proceed by (3), (4), and (6) as well as a reaction such as

$$CH_3+CH_3CH_2CHO=CH_4+CH_3CHCHO. \quad (14)$$

It may be expected that this reaction involving abstraction from a secondary carbon atom would have an activation energy of 7 to 8 kcal/mole if an analogy may be made to similar type structures studied by Trotman-Dickenson, Birchard, and Steacie.[7] The propionaldehyde radical produced in (14) would conceivably have considerable stability as compared to the propionyl radical produced by reactions of type (3) and thus be removed almost completely by radical combination rather than propagating a chain as in (5). That mechanisms such as (3) and (14) are competing is indicated by the much shorter chain lengths found for propionaldehyde than for acetaldehyde at comparable temperatures. This argument is of course not a compelling one since it is also possible that the propionyl radical is more stable thermally than the acetyl radical.

ACKNOWLEDGMENT

We wish to express our appreciation to the Research Corporation for financial aid and to Dr. Amos Newton and Mrs. Frances T. Jewel of the Radiation Laboratory of the University of California for assistance with the mass spectrometric analyses.

[6] A. F. Trotman-Dickenson and E. W. R. Steacie, J. Chem. Phys. **18**, 1097 (1950).

[7] Trotman-Dickenson, Birchard, and Steacie, J. Chem. Phys. **19**, 163 (1951).

Rotational Energy Transfer in H_2†

ROBERT BROUT*
Department of Chemistry, Columbia University, New York, New York
(Received December 11, 1954)

Rotational energy deactivation probabilities have been calculated for H_2 using the quantum-mechanical method of distorted waves. Approximate procedures have been indicated for further extensions of these calculations to other symmetric diatomic molecules. Comparison with data from sound dispersion measurements shows good agreement between theory and experiment.

I. INTRODUCTION

Of great importance in research in chemical kinetics, transport phenomena and the theory of the propagation of sound and shock waves through gases are the transition probabilities for energy interchange to and from various modes of motion of molecules. The following is a calculation of rotation-translation energy interchange upon collision of diatomic molecules. Such calculations have been made with some success for translation-vibration energy interchange upon collision,[1] but to this author's knowledge no numerical results have been published for the rotation problem.[2] Along with workers on the vibration problem we will idealize one of the molecules as a mass point, the other, the scattering center, a rotating diatomic rotor. Unlike the vibrational problem, the rotational one must be considered in three dimensions, hence considerably complicating the situation.

We will employ the method of distorted waves of quantum mechanics, this being the suitable approximation for massive particles at thermal energies. It is to be noted that the Born approximation would be unsatisfactory for this calculation as it does not take proper cognizance of the classical turning point. This indeed has been borne out by calculations.

As fine data on sound dispersion in H_2 have been obtained,[3] we will test our calculation against these data, proper care being taken to sift out the ortho and para cases individually.

II. THE POTENTIAL BETWEEN TWO H_2 MOLECULES

A calculation of the potential between two H_2 molecules has been carried out by de Boer[4] using a valence bond approximation, which should be valid at large interatomic distances. The results of his calculations are

$$V=\sum V_{ij}; \quad V_{ij}=C_{ij}-\frac{J_{ij}}{2}.$$

C_{ij}=Coulombic interaction between wave functions centered on i and j. J_{ij}=resonance interaction between wave functions centered on i and j. i and j are on different molecules and the sum is over the four possible interactions.

De Boer has calculated

$$V_{ij}=V_0e^{-3.53r}.$$

As we have shrunk one molecule into a mass point, we essentially average over all orientations of one of the molecules. By symmetry, de Boer's potential will then reduce to

$$V=V_0'(e^{-\alpha r_1}+e^{-\alpha r_2}).$$

If a_0 is half the interatomic distance in H_2(a_0=0.370A), then by the law of cosines

$$r_1=(r^2+2a_0r\cos\gamma+a_0^2)^{\frac{1}{2}},$$
$$r_2=(r^2-2a_0r\cos\gamma+a_0^2)^{\frac{1}{2}},$$

where r is the distance of mass point to the center of mass of the molecule, and γ the angle between the incident direction of the mass point and the figure axis of the molecule.

As interest is in distances larger than the turning point which is about 2.6A, the roots can safely be expanded.

$$r_1=r+a_0\cos\gamma,$$
$$r_2=r-a_0\cos\gamma,$$

whence

$$V=V_0e^{-\alpha r}\cosh(\alpha a_0\cos\gamma).$$

If the cosh is expanded,

$$V=V_0'\left(1+\frac{(\alpha a_0)^2}{2!}\cos^2\gamma+\frac{(\alpha a_0)^4}{4!}\cos^4\gamma+\cdots\right).$$

Putting $\alpha a_0=0.370\times3.53=1.30$,

$$V=V_0'e^{-\alpha r}(1+0.85\cos^2\gamma+0.12\cos^4\gamma+\cdots).$$

This is further approximated by dropping the $\cos^4\gamma$ term, i.e., the theory is developed in terms of the ex-

† Submitted in partial fulfillment for degree of Doctor of Philosophy in Faculty of Science, Columbia University.

* U. S. Atomic Energy Commission, predoctoral fellow, 1951–1953. Present address: Department of Chemistry, University of Rochester, Rochester, New York.

[1] For a good review see C. Zener, Second Report on Contact Catalysis Natl. Research Council (U. S.), Reprint and Circ. Ser., No. 50, Washington, D. C. (1934).

[2] Recently Hirschfelder and Hornig have published a preliminary report of their work based on a time dependent perturbation method akin to that of C. Zener, Phys. Rev. **38**, 277 (1931); J. Hirschfelder and J. Hornig, University of Wisconsin ONR Report—3—44-A.

[3] I. Zartmann, J. Acoust. Soc. Am. **21**, 171 (1949).

[4] J. de Boer, Physica **9**, 363 (1942).

pansion parameter $(\alpha a_0)^{2n}/n!$ and only first-order terms are taken.

Dropping the $\cos^4\gamma$ term, the above can be rearranged to an expansion in spherical harmonics.

$$V=V_0''(1+0.45P_2(\cos\gamma))$$
$$=V_0(r)+V_2(r)P_2(\cos\gamma),$$

where

$$V_0=V_0''e^{-\alpha r},$$
$$V_2=0.45V_0''e^{-\alpha r}.$$

Let the polar and azimuthal angles of the incident direction and the figure axis of the molecule with respect to some space fixed axis be, respectively, θ, φ and χ, ζ.

Then, by the addition theorem of spherical harmonics,

$$V=V_0+V_2\sum_{-2}^{+2}((2-|m|)!/(2+|m|)!)$$
$$\times P_2^{|m|}(\cos\theta)P_2^{|m|}(\cos\chi)e^{im(\varphi-\zeta)}. \quad (1)$$

We will regard the second term as a perturbation. It will turn out to be the transition inducing term.

For symmetric diatomic molecules other than H_2, it can readily be seen that, to the approximations presented here, V can always be written in the form

$$V=V_0[1+\lambda P_2(\cos\theta)],$$

where λ may be considered as a parameter expressing the deviation of the potential from spherical symmetry.

III. DEVELOPMENT OF THE CROSS SECTION

Using the potential found in the previous section we may now write our Hamiltonian

$$H=H^0+H',$$

where $H^0=H_{\text{rot}}-(\hbar^2/2\mu)\nabla^2+V_0$; H'=second term of (1), considered a perturbation; μ=reduced mass of the two molecules=m_{proton}; ∇^2=Laplacian of the center of mass coordinates; H_{rot}=Unperturbed Hamiltonian of the rotor. Our wave equation is now $H\psi(\chi,\psi;r,\theta,\varphi)=E\psi$. Letting $\psi=\psi^0+\psi'$, we have

$$H^0\psi^0=E\psi^0, \quad (2)$$

$$H^0\psi'=-H'\psi^0. \quad (3)$$

Further, let

$$\psi^0=\Phi_{n_0m_0}(\chi,\psi)F^0(\theta,\varphi,r),$$

where $H_{\text{rot}}\Phi_{nm}=E_n\Phi_{nm}$; i.e., n_0 represents the initial total angular momentum of the rotor, m_0 represents the initial magnetic quantum number. Then,

$$[\nabla^2+k_0^2-(2\mu V_0/\hbar^2)]F^0=0, \quad (4)$$

where

$$k_0^2=(2\mu/\hbar^2)(E-E_{n0}).$$

Further, let

$$\psi^{(1)}=\sum_{n,m}\Phi_{n,m}(\chi,\zeta)F_{n,m}(\theta,\varphi,r),$$

whence, from (3)

$$\sum_{n,m}(\nabla^2-(2\mu V_0/\hbar^2)+k_n^2)F_{nm}\Phi_{nm}$$
$$=-(2\mu/\hbar^2)H^{(1)}F^0\Phi_{n_0m_0},$$

where $k_n^2=(2\mu/\hbar^2)(E-E_n)$. Taking matrix elements,

$$(\nabla^2-(2\mu V_0/\hbar^2)+k_n^2)F_{nm}$$
$$=-(2\mu/\hbar^2)F^0(\Phi_{nm}|H'|\Phi_{n_0m_0}). \quad (5)$$

To evaluate the matrix element,

$$\Phi_{nm}=N_{nm}{}^{\frac{1}{2}}P_n^{|m|}(\cos\chi)e^{im\zeta},$$

where N_{nm} is a normalizing constant, $P_n^{|m|}$ is the associated Legendre polynomial in the customary notation. Whence,

$$(n_0m_0|H'|nm)$$
$$=N_{n_0m_0}{}^{\frac{1}{2}}N_{nm}{}^{\frac{1}{2}}\int\int e^{i(m-m_0)\zeta}P_n^{|m|}(\cos\chi)P_{n_0}^{|m_0|}(\cos\chi)$$
$$\times\sum_{m'=-2}^{+2}((2-|m|)!/(2+|m|)!)e^{im'(\varphi-\zeta)}$$
$$\times P_2^{|m'|}(\cos\theta)P_2^{|m|}(\cos\chi)d\zeta d(\cos\chi).$$

This vanishes unless $m-m_0=\Delta m=m'$, where $|\Delta m|\leq 2$. Hence,

$$(n_0m_0|H'|nm)=N_{nm}{}^{\frac{1}{2}}N_{n_0m_0}{}^{\frac{1}{2}}(P_{n_0}^{|m_0|}|P_2^{|\Delta m|}|P_n^{|m|})$$
$$\times\left(\frac{(2-|\Delta m|)!}{(2+|\Delta m|)!}\right)P_2^{\Delta m}(\cos\theta)e^{i\Delta m\varphi}. \quad (6)$$

If in (5), we let the right-hand side be $f(r,\theta,\varphi)$, via the construction of the appropriate Green's function, the F_n^m which has proper asymptotic behavior is given by[5]

$$F_{nm}(r,\theta,\varphi)\rightarrow(1/4\pi)(e^{ikr}/r)$$
$$\times\int\mathfrak{F}_{nm}(r',\pi-\Theta)f(r',\theta',\varphi')d\tau', \quad (7)$$

where $\cos\Theta=\cos\theta\cos\theta'+\sin\theta\sin\theta'\cos(\varphi-\varphi')$, θ is the scattering angle. $\mathfrak{F}(r,\theta)$ is the solution of the homogeneous equation which has the asymptotic behavior $e^{ikz}+f_{nm}(\theta)(e^{ikr}/r)$. They are the distorted waves. It is evident from (4) that

$$F_{n_0m_0}=\mathfrak{F}_{n_0m_0}. \quad (8)$$

Inserting (6) and (8) into (7),

$$F_{nm}\rightarrow(1/4\pi)(e^{ik_nr}/r)$$
$$\times(2\mu/\hbar^2)N_{n_0m_0}{}^{\frac{1}{2}}N_{nm}{}^{\frac{1}{2}}(P_n^{|m|}|P_2^{|\Delta m|}|P_{n_0}^{|m_0|})$$
$$\times\left(\frac{(2-|\Delta m|)!}{(2+|\Delta m|)!}\right)I_{nn_0}{}^{\Delta m}(\theta,\varphi),$$

[5] N. Mott and H. Massey, *Theory of Atomic Collisions* (Oxford University Press, London, 1933), Chap. VI.

where

$$I_{nn_0}{}^{|\Delta m|}(\theta,\varphi)=\int \mathfrak{F}_n(r',\pi-\Theta)V_2(r')P_2{}^{|\Delta m|}(\cos\theta') \times e^{i|\Delta m|\varphi}\mathfrak{F}_0(r',\theta')d\tau'. \quad (9)$$

Thus we have found the desired cross section, *viz.*,

$$\sigma_{n_0m_0}{}^{nm}(\theta,\varphi)=(1/4\pi)^2(2\mu/\hbar^2)^2 \times(k_n/k_{n_0})|M_{n_0m_0}{}^{nm}|^2|I_{nn_0}{}^{|\Delta m|}|^2, \quad (10)$$

where

$$M_{n_0n_0}{}^{nm}=N_{n_0m_0}{}^{\frac{1}{2}}N_{nm}{}^{\frac{1}{2}}(P_n{}^{|m|}|P_2{}^{|\Delta m|}|P_{n_0}{}^{|m_0|}) \times((2-|\Delta m|)!/(2+|\Delta m|)!).$$

IV. DISTORTED WAVE CALCULATION

For the distorted waves, one uses the partial wave expansion[6]

$$\mathfrak{F}_0=\sum_s(2s+1)i^s\exp(i\delta_s{}^0)f_s{}^0P_s(\cos\theta),$$

where $f_s{}^0$ satisfies the equation

$$[\nabla_r{}^2+k_0{}^2-(2\mu V_0(r)/\hbar^2)-(s(s+1)/r^2)]f_s{}^0(r)=0,$$

which has the asymptotic behavior

$$\cos\delta_s{}^0 j_s(k_0r)+\sin\delta_s{}^0 n_s(k_0r),$$

where j_s and n_s are the spherical Bessel and Neumann functions defined in Shiff.[6]

Also

$$\mathfrak{F}_n(r,\pi-\Theta)=\sum_s(2s+1)(-i)^s\exp(i\delta_s{}^n)f_s{}^nP_s(\cos\Theta).$$

Since Θ is the angle between vectors (θ',φ') and (θ,φ) we can use the addition formula of spherical harmonics, giving

$$\mathfrak{F}_n(r,\pi-\Theta)=\sum_{s,|m|\le s}[(2s+1)(-i)^s\exp(i\delta_s{}^n) \times f_s{}^n((s-|m|)!/(s+|m|)!) \times e^{im(\varphi-\varphi')}P_s{}^{|m|}(\cos\theta)P_s{}^{|m|}(\cos\theta')].$$

Substituting into (9),

$$I_{nn_0}{}^{|\Delta m|}=\sum_{\substack{s,s'\\|m|\le s}}[(2s+1)(2s'+1)\exp(i(\delta_s{}^n+\delta_{s'}{}^0)) \times((s-|m|)!/(s+|m|)!)e^{im\varphi}P_s{}^{|m|}(\cos\theta) \times\int d\tau' f_s{}^n f_{s'}{}^{n_0}V_2P_s{}^{|m|}P_2{}^{|\Delta m|}P_{s'}e^{i(\Delta m-m)\varphi'}.$$

Integration over φ' immediately gives only one term in the m summation, *viz.*, $m=\Delta m$. Integration over θ leaves three terms in the s' summation, *viz.*, $s=s'$, $s'\pm2$.

[6] L. Shiff, *Quantum Mechanics* (Mc-Graw Hill Book Company, Inc., New York, 1948), Chap. V.

Defining

$$a_{ss'}{}^{\Delta m}=(2s'+1)(P_s{}^{|\Delta m|}|P_2{}^{|\Delta m|}|P_{s'}), \quad (11)$$

$$(n_0s'|V_2|ns)=\int f_s{}^0 f_s{}^n V_2r^2dr, \quad (12)$$

we have

$$I_{nn_0}{}^{\Delta m}=2\pi\sum_s[(2s+1)((s-|\Delta m|)!/(s+|\Delta m|)!) \times\exp(i\delta_s{}^n)e^{i\Delta m\varphi}P_s{}^{|\Delta m|}(\cos\theta) \times[\exp(i\delta_s{}^0)a_{ss}{}^{\Delta m}(n_0s|V_2|ns) +\exp(i\delta_{s\pm2}{}^0)a_{ss\pm2}{}^{\Delta m}(n_0s\pm2|V_2|ns)]. \quad (13)$$

We now substitute (13) into (10) and integrate to find a total cross section, *viz.*,

$$\sigma=\int\sigma(\theta,\varphi)d(\cos\theta)d\varphi.$$

The angular integration involves

$$\int P_s{}^{|\Delta m|}P_{s'}{}^{|\Delta m|}d(\cos\theta) =\delta_{ss'}((s+|\Delta m|)!/(s-|\Delta m|)!)2(-1)^{\Delta m}/(2s+1),$$

whence

$$\sigma=\pi|M_{n_0m_0}{}^{nm}|^2(2\mu/\hbar^2)^2[\sum_s(2s+1) \times((s-|\Delta m|)'/(s+|\Delta m|)!B_s{}^2](k_n/k_{n_0}), \quad (14)$$

where

$$B_s{}^2=|\exp(i\delta_s{}^0)a_{ss}{}^{|\Delta m|}(n_0s|V_2|ns) +\exp(i\delta_{s\pm2}{}^0)a_{ss\pm2}{}^{\Delta m}(n_0s|V_2|ns\pm2)|^2. \quad (15)$$

The $a_{ss'}{}^{\Delta m}$ defined by (11) are easily calculated using the customary recurrence relations of Legendre polynomials. They will not be explicitly presented here. Suffice it to say that for large s, $a_{ss'}{}^{\Delta m}\sim0(s^{\Delta m})$.

It only remains to find the distorted partial radial waves f_s, their phase shifts δ_s and

$$\int f_s{}^{n_0}e^{-\alpha r}f_{s'}{}^n r^2dr.$$

The f's are solutions of

$$[1/r^2(d/dr)(r^2(d/dr))+k^2-(2\mu V_0/\hbar^2)e^{-\alpha r} -(s(s+1)/r^2)]f_s(r)=0.$$

This equation is unsolvable except for the case $s=0$. However, as α is very large, the potential rises extremely rapidly in the region of the turning point. For energies $E_{\text{inc}}=kT$, $k=3.51\text{A}^{-1}$ compared to $\alpha=3.53\text{A}^{-1}$. Thus for thermal incident energies, λ is roughly comparable with the space decay rate of the potential, i.e., about one wavelength/2π can fit into the region of varying potential. Hence the wave does not feel the potential for

very much of its history. This is a hard sphere type collision; the distorted wave will be approximated by rigid wall type wave functions, *viz.*,

$$f_s=\cos\delta_s j_s-\sin\delta_s n_s,$$
$$\tan\delta_s=j_s(kr_0)/n_s(kr_0), \tag{16}$$

where r_0 is the turning point.

As $\int V_2 e^{-\alpha r} f_0^s f_n^{s'} r^2 dr$ is integrated from the turning point, the value of V at the turning point is T, the kinetic energy

$$V(r_0)=V_0 e^{-\alpha r_0}=T,$$
$$V(r)=V_0 e^{-\alpha r}=Te^{-\alpha(r-r_0)}.$$

However, as there are two turning points under consideration, the incident and outgoing waves having different energy, one must somehow take a mean of the two effects. We will take a mean of the turning points or what is equivalent,

$$V=(E_{\text{inc}}E_{\text{out}})^{\frac{1}{2}}e^{-\alpha(r-r_0)},$$

where r_0 is the classical kinetic theory diameter.

Hence $(f_{n_0}^s|V_2|f_n^{s'})$ is approximated by

$$0.45(E_{\text{inc}}E_{\text{out}})^{\frac{1}{2}}\int_{r_0}^{\infty} e^{-\alpha(r-r_0)} f_{n_0}^s f_n^{s'} r^2 dr,$$

where

$$f_n^s=\frac{n_s(k_n r_0)j_s(k_n r)-j_s(k_n r_0)n_s(k_n r)}{(j_s^2(k_n r_0)+n_s^2(k_n r_0))^{\frac{1}{2}}}.$$

Unfortunately, only the $(f_{n_0}^0|V_2|f_n^0)$ integral is feasible in closed form. Hence these integrals were done numerically for two cases, the 2→0 deactivation and 3→1 deactivation in H_2 with incident energy kT ($T=300°K$).

For the 2→0 case, $k_2=3.51A^{-1}$, $k_0=5.75A^{-1}$.

For the 3→1 case, $k_3=3.51A^{-1}$, $k_1=6.85A^{-1}$.

r_0, the classical turning point, is taken as 2.72A, this being the kinetic collision diameter accepted for H_2.

Calculations were carried out to 1 percent accuracy.

We abbreviate

$$\int_{r_0}^{\infty} r^2 dr f_s^{n_0} f_{s'}^{n} = g_{ss'}^{n_0 n}.$$

In both cases the $g_{00}^{n_0 n}$, calculated numerically, checked with the exact integral to better than 1 percent.

$$g_{00}^{n_0 n}=1/k_{n_0}k_n\int_{r_0}^{\infty}\sin k_0(r-r_0)\times\sin k_n(r-r_0)e^{-\alpha(r-r_0)}dr$$
$$=\alpha/k_{n_0}k_n[(1/(\alpha^2+(k_{n_0}+k_n)^2)-(1/(\alpha^2+(k_{n_0}-k_n)^2)]. \tag{17}$$

Because of the rapid asymptotic approach of the spherical Bessel functions for moderate s and our relatively large values of kr_0 [the first maximum of $j_s(kr_0)$ occurs at $s\approx kr_0$], the values of these integrals are fairly constant and then drop rather suddenly for $s>10$, e.g., $g_{00}^{20}=4.07$, $g_{55}^{20}=4.10$, $g_{99}^{20}=3.80$. Similar constancy is obtained for $g_{ss\pm2}^{nn_0}$, but not quite so pronounced as the above. At any rate in approximate work, one may take $g_{ss'}^{nn_0}=g_{00}^{nn_0}$ for s or $s'\leq k_{kT}r_0$ and $=0$ for both $s, s'>k_{kT}r_0$, where $k_{kT}=(2\mu kT/\hbar^2)^{\frac{1}{2}}$, $r_0=$classical turning point and $g_{00}^{nn_0}$ is given by Eq. (16). From Eq. (15) it is seen that strong interference terms arise for $\delta_s\neq\delta_{s\pm2}$, where $\tan\delta_s$ is given by (16). It can readily be shown that this interference drops out in the region where $s\approx kr_0$. It turned out in the final calculation that terms $8\leq s\leq 12$ contributed strongly to the sum (15) and the rest but negligibly. In future approximate work one may form an approximation to the transition probability through the above considerations.

V. NUMERICAL RESULTS

We will make the abbreviation

$$A_{nn_0}^{\Delta m}=\sum_s(2s+1)((s-|\Delta m|)!/(s+|\Delta m|)!)B_s^2.$$

Our calculations using the $a_{ss'}^{\Delta m}$ from (11), the $g_{ss'}^{n_0 n}$ numerically calculated and the phase shifts calculated from formula (16), have yielded for incident energy kT

$$A_{20}^{0}=2.95\times10^{-3}A^6,$$
$$A_{31}^{0}=0.91\times10^{-3}A^6.$$

It is to be noted that the ratio of the squares of the $g_{00}^{nn_0}$ is

$$|g_{00}^{02}|^2/|g_{00}^{13}|^2=16.6/6.25=2.66,$$

whereas the ratio of A's is 3.24. Though the agreement is far from exact, it indicates that we can indeed use the $g_{00}^{nn_0}$ term as a barometer to calculate other effects such as energy dependence, effect of moment of inertia, etc., i.e., we let

$$A_{nn_0}^{0}\approx|g_{00}^{nn_0}|^2\times2\times10^2.$$

In order to calculate a cross section, we now rewrite formula (10)

$$\sigma_{n_0m_0}^{nm}=\pi|M_{n_0m_0}^{nm}|^2k_n^2k_{n_0}^2A_{nn_0}^{\Delta m}(k_n/k_{n_0})\times0.45^2,$$

where we have used the formula

$$(2\mu/\hbar^2)(E_nE_{n_0})^{\frac{1}{2}}=k_nk_{n_0}.$$

Transitions for which $\Delta m=0$

For $n_0=2$, $n=0$,

$$M_{20}^{00}=(1/2)^{\frac{1}{2}}(1/2)^{\frac{1}{2}}\int_{-1}^{+1}P_0P_2P_2dx=(1/5)^{\frac{1}{2}},$$

$A_{20}^{0}=2.95\times10^{-3}A^6$ for incident energy kT,

$\sigma_{20}^{00}=2.49\times10^{-1}A^2$,

$\sigma_{\text{kin}}=23.2A^2$.

The transition probability P_{20}^{00} is given by

$P_{20}^{00}=\sigma_{20}^{00}/\sigma_{\text{kin}}=1.07\times10^{-2}$ for incident energy kT.

For $n_0=3$, $n=1$,

$$M_{30}^{10}=(3/2)^{\frac{1}{2}}(7/2)^{\frac{1}{2}}\int_1^{+1}P_1P_2P_3$$
$$=(3/4)(1/3)^{\frac{1}{2}}(1/7)^{\frac{1}{2}}(12/5),$$

$M_{31}^{11}=M_{3-1}^{1-1}=(3/2)M_{30}^{10}$,

$A_{31}^{0}=0.909\times10^{-3}\text{A}^6$ for incident energy kT,

$\sigma_{30}^{10}=1.01\times10^{-1}\text{A}^2$,

$P_{30}^{10}=4.33\times10^{-3}$,

$P_{31}^{11}=P_{3-1}^{-1-1}=(3/2)P_{30}^{10}$.

Transitions for Which $\Delta m\neq0$

It is seen from (11) that for large s, $a_{ss'}^{0}\approx0(1)$, $a_{ss'}^{(1)}\approx0(s)$, and $a_{ss'}^{(2)}\approx0(s^2)$. In the expression for the total cross section given by formula (14), it is seen that these powers of s are canceled out by the factors $(s-|\Delta m|)!/(s+|\Delta m|)!$, hence making all coefficients 0(1). Thus it is a good approximation to let $A_{nn_0}^{\Delta m}=A_{nn_0}^{0}$. In what follows this approximation will be made.

It only remains to calculate the matrix elements $M_{2m_0}^{0m}$ and $M_{3m_0}^{1m}$ as defined in 10, in order to estimate transition probabilities for $\Delta m\neq0$.

For $M_{2m_0}^{0m}$, there are only four possibilities, *viz.*, $m_0=\pm1$, $m=0$ and $m_0=\pm2$, $m=0$:

$$M_{2\pm1}^{00}=(1/6)^{\frac{1}{2}}M_{20}^{00},$$
$$M_{2\pm2}^{00}=(1/24)^{\frac{1}{2}}M_{20}^{00}.$$

For $M_{3m_0}^{1m}$, there are six possible transitions for $\Delta m=1$, *viz.*, $\pm1\to0$, $0\to\pm1$, $\pm2\to\pm1$ and six possible transitions for $\Delta m=2$, *viz.*, $\pm2\to0$, $\pm3\to\pm1$, $\pm1\to\mp1$:

$$M_{3\pm1}^{10}=(4/27)^{\frac{1}{2}}M_{30}^{10},$$
$$M_{3\pm2}^{1\pm1}=(5/27)^{\frac{1}{2}}M_{30}^{10},$$
$$M_{30}^{1\pm1}=(1/18)^{\frac{1}{2}}M_{30}^{10},$$
$$M_{3\pm2}^{10}=(5/216)^{\frac{1}{2}}M_{30}^{10},$$
$$M_{3\pm3}^{1\pm1}=(5/72)M_{30}^{16},$$
$$M_{3\pm1}^{1\mp1}=(1/72)M_{30}^{10}.$$

Mean Transition Probabilities

In order to calculate mean transition probabilities, it is necessary to add all contributions for the various Δm transitions. Thus

$$P_{20}=\sum_{\Delta m}P_{20}^{\Delta m}/5,$$

$$P_{31}=(1/7)(P_{30}^{10}+P_{3\pm1}^{1\pm1}+P_{3\pm1}^{10}+P_{3\pm2}^{1\pm1}$$
$$+P_{30}^{1\pm1}+P_{3\pm3}^{1\pm1}+P_{3\pm2}^{10}+P_{3\pm1}^{1\mp1}).$$

Using the approximation $A_{n_0n}^{\Delta m}=A_{n_0n}^{0}$ and the above calculation for the matrix elements,

$$P_{20}=3.04\times10^{-3},\quad P_{31}=2.96\times10^{-3}.$$

VI. COMPARISON WITH EXPERIMENT

In order to compare with experiment, it is necessary to interpret the sound dispersion data obtained by Zartmann.[3] It will be assumed that *ortho-* and *para-*hydrogen are separately two-state gases. This assumption is justified by the populations of the rotational levels of H_2 at room temperature, given in Table I. For a two-state gas the relaxation time τ is given by the formula[7]

$$\tau^{-1}=\gamma Z(1+\xi),$$

where $\xi=(g(\epsilon_n)/g(\epsilon_0))\exp[-(1/kT)(\epsilon_n-\epsilon_{n0})]$, $g(\epsilon_n)$ = degeneracy of the quantum state, Z = mean number of collisions undergone by a molecule/second, γ = probability of deactivation. τ^{-1} is obtained experimentally and is equal to $\omega_{\max}$, where $\omega_{\max}$ is the circular frequency where the absorption is a maximum. Zartmann[3] has observed $\omega_{\max}=10$ megacycles at one atmosphere pressure. Now $(1/4)(3\xi_{ortho}+\xi_{para})=0.20$ and $Z=1.58\times10^{10}$ sec^{-1} for H_2, hence one can calculate $\bar{\gamma}$ for *ortho* and *para*-H_2.

$$\bar{\gamma}_{\text{exp}}=\frac{\omega_{\max}}{Z(1+0.20)}=3.3\times10^{-3}.$$

If we take a weighted mean of P_{20} and P_{31} calculated in the previous section we find

$$\gamma_{\text{th}}=3.0\times10^{-3}.$$

It is seen that the theory is in excellent agreement with experiment, verifying a persistence of rotation unexpected classically. This is due to the large rotational level spacing of H_2, which in turn is due to its abnormally small moment of inertia.

VII. ACKNOWLEDGMENTS

I would like to express my gratitude to Professor George E. Kimball for his guidance of this research and more generally of my scientific education. Thanks are due Professor Hans Bethe of Cornell University for many helpful suggestions proffered in the course of a

TABLE I.

Gas	Level	Population on basis of 1 at 300°K
ortho	$S=1$	0.878
	3	0.121
	5	0.001
para	0	0.514
	2	0.470
	4	0.016

[7] See, for example, H. Kneser, Ergeb. exakt. Naturw. 22 (1949).

conversation regarding this problem. Lastly, I would like to thank the U. S. Atomic Energy Commission for their support while this research was being carried out.

Note added in proof.—Recent calculations by Takayanaki [Progr. Theoret. Phys. Japan] have been called to the author's attention. The methods used in these papers are quite similar to those presented here. The main difference is the rigorous numerical procedure that we carried out to all contributing distorted waves. It might be added here that our numerically calculated distorted waves gave a phase shift that compared very well with that calculated by the W.K.B. method using the true exponential potential rather than the superimposed rigid wall. This agreement as well as the agreement of Takayanaki calculations using a classical approximation points up the insensitivity of the distorted waves to steepness of the potential, a result expected with massive particles.

THE JOURNAL OF CHEMICAL PHYSICS VOLUME 22, NUMBER 5 MAY, 1954

The Infrared Spectrum of Disilane

H. S. GUTOWSKY AND E. O. STEJSKAL
Noyes Chemical Laboratory, University of Illinois, Urbana, Illinois

(Received December 14, 1953)

The infrared absorption spectrum of Si_2H_6 gas has been observed from 350 to 4000 cm^{-1}. Four of the five infrared active fundamentals have been found and assigned (ν_5 and ν_6, $\parallel$ bands at 2154.4 and 842.7 cm^{-1}; ν_7 and ν_8, $\perp$ bands at 2181.1 and 945.7 cm^{-1}). The Q branches of ν_7 and ν_8 were observed with moderate dispersion and the spacings measured as 2.43_5 and 3.42 cm^{-1}. These spacings are consistent with the Coriolis interaction in a symmetric top without internal rotation, but they do not agree with the spacings predicted by assuming free internal rotation. The general appearance of ν_7 and ν_8 in disilane is similar to these bands in ethane, suggesting comparable potential barriers to internal rotation. In the course of the experiments it was found that disilane decomposes slowly at room temperature into SiH_4 and that in the preparation of disilane from Si_2Cl_6, the Si—Si bond is cleaved by an excess of $LiAlH_4$, producing SiH_4.

INTRODUCTION

RELATIVELY little structural information is available for disilane, Si_2H_6, even though it is the silicon analog of ethane and as such could be of some significance in comparing the chemistry of carbon and silicon. Brockway and Beach[1] made an electron diffraction study of disilane and found the Si—Si bond distance to be 2.32±0.03A. The Raman spectrum of the gas was observed by Stitt and Yost.[2] Three lines were found including a Si—Si stretching fundamental of 434.5 cm^{-1} from which Anderson and Burg[3] estimated a corresponding force constant of 1.7×10^5 dyne cm^{-1}. More recently, the reaction between lithium aluminum hydride and Si_2Cl_6 was discovered by Finholt[4] to be a convenient method of preparing disilane and this encouraged us to investigate its infrared absorption spectrum.

EXPERIMENTAL

In our preparation of disilane several modifications of the reaction between lithium aluminum hydride and hexachlorodisilane[5] were tried. As described by Finholt the reaction was carried out by slowly adding a 15 percent excess of a solution of $LiAlH_4$ in diethyl ether to Si_2Cl_6 also dissolved in ether, cooling and stirring the reaction mixture; the yield reported was 87 percent of that predicted from the Si_2Cl_6 used. Our first preparation followed this general procedure; the low dispersion infrared spectrum of the product exhibited traces of SiH_4 and ether besides the characteristic spectrum of Si_2H_6. After this sample had been sealed in a Pyrex bulb for 18 months, its infrared spectrum was re-examined revealing that the gas was now SiH_4, with a trace of ether but no Si_2H_6. All of the sample condensed in liquid nitrogen so it is inferred that the decomposition is described by a stoichiometric equation such as $2Si_2H_6 \rightarrow 3SiH_4+Si$. A light greyish deposit was found in the storage bulb and presumably was Si or else[6] $(SiH)_x$.

The instability of disilane was shown also by several reactions in which a solution of Si_2Cl_6 was added to a solution of $LiAlH_4$ so that an excess of the latter was always present. In this event, the product was exclusively SiH_4, the Si—Si bond being cleaved in the course of the reaction. The product was identified by determining the gas density and also by comparing its infrared spectrum with data[7] published for SiH_4. In these reactions either tetrahydrofuran or di-*n*-butyl ether was employed as the solvent.

[1] L. O. Brockway and J. Y. Beach, J. Am. Chem. Soc. **60**, 1836 (1938).
[2] F. Stitt and D. M. Yost, J. Chem. Phys. **5**, 90 (1937).
[3] T. F. Anderson and A. B. Burg, J. Chem. Phys. **6**, 586 (1938).
[4] Finholt, Bond, Wilzbach, and Schlesinger, J. Am. Chem. Soc. **69**, 2692 (1947).
[5] Available commercially from Anderson Laboratories Inc., Adrian, Michigan.
[6] D. T. Hurd, *An Introduction to the Chemistry of the Hydrides* (John Wiley and Sons, Inc., New York, 1952), p. 106.
[7] W. B. Steward and H. H. Nielsen, Phys. Rev. **47**, 828 (1935); Tindal, Straley, and Nielsen, Phys. Rev. **62**, 151 (1942).

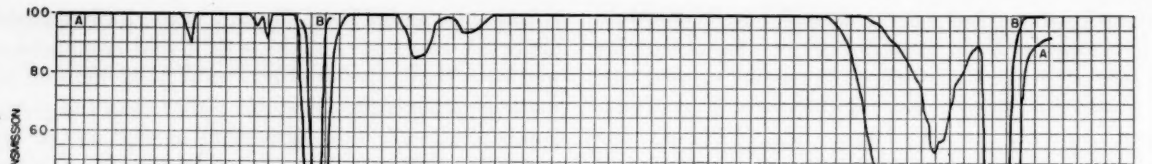

FIG. 1. The low dispersion infrared spectrum of Si_2H_6 gas.

The reactivity of the silicon hydrides is well known; they are spontaneously combustible in air. However, the relative instability of the Si—Si bond does not appear[6] to have attracted much attention previously. Yet this instability is no doubt associated directly with such chemical properties of silicon as its tendency to form siloxanes but not silicon analogs of the long chain hydrocarbons. The Si—Si bond stretching force constant of 1.7×10^5 dyne cm^{-1} is to be compared with the C—C constant of 4.5×10^5, and the C—I constant[8] of 2.7×10^5 dyne cm^{-1}.

The spectrum of disilane was observed with two instruments: a Perkin-Elmer model 21 double-beam recording spectrophotometer utilizing a NaCl prism, and a Perkin-Elmer model 112 single-beam, double-pass spectrometer with NaCl, LiF, KBr, and CsBr prisms. The sample cells for the gas were 10 cm long and contained KBr windows; all observations were made at room temperature. The model 21 instrument was used primarily for survey work and to locate some of the overtone and combination bands; the calibration is good to about ±15 cm^{-1} at 3000 cm^{-1} and ±1 cm^{-1} at 650 cm^{-1}. The LiF prism in the model 112 instrument was used to analyze the absorption at 2150 cm^{-1} (ν_5 and ν_7). It was calibrated mainly against the CO band in the vicinity of 2150 cm^{-1} and also against the atmospheric CO_2 absorption at 2350 cm^{-1}; in this region the accuracy is the order of ±0.1 cm^{-1}. The NaCl prism in the model 112 instrument was calibrated against water vapor absorption and NH_3. The absorption of disilane about 900 cm^{-1} (ν_6 and ν_8) was analyzed with the NaCl prism, and in this region the accuracy is ±0.3 cm^{-1}. A search for low-lying bands was made to 350 cm^{-1} with KBr and CsBr prisms, but with negative results.

TABLE I. The infrared and Raman spectra of Si_2H_6 gas.

Raman $\Delta\nu$ cm^{-1}	Infrared ν cm^{-1}	Assignment
434.5 m, sharp		ν_3
	842.7 s, ∥	ν_6
910–935 w, diffuse		ν_2
	945.7 m, ⊥	ν_8
	1775 w	$\nu_2+\nu_6$
	1860 w	$\nu_2+\nu_8$
	2154.4 m, ∥	ν_5
2163 s, sharp		ν_1
	2181.1 m, ⊥	ν_7
	2502 w	?
	2585 vw	$\nu_3+\nu_5$
	3045 w	$\nu_6+\nu_7$

[8] G. Herzberg, *Infrared and Raman Spectra of Polyatomic Molecules* (D. Van Nostrand Company, Inc., New York, 1945), pp. 193, 391, 424, 438.

RESULTS AND DISCUSSION

Assignment of Fundamentals

The low dispersion infrared spectrum of Si_2H_6 gas is shown in Fig. 1. The partially resolved absorption about 2150 cm^{-1} is reproduced in Fig. 2 and that in the vicinity of 950 cm^{-1} in Fig. 3. The Raman data and the gross features of the infrared spectrum are summarized in Table I, which also includes the frequency assignments. The fundamental modes of vibration and the selection rules are listed in Table II, assuming D_{3d} symmetry.

The Raman data are unfortunately incomplete; the three lines observed at displacements of 2163, 910–955, and 434.5 cm^{-1} correspond most likely to the totally symmetric A_{1g} vibrations, from intensity considerations. Their assignments[2] as Si—H stretching, SiH_3 bending, and Si—Si stretching vibrations, respectively, are reason-

TABLE II. The fundamental vibrations of Si_2H_6.

Species D_{3d}	Designation	Description	Activity	Assigned frequency
A_{1g}	ν_1	Si—H stretching	R. pol.	2163 cm^{-1}
	ν_2	SiH_3 bending		910–955
	ν_3	Si—Si stretching		434.5
A_{1u}	ν_4	torsion	Inactive	
A_{2u}	ν_5	Si—H stretching	I. ∥	2154.4
	ν_6	SiH_3 deformation		842.7
E_u	ν_7	Si—H stretching	I. ⊥	2181.1
	ν_8	SiH_3 deformation		945.7
	ν_9	SiH_3 rocking		
E_g	ν_{10}	Si—H stretching	R. depol.	
	ν_{11}	SiH_3 deformation		
	ν_{12}	SiH_3 rocking		

able. The assignment is supported by comparison with the results on ethane[9] and on silane.[7]

Of the four strongest infrared bands two, at 2154.4 and 842.7 cm^{-1}, have the well-defined PQR branch structure expected for $\parallel$ bands of symmetric-top molecules.[8] These frequencies agree very well with the A_{1g} Si—H stretching and SiH_3 bending frequencies and with the frequencies observed for similar motions in[7] SiH_4 and in[10] SiH_3Cl. So the two bands are assigned as the $\parallel A_{2u}$ fundamentals ν_5 and ν_6. Supporting evidence is given by the separation of the maxima of the P and R branches, which is 18.5 cm^{-1} in ν_5 and 19.2 in ν_6. If one assumes the electron diffraction[1] Si—Si distance of 2.32A and the microwave results[11] for the configuration of the SiH_3 group in SiH_3Cl (Si—H, 1A; H—Si—H angle, 110° 57′), the rotational constants A and B of disilane are calculated to be 1.369 and 0.173 cm^{-1}, respectively. This value of B yields an estimated[8] $P-R$ maxima separation of 17 cm^{-1} which agrees sensibly with observation.

The other two strong infrared bands have well resolved Q branches characteristic of $\perp$ bands of symmetric top molecules.[8] Moreover, in the band about 950 cm^{-1} there is a bare indication that every third line may have a slightly enhanced intensity, as expected for a molecule with three nuclei of nonzero spin about a threefold symmetry axis. The band near 2180 cm^{-1} is undoubtedly a Si—H stretching frequency, while that near 950 cm^{-1} is close to the A_{2u} SiH_3 deformation frequency of 842.7 cm^{-1}. Therefore the two $\perp$ bands are assigned as the $\perp E_u$ fundamentals ν_7 and ν_8.

There remains the infrared active SiH_3 rocking mode, ν_9, which is unassigned. In SiH_3Cl the analagous vibration has been found[10] at 770 cm^{-1}. However, a careful check of the spectrum of disilane over the region from 1100 to 700 cm^{-1} and also the survey with KBr and CsBr prisms to 350 cm^{-1} revealed no absorption that could be attributed to ν_9. The three SiH_3 bands found (ν_2, ν_6, and ν_8) range only from 840 to 950 cm^{-1} and one is tempted to say that ν_9 is obscured by the very intense $\parallel$ band at 842.7 cm^{-1}. The three Raman active E_g fundamentals also have not been observed, and with four fundamentals missing, the assignments suggested for the combination bands in Table I are at best provisional.

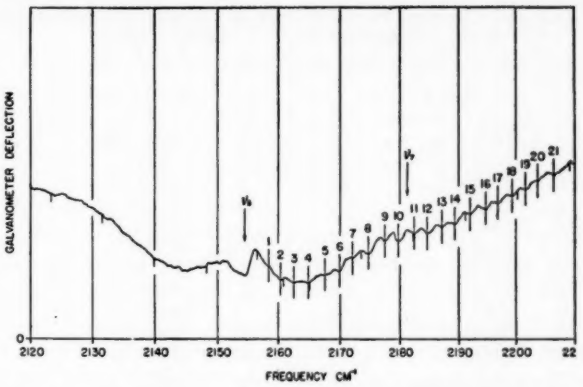

FIG. 2. The fundamental $\parallel$ band ν_5 and the fundamental $\perp$ band ν_7 of Si_2H_6 gas with moderate dispersion. The gas pressure was 0.3 cm in a 10 cm long cell; the slit width was 85μ.

Fine Structure of the $\perp$ Bands ν_7 and ν_8

It may be seen in Figs. 2 and 3 that the double-pass optics in the model 112 instrument were adequate to resolve the line-like Q branches of the $\perp$ bands ν_7 and ν_8. The observed lines are listed in Table III along with tentative assignments. Besides assisting in the determination of the fundamental frequencies, the resolved fine structure provides evidence bearing upon the question of hindrance to rotation of the SiH_3 groups about the Si—Si bond.

The band ν_7 partially overlaps ν_5 and this, as well as the rather erratic intensities of the various Q branches,

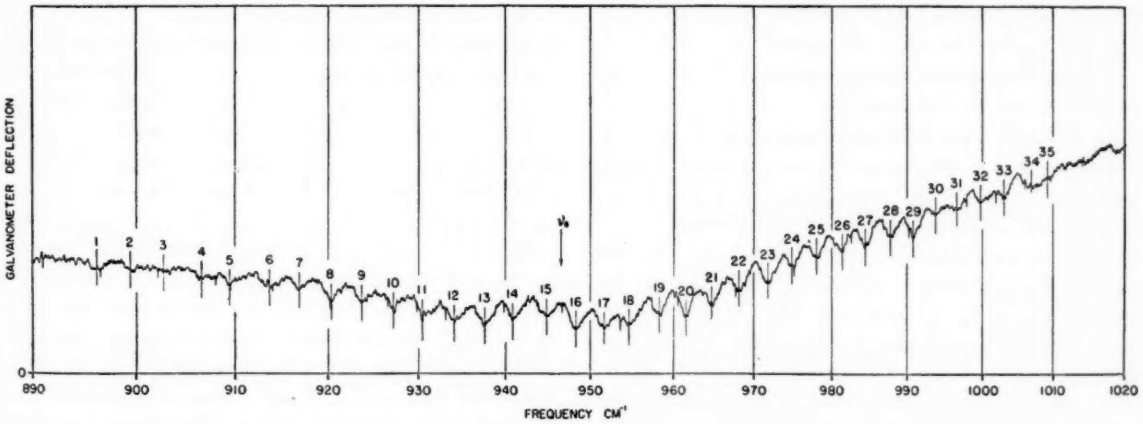

FIG. 3. The fundamental $\perp$ band ν_8 with moderate dispersion. The gas pressure was 1.4 cm in a 10 cm long cell; the slit width was 111μ.

[9] L. G. Smith, J. Chem. Phys. **17**, 139 (1949).
[10] A. Monfils, J. Chem. Phys. **19**, 138 (1951).
[11] Dailev, Mays, and Townes, Phys. Rev. **76**, 136 (1949); A. H. Sharbaugh, Phys. Rev. **74**, 1870 (1948).

TABLE III. Observed wave numbers and provisional assignments of the Q branches[a] in the $\perp$ bands ν_7 and ν_8.

	Band ν_7	
1	2158.5 cm^{-1}	$^PQ_{10}$
2	2160.4	$^PQ_9$
3	2162.6	$^PQ_8$
4	2165.0	$^PQ_7$
5	2167.7	$^PQ_6$
6	2169.7	$^PQ_5$
7	2172.1	$^PQ_4$
8	2174.8	$^PQ_3$
9	2177.5	$^PQ_2$
10	2179.8	$^PQ_1$
11	2182.5	$^RQ_0$
12	2184.7	$^RQ_1$
13	2187.1	$^RQ_2$
14	2189.3	$^RQ_3$
15	2191.9	$^RQ_4$
16	2194.7	$^RQ_5$
17	2196.8	$^RQ_6$
18	2199.2	$^RQ_7$
19	2201.6	$^RQ_8$
20	2203.6	$^RQ_9$
21	2206.4	$^RQ_{10}$

	Band ν_8	
1	896.0 cm^{-1}	$^PQ_{15}$
2	900.0	$^PQ_{14}$
3	903.0	$^PQ_{13}$
4	906.5	$^PQ_{12}$
5	909.0	$^PQ_{11}$
6	913.5	$^PQ_{10}$
7	917.0 cm^{-1}	$^PQ_9$
8	920.0	$^PQ_8$
9	923.5	$^PQ_7$
10	927.0	$^PQ_6$
11	930.5	$^PQ_5$
12	934.0	$^PQ_4$
13	937.5	$^PQ_3$
14	941.0	$^PQ_2$
15	945.0	$^PQ_1$
16	948.0	$^RQ_0$
17	951.5	$^RQ_1$
18	954.5	$^RQ_2$
19	958.0	$^RQ_3$
20	961.5	$^RQ_4$
21	965.0	$^RQ_5$
22	968.5	$^RQ_6$
23	972.0	$^RQ_7$
24	975.0	$^RQ_8$
25	978.0	$^RQ_9$
26	981.5	$^RQ_{10}$
27	984.5	$^RQ_{11}$
28	988.0	$^RQ_{12}$
29	991.0	$^RQ_{13}$
30	994.0	$^RQ_{14}$
31	996.5	$^RQ_{15}$
32	999.5	$^RQ_{16}$
33	1003.0	$^RQ_{17}$
34	1007.0	$^RQ_{18}$
35	1009.5	$^RQ_{19}$

[a] The assignments ^PQ_n and ^RQ_n refer to ΔK's of -1 and $+1$, respectively, while the subscript n gives the K value for the lower state.

makes it difficult to determine the zero branch. Strictly as a guess "line" 11 at 2182.5 cm^{-1} is chosen as $^RQ_0$. Theoretically, the zero sub-lines of the Q branches of a $\perp$ band of a symmetric top molecule without internal rotation are given by[8]

$$\nu=\nu_0+A'(1-2\zeta)-B'\pm 2\{A'(1-\zeta)-B'\}K+\{(A'-B')-(A''-B'')\}K^2. \quad (1)$$

The observed Q branches of ν_7 are fitted very well by the straight line

$$\nu=2182.3\pm 2.435K. \quad (2)$$

Equation (2) suggests that anharmonic and rotation-vibration interaction effects are within our experimental error and can be neglected. On this basis, Eqs. (1) and (2) were solved simultaneously by introducing the A and B values calculated above from the electron diffraction and microwave structural data, giving approximate values for ζ_7 and ν_{07}. The result for the Coriolis interaction constant ζ_7 is -0.01 and for ν_{07}, 2181.1 cm^{-1}.

In the case of ν_8 the choice of the zero branch is somewhat confused by irregularities in the unresolved background of P and R branches. However, of the "lines" 13 to 18, 13, and 16 appear slightly more intense; and because 16 is at the maximum of the absorption it is assigned as $^RQ_0$. The observed Q branches are fitted quite well by the straight line

$$\nu=947.8\pm 3.42K, \quad (3)$$

at least through line 26. The computed values for higher frequencies are too large, suggesting that the K^2 term in Eq. (1) may be important. However, the higher frequency lines are weak and the precision low, so it does not seem worth while to include a K^2 term in fitting the data. From Eqs. (1) and (3) we find ζ_8 to be -0.37 and ν_{08}, 945.7 cm^{-1}.

Restriction of Internal Rotation in Si_2H_6

In the discussion above it has been assumed that disilane behaves as a rigid symmetrical top without internal rotation of the SiH_3 groups. We shall now review the evidence supporting such a view. Qualitatively, the structure of the $\perp$ bands ν_7 and ν_8 for disilane resembles very closely that found for ethane[9] which has a sizable barrier to internal rotation. The Q branches in disilane are relatively sharp considering the moderate dispersion of the spectrometer. Moreover, the values obtained above for the Coriolis interaction constants ζ_7 and ζ_8 in disilane are -0.01 and -0.37, which compare favorably with the values[9] 0.095 and -0.331 for the equivalent bands in ethane.

Howard[12] has shown in the case of free internal rotation, when two degenerate frequencies of different symmetry are themselves accidentally degenerate, that the spacing of the Q branches of a $\perp$ band is given by $[4A(1-\zeta)-2B]$ rather than by the term $[2A(1-\zeta)-2B]$ in Eq. (1) which applies to a rigid symmetric top. Moreover, when the rotation is free the Q branches themselves have a fine structure spacing of $2B$. In fact, $\perp$ bands of this sort have been observed for dimethyl mercury,[13] zinc,[13] and cadmium[14] and also for dimethyl acetylene.[13] And for these compounds there is independent evidence that the methyl groups are free to rotate.

The observed Si—H stretching vibrations of disilane range only from 2154 to 2182 cm^{-1}, so it is probable that the unobserved E_u fundamental ν_{10} will be very close to ν_7. And a similar argument holds for ν_{11} and ν_8. Accordingly, if the rotation in disilane were free, we would expect the Q branch spacings in ν_7 and ν_8 to be given by Howard's equation.[12] This is possible, in principle, by adjusting the value of ζ, and this procedure leads to values for ζ_7 and ζ_8 of 0.49 and 0.31, respectively. Now in the case of ethane, the observed[9] ζ's agree very well with the values found[8] in the methyl halides. Data on the halosilanes are limited, but ζ's can be calculated for SiH_3Cl from the Q branch spacings and the A and B values of 2.74 and 0.22 cm^{-1} from microwave spectra.[11] The Q branch spacings observed[10] in SiH_3Cl are 5.48 and 6.18 cm^{-1} for the $\perp$ Si—H stretching and SiH_3 deforma-

[12] J. B. Howard, J. Chem. Phys. **5**, 451 (1937).
[13] Boyd, Thompson, and Williams, Discussions Faraday Soc. **9**, 154 (1950).
[14] Boyd, Williams, and Thompson, Nature **167**, 766 (1951).

tion bands, and the corresponding ζ's are -0.08 and -0.21. These values are in much better agreement with the values for disilane of -0.01 and -0.37, assuming hindered rotation, than with the values of 0.49 and 0.31 based upon free rotation. Also, in symmetric top molecules with MH_3 groups the M—H stretching vibrations do not usually interact appreciably with the rotation, and the free rotation value of 0.49 for ζ_7 is physically unreasonable. Similar arguments have been applied successfully to the dimethyl metal alkyls[13,14] and dimethyl acetylene.[13]

A final argument favoring restricted rotation in disilane is the absence of any resolved structure or extensive broadening of the Q branches themselves. Howard's analysis suggests a fine structure spacing of $2B$ in the event of free rotation. This spacing is less than the resolving power of the spectrometer we used, but if the fine structure were present, the Q branches should be broader than observed. Moreover, in the dimethyl compounds with free internal rotation an irregular fine structure was found[13,14] with spacing larger than $2B$, for which no detailed interpretation has apparently been given. In any event, the resolution in our experiments would have revealed any fine structure in disilane similar to that in the dimethyl compounds with free rotation. It is unfortunate that the other $\perp$ fundamental has not been found and resolved, for application of the sum rule[15] for the ζ's would give unequivocal evidence as to whether the internal rotation is free or restricted. One might also assume a value for ν_9 and compute[15] the ζ's directly from the normal or symmetry coordinates. The evidence available at present may not be considered conclusive, yet it seems most probable that there is a barrier to internal rotation in disilane, of magnitude comparable to that in ethane.

DISCUSSION

Potential barriers to internal rotation about single bonds have been observed in a number of simple molecules,[16,17] and several theories and types of interaction have been proposed[18,19] to account for the experimental results. Disilane appears to have particular merit in testing some of the postulated interactions. For instance, double-bond character is certainly of much less importance in the Si—Si bond than in the C—C. So comparable hindrance to internal rotation in disilane and ethane is evidence that in these compounds the potential barriers are not associated primarily with multiple bond character.

Also, disilane is a good intermediate case for establishing the dependence of the potential barriers upon interatomic distance. In ethane, where the barrier is about 3 kcal, the end to end interproton distance is 2.28A. In dimethyl acetylene and the dimethyl metal alkyls, where the rotation is free, the distances are about 4.85 and 5.15A. In disilane, where the potential barrier appears to be the same order as that in ethane, the distance is 3.25A.

Lassettre and Dean[19] have proposed that most of the potential barrier to rotation results from interaction between the electric quadrupole moments of the bonds in adjacent groups. Thus in ethane the barrier arises mainly from the angular dependence of repulsive quadrupole-quadrupole interactions of the C—H bonds at opposite ends of the molecule. These interactions vary inversely as the fifth power of the distance; but in disilane this is partially compensated by the increase of the quadrupole moment as the square of the bond length. The dimensional proportions of disilane are very much the same as in ethane, while the scale is about 1.5 times as large. So a simple estimate of the barrier in disilane can be made by assuming the results for ethane, applying the scale factor, and introducing an approximate quadrupole moment for the Si—H bond. In this manner,[19] the potential barrier in disilane is estimated to be the order of 1 kcal, which is consistent with the experimental findings.

ACKNOWLEDGMENT

This research was supported in part by a grant-in-aid from E. I. duPont de Nemours and Company. The instability of disilane and its decomposition to silane were found through experiments performed by C. J. Hoffman and P. G. Pallmer, Jr.; we gratefully acknowledge their interest and help in the early stages of the work.

[15] D. R. J. Boyd and H. C. Longuet-Higgins, Proc. Roy. Soc. (London) **213A**, 55 (1952).
[16] Gordy, Smith, and Trambarulo, *Microwave Spectroscopy* (John Wiley and Sons, Inc., New York, 1953), p. 106.
[17] E. Blade and G. E. Kimball, J. Chem. Phys. **18**, 630 (1950).
[18] C. A. Coulson, *Valence* (Clarendon Press, Oxford, 1952), p. 314.
[19] E. N. Lassettre and L. B. Dean, Jr., J. Chem. Phys. **17**, 317 (1949); see also L. J. Oosterhoff, Discussions Faraday Soc. **10**, 79 (1951).

Letters to the Editor

THIS section will accept reports of new work, provided these are terse and contain few figures, and especially few half-tone cuts. The Editorial Board will not hold itself responsible for opinions expressed by the correspondents. Contributions to this section should not exceed 600 words in length and must reach the office of the Editor not later than the 15th of the second month preceding that of the issue in which the Letter is to appear. No proof will be sent to the authors. A publication charge of $10.00 per Letter is made which, when honored, will entitle the Institution to 100 free reprints.

An Explanation of Certain Types of Curves Found in High-Frequency Techniques*

H. W. HAMME, E. L. GROVE, AND J. L. KASSNER
Division of Analytical Chemistry, University of Alabama, University, Alabama
(Received September 15, 1953)

THE high-frequency conductance and susceptance were measured for certain coil-type containers used in "high-frequency techniques" over a range of frequencies. At a certain narrow frequency band, or bands depending on the coil, there appears a sharp maximum of conductance accompanied by a sudden drop then rise of the susceptance values. If pure water is added to the container (which represents an increase in the over-all capacitance of the coil) the conductance and capacitance maxima shift to a lower frequency. This band represents a region of high sensitivity for titration or other measurement purposes, which is also the region of maximum absorption of energy.

If the distilled water is replaced with a dilute electrolyte as HCl (Fig. 1) the peak or peaks are shifted to a lower frequency due to the change in the composition of the core of the coil. The region of maximum sensitivity appears to be a function of the type and size of the coil, the solvent, the solute, and its concentration, and the distributive capacity between the coil and its case.

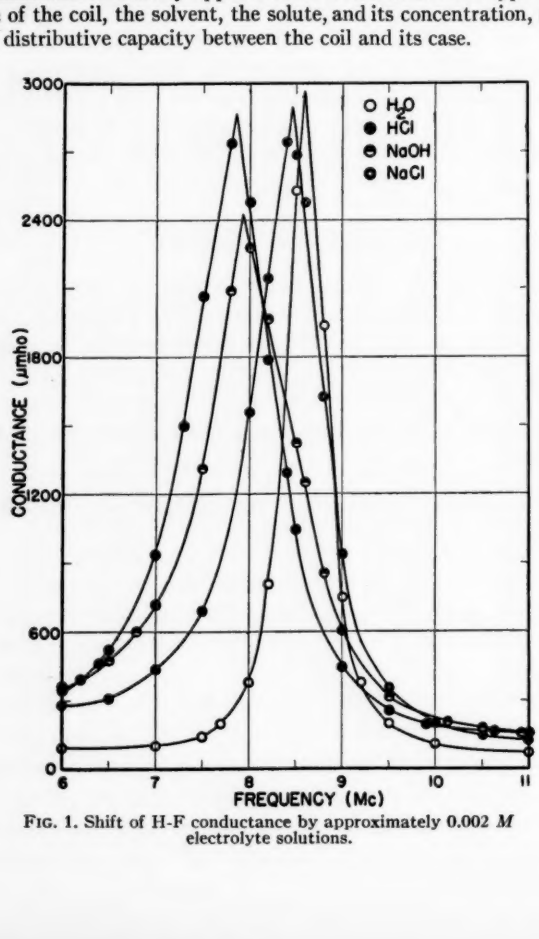

FIG. 1. Shift of H-F conductance by approximately 0.002 *M* electrolyte solutions.

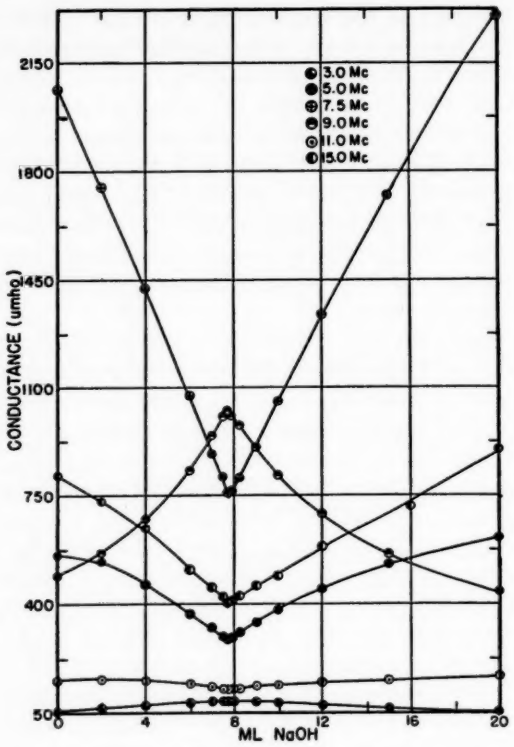

FIG. 2. Titration of HCl with NaOH at various frequencies.

In this work a 0.0015*N* HCl solution caused a shift of the H-F conductance maximum from 8.6 to 7.9 mc (Fig. 1). A similar solution of NaOH caused a similar shift, while the NaCl maximum shifted about 0.4 mc.

The literature contains examples of titrations[1–6] using both coil and condenser-type vessels with various shaped curves. However, Hall[3] was the first to call attention to the fact that certain titration systems gave different shaped curves at different frequencies which was as yet unexplained.

The V-shaped curve (Fig. 2) at 7.5 mc may be considered due to the drop in the H-F conductance toward the salt line as the concentration of the acid is decreased and then to the increase in conductance as an excess of NaOH is added. At 9 mc the same titration produces an inverted V. The H-F conductance increases as the concentration of the acid is reduced to approach the salt curve and again decreases as excess NaOH is added. The closer the salt curve is to the acid and base curves at a given frequency, the smaller the value of the slope of the titration curve. Thus, at 11 mc there would be very little change of slope at the end point.

Preliminary work with condenser-type cells of the type reported in the literature appears to be giving similar results.

* This research was supported by the U. S. Atomic Energy Commission.
[1] Anderson, Bettie, and Revinson, Anal. Chem. **22**, 743–6 (1950).
[2] W. J. Blaedel and H. V. Malmstadt, Anal. Chem. **22**, 734–42 (1950).
[3] J. Hall and J. Gibson, Jr., Anal. Chem. **23**, 966–8 (1951).
[4] F. W. Jensen and A. L. Parrack, Texas Eng. Exp. Sta. Bull. **92** (1946).
[5] C. N. Reilley and W. H. McCurdy, Jr., Anal. Chem. **25**, 88–90 (1953).
[6] West, Burkhalter, and Broussard, Anal. Chem. **22**, 469–71 (1950).

The C–C Bond Dissociation Energies in Cyclanes

H. O. PRITCHARD AND A. F. TROTMAN-DICKENSON
Chemistry Department, University of Manchester, Manchester 13, England
(Received December 4, 1953)

IN a recent letter Seubold[1] has claimed to have estimated the C–C bond dissociation energies in the cyclanes from cyclopropane to cyclononane to an accuracy of approximately ±2 kcal

and, moreover, has claimed that the calculated values agree with existing experimental data. We wish to point out first that the method by which he estimates the bond strengths in cyclopropane and cyclobutane is unsuitable, and second, that he has neglected important experimental evidence on these compounds. Our objections may be summarized as follows.

1. It has been tacitly assumed that the activation energies of the reverse reactions by which the biradicals form cyclanes are zero; this is unrealistic. Seubold has estimated the heat of formation of the trimethylene and *cis*-tetramethylene biradicals in which the C−C−C bond angles are tetrahedral and hence calculated the heats of the reactions by which these radicals are formed from the cyclanes. He then identifies the heats of these reactions with the dissociation energies of the C−C bonds. However, a bond is usually said to be broken when the attraction between the two centers is of the order of kT. It is not known, and there appears to be no reliable way of estimating at what C−C−C angle the attractive force between the centers is of this order, but there is no reason to suppose that this point is reached when the angles in the radicals are exactly tetrahedral: it can hardly be so for both compounds even if it is true for one. Probably, there is still considerable strain in the radicals when the configuration is such that the bond strengths are of the order of kT, at which point the activation energies of the recombinations are zero. These strained radicals will have higher heats of formation which would yield higher values for the calculated C−C bond dissociation energies. Conversely, the reactions by which the biradicals with tetrahedral angles form cyclanes may have substantial energies of activation. An attempt to calculate this energy barrier, based on an empirical strain-energy–bond-angle relationship, led to the conclusion that it would be negligible;[2] this conclusion is probably invalid, however, because of the significant deviations in the cyclopropane and cyclobutane bond lengths from the alkane values,[3] which were not taken into account in the calculation.

2. It is unjustifiable to correlate, as Seubold does, the low "heat of dissociation" of cyclopropane with the ease of reaction of cyclopropane and its derivatives. The isomerization of cyclopropane to propylene occurs cleanly at about 490°C with an activation energy of 65 kcal and an A factor of $10^{15.17}$.[4,5] Despite the application of sensitive tests no evidence can be found for the existence of biradicals in the system;[6] moreover, there are good theoretical reasons for supposing that the fission of the C−C bond is not the rate-determining step in the isomerization.[7] Similarly, there is no evidence that biradicals are formed when cyclobutane decomposes to ethylene for which the activation energy is 62.8 kcal and the A factor $10^{15.71}$ sec^{-1}. When gases such as toluene or hydrogen are added to the reaction system, no effects compatible with the presence of free radicals are observed.[2,8] The A factors for dissociation into biradicals are not likely to be less than 10^{13} sec^{-1} in either case, so that if the proposed radical processes had activation energies of 65 and 63 kcal, respectively, the reactions would occur to the extent of about ½ percent by such mechanisms, which would be readily observable. Thus, we should place lower limits of 65 and 63 kcal on the respective dissociation energies, at variance with our general experience of these compounds. In actual fact, such arguments tell us nothing about dissociation energies, because both radical mechanisms would show quasi-unimolecular falloff in the pressure range used for the activation energy determinations,[4,5,8] and until the extent of such falloff is calculated, we are precluded from placing any limits on the C−C dissociation energies in cyclopropane and cyclobutane.

[1] F. H. Seubold, J. Chem. Phys. **21**, 1616 (1953).
[2] Pritchard, Sowden, and Trotman-Dickenson, Proc. Roy. Soc. (London) **A218**, 416 (1953).
[3] C. A. Coulson, J. Phys. Chem. **56**, 314 (1952).
[4] T. S. Chambers and G. B. Kistiakowsky, J. Am. Chem. Soc. **56**, 399 (1934).
[5] E. S. Corner and R. N. Pease, J. Am. Chem. Soc. **67**, 2067 (1945).
[6] Pritchard, Sowden, and Trotman-Dickenson, Proc. Roy. Soc. (London) **A217**, 563 (1953).
[7] N. B. Slater, Proc. Roy. Soc. (London) **A218**, 224 (1953).
[8] F. Kern and W. D. Walters, Proc. Natl. Acad. Sci. (Washington) **38**, 937 (1952).

Carbon-Carbon Bond Dissociation Energies in the Cycloalkanes

FRANK H. SEUBOLD, JR.,
Department of Chemistry, Northwestern University, Evanston, Illinois
(Received January 19, 1954)

WITH reference to the accompanying letter of Pritchard *et al.*, the following comments concerning the earlier communication with this title[1] are in order.

The newer values of Stevenson[2] for the dissociation energies of the terminal carbon-hydrogen bonds in propane, 99 kcal/mole, and in butane, 101 kcal/mole, are supported by the pyrolytic studies of Szwarc,[3] and appear to be more accurate than those reported by Skinner. Accordingly, the table of dissociation energies has been revised, and values for the corresponding acyclic compounds have been included for comparison. To serve as a criterion for the importance of intramolecular interactions when suitable experimental methods have been devised to test them, the cyclic cases have been recalculated for dissociation to both the coiled and extended configurations of the diradicals. Implicit in all these calculations is the assumption that the activation energy for recombination is zero. There is ample evidence for this assumption in the case of open chain compounds, and little reason to doubt its validity for cyclic compounds, since the published experimental evidence points to the ready cyclization of even trimethylene radicals (Table I).[4]

TABLE I.

Compound	D(C−C)[a]	kcal/mole[b]
$C_2H_6 \rightarrow 2CH_3$		85
cyclopropane	57	57
n-$C_3H_8 \rightarrow CH_3 + C_2H_5$		83
cyclobutane	70	64
n-$C_4H_{10} \rightarrow 2C_2H_5$		81
cyclopentane	92	80
n-$C_5H_{12} \rightarrow C_2H_5 + C_3H_7$		83
cyclohexane	95	87
n-$C_6H_{14} \rightarrow 2C_3H_7$		85
cycloheptane	93	81
n-$C_7H_{16} \rightarrow C_3H_7 + C_4H_9$		87
cyclooctane	93	77
n-$C_8H_{18} \rightarrow 2C_4H_9$		89
cyclononane	94	75

[a] To coiled conformation.
[b] To extended conformation.

That trimethylene, or at least substituted trimethylene radicals, may rearrange as well as cyclize with closely similar rates has recently been demonstrated in the photolysis of methyl cyclopropyl ketone,[5] in which the major process, $\Phi = 0.32$, is the rearrangement to methyl propenyl ketone. The reaction is best explained by initial formation of the biradical, in which hydrogen atom migration to form the conjugated ketone takes place at about half the rate of recombination. The quantum yield at 2654A remains essentially constant from 25°–150°. These observations indicate that the cyclopropane carbon-carbon bond is considerably weaker than that in cyclobutane, since photolysis of methyl cyclobutyl ketone under the same conditions yields no rearranged ketone, but only cyclic products with, at higher temperatures, some ethylene from decomposition of cyclobutyl radicals.[6]

The observed activation energy of 65 kcal/mole for the isomerization of cyclopropane to propylene at 490° does not necessarily pose a lower limit for D(C−C) in cyclopropane. The isomerization has a large pre-exponential factor, $\log A = 15.2$, making it quite possible that at this high temperature the quasi-unimolecular process can outweigh the lower activation energy bond fission which may have a pre-exponential factor even lower than the "normal" value, $\log A = 13$, for unimolecular dissociations. Approximate calculation of the entropy changes in the dissociations

of cyclic and acyclic compounds shows a far smaller change in the former case, quite possibly even a negative value when the loss of one translational degree of freedom in the transition state is considered.

A major argument brought forward for the absence of free radicals in the cyclopropane isomerization is the failure to detect them by the inclusion of toluene as a radical trap. The attack of methyl radicals on toluene requires an appreciable activation energy, about 7 kcal/mole, and has a low steric factor, about 10^{-4}. Either recyclization or rearrangement of trimethylene radicals, exothermic, intramolecular processes, should proceed much more rapidly than attack on toluene by analogy with the results of the methylcyclopropane photolysis. It is doubtful if even nitric oxide could show the presence of diradicals, since even in the case of methyl radicals the rate constant for combination is 1000 times that for reaction with the inhibitor.

The results of Pritchard *et al.*, show that the isomerization of cyclopropane is in the main a quasi-unimolecular process occurring without the intervention of biradicals, but do not, as shown above, necessarily establish a lower limit for the carbon-carbon bond dissociation energy of cyclopropane. Similar considerations apply in the case of cyclobutane.

[1] F. H. Seubold, Jr., J. Chem. Phys. **21**, 1616 (1953).
[2] D. P. Stevenson, Trans. Faraday Soc. **49**, 867 (1953).
[3] C. H. Leigh and M. Szwarc, J. Chem. Phys. **20**, 407 (1953).
[4] C. E. H. Bawn and R. F. Hunter, Trans. Faraday Soc. **34**, 608 (1938).
[5] J. N. Pitts and I. Norman, Los Angeles Meeting, American Chemical Society, May, 1953.
[6] J. N. Pitts and I. Norman, Chicago Meeting, American Chemical Society, September, 1953.

The Ionization Potentials and Electronic Structures of Methyl and Ethyl Fluoride*

C. A. McDowell and B. C. Cox†
Department of Inorganic and Physical Chemistry, University of Liverpool, Liverpool 3, England
(Received January 11, 1954)

SOME years ago Mulliken[1] suggested that the electronic structures of the alkyl halides were best described in terms of a certain kind of localized molecular orbitals and showed that such a description was in agreement with the known spectroscopic data. Mulliken[1] gave the following molecular orbital formula for the normal ground state of the methyl halides (the inner electrons of the halide atom being omitted):

$$(1s_c)^2[sa_1]^2(ns_Xa_1)^2[\pi e]^4[\sigma a_1]^2(np\pi_Xe)^4, {}^1A_1. \quad (1)$$

The $(np\pi_Xe)$ nonbonding orbital is largely localized on the halogen atom, and the $[\pi e]$ orbital completely, and the $[sa_1]$ largely localized in the methyl group. $[\sigma a_1]$ is the main C–X bonding orbital. This formulation indicates that the minimum ionization potential of methyl chloride, bromide, and iodide, corresponds to the removal of an electron from the $(np\pi_Xe)$ nonbonding orbital.

For methyl fluoride a similar formulation was suggested but because of the very high ionization potential of the fluorine atom ($I=17.42$ v)[2] it is obvious that the term value of the $(2p\pi_Fe)$ nonbonding electrons of the fluorine atom will be much lower than that of either the $[\pi e]$ or the $[\sigma a_1]$ orbitals. The term value of the degenerate $[\pi e]$ orbital will be approximately equal to the negative of the ionization potential of methane.

One of the consequences of these ideas of Mulliken's is that the ionization potential of methyl fluoride should be approximately equal to that of methane if in the former molecule there is only slight interaction between the $[\pi e]$ and $(2p\pi_Fe)$ orbitals as is apparently the case in the other methyl halides.[3] Some time ago we determined the ionization potential of methyl fluoride by the electron impact method in a mass spectrometer and obtained the value 12.84 ± 0.03 (s.d.) v. Since this is very close to the ionization potential of methane (13.12 v),[4] it is apparent that Mulliken's views are correct. Furthermore, the closeness of these two values indicates that there is only slight interaction between the $[\pi e]$ and $(2p\pi_Fe)$ orbitals in methyl fluoride.‡

In the cases of ethyl chloride, bromide, and iodide, it is clear that as with the corresponding methyl compounds, the minimum ionization potential refers to the removal of an electron from the nonbonding $(np\pi_Xe)$ orbital localized on the halogen atom. With ethyl fluoride, however, for the same reasons as given above in the case of methyl fluoride, it follows that the minimum ionization potential must refer to the removal of a bonding electron. Ethyl fluoride belongs to the point group C_s and so the degenerate $[\pi e]$ orbital of the methyl group will be split into two new orbitals $[xa'']$ and $[ya']$ of the group C_s. These orbitals will have practically the same term value as the $[\pi e]$ orbital of the CH_3F molecule. There will also be a bonding orbital $[ya']$ localized in the carbon-carbon bond with a term value approximately equal to that of the $[\sigma+\sigma, a_1]$ bonding orbital of ethane. Since the first ionization potential of ethane is thought[3,5] to refer to the removal of an electron from the $[\sigma+\sigma, a_1]$ orbital the term value of the $[ya']$ orbital will, therefore, be approximately -11.83 v ($I_{C_2H_6}$).[6]

Using the same methods as with methyl fluoride we have determined the ionization potential of ethyl fluoride to be $12.00+0.04$ (s.d.) v. As this is so very close to the ionization potential of ethane it is likely that it refers to the energy required to remove an electron from the orbital localized in the carbon-carbon bond.

* This work was assisted in part by a grant from the Hydrocarbons Research Group of the Institute of Petroleum.
† In receipt of a Maintenance Grant from the Department of Scientific and Industrial Research.
‡ Alternatively it can be said that the inductive and mesomeric effects are approximately equal.
[1] R. S. Mulliken, Phys. Rev. **47**, 413 (1935).
[2] Charlotte E. Moore, Circular No. 467, National Bureau of Standards, Washington D. C.
[3] R. S. Mulliken, J. Chem. Phys. **3**, 517 (1935).
[4] C. A. McDowell and J. W. Warren, Disc. Faraday Soc. **10**, 53 (1951).
[5] G. G. Hall, Proc. Roy. Soc. (London) **A205**, 541 (1951).
[6] C. A. McDowell and B. C. Cox (unpublished experiments).

Nuclear Quadrupole Resonances in Solid Aryl Bromides and Iodides*

R. G. Barnes, O. B. Miller,† and F. O. Wooten
University of Delaware, Newark, Delaware
(Received February 24, 1954)

NUCLEAR quadrupole resonances of bromine and iodine have been located in a number of polycrystalline solids by the use of an externally quenched super-regenerative spectrometer operating in the frequency range 100–350 mcps. The experimental data are presented in Table I. Frequencies were measured by harmonic multiplication of the output of a BC-221 frequency meter. An estimated error of ±20 kcps should be assigned to each resonance. In two cases resonances became so weak at liquid nitrogen temperature that no significant measurement was possible. Room temperature measurements are given for these compounds. On the assumption that the weakening was due to strains developed in the crystal structure, these samples were annealed for several days at dry ice temperature but without effect. The frequencies of the Br^{79} resonances were also measured, the ratio $\nu(Br^{79})/\nu(Br^{81})$ agreeing with the published value[1] within the experimental error. Only the low-frequency I^{127} resonances are reported here. We hope in the near future to extend the range of operation of the spectrometer to include the higher iodine resonances.

In general, the resonances can be satisfactorily correlated with Hammett's sigma parameter as has been done for many Cl^{35} resonances.[2] Zeldes and Livingston have pointed out[3] that in the alkyl halides the resonance frequency increases as the number of substituted halogens is increased. The resonance observed for the

bromine in the methyl group in α-bromoacetophenone agrees very well with this rule, falling between the values for methyl bromide and dibromomethane but closer to the latter. The closeness of the resonance frequency in *p*-bromoacetophenone to that in the α form is surprising. This resonance also deviates most from the simple rule that the Br^{81} frequency is 6½ times the Cl^{35} frequency in the same structure. The Cl^{35} resonance in *p*-bromobenzenesulfonyl chloride has been reported.[4]

TABLE I.

Compound	Resonance frequency at 77°K mcps	Approximate signal-noise ratio
	$\nu(I^{127})$	
m-$IC_6H_4NO_2$	291.160	10
o-IC_6H_4COOH	297.791	10
m-IC_6H_4COOH	278.570	10
	$\nu(Br^{81})$	
o-BrC_6H_4COOH	234.450[a]	2–3
p-$BrC_6H_4NH_2$	221.850	10
p-$BrC_6H_4SO_2Cl$	236.665	5
p-$BrC_6H_4COCH_3$	231.107	2–3
α-$C_6H_4COCH_2Br$	230.656	10
$CH_2BrCOOH$	232.425[a]	2–3

[a] Measured at room temperature.

Two of the compounds (*m*-iodonitrobenzene and bromoacetic acid) show unusually large temperature dependences which could indicate the existence of phase changes in their crystal structures. A more careful investigation of these resonances is now in progress.

* Work supported by the U. S. Office of Ordnance Research and the Research Corporation.
† Frederick Gardiner Cottrell fellow.
[1] H. G. Dehmelt and H. Kruger, Z. Physik **129**, 401 (1951).
[2] H. C. Meal, J. Am. Chem. Soc. **74**, 6121 (1952).
[3] H. Zeldes and R. Livingston, J. Chem. Phys. **21**, 1418 (1953).
[4] P. J. Bray and P. J. Ring, J. Chem. Phys. **21**, 2226 (1953).

The Effect of Iodine on the Infrared Spectra of the Alkyl Iodides*

ROBERT H. SCHULER
Chemistry Department, Brookhaven National Laboratory, Upton, Long Island, New York
(Received February 2, 1954)

THE interaction of iodine with various donor molecules has received wide interest within the past several years, the emphasis being largely on the effect of solvation on the visible and ultraviolet absorption spectra.[1] Recently this interest has been extended to measurements in the infrared where small spectral displacements, particularly in the case of oxygenated species, have been observed in certain vibrational bands of the donor molecule.[2,3] Since iodine in alkyl iodide solutions has a strong absorption in the ultraviolet[4] and has the visible absorption maximum displaced from 520 mμ to 480 mμ,[5] the present investigation was undertaken to study the effect of solvation on the infrared spectrum of these solutions. Since the effects in the visible and ultraviolet regions indicate a high degree of solvation, it would be expected that any changes arising from the solvation would be quite pronounced in these systems. The alkyl iodides have an additional advantage in having a very high solubility for iodine.

Iodine solutions in methyl iodide (14.2 *M* CH_3I+1.94 *M* I_2) and in ethyl iodide (11.0 *M* C_2H_5I+1.94 *M* I_2) have been examined in cells of 0.1-mm path length. There is no evidence that the presence of iodine introduces any major changes in the spectrum of the solvent in the region from 2–15μ.[6] Extension of the measurements to 26μ, using a Baird model *B* double beam infrared spectrophotometer equipped with potassium bromide optics, shows only a very slight shift toward longer wavelength in the band corresponding to the C—I stretching frequency (530 cm^{-1} for CH_3I and 508 cm^{-1} for C_2H_5I). The spectrum from 13–22μ for the ethyl iodide-iodine solution, along with that for ethyl iodide (12.4 *M*) is given in Fig. 1. The absorption at 13.5μ, which is not apparently changed by the presence of the iodine, serves for convenient wavelength and intensity calibration.

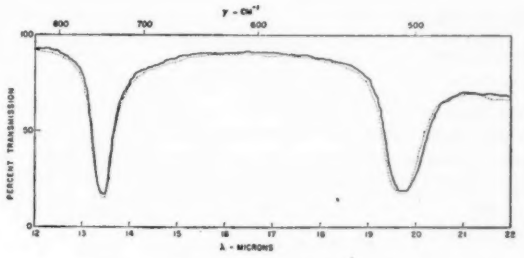

FIG. 1. Infrared absorption spectrum of ethyl iodide (12.4 *M*), dashed curve; and of ethyl iodide (11.0 *M*)—iodine (1.94 *M*) solution, solid curve.

As is seen in Fig. 1, the effect observed is very small, the absorption curve for the solution being barely distinguishable from that for the solvent. The shift (1–2 cm^{-1}) has been confirmed by direct comparison of the solution and the solvent in the double beam instrument. The differential absorption shows that the solution absorbs less strongly than the solvent just below 19.9μ and more strongly just above. Although the corresponding methyl iodide absorption is considerably narrower, the effect of iodine, though real, appears to be even less pronounced.

As in the case of the oxygenated donor molecules, solvation affects only the vibrational modes directly associated with the solvation.[2] The effects are extremely small, in contrast to the pronounced changes in the visible and ultraviolet region. There is no evidence of any change in bond type but rather only to a perturbation of the C—I stretching frequency by the presence of the iodine. Qualitatively the effect appears to be the displacement of the entire band toward lower vibration frequency.

The author wishes to thank Mr. Morris Slavin for his aid and suggestions and Mr. Robert M. Moynihan of Purdue University for making the measurements in the sodium chloride region.

* Research carried out under the auspices of the U. S. Atomic Energy Commission.
[1] See R. S. Mulliken, J. Phys. Chem. **56**, 801 (1952) for a comprehensive resume of donor-acceptor interactions.
[2] Glusker, Thompson, and Mulliken, J. Chem. Phys. **21**, 1407 (1953).
[3] Pimentel, Jura, and Grotz, J. Chem. Phys. **19**, 513 (1951), have reported complicated effects of solvation in mesitylene solutions which, however, Ham, Rees, and Walsh, J. Chem. Phys. **20**, 1336 (1952) attribute to impurities present in the mesitylene. Ham, Rees, and Walsh, Nature **169**, 110 (1952) and Glusker, Thompson, and Mulliken (see reference 2) report no observable effects of iodine solvation on the infrared spectrum in the case of benzene.
[4] R. M. Keefer and L. J. Andrews, J. Am. Chem. Soc. **74**, 1891 (1952).
[5] D. E. Schuler and R. H. Schuler, J. Am. Chem. Soc. (to be published).
[6] A detailed examination of this region shows a slight shift toward longer wavelengths of the weak band at 990 cm^{-1} in the case of ethyl iodide.

Nonempirical Calculation of the Diamagnetic Anisotropy of Benzene

TAKASHI ITOH, KIMIO OHNO, AND HIROYUKI YOSHIZUMI
Department of Physics, Faculty of Science, University of Tokyo, Tokyo, Japan
(Received February 24, 1954)

THE large anisotropy of the diamagnetic susceptibility of aromatic compounds, which is attributed mainly to the free migration of π electrons, has been investigated by Pauling,[1] London,[2] and others from the semiempirical point of view, and the calculated ratios of the anisotropies of various molecules to that of benzene are in fairly good agreement with experiment.

As to the absolute value of the anisotropy of benzene, computations were made by Kambe,[3] and Fujii and Shida[4] using the antisymmetrized LCAOMO method. Taking configuration interaction into account, we have extended these treatments.

We used all the configurations arising from excitation of one or two electrons from the lowest configuration, namely, nine $^1A_{1g}$ states and three $^1A_{2g}$ states. It is to be noted that $^1A_{1g}$ and $^1A_{2g}$ states interact with each other in the presence of an external magnetic field.

TABLE I. Diamagnetic anisotropy of benzene.

$\Delta\chi''_{\text{calc}}$[a]	$-21.70\left(\frac{2\pi eS}{6hc}\right)^2$ [d,e]	64.0%
$\Delta\chi'_{\text{calc}}$[b]	−20.13	59.4
$\Delta\chi_{\text{calc}}$[c]	−16.80	49.6
$\Delta\chi_{\text{obs}}$	−33.9	100

[a] The value when only the ground configuration is considered.
[b] The value with configuration interaction among nine $^1A_{1g}$ states.
[c] The value with configuration interaction among nine $^1A_{1g}$ and three $^1A_{2g}$ states.
[d] S is the area of benzene ring.
[e] The unit is erg per gauss^2 per mole.

The Hamiltonian is

$$\mathbf{H}=\sum_{\nu=1}^{6}\left\{\frac{h^2}{8\pi^2 m}(i\nabla_\nu+\boldsymbol{\alpha}_\nu)^2+\sum_{k=1}^{6}V_{k\nu}\right\}\sum_{\substack{\nu,\mu=1\\ \nu<\mu}}^{6}\frac{e^2}{r_{\mu\nu}}.$$

$\boldsymbol{\alpha}_\nu=(2\pi e/hc)\mathbf{A}_\nu$: $\mathbf{A}_\nu$ is the vector potential at the position of the νth electron.

As usual, we use molecular orbitals of the following form:

$$\phi_l=(6\sigma_l)^{-\frac{1}{2}}\sum_{k=1}^{6}\exp\left\{\frac{2\pi i}{6}kl+i(\boldsymbol{\alpha}_k\cdot\mathbf{r}_\nu)\right\}\chi_k(r_\nu),$$

$$l=0,\ \pm1,\ \pm2,\ 3,\quad \phi_l^*\neq\phi_{-l}.$$

σ_l: normalization factor.

$\boldsymbol{\alpha}_k=(2\pi e/hc)\ \mathbf{A}_k$: $\mathbf{A}_k$ is the vector potential at the position of the kth carbon ion.

$\chi_k(r_\nu)$: the $2p\pi$ AO of the kth carbon atom.

In calculating the matrix element, the integrals containing the exponential factor $\exp\{i(\boldsymbol{\alpha}_k\cdot\mathbf{r}_\nu)\}$ are, for simplicity, approximated in the following manner:

$$\int\exp\{i(\boldsymbol{\alpha}_k-\boldsymbol{\alpha}_m\cdot\mathbf{r}_\nu)\}\chi_k\chi_m d\tau=\exp\left\{i\left(\partial_k-\boldsymbol{\alpha}_m\cdot\frac{\mathbf{R}_k+\mathbf{R}_m}{2}\right)\right\}\int\chi_k\chi_m d\tau,$$

where $\mathbf{R}_k$ and $\mathbf{R}_m$ are the position vectors of the kth and the mth carbon atom, respectively. Then, all the necessary integrals are to be taken from the paper by Parr, Craig, and Ross.[5]

The anisotropy of the diamagnetic susceptibility is given by

$$\chi=-\frac{\partial^2(W-W_0)}{\partial H^2},$$

where W is the energy of the ground state, and W_0 is six times the energy of a $2p\pi$ electron of an isolated carbon atom in the magnetic field. The results of numerical computation are given in Table I. As can be seen, the effect of configuration interaction is not large.

The discrepancy between calculated and observed values may be due to the following approximations: (1) LCAO approximation for the MO. (2) Approximation for the integrals containing the vector potential. (3) Approximation involved in the values of the many center integrals. (4) Neglect of σ electrons.

A full report will be published shortly in the *Journal of the Physical Society of Japan*.

We express our hearty thanks to Professor M. Kotani for his constant interest in this work and to Professor D. P. Craig for sending us the unpublished computation from his paper.[5]

[1] L. Pauling, J. Chem. Phys. **4**, 673 (1936).
[2] F. London, J. phys. et radium **8**, 397 (1937).
[3] K. Kambe, Reports of the University of Electro-Communication, No. 1 143 (1950) (In Japanese).
[4] S. Fujii and S. Shida, Bull. Chem. Soc. Japan, **24**, 242 (1951).
[5] Parr, Craig, and Ross, J. Chem. Phys. **18**, 1561 (1950).

Light Scattering of Spherical Colloidal Particles*

WILFRIED HELLER AND WILLIAM J. PANGONIS†
Chemistry Department, Wayne University, Detroit, Michigan
(Received February 24, 1954)

THE Mie equations were used for obtaining the following quantities for spherical colloidal particles, considering $\alpha=0.2(0.2)7.0$ and $m=1.05(0.05)1.30$[1]: (a) the reduced specific turbidity, $(\tau/c)_0$; (b) the reduced specific scattering at an angle of 90° $(I_{90}/I_0c)_0$; (c) the "scattering ratio," at 90°, for orthogonal electric vectors of the incident beam $(I_{\parallel}/I_{\perp})_0$; (d,e) the mean "wavelength exponents" of (a) and (b),[2] $(\Delta\log f(\lambda)/\Delta\log\lambda)_0$, for the λ range 4370–5461 a.u.; (f,g) the differential exponents of (a) and (b), $(d\log f(\lambda)/d\log\lambda)_0$, at 5461 a.u.; (h) the intensity ratio at two selected symmetrical angles $(I_{45}/I_{135})_0$ (dissymmetry). These data have been reported at several occasions,[3] but a detailed publication had to be delayed repeatedly for purely external reasons. For practical size determinations on colloidal particles, dispersed in a liquid, the specific turbidities are of primary interest because they alone were found to follow a monotonic curve throughout the major part of the colloidal range. In addition, the experimental method involved is quite simple.[4] Pending publication of the entire material, the latter data are made available, for general application, in Table I. They apply to the green mercury line (5461 a.u.), assuming a density of 1.000 for the scattering material. Division of these data by the actual density makes them

TABLE I.

α \ m	1.05	1.10	1.15	1.20	1.25	1.30
			$(\tau/c)_0$ cm^{-1}			
0.2	0.0263	0.1040	0.2288	0.3978	0.6076	0.8540
0.4	0.2025	0.8005	1.7761	31.069	4.7698	6.7694
0.6	0.6376	2.5411	5.6852	10.027	15.523	22.109
0.8	1.3671	5.5159	12.454	22.184	34.617	49.723
1.0	2.3645	9.5908	21.828	39.619	61.643	89.097
1.2	3.5203	14.353	32.814	59.068	93.263	135.28
1.4	4.7236	19.282	44.099	79.348	125.17	181.35
1.6	5.9352	24.010	54.640	98.447	155.16	224.99
1.8	7.0003	28.509	65.114	117.29	186.01	272.59
2.0	8.0964	33.091	76.074	138.45	222.61	331.40
2.2	9.2485	38.118	88.593	163.14	264.70	394.62
2.4	10.535	43.701	102.37	188.99	304.45	445.31
2.6	11.853	49.597	116.07	212.21	335.79	480.93
2.8	13.242	55.175	128.44	231.64	361.83	516.16
3.0	14.606	60.684	139.54	249.77	389.76	566.50
3.2	15.912	65.704	150.37	268.79	420.70	599.77
3.4	17.163	70.647	161.62	289.31	449.05	628.54
3.6	18.395	75.731	173.10	308.04	471.44	649.12
3.8	19.640	80.843	184.19	324.57	491.12	672.86
4.0	20.909	85.960	194.79	340.06	511.84	698.60
4.2	22.192	90.953	204.63	355.49	535.93	714.94
4.4	23.473	95.805	214.40	370.17	547.15	721.95
4.6	24.819	100.52	223.82	383.14	559.21	731.21
4.8	25.970	105.16	232.56	385.04	572.03	744.09
5.0	27.192	109.70	241.46	407.42	585.25	747.86
5.2	28.389	114.28	250.02	418.73	593.98	740.82
5.4	29.592	118.71	258.59	429.47	597.38	735.74
5.6	31.040	123.19	266.45	436.07	600.58	737.13
5.8	32.038	127.55	273.96	442.96	606.82	735.14
6.0	33.239	131.74	280.23	450.88	611.78	720.27
6.2	34.3970	135.58	286.68	457.17	609.19	698.69
6.4	35.5643	139.54	293.40	463.43	603.39	687.61
6.6	36.6999	143.53	299.82	466.29	600.75	681.43
6.8	37.8550	147.49	305.15	469.06	599.60	661.32
7.0	39.1266	152.46	310.44	472.51	593.77	630.50

applicable to any system within the range of α and m values defined,[5] provided the medium is water at 25°C.

Comparison of these data with extensive experimental results obtained in this laboratory on 20 monodisperse Dow polystyrene and polyvinyl toluene lattices—first by Epel[6] and later on by Tabibian[7]—showed excellent agreement with electron microscopic data for particle diameters up to 2500 a.u. and an agreement within about 10 percent for much larger particles (up to 7700 a.u.), using a precision apparatus constructed in this laboratory in conjunction with Herrington.[8]

* This work was carried out with the support of the U. S. Office of Naval Research.

† Present address: Film Department, E. I. du Pont de Nemours and Company, Buffalo, New York.

[1] $\alpha = d\pi/\lambda$, where d is the diameter of the particles and λ is the actual wavelength in the scattering system; m is the refractive index of the scattering material relative to that of the medium.

[2] W. Heller and E. Vassy, J. Chem. Phys. **14**, 565 (1946).

[3] For example, International Congress of Pure and Applied Chemistry, September 10–13, 1951, New York; Phys. Rev. **86**, 645 (1952); Congress on "Radiations et Macromolecules," University of Strasbourg, France, June 9–11, 1952.

[4] W. Heller and H. B. Klevens, Phys. Rev. **67**, 61 (1945).

[5] $\alpha = 7.0$ corresponds to a diameter of 9131 a.u. for $\lambda = 5461$ a.u. if the dispersing medium is water at 25°C. Extension of the data, up to a diameter of 13 000 a.u. is now in progress in collaboration with the Wayne University Computation Laboratory.

[6] W. Heller and J. N. Epel, International Congress of Pure and Applied Chemistry, September, 1951, New York, N. Y.

[7] W. Heller and R. Tabibian, 125th Meeting of the American Chemical Society, March, 1954, Kansas City, Kansas.

[8] W. Heller and K. Herrington, 116th Meeting of the American Chemical Society, September, 1949, Atlantic City, New Jersey.

Microwave Spectrum and Barrier to Internal Rotation of Nitromethane

EILEEN TANNENBAUM, RUSSELL D. JOHNSON,* ROLLIE J. MYERS, AND WILLIAM D. GWINN
Department of Chemistry, University of California, Berkeley, California

(Received March 2, 1954)

MANY lines have been observed in the microwave spectrum of nitromethane (CH_3NO_2) between 16 000 and 45 000 mc/sec. In the region from 30 000 to 34 000 mc/sec about ten of these lines can be assigned as $J=1$ to $J=2$ transitions on the basis of their characteristic Stark effects. Attempts were made to assign some of these transitions with rigid asymmetric rotor energy levels but a satisfactory rigid rotor assignment could not be made. It is possible to assign these $J=1$ to $J=2$ transitions with the inclusion of a term for the restricted mode of internal rotation in the Hamiltonian, and the results of these assignments are given in Table I.

TABLE I. Assigned $J=1$ to $J=2$ lines for nitromethane.

K	k	Calculated frequency[a] $V_6=0.00$ cal/mole	Calculated frequency[a] $V_6=6.00$ cal/mole	Experimental frequency mc/sec
0	0	30 010.7	30 011.5	30 035.6
±1	∓1	32 033.4	32 034.1	32 034.1
±1	±1	33 642.5	33 643.5	33 643.5
0	±2	32 959.8	32 959.8	32 959.2
±1	±3	33 174.4	33 474.6	33 476.5
∓1	∓3	33 174.4	31 676.2	31 677.3
±1	∓3	32 491.6	32 191.4	32 189.7
∓1	±3	32 491.6	33 989.8	33 988.5
0	±4	32 856.6	32 856.6	32 859.5

[a] Calculated using $b+c=16\,419.3-0.32\ k^2$, $b-c=4666.0$ mc/sec, $a(NO_2)=13\,277.5$ mc/sec, $a(CH_3)=160\times10^3$ mc/sec (assumed).

The K quantum number in Table I is the usual symmetric top designation, and it corresponds to the total angular momentum quantized along the axis of internal rotation of a symmetric top molecule. The k quantum number corresponds to the angular momentum of the methyl group quantized along the axis of internal rotation of a free internal rotor. The selection rules for dipole radiation in nitromethane are given very closely by $\Delta K=0$, $\Delta k=0$, and the zero nuclear spin of the O^{16} atoms in nitromethane allows only the states for which $|K-k|$ is even to be populated. The barrier to internal rotation about the symmetry axis of the CH_3 and NO_2 group was taken to have the form $V=V_6(1-\cos 6\phi)$, and the energy levels of such a restricted internal rotor were determined by a matrix formulation similar to that of Burkhard and Dennison.[1]

It can be seen from Table I that the majority of the $J=1$ to $J=2$ transitions are affected only very slightly by the low barrier of nitromethane. In the case of the $K=1$, $k=3$ transitions a degeneracy is removed by a sixfold barrier, and the four transitions obtained are a sensitive function of this barrier term. The value for the barrier which gives the best agreement between the calculated and observed spectrum is $V_6=6.00\pm0.03$ cal/mole. This value is considerably smaller than the previous upper limit of 800 cal/mole.[2] The appreciable discrepancy between the calculated and observed $K=0$, $k=0$ frequency may be caused by the presence of a twelve-fold potential term or by neglected centrifugal distortion effects. The assignment of the lines is further substantiated by the fact that all the $K=1$ lines have both first- and second-order Stark components, while the $K=0$ lines all have only second-order ones.

From the averages of the $K=1$, $k=1$, and $k=3$ frequencies the effect of the centrifugal distortion of the methyl group on $(b+c)$ can be determined. The value obtained for the centrifugal distortion constant, $D_{Jk}=0.16$ mc/sec, compares very favorably with the value of D_{JK} observed for the methyl halides. The $J=0$ to $J=1$ transitions are not split directly by the barrier and their frequencies would all be equal to $(b+c)$ except for the effects of centrifugal distortion. A line was observed at $16\,420\pm1$ mc/sec which was accompanied by a series of overlapping lines spaced out toward lower frequencies. The individual lines were not resolved, but their spacing is consistent with the D_{Jk} value determined from the $J=1$ to $J=2$ lines.

Further work is being done on nitromethane which will include the deuterated species. It is hoped that a complete structure can be determined for the molecule with the data from this additional isotopic species.

* Present address: Dow Chemical Corporation, Midland, Michigan.

[1] D. G. Burkhard and D. M. Dennison, Phys. Rev. **84**, 408 (1951).
[2] W. M. Jones and W. F. Giauque, J. Am. Chem. Soc. **69**, 983 (1947).

Fractionation of Oxygen Isotopes during the Formation of Metal Oxide Films

MALCOLM DOLE AND G. A. LANE
Department of Chemistry, Northwestern University, Evanston, Illinois

(Received March 1, 1954)

IN a research studying the isotopic composition of oxygen and nitrogen in air taken from high altitudes,[1] it became necessary to study the possibility of oxygen isotope fractionation during the chemisorption or "cleanup" of oxygen by metal surfaces at room temperature. When pure oxygen is exposed to a freshly reduced surface of steel or copper, a rapid reduction in the oxygen pressure occurs, followed by a slowing down in the chemisorption process until the pickup of oxygen becomes slow, very slow in the case of copper.

If w_g represents the weight fraction of oxygen unreacted after time t, w_m the weight fraction of oxygen chemisorbed, y_0, y_g, and y_m the atom percentages of O^{18} in the initial gas at zero time, in the gas phase after time t, and in the oxygen chemisorbed on the metal, respectively, and x_0, x_g, and x_m similar percentages for the isotope of mass 16, then material balance requires that

$$x_0 = w_g x_g + w_m x_m \tag{1a}$$

$$y_0 = w_g y_g + w_m y_m. \tag{1b}$$

A fractionation factor can be defined by the expression

$$\alpha = y_m x_m / y_m x_g. \tag{2}$$

It is easy to show that in the case that x_0/x_g approximates unity, which was amply true in the research reported here,

$$\alpha=\frac{y_g-w_g y_g}{y_0-w_g y_g}. \quad (3)$$

Data for α obtained on copper and steel at room temperature are given in Table I.

TABLE I. Fractionation factors for the chemisorption of oxygen on steel and copper.

Exp. no.	Oxygen pressure initial mm	Oxygen pressure final mm	w_g	% O^{18} y_0	% O^{18} y_g	α
Fe-1	103.0	30.0	0.291	0.2050	0.2090	1.028
Fe-2	102.8	88.2	0.858	0.2050	0.2057	1.025
Fe-3	67.0	65.0	0.970	0.2050	0.2051_8	1.025
Cu-1	647.3	588	0.908	0.2043	0.2056	1.074
Cu-2	125.1	92.8	0.742	0.2043	0.2074	1.061
Cu-3	124.7	95.0	0.762	0.2043	0.2070	1.058
Cu-4	95.8	88.3	0.922	0.2043	0.2051	1.052

After the initial exposure to oxygen, the steel was not further reduced, but the copper samples were reduced with hydrogen between experiments Cu-1 and Cu-2, Cu-2 and Cu-3, but not between Cu-3 and Cu-4.

More experiments will be done under more carefully controlled conditions, for different extents of oxidation, at different temperatures and on different metals. At the present time the results indicate (1) that a significant fractionation occurs and (2) that the fractionation factor is significantly different for two different metals. It is hoped that oxygen isotope fractionation studies will shed further light on the mechanism of oxide film formation.

The mass spectrometer used in the oxygen isotope measurements was purchased from funds allocated by the Air Force Cambridge Research Center for the high altitude research. We are indebted to the Abbott Research Fund of Northwestern University for a grant in direct support of this work.

[1] Dole, Lane, Rudd, and Zaukelies, paper submitted to the *Geochimica et Cosmochimica Acta*.

Proton Relaxation in Mn^{++} Aqueous Solutions

JOHN R. ZIMMERMAN
Magnolia Petroleum Company, Field Research Laboratories, Dallas, Texas
(Received March 5, 1954)

BLOEMBERGEN, Purcell, and Pound[1] have predicted the influence of paramagnetic ions on both the longitudinal (T_1) and transverse (T_2) relaxation times of the protons of an aqueous solution. A summary of their results shows that (a) $1/T_1 \propto N_{\text{ion}}$, where N_{ion} is the paramagnetic ion concentration, and (b) in the region where T_1 and T_2 are proportional, the relation $T_1/T_2 \sim$ unity. They very satisfactorily verified these results for the cases of the Cu^{++} and Fe^{+++} aqueous solutions.

We have further substantiated these conclusions for a large number of relaxing agents including such paramagnetic ions as Fe^{++}, Co^{++}, Ni^{++}, and V^{++++}. It might be of interest to those engaged in studies making use of the paramagnetic relaxation mechanism to point out an apparent deviation to such well-behaved systems.

In the case of an Mn^{++} aqueous solution, the ratio T_1/T_2 is not of the order of unity, but instead, $T_1/T_2 \sim 10$, as may be observed in Fig. 1, Curves I and II. This result is especially interesting since the longitudinal (T_1) relaxation times of the Fe^{+++} and Mn^{++} aqueous solutions are in good agreement (compare Curves I and III). Magnetic moment calculations of the Mn^{++} ion based on relaxation[1] theory agree with magnetic susceptibility measurements.[2] Furthermore, although this large value of T_1/T_2 does exist for the Mn^{++} ion, the line-width parameter (T_2) is still inversely

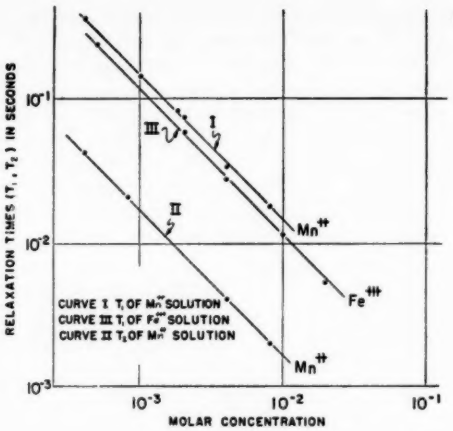

FIG. 1.

proportional to the paramagnetic ion concentration. The "abnormal" line broadening occurs in Mn^{++} aqueous solutions prepared from both manganous sulfate and manganous chloride compounds, and so it would appear in these instances that such a deviation is at least not primarily due to the presence of certain anions.

Further remarks at this time are primarily conjecture. It is quite possible that the Mn^{++} may form a complex with the water molecule through the oxygen in such a manner as to leave one of the hydrogens with a low covalent bond energy. This is to be distinguished from electrostatic hydration of a metallic ion by water molecules. With this assumption a reasonable qualitative interpretation of the line broadening might be that a random change of state of the protons of the water molecules occurs. The loosely attached proton of the complex would serve as an exchange mechanism for the water protons to exist in both the chemical environment of the water molecule and the large static chemical environment of the loosely coupled proton position. These arguments are similar in some respects to rapid exchange rate phenomena relating to complex ion studies.[3] Further work relating to this apparent deviation in resonance line broadening is continuing.

[1] Bloembergen, Purcell, and Pound, Phys. Rev. **73**, 679 (1948).
[2] G. J. Gorter, *Paramagnetic Relaxation* (Elsevier Publishing Company, Inc., New York, 1947), p. 15.
[3] J. R. Zimmerman, J. Chem. Phys. **21**, 1605 (1953).

Bromine Nuclear Quadrupole Resonances*

P. J. BRAY
Department of Physics, Rensselaer Polytechnic Institute, Troy, New York
(Received March 2, 1954)

THE pure quadrupole spectra of the Br^{79} and Br^{81} nuclei have been detected in a number of organic compounds. A self-quenching superregenerative spectrometer was employed for these investigations in the 200 to 300 megacycle per second region. Br^{81} resonance frequencies, signal-to-noise ratios observed, and the measurement temperature are given in Table I. Except for two cases noted in the table, the possible uncertainty in measurement attached to each frequency is attributable to the uncertainty in obtaining exact superposition on the oscilloscope of the quadrupole resonance pip pattern and the external oscillator (TS 175/U) pip pattern. The Br^{79} resonances were also observed.

Since location in this laboratory of the resonances in *p*-bromoaniline, *p*-bromoacetophenone, *o*-bromobenzoic acid, bromoacetic acid, and *p*-bromobenzenesulfonyl chloride, a communication[1] has been received which lists the frequencies for these compounds and some others. Consequently, the *p*-bromoaniline, bromoacetic acid, and *p*-bromobenzenesulfonyl chloride resonances are included in

TABLE I.

Compound	Frequency (megacycles per second)	Temperature	Approximate signal-to-noise ratio
p-bromoaniline[a] p-$BrC_6H_4NH_2$	221.862 ±0.015	Liquid nitrogen	45
m-bromoaniline[b] m-$BrC_6H_4NH_2$	222.614 ±0.010	···	20
o-bromoaniline[a,c] o-$BrC_6H_4NH_2$	220.255 ±0.015	···	2–3
p-bromoaniline hydrochloride p-$BrC_6H_4NH_2 \cdot HCl$	232.043 ±0.015	···	20
p-bromoanisole[b,c] p-$BrC_6H_4OCH_3$	226.690 ±0.015	···	6
o-bromoanisole[b,c] o-$BrC_6H_4OCH_3$	233.250 ±0.020	···	6
p-bromoacetanilide[a] p-$BrC_6H_4NHCOCH_3$	226.805 ±0.010	···	8–10
p-bromoacetophenone[a,c,d] p-$BrC_6H_4COCH_3$	230.670 ±0.065	···	4
α-bromo-*p*-chloroacetophenone[a] $ClC_6H_4COCH_2Br$	233.162 ±0.010	···	15
2,4,6-tribromoaniline $Br_3C_6H_2NH_2$	233.563 ±0.010 230.752 ±0.010 230.095 ±0.010	··· ··· ···	12–14 12–14 12–14
p-bromobenzenesulfonyl chloride[a] p-$BrC_6H_4SO_2Cl$	236.642 ±0.010	···	22–25
o-bromobenzoic acid[a,c,d] o-BrC_6H_4COOH	234.185 ±0.075	20°C	5–8
bromoacetic acid[a] $CH_2BrCOOH$	232.485 ±0.025	20°C	15–16

[a] Compound melted into vial—solid at room temperature.
[b] Liquid at room temperature.
[c] Resonance is broad and diffuse—some difficulty in picking resonance pip on the oscilloscope.
[d] Very difficult to be certain of resonance pip—frequency range given includes total spread of observed values.

Table I simply to show the large signal-to-noise ratios achieved here (a factor between 4 and 8 times larger than those obtained with the externally quenched spectrometer[1]). The frequencies agree generally within experimental error with the earlier results.[1]

In the cases of *o*-bromobenzoic acid and *p*-bromoacetophenone, the present measurements disagree with the communicated values[1] by 200 to 500 kilocycles per second. These resonances are both weak, making proper selection of the resonance frequency difficult. It would be relatively easy for these measurements to be in error by an amount equal to the quench frequency (approximately 150 kilocycles per second here) but further deviations are not probable. In both cases, slightly better signal-to-noise ratios were obtained with the self-quenched spectrometer.

The *o*-bromoaniline resonance is quite out of line with the *para*-, *meta*-, *ortho*-progression of frequencies expected on the basis of Hammett's sigma values.[2,3] This may be due to the effect of crystalline structure differences between the compounds. The anisole resonances appear in the expected order.

The considerable difference between the bromoaniline values and the *p*-bromoaniline hydrochloride frequency is not surprising in view of the considerable change in bonding introduced by the extra proton and chlorine.

The chlorine quadrupole resonances in α-bromo-*p*-chloroacetophenone[4] and *p*-bromobenzenesulfonyl chloride[5] have been reported.

An even number of resonances was expected in 2,4,6-tribromoaniline since the two bromines in *ortho*-positions should be equivalent. The appearance of three resonances is not yet definitely assigned to a known cause. Room temperature measurements (21°C) on these resonances yield values of 230.685, 227.875, and 227.569 megacycles per second. It is interesting to note that (if there is no crossing over) it is the highest and middle frequency resonances which change with temperature at the same rate, while the lowest frequency resonance changes at a rate approximately 12 percent slower. Further work is in progress on this compound.

Temperature dependence studies of most of the reported bromine resonances are in progress in this laboratory. Investigations are also under way on a large number of compounds related to those listed in Table I. These results will appear later.

I wish to thank Dr. S. C. Bunce of the Department of Chemistry for his generous aid in locating and purifying some of the compounds used in this work.

* Research supported by a grant-in-aid from the Rensselaer Polytechnic Institute Research Grants Committee.

[1] Barnes, Miller, and Wooten, *Nuclear Quadrupole Resonances in Solid Aryl Bromides and Iodides* (University of Delaware, Newark, Delaware).
[2] L. P. Hammett, *Physical Organic Chemistry* (McGraw-Hill Book Company, Inc., New York, 1940).
[3] H. C. Meal, J. Am. Chem. Soc. **74**, 6121 (1952).
[4] P. J. Bray and D. Esteva, J. Chem. Phys. (to be published).
[5] P. J. Bray and P. J. Ring, J. Chem. Phys. **21**, 2226 (1953).

The Time Effect in the Fracture of Glass from the Standpoint of Nucleation Theory

TAKEO YOKOBORI
Institute of Science and Technology, University of Tokyo, Komaba-machi, Meguro-ku, Tokyo, Japan
(Received March 8, 1954)

THE interpretation of the delayed time of fracture of glass has been attempted by many investigators.[1–6] Among others, Preston[1] and Orowan[2] attributed this effect to atmospheric attack of the surface of glass. On the other hand, Saibel,[3] Tailor,[4] and Hodgdon and his co-workers[5] considered the problem from the standpoint of chemical reaction-rate theory. It seems, however, to be unreasonable to treat the wide range of breaking time, such as from 10^{-2} sec to 10^{4} sec in terms of a single physical process. For short loading time, the author proposes to treat this problem from the standpoint of nucleation theory. Although Fisher[7] has already treated the fracture of glass based on this theory and derived interesting results, it is concluded that there exists practically no time effect, and the calculated fracture stresses generally exceed the maximum experimental stresses.

The present treatment is an attempt to modify Fisher's theory by taking the effect of the Griffith[8] crack into account. In this case the stress concentration by this crack plays an important role. As a first approximation, a single value q of stress concentration is taken as the average value, although it should be expressed in the form of distribution function. Consequently, based on nucleation theory the delayed time is given by

$$t=\frac{h}{ZkT}\exp[(\Delta f_1{}^*+\pi^3\sigma^3E^2/6(1-\nu^2)q^4S^4)/kT], \qquad (1)$$

where Z is the number of molecules which are concentrated in the neighborhood of the apex of the Griffith cracks and are the origins of initiating nuclei of critical size. Other notations are the same as in Fisher's paper.[7] It is to be noted that Z may be much smaller than the total number N of molecules involved in the specimen as assumed to be the origins of crack nuclei by Fisher.[7] Hence, the free energy of activation, $\Delta f_1{}^*$, cannot be neglected compared with $kT/n(ZkTt/h)$ in Eq. (1). The value of q, $\Delta f_1{}^*$, and Z are calculated by fitting Eq. (1) to the data of Baker and Preston[9] and are listed in Table I. As seen from Fig. 1, the smooth curves calculated are in good agreement with the data for short breaking time, such as, from 10^{-2} sec to 1 or 10 sec, where the effect of atmospheric attack may be assumed very slight. For breaking time longer than 1 sec or 10 sec, another factor such as chemical attack will become predominant. This may be predicted by more appreciable decay in strength as shown by dotted lines in Fig. 1. In the absence of little knowledge about Z, the

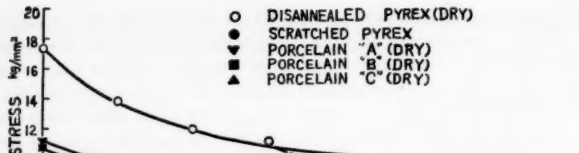

FIG. 1. Comparison of theory and the experimental data of Baker and Preston. The smooth curves are theoretical.

value of Z corresponding to the value[10] about 20 kcal per mole of Δf_1^* may be the most reasonable among the three groups of Z in Table I. In this treatment, the effect of applied stress upon

TABLE I. Values of stress concentration factor q, and the free energy of activation Δf_1^*. ($E=6(10)''$ dynes/cm², $\sigma=100$ ergs/cm² and $\nu=0.25$ are assumed.)

Material	q	Δf_1^* (kcal/mole) $(Z=10^4)$	$(Z=10^8)$	$(Z=10^{12})$
Disannealed Pyrex (dry)	45.4	19.6	25.0	30.8
Scratched Pyrex (wet)	85.6	19.6	25.0	30.8
Porcelain *A* (dry)	59.6	18.9	24.4	30.0
Porcelain *B* (dry)	62.0	18.9	24.4	30.0
Porcelain *C* (dry)	88.1	19.0	24.5	30.1

Δf_1^* was assumed to be small and neglected. When this effect is appreciable, Eq. (1) will be suitably modified. For the case of constant rate of loading, the statistical treatment[11] will be available as applied to other phenomena.

[1] F. W. Preston, J. Appl. Phys. **13**, 623 (1942).
[2] E. Orowan, Nature **154**, 341 (1944).
[3] E. Saibel, J. Chem. Phys. **15**, 760 (1947).
[4] N. W. Tailor, J. Appl. Phys. **18**, 943 (1947).
[5] Hodgdon, Stuart, and Bjorklund, J. Appl. Phys. **21**, 1156 (1950).
[6] C. Gurney, Proc. Phys. Soc. (London) **59**, 169 (1947).
[7] J. C. Fisher, J. Appl. Phys. **19**, 1062 (1948).
[8] A. A. Griffith, Phil. Trans. Roy. Soc. **221A**, 163 (1920).
[9] T. C. Baker and F. W. Preston, J. Appl. Phys. **17**, 179 (1946).
[10] Kuan-Ham Sun, J. Am. Ceram. Soc. **30**, 277 (1947).
[11] T. Yokobori, Phys. Rev. **88**, 1423 (1952).

Kinetics of the Reaction of Sodium Bromomalonate with Thiosulfate

EDWARD S. AMIS AND WILSON J. BROACH
Chemistry Department, University of Arkansas, Fayetteville, Arkansas
(Received March 4, 1954)

BROACH and Amis[1] have studied the dielectric constant and salt effects upon the ethyl bromomalonate-thiosulfate reaction. This note deals with the rate of the sodium bromomalonate-thiosulfate reaction as a function of the dielectric constant in methyl alcohol-water media at temperatures of 25.00±0.02° and 45.00±0.02°C. The experimental procedure was essentially that described in the former publication.

In Fig. 1 are plotted the data of runs showing the effect of the dielectric constant of the solvent upon the reaction at 45°C. Here the reciprocals of the concentrations of one of the two reactants initially present at equal concentrations (0.01000 mole per liter) are plotted against time. It is observable from the plots that the reaction does not conform to a second-order reaction over the whole range of time. The reaction is neither an SN_1 nor a simple SN_2 type. The rates are second order over the greater portion of the time since, after an initial period of changing slope, the curves become straight lines. The slopes of the straight portions of the lines have been obtained and the corresponding second-order velocity constants calculated.

These second-order rate constants as functions of temperature and of dielectric constant are presented in Table I. If a plot of the

TABLE I. Velocity constants of the sodium bromomalonate and thiosulfate ion reaction as a function of the dielectric constant.

25.00°C			45.00°C		
D	k'	$\log k'+3$	D	k' 1/mole-min	$\log k'+2$
78.5	0.21×10^{-2}	0.3222	71.5	0.0227	0.3560
71.0	0.34×10^{-2}	0.5315	64.2	0.0318	0.5024
62.9	0.56×10^{-2}	0.7482	56.5	0.0485	0.6857
54.0	0.99×10^{-2}	0.9956	47.7	0.0545	0.7364
43.9	1.34×10^{-2}	1.1271	43.2	0.0855	0.9320

logarithms of these specific velocity constants at either temperature *versus* the corresponding values of the reciprocals of the dielectric constants is made, a straight line is obtained in the region of high dielectric constant. The slopes, however, are in a direction opposite to that predicted by the Scatchard theory for ionic reactants of like sign.

Bedford, Mason, and Morrell[2] and Bedford, Austin, and Webb[3] studied the reactions of sodium bromomalonate and of sodium bromosuccinate with sodium thiosulfate as functions of ionic strength. They found the change of rate constant with increasing ionic strength to be in a direction opposite to that predicted by the Bronsted-Christiansen theory and attributed this to an orientation effect which LaMer and Kamner[4] had previously postuated for the bromoacetate-thiosulfate reaction.

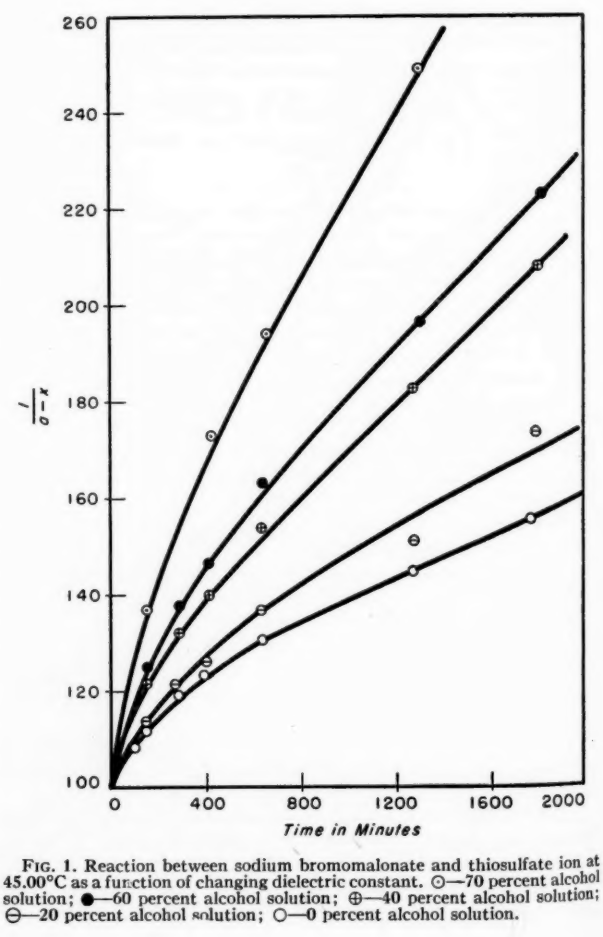

FIG. 1. Reaction between sodium bromomalonate and thiosulfate ion at 45.00°C as a function of changing dielectric constant. ⊙—70 percent alcohol solution; ●—60 percent alcohol solution; ⊕—40 percent alcohol solution; ⊖—20 percent alcohol solution; ○—0 percent alcohol solution.

Comparison of Rates.—A comparison of the rates of the ethyl bromomalonate-thiosulfate reaction and the sodium bromomalonate-thiosulfate reaction shows that the former reaction is almost one hundred thousand times as fast as the latter. For example, the specific velocity constant of the ethyl bromomalonate-thiosulfate reaction at 25.00°C in 20.4 weight percent of methanol in water solvent of dielectric constant 69.0 was found to be 3.93×10^{2} 1/mole-min (see Broach and Amis, reference 1). The specific velocity constant of the bromomalonate ion-thiosulfate ion reaction at 25.00°C in 16.2 weight percent methanol in water solvent of dielectric constant 71.0 is from the table 3.4×10^{-3} 1/mole-min. The conditions are approximately the same for the two cases. The ratio of the velocity constants in these examples is 1.16×10^{5}. This enormous difference in the velocity of these two reactions is perhaps due to the electrostatics. When the negative divalent thiosulfate ion approaches the ethyl bromomalonate dipolar molecule, it does not encounter the great Coulombic repulsion that it meets in approaching the negative divalent monobromomalonate ion.

[1] Wilson J. Broach and Edward S. Amis, J. Chem. Phys. (to be published).
[2] Bedford, Mason, and Morrell, J. Am. Chem. Soc. **56**, 280 (1934).
[3] Bedford, Austin, and Webb, J. Am. Chem. Soc. **57**, 1408 (1935).
[4] Victor K. LaMer, and Mildred E. Kamner, J. Am. Chem. Soc. **53**, 2832 (1931); **57**, 2669 (1935).

The Resonance Energy of Graphite

GORDON M. BARROW
Department of Chemistry, Northwestern University, Evanston, Illinois
(Received March 15, 1954)

ALTHOUGH the resonance energies of the polynuclear aromatic hydrocarbons have been the subject of numerous investigations, it has not been generally recognized that data and methods are now available, so that a fairly reliable experimental resonance energy of the limit of this series of compounds, graphite, can be obtained. In considering a number of compounds, Wheland[1] obtained poor agreement between calculated and experimental resonance energies for the case of graphite, and we are now able to show that, as he suggested, the "experimental" value was in error and his calculated value is actually in good agreement with that observed.

To obtain the ordinary resonance energy, as defined, for example, by Pauling[2] or by Wheland,[3] one can calculate from a set of bond energies the heat of formation to be expected in the absence of resonance and can compare this with the observed heat of formation. In view of the variation in heat of formation of branched hydrocarbons and in particular in view of the apparent difference in bond energy in the hydrocarbons and in diamond, it is important, particularly in the case of graphite, to take into account this branched chain effect so that the difference between the observed and calculated heats of formation may be attributed entirely to the ordinary resonance energy. Mulliken and Parr[4] have recently suggested a satisfactory empirical equation for the heats of formation of hydrocarbons. Using the form and notation of their equation, we obtain for the heat of formation at 25°C in kcal/mole the expression:

$$\Delta H_f^0(298°\mathrm{K}) = -4.14N_{C-H}+4.90N_{C-C}+26.50N_{C=C}-0.78n-\Delta,$$

where n is defined by Mulliken and Parr, and accounts for the branching effects, and the resonance energy appears as a positive value for Δ. The above formula fits the heat of formation data,[5] for example, of all the hexanes, heptanes, and hexenes with an average deviation of 0.6 kcal per mole and also gives the correct heat of formation for diamond and seems reliable to about 0.2 kcal per gram atom of carbon, even in highly branched systems.

Application of the above formula to graphite requires a calculation of the energy of the process of separating the layers of graphite molecules to a hypothetical ideal gas state. From the known heats of sublimation of naphthalene[6] and several higher aromatic compounds,[7] a value of about 1.6 kcal per gram atom of carbon can be estimated for this process. A calculation of the interlayer binding in graphite by Brennan[8] gives a value of 4 kcal per gram atom, but this seems rather high.[9]

The heat of formation of the "ideal gas state" graphite can therefore be taken as about 2 kcal per gram atom to be compared with the value calculated by the formula with $N_{C-C}=1$, $N_{C=C}=\frac{1}{2}$, and $n=8$ of 11.9 giving a resonance energy of 10 kcal per gram atom. This is to be compared, for instance, to a resonance energy of benzene of 36 kcal per mole obtained by the same method.

It is of interest to note the larger resonance energy per carbon atom in the larger molecule and that, therefore, the resonance energies of the polynuclear aromatic molecules do not increase in a simple linear manner with the number of carbon atoms, as might have been assumed from the first few members of the series. Furthermore, the molecular orbital calculation of Wheland[1] gives the resonance energy of benzene as 2.00β, and, therefore, $\beta=18$, and the resonance energy of graphite as 0.58β which corresponds to $\beta=17$. The discrepancy in the original comparison is essentially removed and the simple molecular orbital treatment yields results consistent with the ordinary resonance energies not only of compounds consisting of one or several aromatic nuclei but also of the limiting member of the series of such compounds, graphite.

[1] G. W. Wheland, J. Chem. Phys. **2**, 474 (1934).
[2] Linus Pauling, *The Nature of the Chemical Bond* (Cornell University Press, Ithaca, 1945).
[3] G. W. Wheland, *The Theory of Resonance* (John Wiley and Sons, Inc., New York, 1944).
[4] R. S. Mulliken and R. G. Parr, J. Chem. Phys. **19**, 1271 (1951).
[5] Selected Values of Properties of Hydrocarbons (Circular of the National Bureau of Standards, C 461, U. S. Government Printing Office, Washington, D. C., 1947).
[6] G. M. Barrow and A. L. McClellan, J. Am. Chem. Soc. **73**, 573 (1951).
[7] A. Magnus and F. Becker, Erdöl u. Kohle **4**, 115 (1951).
[8] Robert O. Brennan, J. Chem. Phys. **20**, 40 (1952).
[9] Y. K. Syrkin and M. E. Dyatkina, *The Structure of Molecules and the Chemical Bond* (Butterworth's Scientific Publications, London, 1950), p. 299.

The Decomposition of Nitrogen Dioxide by Neutron Irradiation

P. HARTECK AND S. DONDES
Department of Chemistry, Rensselaer Polytechnic Institute, Troy, New York
(Received March 15, 1954)

THE reaction scheme of nitrogen dioxide, when illuminated with ultraviolet light, is[1]

$$NO_2+h\nu=NO+O, \quad (1)$$

$$NO_2+O=NO+O_2, \quad (2)$$

$$2NO+O_2=2NO_2. \quad (3)$$

However, when nitrogen dioxide is primarily dissociated by ionizing radiation also as

$$NO_2+h\nu=N+O+O, \quad (4)$$

then the question arises whether the nitrogen atoms react only as follows:

$$NO_2+N=2NO. \quad (5)$$

(Normally, the ions produced are considered to neutralize quickly, and only the atoms and radicals formed therefrom are considered in chemical reactions.[2]) Thus, if nitrogen dioxide is irradiated with a very strong source, the products should reform nitrogen dioxide, and the nitrogen dioxide should have an unlimited lifetime if irradiated. To prove this, we sealed purified nitrogen dioxide in quartz vessels and irradiated the gas with neutrons in the Brookhaven National Laboratory reactor. However, analysis of the decomposition products indicated that only 90 percent of the nitrogen dioxide recombined to the original. Therefore, the nitrogen dioxide, which decomposed according to reaction (4) did not react completely according to reaction (5). Experimentally, the products found in this reaction were: nitrogen dioxide remaining, almost equal quantities of nitrogen plus oxygen, and nitrous

oxide. The nitrous oxide could have been obtained from the following most probable reaction:

$$NO_2+N=N_2O+O+43 \text{ kcal}, \quad (6)$$

and the nitrogen from the following two reactions:

$$N_2O+h\nu=N_2+O, \quad (7)$$

$$NO_2+N=\text{(a) } N_2+2O+3.5 \text{ kcal} \quad (8a)$$

$$\text{(b) } N_2+O_2+120.7 \text{ kcal}. \quad (8b)$$

(Reaction (7) alone could not account for the amount of nitrogen formed.)

If the heat of dissociation of nitrogen dioxide is 221.5 kcal,[3] then reactions (5), (6), and (8a,b) are exothermic, and with almost equal amounts of the products these reactions should only have a small heat of activation, since it is not probable that reasonably large heats of activation should have almost the same values. However, this statement deserves further investigation, since the entire gas is nitrogen dioxide, and the primarily formed energetic atoms may react with the nitrogen dioxide before becoming thermal.

Reactions (6) and (9) (the latter in publication),

$$N_2+O+M=N_2O+M+40 \text{ kcal}, \quad (9)$$

deserve special interest, since they may explain the formation of nitrous oxide in the atmosphere as a photochemical equilibrium.

Acknowledgment is made to the U. S. Atomic Energy Commission [Contract At(30-3)-52] for financial assistance.

[1] R. G. W. Norrish, J. Chem. Soc. 1158 (1929).
[2] J. O. Hirschfelder and H. S. Taylor, J. Chem. Phys. **6**, 783 (1938).
[3] Values for the heats of dissociation obtained from A. G. Gaydon, *Dissociation Energies* (Dover Publications, Inc., New York, 1950).

Theory of Absorption Spectra of Catacondensed Hydrocarbons According to Platt's Circular Model of Free Electrons

GENTARO ARAKI AND TOMOKAZU MURAI
Faculty of Engineering, Kyoto University, Yosida, Kyoto, Japan
(Received March 15, 1954)

SPECTRAL levels of the series of catacondensed ring systems, in which no carbon atom belongs to more than two rings and every carbon is on the periphery of the conjugated system, was successfully classified by Platt.[1] He made use of the orbital ring quantum number on the assumption of a circular perimeter. No theoretical calculation of energy levels was carried out by him. We have calculated the excitation energy for this system, taking into account the interaction between π electrons, according to his idea. To take into account the interaction was an essential improvement for this model which enables us to obtain a satisfactory agreement between theory and experiment. The short account of the calculation will be given in what follows.

The orbitals and levels of a free electron moving in a circle are given by (in atomic units)

$$\varphi_q(x)=L^{-\frac{1}{2}}\exp(2\pi iqx/L), \qquad \epsilon(n)=2(\pi/L)^2q^2, \quad (1)$$

where q is the orbital ring quantum number, $0, \pm1, \pm2, \cdots$, and L is the perimeter length. We assume that all levels up to $\pm n$ are occupied by π electrons in the ground state ^1A of a catacondensed system. Then n is equal to the number of benzene rings contained in the system. The total number of π electrons is $2(2n+1)$. The perimeter length is equal to $2(2n+1)l$ where l is the bond length between two carbons. The lower excited states are $^{1,3}B$ and $^{1,3}L$. If we take into account the Coulomb interaction between π electrons, we can calculate the energy of the total system of $2(2n+1)$ π electrons for these ground and excited states by making use of the standard method.

The direct integrals are independent of orbitals because the electron density is constant throughout the circle. The exchange integrals depend only on the difference between orbital ring quantum numbers of two orbitals. These integrals are all divergent, but it is not a difficulty of the present model. The divergence comes from the assumption that π electrons move one-dimensionally in a circle, while the Coulomb interaction is only significant in the three-dimensional space. Therefore, we introduce r_0 as a cut-off radius for the interaction, and we shall make use of r_0 as only one parameter contained in the present model. We have thus the energy values for B and L states as follows:

$$\begin{aligned} E(^1B)&=E(^1A)+\epsilon(2n+1)-\epsilon(n)+2D(1)-D(2n+1)\\ E(^3B)&=E(^3L)=E(^1B)-2D(1)\\ E(^1L)&=E(^3L)+2D(2n+1)=E(^1B)+2D(2n+1)-2D(1), \end{aligned} \quad (2)$$

where D is the exchange integral given by (in atomic units),

$$D(n)=(2/L)\Big[\log\cot(\pi/2)(r_0/L) - \sum_{k=1}^{n} 2(2k-1)^{-1}\cos\{(2k-1)\pi r_0/L\}\Big]. \quad (3)$$

In the present model, in which the perimeter is distorted into a circle, two levels B_a and B_b coincide, and L_a and L_b, too, because matrix elements of the Coulomb interaction between two states having positive and negative orbital ring quantum numbers completely vanish on account of the circular symmetry. If we consider the deviation, from a circle, of the molecular shape the matrix elements of the Coulomb interaction do not vanish and B and L states, respectively, split into two levels. The calculated wavelength of absorption spectra on assuming $r_0/l=0.68$ is compared with experiment[2] in Table I where we adopt the bond length of benzene as the value of l, namely 1.4A. The agreement is quite satisfactory.

TABLE I. Absorption spectra $E(^1B)-E(^1A)$. n = number of rings. λ = wavelength in $m\mu$.

Substance	n	λ_{calc}	λ_{obs}
Benzene	1	186	185
Naphthalene	2	214	220
Anthracene	3	245	256
Naphthacene	4	276	272
Pentacene	5	307	310

The full account will be published later in *Progress of Theoretical Physics (Kyoto)*.

[1] J. R. Platt, J. Chem. Phys. **17**, 484 (1949).
[2] H. B. Klevens and J. R. Platt, J. Chem. Phys. **17**, 470 (1949).

Erratum: Intensities of Vibration-Rotation Bands

[J. Chem. Phys. **21**, 373 (1953)]

ROBERT C. HERMAN AND KURT E. SHULER
Applied Physics Laboratory, The Johns Hopkins University, Silver Spring, Maryland

EQUATION (3) should read:

$$|(v''|u|v''+n)|^2\cong\frac{r_e^2B_ex_e^{n-1}}{\omega_e}\frac{(v''+n)!}{n^2v''!}\left[1+nv''x_e+\frac{n}{2}(n+1)x_e\right]. \quad (3)$$

Equation (4) should read:

$$|(v''|u|v''+n)|^2\cong|(0|u|n)|^2\frac{(v''+n)!}{n!v''!}(1+nv''x_e), \quad (4)$$

where the change consists in the replacement of $(1+v''x_e)$ in the original equations by the expressions $[1+nv''x_e+n/2(n+1)x_e]$ and $(1+nv''x_e)$ with $n=v'-v''$ in Eqs. (3) and (4) above. Since these equations are valid only for $(v'+v'')x_e\ll1$, the above change will not significantly affect the values of the matrix elements. We are very much indebted to Dr. P. A. Fraser for calling our attention to these corrections.

Bending Fundamental of NO_2

MELVIN BROWN* AND M. KENT WILSON
Mallinckrodt Chemical Laboratory, Harvard University, Cambridge, Massachusetts
(Received March 5, 1954)

RECENTLY Moore has investigated the infrared spectrum of NO_2 under high dispersion in the 1.4–3.4μ region.[1] The results of this work combined with those obtained from the bending fundamental yielded the ground-state parameters and a complete set of quadratic anharmonicity coefficients. The present paper communicates the results of the investigation under prism dispersion of the bending fundamental ν_2.

Experimental.—The spectra were taken with a Perkin-Elmer Model 12C spectrometer equipped with NaCl and KBr prisms and a Baird Associates spectrophotometer with NaCl optics.

Commercial nitrogen dioxide was repeatedly redistilled until a crystalline white solid was obtained when the distillate was frozen in a trap immersed in a solid carbon dioxide-acetone mixture. To minimize overlapping absorption by the strong N_2O_4 band at 684 cm^{-1} the absorption cells were held at 175°±2°C.

The data obtained replotted on a linear frequency scale are given in Fig. 1. The positions of the Q branches are listed in the second column of Table I.

TABLE I. Rotational structure of the bending fundamental of NO_2.

Assignment P_Q	Observed (cm^{-1})	Smoothed curve (cm^{-1})
10	639	639
9	647.5	647
8	656	656
7	(667)	666
6	676	677
5	688	688
4	700	700.5
3	714.5	714.5
2	730.5	728
1	742	743
R_Q		
0	761	758.0
1	772.5	774.5
2	791.5	791.5
3	809	809
4	826.5	826.5
5	844	844
6	861	861
7	878.5	878.5
8	897	897

Discussion.—The electron diffraction investigation of NO_2[2] and the rotational structure of the bending mode indicate that nitrogen dioxide is very close to a symmetric top. Accordingly, the bending fundamental was analyzed to this approximation. To compensate partly for the deviation from a symmetric top the positions of the Q branches were plotted as a function of K and a smooth curve drawn through the points. The frequencies read from this smooth curve (column 3 of Table I) were then used to calculate the combination differences which are plotted as a function of K^2 in Fig. 2. The position of the band origin was determined by plotting the sum ${}^RQ_K+{}^PQ_{K+1}$ *versus* $K^2(K+1)^2$ as illustrated in Fig. 3. The value of ν_0 as well as the constants $(A-B)$ and D_K in both the upper and lower states are listed in Table II.

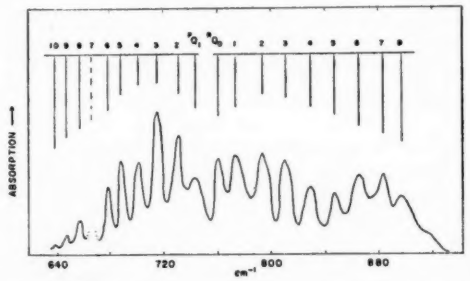

FIG. 1. The bending fundamental of NO_2. The background absorption near 880 cm^{-1} is due to nitric acid, and the dashed part of the curve indicates region observed by CO_2.

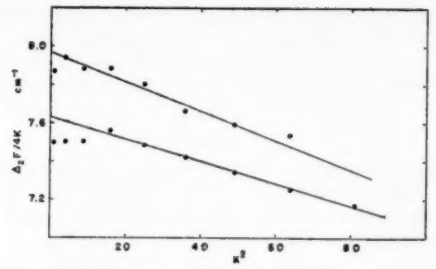

FIG. 2. Determination of the rotational constants of NO_2. The top curve refers to the upper state and the bottom curve refers to the ground state.

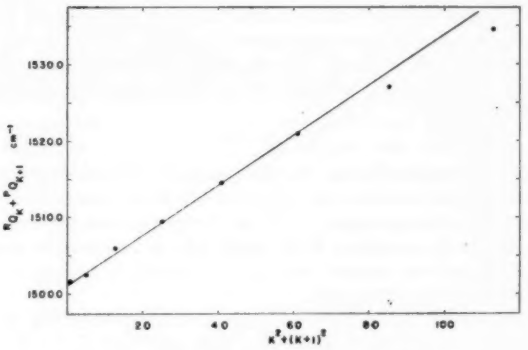

FIG. 3. Determination of the band origin for ν_2 of NO_2.

TABLE II. Rotational constants of NO_2 and band center for ν_2.

$A''-\bar{B}''$	$=7.63\pm0.05$ cm^{-1}
D_K''	$=2.9\times10^{-3}$ cm^{-1}
$A'-\bar{B}'$	$=7.97\pm0.05$ cm^{-1}
D_K'	$=3.8\times10^{-3}$ cm^{-1}
$(A'-'\bar{B})-(A''-\bar{B}'')^a$	$=0.33$ cm^{-1}
ν_0	$=750.6\pm0.3$ cm^{-1}

[a] From plot of ${}^RQ_K+{}^PQ_{K+1}$.

Since the data obtained in this investigation have been incorporated into a much more extensive paper on NO_2 by Moore,[1] it will suffice here to remark that the value of the small moment of inertia as obtained from ν_2 agrees well with that calculated from the structural parameters derived from the electron diffraction investigation.[2]

* Now at Western Reserve Medical School, Cleveland, Ohio.
[1] G. Moore, J. Opt. Soc. Am. **43**, 1045 (1953).
[2] Claesson, Donohue, and Schomaker, J. Chem. Phys. **16**, 207 (1948).

Excess Heats and Volumes of Mixing

P. MEARES
Chemistry Department, University of Aberdeen, Scotland
(Received March 11, 1954)

IN view of the recent letter of Thacker and Rowlinson,[1] it is noteworthy that many mixtures are known for which the excess enthalpy and volume of mixing have opposite signs. The purpose of this communication is to discuss briefly the data for some of these, examined by the writer,[2,3] together with the data of Thacker and Rowlinson.

In an earlier discussion[2] the existence of three effects contributing to the volume change on mixing was demonstrated. One of these,

concerned with molecular packing, is absent when the component molecules are of similar sizes. Restricting this discussion to such mixtures, two effects remain. Scatchard[4] has shown that the internal energy change on mixing ΔU is related to a volume change ΔV_f by

$$\Delta V_f = \kappa \Delta U, \quad (1)$$

where κ is the isothermal compressibility of the mixture. ΔV_f is therefore similar in sign to the energy and enthalpy of mixing. A further contribution ΔV_c arises from the differences between the compressibilities and cohesive energy densities, L, of the pure components and of the mixture. This can be expressed by[2]

$$\Delta V_c = v_1 v_2 (L_1 - L_2)(\beta_1 - \beta_2), \quad (2)$$

where v_1 and v_2 are the volume fractions of components 1 and 2 in the mixture, and β_1 and β_2 are the compressibilities of single or small groups of molecules of types 1 and 2 in the mixture. These are not susceptible to measurement or precise definition, but will clearly be smaller than the corresponding macroscopic compressibilities κ_1 and κ_2. The simplest reasonable assumption is that for random mixing

$$\beta_1 = k\kappa_1, \text{ etc.}, \quad (3)$$

where the constant, k, has the same value for all substances. It is a matter of observation that when ΔV_c is large enough to be significant, it is always negative. When the component molecules are very unlike in molecular force fields, ΔV_c is numerically greater than ΔV_f, and the enthalpy and volume changes in an endothermal mixture have opposite signs.

By a suitable choice of the constant, k, the foregoing argument is placed on a basis for comparison with experiment. In Table I

TABLE I.

Mixture	ΔV_f ml/ml	ΔV_c ml/ml	ΔV_{calc} ml/ml	ΔV_{obs} ml/ml	ΔH_{obs} cal/ml
Ethyl benzene+*o*-xylene	+0.0003	−0.0005	−0.0002	−0.0002	+0.075
Ethyl benzene+tetralin	+0.0004	−0.0009	−0.0005	−0.0007	+0.067
Ethyl benzene+dimethyl phthalate	+0.0036	−0.0061	−0.0025	−0.0024	+0.985
Ethyl benzene+diethyl phthalate	+0.0017	−0.0039	−0.0022	−0.0020	+0.371
Ethyl benzene+dipropyl phthalate	+0.0011	−0.0026	−0.0015	−0.0018	+0.200
Ethyl benzene+dibutyl phthalate	+0.0005	−0.0023	−0.0018	−0.0015	+0.045
1:3 Butanediol diacetate +dimethyl phthalate	+0.0005	−0.0028	−0.0023	−0.0012	+0.093
1:3 Butanediol diacetate +dimethylglycol phthalate	+0.0011	−0.0033	−0.0022	−0.0011	+0.356

data are given for eight mixtures, taken from references 2 and 3, which have approximately equal-sized component molecules and opposite signs for the heat and volume changes on mixing. The mixtures contain equal volumes of the two components. To calculate ΔV_c, k has been taken throughout as 0.4, a physically reasonable value. The calculation of ΔV_f has been described previously.[5] ΔV_{calc} is the sum $(\Delta V_f + \Delta V_c)$. Its good agreement with ΔV_{obs} should not be too highly stressed, as k was chosen to represent the data.

The calculation cannot be extended in such detail to the mixtures of Thaker and Rowlinson as the heats of mixing, though stated to be positive, are not available. An estimate of ΔV_f has been made by combining (1) with the Hildebrand regular solution equation,[6]

$$\Delta V_f = \kappa v_1 v_2 (L_1^{\frac{1}{2}} - L_2^{\frac{1}{2}})^2. \quad (4)$$

Calculation of ΔV_c has been carried out using for *n*-pentane and *n*-hexane the cohesive energies compiled by Hildebrand and Scott,[6] and isothermal compressibilities derived from adiabatic compressibilities[7] (i.e., C_5H_{12} $\kappa = 177\times10^{-6}$ megabar^{-1}, C_6H_{14} $\kappa = 146\times10^{-6}$ megabar^{-1}). Volume fractions have been taken as 0.5 as this will be near the composition for maximum contraction.[1,2] Similar calculations for three mixtures examined at 0°C by Mathot and Desmyter[8] have also been made. 180×10^{-6} megabar^{-1} was taken for the compressibility of neopentane; the other compressibilities were obtained as before.[5] These calculated values of ΔV are compared with the observed values in Table II. The agreement is

TABLE II.

Mixture	ΔV_f ml/ml Eq. (4)	ΔV_c ml/ml	ΔV_{calc} ml/ml	ΔV_{obs} ml/ml	H_{obs}
Ethyl benzene+*n*-pentane	+0.0044	−0.0093	−0.0049	−0.0052	+ive
Ethyl benzene+*n*-hexane	+0.0028	−0.0050	−0.0022	−0.0013	+ive
o-xylene+*n*-pentane	+0.0048	−0.0148	−0.0100	−0.0063	+ive
Neopentane+benzene	+0.0104	−0.0170	−0.0066	−0.0048	+ive
Neopentane+cyclohexane	+0.0038	−0.0074	−0.0036	−0.0105	+ive
Neopentane+carbon tetrachloride	+0.0070	−0.0130	−0.0060	−0.0049	+ive

satisfactory, considering the uncertainty in ΔV_f from (4). This equation will usually underestimate ΔV_f,[3,5] and this is supported by the fact that ΔV_{calc} is usually larger than ΔV_{obs}, except for neopentane+cyclohexane where the divergence is surprisingly large.

Consideration of the physical relation between cohesive energy density and compressibility in terms of molecular force and volume parameters shows that the behavior of $(\Delta V_f + \Delta V_c)$ for various mixtures follows closely the predictions of Prigogine and Bellemans,[9] based on the cell model for mixtures of molecules of slightly different sizes.

[1] R. Thacker and J. S. Rowlinson, J. Chem. Phys. **21**, 2242 (1953).
[2] P. Meares, Trans. Faraday Soc. **45**, 966 (1949).
[3] P. Meares, Trans. Faraday Soc. **49**, 1133 (1953).
[4] G. Scatchard, Trans. Faraday Soc. **33**, 160 (1937).
[5] P. Meares, Trans. Faraday Soc. **45**, 1066 (1949).
[6] J. H. Hildebrand and R. L. Scott, *Solubility of Non-electrolytes* (Reinhold Publishing Corporation, New York, 1950), 3rd edition.
[7] W. Schaaffs, Z. physik. Chem. **194**, 28 (1944).
[8] V. Mathot and A. Desmyter, J. Chem. Phys. **21**, 782 (1953).
[9] I. Prigogine and A. Bellemans, Faraday Soc. Disc. **15**, 80 (1953).

Thermodynamic Functions of Hydrogen Isocyanate

NORBERT W. LUFT AND OM P. KHARBANDA
Simon-Carves Ltd., Cheadle Heath, Stockport, England
(Received March 18, 1954)

A LIKELY side reaction in a nitrogen-containing system at high temperatures is a radical combination according to

$$NH + CO \rightarrow HNCO, \quad (1)$$

and for kinetic considerations the thermodynamic functions of hydrogen isocyanate are required. These can now be obtained statistically from known[1,2] molecular parameters and vibrational frequencies, *viz.*, fundamentals $\omega = 572$, 670, 797, 1327, 2274, 3531 cm^{-1}, and moments of inertia $I\times10^{40} = 0.9157$, 76.36, 77.276 g cm^2. The functions were calculated for an ideal gas of HNCO molecules at a total pressure of 1 atmos by using the familiar approximation of the harmonic oscillator and rigid rotator (Table I).

TABLE I. Calculated thermodynamic functions of ideal HNCO gas at 1 atmos.

T°K	S^0	$-(F^0-H_0^0)/T$	$(H^0-H_0^0)/T$	C_p^0
298.16	56.92	48.14	8.78	10.73
300	56.97	48.19	8.78	10.75
400	60.26	50.81	9.45	12.08
500	63.06	52.98	10.08	13.12
600	65.54	54.88	10.66	13.93
800	69.72	58.08	11.64	15.19
1000	73.22	60.77	12.45	16.12
1200	76.23	63.10	13.13	16.84
1400	78.86	65.16	13.70	17.39
1500	80.06	66.12	13.94	17.61

The accuracy of the calculated figures is regarded as satisfactory since the basic molecular parameters and vibrational frequencies do not involve any major uncertainties. The only frequency which has not yet been located precisely is the nonplanar bending frequency ω_6 of species a'', for which Herzberg and Reid's[1] value of 670 cm^{-1} has been accepted in the present calculations.

The assignment of some overtone bands is less certain, and the problem of inversion doubling, especially in the bending frequency ω_3, has not been looked into so far. By a method outlined earlier,[3] the inversion barrier in HNCO is estimated to be as low as $V_\pi = 5.6$ kcal/mole, i.e., of the same order of magnitude as in NH_3. Judging from the experience[4] with NH_3, however, it may be concluded that below 1500°K such inversion doubling would not affect the thermodynamic functions significantly.

[1] G. Herzberg and C. Reid, Disc. Faraday Soc. **9**, 92 (1950).
[2] W. J. O. Thomas, Trans. Faraday Soc. **49**, 855 (1953).
[3] N. W. Luft, Disc. Faraday Soc. **14**, 114 (1953).
[4] K. S. Pitzer, J. Chem. Phys. **7**, 251 (1939).

$BaTiO_3$-KF Phase Diagram

CLARENCE KARAN
International Business Machines Corporation, Poughkeepsie, New York
(Received March 15, 1954)

IT has been found that on the $BaTiO_3$ rich side of the eutectic composition, the liquidus temperatures[1] obtained by the differential thermal analysis techniques are low. This was also pointed out to the author by workers at Bell Telephone Laboratories.[2] Depression of the liquidus, it is believed, was introduced by supersaturation which was apparently relatively constant throughout the various determinations, hence escaping early detection.

Work is being continued on this system and it is hoped that a complete phase equilibrium diagram, for the KF-rich end at least, will be obtained. As an interim measure, more nearly correct liquidus temperatures have been determined by straightforward solubility measurements. Solubility data appear in Table I.

TABLE I. Mole percent solubility of $BaTiO_3$ in KF *vs* temperature.

Temp., °C	1000	1050	1100	1150	1200	1250	1300
$BaTiO_3$, mole %	4	6	9	12½	17	22½	28½

[1] C. Karan and B. J. Skinner, J. Chem. Phys. **21**, 2225 (1953).
[2] Private communication from S. O. Morgan, based on unpublished work of S. S. Flaschen.

Erratum: Heats of Combustion and Formation of Some Organosilicon Compounds

[J. Chem. Phys. **19**, 1330 (1951).]
TOSHIO TANAKA, UKIKO TAKAHASHI, ROKURO OKAWARA, AND TAKEO WATASE
Institute of Industrial Chemistry, Faculty of Engineering, Osaka University, Osaka, Japan
(Received March 15, 1954)

IN Table I of the paper referred to above, $-\Delta H_R$ and $-\Delta H_f^0$ are to be amended as shown in Table I. In this table we adopted the value −208 kcal $mole^{-1}$ instead of the older value used in our previous paper for the heat of formation of silica.

TABLE I. Molar heat of combustion and formation at 20°C.

Substance	$-\Delta H_R$ kcal $mole^{-1}$	$-\Delta H_f^0$, kcal $mole^{-1}$ obs
Hexamethylcyclotrisiloxane	1407	396
Hexaphenylcyclotrisiloxane	4810	225
Diethylsilanediol	782	212
Dimethyldiethoxysilane	1119	200
Di-*n*-propyldiethoxysilane	1751	217

Polar Solvent Effects on the Absorption Spectra of Metallic Complexes

KAZUO NAKAMOTO, MASAHISA KOBAYASHI, AND RYUTARO TSUCHIDA
Department of Chemistry, Faculty of Science, Osaka University Nakanoshima, Kita, Osaka, Japan
(Received March 11, 1954)

ABSORPTION spectra of metallic complexes generally have two absorption bands, the first lies in the visible region, and the second in the near ultraviolet. Adjacent to these bands, many complexes show strong absorptions usually designated as the cpecific band. One of the authors, Tsuchida, has previously dissussed their origins in terms of electronic structure. According to Tsuchida,[1] the first band is due to *d* or *f* electrons in an unsaturated shell of the central metallic ion, the second band is attributed to coordination electrons, and the specific band is caused by the ligand itself.

After study of quantitative correlation between the first and the second bands, Soné[2] has concluded that both bands should be ascribed to the same origin. Inamura and Kondo[3] studied the absorption spectra of Ir^{III} and Ir^{IV} complexes and suggested that both bands may be due to the coordination electrons. However, the optical rotatory dispersion of *d* [Co *en*$_3$]Br_3 [4] shows that the contribution of each band to the rotatory power is remarkably different. Moreover, the dichroism of Co-praseo salt[5] in the case that the bands have inverted dichroic properties. As stated above,

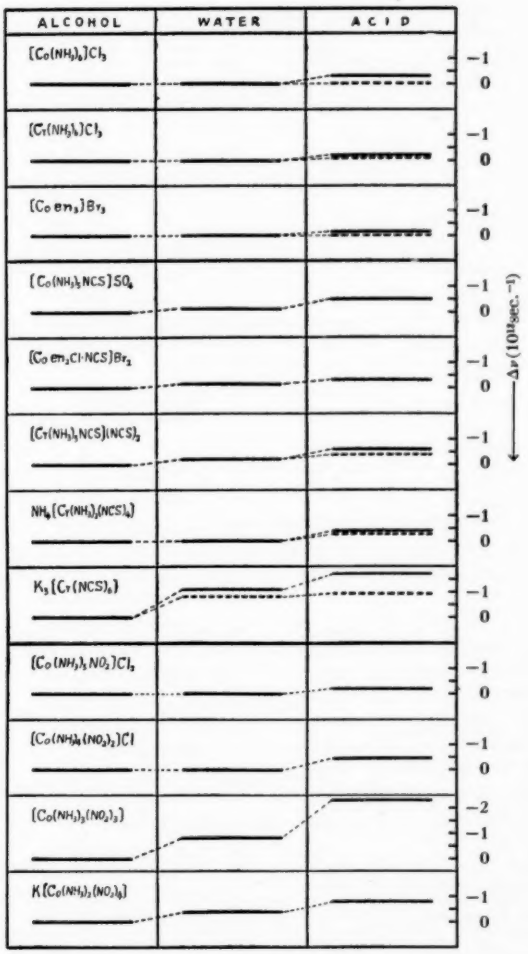

FIG. 1. The solvent behavior of the first and the second bands: ———, first band; – – – – –, second band. (In the case of nitro and some rhodanato complexes, overlapping of the second band by the strong specific band prevents measurement of the second band maximum.)

the origins of the absorption bands in metallic complexes have been a subject of much discussion and conflicting evidence.

The present work was undertaken to investigate the relation between the type of bands and their behavior in a series of polar solvents. Measurements of absorption spectra of typical metallic complexes in alcoholic solution, water, and acetic acid solution were made using a Beckman Model DU spectrophotometer. In order to compare the magnitude of the relative shift, the maxima of the first and the second bands in an alcoholic solution are shown on the same level in Fig. 1. The figure shows definitely that both bands become progressively more bathochromic as the solvent is changed in the order, alcohol, water, and acetic acid (red shift). The only difference between them is that the first band is generally shifted more markedly than the second band.

The solvent behavior of the specific band is, however, in the opposite direction to the first and the second bands as is shown in Fig. 2. That is, the band becomes progressively more hypsochromic in the same order of the solvents (blue shift). Irregularity is found in rhodanato complexes, but it may be due to some special interaction between the rhodanato group and acetic acid.

If we compare our results with that of McConnell,[6] we find that the first and the second bands correspond to the $\pi-\pi$ absorption, whereas the specific band corresponds to the $n-\pi$ absorption. In fact, absorption spectra of amine and ethylenediamine complexes which have bound lone pair electrons for coordination do not show the specific bands, while the complexes which have CN^-, NO_2^-, ONO^-, H_2O, NCS^-, SO_4^{--}, NO_3^-, OH^-, $C_2O_4^{--}$, CO_3^{--}, Cl^-, CrO_4^{--} Br^-, I^-, etc., as ligands always indicate their own specific bands. This fact suggests that the specific absorption originates in the lone pair electrons of the ligands. In regard to the first and the second bands, however, a conclusion cannot be drawn at the present time as to whether both of them should be ascribed to the same type of electrons or not. Experimental work is now in progress which may lead to a better theoretical explanation.

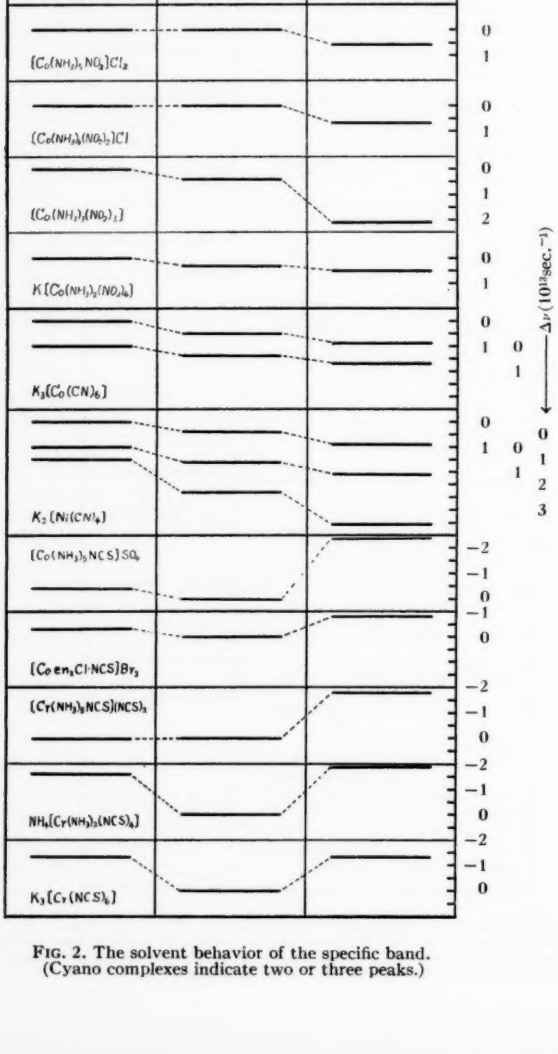

FIG. 2. The solvent behavior of the specific band. (Cyano complexes indicate two or three peaks.)

[1] R. Tsuchida, Bull. Chem. Soc. Japan **13**, 388, 436, and 471 (1938).
[2] K. Soné, J. Chem. Soc. Japan **71**, 270, 316, and 364 (1950).
[3] Y. Inamura and S. Kondo, J. Chem. Soc Japan **72**, 787 and 840 (1951).
[4] M. Kobayashi, J. Chem. Soc. Japan **72**, 787 and 840 (1950).
[5] S. Yamada and R. Tsuchida, Bull. Chem. Soc. Japan **25**, 127 (1952).
[6] H. McConnell, J. Chem. Phys. **20**, 700 (1952).

Nuclear Quadrupole Resonance in Ethyl Chloroformate and Ethyl Trichloroacetate*

T. L. WEATHERLY AND QUITMAN WILLIAMS
School of Physics, Georgia Institute of Technology, Atlanta, Georgia
(Received March 18, 1954)

PURE quadrupole resonance has been observed in ethyl chloroformate and ethyl trichloroacetate at liquid nitrogen temperature. Observations were made using a simple regenerative oscillator, Zeeman modulation, and a phase-sensitive detector. Frequencies were measured with a Signal Corps BC-221 frequency meter calibrated against radio station WWV. The Cl^{35} resonance frequencies are listed in Table I along with the resonance frequencies for trichloroacetyl chloride reported by Allen.[1]

TABLE I

1. Ethyl chloroformate	$Cl-\overset{\overset{O}{\|}}{C}-O-C_2H_5$	33.858
2. Trichloroacetyl chloride[a]	$Cl-\overset{\overset{O}{\|}}{C}-CCl_3$	33.721 40.132 40.473 40.613
3. Ethyl trichloroacetate	$C_2H_5-O-\overset{\overset{O}{\|}}{C}-CCl_3$	40.200 40.339

[a] Data from reference 1.

Comparison of the structural formulas and resonance frequencies for these molecules illustrates the effect of chemical bonding on nuclear quadrupole resonance pointed out by Livingston[2] and Allen.[3] In molecules 1 and 2 the chlorine atoms on the left end have almost identical bonding to the carbon atom and their resonance frequencies are almost the same. In molecules 2 and 3 the CCl_3 groups have almost identical bonding to the molecule, and again the resonance frequencies for the chlorine atoms are about the same.

The existence of two resonances for the CCl_3 group of ethyl trichloroacetate and three for the same group in trichloroacetyl chloride is probably a result of the difference in crystal structure of the two molecules.

* Sponsored by the Office of Ordnance Research, U. S. Army.
[1] H. C. Allen, J. Am. Chem. Soc. **74**, 6074 (1952).
[2] Ralph Livingston, J. Phys. Chem. **57**, 496 (1953).
[3] H. C. Allen, J. Phys. Chem. **57**, 501 (1953).

Erratum: Author Index to Volume 21

[J. Chem. Phys. **21**, 2249 (1953)]

THE first line after the name of "Clark, Joan R." should read:

Cleveland, Forrest F. (see Bernstein, Richard B.)—1778, 1903(L).

The Molecular Structure of 1,1,2,2-Tetrafluorodichloroethane

M. IWASAKI, S. NAGASE, AND R. KOJIMA
The Government Industrial Research Institute, Nagoya, Japan
(Received February 8, 1954)

UNDER superatmospheric pressures, CF_2Cl-CF_2Cl was obtained by the fluorination of C_2Cl_6 with SbF_3 in the presence of an $SbCl_5$ catalyst. The product was distilled at 4°C. The purity of this sample was tested by an infrared absorption spectrum.[1]

The molecular structure of gaseous CF_2Cl-CF_2Cl was investigated with the electron diffraction method. The diffraction camera[2] used had a rotating sector, the aperture of which was proportional to S^2. The diffraction pattern was measured up to $S=22$ by a recording microphotometer. A procedure similar to that employed by Karle[3] was used for deriving the radial distribution curve from a microphotometer record. The radial distribution curve thus obtained from the experimental intensity curve is shown in Fig. 1. The bond distances and bond angles determined from this are as follows:

$$\begin{aligned} &C-F=1.33A, && \angle CCF=108° \\ &C-Cl=1.74A, && \angle FCF=108° \\ &C-C=1.45A \text{ (assumed)}, && \angle ClCF=110°30'. \end{aligned}$$

The C−C single bond distance was assumed to be 1.45A, appreciably smaller than the normal value 1.54A. Unless this short distance is assumed, one cannot give reasonable interpretation of the radial distribution curve. It is because the positions of a peak at 2.15A and those lying between 3A and 4.5A show values smaller than those expected for a model having a normal C−C bond distance; the former peak corresponds to the nonbonded C···F distance, while the latter to the long inter-halogen distances.

This shortening of the C−C bond distance has already been found in some fluorinated hydrocarbons, *viz.*, CHF_2-CHF_2, $CH_3CF_2CH_3$, $CF_3CF_2CF_3$, and CF_3CH_2Cl.[4] Other bond distances and bond angles have reasonable values compared with the structures of similar fluorinated hydrocarbons.[4]

Two rotational isomers, *trans* and *gauche*, are expected in this molecule as in related halogenated ethanes. In fact, the peak at 4.24A corresponds to *trans*-(Cl···Cl) distance characteristic of

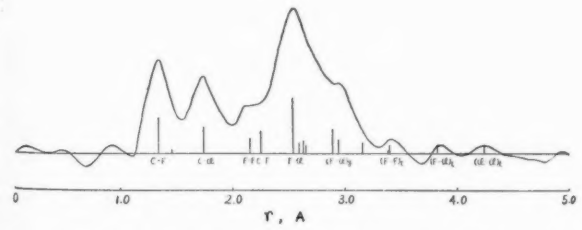

FIG. 1. The radial distribution curve of 1 1,2,2-tetrafluorodichloroethane.

the *trans*-form, and the peak at 3.84A to *trans*-(F···Cl) distance characteristic of the *gauche*-form. These two peaks show evidently the existence of the two rotational isomers. From the ratio of the heights of these two peaks, one can roughly estimate the abundance ratio of the two isomers. Hence, this molecule can be considered to be a nearly equimolecular mixture of the *trans*- and *gauche*-forms. From Raman[5] and infrared[6] spectroscopic data, the existence of rotational isomers has already been confirmed.

The abscissa of the vertical lines shown in Fig. 1 are the interatomic distances calculated from the results mentioned above while the heights are drawn proportional to Z_iZ_j/r_{ij}. The agreement with the peaks in radial distribution curve is very good in regard to the positions and the heights.

This experiment was carried out using an apparatus in Nagoya University. We would like to express our gratitude to Professor M. Kubo and Dr. M. Kimura for giving us facilities to use the apparatus. Thanks are also due Mr. S. Saheki for his measurement on the infrared absorption spectrum.

[1] An infrared absorption spectrum was obtained on a Perkin-Elmer Model 12C spectrometer in the Government Chemical Industrial Research Institute, Tokyo.
[2] Annual Meeting of the Chemical Society of Japan held in April, 1953. Morino, Kimura, and Iwasaki, "Construction of an electron diffraction camera with a rotating sector." This apparatus has recently been set up in the Chemical Department, Faculty of Science, Nagoya University, Nagoya, Japan.
[3] I. L. Karle and J. Karle, J. Chem. Phys. **17**, 1052 (1949); **18**, 957 (1950).
[4] J. H. Simones, *Fluorine Chemistry* (Academic Press Inc., New York, 1950), Vol. 1, p. 348.
[5] G. Glockler and C. Sage, J. Chem. Phys. **8**, 291 (1940).
[6] D. Simpson and E. K. Plyler, J. Research Natl. Bur. Standards **50**, 223 (1953).

Equivalence of Chang's and Nakamura's Theories of Hindered Rotation in Molecular Crystals

HUBERT M. JAMES, *Purdue University, Lafayette, Indiana*
AND
THEODORE J. KRIEGER, *Battelle Memorial Institute, Columbus, Ohio*
(Received February 18, 1954)

THEORIES of "rotational" transitions in crystals have been developed by Chang[1] and by Nakamura,[2] both following the general ideas of Bethe's[3] treatment of order-disorder transitions in alloys. The two formulations of the theory are rather dissimilar in appearance, Nakamura's being the more elegant, and Chang's following more closely the pattern of Bethe's original work. When applied to identical crystal models, consisting of molecules with next-neighbor coupling energy proportional to $\cos\theta_{ij}$, they obtain the same values for the transition temperature, but different values for the discontinuity in C_v at the transition point. In discussing this discrepancy, Nakamura has suggested that Chang's theory is not correctly modeled after Bethe's approximation. We wish to point out that Chang's theory and Nakamura's are in fact equivalent, and that the discrepancy in values of ΔC_v is due to a numerical error in Chang's work.

The basic function in Nakamura's theory is $g_a(\omega_i)$, which gives the distribution of orientations ω_i for molecule i on an a site in the lattice. This is determined by the consistency condition

$$\int K(\omega,\omega')[g_b(\omega')]^{(z-1)/z}d\omega'=\lambda[g_a(\omega)]^{1/z}, \tag{1}$$

where

$$K(\omega,\omega')=\frac{1}{4\pi}\exp\left[-\frac{J}{2kT}\cos(\omega,\omega')\right], \tag{2}$$

and $g_b(\omega')$ is the distribution of orientations of a molecule on a b site, this function being identical with g_a if $J<0$, and differing by a reflection in the xy plane if $J>0$. As usual, z is the number of b sites surrounding an a site.

Nakamura formulates his theory by considering only a pair of next-neighbor molecules, but Chang considers a central molecule and all its next neighbors, which form the "outer shell." The basic function of Chang's theory is $g(\omega_i)$, which is not itself a distribution function, but a weight function that represents the weight given to orientation ω_i of an outer-shell molecule by its interaction with its $z-1$ next neighbors that lie outside the outer shell; the effect of coupling to the central molecule in determining the orientational distribution of this outer-shell molecule is considered separately. Nakamura's criticism of Chang's theory seems to be based on identification of Chang's $g(\omega)$ with his own $g_a(\omega)$. Actually, since $g_a(\omega)$ represents the orienting effect of interaction with z neighbors, $g(\omega)$ the effect of interaction with only $z-1$ neighbors, one must expect $g(\omega)$ to be proportional to $[g_a(\omega)]^{(z-1)/z}$. Since $g_a(\omega)$ and $g(\omega)$ both integrate to 4π, in the respective theories, the precise relation between them is

$$g(\omega)=4\pi[g_a(\omega)]^{(z-1)/z}\Big/\int[g_a(\omega)]^{(z-1)/z}d\omega. \tag{3}$$

In terms of Chang's function $g(\omega)$, Nakamura's consistency condition becomes, for $J<0$,

$$\int K(\omega,\omega')g(\omega')d\omega'=\lambda'[g(\omega)]^{1/(z-1)}. \quad (4)$$

Chang's consistency relation is expressible as

$$\int d\omega' K(\omega,\omega')g(\omega)\left[\int d\omega'' K(\omega',\omega'')g(\omega'')\right]^{z-1} = \int\left[d\omega' K(\omega,\omega')g(\omega')\right]^{z}. \quad (5)$$

It is easily seen that Eq. (5) follows from Eq. (4), but it is not evident that the converse is true. Thus every solution obtained in Nakamura's formulation will be a solution in Chang's formulation, but we cannot exclude the possibility that Chang's approach might lead to other solutions without physical significance. Our own work on transitions in systems with a more general type of molecular interaction[4] is based on a consistency condition that leads to Eq. (4) with an appropriately generalized form of $K(\omega,\omega')$ [see Eq. (8.11) of reference 4]; it is thus equivalent to Nakamura's condition.

Nakamura writes

$$g_a(\omega)=1+\sum_{\tau=1}^{\infty} c_\tau P_\tau(\cos\theta), \quad (6)$$

converts Eq. (4) to a set of conditions on the c_τ, and solves these assuming $c_\tau=O(c_1{}^\tau)$. Chang writes

$$g(\omega)=1+\sum_{\tau=1}^{\infty} a_\tau P_\tau(\cos\theta), \quad (7)$$

converts Eq. (5) to a set of conditions on the a_τ, and solves these assuming $a_\tau=O(a_1{}^\tau)$. We have verified by direct comparison that these solutions are entirely equivalent,[5] and that Chang's expression for ΔC_v is equivalent to Nakamura's; our numerical calculations check those of Nakamura, rather than those of Chang.

[1] T. S. Chang, Proc. Cambridge Phil. Soc. **33**, 524 (1937).
[2] T. Nakamura, J. Phys. Soc. Japan **7**, 264 (1952).
[3] H. A. Bethe, Proc. Roy. Soc. (London) **A150**, 552 (1935).
[4] H. M. James and T. J. Krieger, J. Chem. Phys. **22**, 796 (1954).
[5] The following misprints in Nakamura's paper should be noted:

Eq. (29) and (30): replace λ_l by $(-1)^l\lambda_l$
Eq. (33): replace $[z/(z-2)]^2$ by $[z/(z-1)]^2$.

Erratum: Magnetic Susceptibilities of Np^{+6}, Np^{+5}, and Np^{+4}

[J. Chem. Phys. **22**, 386–393 (1954)]

DIETER M. GRUEN AND CLYDE A. HUTCHISON, JR.
Institute for Nuclear Studies, Department of Chemistry, and Argonne National Laboratory, University of Chicago, Chicago, Illinois

FOOTNOTE number 11 should be replaced by the following:

A more detailed form of this paper (or extended version, or material supplementary to this article) has been deposited as Document number 4234 with the ADI Auxiliary Publications Project, Photoduplication Service, Library of Congress, Washington 25, D. C. A copy may be secured by citing the Document number and by remitting \$3.75 for photoprints, or \$2.00 for 35-mm microfilm. Advance payment is required. Make checks or money orders payable to; Chief, Photoduplication Service, Library of Congress.

Announcement

IN accordance with the By-Laws, By-Law III, Sections 6c and 6d, the Nominating Committee has informed me of nominations for the new officers of the Division of Chemical Physics, and I have cast a ballot whereby they are elected. These new officers, accordingly, are J. G. Kirkwood as Vice-Chairman, and C. H. Townes as Executive Committee member.

The complete new list of officers, with the year in which they will cease from their offices, is as follows.

E. H. Nielsen	Chairman (1955)
J. G. Kirkwood	Vice-Chairman (1955)
Bryce Crawford, Jr.	Secretary (1955)
F. G. Brickwedde	Treasurer (1955)
C. H. Townes	Executive Committee (1957)
A. A. Frost	Executive Committee (1956)
K. S. Pitzer	Executive Committee (1956)
D. F. Hornig	Executive Committee (1955)
J. O. Hirschfelder	Executive Committee (1955)

BRYCE CRAWFORD, JR.
Secretary